An Experimental Parametric Analysis of Particle Dampers for Optimizing their Applications

D I S S E R T A T I O N
zur Erlangung des akademischen Grades

Doktoringenieur
(Dr.-Ing.)

von M.Sc. Braj Bhushan Prasad
geboren in Gaya, Indien

genehmigt durch die Fakultät für Maschinenbau
der Otto-von-Guericke-Universität Magdeburg

Gutachter:
1. Prof. Dr.-Ing. Elmar Woschke
2. Prof. Dr.-Ing. André Katterfeld
3. Dr.-Ing. Fabian Duvigneau

Promotionskolloquium am 11.08.2025

Abstract

Particle damping is a passive vibration mitigation technique that harnesses the inherent dissipative properties of granular materials. By strategically incorporating these materials into vibrating structures, significant energy dissipation can be achieved through particle-particle and particle-wall collisions. However, the complex interactions between particle properties, cavity geometry, packing arrangement, and excitation conditions have made it difficult to develop a comprehensive design framework. This work addresses these challenges through extensive experimental investigations, identifying key design parameters and their effects on vibration reduction, ultimately establishing a robust framework for optimizing particle damper performance.

Advancements in particle damping are presented, focusing on overcoming the limitations of conventional particle dampers made from traditional granular materials (e.g. steel and lead). While these dampers effectively reduce vibration amplitudes in high-frequency ranges, their performance at low frequencies is often limited. A significant contribution of this thesis is the development of recycled rubber particle dampers (RRPDs) made from automotive tire waste. These dampers not only reduce vibrations across both high- and low-frequency ranges but also minimize additional mass, making them suitable for the lightweight industry. Additionally, this study examines the impact of polydisperse granular materials on vibration attenuation, an area underexplored in previous studies. The findings indicate that both particle size and particle size distribution are critical to optimizing damper efficiency.

Another significant challenge in the field of particle damping is the inadequate kinetic energy generated by the main structure, which often fails to mobilize the granular particles within the damper. Without sufficient kinetic energy, the granular materials cannot effectively interact through particle-particle and particle-wall collisions, limiting the overall damping performance. To overcome this issue, three innovative passive design variants are introduced in this thesis, namely: the thin wall cavity (TWC), the thin wall cavity with additional sheets (TWC-AS), and the ring cavity (RC). These designs effectively introduce additional kinetic energy into the granular materials, enhancing their mobilization and improving damping performance.

The long-term reliability of particle dampers, particularly under prolonged loading conditions, has remained largely unexplored. To address this, an extensive durability test was conducted to evaluate the performance of dampers incorporating rubber granulates under high-amplitude cyclic loading and varying temperature conditions over an extended period. The results showed that, even after prolonged exposure to these challenging conditions, the dampers retained their vibration attenuation capabilities. This demonstrates that rubber granulate-based particle dampers are not only effective in the short term but are also capable of sustaining performance under long-term loading conditions, making them a promising solution for real-world engineering applications.

Lastly, this work bridges the gap between laboratory research and industrial applications by testing the examined design parameters on full-scale structures, such as wind turbine generators, blades, and electric vehicles. The results show that particle dampers, designed according to the proposed framework, can be effectively implemented in large-scale engineering systems.

This thesis provides valuable new insights and introduces innovative advancements in particle damping technology. These developments enhance the efficiency and durability of particle dampers, addressing key limitations and optimizing their performance. Furthermore, the research offers practical and effective solutions for applying particle damping in industrial-scale structures, demonstrating its efficiency in improving the performance and reliability of engineering systems in real-world applications. Through these contributions, this work significantly advances both the theoretical understanding and practical implementation of particle damping technology.

Kurzfassung

Partikeldämpfer stellen ein passives Verfahren zur Reduktion mechanischer Schwingungen dar, dessen Wirkprinzip auf den dissipativen Eigenschaften granularer Materialien beruht. Durch die gezielte Integration dieser Materialien in schwingungsbeanspruchte Strukturen erfolgt eine effiziente Energiedissipation infolge von Partikel-Partikel- sowie Partikel-Wand-Kollisionen. Die Entwicklung eines übertragbaren und umfassenden Gestaltungsansatzes für Partikeldämpfer wird jedoch durch die komplexen Wechselwirkungen zwischen partikelbezogenen Materialeigenschaften, Kavitätsgeometrie, Packungsdichte und den jeweiligen Anregungsbedingungen erheblich erschwert. Die vorliegende Arbeit setzt sich mit diesen Herausforderungen auseinander, indem sie auf systematische experimentelle Untersuchungen zurückgreift, zentrale Einflussparameter sowie deren Wirkung auf die Schwingungsdämpfung herausarbeitet und auf dieser Grundlage ein robustes Optimierungskonzept für die Auslegung von Partikeldämpfern entwickelt.

Aufbauend auf diesen Grundlagen werden im weiteren Verlauf neue Entwicklungen im Bereich der Partikeldämpfer vorgestellt, die darauf abzielen, die Beschränkungen konventioneller Dämpfungskonzepte zu überwinden. Während herkömmliche Partikeldämpfer zwar eine wirksame Reduktion von Schwingungsamplituden im Hochfrequenzbereich ermöglichen, zeigen sich oftmals Defizite hinsichtlich der Dämpfung im Niederfrequenzbereich. Ein wesentlicher Beitrag dieser Arbeit liegt daher in der Entwicklung gummibasierter Partikeldämpfer (Recycled Rubber Particle Dampers, RRPDs), die aus Altreifenmaterial gefertigt werden. Diese Dämpfer erlauben eine effiziente Schwingungsreduktion sowohl im Hoch- als auch im Niederfrequenzbereich, wobei die zusätzliche Masse gering bleibt – ein entscheidender Vorteil für Leichtbauanwendungen. Ergänzend erfolgt eine Analyse des Einflusses polydisperser granularer Materialien auf die Schwingungsdämpfung, einem bislang nur unzureichend adressierten Forschungsaspekt. Die erzielten Ergebnisse verdeutlichen, dass sowohl die absolute Partikelgröße als auch die Partikelgrößenverteilung maßgebliche Parameter für die Optimierung der Leistungsfähigkeit von Partikeldämpfern darstellen.

Darüber hinaus wird eine weitere zentrale Herausforderung adressiert, die in der begrenzten Mobilisierung granularer Partikel liegt. Diese tritt infolge einer unzureichenden kinetischen Energie der Hauptstruktur auf und reduziert die Effizienz der Schwingungsdämpfung. Zur Lösung dieses Problems werden drei innovative passive Konstruktionskonzepte vorgestellt: die Dünnwandkavität (Thin-Walled Cavity, TWC), die Dünnwandkavität mit zusätzlichen Platten (TWC with Additional Sheets, TWC-AS) sowie die Ringkavität (Ring Cavity, RC). Diese Ansätze verbessern die Energieübertragung auf die Partikel, intensivieren deren Bewegung und steigern dadurch die Dämpfungsleistung signifikant.

Ein weiterer Schwerpunkt dieser Arbeit liegt auf der Untersuchung der langfristigen Zuverlässigkeit von Partikeldämpfern, die bislang nur unzureichend erforscht ist. Zu diesem Zweck wurde ein umfangreicher Dauertest durchgeführt, bei dem die Leistungsfähigkeit gummigranulatbasierter Partikeldämpfer unter zyklischen Hochamplitudenbelastungen sowie variierenden Temperaturbedingungen über einen längeren Zeitraum systematisch bewertet wurde. Die Ergebnisse zeigen, dass die untersuchten Dämpfer auch nach langandauernder Beanspruchung ihre schwingungsdämpfenden Eigenschaften beibehalten. Damit wird nachgewiesen, dass Partikeldämpfer auf Basis von Gummigranulat nicht nur kurzfristig wirksam sind, sondern auch unter Langzeitbelastung eine stabile Leistungsfähigkeit aufweisen und sich somit als besonders vielversprechende Lösung für ingenieurtechnische Anwendungen qualifizieren.

Abschließend wird eine Brücke zwischen laborbasierten Untersuchungen und industriellen Anwendungen geschlagen, indem die identifizierten Designparameter an großtechnischen Strukturen wie Windturbinen-Generatoren, Rotorblättern und Elektrofahrzeugen evaluiert werden. Die Ergebnisse belegen, dass Partikeldämpfer, die auf Grundlage des entwickelten Designrahmens konzipiert wurden, erfolgreich in großskaligen ingenieurtechnischen Systemen implementierbar sind.

Zusammenfassend generiert diese Dissertation neue wissenschaftliche Erkenntnisse sowie innovative Konzepte zur Weiterentwicklung der Partikeldämpfertechnologie. Die erzielten Resultate leisten einen Beitrag zur Steigerung der Effizienz und Langlebigkeit von Partikeldämpfern, indem bestehende Beschränkungen gezielt adressiert und die Leistungsparameter systematisch optimiert werden. Darüber hinaus werden praxisorientierte Lösungsansätze für den industriellen Einsatz bereitgestellt, welche die Effektivität der Partikeldämpfung zur Erhöhung der Leistungsfähigkeit und Zuverlässigkeit technischer Systeme in realen Anwendungen nachweisen. Damit erbringt die vorliegende Arbeit einen substantiellen Beitrag sowohl zur theoretischen Fundierung als auch zur praktischen Implementierung der Partikeldämpfertechnologie.

Contents

Figures

Tables

Notation

Latin Symbols

a_0	Fourier series coefficient
a	radius of circular contact area
a_m	Fourier series coefficient
b	half-width of the rectangular profile
b_{d}	effective damping parameter
b_m	Fourier series coefficient
c_m	complex valued Fourier coefficients
$d10$	effective diameter
$d50$	median particle size
$d90$	coarse fraction
e_n	coefficient of restitution
E^*	equivalent Young's moduli
E_{diss}	dissipated energy
ΔE_f	energy loss due to friction
ΔE_n	energy dissipation due to normal impact
ΔE_t	energy dissipation due to tangential impact
E_{max}	maximum dissipated energy
F	force signal acting on the wall
$F(t)$	total force exerted by the particles
$F(\omega)$	signal in frequency domain
f	impulse signal
$f(x)$	real valued function
$f(t)$	continuous-time signal
$f[n]$	discrete-time signal
$F[n]$	discrete Fourier transform
f_c	center frequency
f_l	lower limit frequency
f_N	Nyquist frequency
f_s	sampling frequency
f_u	upper limit frequency
$f_W(t)$	windowed signal
i	imaginary number
ΔL	level error
L	period
l	contact length
m	mass of particle
$N(t)$	noise component
P	average power transmission
P_{diss}	power dissipated
P_{max}	maximum power
R	radius of spheres
R_{eff}	equivalent radius

$S(t)$	signal component
T	vibration period
V	container velocity amplitude
V^*	complex velocity amplitude
v	surface velocity
v_n	relative normal velocity between two particles
v_t	relative tangential velocity between two particles
$W(n)$	Hanning window function
$W(t)$	window function in time domain
$W(\omega)$	window function in frequency domain
X	amplitude
$\dot{x}$	particle velocity

Greek Symbols

Ω	excitation angular frequency
δ_t	overlap distance between two contacting particles
η	loss factor
ω	angular frequency
ω_0	fundamental frequency
$\mathcal{O}$	Landau notation
σ	RMS value
ν	Poisson's ratio
ζ	coefficient of friction

Abbreviations

AC	alternating current
CFRP	carbon-fiber-reinforced plastic
DC	direct current
DEM	discrete element method
DFT	discrete Fourier transform
ELT	end-of-life tires
EPDM	ethylene propylene diene monomer
EV	electric vehicle
FFT	fast Fourier transform
FEM	finite element method
FPID	finite particle impact damper
FRF	frequency response function
GFRP	glass-fiber-reinforced plastic
HCDP	honeycomb damping plate
HMPD	hard material particle damper
HPD	hybrid particle damper
ICE	internal combustion engine
IFAM	institute for manufacturing technology & advanced materials
LSV	laser scanning vibrometer
MBD	multi-body dynamics
MLW	mainlobe width
MU	multi-unit
MUPD	multi-unit particle damper
NPOD	non-destructive particle damper
NVH	noise, vibration and harshness
PCB	printed circuit board

PC	polycarbonate
PEC	pre-existing cavity
PEM	power electronic module
PP	polypropylene
PSD	particle size distribution
PVC	polyvinyl chloride
PWM	pulse width modulation
RC	ring cavity
RG	rubber granulate
RP	rubber powder
RPM	rotation per minute
RMS	root mean square
RRPD	recycled rubber particle damper
SDOF	single degree of freedom
SNR	signal-to-noise ratio
SL	sum level
SLA	sidelobe attenuation
SU	single unit
TLCD	tuned liquid column damper
TLD	tuned liquid damper
TMD	tuned mass damper
TWC	thin wall cavity
TWC-AS	thin wall cavity with additional sheets
WTS	wind turbine stator

1 Introduction

This chapter provides an overview of various vibration control techniques, highlighting their applications, benefits, and limitations. It establishes a foundational understanding of methods for reducing unwanted vibrations in engineering systems. The focus then shifts to particle dampers, offering a summary of their fundamental principles as a specialized vibration control method. Additionally, the chapter outlines the research motivation, key objectives, and the overall thesis structure, guiding the reader through the subsequent chapters. The primary goal is to demonstrate the advantages of particle damping over conventional passive damping techniques while also setting the context and direction for the thesis.

1.1 Vibration control methodologies

Vibrations in structures can arise from various sources, including mechanical forces, environmental disturbances, and electrical or thermal fluctuations. In many cases, vibrations are unwanted side effects that can compromise system performance, durability, and user comfort. Consequently, mitigating vibration in the development of mechanical devices or machines is a critical engineering challenge.

A prime example of the challenges posed by vibration is the offshore wind energy sector. Wave- and wind-induced vibrations can significantly affect the lifespan and efficiency of turbine components [1]. Similarly, in onshore wind turbines, the rotational motion of the internal components generates vibrations that propagate throughout the turbine, ultimately resulting in noise pollution within the surrounding environment. This acoustic output can have detrimental effects on human health and well-being, including sleep disturbances, headaches, and increased stress levels [2–4]. Similarly, vibration and associated acoustic noise are paramount considerations in vehicle design, consistently ranking among the top five critical attributes along with safety, performance, handling, and fuel efficiency [5]. Mitigating vibration and noise in commercial vehicles is essential to improve passenger comfort, driving experience, and overall vehicle performance [6, 7]. Vibration control is essential not only for large-scale machinery, but also for delicate components. For example, printed circuit boards in spacecraft can be subjected to extreme vibrational forces during launch, which can potentially damage electronic components [8]. Increasing global attention is being directed toward the environmental impact of industrial vibrations and the related acoustic noise, especially in sensitive marine ecosystems. For instance, vibrations and noise from shipping are recognized as major disturbances, with their effects potentially intensified by climate change. The expanding offshore wind industry has introduced new vibration and acoustic challenges, affecting marine life [9]. As a result, developing strategies to mitigate and control unwanted vibrations has become a central challenge and opportunity across multiple industries.

To reduce vibration amplitude in mechanical structures, various control approaches have been developed over the years. Three main techniques have emerged as widely used for mitigating undesired vibration: passive, active, and semi-active or hybrid control [10], see Figure 1.1. The choice between passive, active, or hybrid vibration control techniques depends on several factors, such as the application area, system requirements, effectiveness, economic considerations, and practicality. However, it is essential to note that each method possesses its strengths and limitations. For instance, active vibration control is generally employed for controlling low-frequency, whereas the passive damping technique is highly effective in reducing high-frequency vibration [10, 11]. In contrast, hybrid vibration control, or semi-active vibration control, is designed by merging the strengths and weaknesses of passive and active vibration control techniques to effectively mitigate vibrations across a wide frequency range [10–12].

Typically, an active vibration control system consists of a coordinated integration of mechanical and electronic components, managed by a computer or microprocessor. The primary elements include the primary structure subjected to disturbances, sensors for vibration detection, controllers for signal processing and control signal generation, and actuators to counteract the disturbance. The system uses actuators to generate opposing forces, thereby attenuating structural vibration. Based on the control algorithm employed, active vibration control techniques can be categorized into three primary groups: feedback, feedforward, and mix control [11], see Figure 1.1. Several experimental studies have demonstrated the efficiency of active damping systems that incorporate piezoceramic patch actuators in reducing the vibration amplitude of flat metal plates [13–15]. Furthermore, in a previous work [16], a velocity feedback control algorithm was employed to reduce the vibration amplitude of the lid of an electric drive power electronic subsystem by up to 12 dB.

While active control methods have demonstrated effectiveness in mitigating vibrations across a wide range of structures, from simple beams [17] to complex space structures [18], and offer benefits such as weight reduction and minimal structural stiffness alteration, their practical implementation is hindered by several challenges. For instance, piezoelectric materials, commonly employed as actuators and sensors in these systems, exhibit limitations in terms of reliability, cost, integration, and power consumption. Moreover, their performance is susceptible to electromagnetic interference and temperature variations [19]. Practical difficulties also arise during the attachment and installation of piezoelectric sensors and actuators to host structures, with the adhesive layer being a critical factor [20].

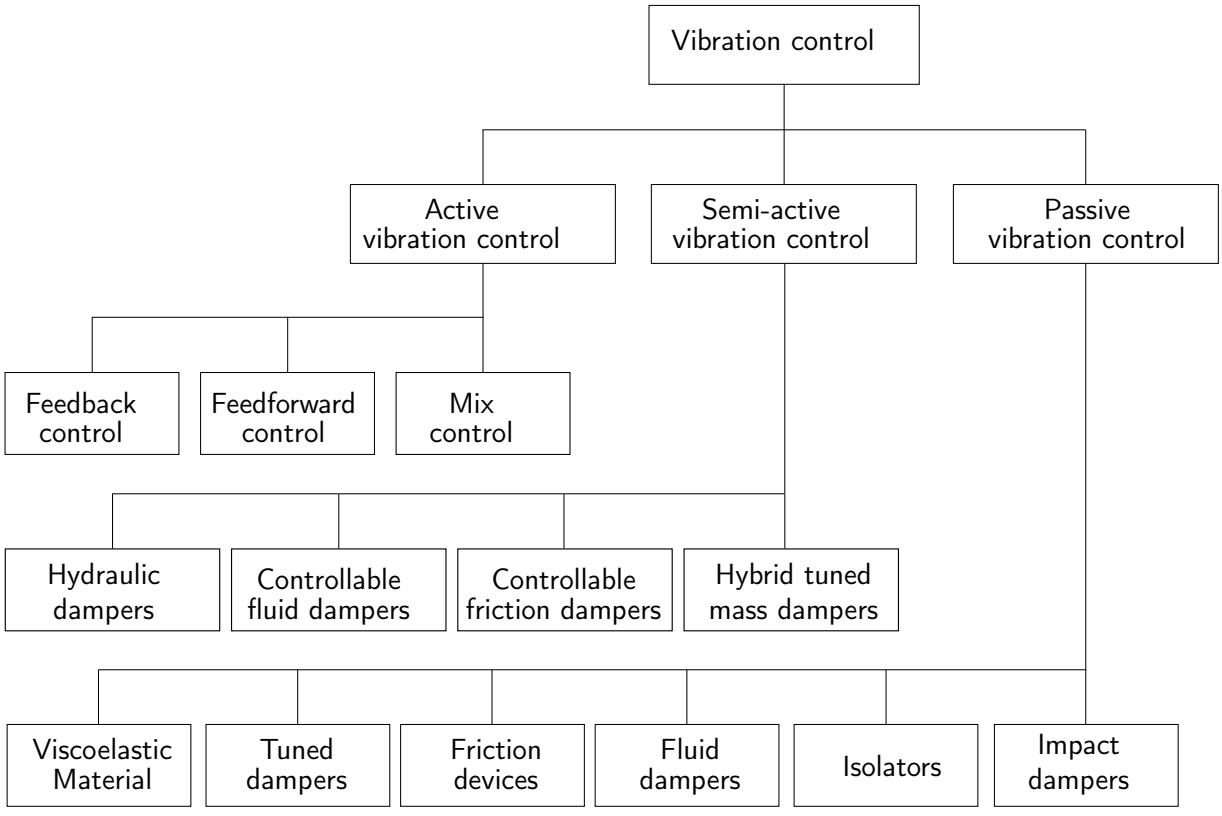

Figure 1.1: Classification of vibration control techniques.

Semi-active control has gained significant attention in recent years due to its economic advantages over active control systems. This is primarily attributed to the lower operational costs associated with semi-active devices, which do not require high-power actuators. Defined as passive components with dynamically adjustable damping properties requiring minimal power input, these devices offer enhanced

resilience compared to active counterparts by maintaining functionality in passive mode during power outages. Control strategies for semi-active systems typically involve adjusting device parameters, such as orifice size in fluid viscous dampers [21], normal force in semi-active friction dampers [22], or current/voltage in magnetorheological dampers [23]. As depicted in Figure 1.1, the majority of semi-active devices can be categorized into four primary types: hydraulic dampers, controllable fluid dampers, controllable friction dampers, and semi-active or hybrid tuned mass dampers [24].

Semi-active vibration control has seen significant advancements in automotive suspension systems [25], civil engineering structures [26], and aerospace components [27]. However, its practical implementation is complex and has inherent limitations. Optimal performance depends on sophisticated control algorithms, which can be affected by changes in system parameters and external factors. Variations in damping and stiffness due to temperature changes or wear can reduce the effectiveness of these algorithms. Unlike passive systems, semi-active systems require additional components, such as sensors, actuators, and control units, which increase complexity and cost [26]. This added complexity can introduce potential failure points, necessitating more frequent maintenance and potentially compromising system reliability.

Unlike active and semi-active counterparts, passive vibration control systems function autonomously without external power or control algorithmic intervention. Their inherent cost-efficiency, low maintenance demands, and robust durability render them prime candidates for industrial applications encompassing automotive [28, 29], aerospace [28], and railway sectors [30]. Fundamentally, these systems dissipate energy through material-induced forces, fluid viscosity, or friction [31]. As illustrated in Figure 1.1, passive vibration control strategies can be categorized into six primary types based on their operational principles: viscoelastic materials, tuned dampers, friction dampers, fluid dampers, isolators, and impact dampers [32].

Viscoelastic dampers use the unique properties of viscoelastic materials to reduce system vibrations by dissipating energy through shear deformation as the material deforms with structural motion [33, 34]. They are broadly categorized into three types: free-layer damping, constrained-layer damping, and tuned viscoelastic dampers [28].

Free-layer damping involves applying a thin viscoelastic layer to one or both sides of a structure, often using spray or adhesive techniques [35]. Constrained-layer damping, or sandwich-layer damping, places the viscoelastic material between a flexible base and a rigid constraining layer, enhancing effectiveness due to shear action within the viscoelastic layer [36, 37]. This method often uses materials like aluminum or steel as constraining layers, making it more effective at reducing vibration amplitude than free-layer methods.

Tuned viscoelastic dampers, which use viscoelastic materials to dissipate energy similarly to tuned mass dampers, have shown up to 2 dB reduction in system response [38]. Comparative studies highlight that all three methods can reduce vibration by $6 - 10$ dB in the $200 - 1000$ Hz range, with constrained-layer dampers potentially lowering system weight by up to 5 kg compared to asphaltic sheets, while free-layer options offer cost savings [39]. While constrained-layer dampers offer the potential for weight reduction compared to asphaltic sheets, the extent of this reduction is dependent on the design and application.

Applications include automotive window damping using laminated glass, aerospace pipeline vibration control, computer hardware stabilization, and vibration reduction in carbon fiber wind turbine blades [40–43].

While viscoelastic dampers have proven effective in diverse industries, their dynamic characteristics are highly sensitive to temperature. In other words, the damping efficiency of viscoelastic dampers may decrease when subjected to extremely high or low temperatures. Moreover, the damping performance of these dampers is dependent on vibration frequency, dynamic load, pre-load, and other environmental conditions such as humidity. Over time, viscoelastic materials are susceptible to degradation, embrittlement, and disintegration due to outgassing and other processes.

Unlike viscoelastic dampers, a tuned mass damper (TMD) is a passive device comprising a small mass, a tuned spring, and a dashpot system attached to a structure. The TMD is specifically calibrated to a target structural frequency, enabling it to resonate out of phase with the structure when that frequency is excited. This phase opposition facilitates energy dissipation through the inertial forces exerted by the damper on the structure, thereby reducing vibrational amplitudes [44].

The TMD was first applied by Hermann Frahm in 1909 to reduce ship hull vibrations and rolling motion [45], and its theoretical foundation was established by Ormondroyd and Den Hartog in 1928 [46]. Den Hartog work from 1940 provided a detailed analysis of TMD tuning and damping parameters [46]. Since then, TMDs have become widely used for vibration, wind-induced oscillation, and noise reduction in mechanical and civil engineering structures [30, 47]. Notable applications include reducing vibration in multi-body vehicle models [48], offshore wind turbines [49], and civil structures globally [50, 51]. However, TMDs face limitations in lightweight mechanical systems due to their increased mass, mechanical feasibility issues, and sensitivity to frequency variations under dynamic conditions [52]. Additionally, their large relative displacements and need for substantial clearances make them unsuitable for broadband damping applications [53].

Friction dampers, introduced by Pall et al. [54, 55] in 1980, are a passive damping technique that reduce vibrations by converting kinetic energy into thermal energy through heat generation at the interface of two contacting surfaces in relative motion [56]. They are robust in harsh environments, do not require tuning for different excitation frequencies, and can act in multiple directions simultaneously. Applications include reducing resonant stresses in turbine blades to prevent high-cycle fatigue [57] and mitigating flexural vibrations in propulsion shafts for ultralight helicopters [58]. Research has also explored combining friction dampers with other damping techniques. Sanati et al. [59] found that integrating friction dampers with viscoelastic materials enhanced performance, while Bagheri et al. [60] demonstrated that friction dampers were more effective at reducing base shear but less effective in controlling lateral displacement compared to metallic dampers.

Despite their advantages, friction dampers suffer from reliability concerns due to uncertainties associated with sliding interfaces [55]. Moreover, their effectiveness is limited to lower frequency vibrations and is contingent upon adequate normal force, friction coefficient, and material durability. Consequently, their practical application is restricted by these factors. Additionally, the performance of friction dampers is susceptible to deterioration arising from alterations in surface conditions.

Fluid dampers utilize the energy-dissipating properties of fluids to convert structural vibrations into heat through mechanisms such as added mass, fluid resistance, and fluid sloshing. They can be customized to absorb specific vibration frequencies and mitigate sudden shocks [32]. In the automotive industry, fluid dampers are a common choice for vibration control [61, 62]. For example, Pistek [63] developed a viscous damper using silicone fluids to reduce vibrations in a V10 diesel engine. These dampers are also widely employed to mitigate the effects of seismic energy on buildings and bridges [64, 65]. While viscous dampers offer advantages like easy installation, adaptability to various loading conditions, and low maintenance, they also present challenges, including high initial costs, temperature sensitivity, leakage, and limited effectiveness at low frequencies. Furthermore, fluid dampers are often restricted in their applications due to their sensitivity to harsh environmental conditions.

Passive vibration isolators represent another approach to vibration control. However, they should not be classified as dampers, as isolation and damping operate through fundamentally distinct mechanisms. While isolation aims to prevent the transmission of vibrations, damping focuses on dissipating vibrational energy. Passive isolators are extensively utilized across diverse industries, from simple rubber feet on vibrating pumps to advanced base isolation systems designed to mitigate seismic forces. These isolators typically consist of a resilient support structure (providing stiffness) and an energy-dissipative element (offering damping). Common materials include elastomers, foam, cork, and steel (springs, pads, cables), with some materials like elastomers and fiberglass providing both stiffness and damping properties [66]. Applications are extensive, ranging from seismic protection using base isolation systems [67, 68] to

vibration reduction in automotive components with rubber isolators [69, 70]. Foam isolators enhance vibration isolation in structures like car seats [71]. While effective for high-frequency vibrations, passive isolators have limitations in low-frequency attenuation and often require significant installation space.

To overcome the limitations of conventional passive damping techniques, particle dampers utilize the energy dissipation properties of granular materials for vibration attenuation. A particle damper is a generalized form of an impact damper, where a container allows unrestricted movement of a single particle. Attached to a vibrating structure, the particle collides with the container walls, transferring momentum from the primary structure to the impact mass, thus reducing vibration amplitude. Figure 1.2 (left) shows a schematic of an impact damper installed on the end of a cantilever beam.

Paget has demonstrated the effectiveness of an impact damper to reduce the vibration amplitude of a turbine blade [72]. Another successful application of an impact damper is in mitigating vibrations in a radar antenna structure. To accurately simulate the antenna's fundamental mode, a prototype was developed. The findings conclusively established the significant efficiency of impact dampers in vibration attenuation [73]. Impact dampers are also employed to reduce vibration amplitude in boring tools or drills [74], cable-stayed bridges [75], and slender mill tools [76]. However, the utilization of an impact damper is constrained due to high levels of noise, impact forces, and sensitivity to excitation amplitude. Additionally, an impact damper can also cause excessive wear to the contact surfaces.

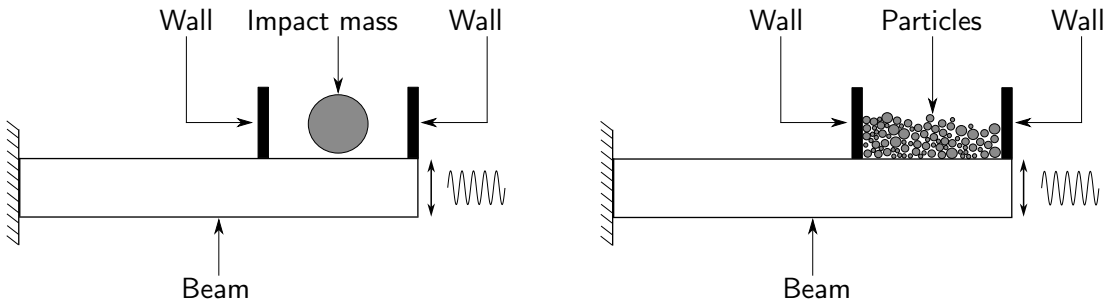

Figure 1.2: Schematic representation of an impact damper (left) and a particle damper (right) mounted on the tip of a cantilever beam under dynamic load.

To overcome the limitations of impact dampers, the particle damping technique can be used as an alternative. This technique involves replacing the single particle in the impact damper with several small auxiliary masses. Hence, particle dampers can be viewed as a broader or more comprehensive version of impact dampers. Particle damping technology is variously referred to as granular, acceleration, or multiple impact damping. For consistency, this thesis will uniformly adopt the term "particle dampers". It is important to clarify that the term "single-particle damper" is frequently associated with impact dampers due to their single impact mass. Nevertheless, in this thesis, impact dampers are distinctly differentiated from particle dampers. Consequently, in this thesis, "particle dampers" specifically refers to dampers that utilize more than one particle. Similar to impact dampers, particle dampers can also be mounted to the vibrating structure, see Figure 1.2 (right).

This section has provided a brief overview of several prevalent passive vibration control techniques, including viscoelastic dampers, tuned mass dampers, friction dampers, fluid dampers, isolators, and impact dampers. While the field of passive damping is vast and encompasses a wider array of devices, this section aimed to establish a foundational knowledge of key techniques. It is acknowledged that metallic dampers and metamaterials represent significant areas of research within passive damping. Nonetheless, due to the scope of this thesis, a detailed exploration of all passive damping techniques is beyond the purview of this work. The presented overview serves as a foundational framework for understanding the fundamental principles of various passive vibration control methods.

1.2 Introduction to particle damping

Particle damping is a passive vibration mitigation technique that leverages the inherent dissipative properties of granular materials. Traditionally, particle dampers consist of granular material confined within an enclosure attached to a vibrating structure. An alternative configuration involves creating small cavities within the vibrating structure, which can be partially filled with granular materials [32]. Despite the potential benefits of both configurations, a standardized design methodology for particle dampers remains elusive, as most existing approaches are predominantly application-specific.

Particle dampers have been classified in diverse manners by various researchers, with some categories showing similarities across different classifications. As an example, Gagnon et al. [77] have classified particle dampers based on their topology. Lu et al. [78] have categorized variants of particle dampers into four primary groups, specifically: basic traditional particle dampers, configuration-improved type particle dampers, material-improved type particle dampers, and combination-type particle dampers.

While there are multiple design variants and approaches for particle dampers, the underlying damping mechanism remains consistent across each design. Upon experiencing vibrations in the primary structure, the kinetic energy of the vibrating structure is transferred to the particle damper, initiating collisions between particles and between particles and cavity walls. Consequently, this process leads to a reduction in the vibration amplitude of the primary structure. Therefore, the energy dissipation in particle dampers can be assessed by examining a combination of loss mechanisms. These mechanisms include collisions between particles and the container walls, collisions between particles, sliding friction among particles, and rolling friction among particles.

Fowler et al. [79] classified the damping mechanism of a particle damper into two primary categories: external and internal damping. External mechanisms encompass friction and impact interactions between the particles and the cavity, while internal mechanisms involve friction and impact interactions among individual particles. The efficiency of these mechanisms might fluctuate based on various system parameters.

Figure 1.3 (left) presents a Discrete Element Method (DEM) model of a particle damper, featuring spherical particles randomly placed in a box. Once static equilibrium (zero velocity) is achieved, harmonic motion is applied to excite the system. The colormap indicates particle velocities, with red representing higher velocities and blue indicating lower velocities. The schematic representation of the DEM model of a particle damper is shown in Figure 1.3 (right). In this figure, a box partially filled with spherical particles is excited by a harmonic force. The random movement of the particles is indicated by arrows, and the friction between particle-particle (μ_p) and particle-wall (μ_w) interactions is also depicted.

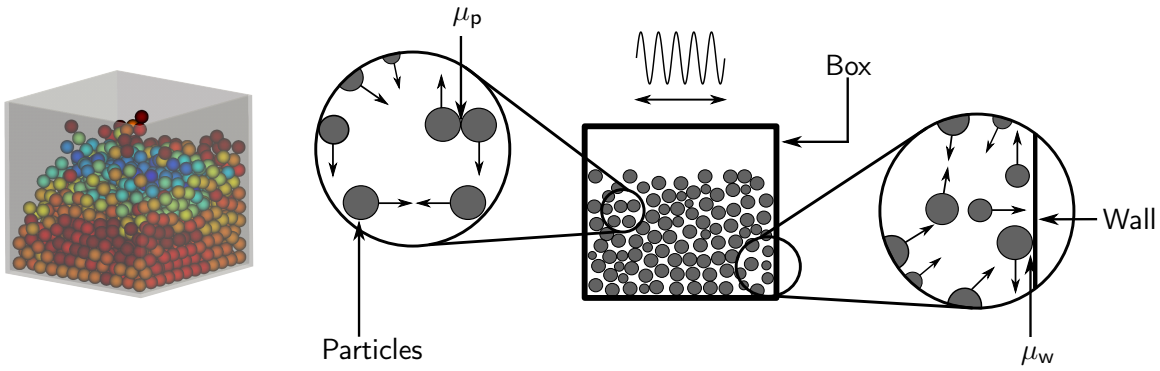

Figure 1.3: (Left) Discrete Element Model (DEM) of a particle damper subjected to harmonic excitation. (Right) Schematic representation of the DEM model, depicting the random movement of particles (arrows) and particle-particle/wall interactions.

Furthermore, the dissipation of energy in a particle damper is also contingent on several other factors.

For example, the choice of granular material in designing a particle damper significantly affects its vibration attenuation capabilities. Additionally, filling ratios, the quantity, shape, and size of particles, and the intensity of excitation play a significant role in reducing the vibration amplitude of a structure. Moreover, particle dampers exhibit highly non-linear behavior. The non-linear behavior can be attributed to a geometric non-linearity resulting from the alteration in the local packing arrangement of particles. Typically, a non-linear contact constitutive model is utilized to explain the force-displacement reaction at the contacts, contributing a material non-linearity to the system. These two sources of non-linearity at the particle level combine to produce an overall non-linear response of the material at a macro-scale.

Particle dampers have gained attention for their simplicity, low maintenance, and cost-effectiveness. They effectively reduce vibrations across a wide frequency range, are reusable, and show minimal sensitivity to temperature variations depending on the granular material used [77]. Compared to conventional damping and active control methods, they offer better weight efficiency and superior vibration attenuation [80]. Studies have shown that particle dampers outperform TMDs and active control systems, particularly in reducing vibrations over a broader frequency spectrum [16, 81].

1.3 Motivation

Particle dampers have emerged as a promising passive vibration control solution, effectively dissipating vibrational energy through particle interactions. Unlike conventional damping mechanisms, they do not rely on viscoelastic materials or fluid-based systems but instead utilize the dissipative effects of viscoelastic collisions and frictional interactions among granular materials within an enclosed cavity. These characteristics make particle dampers particularly advantageous in applications where conventional damping materials may degrade over time, broadband damping is required, or additional weight and complexity must be minimized. However, despite their potential benefits, their widespread industrial adoption remains limited, primarily due to the lack of a comprehensive design framework that accounts for real-world constraints and operational conditions.

Existing research on particle dampers has provided valuable insights into their fundamental working principles and performance characteristics. However, much of this research has been conducted in controlled laboratory environments, often using simplified structural models and focusing on a limited range of materials (see Chapter 2). As a result, the applicability of these findings to practical engineering applications remains constrained. One of the primary limitations is the predominant use of high-density materials, such as steel and tungsten, which, while effective in energy dissipation, pose practical challenges in weight-sensitive applications. Low-density granular materials, which could offer viable alternatives, have not been adequately explored. Moreover, the effectiveness of particle dampers at lower vibration frequencies remains a challenge, as the mobilization of particles under such conditions is often insufficient to induce the desired level of damping.

Another significant challenge in the design and optimization of particle dampers is ensuring the effective mobilization of granular materials within the damping cavity. Although the vibrational energy of the main structure can induce particle motion, the degree of mobilization is strongly influenced by factors such as excitation frequency, amplitude, and the physical properties of the granular medium. At lower frequencies, in particular, the available kinetic energy may be insufficient to overcome inter-particle friction and adhesion forces, resulting in suboptimal energy dissipation. To mitigate this limitation, researchers have investigated semi-active enhancement techniques, such as the use of electromagnetic fields to externally manipulate particle movement. However, these approaches introduce additional complexity, require external power sources, and are often restricted to specific material compositions, limiting their practicality in broader engineering applications. Therefore, developing innovative passive design strategies that inherently promote particle mobility remains a critical area of research.

Furthermore, the long-term durability of granular materials under repeated cyclic loading remains an area of concern. The mechanical properties of particles may change over time due to continuous

collisions, abrasion, and environmental factors such as humidity and temperature fluctuations. While existing studies have primarily focused on the immediate damping characteristics of particle dampers, little attention has been given to their performance degradation over prolonged operational periods. Addressing this gap is crucial for ensuring the reliability and longevity of particle dampers in industrial applications.

Given these challenges, this thesis aims to advance the state of the art in particle damper technology by systematically addressing the limitations identified in existing studies. A key objective is to explore novel materials, including unconventional granular media, that can enhance damper performance while mitigating the practical limitations associated with high-density materials. Additionally, the research will investigate the role of particle size distribution, filling ratios, particle shape, and environmental factors in influencing damping efficiency. Understanding these parameters will allow for the development of optimized designs tailored to specific engineering applications. Finally, the practical implementation of particle dampers will be demonstrated in industrial contexts, such as wind turbines and electric drives, to validate their effectiveness in mitigating operational vibration amplitude.

By addressing these key research areas, this study aims to establish a robust and comprehensive framework for the design and implementation of particle dampers in engineering applications. The insights gained from this research will contribute to the broader adoption of particle dampers across multiple industries, fostering the development of more efficient, reliable, and sustainable vibration mitigation solutions. Ultimately, the advancement of particle damper technology has the potential to play a significant role in enhancing the performance and longevity of mechanical systems, reducing maintenance costs, and promoting safer and more sustainable engineering practices.

1.4 Outline of the dissertation

This thesis comprises thirteen chapters organized into three main parts to systematically investigate the vibration attenuation properties of particle dampers and develop a robust design framework.

Part 1: Foundation and research gaps (Chapters 1 - 4)

- Introduces the motivation, theoretical background, and identifies research gaps in particle damper technology.

Part 2: Experimental investigations at the laboratory scale (Chapters 5 - 10)

- Chapter 5: Experimental analysis of various granular materials, including recycled rubber particle dampers (RRPDs), hard material particle dampers (HMPDs), and hybrid particle dampers (HPDs), examining the effects of particle size, filling ratios, and humidity on performance.
- Chapter 6: Optimizes particle damper designs for large hollow structures, proposing three passive variants, namely: thin wall cavity (TWC), TWC with additional sheets (TWC-AS), and ring cavity (RC) to enhance vibration mitigation.
- Chapter 7: Evaluates long-term durability under dynamic conditions by subjecting particle dampers to millions of cycles and temperature variations, assessing performance degradation.
- Chapter 8: Investigates particle dampers on rotating components, using a scaled rotor blade to examine vibration mitigation across varying rotational speeds.
- Chapter 9: Tests particle damping concepts for vibration control in wind turbine generator specimens, establishing foundational data for industrial application.
- Chapter 10: Explores three particle damper designs for wind turbine blades through laboratory testing to identify the optimal approach for industrial scaling.

Part 3: Industrial implementation (Chapters 11 - 13)

- Chapter 11: Evaluates particle dampers on a commercial wind turbine component, assessing their real-world applicability.
- Chapter 12: Expands industrial testing to electric drives, bridging lab-to-industry transitions and demonstrating practical viability.
- Chapter 13: Summarizes findings, conclusions, and outlines potential research directions, contributing significantly to the application of particle dampers in complex engineering systems.

This structure facilitates a clear, progressive understanding of particle damper technology from foundational research to practical applications, ultimately aiming to drive adoption in industrial contexts.

2 State of the art in particle dampers

This chapter offers a comprehensive overview of the current state of the art on particle dampers. It critically assesses the analytical, numerical, and experimental techniques used to investigate their behavior, emphasizing their advantages and limitations. The primary objective is to elucidate the diverse approaches employed to study the design parameters that govern particle damper effectiveness and to explore the various methods used to analyze their damping mechanisms.

2.1 Introduction

In contrast to the well-established theoretical frameworks that exist for conventional dampers, such as viscoelastic dampers and TMDs, there is currently no universally accepted theory for studying the behavior of particle dampers. As a result, researchers rely heavily on analytical, numerical, and experimental approaches to fully understand the dynamic behavior of systems incorporating particle dampers. Each of these methods offers unique insights and plays an important role in the study of particle dampers. Analytical models, while useful in providing a fundamental understanding of particle damping behavior, often face limitations that restrict their ability to fully capture the complexities of the system. As a result, experimental validation becomes necessary to verify the outcomes of these models. Additionally, numerical simulations emerge as a powerful theoretical tool for gaining deeper insights into the mechanisms governing particle damping.

This chapter provides a detailed review of the various research methodologies employed in the study of particle dampers, with particular emphasis on the analytical, numerical, and experimental approaches found in the literature. Although the primary focus of this thesis is the experimental analysis of particle damper design parameters, it is important to contextualize the experimental work within the broader research landscape, where analytical and numerical methods also play significant roles in advancing the understanding of particle damping mechanisms.

2.2 Analytical method of particle damper

This section provides a critical review of analytical modeling techniques applied to particle dampers. As highlighted in Section 1.2, the inherently nonlinear energy dissipation characteristics of particle dampers significantly limit the applicability of analytical methods for design and analysis. Consequently, their utility is restricted to specific and simplified scenarios [78].

Several researchers have developed analytical models for an impact dampers [82–84]. While these models provide a reasonable estimate for the external friction and impact interaction between particles and the cavity, they are not well-suited for representing the internal friction and impact interaction among individual particles.

Fowler et al. [79] utilized an equivalent single degree of freedom (SDOF) dashpot system to model a beam. They employ a modified version of the Hertz method to quantify the force between colliding bodies. In cases of oblique impacts, the forces are measured using Coulomb's law. However, the authors have employed an approach closely resembling the DEM to address the motion of individual particles.

Olson [85] has developed a mathematical model to perform analytical evaluations of the particle damper design. He used a generalized Maxwell model to characterize the viscoelastic behavior of granular materials. In his model, he considered the normal forces and shear forces as independent quantities. The validity of the mathematical model is confirmed through the simulation of laboratory tests conducted on a cantilevered beam. The theoretical model closely aligns with the experimental findings. However, the model assumes that the enduring contacts exert a more substantial influence on the overall damping compared to oblique impacts. Therefore, the model disregards the shear forces produced during oblique impacts. Overall, the particle damper model has successfully predicted the general trend. Nevertheless, there is a tendency to overestimate the degree of attenuation, especially when handling multi-particle dampers.

Saeki [86] has proposed an analytical model that is based on the DEM for evaluating the effectiveness of a multi-unit particle damper. He has employed the Hertzian contact theory to model the normal component of the contact forces, while Coulomb's law of friction is utilized to model the tangential component. Furthermore, to evaluate the behavior of the entire system, integration of the primary systems equations of motion has been carried out. Moreover, to simplify the analysis, they made the assumption of uniform behavior for each unit, thereby reducing the analysis to the number of particles within a single container. The model proposed by Saeki has the capability to simulate the damping performance of a multi-unit particle damper within a horizontally vibrating system. The effectiveness of the model has been verified by the experimental study, which is equivalent to a SDOF system.

Zalewski et al. [87] have presented a theoretical model for a vibrating granular beam by combining the classical Euler-Bernoulli beam theory with the Kelvin-Voigt material model. To verify their theoretical model, they carried out an experimental study on a special granular structure that is comprised of a steel core and molded material. The molded material gives the beam a rectangular cross-sectional shape and creates an envelope around the steel core. The space inside the envelope is used to enclose polypropylene cylindrical grains. They used a vacuum pump to alter the internal pressure of the structure to modify the elastic and dissipative properties of the system. The suggested rheological model demonstrates a strong correlation between the experimental and numerical data.

Szmidt et al. [88] has used the experimental and theoretical model of Zalewski et al. [87] to carry out a forced vibration analysis. The study shows a good agreement between the numerical and analytical investigations.

Based on the overview above, it becomes evident that analytical models of particle dampers are uncommon and are restricted to highly idealized scenarios. The complex and non-linear dynamics arising from particle-particle and particle-wall collisions, characterized by abrupt changes in particle motion, render analytical solutions intractable for most practical applications. Consequently, while analytical models can provide valuable insights under specific conditions, numerical methods are indispensable for a theoretical understanding of particle damper behavior. The subsequent section offers a detailed examination of numerical modeling techniques employed in particle damper research.

2.3 Numerical method of particle damper

While this thesis prioritizes an experimental approach, a critical review of existing numerical methods remains essential. Given the limited availability of analytical solutions for particle dampers, and the fact that most analytical approaches depend on numerical methods to solve the equations (see Section 2.2), numerical simulations have become the primary tool for developing a theoretical understanding of the particle damper concept. Furthermore, by reviewing the numerical approach to designing a particle damper, it becomes clear which design parameters can be assessed through numerical simulations, thereby minimizing the need for experimental investigations. Additionally, analyzing numerical modeling can aid in interpreting and understanding the results of experimental investigations.

The DEM has emerged as a powerful computational tool for investigating the dynamics of granular systems across various disciplines, including mining operations [89], mixing and milling processes [90, 91], geotechnical engineering [92, 93], food processing applications [94], and material handling [95]. This method excels at capturing the motion and interactions of individual particles within an assembly. Recognizing this strength, researchers have increasingly explored the application of DEM to simulate particle damper systems in the field of structural control. Consequently, DEM has gained significant traction in recent years for investigating the design parameters influencing particle damper performance. Additionally, DEM simulations are being employed to study the energy dissipation mechanisms within these devices.

Pioneered by Cundall and Strack [96], DEM adopts a Lagrangian approach, explicitly tracking the time-dependent position of each individual particle within the system. This approach falls under the category of discontinuum mechanics, focusing on the interactions between discrete bodies. The core principle of this method lies in the interactions between discrete bodies. A contact detection algorithm identifies interactions between particles. Subsequently, contact force laws are applied to these interactions. These laws typically incorporate spring forces, damping forces, and frictional forces. By summing the forces and moments acting on each individual particle, the resulting acceleration is calculated. By numerically integrating the acceleration over a small time step, the updated velocities of all particles are determined. Subsequently, integrating these velocities yields the new positions of all particles. The integration is carried out using the central difference method with sufficiently small time steps, Δt. It is important to emphasize that the stability of the solution to these equations is contingent upon the time step being smaller than the critical time step, i.e., $\Delta t \leq t_{\text{crit}}$ [1]. The updated positions then influence subsequent contact detection, potentially creating new contacts or resolving existing ones. This iterative process, which includes contact detection, force calculation, and position update, is fundamental to the DEM simulation cycle.

The numerical studies of a particle damper can be broadly categorized into two groups: analysis of structure-independent particle dampers and structure-integrated particle dampers [97]. The former operates independently of any supporting structure, while the latter is either attached to or embedded within the primary vibrating structure. Instead of "structure-independent particle damper," the term "non-destructive particle damper" (NOPD) is also commonly used in numerical studies [98, 99]. However, in experimental studies, their characteristics can differ depending on the test specimen used to analyze NOPDs. The term NOPD was first coined by Panossian [32], who demonstrated the efficiency of particle dampers in reducing the high amplitude vibrations of the space shuttle main engine liquid oxygen inlet tee. To illustrate this, he drilled four 1 mm diameter holes inside one of the liquid oxygen inlet tees and partially filled it with granular materials of different types. A detailed account of the author's experimental study and its results will be presented in Section 2.4, which is dedicated to the experimental review.

One of the primary reasons for choosing structure-independent particle dampers for numerical studies is that many aspects of particle damper behavior can be analyzed solely with DEM simulations, without the need to combine DEM with other continuum-based methods like the finite element method (FEM). A key area of study involves the relationship between the motion modes of the granular material and the resulting energy loss within the damper. Another important aspect of investigation is the influence of particle shape on vibration attenuation. By varying the shape of the particles within the damper, researchers can assess the impact on vibration reduction. Additionally, these dampers are widely employed to evaluate the overall performance of particle dampers across the amplitude-frequency domain. However, a major limitation of this approach lies in its representation of the container. DEM typically assumes a rigid container for the particles, neglecting any potential deformation during

[1] The selection of the time step is a crucial aspect in DEM simulations. It must be chosen sufficiently small to address two primary concerns: first, to prevent excessive particle overlaps that could lead to unrealistically high interaction forces, and second, to mitigate the influence of disturbance waves, such as Rayleigh waves, which can affect the accuracy of the simulation.

particle-wall interactions. Consequently, container excitation, regardless of particle presence, yields identical motion. This inherent rigidity restricts the analysis of real-world scenarios, such as the effects of particle impacts on container walls. Furthermore, validating this numerical approach necessitates alternative experimental studies that differ slightly from those directly measuring surface velocity or acceleration levels of the structure, significantly restricting the ability to directly compute vibration attenuation. Additionally, this approach prevents the analysis of the frequency response of particle dampers. In DEM, as previously noted, the cavity is treated as perfectly rigid, meaning it undergoes no deformation. As a result, the frequency response function (FRF) holds no significance, since it inherently describes the relationship between force and displacement, velocity, or acceleration, all of which depend on structural deformation. Despite this restriction, the extensive application of structure-independent dampers in parametric studies highlights their critical role in advancing our understanding of these devices.

To address the aforementioned limitations, researchers often study integrated particle dampers, which requires coupling DEM with a continuum-based method, such as FEM [100] or the Multi-Body dynamics (MBD) [101] approach. This combined approach offers significant advantages. It allows for the simulation of a wider variety of vibration scenarios, providing a more comprehensive understanding of the damper's behavior under real-world conditions. FEM, in particular, enables the direct simulation of the container's deformation and surface velocity, offering valuable insights into the interaction between the particles and the structure. Additionally, this approach facilitates the modeling of multi-unit (MU) dampers or enclosures with multiple cavities, which can be crucial for applications involving complex geometries.

This review is organized into three sections. The first section examines the diverse computational methods utilized in DEM simulations to quantify energy dissipation within structure-independent particle dampers (Section 2.3.1). The second section (Section 2.3.2) provides a comprehensive overview of existing models for structure-independent particle dampers, which are widely utilized to study various design parameters of particle dampers. The final section (Section 2.3.3) explores contemporary research on coupling methodologies for particle damper design.

2.3.1 Energy dissipation in structure-independent particle dampers

Several methodologies exist for quantifying energy dissipation within DEM simulations. While these approaches vary in specific details, they fundamentally rely on parameters extracted directly from the simulation data. Typically, these parameters encompass contact forces between particles and boundaries, as well as particle velocities in both normal and tangential directions. Considering the various methods for computing energy dissipation, it is crucial to thoroughly understand these techniques before exploring the impact of different particle damper parameters using DEM simulations.

The complex power method, introduced by Yang et al. [102] in conjunction with DEM simulations, offers a well-established approach for characterizing the loss factor of structure-independent particle dampers [103]. This approach allows for the indirect quantification of the energy dissipation properties of the particle damper [99, 103–107]. Furthermore, this method has been widely used for analyzing motion modes or phases within granular materials, which are known to influence the damping behavior of particle dampers.

Within the complex power method, the computation of energy dissipation relies on the excitation force applied to the particle damper and the container's resulting velocity. In the context of DEM simulations, the container's excitation is typically known, allowing for the straightforward computation of its velocity. For instance, if the structure-independent particle damper undergoes sinusoidal motion described by

$$x = X \sin(\Omega t), \tag{2.1}$$

with amplitude X and angular frequency $\Omega = 2\pi f$, then the container's velocity can be readily determined as

$$\dot{x} = V\cos(\Omega t), \tag{2.2}$$

with container velocity amplitude $V = X\Omega$. The total force driving the system is the combined effect of the container's inertia and the contact forces exerted by the particles on the container walls in the direction of excitation. Furthermore, in a system undergoing forced harmonic motion, the average power transmitted through a component can be expressed mathematically as

$$P = \frac{1}{2}FV^*. \tag{2.3}$$

Performing a Fast Fourier Transform (FFT) on the force signal acting on the container wall in the excitation direction yields the complex amplitude F. The conjugate complex amplitude (V^*) of the velocity signal for the particle damper container velocity is obtained through another FFT. The real part of Eq. (2.3) corresponds to the power dissipated (P_{diss}) during a cycle. Additionally, the imaginary part allows for the extraction of the maximum power (P_{max}) stored within a single cycle. Finally, the damping loss factor, a widely used parameter for quantifying the damping efficiency of materials, can be determined using the following equation

$$\eta = \frac{\text{Energy dissipated in a cycle per radian}}{\text{Maximum energy stored in a cycle}} = \frac{P_{\mathsf{diss}}}{P_{\mathsf{max}}} = \frac{\mathsf{Real}(P)}{\mathsf{Imag}(P)}. \tag{2.4}$$

Building on similar approaches, Chen et al. [108] and Duan et al. [104] explicitly compute energy dissipation in both normal and tangential directions for particle dampers. Their formulations additionally account for energy losses due to friction. Energy dissipation (ΔE_{n}) due to normal impact between particles i and j can be expressed as

$$\Delta E_{\mathsf{n}} = \frac{1}{2}\frac{m_i m_j}{m_i + m_j}\left(1 - e_{\mathsf{n}}^2\right)\left|\Delta v_{\mathsf{n}}\right|^2, \tag{2.5}$$

where m_i and m_j represent the masses of the i^{th} and j^{th} particles, respectively, and e_{n} is the coefficient of restitution. The term v_{n} denotes the relative normal velocity between the particles. Furthermore, assuming no tangential slip during particle collisions, the dissipated tangential impact energy (ΔE_{t}) can be calculated using

$$\Delta E_{\mathsf{t}} = \frac{1}{2}\frac{m_i m_j}{m_i + m_j}\left(1 - e_{\mathsf{n}}^2\right)\left|\Delta v_{\mathsf{t}}\right|^2, \tag{2.6}$$

v_{t} denotes the relative tangential velocity between the particles. If the applied tangential force exceeds the maximum static friction force between two contacting particles, relative motion (i.e., slip) will occur. In this regime, the energy dissipated in the tangential direction becomes non-conservative and cannot be directly accounted for. Friction introduces a power term with a negative sign, signifying energy loss. The magnitude of this energy loss due to friction can be determined as follows

$$\Delta E_{\mathsf{f}} = \xi\left|F_{nij}\delta_{\mathsf{t}}\right|, \tag{2.7}$$

where, ξ is the coefficient of friction between i and j. δ_{t} denotes the overlap distance between two contacting particles. Building upon relationships established in Eqs. (2.5) - (2.7), the average power dissipation over a single vibration period, T, can be expressed as

$$P = \frac{\sum \Delta E_{\mathsf{n}} + \sum \Delta E_{\mathsf{t}} + \sum \Delta E_{\mathsf{f}}}{T}. \tag{2.8}$$

Saluena et al. [109, 110] introduced an effective damping parameter, denoted by b_{d}, to quantify energy dissipation in a structure-independent particle damper. This parameter is proportional to the ratio

between the average energy dissipated per cycle and the average translational kinetic energy of the entire granular system with total mass m. Mathematically, the effective damping parameter is defined as

$$b_{\mathsf{d}} = \frac{\frac{1}{T}\int_T W_{\mathsf{diss}}(t)\,dt}{2\sum_n m_n \int_T v_n^2(t)\,dt}. \tag{2.9}$$

However, Saluena et al. [109, 110] do not address the calculation of the average dissipated power directly from the results of DEM or molecular dynamics simulations.

Pourtavakoli et al. [111], characterized damping performance by the relative energy dissipated per cycle, represented by the ratio $\left(\frac{E_{\mathsf{diss}}}{E_{\mathsf{max}}}\right)$. E_{diss} represents the energy dissipated by the damper in a single oscillation cycle. This value depends on the oscillation amplitude and can be calculated as

$$E_{\mathsf{diss}} = \int_T \dot{x}(t)F(t)\,dt. \tag{2.10}$$

Analogous to the complex power method, the term $F(t)$ in Eq. (2.10) is defined as the total force exerted by the particles on the side walls of the damper, acting in the direction parallel to particle motion. $\dot{x}(t)$ represents the particle velocity averaged over a single cycle of period T. E_{max} is the maximum energy dissipation potential per cycle and is estimated assuming inelastic collisions between all particles and the wall at their maximum relative velocity. It can be computed as

$$E_{\mathsf{max}} = 4mA^2\omega^2, \tag{2.11}$$

where, m represents the total mass of all particles within the granular system. A denotes the oscillation amplitude of the excitation force, and ω signifies the angular frequency.

The methodologies presented for calculating loss factors in particle dampers have emerged as highly effective and insightful tools for evaluating the impact of various parameters on the damping performance of these systems. These approaches, which focus on quantifying energy dissipation, have been extensively utilized in a wide range of studies to investigate how different factors influence the behavior and efficiency of particle dampers. Among the key parameters examined are the excitation frequency, which has been explored in studies such as those by Wong et al. [103] and Meyer et al. [106], highlighting its critical role in determining the dynamic response of particle dampers. Additionally, the shape of the particles has been also identified as an another significant factor, as demonstrated by Terzioglu et al. [112], who investigated how variations in particle geometry affect energy absorption and damping characteristics. The quantity of particles within the damper has also been a focal point of research, with Meyer et al. [106] providing insights into how the number of particles influences the overall damping performance. Furthermore, the inter-particle friction coefficient, which governs the interactions between individual particles, has been extensively studied by Wong et al. [103, 113], revealing its importance in determining the energy dissipation mechanisms within the damper. Lastly, the dimensions of the enclosing cavity, which houses the particles, have been shown to play a crucial role in the effectiveness of particle dampers, as evidenced by the work of Ito et al. [114], who examined how cavity size and shape impact the damping behavior.

2.3.2 Review of structure-independent particle dampers

The previous section explored various approaches used to compute energy dissipation in a particle damper through DEM. It also highlighted that these methodologies have been applied in various studies to examine the influence of different particle damper design parameters. However, their specific impact on damping efficiency has not been discussed. Therefore, this section reviews existing numerical studies that employ DEM to analyze structure-independent particle dampers. The focus lies on investigations that utilize DEM to systematically evaluate how various design parameters, such as

particle characteristics (shape, size, material), cavity geometry, and vibration mode of granular materials, influence the damping efficiency of these devices. This emphasis on design parameters is driven by their direct impact on a particle damper's performance and their crucial role in facilitating the study and design of such dampers at both laboratory and real-world scales. Discussions on computational efficiency are also included. However, this section excludes literature on contact detection algorithms, contact models, and time step selection. While these aspects are relevant to DEM simulations, they are considered numerical and mathematical concerns that require a separate approach and thus fall outside the primary focus of this thesis.

2.3.2.1 Particle shape

Particle shape is a critical parameter in DEM, significantly influencing their predictive capabilities. Accurate representation of particle geometry is essential for reliable results [115]. However, in the concept of particle dampers, it is unclear whether particle shape affects the damping efficiency.

Sanchez et al. [116] used a two-dimensional, open-source DEM code to investigate how particle fragmentation and fusion affect vibration response. They simulated fragmentation by replacing hexagonal particles with triangles, finding it had no impact on damping performance. In contrast, fusion of square particles into larger ones degraded vibration attenuation. The study also examined particle shape (triangular, square, hexagonal) and found it did not significantly influence vibration attenuation. While their numerical simulations offer insights into vibration reduction through fragmentation and fusion, experimental verification is needed to confirm the models' validity.

Particle shape's impact on vibration attenuation in particle dampers was also explored by Pourtavakoli et al. [111] employing a multisphere method to model five distinct geometries (rods, squares, rings, crosses, and L-shapes). To quantify the complexity of these shapes, the authors have utilized four parameters: aspect ratio, circularity, convexity, and solidity. Damping performance was evaluated using Eq. (2.10) - (2.11). Their numerical investigations indicated that the critical excitation amplitude, corresponding to the maximum damping efficiency, was independent of particle shape. However, below a certain critical amplitude, in the gas-like regime, spherical particles dissipated energy more effectively than complex-shaped particles of equal mass. In this region, the damper's efficiency exhibits a dependence on the shape of the particles.

Terzioglu et al. [112] studied the impact of particle sphericity on granular dampers in the bouncing bed motional phase, identified as the optimal energy dissipation zone [117]. The bouncing bed phase is defined in Section 2.3.2.3. Using a multi-sphere approach, they created oblate and prolate spheroid particles by varying the aspect ratio of an ellipse, examining eight different aspect ratios. Their findings showed that particle shape significantly affects energy dissipation in granular dampers during the bouncing bed phase, with both experimental and numerical results showing consistent trends.

Despite the recognized importance of particle shape, research investigating its influence on damping performance remains scarce. This scarcity can be attributed to two primary challenges associated with incorporating non-spherical particles into DEM simulations. Firstly, modeling complex shapes presents significant difficulties compared to the simplicity of spheres [118]. Secondly, the computational cost associated with non-spherical shapes can be substantial. Sinnott et al. [119] demonstrated that super-quadrics particles can increase computation time by a factor of 2 to 3, with some cases exceeding 10-fold. Similarly, ellipsoidal particles require roughly four times the computational resources compared to spherical particles [120].

Several methods exist for modeling non-spherical particles, with the multisphere method being a well-established technique [121, 122]. This method models complex particle shapes by clustering spheres of various sizes into clumps. Clumps, treated as single entities, allow spheres to overlap and maintain fixed distances, avoiding internal contact force calculations. They stay unbreakable during simulations and are compatible with efficient algorithms for contact detection and interaction points.

The primary advantage of clumps lies in their compatibility with efficient algorithms designed for contact detection and interaction point determination, originally developed for spherical particles. However, accurately modeling intricate geometries (sharp edges, smooth surfaces) with clumps necessitates a large number of spheres, consequently increasing computational cost. Any particle shape can be used in clumps, but non-spherical components reduce computational benefits. A major challenge is determining the optimal number of spheres needed to approximate real particles [123]. Sphere overlap can cause discrepancies in mass and inertia, and while density adjustments can fix mass issues [122], inertia discrepancies are harder to correct [124]. Parteli [125] introduced analytical equations to compute the mass and moment of inertia of intricate particles made with the multisphere method. These equations apply under the condition that each clump's sphere-sphere overlap involves at most two spheres. The method entails excluding surplus contributions from sphere intersections to accurately find the mass and moment of inertia of each particle. Besides clumps, ellipsoids are the simplest non-spherical models used in DEM simulations, with superquadrics and polyhedrons providing additional options for modeling complex shapes [124].

From the above discussion it can be concluded that the influence of particle shape on particle damper performance has been studied, but accurately modeling realistic particle shapes in DEM simulations remains challenging. Furthermore, existing literature presents conflicting views on the effect of shape, with Sanchez et al. [116] suggesting minimal influence and Pourtavakoli et al. [111] proposing a motion mode dependent effect. However, neither provided experimental validation. Conversely, Terzioglu et al. [112] demonstrated the importance of shape through combined experimental and numerical studies. Both Terzioglu et al. [112] and Pourtavakoli et al. [111] highlight the impact of particle shape on the performance of particle dampers, showing that this effect is closely tied to the motion mode of the particles. However, the studies differ in identifying the specific motion phase where particle shape plays a significant role. Moreover, considering particle shape during calibration is crucial as it impacts bulk material properties. Modifying particle shape after calibration requires time-consuming recalibration [124]. Therefore, the combined challenges of accurately representing particle shapes and the associated calibration burden limit comprehensive exploration of particle shape effects on particle damper performance using DEM simulations.

2.3.2.2 Numerical parametric analysis

It is well-established that parameters such as material properties, filling ratios, container geometry, and excitation levels significantly influence the vibration attenuation capabilities of particle dampers. While the majority of DEM-based research on particle dampers has focused on refining contact models for accurate numerical simulations [126–129], considerable attention has also been devoted to contact detection algorithms [130, 131]. Although parametric studies are not the primary focus of most DEM investigations, a substantial body of literature explores the impact of the aforementioned parameters on particle damper performance. This section provides a comprehensive overview of the current state-of-the-art in this regard.

Mao et al. [132, 133] conducted numerical simulations on an SDOF system to study particle movement within a container, concluding that particle damping results from both impact and friction damping. They tested packing ratios of 95%, 50%, and 25%, finding that the 95% ratio is ineffective due to minimal clearance between particles and walls, making friction damping more significant than impact damping. The 25% packing ratio showed the highest damping efficiency, while energy dissipation remained constant for the 50% and 95% ratios.

Wong et al. [103, 113] investigated the energy dissipation mechanisms in particle dampers using the DEM and the complex power method. The DEM model is constructed using a Perpex cylinder casing enclosing steel particles of four varying diameters (3.0 mm, 2.5 mm, 2.0 mm, and 1.5 mm). Through their simulations, they identify friction as the dominant energy dissipation mechanism within the studied dampers, based on approximated material parameters. The validity of these numerical findings

is further supported by experimental results. Additionally, the simulations reveal a significant impact of contact stiffness (although the experimental stiffness value remains undetermined) between particles and damper walls on the power dissipation.

Ito et al. [114] studied how vessel shape (rectangular, pentagonal, semicircular) affects vibration reduction. The semicircular vessel had the lowest amplification ratio, and a compartmentalized rectangular vessel performed better than a standard one. They also found that more particles improved vibration attenuation due to reduced clearance between particles and the vessel wall. While the simulations provided useful insights, experimental verification is needed to confirm the findings.

Lu et al. [134] used DEM simulations to study how different system parameters affect a particle damper. They simulated a container partially filled with 6 mm spherical particles subjected to horizontal harmonic excitation. They studied the effect of material properties on particle damper performance by varying particle density and found that the damper's performance was minimally affected by particle material. However, several experimental studies have shown that material properties play a significant role in particle damper performance [7, 8]. Nevertheless, the quantity of particles significantly influenced the damper's behavior. Additionally, higher excitation levels improved damping efficiency.

Duan et al. [104] used 3D DEM simulations to examine energy dissipation in particle dampers under vertical excitation. They modeled a cylindrical container with 250 stainless steel spheres (1.5 mm radius) and calculated average loss power using Eq. (2.8), implementing a velocity-dependent restitution coefficient. The results showed that energy dissipation depends on the velocity amplitude of the excitation load. The comparison between the simulation and experimental results indicates a reasonable quantitative agreement in loss power at higher acceleration levels. However, at lower acceleration, the discrepancy is significantly larger. Incorporating a velocity-dependent restitution coefficient improves the alignment between simulation and experimental results. The authors conclude that DEM can be used not only for qualitative analysis but also for quantitative analysis, provided the model is sufficiently accurate.

Meyer et al. [106] investigated the influence of particle material on the loss factor of particle dampers using the complex power method in conjunction with DEM simulations. They employed three distinct materials for the spherical particles: steel, tungsten, and polypropylene. Their findings revealed no significant impact of these material choices on the loss factor of the damper. To further explore this aspect, the authors varied the particle density across a wide range (7800 $\frac{\text{kg}}{\text{m}^3}$ to 900 $\frac{\text{kg}}{\text{m}^3}$ and 19250 $\frac{\text{kg}}{\text{m}^3}$) and the Young's modulus (210 GPa to 1.1 MPa and 1000 GPa). These variations also showed negligible effects on the loss factor. These results suggest that, within the scope of this study, particle material properties may not be a critical factor for optimizing particle damper performance. Meyer et al. [135] observed similar results regarding particle material properties (Young's modulus and density) in a separate study investigating different particle configurations within the damper.

Luo et al. [136] investigated the effects of particle size and filling ratio on energy dissipation in dampers using DEM simulations. They computed the energy dissipation mechanism with Eqs. 2.5 - 2.7 and evaluated four particle sizes: 2 mm, 3 mm, 4 mm, and 5 mm. They found that energy loss depends on particle size, with 3 mm being optimal. An 80% filling ratio was also identified as best for reducing vibration amplitude. Experimental studies confirmed the damper's effectiveness, but the study did not compare experimental and simulation results.

Song et al. [137] conducted both numerical and experimental studies on the effect of various particle damper parameters on vibration reduction. Using a cylindrical cavity (94 mm diameter, 80 mm height) filled with discrete particles, they evaluated energy dissipation as per Chen et al. [108] and Duan et al. [104] They tested four materials (lead, steel, glass, and rubber), finding lead most effective and rubber least effective. The study also investigated nine filling ratios (10% to 90%), with 80% providing the best vibration reduction. Particle sizes (4 mm, 6 mm, 8 mm, 10 mm, 12 mm) were tested, with 8 mm proving most effective. Numerical and experimental results were consistent, though

a quantitative comparison was not provided, which would enhance the model's validation.

A review of numerical parametric analyses reveals conflicting findings regarding the optimal filling ratio for particle dampers. For example, Mao et al. [132, 133] reported that a 25% filling ratio yields the most effective vibration attenuation, whereas higher filling ratios ranging from 50% to 95% were found to be largely ineffective in reducing vibration amplitude. In contrast, studies conducted by Luo et al. [136] and Song et al. [137] indicate that an 80% filling ratio provides the highest damping efficiency. The discrepancy in findings, particularly the deviation observed in the results of Mao et al. [132, 133], may be attributed to the simplifications introduced in their numerical model, which could have influenced the accuracy of their predictions. Another area of discrepancy concerns the influence of material properties on the damping performance of particle dampers. Both Duan et al. [104] and Meyer et al. [106] have reported that variations in material density have a negligible impact on damping efficiency. However, several experimental studies suggest that the choice of material plays a crucial role in the design and performance of particle dampers. Investigating the role of different granular materials in particle damper design is also a key focus of this thesis. The divergence observed in numerical studies may stem from the fact that they primarily account for changes in material density while neglecting other critical properties, such as viscoelastic behavior, which are typically not directly incorporated into the DEM simulations.

From the above review it can be concluded that studying the influence of parameters such as particle size, filling ratio, and material properties on the damping performance of particle dampers presents significant challenges, as these aspects can only be effectively investigated through experimental methods. In contrast, analyzing the effect of parameters such as motion mode is more conveniently conducted using the DEM rather than experimental approaches. The following section presents a numerical study focused on the influence of motion mode.

2.3.2.3 Motion mode

The motion mode of granular materials constitutes another frequently investigated parameter in conjunction with structure-independent particle dampers using DEM simulations. Experimental exploration of the influence of particle motion on damper efficiency presents significant challenges, thereby necessitating the extensive use of DEM simulations as a valuable tool for these studies. While a substantial body of research has focused on the granular material's state within the damper, this topic will be briefly addressed in this thesis. The motion mode, often termed the state of the granular material, can exhibit characteristics akin to solids, fluids, or gases under varying conditions. This section provides a concise review of the literature on how this state affects the damping performance of particles.

Saluena et al. [109, 110] employed molecular dynamics simulations to investigate the motion of granular materials in partially filled, two-dimensional containers subjected to horizontal vibrations. Their primary focus was on the rate of energy dissipation within the particle assembly. The study identified three distinct motion regimes: solid-like, convective, and gas-like. A significant enhancement in energy dissipation was observed during the solid-liquid transition phase of the particle bed.

Zhang et al. [98] investigated the link between NOPD damping effectiveness and granular bed motion using DEM. They modeled a cylindrical container (20×60 mm^2) with 3 mm monodisperse steel spheres. To characterize energy dissipation, they used the effective damping parameter (Eq. 2.9) in their simulation and found a consistent trend with experimental data. The study concluded that NOPD's damping effectiveness is closely tied to the motion patterns of the granular material, achieving optimal damping during the transition from the "Leidenfrost state" to the "buoyancy convection state." The Leidenfrost state involves dense particle clusters suspended above fast-moving particles, while buoyancy convection combines the Leidenfrost effect with convection in suspended granular layers. The study focused exclusively on first-mode vibrations. Building on their previous work, Zhang et

al. [138] examined the effect of particle motion mode on damping efficiency in a 100 mm $\times$ 6 mm $\times$ 50 mm container. Noting that container geometry affects particle motion modes, they used 2000 monodisperse steel spheres (2 mm diameter) and subjected the system to vertical harmonic motion. Using Eq. 2.9 to characterize damping behavior, they observed six particle motion modes, compared to seven in their prior study [98]. Consistent with earlier findings, the Leidenfrost state provided the best damping, while the solid-like state had the least. They stress the importance of careful calibration for contact parameters in DEM to avoid unrealistic damping predictions.

Yin et al. [139] also used DEM to study the effect of granular motion modes on the loss factor of NOPDs. They modeled a closed cylinder with 500 steel spheres (3.5 mm diameter) and classified the motion modes into seven groups: solid-like state, local fluidization, global fluidization, convection, Leidenfrost effect state, buoyancy convection, and bouncing bed, aligning with Zhang et al. [98] definitions. Their study showed that the loss factor varies with excitation intensity and frequency for each mode. They found that NOPDs achieve optimal damping in the buoyancy convection state. However, these results are based on numerical simulations, and experimental validation is needed.

Meyer et al. [106] employed DEM to investigate the reduced loss factor of monodisperse particle dampers. They utilized the complex power method for data analysis, focusing on how various particle motion modes influence vibration attenuation. Their study involved a cubic aluminum box filled with 550 steel particles of 2.5 mm radius. The authors observed distinct motion modes depending on the intensity of the container's excitation. They found that the bouncing bed mode and the transition from local to global fluidization resulted in high reduced loss factor values.

It can be concluded that particle motion modes in DEM studies depend on factors like cavity geometry, excitation direction, frequency, amplitude, and material configurations. Various studies have identified different motion regimes: Saluena et al. [109, 110] found three regimes (solid-like, convective, and gas-like) in a horizontally vibrated system; Zhang et al. [98] observed seven modes in a vertically excited 3D system and six in a quasi-2D simulation; Meyer et al. [106] identified five modes in a horizontally vibrated cubic container. The optimal damping mode varies across studies. While numerical studies offer valuable insights for particle design, experimental validation is lacking. No published work directly links particle motion mode to damping efficiency in particle dampers, although some experimental studies have explored motion patterns in vibrated containers. Eshuis et al. [140] observed eight motion modes for glass beads in a quasi-2D container, and Ansari et al. [141] found similar results with monodisperse particles. While the investigation of granular motion under extreme excitation forces, such as those induced by shaking table tests, offers valuable insights, the occurrence of such intense vibrations in real-world mechanical structures is infrequent. Consequently, it is rare that granular materials will attain states resembling bouncing bed or gaseous conditions under typical operating circumstances.

2.3.3 Review of structure-integrated particle damper

Although the DEM has been successful in analyzing particle damper behavior and vibration reduction mechanisms, current research primarily centers on the dynamics of the particles themselves, often disregarding their interaction with the impacted mechanical structures. This limitation arises from DEM's treatment of contact surfaces as massless rigid bodies, hindering the modeling of dynamic deformation within the mechanical structures. However, the complex interaction between these structures and the granular material particles significantly influences energy dissipation and the overall effectiveness of vibration attenuation. To address this, DEM necessitates integration with other methods like the FEM or MBD. This section reviews the literature on the combined approach of coupling DEM with such continuum methods to achieve simultaneous modeling of both particle and mechanical structural dynamics.

2.3.3.1 Coupled numerical modeling techniques

Meyer et al. [100] investigated the damping behavior of particle dampers for various eigenfrequencies of basic structures using a combined DEM and reduced FEM approach. The particle damper design consists of a cubic aluminum box filled with steel spheres (5 mm radius) attached to the midpoint of a free-free beam. To achieve coupling, the FEM captures the movement of the particle box and transmits it to the DEM model. This excitation allows for calculation of particle interactions and resulting forces on the container walls. These forces and moments are then transferred back to the FEM model. The combined accelerations (particle and modal states) are then used to obtain the complete system's frequency response. The authors achieved good agreement between experiment and simulation for the system without a particle damper. Introducing particles to the system resulted in a significant increase in damping, with qualitative agreement between experiment and simulation observed. However, the most significant discrepancies occurred at high damping values, where the simulation overestimated the damping effect. Their study concludes that a single, optimal particle damper design for all eigenfrequencies is unlikely. Instead, achieving optimal performance necessitates a trade-off between various factors.

Lin et al. [142] employed a coupled DEM and FEM approach to investigate design parameters for particle dampers aimed at reducing vibration amplitudes in railway tracks caused by wheel-rail contact. The particle damper, modeled using DEM, consisted of multiple cavities filled with stainless steel spheres (5 mm diameter) and was attached to both sides of the FEM-simulated rail track. The study explored the effect of three particle sizes (4 mm, 5 mm, and 6 mm) on performance, identifying 5 mm as the optimal size. They further investigated four filling ratios (10%, 20%, 30%, and 40%) for the 5 mm particles using their coupled simulation approach. The results concluded that a particle damper with 5 mm particles and a 30% filling ratio achieved the most significant energy dissipation. While the experimental study verified the simulation for a single resonance frequency, the authors did not elaborate on the DEM-FEM coupling strategy employed. Additionally, it remains unclear whether the design of the particle damper cavities was performed using FEM.

Lio et al. [143] investigated the energy dissipation mechanism of a spring-mass-damper-slider system with a particle damper using a two-way coupled DEM-MBD model. Within this model, the hollow box is represented by the MBD, while the particles and their interactions with the box are captured by the DEM. This two-way coupling allows for a dynamic exchange of forces and displacements. Particle-wall contact forces calculated by DEM affect the movement of the hollow box (MBD). Furthermore, hollow box displacements from MBD are then fed back to DEM as updated boundary conditions for the particles. The authors validated their numerical model through experimental comparison, demonstrating reasonable agreement. Their study concludes that the damping effect primarily arises from the contact forces generated during particle-box interactions. These forces act as resistive forces on the hollow box, dissipating energy and hindering its motion. Additionally, they mentioned that energy loss within the particles themselves is mainly due to contact friction and damping when struck by the hollow box.

In a recent study by Xia et al. [144], a DEM-FEM coupling strategy was employed to investigate the effectiveness of particle dampers in reducing vibration amplitude within a simplified, scaled-down model of a satellite load-bearing cylinder. The authors explored the effect of four distinct particle materials (ceramic, iron-based alloy, lead-based alloy, and tungsten-based alloy) on the cylinder's vibration characteristics. Numerical simulations revealed that iron-based alloy particles exhibited the most significant reduction in vibration amplitude compared to the other materials tested. Furthermore, the study examined the impact of particle diameter on vibration attenuation. Iron-based alloy particles of three different diameters (2 mm, 3 mm, and 4 mm) were investigated. The results indicated that 3 mm diameter particles were most effective in reducing vibration compared to 2 mm and 4 mm counterparts. Additionally, an optimal filling ratio of 80% was identified for maximum vibration mitigation. To validate the numerical model, experimental studies were conducted. While the trend for vibration reduction remained consistent between the experimental and numerical results, a significant

discrepancy in magnitude was observed. The vibration mitigation values obtained from the numerical model consistently exceeded those measured experimentally. It is noteworthy that the study employed spherical particles for both the numerical and experimental investigations. Additionally, only iron-based alloy particles were used in the experimental validation, as this material demonstrated the most promising results in the DEM-FEM simulations.

2.3.4 Summary and discussion of numerical methods

This review comprehensively examines particle damper modeling techniques, focusing on the DEM and combined numerical approaches (e.g., DEM-FEM or DEM-MBD). While the reviewed literature highlights the ability of numerical approaches to provide insightful understanding of particle damper behavior, it also identifies several significant challenges associated with these methods.

Particle shape presents a significant challenge in the DEM modeling of particle dampers. While spherical particles are widely adopted due to their computational efficiency (as detailed in Section 2.3.2.1), other geometries, such as clumps, ellipsoids, superquadrics, and polyhedrons, can also be incorporated. However, these complex shapes present computational difficulties and are consequently less frequently employed. Furthermore, the available options for non-spherical shapes remain limited, hindering the ability to accurately represent the diverse particle morphologies encountered in real-world applications.

Particle size presents another substantial challenge for the numerical modeling of particle dampers. While accurate modeling of particle size might be achievable for laboratory-scale setups with a relatively small number of particles (as evidenced by the reviewed literature), replicating real-world particle damper designs or even some laboratory experiments can become computationally intractable due to the vast number of particles involved. Industrial applications often utilize billions to trillions of particles, exceeding the capabilities of current computing power and likely remaining infeasible in the foreseeable future, even considering exponential growth in computational resources [124]. This limitation arises from the sheer number of particle interactions that need to be simulated, significantly increasing computational demand and hindering practical implementation.

Calibration of material input parameters remains a critical challenge for DEM simulations of particle dampers. The reviewed literature often lacks explicit discussion regarding parameter calibration, making it difficult to assess the reliability of the modeling results. Natural bulk materials exhibit inherent variability due to external conditions and geographic location, further complicating the process of obtaining accurate input values. Calibration can often be the most time-consuming aspect of a DEM simulation project, and some studies have identified it as the primary obstacle to wider industrial adoption of DEM for particle dampers.

Interestingly, some DEM simulations reported in the literature suggest that material choice, density, and Young's modulus have minimal influence on particle damper energy dissipation. However, this thesis will subsequently demonstrate that the selection of granular material plays a critical role in designing an efficient particle damper.

Additionally, it has been observed that combined numerical approaches, such as DEM-FEM and DEM-MBD couplings, offer advantages over DEM simulations alone. However, these benefits come at the cost of increased computational time. Moreover, coupling strategies inherit all the challenges associated with DEM modeling, except for the rigidity issue of mechanical structures, which is resolved in coupled numerical approaches. During the concept development phase of the particle damper design strategy presented in this thesis (experimentally), it was found that the discretization of the mechanical structure in FEM modeling should be kept as coarse as possible to reduce computational time. However, this coarse mesh during the concept design phase can lead to inaccurate results.

While numerical approaches offer valuable insights into particle damper behavior, their limitations necessitate complementary experimental studies for a comprehensive understanding. Numerical sim-

ulations can struggle to fully capture the effects of all relevant parameters, particularly for complex real-world scenarios with a vast number of particles. Therefore, laboratory experiments remain a crucial tool in developing and validating particle damper designs. These experiments allow researchers to observe and quantify the behavior of the damper under controlled conditions, bridging the gap between numerical predictions and real-world applications.

2.4 Experimental approach of particle damper

The review of numerical modeling techniques applied to particle damper design reveals both the strengths and shortcomings of this approach, underscoring the necessity of complementary experimental investigations. Section 2.2 and Section 2.3 have demonstrated the limited success of analytical and numerical methods in predicting particle damper performance and optimizing designs for practical applications. Consequently, an experimental approach is deemed more promising for advancing the field of particle damper design.

Experimental investigations into particle damper design and energy dissipation can be categorized into two primary approaches. The first involves the study of particle damper parameters using isolated, structure-independent configurations. These experiments often serve as benchmarks for validating numerical models. However, due to their idealized conditions, including simplified cavity geometry and particle characteristics, this category of research will not be extensively reviewed in this section. In contrast, the second approach focuses on evaluating overall damping performance and design parameters within the context of integrated structural systems. This section will primarily concentrate on the latter category of experimental studies.

The literature review of the experimental investigations of particle damper design in this thesis is categorized based on reported application areas, such as aerospace, automotive, and machinery fields. Furthermore, several studies have examined the influence of various particle damper parameters using beam- or plate-like structures as primary systems. These investigations often lack a specific application focus, concentrating mainly on parameter analysis at the laboratory scale. This thesis will also include a review of such studies.

2.4.1 Particle dampers application in aerospace field

Panossian [32] has introduced the NOPD concept, which involves the creation of small cavities within a vibrating structure that can be partially filled with granular materials. The effectiveness of this concept is demonstrated by reducing the vibration amplitude of a space shuttle main engine liquid oxygen inlet tee. To design the NOPD he used four different kinds of granular materials, namely: steel balls, zirconium oxide ceramic balls, nickel powder, and tungsten powder. In order to enclose these granular materials, Panossian drills four 1 mm diameter holes in the liquid oxygen inlet tee splitter and partially fills them with steel balls of varying sizes (0.18 mm, 0.28 mm, and 0.58 mm), zirconium oxide ceramic balls (0.25 mm), nickel powder, and tungsten powder. The experimental results indicate that the tungsten powder exhibits significantly higher vibration attenuation compared to the other materials. However, it is important to note that the damping performance of these materials is not straightforward and exhibits slight variations in damping capabilities across different mode shapes. Notably, the steel balls with a diameter of 0.18 mm demonstrate superior vibration attenuation capabilities at 3807 Hz and 4309 Hz compared to other materials, while the nickel powder performs better at 4257 Hz. Therefore, based on these findings, the author concludes that the vibration attenuation achieved through particle dampers is a complex function influenced by material properties and various parameters that need further investigation.

Simonian [145] used the particle damping technique in the aerospace sector, demonstrating its remarkable damping capability under random vibration conditions. The study shows that particle

dampers, specifically those containing lead shot, are significantly efficient in reducing the vibration amplitude compared to conventional passive dampers like viscoelastic materials or viscous fluids.

Michon et al. [146] substituted traditional, heavy solid particles with lighter, hollow ones to enhance the damping performance of a honeycomb beam while minimizing added mass. Their approach significantly improved overall damping. However, their experimental honeycomb cantilever beam exhibited no damping effect for its first vibration mode when partially filled with hollow particles. The authors explored three filling ratios (50%, 80%, and 100%), determining that 80% provided optimal damping efficiency. Nevertheless, the study lacks crucial details about the particle shape, size, and the nature of the granular material, such as whether it was monodisperse or polydisperse.

The particle damper concept has been successfully implemented in the aerospace industry by Veeramuthuvel et al. [8]. The authors affixed a square-shaped particle damper capsule onto a printed circuit board (PCB) that experiences significant vibrations during spacecraft launch. The vibration attenuation performance of three distinct granular materials, namely tungsten carbide, stainless steel, and aluminum alloy, was tested in their study. In their experimental studies, they observed that materials with higher densities exhibit greater damping efficiency. Furthermore, they conducted a study to examine the impact of packing ratio on vibration mitigation and found that a packing ratio of 60% effectively reduced vibrations for all the materials they studied. In addition, they observed that regardless of the granular materials used, a packing ratio of 100% is not effective in reducing the vibration amplitude.

Bustamante et al. [147] investigated the potential of elastomer particles to mitigate vibration in beams and plates. They employed two elastomer types, A and B, with the latter further categorized by size. However, the study lacked detailed material and particle characterization. Elastomer A demonstrated vibration reduction in the 30 - 40 Hz range for beams, while Elastomer B exhibited optimal damping between 60 - 90 Hz. Interestingly, a shift in peak damping to 80 - 120 Hz was observed, attributed to the increased stiffness of Elastomer B compared to Elastomer A and smaller Elastomer B particles. Similar findings were observed for plates, with maximum attenuation reaching 24 dB. The damping performance varied across frequencies, with some peaks experiencing significant reduction, others minor attenuation, and some remaining unaffected. To assess real-world applications, the authors applied the particle damper to a scaled aircraft floor panel comprising a honeycomb aluminum core and epoxy skins. Sixty evenly spaced dampers significantly reduced vibrations. The particle damper's performance matched a commercial damping layer, excelling at mid-range frequencies but slightly underperforming at higher ones.

Ye et al. [148] studied the vibration damping performance of a multi-unit particle damper (MUPD) on an aluminum alloy bracket structure, a common component in spacecraft, subjected to both harmonic and random excitation. The MUPD was externally mounted on the top of the bracket. The authors evaluated the vibration attenuation capabilities of four different granular materials: 2.0 mm steel particles, 2.0 mm lead particles, 0.048 mm stainless steel powder, and 0.5 mm tungsten carbide powder. Their findings revealed that tungsten carbide powder exhibited the most effective vibration damping, followed by stainless steel powder, lead particles, and lastly, steel particles. Additionally, the study concluded that the cavity's structural design significantly influences the damping behavior of the particle damper.

Xia et al. [144] utilized iron-based alloy particles to design a particle damper for mitigating vibration amplitude in a simplified, scaled-down model of a satellite load-bearing cylinder. The cylinder comprised four layers, and the study examined the effect of particle damper placement by strategically mounting four dampers at each layer. Their findings revealed that attaching particle dampers to the first layer of the cylinder yielded the most significant reduction in structural vibration amplitude. Notably, this configuration achieved substantial vibration attenuation around the resonance frequencies of 199.3 Hz, 308.75 Hz, and 398.75 Hz.

2.4.2 Particle dampers application in automotive field

Duvigneau et al. [149] demonstrated the effectiveness of particle dampers in reducing the vibration amplitude of an automotive engine oil pan. Their experimental study revealed that using sand with an average particle size of 0.3 mm resulted in a significant reduction in oil pan vibration. The authors conducted separate measurements of the vibration response when the oil pan was filled with water and sand, respectively. This experiment aimed to establish that the primary factor responsible for vibration attenuation was the particle damping mechanism rather than just the added mass of sand. Additionally, they have also shown that the addition of sand particles can increase the vibration attenuation of the oil pan to a certain extent.

Koch et al. [150] extended the research conducted by Duvigneau et al. [149] by introducing a honeycomb structure to replace the original bottom of the oil pan bottom. This modification allowed them to investigate the influence of granular materials distribution on the vibration behaviour of the system. Furthermore, the honeycomb bottom has been used to keep the mass of the entire structure filled with granular materials either equal to the total mass of the original structure or to make it lighter than the original mass. Moreover, they have studied the influence of three different sizes of sand particles on the oil pan vibration attenuation. To achieve this, they utilized three different sizes of sand particles in their investigation. The experimental study reveals that larger sand particles exhibit higher damping efficiency. Additionally, the results demonstrate that a larger angle of repose can contribute to achieving higher damping. Furthermore, they suggest that the optimal placement for the granular material filling is the location where the vibration amplitude is higher. The effectiveness of this concept was then demonstrated through testing on a running engine test bench.

Koch et al. [7] have also investigated the vibration attenuation performance of eight different granular materials, namely: rubber granulate, sand, corundum, glass balls, silicon, gelatin gel, polystyrene, and glass with two different grain sizes. The experimental studies have shown that the rubber granulate damping performance is significantly higher in comparison to the other granular materials under investigation.

Liming et al. [151] explored the use of particle dampers to mitigate cab vibration in mining trucks. Their study investigated the placement of a particle damper within the driver's seat base. This implementation achieved a significant reduction in vibration amplitude of the seat base, reaching nearly 30%. The research employed a dual testing approach, utilizing both laboratory and real-world truck testing. The findings revealed a more pronounced effect of particle damping technology at higher engine speeds (2200 rpm) compared to lower speeds (750 rpm).

2.4.3 Particle dampers application in machinary field

Xu et al. [152] have successfully demonstrated the application of particle damping technique to reduce the dynamic response of a banknote machine. The authors applied the particle damping technique to the banknote machine by drilling ten 3 mm diameter holes on the machine shaft and completely filling them with 0.5 mm diameter tungsten particles. Based on their experimental investigation, the particle damper exhibits remarkable effectiveness within the frequency range of 4000-6000 Hz, capable of reducing the vibration amplitude of the primary structure by up to 40 dB. Nevertheless, within the frequency range of 0-2000 Hz, the tungsten particles exhibit only moderate damping capabilities. Moreover, a noise reduction of 6 dB(A) has been also achieved.

Sims et al. [153] investigated the application of a particle damper for mitigating chatter during milling operations. The damper was a 35 mm diameter, 60 mm deep cavity filled with steel particles (0.18-0.24 mm). Their results demonstrated a significant enhancement in chatter stability when the damper was applied to a flexible workpiece. Without the damper, machining with an axial depth of cut exceeding 0.10 mm was generally impossible. In contrast, with the damper, machining at depths of up to 7.00 mm was achievable. The study concluded that particle dampers can dramatically improve the

chatter stability of flexible workpieces. Nevertheless, it is evident that predictions based on laboratory results diverged significantly from the outcomes of the machining trials.

Chan et al. [154] investigated the use of particle dampers to mitigate vibrations in the bond arm of a die bonding machine. They attached enclosures filled with tungsten particles to the bond arm at two distances from its free end and observed a successful reduction in the primary structure's vibration amplitude. Their study focused on the influence of particle size on vibration attenuation. They found that larger particles provided slightly better damping around 430 Hz, although the differences were not substantial. At higher frequencies (1940 Hz and 4550 Hz), the effect of particle size became even less significant. Additionally, the choice of enclosure material played a role. Aluminum enclosures outperformed hard plastic counterparts when filled with tungsten particles. Furthermore, they investigated the optimal positioning of the particle dampers on the bond arm. Their analysis revealed that the placement should consider the modal amplitude of the structure to achieve maximum damping at the desired frequency.

Kumar et al. [155] employed copper (2.36 mm and 4.75 mm) and lead (3.2 mm and 4.75 mm) spherical particles to reduce the vibration amplitude in a boring bar. Their findings revealed that copper particles damping efficiency is significantly higher than the lead particles. Furthermore, they observed that larger-sized particles were more effective for reducing the vibration amplitude of the structure.

Another application of particle dampers to reduce the vibration amplitude from a boring bar has been investigated by Muthu et al. [156]. Their damper employed 1 mm cast iron spherical particles contained within a cylindrical acrylic casing. The damper was positioned at three different distances from the boring bar's free end, while particle packing density was varied between 25%, 50%, and 75%. Results demonstrated that a 50% packing ratio yielded the most substantial vibration reduction. Interestingly, the damper's position did not affect its damping efficiency when using the optimal 50% packing ratio.

Goehler et al. [157] developed a particle damper by filling stainless steel hollow spheres with ceramic powders. To evaluate its performance, they constructed a prototype milling slide using these particle-filled spheres instead of traditional steel sheets. Compared to the conventional design, their particle damper enhanced damping by a factor of five, doubled stiffness, and reduced mass by 10%. Nevertheless, the authors asserted that optimizing the sphere filling level and slide design to accommodate the unique properties of the particle-filled sheets could further elevate the damping capabilities of their hollow sphere-based particle damper.

Xiao et al. [158] explored the use of a particle damper to reduce vibration amplitude in gear transmissions under centrifugal forces. Their design employed stainless steel balls (3 mm diameter) housed within eight drilled holes (15 mm diameter) on the gear surface. Baffle rings prevented ball loss. The study revealed a positive correlation between rotational speed and energy dissipation within the damper. Additionally, they found that filling ratios below 50% were ineffective in mitigating vibrations. Notably, the optimal filling ratio varied with rotational speed, ranging from 60% at 300 rpm to 80% at 1100 rpm.

Jin et al. [159] investigated the use of particle dampers for vibration attenuation in pipelines at a laboratory scale. They designed and tested dampers containing cast iron balls of three sizes: 1 mm, 2 mm, and 3 mm. The study compared the effectiveness of single-unit and multi-unit damper configurations. Their findings demonstrated that 1 mm and 2 mm balls offered superior vibration mitigation compared to 3 mm balls. Notably, when achieving the optimal particle filling ratio, the vibration attenuation performance of both single-unit and multi-unit systems was found to be nearly equivalent. Furthermore, the authors successfully validated the particle damper concept on an original-scaled hydraulic power source pipeline.

Particle damper also finds its application in reducing the vibration amplitude of a tensegrity prism [160]. Furthermore, three different materials are used to design the particle damper. They used steel spheres with a diameter of 7 mm, 3D-printed spheres also 7 mm in diameter, and glass spheres with four different diameters: 5 mm, 6 mm, 7 mm, and 8 mm for particle damper design. The results indicated that

smaller particles exhibited a higher vibration attenuation. Comparatively, the vibration attenuation of glass spheres is notably higher than that of other materials, particularly at higher excitation magnitudes. Moreover, the 3D-printed spheres demonstrate lower damping capability than glass spheres but still surpass the damping performance of steel spheres.

Wang et al. [161] have successfully employed a particle damper to reduce the amplitude of pipeline vibrations. The damping performance of three different materials, namely steel balls, aluminum balls, and glass balls, was examined. The results indicate that the vibration attenuation capacity of steel balls significantly surpasses that of aluminum and glass balls. Moreover, they have determined that an ideal filling ratio for the design of a particle damper falls within the range of 70% -90%. Moreover, their research has demonstrated that the influence of boundary conditions is negligible.

In a recent study by Ye et al. [162], particle dampers were implemented on a scaled model of a container crane to investigate their effectiveness in vibration attenuation. The dampers consisted of chambers partially filled with spherical granular materials and attached to the crane structure. The influence of four materials (10 mm diameter) – lead, glass, aluminum, and steel – on vibration reduction was examined. Results indicated that lead exhibited the most significant reduction in vibration amplitude compared to the other materials. Furthermore, Ye et al. [162] investigated the effect of filling ratio on vibration mitigation using steel balls (10 mm diameter) within the damper chambers. They tested four filling ratios: 20%, 40%, 60%, and 80%, with an additional test at 100% (full chamber). The optimal vibration suppression effect was achieved at a filling ratio of 60%. Additionally, the influence of particle size on vibration attenuation was explored using particles of varying diameters (6 mm, 8 mm, 10 mm, and 12 mm). The study found a positive correlation between particle size and vibration mitigation, with larger particles demonstrating a greater reduction in vibration. While the study provides valuable insights, it mainly focuses on time-acceleration data, lacking analysis of the effective frequency range.

2.4.4 Particle dampers application in wind turbine

Stauber et al. [163] has used elastomer particle damper to reduce the vibration amplitude of a wind turbine tower. They proposed that particles with rough and textured surfaces are beneficial for energy dissipation. Through experimental investigations, they demonstrated that particle dampers containing elastomer particles can substantially reduce vibration amplitude within the frequency ranges of 100 Hz to 600 Hz.

Sandanshiv et al. [164] demonstrated the efficacy of particle dampers in mitigating vibration amplitudes within wind turbine blades. The study employed external particle dampers mounted on all three blades, each containing 9 mm steel balls enclosed within a polypropylene container. The authors evaluated four different damper locations and three rotational speeds (60 rpm, 70 rpm, and 80 rpm). Their findings revealed that particle dampers positioned near the blade root offered the most significant vibration attenuation at the lowest rotational speed (60 rpm).

2.4.5 Influence of various parameters on particle damper performance

Schmidt [165] evaluated the loss factors of five materials: dry sand (0.3-1 mm), glass beads (1 mm), brick fragments (0-10 mm), coal slag (0-15 mm), and iron filings (3-15 mm). Sand and glass beads, characterized by uniform, smooth grains, exhibited average loss factors of 0.12 and 0.15, respectively. Coal slag achieved the highest loss factor of 0.25, though this required a thicker layer (4.0 cm) compared to the 3.2 cm layers of sand, glass beads, and brick fragments. Notably, coal slag also demonstrated a loss factor of 0.21 in a thinner layer. Iron filings (3.5 cm layer) reached a loss factor of 0.14. These values were measured within the 200-500 Hz frequency range. Contrary to expectations, loss factors increased below 200 Hz. Additionally, the study revealed that thicker material layers generally corresponded to lower loss factors.

Wolf [166] investigated the potential of sand to attenuate vibrations in ceiling, wall, and floor panels of a sonic fatigue facility. To conduct experiments, scaled beams were used as models. Sand was contained in large boxes bolted to the steel beam. Results indicated significant vibration amplitude reduction at 280 Hz, 690 Hz, 1220 Hz, and 1830 Hz. Additionally, a decrease in vibration amplitude at 40 Hz was observed when six sand-filled boxes were attached. Furthermore, it has been observed that the loss factors varied between horizontal and vertical beam orientations. It is important to note that adding sand increased system weight by 30%. Furthermore, inconsistencies in loss factor values were observed across different measurement techniques and acceleration levels. While some instances showed agreement, a clear trend remained elusive.

Sun et al. [167] investigated the damping capabilities of sand when applied to plate and beam structures. Their results showed that increasing sand layer thickness on plates initially reduces vibrations but exceeding a certain threshold reverses this effect. The authors attribute this to the relationship between sand loss factor and static pressure, as described by Schmidt [165]. This implies that the loss factor varies with sand layer thickness. For beam-like structures, they observed that the loss factors were roughly proportional to the amount of sand present. Additionally, they found that the damping properties of a sand-containing plate are also influenced by how the structure is suspended. For example, they noted that the loss factor decreases when the sand-covered plate is suspended vertically.

Cempel et al. [168] examined how various arrangements of shot packing affect the reduction of vibrations in an aluminum cylinder. In total, eight different shot-filling configurations were analyzed and the mass of the shot in each configuration was kept the same. The study revealed that optimal and consistent vibration attenuation can be obtained by either randomly dispersing the shots within the container or densely packing them in a plastic bag. However, the authors fail to provide details concerning the material composition of the shots. Their focus was solely on the packaging material.

Papalou et al. [169] conducted a study where they designed a particle damper using steel balls and successfully demonstrated the significant impact of particle size on vibration attenuation. The steel balls (1.6 mm, 3.2 mm, and 12.7 mm) were contained within the cavity formed by four aluminum edge brackets. One bracket was securely attached to the vibrating plate, while the other three were adjustable, allowing modifications to the particle damper's size. Additionally, the authors have demonstrated that the correlation between the mass ratio and the vibration response of the system is non-linear. Interestingly, when the excitation level is high enough to overcome friction forces between the particles, the vibration response of the system becomes independent of the excitation intensity. However, the direction of excitation does not impact the performance of particle damping. Additionally, they found that smaller particle sizes led to decreased influence of container size and excitation intensity, expanding the optimal design space.

Papalou et al. [170] have carried out the above work to investigate the influence of a particle damper when subjected to harmonic excitation at its base. The excitation amplitude remained constant, while the frequency was varied. The results showed significant vibration attenuation. Additionally, it has been noted that substituting the solid particle in a single-particle damper (impact damper) with smaller particles of the same mass yields significant improvement in reducing interface material deterioration, reducing high noise levels, and making the particle damper less sensitive to container size and excitation amplitude.

Holkamp et al. [171] have conducted experimental investigations on the damping properties of particle dampers using a cantilever beam with drilled holes. The study aimed to identify and analyze various parameters that influence the damping efficiency of particle dampers, focusing on different particle materials and shapes. Tungsten carbide cobalt, aluminum, titanium, stainless steel, and glass beads were examined as potential damping materials. The experimental results revealed that steel, tungsten, and titanium exhibited similar capabilities in reducing the vibration amplitude of the cantilever beam. Conversely, glass beads exhibited significantly higher vibration attenuation compared to aluminum.

Furthermore, the influence of particle shape on vibration attenuation was found to be negligible. Additionally, it was observed that increasing the mass of the granular material beyond a certain threshold did not yield any additional damping effects. The influence of filling ratio on damping was also explored. Six distinct tungsten filling ratios of 45%, 67%, 78%, 89%, 100%, and 111% were examined. The lattermost was achieved by loosening the set screws. Optimal damping performance was observed at the filling ratio of 45%. A relatively stable damping response was noted within a range of 67% to 78% volume fraction. Conversely, damping capacity was significantly reduced at both 100% and 111% volume fractions, irrespective of force amplitude.

Tomlinson et al. [172] employed a particle damper composed of 0.8 mm diameter steel balls to mitigate the vibration response of a mild steel plate. In their experimental investigation, they utilized a hollow steel cylinder with varying aspect ratios to construct the particle damper. The study revealed that the geometry of the particle damper significantly influences the vibration attenuation. The main focus of their studies was to create a particle damper capable of withstanding high temperatures up to 600 degrees Celsius. Additionally, they aimed to effectively reduce the vibration amplitude of a discharge nozzle within the frequency range of 400 Hz to 1000 Hz.

Yang et al. [173] successfully applied a particle damper to mitigate vibration amplitude in a clamped aluminum beam. Employing 200 brass balls (1.6 mm), they constructed the particle damper. Their findings indicate that gap size significantly influences the damper's efficacy. To explore this, they tested seven gap sizes: 0 mm, 0.25 mm, 0.50 mm, 0.75 mm, 1.0 mm, 1.50 mm, and 2.0 mm, corresponding to filling ratios from 100% (1.0 mm gap) to 65% (2.0 mm gap). Results indicated that increasing gap size enhanced damping efficiency up to an optimal point, beyond which performance declined.

Nayfeh et al. [174] filled rectangular box and U-channel beams with 3M glass microbubbles (average size: 0.065 mm). The box beam's mass increased by 2.3%, while the U-channel's increased by 3.3%. For the box beam, damping slightly improved in the first two modes but significantly increased in modes three to six. The fifth mode exhibited pronounced TMD-like behavior with a new mode appearing. The U-channel beam also showed TMD-like behavior near the fourth mode, minimal damping in the sixth mode, and moderate damping in higher modes. The authors further investigated the impact of varying granular material layer thickness from 0.0013 mm to 0.0009 mm, observing TMD-like behavior in the fifth mode and strong damping in the first mode. However, the specific placement of the material within the beams was not detailed in the study.

The significance of particle interface friction in the damping capabilities of a particle damper has been experimentally investigated by Rongong et al. [175]. To illustrate this, the authors conducted experiments by mixing light and heavy oil with the particles and then compared their damping efficiency with that of dry particles. The results revealed that dry particles can achieve significantly higher vibration reduction compared to particles mixed with light and heavy oil. Additionally, they employed an electromagnet to generate magnetic flux, enabling the alteration of contact forces within the particle damper. The introduction of a magnetic field resulted in a slight enhancement of damping efficiency. Furthermore, the paper explores various techniques, such as incorporating a cellular honeycomb structure within a disk-shaped particle damper and applying a magnetic field, as means to modify the static pressure distribution and further improve the damping capabilities of the particle damper. Additionally, the study examined the influence of particle material on the damping performance of particle dampers. To this end, steel and lead particles with a diameter of 1.6 mm were used. The results indicated a similar damping trend, leading the authors to conclude that impact behavior is not a primary factor in particle damper design. However, this contradicts findings by Olson [85] and Saeki [86], among others, who emphasized the crucial role of contact forces generated by particle collisions in reducing vibration amplitude.

Marhadi et al. [176] investigated the influence of particle material and size on the vibration damping of a cantilever beam. A particle damper was attached to the beam's free end and tested with four spherical materials: lead, steel, glass, and tungsten carbide spheres, as well as three powder-like materials:

lead dust, steel dust, and sand. For spherical particles, material choice impacted specific damping capacity with lower particle counts but became less significant as the number increased. Powder-like materials exhibited similar damping capacities regardless of material. Steel dust damped significantly less than steel spheres, while lead dust and spheres showed comparable damping. To study particle count effects, glass spheres of 0.5 mm, 1.12 mm, and 3 mm diameter were used. When excitation amplitude was below the critical level, damping was consistent across particle numbers. However, with higher excitation, 50 particles showed significantly lower damping compared to 1035 and 11000 particles, which exhibited similar damping.

Zhao et al. [177] investigated the influence of particle filling on the dynamic characteristics of the NOPD frames through free vibration experiments. The authors have filled the cavities with sand particles ranging in size from 1.6 mm to 3.15 mm. They employed three distinct particle arrangement schemes to explore the effects of particle filling ratio and scheme on the frame's damping properties. Their findings revealed a significant increase in damping across all filling schemes compared to the initial state, highlighting the substantial impact of particle filling ratio on structural damping. Interestingly, they observed a trend where out-of-plane vibration damping increments generally surpassed those for in-plane vibration under identical particle filling schemes and ratios. Finally, their study concluded that the most effective strategy to achieve the most significant particle damping effect involves placing particles within cavities of components exhibiting large vibration displacements.

Booty et al. [178] used a suspended steel plate to experimentally investigate the influence of various particle damper parameters on reducing vibration amplitude. Firstly, they demonstrate the superiority of lead particles over steel counterparts in mitigating vibration amplitude, highlighting the critical role of material selection. Secondly, they investigate the impact of container material, exposing the limitations of non-metallic options like rubber balloons and latex bags compared to the efficacy of metal containers. Furthermore, their comparative analysis of copper particles (4 mm diameter) and copper powder forms unveils that copper powder, despite its smaller size, exhibited slightly better vibration damping. This effect was particularly pronounced below 1 kHz and in the range between 2.5 kHz and 4.5 kHz. These findings highlight the complex interplay between particle size, morphology, and frequency response in vibration damping applications. Finally, the authors explore the influence of particle shape on vibration attenuation, contrasting large, irregular solid particles with machine swarf. Their findings suggest that, for practical applications, prioritizing particles with regular shapes can be highly advantageous. Additionally, the study conducted a comparative analysis of particle dampers with viscoelastic damping layers and acoustic black holes. Results indicate that both damping methods are effective at higher frequencies, while particle dampers exhibit superior performance at lower frequencies. However, the specific frequency ranges for these classifications were not provided by the authors.

2.4.6 Summary and conclusion of experimental approach

The experimental review in the previous section highlights a diverse range of studies evaluating the performance of particle dampers under different operating conditions. A summary of these investigations is provided in Table 2.1 - 2.2. Research has focused on key parameters affecting damper efficiency, including particle material, size, shape, and filling ratio, across a range of applications. Despite extensive research, many studies present conflicting results, making it difficult to draw universally applicable conclusions on the optimal design and performance characteristics of particle dampers.

For instance, Michon et al.[146] found that an 80% filling ratio was the most effective in reducing structural vibration. In contrast, Muthu et al.[156] identified 50% as the optimal level for maximizing damping efficiency in particle dampers. Likewise, Veeramuthuvel et al.[8] determined that a 60% filling ratio provided the best vibration reduction for a PCB. A similar pattern was noted by Ye et al.[162], who observed that 60% was ideal for minimizing vibrations in a scaled container crane model. Conversely, Wang et al. [161] reported that the most effective range lies between 70% and 90%, suggesting that optimal performance is influenced by system-specific parameters and operating conditions. These

varying outcomes may be attributed to differences in cavity size, excitation force, and boundary conditions. Therefore, it is crucial to explore whether optimal filling ratios can be identified.

Similarly, the choice of granular materials for particle dampers has led to mixed findings. Commonly used substances include steel balls, lead, copper, aluminum, and sand, yet direct comparisons of their damping effectiveness are scarce in most studies. A review of experimental approaches shows that many investigations have only considered one to three materials when evaluating their impact on vibration reduction. Notably, Koch et al.[7] and Schmidt[165] examined six and five different granular options, respectively, while Panossian [32] assessed multiple materials, concluding that all contributed to vibration attenuation, though their efficiency varied across frequency ranges. This variability has made it difficult to determine a universally superior material for damper design. Veeramuthuvel et al.[8] proposed that denser materials enhance damping performance, a claim reinforced by Ye et al.[162], who found lead to be considerably more effective than steel. They also reported that powder-based materials outperformed spherical particles in vibration mitigation. Contradicting these observations, Rongong et al.[175] found no significant difference between lead and steel, while Marhadi et al.[176] noted that the damping ability of powdered materials remained unchanged regardless of composition. These conflicting results highlight the ongoing uncertainty surrounding the optimal granular material for particle dampers.

Particle size is another critical parameter influencing the performance of particle dampers, and the review presented above highlights contradictory findings in this regard. The size of granular materials plays a significant role in determining their ability to dissipate vibrational energy, yet there is no clear consensus on the optimal particle size for achieving maximum damping efficiency. For example, Kumar et al. [155] observed that using granular materials with a larger particle size leads to more effective vibration mitigation. However, in direct contrast to these findings, Jin et al. [159] reported that granular materials with larger particle sizes are ineffective in reducing vibration amplitude.

Additionally, while particle dampers have been proven to effectively reduce vibration amplitude in controlled laboratory experiments, particularly when applied to simplified structures such as beams and plates, their implementation in full-scale structures under real-world operating conditions remains limited. Most studies have focused on small-scale experimental setups, where the boundary conditions and external influences can be carefully controlled. In these settings, particle dampers have shown promising results in terms of vibration mitigation. However, the transition from laboratory-scale demonstrations to practical applications in complex engineering structures presents several challenges. One of the key difficulties in scaling up particle dampers lies in their unpredictable behavior under varying environmental conditions, such as temperature fluctuations, humidity, and dynamic loads encountered in real-world scenarios. Additionally, the effectiveness of particle damping in large structures depends on factors such as the distribution of particles, the mode shapes of vibration, and the interaction between the damper and the host structure. These complexities make it challenging to replicate the success observed in laboratory experiments when applied to industrial machinery, aerospace components, automotive structures, or civil engineering applications.

From the above discussion it can be concluded that despite their potential, particle dampers still face significant hurdles in terms of consistent design guidelines and practical application. The inconsistencies observed in experimental results underscore the need for further research to address these gaps and develop clearer recommendations for their optimization and use in engineering applications. These research gaps will be further explored in the next chapter, where a proposed approach to advancing particle damper technology is discussed.

Table 2.1: Summary of experimental methods for particle damper (Part I).

Reference	Year	Material	Particle diameter [mm]	Frequency [Hz]	Filling ratio [%]	Lab specimen
		sand	0.3 - 1.0			
		Glass beads	1.0			
Schmidt [165]	1954	Brick fragments	0 - 10.0	200 - 500	-	-
		Coal slag	0 - 15.0			
		Iron filings	3.0 - 15.0			
Wolf [166]	1962	Sand	-	40 - 1830	-	Beam
Sun et al. [167]	1986	Sand	-	20 - 10000	-	Plate and beam
		Steel balls	0.18, 0.28, 0.58			
Panossian [32]	1992	Zirconium oxide ceramic balls	0.25	3000 - 6000	-	Inlet Tee
		Nickel & Tungsten powder	-			
Cempel et al. [168]	1993	-	-	-	-	Closed cylinder
Papalou et al. [169]	1996	Steel balls	1.6, 3.2, 12.7	-	-	Plate
Papalou et al. [170]	1998	Steel balls	1.6, 6.4, 12.7	-	-	Plate
		Aluminum	0.045 - 0.075		45%,	
		Tungsten carbide cobalt	0.045 - 0.075	-	78, 89	
Holkamp et al. [171]	1998	Titanium	0.053 - 0.15		100, 111	Beam
		Stainless steel	0.045 - 0.106		100, 111	
		Glass beads	0.028 - 0.84		67	
Tomlinson et al. [172]	2001	Steel spheres	0.8	400 - 1000	95	Plate
Yang et al. [173]	2002	Brass balls	1.6	314 - 326	65 - 100	Beam
Nayfeh et al. [174]	2002	Glass microbubbles	0.065	0 - 3000	-	Beam
Xu et al. [152]	2004	Tungsten carbide	0.5	30-12500	-	Note Machine
Simonian [145]	2004					
Rongong et al. [175]	2005	Steel & lead	1.6	-	-	SDOF test rig
Sims et al. [153]	2005	Steel	0.18 - 0.24	-	-	I-shaped beam
		Lead spheres	1.2			
		Steel spheres	1.17	-		
		Glass spheres	0.5, 1.12, 3.0			Beam
Marhadi et al. [176]	2005	Tungsten carbide	0.5	-	-	Beam
		Sand	0.2			
		Steel dust	0.5			
		Lead dust	0.2			
Chan et al. [154]	2006	Tungsten	0.30 - 0.50, 0.50 - 0.71	430 - 4550	50	Bond arm
			0.71 - 1.00, 1.00 - 1.40		75, 90	
					5, 10	
Zhao et al. [177]	2011	Sand	-		15, 20	Frame
			0.16 - 0.315		25, 30, 35	
					40, 45, 50	

Table 2.2: Summary of experimental methods for particle damper (Part II)

Reference	Year	Material	Particle diameter [mm]	Frequency [Hz]	Filling ratio [%]	Lab specimen
Kumar et al. [155]	2011	Copper	2.36, 4.75	-	-	Boring bar
		Lead	3.2, 4.75			
Michon et al. [146]	2013	Soft hollow particles	-	10 - 1500	50, 80, & 100	Beam
Goehler et al. [157]	2014	steel with ceramic powders	-	-	-	Milling slide
		Lead & steel spheres	-		-	
Booty et al. [178]	2014	Copper balls	4.0	0 - 7000	-	Plate
		Copper powder	-		-	
Stauber et al. [163]	2016	Elastomer	-	0 - 600	-	Plate
		Tungsten carbide	0.5, 0.8, & 1.0		-	
Veeramuthuvel et al. [8]	2016	Stainless steel	0.5, 0.8, 1.0 & 1.2	50 - 250	30, 60, & 100	Printed circuit board
		Aluminium alloy	0.1 & 1.2		-	
Xiao et al. [158]	2016	stainless steel	3.0	-	60 & 90	Gear
Koch et al. [150]	2017	Sand A	0.1 - 0.3	0 - 1500	-	Oil pan
		Sand B	0.1 - 0.48		-	
		Sand C	0.7 -1.2		-	
Bustamante et al. [147]	2016	Elastomer	20 - 2000	-	-	beam & plate
Duvigneau et al. [149]	2018	Sand	0.3	350 - 1600		Oil pan
Liming et al. [151]	2018					
Koch et al. [7]	2019	Sand	-	-	-	Oil pan
		Granular rubber	-	-		
		Granular glass	0.2-0.4 & 0.4 – 0.6	-	-	
		Corundum	-	0 - 500	-	
		Polystyrene	-	-	-	
		Glass balls	3.0	-	-	
Sandanshiv et al. [164]	2019	Steel	9.0	0 - 1000	-	Scaled rotor blade
Muthu et al. [156]	2020	Cast iron	1.0	-	20, 50, & 75	Boring bar
Jin et al. [159]	2021	Cast iron	1.0, 2.0, & 3.0	300 - 440	-	Pipeline
Ye et al. [148]	2022	Stainless steel	2.0	-	-	Bracket structure
		Lead particles	2.0	-		
		Stainless steel powder	0.048	10 - 2000	-	
		Tungsten carbide powder	0.5		-	
		, steel	7.0	-	-	
An et al. [160]	2022	3D-printed spheres	7.0	20 - 240		Tensegrity prism
	2022	Glass	5.0, 6.0, & 7.0	10 - 2000		
		steel	1.0	-	-	
Wang et al. [161]	2023	Aluminum	1.0	10 - 2000	20, 40, 60, 80, 90 & 100	Pipe
		Glass	1.0			

3 Research gap analysis and objective setting

The preceding literature review has thoroughly examined different methods for studying particle damper design parameters. While numerical simulations have been widely explored, their ability to accurately predict real-world behavior is somewhat limited. Additionally, a thorough examination of experimental methodologies for particle damper design has been conducted.

Building on these findings, this chapter will identify critical research gaps and define the specific objectives of this thesis. Additionally, it will discuss how these gaps have been addressed throughout the study. This chapter outlines four key research questions that emerged from a thorough review of the existing literature. Each question is examined in detail within four distinct subsections. However, it's important to note that these four overarching questions serve as a foundation for addressing several more specific research gaps that will be explored throughout this thesis.

3.1 Particle damper performance limitations due to granular media

Section 2.4 provides a comprehensive analysis of the various granular materials commonly used in the design of particle dampers, with a particular focus on high-density materials such as steel, lead, and tungsten. These materials are frequently favored in the design process due to their effectiveness in minimizing vibration amplitudes, as supported by the findings presented in Tables 2.1 and 2.2. In addition to these materials, tungsten powder and sand are also highlighted in the literature for their vibration-reducing properties. However, despite their effectiveness in this regard, the inherently high density of these materials poses certain limitations, particularly when designing for lightweight applications where minimizing mass is a critical requirement. Furthermore, while these granular materials exhibit strong performance in attenuating vibrations at higher frequencies, they are notably less effective when addressing vibrations at lower frequencies. This reduction in efficiency could be attributed to the specific selection of granular materials in particle damper design, suggesting that material choice plays a key role in determining the frequency range over which the damper performs optimally. As such, the study of these materials in the context of both high- and low-frequency applications remains an important consideration for advancing particle damper technology.

Elastomeric granular materials have shown significant potential for reducing vibrations at lower frequencies in a range of specific applications. Despite their promising capabilities, a notable limitation in much of the existing research is the absence of comprehensive characterization of the granular material properties being used. Key attributes, such as the particle size distribution and whether the particles are monodisperse or polydisperse, are often left unspecified, leaving gaps in understanding how these materials behave under different conditions. For instance, Stauber et al. [163] implemented an elastomer particle damper designed to operate within the frequency range of 100 to 600 Hz, yet they did not provide any details regarding the characteristics of the particles themselves. Similarly, Bustamante et al. [147] utilized elastomer particles to reduce vibrations in beams and plates within a lower frequency range of 30 to 120 Hz, but once again, critical information about the particle properties was not disclosed. Koch et al. [7] also employed rubber particles in their vibration damping studies, focusing on dampers that were effective starting from 100 Hz, but they, too, did not report the material properties.

In addition to the lack of detailed particle characterization, another challenge in comparing the findings from various studies is the variability in experimental conditions. Differences in the test specimens

used, the boundary conditions applied, the excitation amplitudes, and the specific frequency ranges investigated can all influence the observed effectiveness of elastomeric granular materials in vibration attenuation. These inconsistencies make it difficult to draw definitive conclusions about the performance of these materials across different contexts. Therefore, it is essential to take these factors into account when comparing and interpreting the results from experimental studies to ensure a more accurate and holistic understanding of the role elastomeric granular materials can play in vibration mitigation. Addressing these gaps in characterization and experimental parameters will be crucial for advancing the practical application of elastomer particle dampers across a broader range of industries and conditions.

Additionally, previous research has primarily focused on spherical particles to explore the effect of particle size on vibration attenuation. However, in practical applications, granular materials often have irregular shapes. Studies investigating the relationship between particle size and vibration reduction have yielded conflicting findings. For example, An et al. [160] reported that smaller glass spheres were more effective at damping vibrations, while Koch et al. [7] found that larger sand particles performed better. This inconsistency could be attributed to differences in the particle types used. An et al. [160] employed monodisperse particles, whereas Koch et al. [7] used polydisperse materials. Furthermore, some studies suggest that higher-density granular materials can be effective across both high and low-frequency ranges, depending on the specific application. Although particle dampers are generally considered broadband damping devices, as shown in Tables 2.1 and 2.2, the same material can exhibit varying effective frequency ranges.

The existing literature on particle damper design is constrained by varying and inconsistent findings concerning the most effective granular materials and their vibration mitigation properties. This lack of consensus leads to uncertainty about how factors such as the type of granular material, particle size, and particle distribution influence damper performance, complicating the design of optimized dampers, particularly for lightweight applications. Additionally, there is a significant gap in comprehensive studies that systematically compare the vibration attenuation effectiveness of different granular materials.

This thesis addresses the identified research gaps through a comprehensive experimental investigation of granular materials under rigorously controlled conditions, detailed in Chapter 5. This standardized experimental methodology facilitates direct comparison of the vibration damping characteristics across diverse materials. Chapter 5 introduces two primary particle damper typologies: recycled rubber particle dampers (RRPDs) and hard material particle dampers (HMPDs), evaluated for their respective vibration reduction efficacy. Recognizing the performance limitations inherent in single-material dampers, this research further investigates hybrid particle dampers (HPDs) as a novel strategy for enhanced vibration attenuation. The strategic combination of distinct granular materials within HPDs presents a promising avenue for improving overall particle damper effectiveness across a broader spectrum of applications.

The concept of hybrid particle damper design has been explored in various contexts. For example, Akbar et al. [179] developed an HPD by integrating a particle impact damper with a Coulomb friction damper. Meyer [97] explored HPD configurations by varying the container material while maintaining a consistent particle material. Chockalingam et al. [180] designed an HPD for chatter suppression in a boring bar, employing a mixture of copper and zinc particles. Their findings demonstrated superior chatter reduction performance for the mixed-particle damper compared to single-material (copper or zinc) configurations.

Within the scope of this thesis, an HPD is defined as a system incorporating two distinct materials, or the same material with varying particle size distributions (PSDs), combined in defined ratios. While the use of mixed-material HPDs has been previously investigated, notably by Chockalingam et al. [180], this area remains relatively underexplored. This scarcity of research underscores the need for a more comprehensive investigation into the performance of HPDs, utilizing diverse combinations of both conventional and unconventional granular materials, which forms one of the key focuses of this work.

3.2 Granular motion enhancement in dampers

Chapter 1 explains that the vibration amplitude of the main structure has a direct effect on the kinetic energy transferred to the granular material within a particle damper. This transfer of energy is critical for activating the particle-to-particle and particle-to-wall collisions, which are the mechanisms that enable the particle damper to reduce vibrations effectively. However, there are scenarios where the main structure's vibration may be insufficient to induce adequate kinetic energy in the granular material, hindering the damping process of the particle damper. To address this limitation, Rongong et al. [175] proposed an innovative solution to enhance the performance of particle dampers. Their approach involved integrating a cellular honeycomb structure with the damper and applying a magnetic field to a disk-shaped particle. This strategy altered the static pressure distribution within the damper, resulting in improved control of vibrations. While this method offers enhanced performance, it is limited by the requirement for magnetic materials and falls into the category of semi-active vibration control. Unlike passive dampers, this semi-active approach requires external power and control systems, which adds complexity but increases the flexibility of the damping process.

It has been widely observed that in most cases, particle dampers are attached externally to vibrating structures. This external attachment approach has become the common configuration for damping vibrations [8, 164, 169]. However, a few researchers have explored the possibility of placing particle dampers internally by drilling holes into the structure and filling them with granular materials [32, 152, 158]. While this internal method of drilling holes and partially filling them with granular substances has proven highly effective in reducing vibrations, it also comes with challenges. The method requires a comprehensive structural analysis to ensure the integrity and strength of the altered structure are not compromised by the modifications. Interestingly, even when the primary structure is naturally hollow, the typical approach has still been to mount particle dampers externally. There has been relatively little exploration of how to utilize the existing hollow space inside such structures for designing particle dampers. For instance, Jin et al. [159] conducted a study focused on the use of external particle dampers to reduce vibrations in pipelines, and their research showed considerable success in lowering vibration amplitudes. Despite these positive results, the external attachment of particle dampers can introduce additional costs and complexities. These include the design of the cavity to house the granular materials, the containment system needed to keep those materials in place, and the need for a reliable connection between the cavity and the main structure. Thus, while external dampers can be effective, they also come with certain drawbacks that merit further investigation into more efficient design alternatives.

Although considerable research has been devoted to the design and performance of particle dampers in small-scale structures, there remains a significant gap in studying their effectiveness in reducing vibrations in large-scale structures. The work of Sandanshiv et al. [164] stands out as one of the few exceptions, where they conducted a laboratory-scale investigation focusing on wind turbine blades, each with a length of 1525 mm. Their findings suggest that particle dampers hold potential for effectively mitigating vibrations in larger-scale applications, including those involving rotational motion. Nevertheless, more comprehensive research is needed to fully explore and optimize the performance of particle dampers in such large-scale settings, ensuring their broader applicability and efficiency.

To overcome these limitations, there is a pressing need for a passive design approach that can effectively induce kinetic energy into the granular material, thereby enhancing the performance of particle dampers without the need for external power or control. Additionally, there is a need for a design strategy that allows the use of particle dampers in large hollow structures while minimizing the added mass of the granular material. To address these challenges, this thesis proposes three passive design variants: the Thin-Wall Cavity (TWC), the Thin-Wall Cavity with Additional Sheets (TWC-AS), and the Ring Cavity (RC) (see chapter 6). These designs aim to increase the relative motion of the granular material, thereby improving the efficiency of the particle damper. Notably, the TWC design variant is particularly suited for integrating particle dampers into large hollow structures, as it can significantly reduce the

additional mass of the structure.

3.3 Durability of particle dampers

Granular materials inside a particle damper are subjected to dynamic forces throughout their entire operational life. These persistent stresses can gradually change the characteristics of the granular media, potentially affecting the damper's wear resistance, durability, and overall performance. Because the effectiveness of particle dampers is closely tied to the condition of the materials they contain, maintaining their long-term performance is becoming more critical. However, a significant challenge remains in understanding how the vibration attenuation of these materials evolves over time under varying dynamic loads, which creates uncertainty in ensuring the consistent reliability of these devices as they are increasingly studied across various fields of application.

To address this important research gap, an in-depth experimental study has been conducted as part of this thesis, detailed extensively in Chapter 7. This study was performed in collaboration with an industrial partner, allowing for a robust investigation that aligns with real-world engineering demands. The primary focus of this research is to evaluate the vibration reduction capabilities of a particle damper both prior to and after it has been subjected to prolonged exposure to millions of high-amplitude dynamic loads and repeated temperature cycling over a period of several months. By simulating these extreme conditions, the study aims to provide critical insights into the long-term performance, wear resistance, and overall durability of particle dampers. The findings of this investigation are intended to offer valuable data that will support the reliable and effective application of particle dampers in practical industrial settings, enhancing their performance under the demanding conditions typically found in real-world operations.

3.4 Lab to industry transition

The efficiency of particle dampers is well-documented in small-scale experimental setups. These studies typically involve simplified models that do not fully capture the complexities of real-world applications. Laboratory experiments often use controlled conditions to isolate specific variables, which, while useful for fundamental understanding, do not always translate directly to industrial-scale applications. One of the key reasons why particle dampers have not been widely tested at industrial scales is due to the highly nonlinear nature of their behavior. The challenges associated with accurately modeling and predicting the performance of particle dampers stem from their sensitivity to a wide range of design parameters. Variables such as particle size, distribution, fill ratio, and the geometry of the damper all interact in complex ways. This interaction can lead to unpredictable and nonlinear behavior, making it difficult to model their efficiency with precision.

Despite these challenges, there are examples where particle dampers have been successfully applied in practical applications. For instance, Xu et al. [152] demonstrated the effectiveness of particle damping in reducing the dynamic response of a banknote machine. Similarly, Liming et al. [151] showed how particle dampers could be used to mitigate vibrations in cab driver seats of mining trucks. Koch et al. [150] also applied particle damping technique to reduce vibration amplitudes in a combustion engine test bench. While these successes highlight the potential of particle dampers, it is notable that they have not yet been widely used in more complex structures, such as wind turbine generators and blades, on an industrial scale. Another emerging area of interest is the application of particle dampers in electric vehicles. While electric vehicles are generally quieter than those with internal combustion engines, they present new challenges in terms of vibration and noise emissions. This raises the question of whether particle dampers could be similarly effective in reducing vibration amplitudes in electric drives, offering a potential solution to these new challenges.

In this thesis, various design strategies have been developed for both wind turbine generators (as discussed in Chapter 9) and wind turbine blades (as discussed in Chapter 10) at a laboratory scale. The concepts introduced in these chapters each have their own distinct advantages and limitations. After conducting a thorough analysis of all these design strategies, in conjunction with the parameter studies detailed throughout this thesis (refer to Chapters 5 - 7), a particle damper was also tested on a wind turbine generator and blade at an industrial scale (refer to Chapter 11). Additionally, the design parameters explored in this thesis will be applied to an electric drive test bench under real boundary conditions and loads, with the aim of reducing vibration amplitude (see Chapter 12).

4 Signal processing for vibration measurement

Signal processing is an extensive and multidisciplinary field that spans across a wide array of applications in different industries, each adopting specialized methodologies that are tailored to meet their unique requirements. Despite the diverse approaches utilized in these fields, there exist certain fundamental principles of signal processing that remain universally applicable and serve as the foundational concepts that underpin numerous applications. These core principles provide the essential framework for understanding and analyzing signals, whether in the context of communication, audio processing, or vibration analysis, among many others.

This chapter is dedicated to exploring these core principles, with a particular emphasis on their relevance to experimental vibration analysis, a key area of focus in this thesis. While a thorough examination of the theoretical foundations of signal processing is not within the scope of this work, the discussion will focus on the key concepts that are most pertinent to the objectives of this thesis. These concepts are not only vital for a deeper understanding of the signal processing techniques employed in the experimental studies but also serve as the basis for the implementation and interpretation of the results presented throughout this thesis.

4.1 Fourier analysis

Fourier analysis provides a framework for decomposing arbitrary functions into a sum of sinusoidal components with distinct frequencies. This decomposition can be achieved through two primary methods, namely: Fourier series and Fourier transform.

In general, Fourier series and Fourier transform are typically applied to continuous functions. However, since digital computers cannot process signals in continuous time, it becomes necessary to approximate the Fourier transform using discrete data points. This is where the discrete Fourier transform (DFT) comes into play, offering a practical method for the numerical approximation and computation of analog signals. Despite its utility, the DFT is computationally intensive for large datasets, as it requires $\mathcal{O}(n^2)$ operations due to the multiplication by a dense $n \times n$ matrix (see Section 4.1.3). To overcome this challenge, James W. Cooley and John W. Tukey introduced the fast Fourier transform (FFT), an efficient algorithm for computing the DFT [181] (see Section 4.1.4). This section provides a concise overview of Fourier series, Fourier transform, DFT, and FFT, emphasizing their crucial roles in experimental vibration analysis.

4.1.1 Fourier series

Consider a function $f : \mathbb{R} \to \mathbb{R}$ that exhibits periodicity over the interval $[-L, L]$, where L represents the period. This periodicity implies that for any real number x, the function satisfies the property $f(x) = f(x + L)$. Fourier's theorem asserts that such a function $f(x)$ can be expressed as the series, known as the Fourier series [181–183]

$$f(x) \approx \frac{a_0}{2} + \sum_{m=1}^{\infty} \left(a_m \cos\left(\frac{m\pi x}{L}\right) + b_m \sin\left(\frac{m\pi x}{L}\right)\right). \tag{4.1}$$

The coefficients a_0, a_m and b_m can be determined by utilizing the orthogonality property between $\sin$ and $\cos$ functions. Additionally, the validity of term-by-term integration of Eq. (4.1) is considered and both sides are multiplied by $\cos\left(\frac{n\pi x}{L}\right)$. The resulting expression is then integrated term-by-term over the interval $[-L, L]$, leading to

$$\int_{-L}^{L} f(x) \cos\left(\frac{n\pi x}{L}\right) dx = \frac{a_0}{2} \int_{-L}^{L} \cos\left(\frac{n\pi x}{L}\right) + \sum_{m=1}^{\infty} a_m \int_{-L}^{L} \cos\left(\frac{m\pi x}{L}\right) \cos\left(\frac{n\pi x}{L}\right) dx + \sum_{m=1}^{\infty} b_m \int_{-L}^{L} \sin\left(\frac{m\pi x}{L}\right) \cos\left(\frac{n\pi x}{L}\right) dx. \tag{4.2}$$

For a fixed integer $n \geq 1$, the orthogonality relations ensure that within the first summation on the right-hand side of Eq. (4.2), only the term corresponding to $m = n$ remains non-zero. As a result, this simplifies the expression to yield the coefficient a_n

$$a_n = \frac{1}{L} \int_{-L}^{L} f(x) \cos\left(\frac{n\pi x}{L}\right) dx \qquad n = 1, 2, 3, \ldots \quad . \tag{4.3}$$

An analogous expression for b_n can be derived by multiplying Eq. (4.2) by $\sin\left(\frac{n\pi x}{L}\right)$ and integrating the resulting expression term-by-term over the interval $[-L, L]$. This yields the coefficient b_n

$$b_n = \frac{1}{L} \int_{-L}^{L} f(x) \sin\left(\frac{n\pi x}{L}\right) dx \qquad n = 1, 2, 3, \ldots \quad . \tag{4.4}$$

The orthogonality relations additionally imply that

$$\int_{-L}^{L} \sin\left(\frac{n\pi x}{L}\right) dx = \int_{-L}^{L} \cos\left(\frac{m\pi x}{L}\right) dx = 0. \tag{4.5}$$

Drawing upon the relation given in Eq. (4.5), the following expression for a_0 can be obtained

$$a_0 = \frac{1}{L} \int_{-L}^{L} f(x)\, dx. \tag{4.6}$$

Algebraic manipulations involving trigonometric sums, as shown in Eq. (4.1), are greatly simplified by adopting complex exponential notation to represent sine and cosine functions. Accordingly, it is natural to utilize Euler's identity to reformulate a Fourier series in its complex form, incorporating complex coefficients. Euler's identity for sine and cosine is expressed as follows for $z \in \mathbb{C}$

$$\cos(z) = \frac{e^{iz} + e^{-iz}}{2} \qquad \text{and} \qquad \sin(z) = \frac{e^{iz} - e^{-iz}}{2i}. \tag{4.7}$$

Let's substitute $z = \frac{m\pi x}{L}$ into Eq. (4.7), which leads to

$$\cos\left(\frac{m\pi x}{L}\right) = \frac{e^{\frac{im\pi x}{L}} + e^{\frac{-im\pi x}{L}}}{2} \qquad \text{and} \qquad \sin\left(\frac{m\pi x}{L}\right) = \frac{e^{\frac{im\pi x}{L}} - e^{\frac{-im\pi x}{L}}}{2i}. \tag{4.8}$$

Substituting Eq. (4.8) in Eq. (4.1) yields

$$
\begin{aligned}
f(x) &= \frac{a_0}{2} + \sum_{m=1}^{\infty} \left[\frac{a_0}{2} \left(e^{\frac{im\pi x}{L}} + e^{\frac{-im\pi x}{L}} \right) + \frac{b_m}{2i} \left(e^{\frac{im\pi x}{L}} - e^{\frac{-im\pi x}{L}} \right) \right] \\
&= \frac{a_0}{2} + \sum_{m=1}^{\infty} \frac{1}{2} \left(a_m + \frac{b_m}{i} \right) e^{\frac{im\pi x}{L}} + \sum_{m=1}^{\infty} \frac{1}{2} \left(a_m - \frac{b_m}{i} \right) e^{\frac{-im\pi x}{L}} \\
&= \frac{a_0}{2} + \sum_{m=1}^{\infty} \left(\frac{a_m - ib_m}{2} \right) e^{\frac{im\pi x}{L}} + \sum_{m=1}^{\infty} \left(\frac{a_m + ib_m}{2} \right) e^{\frac{-im\pi x}{L}}.
\end{aligned} \tag{4.9}
$$

To simplify Eq. (4.9), a new variable is introduced. This variable is defined to represent the combined expression within parentheses. Furthermore, the constant term $(\frac{a_0}{2})$ is denoted as c_0. This leads to

$$
c_0 = \frac{a_0}{2}, \quad c_m = \left(\frac{a_m - ib_m}{2} \right), \quad c_m^* = \left(\frac{a_m + ib_m}{2} \right). \tag{4.10}
$$

Then Eq. (4.9) can be formulated as

$$
f(x) = c_0 + \sum_{m=1}^{\infty} c_m e^{\frac{im\pi x}{L}} + \sum_{m=1}^{\infty} c_m^* e^{\frac{-im\pi x}{L}}. \tag{4.11}
$$

Note that the negative frequency terms (c_{-m}) are introduced so that

$$
\sum_{m=1}^{\infty} c_m^* e^{\frac{-im\pi x}{L}} = \sum_{m=1}^{\infty} c_{-m} e^{\frac{-im\pi x}{L}}. \tag{4.12}
$$

Therefore, for a function $f : \mathbb{R} \to \mathbb{R}$, periodic over the interval $[-L, L]$ (where L is the length of period), the Fourier series in complex exponential form can be expressed as

$$
f(x) = \sum_{m=-\infty}^{\infty} c_m e^{\frac{im\pi x}{L}}, \tag{4.13}
$$

where c_m is the Fourier coefficient and can be computed by plugging Eq. (4.10) in Eq. (4.3) and Eq. (4.4)

$$
c_m = \frac{1}{2} \left[\frac{1}{L} \int_{-L}^{L} f(x) \cos \left(\frac{m\pi x}{L} \right) \, dx - \frac{i}{L} \int_{-L}^{L} f(x) \sin \left(\frac{m\pi x}{L} \right) \, dx \right]. \tag{4.14}
$$

Using Eq. (4.7) in Eq. (4.14) gives

$$
c_m = \frac{1}{2} \left[\frac{1}{L} \int_{-L}^{L} f(x) \left(\frac{e^{\frac{im\pi x}{L}} + e^{\frac{-im\pi x}{L}}}{2} \right) \, dx - \frac{i}{L} \int_{-L}^{L} f(x) \left(\frac{e^{\frac{im\pi x}{L}} - e^{\frac{-im\pi x}{L}}}{2} \right) \, dx \right]. \tag{4.15}
$$

Thus, the complex valued Fourier coefficients are given by

$$
c_m = \frac{1}{2L} \int_{-L}^{L} f(x) e^{\frac{-im\pi x}{L}} \, dx. \tag{4.16}
$$

4.1.2 Fourier transforms

The Fourier series discussed so far applies to periodic functions. However, it can be extended to aperiodic functions by initially considering the function over a finite interval, $[-L, L]$, and then allowing

$L \to \infty$. This approach is intuitive, as an aperiodic function can be viewed as one that repeats only at infinity, effectively meaning it does not repeat at all [184].

In vibration analysis, signals are typically measured in the time domain. Therefore, if the Fourier series has a period of $2T$, then Eq. (4.13) and Eq. (4.16) can be expressed as

$$f(t) = \sum_{m=-\infty}^{\infty} c_m e^{im\frac{\pi}{T}t}. \tag{4.17}$$

$$c_m = \frac{1}{2T}\int_{-T}^{T} f(x)e^{-im\frac{\pi}{T}t}\,dt. \tag{4.18}$$

Eq. (4.18) can be expressed as

$$2T\,c_m = \int_{-T}^{T} f(x)e^{-im\frac{\pi}{T}t}\,dt. \tag{4.19}$$

As $T \to \infty$, the fundamental frequency $\omega_0 = \frac{2\pi}{T}$ approaches zero, causing the discrete quantity $m\omega_0$ to become continuous and capable of assuming any real value, given that m spans the range $\pm\infty$. To accommodate this transition, a new variable $\omega = m\omega_0$ is introduced and $F(\omega) = 2T\,c_m$ is defined. Substituting these expressions into Eq. (4.19)results in the analysis equation for the Fourier Transform, also known as the Forward Fourier Transform.

$$F(\omega) = \mathcal{F}(f(t)) := \int_{-\infty}^{\infty} f(t)e^{-i\omega t}\,dt. \tag{4.20}$$

Similarly, the Inverse Fourier Transform can be derived. As $T \to \infty$, the relation $\frac{1}{T} = \frac{\omega_0}{2\pi}$ holds. Given that ω_0 becomes negligibly small for large T, it can be replaced by the differential quantity $d\omega$. As in the previous derivation, $\omega = m\omega_0$ and $F(\omega) = 2T\,c_m$ is set. By substituting these expressions and replacing the summation with an integral, the Inverse Fourier Transform is obtained.

$$\mathcal{F}^{-1}(F(\omega)) := \frac{1}{2\pi}\int_{-\infty}^{\infty} F(\omega)e^{i\omega t}\,d\omega. \tag{4.21}$$

4.1.3 Discrete Fourier transform (DFT)

The DFT is a discrete analogue of the continuous Fourier transform, tailored for signals represented by a finite sequence of N samples. Consider a continuous-time signal $f(t)$. When sampled at regular intervals of Ts seconds, a discrete-time sequence $f[n]$ is obtained, where $n = 0, 1, \cdots, N-1$. The Fourier Transform of $f(t)$ is given by Eq. (4.20). However, since we only have the discrete samples $f[n]$, the integral in Eq. (4.20) is approximated by a summation, leading to the DFT [185]

$$\begin{aligned} F(\omega) &= \int_{0}^{(N-1)Ts} f(t)e^{-i\omega t}\,dt \\ &= f[0]e^{-i0} + f[1]e^{-i\omega Ts} + \cdots f[k]e^{-i\omega kTs} + \cdots f(N-1)e^{-i\omega(N-1)Ts} \\ &= \sum_{k=0}^{N-1} f[k]e^{-i\omega kTs}. \end{aligned} \tag{4.22}$$

$$F[n] = \sum_{k=0}^{N-1} f[k]e^{-i\frac{2\pi}{N}nk} = \sum_{k=0}^{N-1} f[k]w^{nk} \qquad n \in 0, 1, \cdots N-1, \tag{4.23}$$

where $w = e^{-i\frac{2\pi}{N}}$. Eq. (4.22) represent the DFT of the sequence $f[k]$ denoted by $F[n]$ and expanding Eq. (4.23) yields the following expression

$$\begin{aligned}
F[0] &= f[0]1 + f[1]1 + f[2]1 + f[3]1 + \cdots + f[N-1]1 \\
F[1] &= f[0]1 + f[1]w + f[2]w^2 + f[3]w^3 + \cdots + f[N-1]w^{(N-1)} \\
F[2] &= f[0]1 + f[1]w^2 + f[2]w^4 + f[3]w^6 + \cdots + f[N-1]w^{(N-2)} \\
F[3] &= f[0]1 + f[1]w^3 + f[2]w^6 + f[3]w^9 + \cdots + f[N-1]w^{(N-3)} \\
&\vdots \\
F[N-1] &= f[0]1 + f[1]w^{(N-1)} + f[2]w^{(N-2)} + f[3]w^{(N-3)} + \cdots + f[N-1]w.
\end{aligned} \tag{4.24}$$

The system of equations can be more concisely represented in matrix form as follows

$$\begin{bmatrix} F[0] \\ F[1] \\ F[2] \\ \vdots \\ F[N-1] \end{bmatrix} = \begin{bmatrix} 1 & 1 & 1 & 1 & \cdots & 1 \\ 1 & w & w^2 & w^3 & \cdots & w^{[N-1]} \\ 1 & w^2 & w^4 & w^6 & \cdots & w^{[N-2]} \\ 1 & w^3 & w^6 & w^9 & \cdots & w^{[N-3]} \\ \vdots & & & & & \\ 1 & w^{[N-1]} & w^{[N-2]} & w^{[N-3]} & \cdots & w \end{bmatrix} \begin{bmatrix} f[0] \\ f[1] \\ f[2] \\ \vdots \\ f[N-1] \end{bmatrix}. \tag{4.25}$$

Each row of the $N \times N$ matrix w requires N complex multiplications and $N-1$ complex additions to compute its dot product with the $N \times 1$ column vector $f[k]$. Consequently, the entire matrix multiplication involves $\mathcal{O}(N^2)$ complex multiplications and $N(N-1)$ complex additions. For large values of N, this computational complexity renders DFT operations computationally intensive, even on high-performance computing systems.

4.1.4 Fast Fourier transform (FFT)

The development of FFT algorithms is primarily motivated by the goal of reducing computational time required for the DFT. FFTs are designed to efficiently perform the DFT, especially for highly composite transform lengths N. Numerous FFT variations exist, including the Cooley-Tukey FFT algorithm, prime factor FFT algorithm, Bruun's FFT algorithm, Bluestein's FFT algorithm, and Goertzel's FFT algorithm, among others. While a comprehensive discussion of each is beyond the scope of this thesis, this section will demonstrate the twiddle factor algorithm, introduced by Gentleman and Sande in 1966, to illustrate the computational advantage of FFT over the DFT. This concept is also used in other FFT algorithms, such as the Cooley-Tukey algorithm [181].

The periodicity of the twiddle factor enables the combination of terms, effectively reducing the number of computationally intensive multiplication steps needed for a specified number of samples. As previously shown, the standard DFT formulation with N values necessitates $\mathcal{O}(N^2)$ multiplications. In contrast, the FFT requires only $\mathcal{O}(Nlog_2(N))$ multiplications [181].

To illustrate the computational efficiency of the twiddle factor algorithm, consider the case where $N = 4$. Each $F[n]$ values can then be computed using Eq. (4.23)

$$F[n] = \sum_{k=0}^{3} f[k]w^{nk}. \tag{4.26}$$

When $N = 4$, the standard DFT requires a total of 16 multiplications. However, by expressing the transformation as a summation in Eq. (4.26), the computation can be efficiently divided into separate odd and even components

$$F[n] = \sum_{\gamma=0}^{1} f[2\gamma] w^{2\gamma k} + \sum_{\gamma=0}^{1} f[2\gamma+1] w^{(2\gamma+1)k}. \tag{4.27}$$

The second twiddle factor can be decomposed into two distinct components

$$w^{(2\gamma+1)k} = w^{2\gamma k} w^{k}. \tag{4.28}$$

expanding the summation notation for $F[0]$ through $F[3]$ and simplifying the resulting expression, we get

$$\begin{aligned} F[0] &= f[0]w^0 + f[2]w^0 + f[1]w^0 w^0 + f[3]w^0 w^0 \\ F[1] &= f[0]w^0 + f[2]w^2 + f[1]w^1 w^0 + f[3]w^1 w^2 \\ F[2] &= f[0]w^0 + f[2]w^4 + f[1]w^2 w^0 + f[3]w^2 w^4 \\ F[3] &= f[0]w^0 + f[1]w^6 + f[1]w^3 w^0 + f[3]w^3 w^6. \end{aligned} \tag{4.29}$$

An analysis of Eq. (4.29) demonstrates that the proposed algorithm necessitates 12 multiplication operations, representing a decrease from the 16 required by the DFT. While this figure remains higher than the ideal $\mathcal{O}(Nlog_2(N))$ multiplication, careful consideration of the repeated multiplications inherent to the equation reduces the actual operation count to 8 for the 4-point problem. As a result, the computational burden of the FFT is roughly halved compared to the DFT [185].

4.2 Signal averaging

Signal averaging is an essential technique in signal processing, designed to enhance the signal-to-noise ratio (SNR) by diminishing unwanted noise within a signal. This technique is based on the principle that, while the true signal remains constant, random noise components tend to cancel each other out when averaged over time or across multiple measurements. As a result, the averaging process enhances the signal, increasing its prominence and facilitating detection.

Signal averaging relies on four key assumptions regarding the signal and noise characteristics. Firstly, the signal and noise components must be uncorrelated. Secondly, accurate temporal alignment of each signal waveform is essential. Thirdly, the noise must be truly random, characterized by a zero mean and a statistical distribution. Finally, a consistent signal component must be present in repeated measurements to enable effective averaging [186, 187].

A widely employed approach to noise attenuation is the application of conventional filtering to restrict the bandwidth of monitoring instruments. If the instrument's bandwidth surpasses that of the desired signals, the excess bandwidth solely contributes to increased noise and can be discarded without incurring any signal loss. Nevertheless, filtering becomes inadequate when signal and noise components coexist within the same frequency band [186].

An input waveform $f(t)$ is considered, consisting of a signal component $S(t)$ and a noise component $N(t)$. Let the n-th repetition of $S(t)$ begin at time t_n, then the input signal can be then expressed as [186, 187]

$$f(t) = S(t) + N(t). \tag{4.30}$$

If a sample of $f(t)$ is taken at intervals of T seconds, then the value of any sample point at the i-th time instance is given by the sum of the signal and noise components

$$f(t_n + iT) = S(t_n + iT) + N(t_n + iT) = S(iT) + N(t_n + iT). \tag{4.31}$$

For a given i and n, $N(t_n + iT)$ is treated as a random variable. It is resonable to assu me that all $N(t_n + iT)$ values have a mean of zero and an identical root mean square (RMS) value, denoted as σ. For different values of n, the noise samples are generally statistically independent. Now, consider the i-th sample point, where the SNR for any specific repetition is given by

$$SNR = \frac{S(iT)}{\sigma}. \tag{4.32}$$

After m repetitions, the value recorded at the j-th memory location is

$$\sum_{n=1}^{m} f(t_n + iT) = \sum_{n=1}^{m} S(iT) + \sum_{n=1}^{m} N(t_n + iT). \tag{4.33}$$

For the i-th sample point, the signal component remains consistent across each repetition, provided that the signal is table and the sweeps are perfectly aligned. In this case the signal component can be written as

$$\sum_{n=1}^{m} S(iT) = mS(iT). \tag{4.34}$$

Following multiple repetitions, the noise component of the input signal exhibits an RMS value of σ. Then, the noise component can be written as

$$\sum_{n=1}^{m} N(t_n + iT) = \sqrt{m\sigma^2} = \sqrt{m}\sigma. \tag{4.35}$$

The SNR after m repetitions is obtained by taking the ratio of Eq. (4.34) and Eq. (4.35) and applying Eq. (4.32)

$$(SNR)_m = \frac{mS(iT)}{\sqrt{m}\sigma} = \sqrt{m}\, SNR. \tag{4.36}$$

Thus, from the above equation, it is evident that signal averaging enhances the SNR by a factor of $\sqrt{m}$.

As recommended by Trimble [186], a two-pronged approach involving conventional bandpass filtering and signal averaging is adopted to effectively reduce noise in the signal. Bandpass filtering serves to improve the input SNR, thereby decreasing the required averaging time. Therefore, both bandpass filtering and signal averaging are implemented throughout this thesis to suppress noise and improve signal clarity.

4.3 Sampling theorem

The precise measurement of vibrations relies on the process of converting analog, continuous signals into digital, discrete forms. This conversion is fundamentally governed by the principles outlined in the sampling theorem, a critical theoretical framework in signal processing. The theorem establishes the conditions under which a continuous signal can be accurately reconstructed from its discrete samples, ensuring fidelity in the representation of the original signal during digital processing. While Nyquist

initially proposed this theorem in 1928, it was Shannon's 1949 work that popularized and clarified its significance, making it a cornerstone of signal processing and vibration analysis [188, 189].

The Nyquist theorem provides a framework for sampling a signal or waveform without any loss of information. Consider a bandlimited signal $f(t)$, where "bandlimited" implies that the Fourier transform of $f(t)$ is restricted to frequencies below a maximum value f_{max} [190]

$$|F(\omega)| = 0 \qquad \forall\, |f| > f_{\mathsf{max}} \tag{4.37}$$

The Nyquist-Shannon sampling theorem stipulates that a continuous-time signal can be perfectly reconstructed from its discrete samples if the sampling rate, f_{s}, exceeds twice the maximum frequency component, f_{max}, present in the signal

$$f_{\mathsf{s}} > 2 \cdot f_{\mathsf{max}}. \tag{4.38}$$

If the condition in Eq. (4.38) is met, no information is lost during the sampling process, and the original signal can, in theory, be perfectly reconstructed from the sampled data. Alternatively, a Nyquist frequency, f_{N}, can be defined based on a given sampling frequency, f_{s} [191]

$$f_{\mathsf{N}} = \frac{f_{\mathsf{s}}}{2}. \tag{4.39}$$

Any signal components with frequencies exceeding the Nyquist frequency will be aliased during the sampling process, leading to irreversible information loss. Such signals are termed undersampled. Conversely, if a signal is strictly bandlimited to frequencies below the Nyquist frequency, it can be perfectly reconstructed from its samples, and the sampling rate is considered oversampled. When a signal is bandlimited to the Nyquist frequency, it is said to be critically sampled.

4.4 Window function

The DFT relies on two fundamental assumptions, namely: periodicity of the sampled data and band-limited continuity. While the former is inherent to the DFT, the latter is often violated in practical applications. This violation, characterized by discontinuities in the time-domain signal, leads to the introduction of spurious harmonic frequencies in the frequency domain, a phenomenon known as spectral leakage. To mitigate the adverse effects of spectral leakage, window functions can be employed. These functions gradually taper the signal's amplitude towards zero at both ends, thereby reducing the abrupt discontinuities and minimizing the generation of spurious frequencies [192].

When a signal $f(t)$ is subjected to windowing, it is multiplied by a window function $W(t)$, yielding a windowed signal $f_W(t)$ in the time domain, expressed as [193]

$$f_W(t) = W(t) f(t). \tag{4.40}$$

In the frequency domain, the described signal windowing corresponds to a convolution between the Fourier transform of the window function and the Fourier transform of the signal [193]

$$F_W(\omega) = W(\omega) \otimes F(\omega). \tag{4.41}$$

However, this convolution results in two primary effects, defined by the window function's spectrum: the main lobe and the side lobes. The main lobe, the dominant part of the spectrum, has a width inversely related to the time-domain window width. A narrower main lobe enhances frequency resolution, while a wider window leads to this narrowing. Side lobes, smaller peaks away from the main lobe, cause spectral

leakage by introducing spurious frequency components that distort the signal. Window functions aim to minimize side lobe amplitude to reduce leakage and improve frequency accuracy. However, reducing side lobes often widens the main lobe, lowering frequency resolution. Thus, selecting an appropriate window function requires balancing frequency resolution with spectral leakage minimization.

Various window functions can be applied depending on the characteristics of the signal being analyzed. In this study, structural dynamics measurements were primarily conducted using the Polytec Laser Scanning Vibrometer (LSV), which offers seven window function options: rectangular, Hanning (Hann), Hamming, Blackman-Harris, Bartlett, flat top, and exponential. Selecting an appropriate window function is a non-trivial task, as each has distinct characteristics and is suited to specific applications. Generally, the Hanning window is suitable for approximately 95% of cases due to its favorable balance between frequency resolution and reduced spectral leakage. When the signal's nature is unknown, the Hanning window is a recommended starting point [194]. In this thesis, the Hanning window has been predominantly utilized in the experimental studies. However, several other window functions were also tested. The findings consistently indicate that the Hanning window is well-suited for the majority of the experiments conducted.

The Hanning window, distinguished by its cosine-shaped profile, is mathematically defined as

$$W(n) = 0.5 - 0.5\,\cos\left(\frac{2\pi n}{N-1}\right) \qquad 0 \leq n \leq N-1. \tag{4.42}$$

The above equation defines a window function where n is the sample index and N is the total number of samples. This function generates a bell-shaped curve that tapers smoothly to zero at both ends. The cosine component ensures a gradual transition between samples, mitigating spectral leakage. The scaling factor 0.5 balances the energy distribution within the window.

The Hanning window provides a balance between frequency resolution and side lobe suppression, making it a versatile tool for signal processing. It is computationally efficient and effective in reducing spectral leakage, improving the accuracy of frequency analysis. However, its performance may be limited in applications requiring exceptional frequency resolution or stringent noise reduction, where other window functions like the Kaiser or Gaussian windows might be more suitable.

In the characterization of window functions, several parameters are commonly utilized, including sidelobe attenuation (SLA), mainlobe width (MLW) expressed as a multiple of the line spacing, and the level error (ΔL) measured at half the line width [195]. These parameters are widely accepted in the scientific community, although they are not universally binding, meaning that alternative definitions and approaches may also be found in the literature. An ideal window function is expected to exhibit several key properties, like it should effectively attenuate the sidelobes, which is represented by a high value of SLA, it should minimize the level error in the amplitudes, indicated by a small value of ΔL, and it should demonstrate high selectivity, which is reflected in a small MLW. The level error (ΔL) arises as a result of the inherent shape of the window function, which leads to a reduction in the amplitude representation of certain frequencies. The parameters for the window functions are summarized in Table 4.1.

Table 4.1: Parameters of various window functions [195].

Window function	**SLA (dB)**	ΔL	**MLW (lines)**
Rectangle	13.3	0	1.62
Hanning	31.5	1.82	3.24
Hamming	42.7	1.75	3.38
Blackman	58.1	1.1	5.87
Flat top	60	0.05	7.01

5 Vibration attenuation performance of granular materials and mixtures

As mentioned in Chapter 2, the energy dissipation mechanism of a particle damper is a highly complex and nonlinear phenomenon. This complexity presents a significant challenge for their design. Furthermore, numerous factors, such as particle size, shape, granular material, and filling ratios, influence its vibration attenuation capability [196, 197]. Among these variables, the choice of granular material employed in the particle damper plays a vital role in determining its efficiency. Moreover, Chapter 2 highlights the prevalence of high-density materials like steel, lead, and tungsten in traditional designs, with limited exploration of alternatives like rubber granulates.

This chapter addresses this gap by introducing the concepts of Recycled Rubber Particle Dampers (RRPDs) and Hard Material Particle Dampers (HMPDs). Also, Chapter 2 highlighted the prevailing approach of using a single material type within particle dampers. To overcome this limitation, this chapter employs the concept of hybrid particle dampers (HPDs). HPDs utilize combinations of different granular materials, aiming to surpass the performance of conventional single-material dampers in vibration control. Additionally, this chapter investigate the effect of moisture content on the behavior of these systems, along with the relationship between vibration response and granular material mass, an aspect that has received limited attention in prior research.

The present chapter builds on previous work [198], offering a deeper exploration of how particle size distribution affects the performance of RRPDs. Additionally, it provides a more comprehensive analysis of the mass-specific vibration control of particle dampers..

5.1 Test specimen development for laboratory evaluation

The design of the test specimen to study the vibration mitigation capability of RRPDs, HMPDs, and HPDs draws inspiration from a stator commonly found in direct-drive wind turbine generators, see Figure 5.1 (left). To enable efficient and practical laboratory testing, a chosen section of the wind turbine stator (WTS) was downsized while maintaining its key geometric features, see Figure 5.1 (right). This downsized version retains the essential aspects of the original stator, allowing for easier handling within a laboratory setting. The chosen configuration was motivated by the aim to utilize a single test specimen for both analyzing particle damper design parameters and extrapolating findings from laboratory-scale experiments to industrial-scale structures (see Chapters 9 and 11).

Prior to finalizing the dimensions of the laboratory test specimen, a series of numerical modal analyses were conducted using the FEM. This investigation comprised three key steps. Initially, a modal analysis was performed on the original, unscaled dimensions of the WTS. This step provided crucial insights into the eigenfrequencies and eigenmodes associated with the original scaled WTS design. Subsequently, modal analyses were conducted on several scaled versions of the test specimen. Scaling involved a uniform reduction of all geometric dimensions, including wall thickness, by predetermined factors. The purpose of this step was to explore how the scaling process affects the modal characteristics of the specimen. The primary objective of analyzing the scaled versions was to identify configurations that captured the maximum number of eigenfrequencies within the designated frequency range of interest (20 Hz - 355 Hz). This information was crucial for selecting the final dimensions of the test specimen.

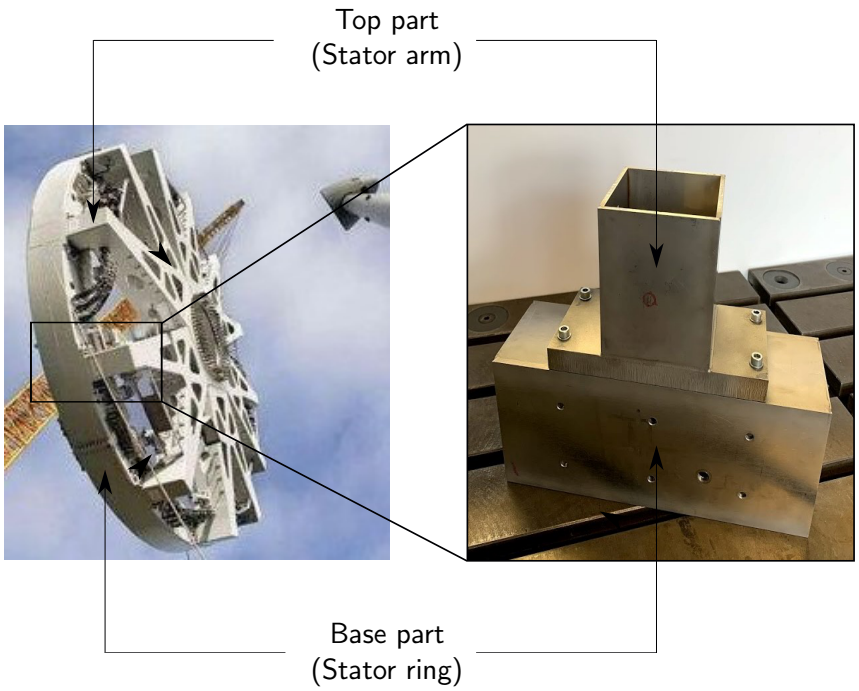

Figure 5.1: Left: Full-scale assembly of a commercial wind turbine stator [199]. Right: Scaled-down test specimen of a wind turbine stator designed for laboratory experiments.

The decision to concentrate on the low-frequency range in this chapter arises from two primary factors. Firstly, as observed in Chapter 2, passive vibration control methods are generally most effective in the high-frequency range. Although the particle damper is a broadband damping concept, Chapter 2 demonstrates that particle damper designs are predominantly effective in the high-frequency range. Therefore, this chapter aims to investigate how particle damper material selection can extend its effectiveness to the low-frequency range. Furthermore, this thesis seeks to translate particle damper technology from the controlled laboratory environment to the real-world complexities of the industrial sector.Wind turbine components were chosen as one of the target applications due to the significant challenges they face with low-frequency vibrations. It is important to note that this chapter prioritizes the low-frequency range relevant to wind turbines. However, the broader applicability of particle dampers is explored in later chapters, investigating their effectiveness in the high-frequency domain as well.

The test specimen illustrated in Figure 5.2 represents a scaled-down version of the original arm from a wind turbine generator, measuring one-fifth the original size. The test specimen comprises two components: the base part, representing the stator ring and features a rectangular cross-section. The upper segment of the test specimen resembles the stator arm of a WTS and exhibits a square-shaped hollow cross-section. In order to conduct experimental investigations concerning the damping performance of granular materials and their mixture, these materials are placed within the existing cavity located in the upper segment of the test specimen, as illustrated in Figure 5.3. The selection of this hollow space is based on experimental studies that investigated various particle damper design methods for implementation in wind turbine generators (see Chapter 9). Additionally, a fixed filling volume of 80% was chosen for all experiments. The selection of this particular filling volume is deliberate, aimed at minimizing the added mass of granular materials while ensuring a significant presence of particles within the cavity, thereby leading to a notable reduction in vibration amplitude. In this chapter, the experimental investigation delves into the impact of 20 distinct granular materials on the structure's vibration response. These materials are classified into two primary categories: recycled rubber particles and hard granular materials. As mentioned previously, this categorization facilitates the introduction of three damper designs: RRPDs, HMPDs and HPDs. It is important to note that additional details

about the test specimen will be provided in Chapter 9.

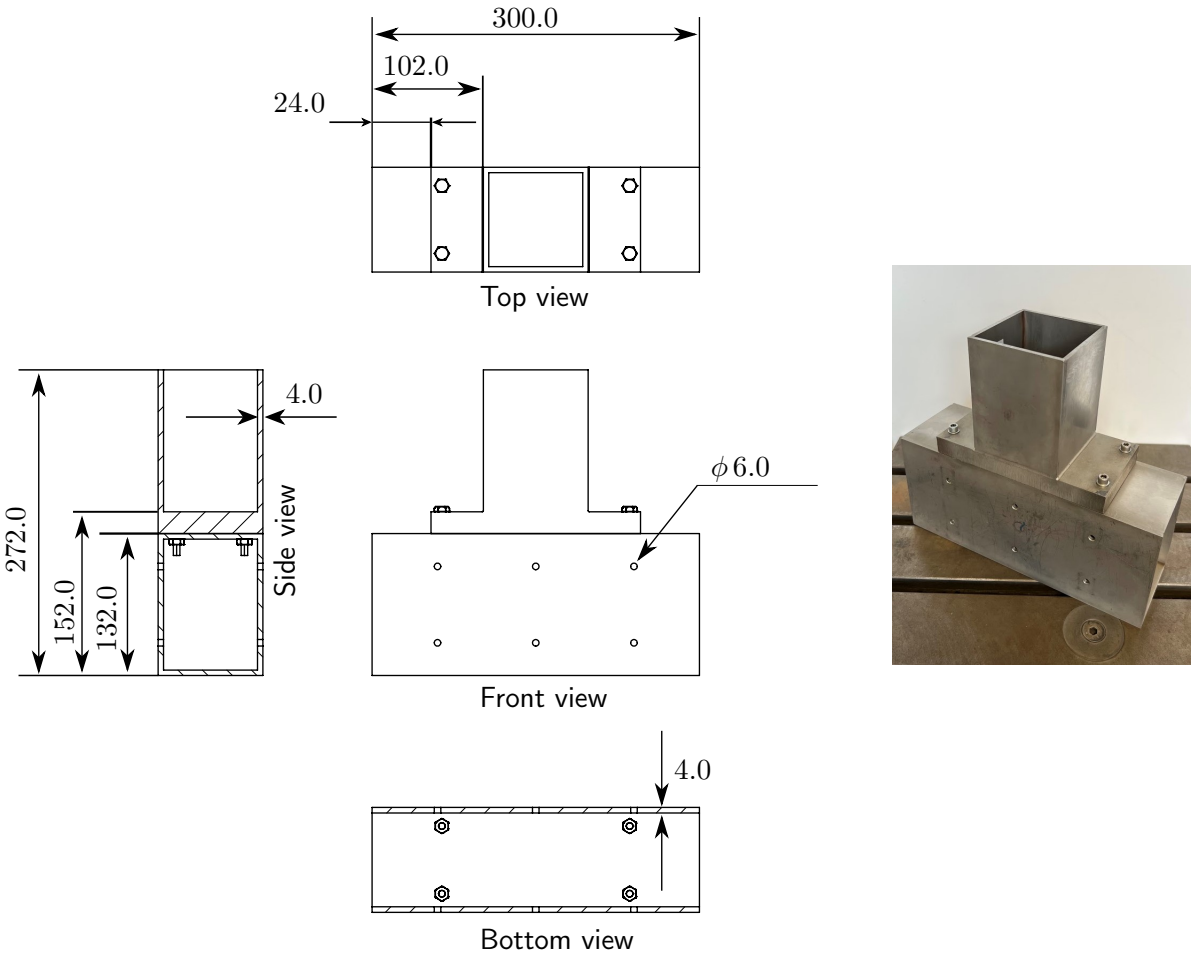

Figure 5.2: Design and dimensions of the test specimens used to evaluate the vibration attenuation properties of RRPDs, HMPDs, and HPDs. All the dimensions are in mm.

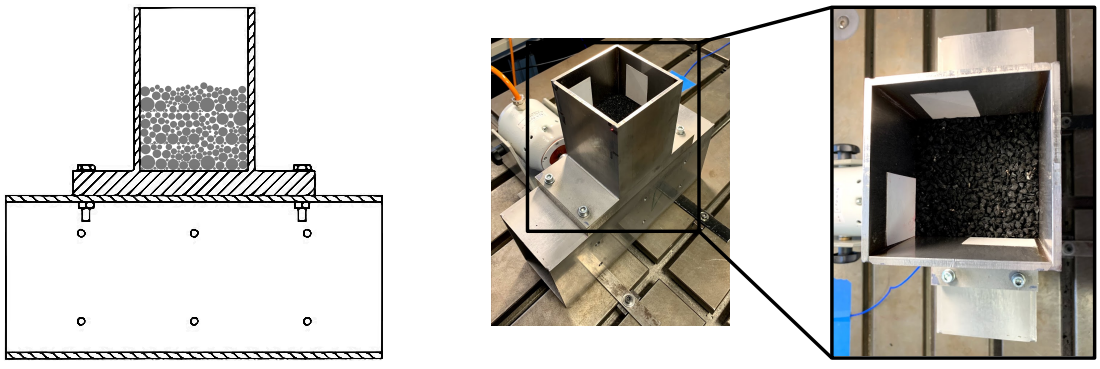

Figure 5.3: Placement of granular material within the upper cavity of the test specimen.

5.2 Material influence on particle damper performance

This section provides a comprehensive and detailed characterization of the granular materials used in the design and development of three specific types of particle dampers: RRPDs, HMPDs, and

HPDs. It includes an in-depth analysis of the particle sizes, examining both the individual particle sizes and their distribution within the polydisperse mixtures. This analysis is crucial for gaining a deeper understanding of how these specific granular configurations contribute to the overall performance and efficiency of the particle damping systems. It is important to note that the measurements of particle size and distribution were performed by the Fraunhofer Institute for Manufacturing Technology and Advanced Materials (IFAM). As such, this section will provide only a brief overview of the measurement techniques employed by IFAM, presented here for the sake of completeness, rather than an exhaustive discussion of the methods used.

5.2.1 Recycled rubber particle dampers (RRPDs)

The development of the RRPDs involves the utilization of rubber granulates (RGs) and rubber powders (RPs) of varying shapes and sizes, as illustrated in Figure 5.4. The materials used in this study can be classified into two distinct categories. The first category comprises RGs obtained from the recycling of end-of-life tires (ELT), along with RPs also derived from the same source. These ELT-based RGs and RPs, depicted in Figure 5.4 (a)-(g) and (j)-(k), respectively. The ELT rubber materials used in this thesis are manufactured by GENAN GmbH.

The second category consists of RGs obtained from the recycling of ethylene propylene diene monomer (EPDM) rubber, as shown in Figure 5.4 (h)-(i). Unlike the ELT-based materials, EPDM RGs are commonly used as filling material for punching bags.

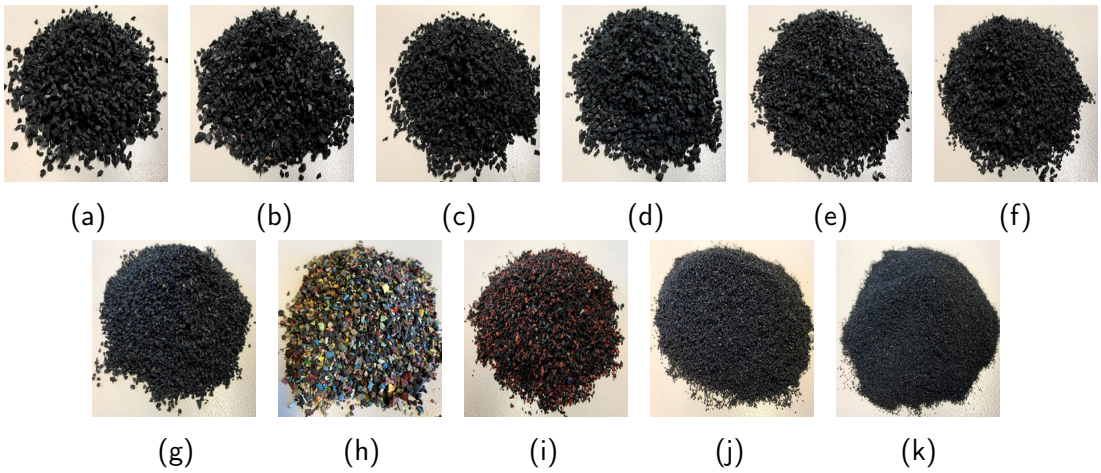

Figure 5.4: Rubber materials for RRPD design: (a) RG 6.4 mm , (b) RG 5.1 mm, (c) RG 4.7 mm, (d) RG 4.6 mm, (e) RG 3.6 mm, (f) RG 2.4 mm, (g) RG 2.3 mm, (h) RG 3.0 mm, (i) RG 2.2 mm, (j) RP 0.8 mm, (k) RP 0.5 mm.

The choice of RGs and RPs for particle damper design is driven by their highly non-linear viscoelastic material properties, which can offer exceptional damping characteristics [7]. Furthermore, both RGs and RPs possess rough and irregular surfaces, which can increase the number of contact points and interacting surfaces, thereby enhancing their damping properties [163, 197]. However, it is crucial to note that RG particles generally have rougher and more irregular surfaces compared to RP particles. Moreover, employing recycled tires not only provides environmental and climate advantages but also introduces a sustainable methodology to particle damper design. In addition to evaluating the overall vibration attenuation capacity of RGs, this study also investigates the influence of rubber particle size on vibration mitigation. However, it is important to acknowledge that the particle size distribution (PSD) of both RGs and RPs is non-uniform, see Figure 5.5 - Figure 5.7. To facilitate a clearer comparison of the PSD between RGs and RPs, the frequency and cumulative curves for each material type are presented separately.

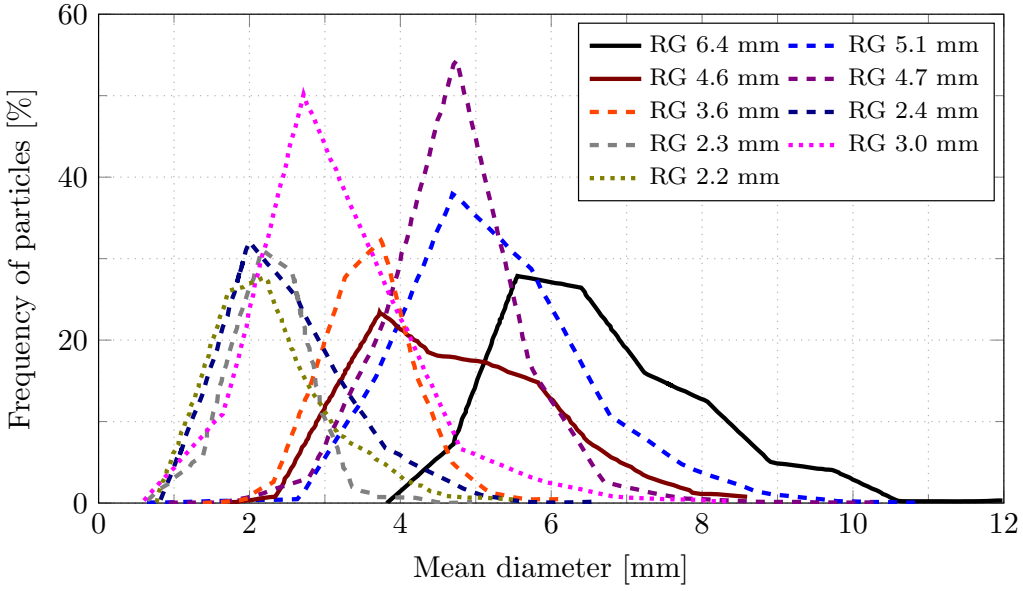

Figure 5.5: Volume-based relative frequency distribution of the investigated ELT and EPDM RGs.

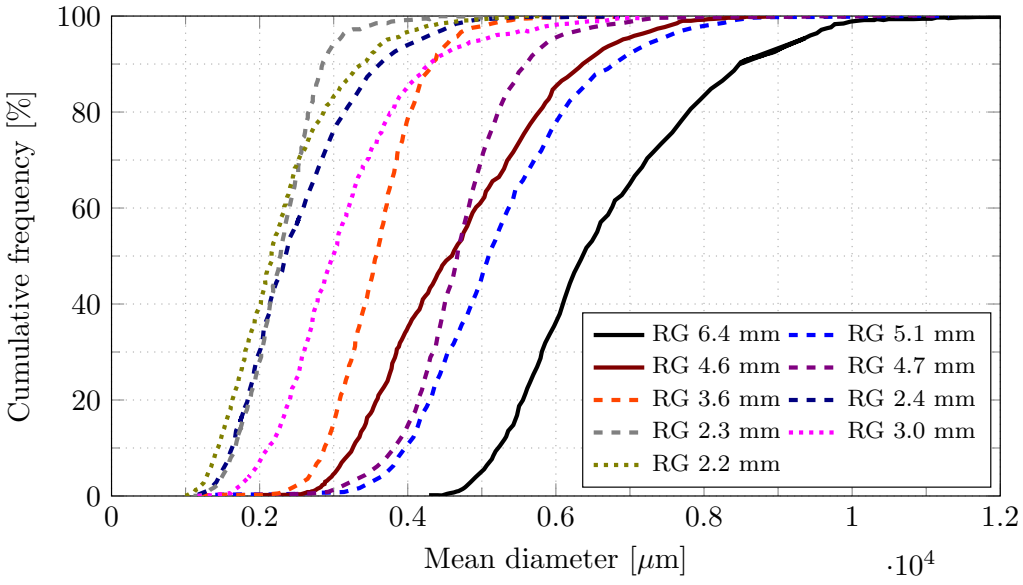

Figure 5.6: Volume-based cumulative frequency distribution of the investigated ELT and EPDM RGs.

Given the polydisperse nature of the RGs and RPs PSD, two approaches can be employed to investigate the influence of particle size on vibration attenuation. The first approach utilizes a single central value, such as the median particle size (d50), to assess its effect on vibration mitigation. The d50 refers to the diameter value that divides the PSD in half, with equal portions of particles exceeding and falling below this size. Importantly, within the context of this thesis, d50 represents the Feret median of the volume distribution, offering a readily interpretable and highly relevant statistic for characterizing PSD. Centralized measures such as mean, median, or mode offer a valuable starting point for understanding particle size. However, a more comprehensive view of the distribution requires additional information about the spread of particle sizes. To achieve this, utilizing both a central value and a measure of dispersion provides a more accurate representation of the PSD [200, 201]. This combined approach

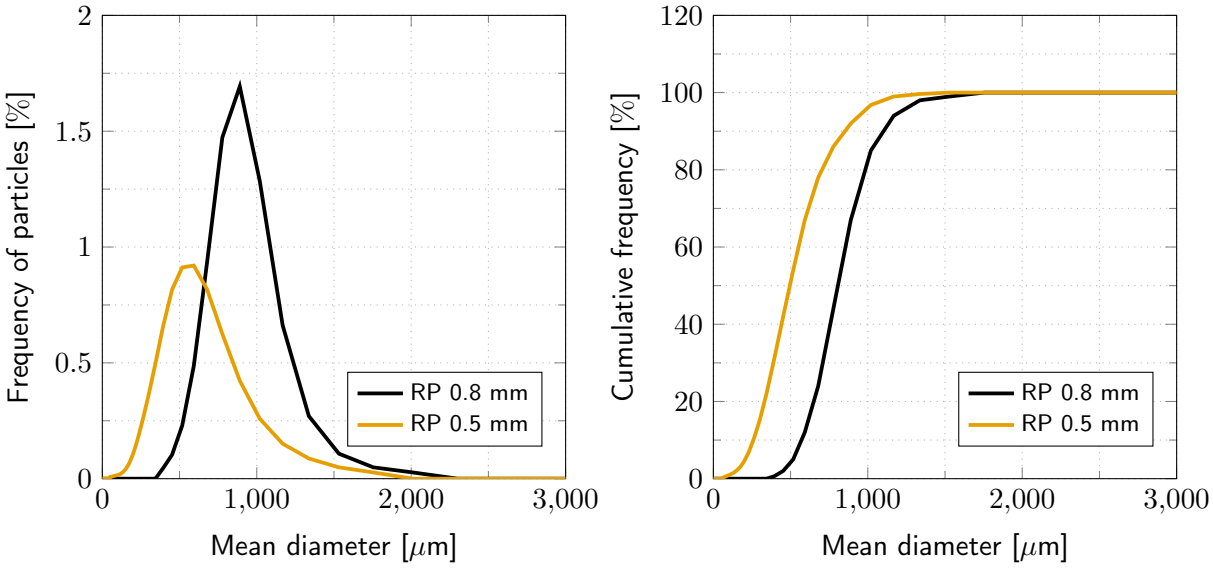

(a) (b)

Figure 5.7: Volume-based relative frequency distribution (a) and cumulative frequency distribution (b) of the investigated ELT and EPDM RGs.

offers a deeper understanding of the variation within the particle population and its potential impact on vibration attenuation.

The analysis of frequency and cumulative curves (Figures 5.5 - 5.6) provides valuable insights into the distribution of the particle population. These curves offer a visual representation and facilitate the extraction of crucial data points such as d10, d50, and d90, thereby providing essential information about the spread of particle sizes. Mathematically, these curves are intimately connected, with the cumulative distribution being derived from the frequency distribution through integration [200].

Table 5.1 summarizes the PSD of RGs and RPs, including their d10, d50, and d90 values. Analogous to d50, d90 represents the particle diameter at which 90% of the distribution falls below in size and 10% falls above. Similarly, d10 signifies the diameter where 10% of the particles are smaller and 90% are larger. A three-point characterization comprising d10, d50, and d90 is considered comprehensive and suitable for most particulate materials. Additionally, the table lists the source materials from which RGs and RPs are manufactured. The naming convention for the rubber particles in Table 5.1 employs a system where the numerical value directly denotes the Feret median diameter of the material. This approach facilitates clear differentiation between individual RGs and RPs, enabling straightforward identification of their key size characteristics.

Although visual inspection of Figure 5.5 - Figure 5.7 allows for a qualitative assessment of the PSD curve's width, quantitative measures of absolute width can be obtained from the cumulative distribution data. A commonly used metric for this purpose is the span, which is calculated using the d90 and d10 values as follows [202]

$$\text{Span} = \text{d90} - \text{d10}. \tag{5.1}$$

Table 5.1 also summarizes the distribution width of each RG and RP along with their bulk density. However, the bulk density values of the EPDM rubber granulates "RG 3.0 mm" and "RG 2.2 mm" are not reported, as these materials were sourced from the study conducted by Koch et al. [7], in which such data were not provided. Particle size analysis also revealed that rubber granulates "RG 4.6 mm" and "RG 6.4 mm" exhibited the widest size distribution among the tested materials, see Figure 5.5 and Figure 5.6. Interestingly, within the rubber powder category, "RP 0.5 mm" particles displayed a broader size range compared to "RP 0.8 mm" particles, see Figure 5.7.

Table 5.1: PSD of RGs and RPs, including their bulk density and source material.

Nomenclature	d10 [mm]	d50 [mm]	d90 [mm]	Absoulte span [mm]	Bulk density [kg/m^3]	Material [-]
RG 6.4 mm	5.25	6.37	8.50	3.25	495	ELT
RG 5.1 mm	3.99	5.10	6.81	2.82	465	ELT
RG 4.7 mm	3.84	4.68	5.62	1.78	455	ELT
RG 4.6 mm	3.28	4.60	6.40	3.12	465	ELT
RG 3.6 mm	2.88	3.58	4.33	1.45	430	ELT
RG 2.4 mm	1.62	2.37	3.61	1.99	430	ELT
RG 2.3 mm	1.67	2.28	2.86	1.19	395	ELT
RP 0.8 mm	0.56	0.79	1.09	0.53	355	ELT
RP 0.5 mm	0.25	0.49	0.85	0.60	340	ELT
RG 3.0 mm	2.13	3.00	4.33	2.20	-	EPDM
RG 2.2 mm	1.44	2.17	3.41	1.97	-	EPDM

The measurement of particle size and distribution was conducted by the Fraunhofer Institute for Manufacturing Technology and Advanced Materials (IFAM). IFAM utilized laser diffraction spectroscopy (Horiba LA950) in accordance with ISO 13320:2009 to determine the geometric dimensions of the RPs. Additionally, the PSD of the RG samples was determined by scanning 1000 - 2000 particles from each sample using a transmitted-light scanner (Microtek ScanMaker i900) and specialized image analysis software (Aquinto a4i Analysis). It is important to note that the PSD data for ELT-RGs and RPs provided by GENAN GmbH differ from the information presented in Table 5.1. This discrepancy may be due to the different measurement methods used for analyzing particle size distribution; GENAN GmbH employed the sieve method for their measurements. Additionally, PSD data for the EPDM RGs were not reported in the study by Koch et al. [7], which necessitated the use of PSD measurements conducted by IFAM for these specific RGs. Therefore, to maintain consistency and ensure data availability, the PSD measurements performed by IFAM will be utilized throughout this thesis for the analysis of vibration attenuation.

5.2.2 Hard material particle dampers (HMPDs)

This section examines the material characteristics of hard granular materials used in the design of HMPDs. For this investigation, nine distinct granular materials, representing a combination of conventional and non-conventional choices, were chosen for this investigation (Figure 5.8).

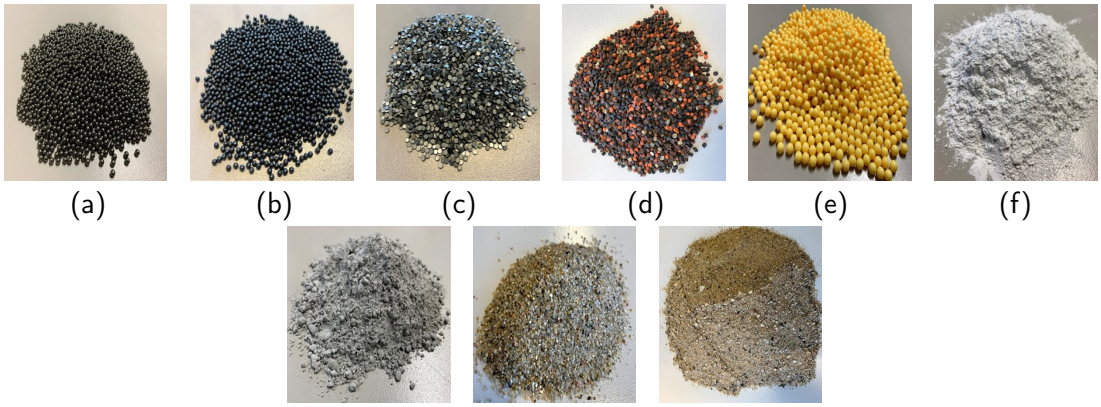

Figure 5.8: Granular materials employed in the design of HMPDs: (a) Steel balls, (b) lead shot, (c) steel chips, (d) plastic cylinders, (e) plastic balls, (f) quartz powder, (g) stone powder, (h) sand coarse, (i) sand mix.

In Chapter 2, a comprehensive overview is provided of the prevalent use of hard granular materials like steel balls and lead shot in particle damper design. In this thesis, the exploration is extended beyond these conventional materials by incorporating unconventional alternatives such as stone powder, plastic balls, and quartz powder. The selection of these materials was guided by their economic viability and commercial accessibility. It is noteworthy that the selected materials, such as steel balls, lead shot, steel chips, plastic balls, and cylinders, are all monodisperse in nature. The specific particle size information for each material can be found in Table 5.2. Unlike the monodisperse materials (steel balls, lead shot, etc.), sand, stone powder, and quartz powder exhibit a natural variation in grain size, akin to rubber granulates. To quantify the distribution for stone powder and quartz powder, laser diffraction (Horiba LA950) measurements were conducted at IFAM according to ISO 13320:2009. The particle size distribution for these materials is illustrated in Table 5.3. Key parameters, including d10, d50, d90, and the width of the distribution, are summarized in Table 5.3 for these materials. In contrast, the average particle size for sand was adopted from the work of Koch et al. [150], as the same sand sample is utilized in this work. The average particle size of coarse sand and sand mix is 0.7 mm and 0.05 mm, respectively. Moreover, the bulk density of the majority of the hard materials is not reported in this work, as these materials were supplied by IFAM without the corresponding bulk density data.

Table 5.2: Particle diameter of monodisperse granular materials for HMPDs design

Material	Steel balls	Lead shot	Steel chips	Plastic cylinders	Plastic balls
Particle diameter [mm]	4.5	3.0	4.0	4.0	6.0

Table 5.3: Particle size of polydisperse granular materials for HMPDs design.

Material	**d10 [mm]**	**d50 [mm]**	**d90 [mm]**	**Absoulte span [mm]**	**Bulk density [kg/m^3]**
Quartz powder	0.00597	0.02365	0.07666	0.07069	-
Stone powder	0.00269	0.01116	0.04283	0.04014	890

5.2.3 Hybrid particle dampers (HPDs)

Conventional particle dampers, which employ a single type of granular material, have been demonstrably successful in mitigating vibration across numerous fields. However, a key consideration is whether the vibration attenuation capabilities of these dampers can be further enhanced without significant design modifications. Hence, this thesis uses the concept of HPDs to address this gap. HPDs leverage a strategically chosen combination of different granular materials within the existing particle damper design. By harnessing the unique properties of each material, HPDs aim to achieve superior vibration mitigation performance compared to conventional single-material dampers. This thesis investigates the potential of HPDs, exploring how the interplay of diverse materials within the damper can lead to enhanced damping effectiveness. The core concept behind the HPDs design lies in utilizing the beneficial properties of both RRPDs and HMPDs within a single damper. The influence of eight different granular material combinations on vibration attenuation performance is investigated in this work, as shown in Figure 5.9.

The initial stage involved the creation of HPDs through the incorporation of hard, spherical particles (e.g., steel balls, lead shot) with irregularly shaped polydisperse rubber particles. It is important to highlight that selecting the rubber particles for this mixture involves comparing the damping effectiveness of different rubber particles within the RRPDs. After conducting this comparison, the rubber granulate showing notable damping performance was selected for designing this HPD. The reason behind combining hard, spherical particles (e.g., steel balls, lead shot) with irregularly shaped rubber particles lies in maximizing particle-particle contact points during collisions within the damper.

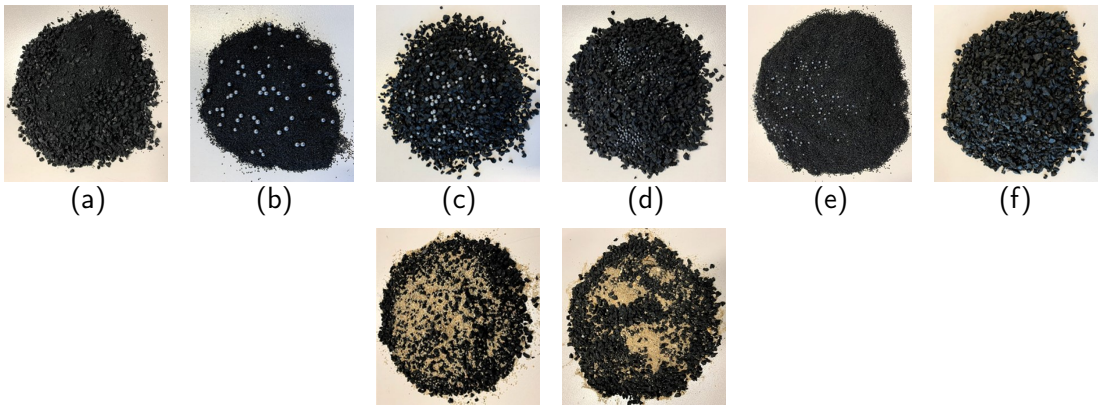

(a) (b) (c) (d) (e) (f) (g) (h)

Figure 5.9: Compositions of granular material mixtures used to design HPDs, with percentages referring to mass fractions: (a) RP 0.8 mm (50%) and RG 4.6 mm (50%) , (b) RP 0.8 mm (75%) and steel balls (25%), (c) RG 4.6 mm (75%) and steel balls (25%) , (d) RG 4.6 mm (75%) and lead shot (25%), (e) RP 0.8 mm (75%) and lead shot (25%), (f) RG 6.4 mm (50%) and RG 4.6 mm (50%), (g) sand coarse (50%) and RG 4.6 mm (50%), (h) sand mix (50%) and RG 4.6 mm (50%).

Compared to a purely spherical media, the introduction of irregularly shaped particles creates a multitude of contact points, enhancing energy dissipation mechanisms. These mechanisms involve increased inter-particle friction and larger deformations within the soft particles upon impact. Ultimately, this leads to a more effective attenuation of vibrations transmitted to the structure.

Furthermore, the RP is blended with lead shot and steel balls. This mixture aims to explore the vibration response of the system when combining the fine particles of soft material with highly efficient hard materials, as depicted in Figures 5.9 (b) and (e). This particular mixture for the HPD can be regarded as an expanded version of the fine particle impact damper (FPID). The FPID emerged as a solution to address limitations associated with conventional impact dampers. Therefore, the FPID can be viewed as an elaboration on the traditional impact damper concept. In an FPID, a single large impact mass coexists within a container filled with numerous fine particles. Due to inter-particle adhesion forces, these fine particles envelop the large mass and undergo substantial inelastic deformations upon impact. These deformations contribute to a significantly enhanced rate of energy dissipation within the damper [203].

Two types of sand are also mixed with RGs to examine their potential in reducing the vibration amplitude of the test specimen, as illustrated in Figures 5.9 (g) and (h). Additionally, a range of RGs with varying average particle sizes is incorporated, along with RP being combined with RG (Figures 5.9 (a) and (f)). This configuration was designed to analyze the effect of particle size disparity within the soft component on the damping behavior.

The design of an HPD necessitates a trade-off between two key factors: minimizing the additional mass and ensuring significant damping. Introducing a large quantity of heavy metallic inclusions (such as steel balls or lead shot) may significantly enhance vibration attenuation, but it also increases the overall weight of the damper. This can be counterproductive in applications where weight reduction is crucial. To address this challenge, the HPD is composed of 25% metallic inclusions and 75% RGs. This ratio offers a balance between achieving substantial vibration mitigation and maintaining a relatively low added mass. For HPD utilizing mixtures of different rubber particle sizes or sand and rubber particles, a 50% mixture ratio is employed. This selection is justified by the minimal mass difference between these materials compared to the substantial disparity between metal and rubber. A $50:50$ ratio allows for a good balance between maximizing particle interactions and maintaining the overall damper mass. This approach of tailoring the material ratio based on the inherent mass difference between components

allows for the development of HPDs that are both lightweight and effective in mitigating vibrations.

5.3 Experimental setup

In this thesis, the laser scanning vibrometer (LSV) plays a central role in evaluating the structural response of the test specimen. The LSV is a contactless measuring device, relying on the Doppler effect to extract valuable insights into the dynamic behavior of a system. This thesis utilizes a Polytec LSV, specifically the PSV-400 model, for experimental investigations. Figure 5.10 presents a schematic illustration of the core experimental setup used throughout this thesis to investigate the system's dynamical response. This setup serves as the foundation for all experimental studies conducted in this thesis, with variations in the shape and boundary conditions of the test specimen implemented to address specific research questions. Details of these variations are provided in the relevant chapters for clarity. Figure 5.11 presents a detailed illustration of the setup specifically used to quantify the damping efficiency of the RRPDs, HMPDs, and the HPDs under investigation.

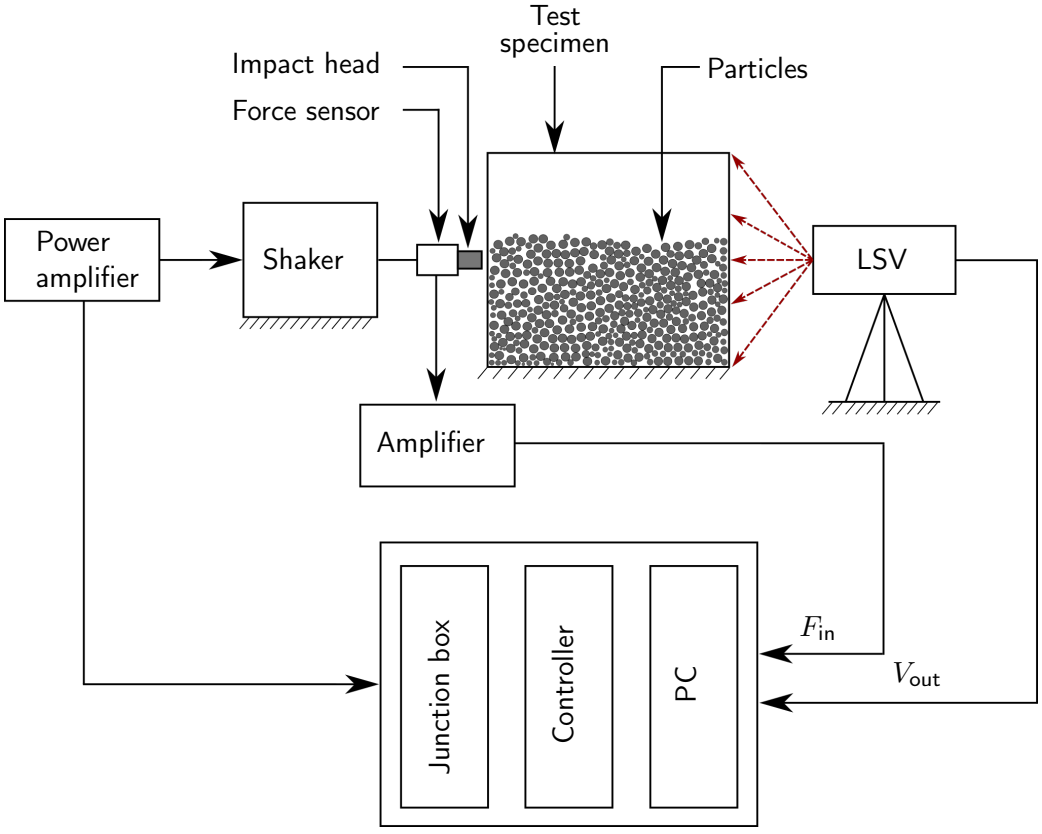

Figure 5.10: Schematic representation of the experimental setup used to measure the vibration response of a test specimen.

The test specimen was excited using an electrodynamic shaker by Tira. To isolate any potential secondary vibrations from the shaker itself, it was securely mounted on an iron frame. This frame, in turn, was connected to the measuring table using identical bolts and sliding blocks, effectively creating a decoupled system. Decoupling ensures consistent measurements across tests, improving accuracy and repeatability. Moreover, it confirms that the measured response comes exclusively from the test specimen, preventing any unintended interactions with the table. Furthermore, to excite the test specimen, an impulse signal was used, driven by the need to capture resonances across the desired frequency range (20 Hz - 355 Hz).

Selection of the optimal excitation point was achieved through an iterative process. The test specimen

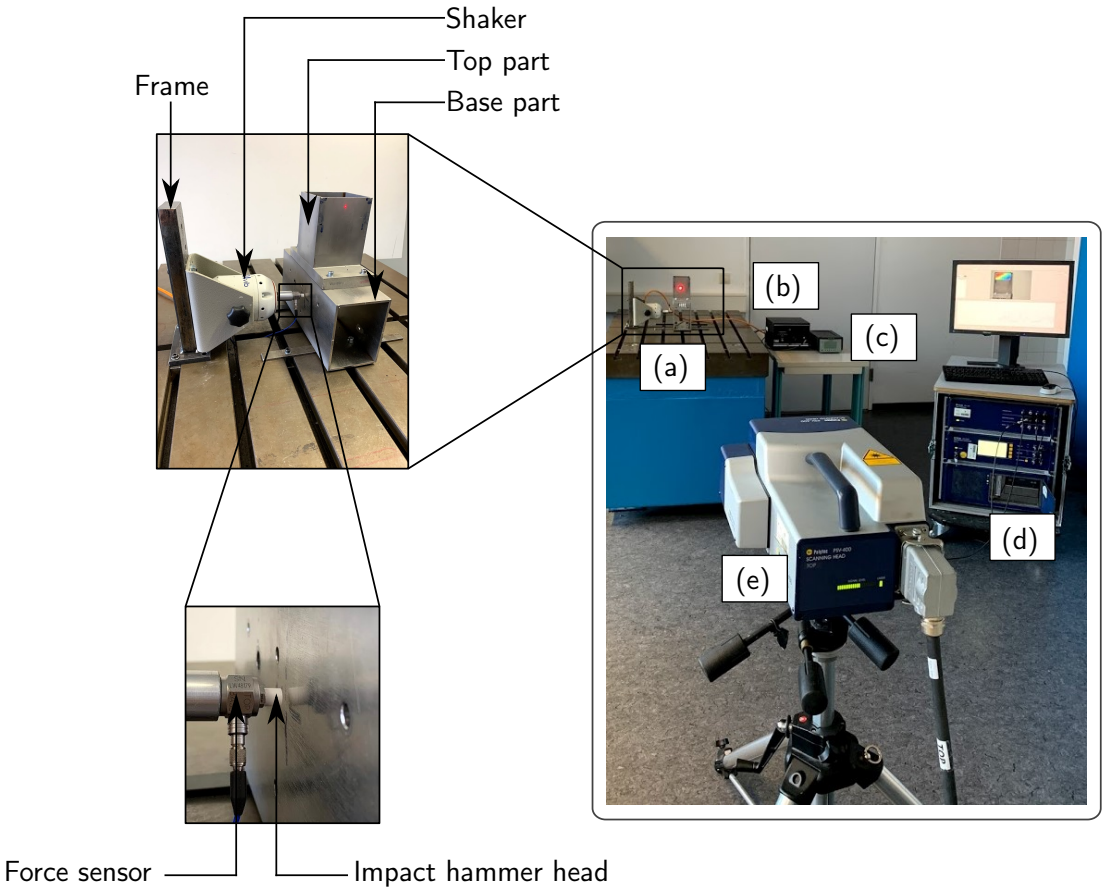

Figure 5.11: Experimental setup for measuring vibration attenuation of RRPDs, HMPDs, and HPDs: (a) Test specimen, (b) shaker power amplifier, (c) force sensor amplifier, (d) control and post-processing unit, (e) laser vibrometer scan head.

was excited at various locations using a modal hammer, and the resulting frequency response functions (FRFs) were visualized in real-time using Polytec software. This real-time spectral analysis enabled the selection of an excitation point that effectively stimulated a broad range of resonant frequencies within the pre-defined frequency band of interest. Additionally, the normal direction was chosen for applying the excitation due to its effectiveness for the specific experiments conducted in this thesis. The limited size of the other specimen surfaces further supported the selection of the normal direction as the most suitable option for inducing vibrations.

Force measurement on the test specimen was achieved using a PCB Piezotronics force sensor, model 208C02, strategically positioned between the shaker and the impulse head, see Figure 5.11. This placement ensured the capture of the forces exerted on the test specimen during excitation. The sensor's output signal was amplified using a Bruel $\&$ Kjær Type 2693 amplifier. Additionally, to provide sufficient power for driving the shaker, a TIRA Type 50009 power amplifier was employed. To avoid double strokes near the point of excitation, a consistent 2 mm gap was maintained between the hammer head and the specimen throughout the experiments. To ensure repeatability, the specimen's base was rigidly fixed during all tests. Furthermore, to measure the out-of-plane surface velocity of the test specimen, the scanning head of the laser scanning vibrometer was positioned horizontally relative to the specimen surface. Additionally, the entire experimental setup remained static throughout the study to maintain consistent frequency response characteristics.

To evaluate the vibration attenuation capabilities of RRPDs, HMPDs, and HPDs, a designated cavity in the upper portion of the test specimen was filled to 80% of its volume with the granular materials

or their predefined mixtures. Moreover, it should be noted that the cavity within the top section remained open, lacking any lid or cover, for the entire duration of the experiments. To further minimize experimental uncertainties, the test specimen's base was firmly secured to the measuring table using two identical beam-like steel structures. These beams acted as a dual isolation system, increasing stability and decoupling the specimen from any potential vibrations from the table. To achieve this, four identical bolts and sliding blocks were used to connect the base to the steel beams. The top section, which housed the granular materials, was attached to the base using four identical sets of bolts, nuts, and washers. To ensure consistent assembly and eliminate any possible variations, a torque wrench was employed throughout the process, guaranteeing a uniform pre-load of 6 Nm for each bolt. This approach was essential because prior investigations during the experimental setup revealed the vibration behavior of the structure is highly sensitive to the bolt-tightening procedure. Inconsistent bolt tightness could introduce unwanted variations in the data.

To establish a robust testing methodology, an initial empirical study was conducted with a reference specimen (without granular materials). This investigation had two main objectives: to identify the optimal experimental settings and to determine the optimal number of scan points. This investigation identified several key factors for optimal experimentation. Firstly, averaging multiple measurements (six per point) improved the SNR by reducing random fluctuations. Secondly, a 1000 Hz low-pass filter was applied to limit the bandwidth of the captured data, further minimizing noise. Moreover, spectral leakage, a potential source of error, was addressed by employing the Hann window function in all subsequent experiments. Finally, crucial parameters like the sampling frequency (12.8 kHz) and frequency resolution (0.781 Hz) were meticulously chosen based on the findings. A summary of these optimized parameters is presented in Table 5.4. The second aspect of the preliminary study focused on the number of scan points. Various configurations were investigated to determine the optimal balance between measurement time and data accuracy. It was revealed through this analysis that 11 scan points, strategically positioned on the top surface of the test specimen, were sufficient for all subsequent experiments.

Table 5.4: List of parameters for data acquisition.

Parameter	Complex average	Cut-off frequency	Sampling frequency	Frequency resolution
Values	6	1000 Hz	12.8 kHz	0.781 Hz

Furthermore, reproducibility and repeatability are crucial aspects of experimental research, as they contribute to the robustness and reliability of findings. To ensure the repeatability and reproducibility of findings in this thesis, experimental conditions were meticulously controlled. Scan point locations, hammer-to-specimen distance, and laser scanning vibrometer position remained constant throughout the experiments.

Repeatability was evaluated by disassembling and reassembling the reference specimen's top section twice while maintaining the secure position of the base. This process assessed the consistency of the setup and identified potential sources of variability. Emphasis was placed on maintaining the structural integrity and proper alignment of the specimen during disassembly and reassembly, ensuring the closest possible replication of the original test conditions. By repeating this process, the stability of the setup was confirmed, and confidence in reproducibility was gained. Furthermore, in order to strengthen the robustness of experimental repeatability, the vibration behavior of the reference specimen was monitored after each granular material measurement set. This proactive approach aided in tracking potential changes in the specimen's response, enabling identification of any deviations from expected behavior. Finally, upon completion of the experiments, the frequency response of the reference specimen was analyzed to comprehensively assess the setup's ability to consistently reproduce the system's response, see Figure 5.12. These FRFs provided strong evidence of the setup's reliability and its capacity to generate consistent and reproducible data.

It is crucial to emphasize that all FRFs within this thesis are expressed in terms of mobility, unless

otherwise specified. Mobility represents the ratio of velocity to applied force and can be determined by:

$$\text{Mobility} = \frac{\text{Velocity}}{\text{Force}} = \frac{v}{f}. \tag{5.2}$$

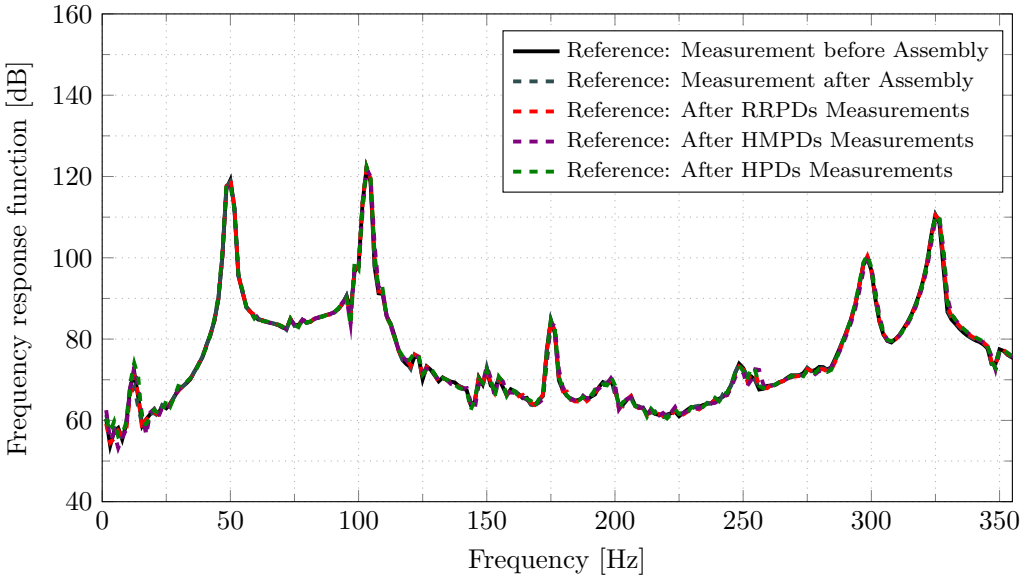

Figure 5.12: Experimental reproducibility as evidenced by consistent outcomes.

It should be noted that the experimental setup depicted in Figures 5.10 - 5.11 represents the culmination of an iterative development process. Prior to this final configuration, numerous alternative setups were explored and rigorously tested. However, these earlier iterations exhibited limitations in terms of reproducibility and repeatability of the measurements. This ongoing evaluation process ultimately led to the selection of the setup presented in Figure 5.10, which demonstrated superior robustness in achieving consistent and reliable results.

5.4 Absolute vibration attenuation

An analysis of the FRFs was conducted to investigate the influence of RRPDs, HMPDs, and HPDs on the resonant behavior of the test specimen. Narrowband and one-third octave band spectra were utilized to examine the FRFs within the frequency range of interest (20 Hz to 355 Hz). The narrowband spectrum served to identify the number of resonance peaks present within this specific frequency band. For example, both the reference test specimen and the specimen filled with RGs and RPs displayed five distinct resonance frequencies within the range of interest below 355 Hz, see Figure 5.13. Furthermore, to gain a more comprehensive understanding of the vibration behavior across the entire frequency spectrum, a one-third octave band plot is employed, see Figure 5.14. This analysis provides an in-depth view of the overall vibration level at each frequency band. For each one-third octave band, the following key frequencies can be expressed in Hz: lower limit (f_l), upper limit (f_u), and center frequency (f_c). These values are related mathematically as follows

$$f_\mathsf{l} = \frac{f_\mathsf{u}}{\sqrt[3]{2}}, \tag{5.3}$$

$$f_\mathsf{u} = \sqrt[3]{2} \cdot f_\mathsf{l}, \tag{5.4}$$

$$f_c = \sqrt{f_l \cdot f_u} = \sqrt[6]{2} \cdot f_l = \frac{1}{\sqrt[6]{2}} \cdot f_u. \tag{5.5}$$

The influence of RRPDs, HMPDs, and HPDs on reducing vibration amplitude is quantified through an amplitude reduction plot. For example, Figure 5.15 illustrates the amplitude reduction plot for the RRPDs. The amplitude reduction plot is generated by subtracting the one-third octave band levels of the reference specimen from those of the specimen filled with granular materials. A horizontal red line at 0 dB serves as a baseline for comparison. Regions above this line indicate an increase in vibration amplitude, while areas below signify a reduction. In this chapter analysis, specific focus is placed on the one-third octave bands surrounding the most prominent resonance peaks identified through narrowband spectrum. These frequency bands are highlighted by gray patches in all figures. This targeted approach allows for a more precise evaluation of the vibration mitigation effectiveness of the granular materials. All data acquired through the experimental investigations were analyzed using MATLAB throughout this thesis.

5.4.1 Recycled rubber particle dampers (RRPDs)

Figures 5.13-5.15 show the FRFs of both the reference specimen and the specimens with the RRPDs. The narrowband spectrum demonstrates that the reference specimen and specimens with RRPDs incorporating RGs and RPs all exhibit five distinct resonance frequencies below 355 Hz. These resonances are located at 50 Hz, 103 Hz, 175 Hz, 298 Hz, and 325 Hz, see Figure 5.13.

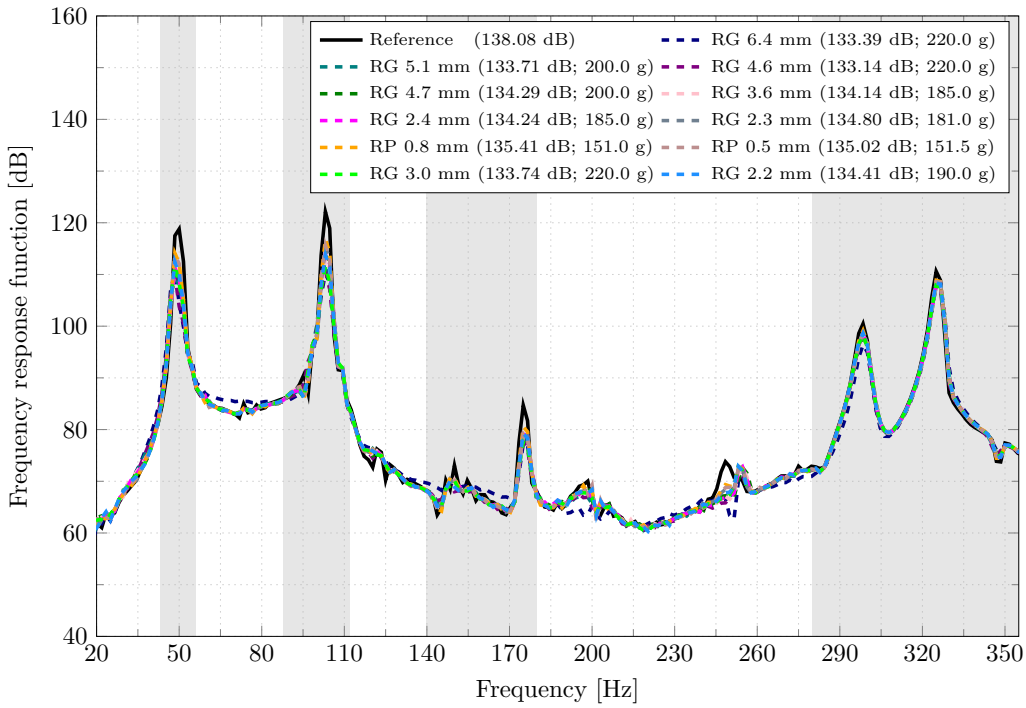

Figure 5.13: Narrowband spectrum of the test specimen with and without RRPDs, incorporating RGs and RPs. The SL value of the surface velocity is given in dB and the mass of the granular filling materials is given in g.

From the one-third octave band spectrum (Figure 5.14), it can be observed that all the RRPDs, irrespective of the type of RGs and RPs, can achieve significant vibration attenuation across the entire frequency range. This observation is consistent regardless of the particle size or shape used. Moreover, the vibration mitigation appears to be particularly pronounced around the initial three central

frequencies within the one-third octave band (50 Hz, 100 Hz, and 160 Hz). This effect is significantly stronger compared to the reduction in vibration amplitude observed near the central frequency of 315 Hz.

The specific magnitude of vibration amplitude reduction for the tested specimen resulting from the various types of RGs and RPs is quantified in Figure 5.15. The results indicate that the overall efficiency of the rubber granulate "RG 4.6 mm" (purple dashed line) in reducing the vibration amplitude of the test specimen is significantly higher compared to the rest of RGs. This observation is further supported by the sum level (SL) value of the surface velocity of the rubber granulate "RG 4.6 mm" (133.14 dB), which is lower compared to other RGs and RPs. A similar vibration mitigation pattern is observed for the rubber granulate "RG 6.4 mm" (represented by the navy dashed line), although it has the drawback of increasing the vibration amplitude in specific white-marked stripes within the one-third octave bands. The sum level of the surface velocity is determined using the following expression.

$$\mathrm{SL} = 20 \log_{10} \left(\sum_{i=1}^{n} 10^{\frac{v_i}{20}} \right), \tag{5.6}$$

where v_i represents the velocity at the ith point.

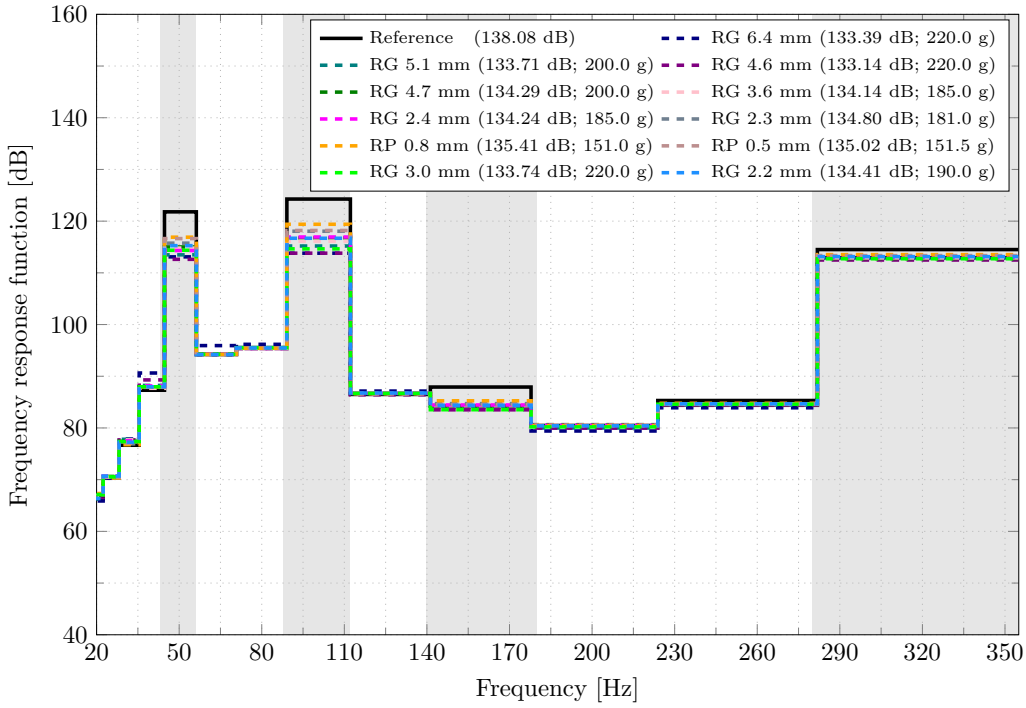

Figure 5.14: One-third octave band of test specimen with and without RRPDs, incorporating RGs and RPs. The SL value of the surface velocity is given in dB and the mass of the granular filling materials is given in g.

To investigate the influence of particle size on the system's vibration response, a comparative analysis was conducted using ELT rubber granulates. The results indicated that rubber granulate with a larger median value exhibited greater effectiveness in reducing the system's vibration response compared to those with a smaller median value. see Figure 5.15 and Table 5.5. This aligns with the findings of Koch et al. [150], who investigated the impact of sand particle size on the vibration attenuation properties of an oil pan. They found that sand particles with a larger average particle size are effective in reducing the vibration amplitude of the oil pan. Furthermore, it has been observed that the overall

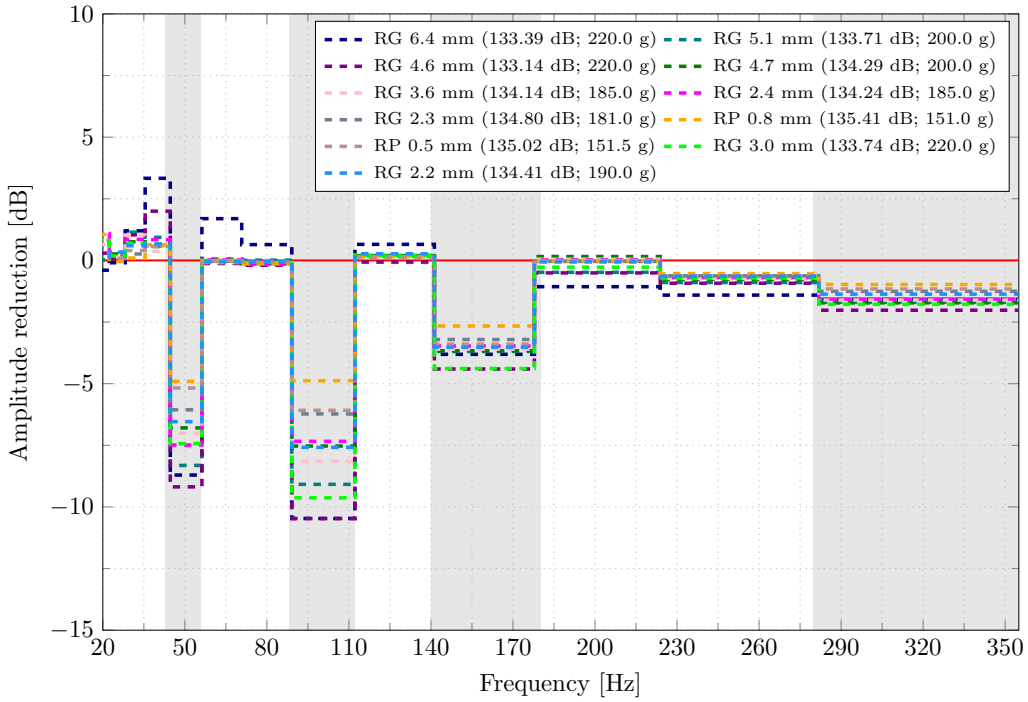

Figure 5.15: Amplitude reduction plot of the test specimen with and without RRPDs, incorporating RGs and RPs. The SL value of the surface velocity is given in dB and the mass of the granular filling materials is given in g.

damping efficiency of the RGs increases with the median particle size up to a certain threshold, beyond which particle size no longer has an influence. This trend is evident as the overall vibration attenuation capability improves when the median particle size increases from "RG 2.3 mm" to "RG 4.6 mm". However, there is a decline in vibration attenuation capability for rubber granulates "RG 4.7 mm" and "RG 5.1 mm", even though their median particle sizes are larger than that of "RG 4.6 mm".

It is important to mention that a discrepancy in the mass of RGs and RPs has been observed even when the filling volume remains constant. This difference likely arises from variations in the bulk density of the particle types. Additionally, the filling process and the settling behavior of the granular material can influence the final packing density and, consequently, the achieved fill height. Due to the random nature of granular material filling, individual RGs and RPs may exhibit variations in packing ratio and particle arrangement within the cavity. Furthermore, the post-filling step of achieving a zero angle of repose to ensure a consistent final height might further alter the internal particle arrangement and packing density. These factors collectively contribute to the observed mass differences between RGs and RPs despite identical filling volumes.

To isolate the effect of mass differences, a controlled comparison was conducted using RGs with identical material mass and filling volume. Specifically, "RG 5.1 mm" (200 g) was compared with "RG 4.7 mm" (200 g). The results showed that "RG 5.1 mm," with its larger particle size, reduced the test specimen's vibration amplitude significantly higher than "RG 4.7 mm." Additionally, rubber granulates "RG 4.6 mm" and "RG 6.4 mm" have similar masses for the given filling volume. Despite their different median particle sizes, both "RG 4.6 mm" and "RG 6.4 mm" exhibited comparable vibration reduction at the central frequencies of 50 Hz and 100 Hz, as well as similar performance at 160 Hz and 315 Hz, as shown in Table 5.5.

Interestingly, in contrast to the findings for RGs, rubber powder with a smaller particle size ("RP 0.5 mm") exhibits greater effectiveness in vibration amplitude reduction compared to its larger counterpart

("RP 0.8 mm"). This aligns with observations reported by Chesla et al. [80], where steel powder with a finer grain size (0.15 mm) demonstrated superior damping performance compared to a coarser variant (0.40 mm). However, it is noteworthy that Chesla et al. [80] solely based their conclusions on average particle size, and no discussion regarding particle size distribution was included.

From the above discussion, it can be seen that analyzing the vibration attenuation capabilities of RRPDs in relation to median particle size provides valuable insights for selecting granular materials based on particle size during damper design. However, the correlation between vibration attenuation and particle size appears less pronounced when comparing rubber granulates ("RG 2.4 mm" and "RG 3.6 mm") to rubber powders ("RP 0.5 mm" and "RP 0.8 mm"). This suggests that median particle size alone is insufficient for characterizing the vibration attenuation performance of polydisperse RRPDs. Moreover, it has been also previously mentioned in Section 5.2 that while single-point metrics like mean, median, or mode can offer a basic understanding of the PSD, they are insufficient for comprehensive PSD characterization, especially for polydisperse samples. For polydisperse materials, a more complete picture of the PSD requires additional parameters such as d10, d50, d90, and distribution span [201].

Table 5.5: Vibration reduction (dB) of RGs and RPs at various resonance frequencies.

RRPDs	50 Hz	100 Hz	160 Hz	315 Hz	Material
RG 6.4 mm	-8.7	-10.5	-3.8	-1.6	
RG 5.1 mm	-8.3	-9.1	-3.7	-1.7	
RG 4.7 mm	-6.8	-7.5	-3.7	-1.7	
RG 4.6 mm	-9.2	-10.5	-4.4	-2.0	ELT
RG 3.6 mm	-7.0	-8.0	-3.6	-1.6	
RG 2.4 mm	-7.5	-7.4	-3.5	-1.6	
RG 2.3 mm	-6.1	-6.2	-3.2	-1.3	
RP 0.8 mm	-4.9	-4.9	-2.7	-1.0	ELT
RP 0.5 mm	-5.2	-6.1	-3.4	-1.2	
RG 3.0 mm	-7.4	-9.6	-4.4	-1.8	EPDM
RG 2.2 mm	-6.5	-7.6	-3.5	-1.4	

Hence, a more in-depth analysis of the relationship between PSD and damping performance of RRPDs is necessary to establish a comprehensive correlation between granular material characteristics and their vibration mitigation capabilities. As mentioned above, although "RG 4.6 mm" exhibited a smaller median particle size compared to "RG 4.7 mm" and "RG 5.1 mm," it demonstrated superior vibration attenuation performance. This discrepancy can be attributed to the broader PSD of "RG 4.6 mm." Supporting this observation, "RG 4.6 mm" and "RG 6.4 mm," which share similar PSD spans (see Table 5.1), exhibited comparable vibration attenuation capacities, see Table 5.5. Furthermore, a comparative analysis of "RG 3.6 mm" and "RG 2.4 mm" indicated a marginally better overall vibration reduction capacity for the former, as evidenced by SL values in Figure 5.15. However, a notable discrepancy was observed near the resonance frequency of 100 Hz, where "RG 2.4 mm" reduced the vibration amplitude of the structure by 0.6 dB less than the rubber granulate "RG 3.6 mm." Considering the broader PSD span of "RG 2.4 mm" (Table 5.1), this anomalous behavior is more likely attributable to experimental uncertainty than to fundamental material differences. Nonetheless, the overall difference in vibration attenuation between the two materials remains negligible.

These findings indicate that the PSD span, rather than solely the median particle size, is a critical determinant of vibration mitigation effectiveness in polydisperse granular materials. This assumption is further supported by a comparison of rubber powders "RP 0.8 mm" and "RP 0.5 mm". Despite its smaller median particle size, "RP 0.5 mm" exhibited superior vibration attenuation compared to "RP 0.8 mm". This discrepancy can be attributed to the wider PSD span of "RP 0.5 mm" relative to "RP 0.8 mm". A similar explanation applies to the study by Chesla et al. [80], where steel powder with a finer grain size exhibited better vibration attenuation than its coarser counterpart. However, the

authors did not identify PSD as a critical factor influencing the vibration mitigation performance of polydisperse materials.

From the above discussion, it can be concluded that the rubber granulate "RG 4.6 mm" exhibits significantly superior overall vibration mitigation performance compared to rubber powders and other rubber granulates. Furthermore, it was observed that both PSD span and median particle size are critical factors influencing the vibration attenuation performance of polydisperse granular materials. Moreover, an intriguing observation regarding the relationship between particle shape and vibration response has emerged. Figure 5.15 demonstrates that all rubber granulates significantly outperform rubber powders in reducing the test specimen's vibration amplitude. This can be attributed to the inherently rougher and more irregular surface textures of rubber granulates compared to powders. Therefore, it can be assumed that the irregular shapes of rubber granulate particles are highly effective in mitigating vibration amplitude within the primary structure. A plausible explanation lies in the increased number of contact points, interacting surfaces, and friction coefficient associated with the rough and irregular shapes of the rubber particles. This translates to enhanced damping efficiency compared to the smoother surfaces of rubber powders.

5.4.2 Hard material particle dampers (HMPDs)

The vibration response of the system, both with and without HMPDs, is shown in Figure 5.16. A notable frequency shift is observed around the first three prominent resonance peaks. This shift can be attributed to the increased mass introduced by the HMPDs, particularly evident with denser materials like lead shot, steel balls, and steel chips. Consequently, the one-third octave bands encompassing these resonant peaks are also shifted. Due to this frequency shift, one-third octave analysis is deemed unsuitable for evaluating vibration attenuation by the HMPDs. Therefore, only narrow-band spectra are presented for further analysis. However, it is important to emphasize that this frequency shift does not impact the analysis of HMPDs, as the primary focus lies on analyzing the impact of the granular materials on vibration attenuation through peak values. As stated previously, rubber granulate "RG 4.6 mm" exhibited the most significant vibration suppression among the tested materials for RRPDs. Hence, to facilitate a direct comparison, the FRF of "RG 4.6 mm" is included alongside the FRFs of the HMPDs in Figure 5.16.

It has been observed that among the investigated materials, rubber granulate "RG 4.6 mm" exhibited the greatest reduction in vibration amplitude (-9.2 dB) around the first resonance peak compared to stiffer granular materials, see Tables 5.5 and 5.6. However, near the second resonance peak, its performance became comparable to spherical lead shot particles (-11.5 dB; maroon dashed line) and plastic cylinders (-11.5 dB; deep pink dashed line), see Table 5.6. All three achieved similar vibration reduction of up to 12 dB. Notably, lead shot particles required nearly 13 times the mass of "RG 4.6 mm" to achieve this effect. This significant mass difference is further emphasized by the absence of any eigenfrequency shift in the system with "RG 4.6 mm" implementation.

At higher resonance frequencies, the performance of hard granular materials becomes more prominent. Notably, near the second resonance peak, stone powder (firebrick dotted line) and quartz powder (cyan dotted line) achieved the highest vibration reduction, reaching 19.9 dB and 16.2 dB, respectively. This trend continued near the third peak, with all three materials (plastic cylinder, stone powder, and quartz powder) demonstrating similar reductions of approximately 16 dB. Furthermore, from the fourth to the fifth resonance peaks, hard granular materials consistently outperformed "RG 4.6 mm" rubber granulate (purple dashed line) in terms of vibration mitigation. Interestingly, within the 20 Hz to 355 Hz frequency range, lead shot (maroon dashed line) and steel balls (blue dashed line) exhibited a significantly higher overall damping efficiency compared to other hard, spherical particles like plastic balls. It should be noted that across the investigated frequency range (20 Hz to 355 Hz), lead particles (maroon dashed line) demonstrated a superior overall damping performance compared to other materials. This is evident from their lower SL value (130.33 dB) compared to rubber granulate "RG 4.6 mm" (133.14 dB;

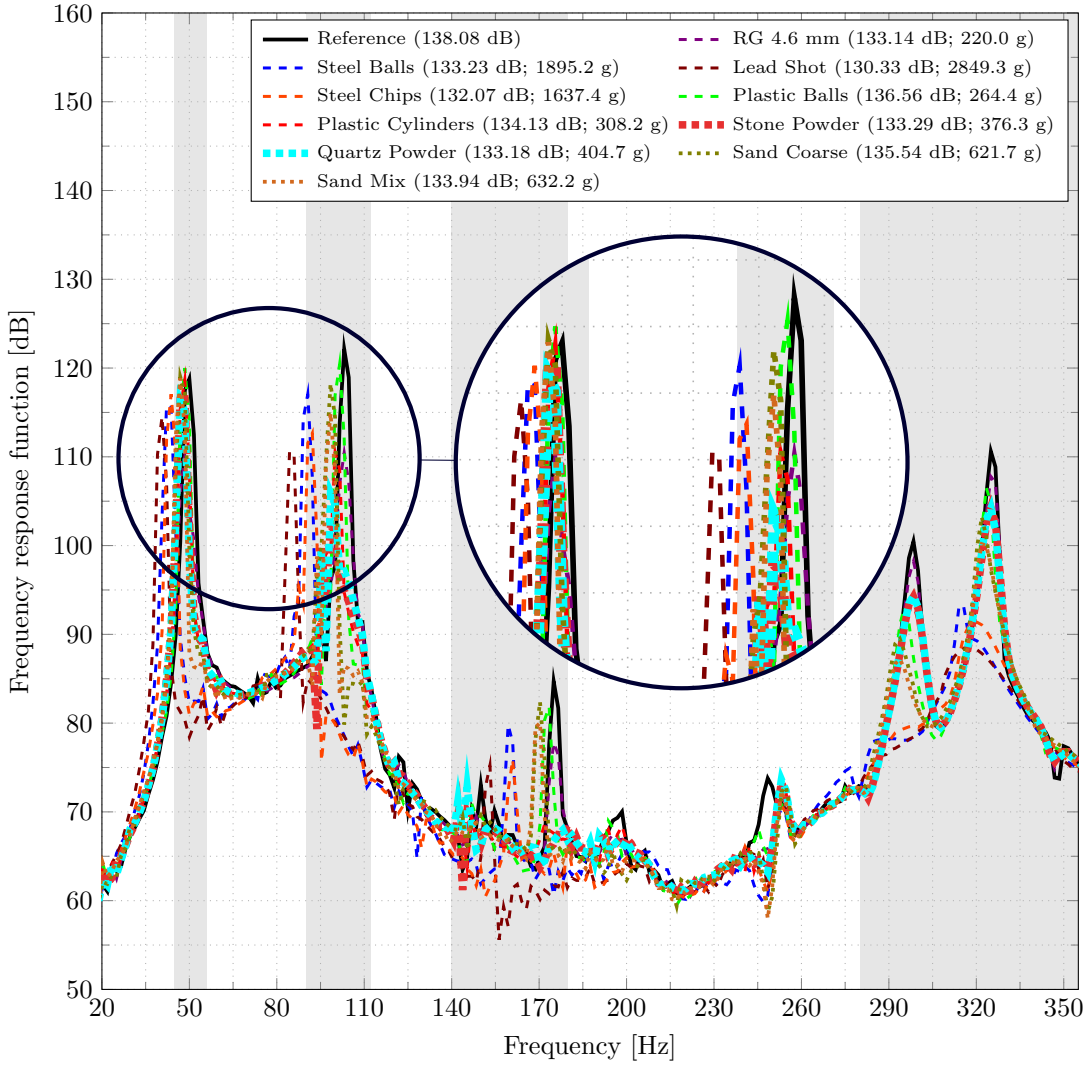

Figure 5.16: Narrowband spectrum of the test specimen with and without HMPDs. The SL value of the surface velocity is given in dB and the mass of the granular filling materials is given in g.

purple dashed line) and other hard, spherical particles such as steel balls (133.23 dB; blue dashed line), plastic balls (136.56 dB; green dashed line), and plastic cylinders (134.13 dB; deep pink dashed line).

An assessment of the overall vibration mitigation performance of various hard materials in fine particle (powder) form indicates that quartz powder (cyan dotted line) and stone powder (firebrick dotted line) exhibit superior damping effectiveness. This enhanced performance can be attributed to the higher number of particles present within the cavity. Compared to other hard materials, quartz and stone powders have a significantly smaller median particle size, resulting in a greater particle count within the same cavity volume. Consequently, the increased particle-particle and particle-wall interactions lead to a substantial enhancement in damping performance. This superior performance can be justified by the lower SL value of quartz powder (133.18 dB) and stone powder (133.29 dB) relative to sand (135.54 dB) and sand mix (133.94 dB). While stone powder and quartz powder exhibit superior vibration attenuation capabilities, their powdered form presents challenges for practical implementation in particle damper designs due to handling difficulties. Moreover, the sand mix outperforms coarse sand, likely due to the presence of shell-like particles within the mix. As these shell particles could not

Table 5.6: Vibration reduction (dB) of HMPDs at various resonance frequencies.

Material	50 Hz	103 Hz	175 Hz	298 Hz	325 Hz
Steel balls	-3.0	-5.1	-4.9	-22.6	-17.4
Lead shot	-4.3	-11.5	-9.5	-23.3	-22.2
Steel chips	-1.7	-9.4	-8.8	-21.3	-19.3
Plastic balls	1.2	-1.6	-2.9	-7.5	-4.1
Plastic cylinders	0.1	-11.5	-16.1	-6.8	-5.6
Stone powder	-2.0	-19.9	-16.2	-6.3	-6.3
Quartz powder	-2.5	-16.2	-16.7	-6.2	-6.4
Sand coarse	0.2	-3.9	-2.3	-10.9	-7.4
Sand mix	0	-7.2	-4.7	-13.3	-10.4

be isolated from the sand mix, their contribution to the overall performance cannot be determined independently. Nevertheless, this suggests a potential synergistic effect from the combined particle types.

Furthermore, plastic cylinders (134.13 dB) demonstrate significantly higher damping compared to plastic balls (136.56 dB). This can be attributed to two factors. Firstly, the particle size of plastic cylinders is smaller than plastic balls, resulting in a larger number of particles within the test specimen cavity for a given volume. This is confirmed by the particle count, where 10 g of plastic cylinders contain 302 particles compared to only 90 particles for plastic balls. Hence, the increased number of particles translates to more contact points and collisions within the cavity, leading to higher frictional losses and enhanced vibration mitigation. Secondly, particle shape can significantly impact vibration attenuation by affecting the contact area, as the contact radius between two objects is determined by their geometry and the applied load. According to Hertzian contact theory, which explains the interaction between two elastic bodies, the contact area differs for spheres and cylinders due to their distinct shapes [204].

For instance, when two elastic spheres of radii R_1 and R_2 are brought into contact under a compressive force F, the resulting circular contact area has a radius a, which can be calculated as follows [205]

$$a = \sqrt[3]{\frac{3\,F R_{\text{eff}}}{4E^*}}, \tag{5.7}$$

where R_{eff} represents the effective or equivalent radius, calculated as

$$R_{\text{eff}} = \frac{1}{R_1} + \frac{1}{R_2}. \tag{5.8}$$

The expression for E^* is given as follows when both bodies are elastic

$$E^* = \frac{1-\nu_1^2}{E_1} + \frac{1-\nu_2^2}{E_2}. \tag{5.9}$$

In Eq. 5.9, E_1 and E_2 denote the Young's moduli of spheres 1 and 2, respectively, while ν_1 and ν_2 represent their corresponding Poisson's ratios.

In case of cylinders, if two circular cylinders with radii R_1 and R_2 are compressed axially by a line load of magnitude F, their contact region assumes a rectangular profile with half-width b determined by

$$b = \sqrt[2]{\frac{4\,F l R_{\text{eff}}}{\pi E^*}}, \tag{5.10}$$

where, l denotes the length of the cylinders when they are in line contact.

In the case of the plastic spheres used in this thesis, both have the same radius of 3.0 mm. Therefore, according to Eq. 5.8, the effective radius for the spheres is calculated to be 1.5 mm. On the other hand, for the cylindrical particles with a radius of 2.0 mm, the effective radius is determined to be 1.0 mm. Without delving into specific details about the forces applied or the material parameters, it can be stated that the contact area for the cylinder-cylinder interaction is substantially larger than that of the sphere-sphere contact. This is primarily due to the additional length factor ($l = 4.7$ mm) introduced in Eq. 5.10.

Even though the effective radius of the spheres is slightly greater than that of the cylinders, the longer contact line formed between the cylinders leads to a larger overall contact area, and consequently, a larger contact radius in general. However, this observation holds true only when the two cylinders are in contact with their axes aligned parallel to each other. If the axes of the two cylinders are inclined or non-parallel, the resulting contact area and the effective contact radius can vary significantly [205]. A schematic representation illustrating the contact points and contact lines for spherical-spherical, cylinder-cylinder, and disc-disc geometries is presented in Figure 5.17.

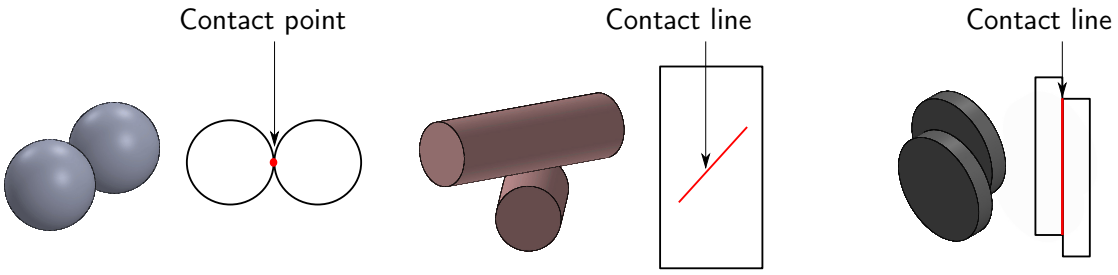

Figure 5.17: Schematic illustration of the contact points and lines for various geometrical shapes.

The aforementioned reasoning accounts for the superior damping performance observed with plastic cylinders (SL value 134.13 dB) compared to plastic balls (SL value 136.56 dB). Apart from this, the plastic cylinder and plastic balls are made up of different kinds of plastic material that has also an effect on vibration attenuation.

A comparison between steel spherical particles (indicated by the blue dashed line) and the flat shape of steel chips (represented by the orange dashed line) further supports the notion that particle shape plays a crucial role in vibration attenuation, see Figure 5.16. Notably, it was observed that a sample containing 10 g of steel balls consists of approximately 30 individual particles, whereas the same mass of steel chips contains around 200 particles. As a result, the test specimen cavity contains higher number of steel chips compared to steel balls for the specified filling volume. Thus, the vibration attenuation provided by the steel chips is greater than that of the steel balls. The relationship between a higher number of particles and increased vibration mitigation has already been discussed above.

Moreover, it is important to highlight that the total mass of the steel chips is 257.8 g less than that of the steel balls. Despite this higher mass, the steel balls demonstrate less effectiveness in vibration mitigation compared to the steel chips. This finding emphasizes that mass alone is not the sole factor influencing the reduction of vibrations within a structure. This conclusion aligns with the findings of Duvigneau et al. [149], who conducted an experiment involving an oil pan filled with equal masses of sand and water. Their study revealed that sand was significantly more effective than water in reducing the vibration amplitude of the oil pan.

In addition, the contact surface area between two steel chips may be significantly larger compared to that between two steel balls (refer to Figure 5.17), which is also a key factor influencing the energy dissipation mechanism in particle dampers.

5.4.3 Hybrid particle dampers (HPDs)

Based on the results of RRPDs and HMPDs testing, the HPDs have been designed to enhance the vibration attenuation of structures. The HPDs combines the energy dissipation properties of two distinct granular materials. For instance, soft, lightweight materials like rubber granulate (e.g., "RG 4.6 mm") are combined with high-density spherical particles (e.g., lead). The concept behind the HPDs is to leverage the damping efficiencies of both RRPDs and HMPDs, thereby enhancing the overall vibration attenuation of the test specimen compared to a particle damper using a single type of granular material. Additionally, the design of HPDs focuses on reducing the total mass of the granular media compared to dampers made exclusively of HMPDs. The effectiveness of the HPDs in reducing vibration amplitude is demonstrated in Figures 5.18 - 5.20.

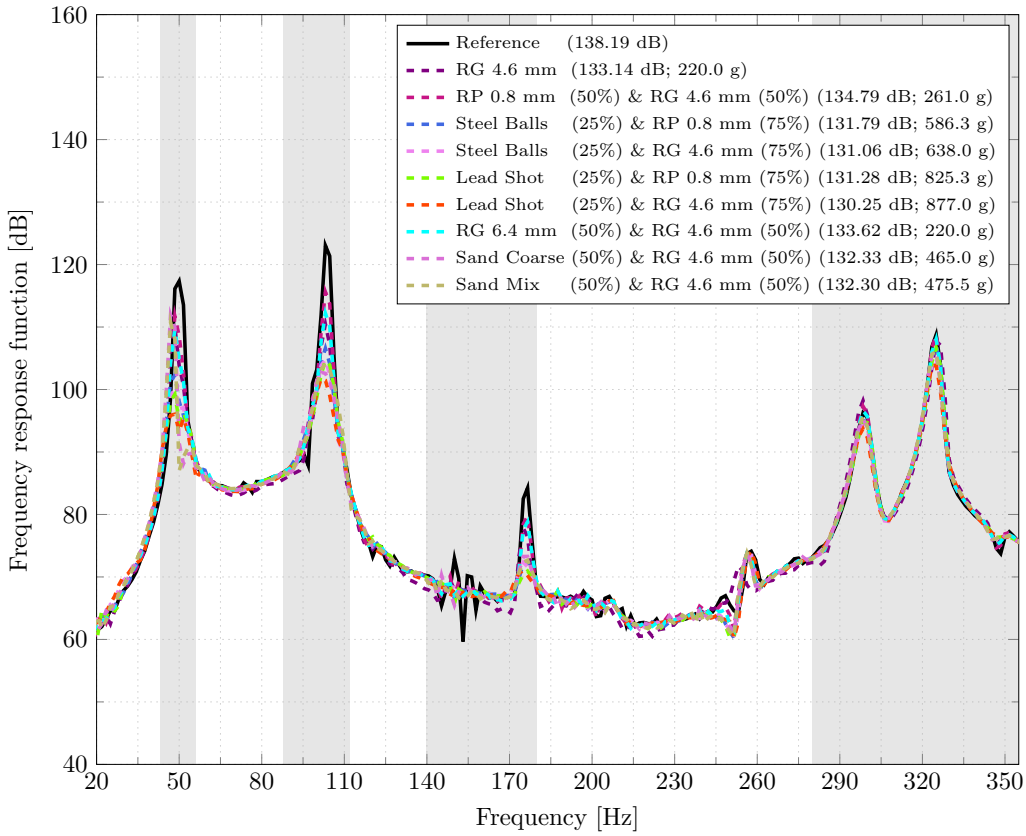

Figure 5.18: Narrowband spectrum of the test specimen with and without HMPDs. The SL values of the surface velocity are given in dB and the mass of the granular filling materials is given in g.

Prior investigations identified lead shot (130.33 dB) as the most effective granular material for vibration attenuation in the HMPDs category. Similarly, rubber granulate "RG 4.6 mm" exhibited exceptional vibration mitigation characteristics among the tested materials in the RRPDs category. To harness the potential of these findings, an HPD design was formulated by combining lead shot and steel balls with rubber granulate "RG 4.6 mm". This configuration aimed to assess the impact of this high-performing mixture on the system's vibration response (see Figure 5.9 (c)-(d)).

Conversely, rubber powder "RP 0.8 mm" demonstrated the lowest damping efficiency within the RRPDs category. To explore the influence of a poorly performing soft material, "RP 0.8 mm" was incorporated into hybrid dampers with both lead shot and steel balls. This design was employed to investigate the damping behavior of HPDs when a low-performing material from the RRPDs category

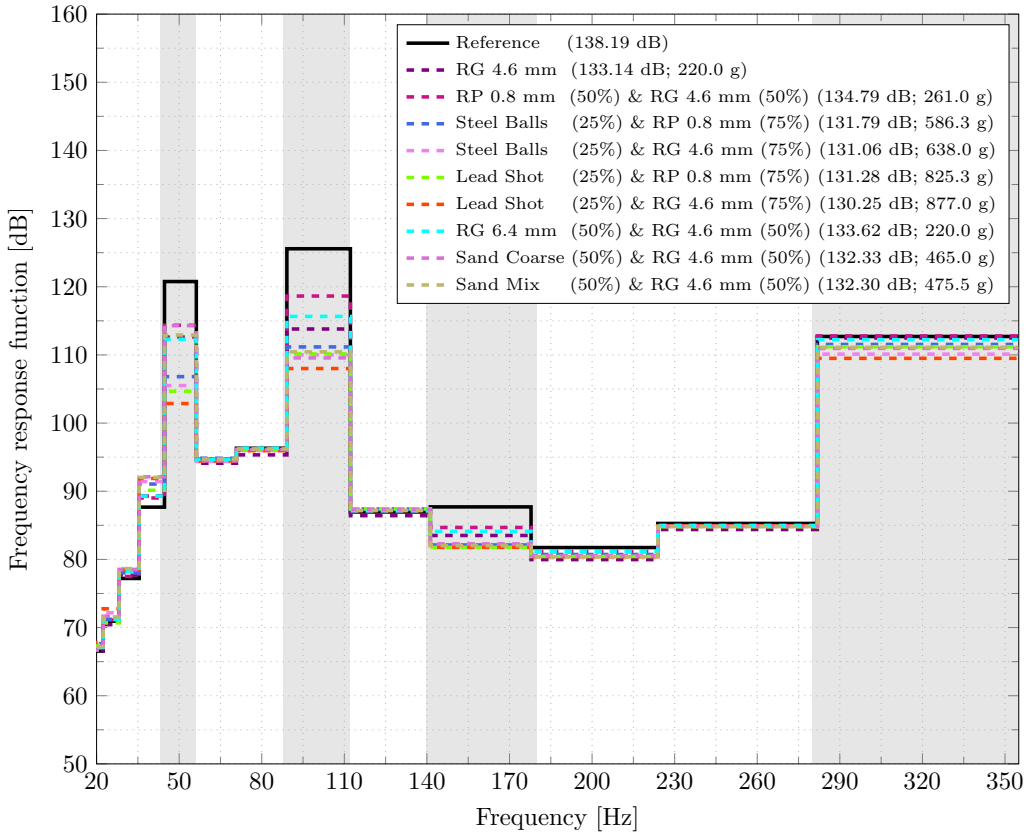

Figure 5.19: One-third octave band spectrum of the test specimen with and without HPDs. The SL values of the surface velocity are given in dB and the mass of the granular filling materials is given in g.

is combined with high-performing materials from the HMPDs category. Furthermore, the second-least performing hard material in the fine particle form (sand) was combined with the high-performing soft material, "RG 4.6 mm". Additionally, a mixture solely composed of "RP 0.8 mm" and "RG 4.6 mm" was evaluated (see Figure 5.9 (a)). Moreover, the rubber granulate "RG 6.4 mm" reduces the vibration amplitude of the test specimen in a very similar fashion as the rubber granulate "RG 4.6 mm", see Figure 5.15. Therefore, another mixture of these two soft materials has been also experimentally investigated.

The selection of material ratios within the HPDs considered practical limitations. Since excessive granular material mass can be detrimental in some industrial applications, a $75\%/25\%$ volume ratio of soft to hard materials was implemented for most mixtures. Notably, the mass of sand is significantly lower (approximately three to four times) compared to steel balls and lead shot. Therefore, a $50\%/50\%$ sand and "RG 4.6 mm" mixture was employed. A similar $50\%/50\%$ ratio was used for the soft-only mixture of "RP 0.8 mm" and "RG 4.6 mm". As discussed previously, the rubber granulate "RG 4.6 mm" has been the favorable granular material for the particle damper design due to its damping and lightweight property. Therefore, for comparison purpose, the FRF of the "RG 4.6 mm" has been also plotted along with the HPDs.

All investigated HPDs effectively reduced vibration amplitude across the test specimen's resonance frequencies (see Figure 5.19). The HPD containing 25% lead shot and 75% rubber granulate "RG 4.6 mm" achieved the most significant reductions. This combination achieved vibration reduction up to 18 dB around the first two resonance frequencies (50 Hz and 100 Hz), see Figure 5.20. Notably,

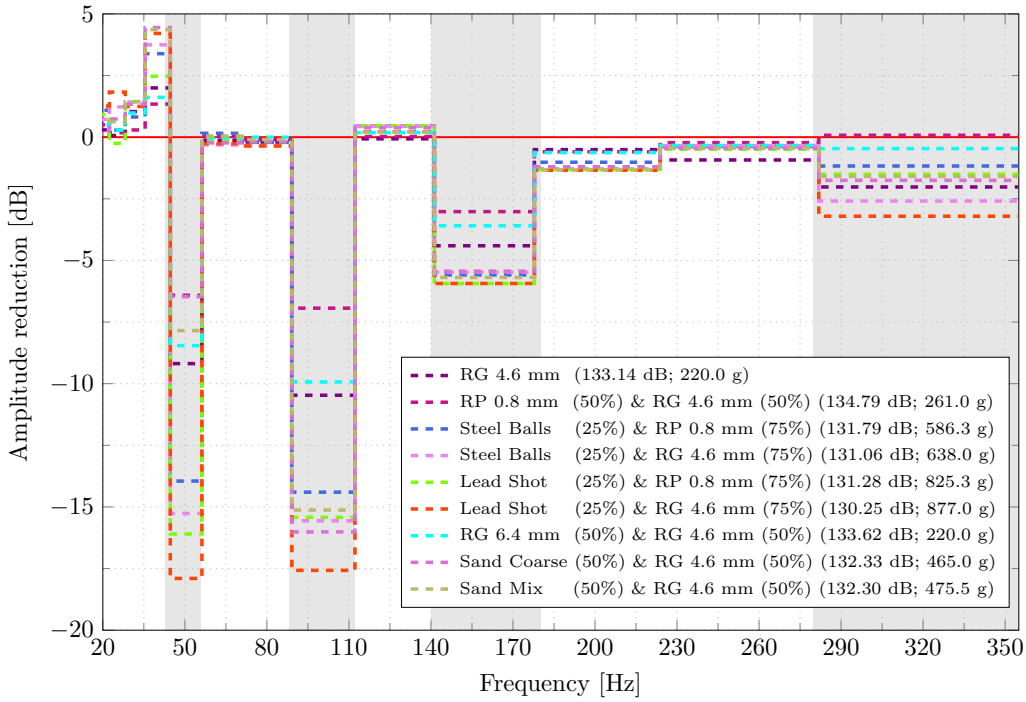

Figure 5.20: Amplitude reduction plot of the test specimen with and without HPDs. The SL values of the surface velocity are given in dB and the mass of the granular filling materials is given in g.

even at higher resonance frequencies (third and fourth), reductions of 6 dB and 3 dB were observed, respectively, surpassing the performance of the RRPD consisting of rubber granulate "RG 4.6 mm".

Around the first three resonance frequencies, the mixture of lead shot and steel balls with rubber granulate and rubber powder shows significantly higher damping efficiency in comparison to the particle damper with the rubber granulate "RG 4.6 mm". Moreover, the findings indicate that combining hard spherical particles (like lead shot or steel balls) with rubber granulate results in a superior vibration reduction performance compared to mixtures of these particles with rubber powder. This improvement is particularly noticeable around the central frequencies of 50 Hz, 100 Hz, and 315 Hz, as illustrated in Figures 5.19 - 5.20. Nevertheless, the vibration attenuation capabilities of both types of mixtures are nearly identical around the central frequency of 160 Hz.

For HPDs made with sand (coarse or mixed) and "RG 4.6 mm" rubber granulate, both mixtures demonstrate very similar vibration attenuation with minimal differences. It is important to note that quartz powder and stone powder were not included in these HPDs, even though they are the best-performing materials in powder form for HMPDs. The reason for this is that mixing these powders with rubber powder or rubber granulate is impractical, as it would be extremely difficult to separate them after the experiment.

The present investigation into HPDs suggests that incorporating hard, spherical particles with irregularly shaped rubber granulate demonstrated enhanced vibration damping. This is primarily attributed to the viscoelastic deformation induced in the rubber particles during impact with the hard particles. While a similar phenomenon occurs when rubber powder is used, its damping effectiveness is slightly lower due to the lack of irregular shapes in the powder. Additionally, the adhesive forces between the fine rubber powder particles and the metallic spheres can potentially form an outer layer, altering the particle deformation and collision behavior. This could impact the overall vibration attenuation capability. In conclusion, the viscoelastic deformation of the rubber component, whether granulate or powder, is

a key factor in the improved damping performance of HPDs. The irregular shape of the granulate appears to contribute to enhanced damping compared to powder. The vibration attenuation of each HPD around central frequencies is summarized in Table 5.7.

Table 5.7: Vibration reduction (dB) of HPDs at various resonance frequencies.

Mixture	50 Hz	100 Hz	160 Hz	315 Hz
RP 0.8 mm (50%) & RG 4.6 mm (50%)	-6.4	-6.9	-3.0	0.1
Steel balls (25%) & RP 0.8 mm (75%)	-13.9	-14.4	-5.6	-1.2
Steel balls (25%) & RG 4.6 mm (75%)	-15.3	-15.6	-5.5	-2.6
Lead shot (25%) & RP 0.8 mm (75%)	-16.1	-15.4	-5.9	-1.5
Lead shot (25%) & RG 4.6 mm (75%)	-17.9	-17.6	-5.9	-3.2
RG 6.4 mm (50%) & RG 4.6 mm (50%)	-8.5	-9.9	-3.6	-0.5
Sand coarse (50%) & RG 4.6 mm (50%)	-6.5	-16.0	-5.4	-1.7
Sand mix (50%) & RG 4.6 mm (50%)	-7.8	-15.1	-5.7	-1.6

5.4.4 HPDs with constant mass

In the previous section, the vibration mitigation performance of HPDs with a constant filling ratio (80%) was examined. However, due to differences in material bulk densities, the mass of each mixture varied. Consequently, in this section, the HPD containing a specific mixture will be evaluated under a constant mass.

To accomplish this, the mass of the granular material in the HPDs was set to 300 g. This mass was selected to ensure that the cavity filling ratio remained below 100%, as it is well known that a filling ratio of 100% can reduce the effectiveness of a particle damper. This reduction occurs because the minimal gap within the cavity restricts the movement of the granular material, which is essential for the proper functioning of particle dampers. Another reason for selecting this specific mass was that it ensured an adequate quantity of hard material particles, such as lead shot and steel balls, within the cavity. A minimum amount of hard particles is crucial for a significant reduction in vibration amplitude, which is effectively achieved with a 300 gram mass.

For this investigation, a mixture of rubber granulate "RG 4.6 mm" and lead spherical particles was selected due to its superior vibration mitigation capability observed previously. Five different ratios of this mixture were formulated to design the HPD, see Table 5.8. In each mixture, the mass of the rubber granulate was increased by 50 g, while the mass of the lead shot was simultaneously reduced by 50 g. It is important to note that, although the material ratios varied, the total mass of the mixture remained constant. This approach was explored to assess how the quantity of metal particles affects the vibration mitigation performance of the HPD. Furthermore, to compare the performance of HPDs, HMPDs, and RRPDs under a constant mass, the vibration mitigation of individual materials, such as rubber granulate "RG 4.6 mm," lead shot, and steel balls, was also evaluated at 300 g. These materials were selected because they demonstrated superior performance compared to others tested materials within their respective categories. The vibration amplitude reduction values for these materials and their mixtures are provided in the Table. 5.8.

The narrow-band spectrum, one-third octave band, and the difference plot for these measurements are presented in the Appendix (see Figures A1.1 - A1.3). The FRFs plot shows slight differences in the number and values of resonance peaks compared to the previously discussed system. These discrepancies are likely due to minor, unavoidable variations introduced when replicating the experimental setup after a considerable time interval, which can result in shifts in the resonance spectrum. It is important to emphasize that changes in the number of resonance frequencies will not affect the current investigation, as the resonance peaks of the reference test specimen and the specimens with RRPDs, HMPDs, and HPDs remain consistent.

Table 5.8: Vibration reduction (dB) of HPDs at a constant mass.

Material	53 Hz	198 Hz	337 Hz
RG 4.6 mm (300 g)	11.7	8.5	3.5
Lead shot (300 g)	7.4	6.9	2.7
Steel balls (300 g)	6.3	5.9	2.8
RG 4.6 mm (50 g) & Lead Shot (250 g)	15.2	7.4	2.1
RG 4.6 mm (100 g) & Lead Shot (200 g)	12.6	6.3	2.2
RG 4.6 mm (150 g) & Lead Shot (150 g)	14.2	8.1	2.9
RG 4.6 mm (200 g) & Lead Shot (100 g)	9.3	8.1	2.7
RG 4.6 mm (225 g) & Lead Shot (75 g)	11.0	9.0	3.4

As evident from the Table. 5.8, rubber granulate "RG 4.6 mm" exhibits a significantly higher reduction in vibration amplitude compared to lead shot and steel balls. The combination of rubber granulate "RG 4.6 mm" (50 g) and lead spheres (250 g) demonstrates the most effective vibration reduction, particularly around the first resonance peak (53 Hz). This effect was superior to other mixing ratios of rubber granulate "RG 4.6 mm" and lead shots tested. Moreover, for the second resonance peak, the mixture containing 225 g of "RG 4.6 mm" and 75 g of lead shot exhibits a significantly higher vibration attenuation efficiency compared to all other HPDs at constant mass and individual materials, like rubber granulate "RG 4.6 mm", steel balls and lead shot. Interestingly, the vibration mitigation of "RG 4.6 mm" itself approaches that of the aforementioned mixture around this peak. A comparable trend has been noted around the third resonance peak, where the vibration reduction value of the rubber granulate "RG 4.6 mm" is slightly higher than that of the other material mixtures, except for the mixture containing 225 g of "RG 4.6 mm" and 75 g of lead shot, which exhibit similar vibration mitigation values.

While the results from the HPDs at a fixed mass provide valuable insights, it is crucial to acknowledge the limitations. Identifying the optimal mixing ratio for broad-band vibration attenuation likely requires extensive experimental investigations. This need for numerous experiments can potentially be mitigated through a well-developed FEM - DEM coupling strategy. However, as discussed in Chapter 2, numerical simulations of particle dampers face significant limitations, with particle shape posing a particular challenge for both DEM and FEM-DEM simulations. However, determining the optimal mixing ratio is a complex challenge that requires further in-depth experimental investigation. Such an in-depth study falls outside the scope of the current thesis, which primarily focuses on the initial exploration of the potential benefits and limitations of HPDs.

5.5 Mass-specific vibration attenuation

Previous sections explored the vibration attenuation characteristics of various materials with a fixed filling ratio of 80%. The results demonstrated that rubber granulate "RG 4.6 mm" exhibited significantly superior overall vibration reduction compared to other rubber granulates and rubber powders. However, for higher frequencies (approximately 175 Hz, 298 Hz, and 325 Hz), HMPDs incorporating granular materials like lead shot, steel balls, steel chips, plastic balls, stone powder, and quartz powder displayed notable vibration attenuation capabilities. It is important to acknowledge a trade-off between the high damping performance of HMPDs and their practical limitations. The increased mass of HMPDs, compared to RRPDs, can be a disadvantage in applications prioritizing lightweight design. To address this, a combined analysis of both the absolute damping value and the mass-specific damping value for each granular material is necessary. Mass-specific vibration attenuation refers to the reduction in vibration amplitude of a structure achieved by a given material per gram. This will establish a comprehensive ranking of their vibration attenuation effectiveness, facilitating the optimal selection of granular materials for specific applications based on the desired balance between damping performance

and weight constraints.

5.5.1 Recycled rubber particle dampers

Table 5.9 provides an overview of the mass-specific vibration reduction values for RRPDs. Notably, the rubber granulate "RG 4.6 mm" exhibits superior performance across all resonance frequencies when compared to other rubber granulates. Interestingly, at the central frequencies of 50 Hz and 100 Hz, the mass-specific attenuation of "RG 6.4 mm" approaches that of "RG 4.6 mm," suggesting a noteworthy overlap in performance at these specific frequencies.

This observation aligns with the trends in absolute vibration attenuation for RRPDs discussed in Section 5.4.1, where it was noted that vibration mitigation generally increases with both the median particle size and the width of the PSD of the rubber granulates. However, a threshold effect appears to be present, as "RG 4.6 mm" achieves peak mass-specific attenuation before a decline is observed at larger particle sizes. This phenomenon has also been noted in relation to absolute vibration values, with previous discussions highlighting the connection between this threshold effect and the PSD width.

Importantly, "RG 6.4 mm" manages to maintain mass-specific attenuation levels that are comparable to those of "RG 4.6 mm" at the central frequencies of 50 Hz and 100 Hz, further reinforcing the similarities in their performance.

Table 5.9: Mass-specific vibration reduction (dB/g) of RRPDs at various resonance frequencies.

RRPDs	50 Hz	100 Hz	160 Hz	315 Hz	Material
RG 6.4 mm	-0.0418	-0.0477	-0.0173	-0.0073	
RG 5.1 mm	-0.0415	-0.0455	-0.0185	-0.0085	
RG 4.7 mm	-0.0340	-0.0375	-0.0185	-0.0085	
RG 4.6 mm	-0.0418	-0.0477	-0.02	-0.0090	ELT
RG 3.6 mm	-0.0378	-0.0438	-0.0195	-0.0086	
RG 2.4 mm	-0.0405	-0.0394	-0.0189	-0.0086	
RG 2.3 mm	-0.0337	-0.0343	-0.0177	-0.0072	
RP 0.8 mm	-0.0325	-0.0325	-0.0179	-0.0066	ELT
RP 0.5 mm	-0.0343	-0.0403	-0.0224	-0.0079	
RG 3.0 mm	-0.0336	-0.0436	-0.02	-0.0082	EPDM
RG 2.2 mm	-0.0342	-0.0400	-0.0184	-0.0074	

The analysis of mass-specific vibration attenuation for RPs reveals a trend that is closely aligned with the findings regarding absolute attenuation. Specifically, this trend demonstrates that "RP 0.5 mm" has a higher mass-specific vibration reduction value compared to "RP 0.8 mm." This relationship indicates that, much like the trends observed in RG, RPs with a larger PSD span (such as "RP 0.5 mm") are more effective at reducing vibration amplitude. This enhanced capability contributes to greater efficiency in diminishing vibration amplitude per gram of material. These results underscore the significance of PSD in determining the performance of RPs for both absolute and mass-specific vibration attenuation.

The trend observed for mass-specific vibration reduction in EPDM RGs mirrors the trend noted for their absolute vibration reduction values. This correlation again suggests that RGs with a larger PSD are generally more effective at reducing the vibration amplitude of the structure per gram of material. However, an exception to this trend occurs at the frequency of 50 Hz, where the mass-specific vibration reduction value for "RG 3.0 mm" is slightly lower than that of "RG 2.2 mm.

From the preceding discussion, it can be concluded that the trends identified in both absolute and mass-specific vibration attenuation within RRPDs exhibit a notable degree of similarity. Hence, understanding these similarities can provide valuable insights into optimizing the design and application of RRPDs for effective vibration mitigation.

5.5.2 Hard material particle damper

An intriguing divergence can be noted when comparing the trends for absolute vibration attenuation and mass-specific vibration attenuation in HMPDs. In the case of absolute vibration reduction, lead shot emerges as the most effective option, outperforming other types of HMPDs consisting of monodisperse materials, as detailed in section 5.4.2. However, when it comes to mass-specific attenuation, the scenario changes significantly. In this context, plastic balls and cylinders exhibit superior performance compared to other monodisperse granular materials. This performance disparity is clearly illustrated in Table 5.10, highlighting the unique effectiveness of plastic materials in achieving enhanced mass-specific vibration attenuation within monodisperse HMPDs. Within the realm of plastic materials, the trend associated with mass-specific vibration attenuation closely mirrors the trend that is observed in the absolute vibration attenuation of these same materials.

The superior mass-specific performance of plastic balls and cylinders in HMPDs compared to lead shot can be attributed to two primary factors: bulk density and material properties. Lead shot possesses a significantly higher bulk density than plastic balls and cylinders. This higher density results in a lower number of lead particles per gram when compared to their plastic counterparts. Since the number of particles directly influences the frequency of impact interactions with the surrounding structure, a reduced particle count inherently diminishes the overall vibration attenuation capability of lead shot.

In contrast, plastic balls and cylinders exhibit distinct material properties that enhance their performance in vibration attenuation. Specifically, plastic balls, due to their lighter weight, require lower frequencies to overcome their inertia and initiate movement. This characteristic contributes to their effectiveness at lower resonance frequencies, approximately around 50 Hz. On the other hand, plastic cylinders necessitate a higher threshold frequency to overcome their moment of inertia. As a result, plastic cylinders demonstrate superior performance at elevated frequencies, specifically at 103 Hz and 175 Hz. Notably, as the frequency increases further to 298 Hz and 325 Hz, the mass-specific damping performance of both plastic balls and cylinders becomes comparable. This suggests that while each material excels in different frequency ranges, their effectiveness in mass-specific vibration attenuation converges at higher frequencies, highlighting the unique advantages of plastic materials in various vibration mitigation applications within HMPDs.

Table 5.10: Mass-specific vibration reduction (dB/g) of HMPDs at various resonance frequencies.

Material	50 Hz	103 Hz	175 Hz	298 Hz	325 Hz
Steel balls	-0.0016	-0.0027	-0.0026	-0.0119	-0.0092
Lead shot	-0.0015	-0.0040	-0.0033	-0.0082	-0.0078
Steel chips	-0.0010	-0.0057	-0.0054	-0.0130	-0.0118
Plastic balls	0.0045	-0.0061	-0.0109	-0.0284	-0.0155
Plastic cylinders	0.0003	-0.0373	-0.0522	-0.0221	-0.0182
Stone powder	-0.0053	-0.0529	-0.0431	-0.0166	-0.0167
Quartz powder	-0.0062	-0.0400	-0.0413	-0.0153	-0.0158
Sand coarse	0.0003	-0.0063	-0.0037	-0.0175	-0.0119
Sand mix	0	-0.0114	-0.0074	-0.0210	-0.0165

In HMPDs that utilize powders and fine particles, such as stone powder, sand, and quartz powder, a strong correlation is evident between the trends of absolute vibration attenuation and mass-specific vibration attenuation. Specifically, at the resonance frequency of 50 Hz, quartz powder demonstrates the highest vibration reduction value per gram among these materials, which aligns closely with the observed behavior of absolute vibration attenuation. This indicates that quartz powder not only excels in absolute terms but also maintains efficiency on a mass-specific basis.

The relationship between absolute and mass-specific vibration attenuation continues to be observed at higher frequencies. At 103 Hz, for instance, stone powder exhibits a superior mass-specific mitigation value compared to other powdered materials, effectively mirroring the trends seen in absolute vibration

attenuation. As the frequency increases further, the trend persists. Around 175 Hz, both stone powder and quartz powder show comparable performance in terms of vibration reduction, demonstrating similar efficacy in both absolute and mass-specific damping scenarios. Likewise, at frequencies of 298 Hz and 325 Hz, a sand mixture reveals analogous vibration reduction characteristics, reinforcing the correlation between absolute and mass-specific attenuation. Finally, at the resonance frequency of 352 Hz, the mass-specific mitigation performance of sand and stone powder becomes comparable.

5.5.3 Hybrid particle damper

A noteworthy discrepancy arises when examining the trends of absolute and mass-specific vibration attenuation in HPDs. Specifically, while the HPD composed of 25% lead shot and 75% "RG 4.6 mm" exhibits superior performance in terms of absolute vibration reduction, as previously discussed, the mass-specific attenuation presents a different trend, see Table 5.11.

In this context, it is observed that the HPD comprising 50% "RG 4.6 mm" and 50% "RG 6.4 mm" outperforms all other HPDs in terms of mass-specific vibration attenuation. This finding highlights the complexity and variability in the performance of HPDs, emphasizing that while lead shot may be more effective for absolute vibration reduction, the composition of rubber granulates yields a more favorable outcome when evaluated on a mass-specific basis. Such discrepancies underscore the necessity of considering both absolute and mass-specific metrics when assessing the overall effectiveness of HPDs for vibration mitigation applications, as the optimal material composition can vary significantly depending on the performance criterion being examined.

Table 5.11: Mass-specific vibration reduction (dB/g) of HPDs at various resonance frequencies.

Mixture	50 Hz	100 Hz	160 Hz	315 Hz
RP 0.8 mm (50%) & RG 4.6 mm (50%)	-0.0245	-0.0266	-0.0116	0.0003
Steel balls (25%) & RP 0.8 mm (75%)	-0.0237	-0.0246	-0.0095	-0.0019
Steel balls (25%) & RG 4.6 mm (75%)	-0.0239	-0.0244	-0.0086	-0.0041
Lead shot (25%) & RP 0.8 mm (75%)	-0.0195	-0.0187	-0.0072	-0.0018
Lead shot (25%) & RG 4.6 mm (75%)	-0.0204	-0.0200	-0.0068	-0.0037
RG 6.4 mm (50%) & RG 4.6 mm (50%)	-0.0384	-0.0451	-0.0163	-0.0021
Sand coarse (50%) & RG 4.6 mm (50%)	-0.0139	-0.0344	-0.0116	-0.0038
Sand mix (50%) & RG 4.6 mm (50%)	-0.0165	-0.0318	-0.0119	-0.0033

This divergence in vibration attenuation trends can be potentially explained by the fact that the concentration of metal particles, such as lead shot or steel balls, in a single gram of this particular mixture may be minimal or even negligible. Despite this low overall mass contribution, it is important to note that at the resonance frequency of 315 Hz, the HPD composed of 25% steel balls and 75% rubber granulate "RG 4.6 mm" demonstrates the highest mass-specific reduction value.

This finding indicates that the presence of metal particles can still exert a significant influence on vibration attenuation performance at specific frequencies, highlighting the complex interactions within the material mixture. Even when the overall number of metal particles is relatively low, their impact on mass-specific vibration reduction can become pronounced under certain conditions. Thus, this underscores the importance of considering the frequency-dependent effects of different material compositions when evaluating the effectiveness of HPDs in mitigating vibrations.

5.6 Further results

It has been observed how selection of granular materials can influence the performance of a particle damper. Nevertheless, once granular material has been selected there are several other design

parameters, which can influence particle damper vibration mitigation capability. This section focuses on two key parameters, namely: filling ratio and moisture effects. The filling ratio plays a critical role in determining the capability of vibration attenuation, as well as contributing additional mass to the system. This aspect is particularly significant for industries where maintaining a lightweight product is a crucial requirement. In addition to the filling ratio, moisture levels can also pose significant concerns during operation, especially in harsh environments or throughout the manufacturing process. Therefore, it is essential to thoroughly examine both parameters within the context of the current setup.

While the influence of filling ratio on vibration attenuation has been investigated in several studies [8, 146, 158], its dependency on specific applications and the geometry of the test specimens warrants a dedicated analysis for the setup presented here. Furthermore, the impact of moisture on the performance of particle dampers in real-world scenarios remains largely underexplored in the existing literature. To begin addressing this, a preliminary experimental investigation was conducted to evaluate the effect of moisture on damper efficiency.

5.6.1 Filling level evaluation

It has been established that the rubber granulate "RG 4.6 mm" exhibited a significant reduction in system vibration response. Therefore, this study focuses on the influence of filling level with this specific rubber granulate. To achieve this, the mass of "RG 4.6 mm" particles within the cavity was progressively increased until near-complete (approximately 100%) filling was achieved. The vibration response of the test specimen for each filling level is presented in Figures 5.21 - 5.23.

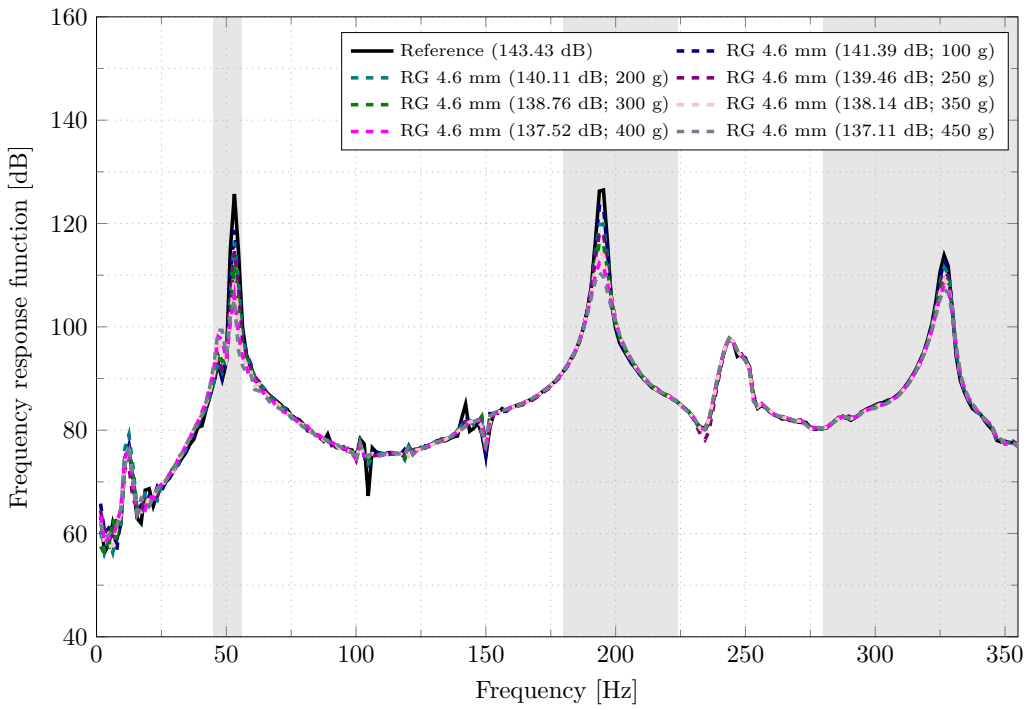

Figure 5.21: Narrow band spectrum of test specimen filled with rubber granulate "RG 4.6 mm"at different filling ratios. The SL values of the surface velocity are given in dB.

The current test system shows slight differences in both the number and magnitude of resonance peaks compared to the FRFs of RRPDs, HMPDs, and HPDs at constant volume. These discrepancies are likely due to minor, unavoidable variations that occurred when replicating the experimental setup after a considerable time gap. Such differences can result in changes to the resonance spectrum. To ensure

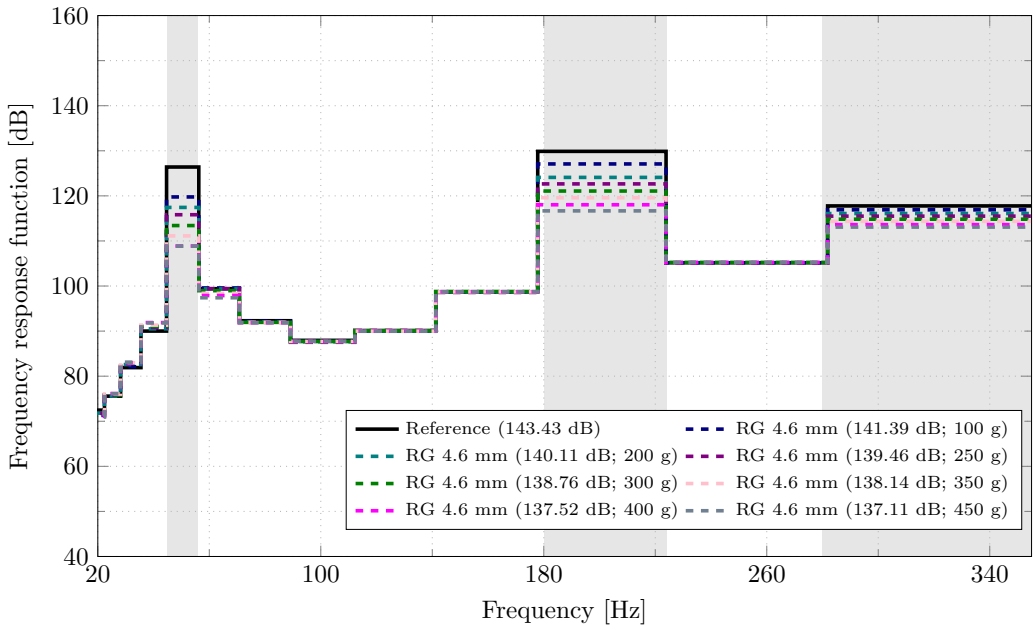

Figure 5.22: One-third octave band of test specimen filled with rubber granulate "RG 4.6 mm" at different filling ratios. The SL values of the surface velocity are given in dB.

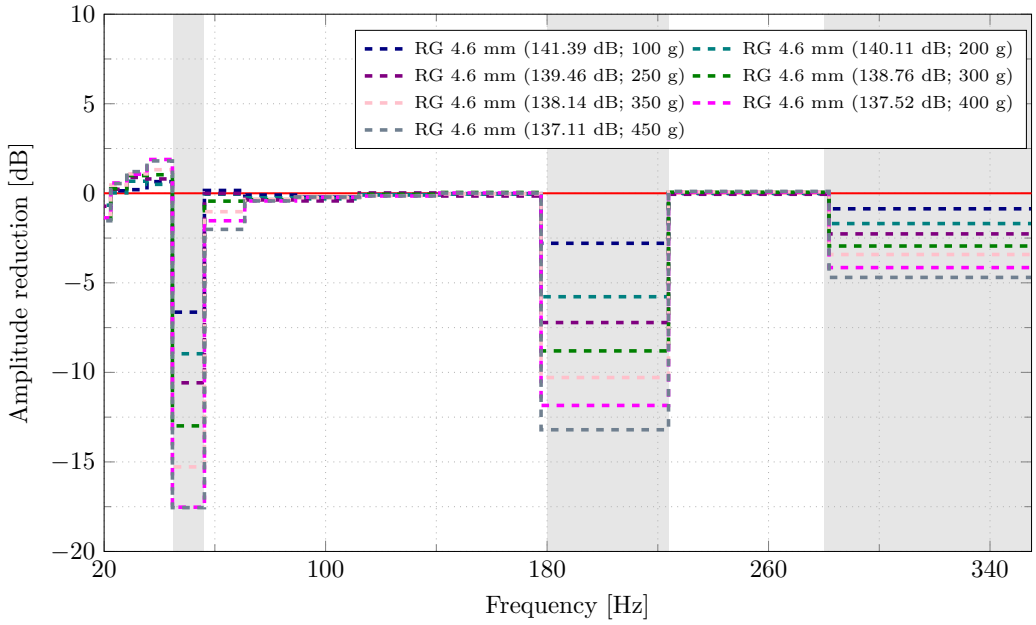

Figure 5.23: Amplitude reduction plot of test specimen filled with rubber granulate "RG 4.6 mm" at different filling ratios. The SL values of the surface velocity are given in dB.

the robustness of the current setup, repeatability tests were conducted, even though the design mirrors the one detailed in Section 5.3. The results of these tests provided strong evidence for the reliability of the experimental configuration. The fact that there might be a different number of resonance frequencies won't affect our current study. This is because the frequency spectra of the reference test specimen and the one filled with rubber granulate "RG 4.6 mm" are the same, since the resonance peaks occur at the same frequencies. To investigate the impact of the filling ratio on the system's

response, the mass of the filling material was gradually increased in the following increments: 100 g, 200 g, 250 g, 300 g, 350 g, 400 g, and 450 g. In this case, 400 g of rubber granulate represents the full 100% filling volume.

At the first resonance frequency (53 Hz), a clear trend is observed in the vibration attenuation capability of the rubber granulate "RG 4.6 mm," which improves as the mass of the granulate is increased from 100 g to 400 g. This improvement can be attributed to the corresponding increase in the number of rubber particles. As the mass of the rubber granulate increases, so does the particle count, leading to a greater likelihood of particle-particle and particle-wall collisions. These collisions play a crucial role in dissipating vibrational energy, thereby enhancing vibration reduction as the material mass increases. Beyond this point, however, there is no further reduction in vibration amplitude, meaning that the vibration mitigation provided by 450 g of rubber granulate is essentially the same as that provided by 400 g. This indicates a threshold in effectiveness at this frequency, after which additional material does not contribute to further attenuation.

Interestingly, a continuous reduction in vibration is observed around the second resonance peak (195 Hz), despite the diminishing effect seen at other frequencies. This behavior may be attributed to the absence of a cavity lid. The presence of a lid eliminates internal gaps, restricting the movement of granular materials and thereby reducing their effectiveness. However, in the current experimental setup, which lacks a lid, the absence of confinement might allow for greater freedom of particle movement. This enhanced mobility could contribute to the observed vibration reduction at the second resonance frequency. Interestingly, the trend in vibration attenuation around the third resonance peak mirrors the behavior seen at the first resonance frequency. Table 5.12 provides a summary of the vibration reduction observed at each resonance peak.

Table 5.12: Vibration reduction (dB) for RG 4.6 mm at various filling ratios.

Filling level	53 Hz	195 Hz	326 Hz
100 g	6.63	2.79	0.87
200 g	8.96	5.78	1.69
250 g	10.58	7.22	2.27
300 g	12.98	8.80	2.94
350 g	15.28	10.28	3.42
400 g	17.52	11.84	4.15
450 g	17.55	13.20	4.70

5.6.2 Influence of moisture

The coefficient of friction, a critical factor influencing damping mechanisms, is known to be sensitive to variations in moisture content [206]. Furthermore, moisture can enhance the adhesion forces between particles [207], potentially altering their movement within the cavity and, consequently, affecting the overall performance of the particle damper. Therefore, this section presents the investigation carried out to study the impact of moisture on the damping behavior of granular materials used in the design of a particle damper.

For this investigation, two specific materials were selected: rubber granulate "RG 4.6 mm" and sand. The reason for selecting the "RG 4.6 mm" has been elaborated on in earlier sections. Notably, ELT rubber granulate, compared to rubber powder, demonstrates a higher capacity for moisture absorption, making it an ideal candidate for assessing the effects of moisture on particle dampers. Conversely, sand was chosen to examine the influence of humidity on fine-grained materials, providing a contrasting perspective in the study of moisture's role in damping performance.

To examine the influence of humidity on the damping performance, the rubber granulate "RG 4.6 mm" was immersed in 28 ml of water for an extended period, allowing the rubber particles sufficient time to

absorb the entire volume of water. This soaking process ensured that the rubber granulate reached its maximum water absorption capacity. In contrast, sand, which has a much higher capacity for water absorption compared to the rubber granulate, was only soaked for a few minutes in 28 ml of water. This shorter soaking duration for sand was sufficient to saturate it without the need for prolonged exposure to water. Following the soaking procedures, the dynamic behavior of the test specimens, which included both dry and humid versions of the rubber granulate and sand, was measured. The results of these measurements are presented in Figures 5.24 - 5.26, illustrating the effects of moisture on the damping characteristics of each material.

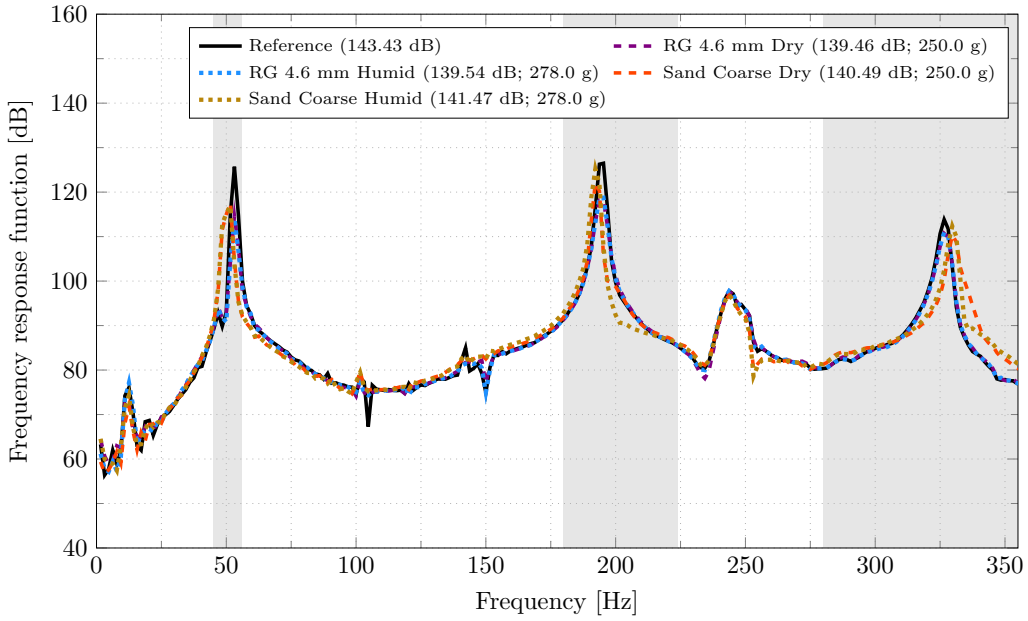

Figure 5.24: Narrow band spectrum of test specimen filled with dry and humid rubber granulate "RG 4.6 mm". The SL values of the surface velocity are given in dB and the mass of the granular filling materials is given in g.

The experimental findings reveal that moisture exerts a minimal influence on the vibration attenuation capacity of the rubber granulate labeled "RG 4.6 mm" across all resonance frequencies. In contrast, humid sand exhibits a noticeable reduction in damping efficiency when compared to its dry counterpart, despite undergoing an 11.2% increase in mass due to water absorption. Notably, the vibration reduction capabilities of both dry and humid sand are quite similar around the first resonance frequency, which occurs near 50 Hz. However, significant disparities of 2.8 dB and 1.3 dB are observed at the second and third resonance frequencies, respectively.

This decline in damping performance for humid sand can be attributed to the adhesion forces that arise between sand particles as a result of moisture. These forces may cause the particles to aggregate, restricting their free movement within the cavity of the damper. Such constrained particle motion could disrupt the effectiveness of the damping mechanism. Therefore, the use of granular materials composed of very fine particles in particle damper applications may present challenges in high-humidity environments.

This brief investigation highlights that mass alone is not the sole factor in reducing the vibration amplitude of the structure when using a particle damper. If it were, one would expect humid sand, which has greater mass than dry sand, to perform better. Moreover, the findings demonstrate how restricting the movement of sand due to humidity can significantly influence the performance of the particle damper. Consequently, the interactions between particles and between particles and the damper

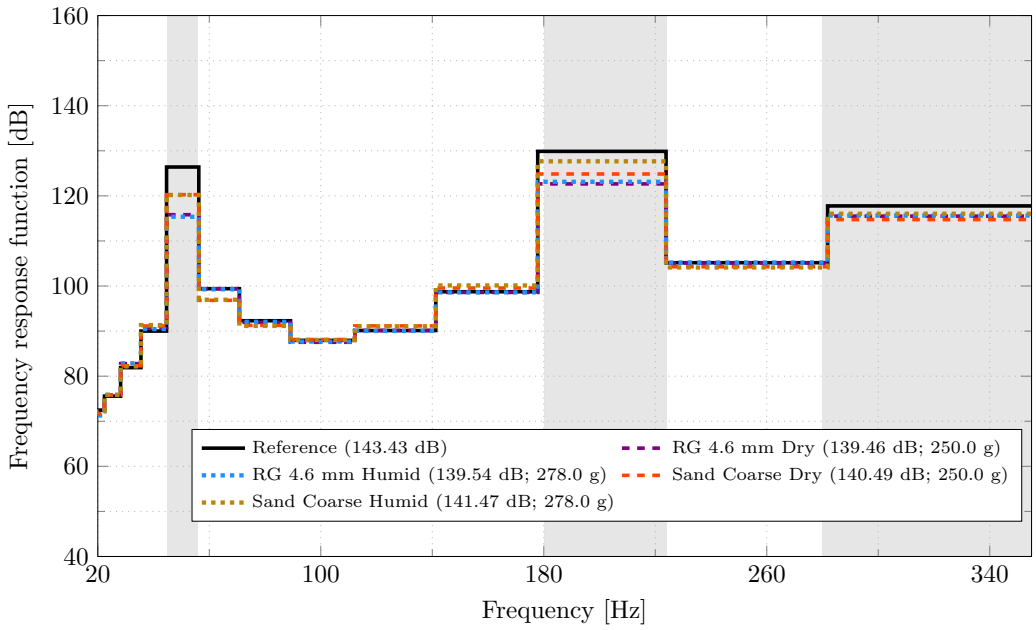

Figure 5.25: One-third octave band of test specimen filled with dry and humid rubber granulate "RG 4.6 mm". The SL values of the surface velocity are given in dB and the mass of the granular filling materials is given in g.

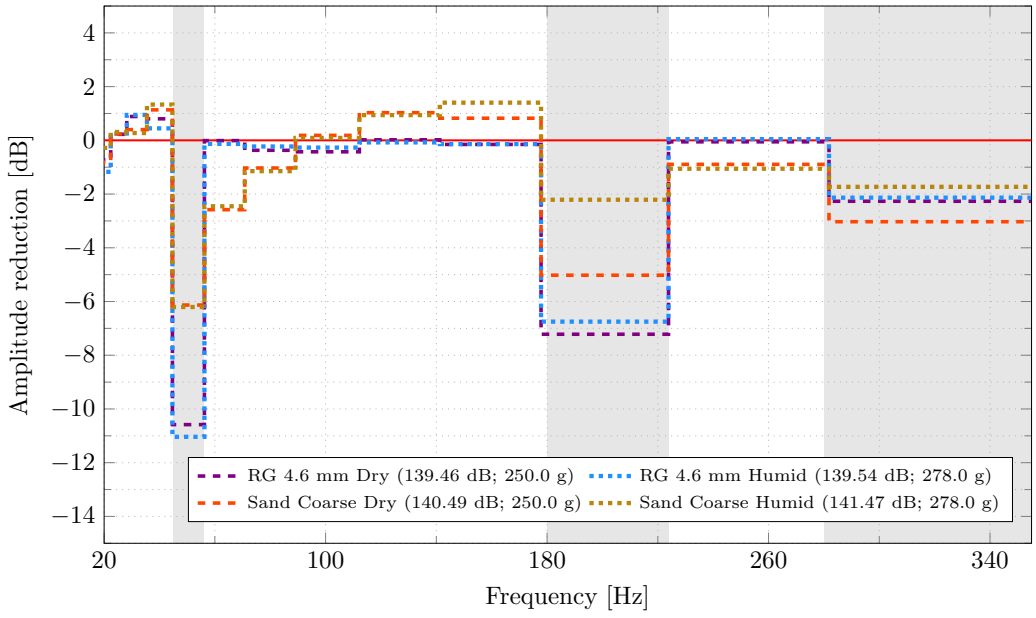

Figure 5.26: Amplitude reduction plot of test specimen filled with dry and humid rubber granulate "RG 4.6 mm". The SL values of the surface velocity are given in dB and the mass of the granular filling materials is given in g.

walls are major contributors to the reduction in vibration amplitude of the structure. A similar study conducted by Rongong et al. [175] examined the effects of mixing particles with oil and found that the damping performance of the particle damper was affected by the oil, as it altered the coefficient of friction of the granular materials.

To further understand these effects, additional experimental investigations are necessary to examine the influence of humidity on even finer particle materials, such as quartz powder, rubber powder, and stone powder. These studies would provide valuable insights into how different materials behave under varying moisture conditions and contribute to optimizing damping performance in diverse applications.

5.7 Discussion and conclusion

This chapter has examined the vibration attenuation capabilities of various granular materials, categorized into two groups: recycled rubber particle dampers (RRPDs) and hard material particle dampers (HMPDs). The motivation for testing these materials arises from the fact that most of the existing literature on particle dampers focuses on conventional, monodisperse materials such as steel, lead, and tungsten (as discussed in Chapter 2). While the performance of particle dampers is influenced by multiple factors, the selection of granular materials is particularly significant. Therefore, it is essential to explore alternative materials to expand the potential applications and effectiveness of particle dampers in diverse contexts.

This thesis presents a finding regarding the role of particle size distribution (PSD) in the vibration attenuation capability of particle dampers. While previous studies have predominantly used monodisperse materials and ignored the influence of PSD, and those that employed polydisperse materials typically focused on average particle size alone [165, 176], this research demonstrates that average or median particle size is insufficient for accurately assessing vibration mitigation.

In case of RRPDs, the experimental analysis reveals that the vibration attenuation capacity of RRPDs is influenced by two critical factors: the median particle size and the PSD. Given that the rubber granulates used in RRPDs are inherently polydisperse, a thorough examination of both characteristics is necessary to accurately evaluate their vibration mitigation potential. It has been found that an increase in the median particle size correlates with improved vibration attenuation. However, there are instances where a larger median particle size does not result in enhanced vibration reduction capabilities for the RRPDs. In these cases, a detailed investigation of the PSD becomes essential. The results suggest that a broader PSD generally contributes to enhanced vibration mitigation performance of the RRPDs. Therefore, it can be concluded that for polydisperse granular materials, such as those used in RRPDs, achieving optimal damping efficiency requires precise determination of both the median or average particle size and the PSD. This contributes a new perspective to the field, revealing that vibration reduction efficiency can be optimized only by a comprehensive evaluation of these two parameters.

This study further explores the impact of nine different hard granular materials on the vibration response of systems equipped with HMPDs. The selected materials were categorized into two distinct forms: monodisperse granulates, which include lead shot, steel balls, plastic balls, and steel chips, and polydisperse powders, encompassing stone powder, sand, and quartz powder. The experimental evaluation of HMPDs reveals that the overall damping efficiency of lead shot, steel chips, and steel balls is significantly superior to that of the other hard granular materials tested. This finding highlights the importance of material selection in enhancing the vibration mitigation capabilities of HMPDs.

Moreover, a comparative analysis of the vibration response of test specimens partially filled with various particle shapes, specifically plastic balls, plastic cylinders, steel balls, and steel chips, indicates that particle shape also plays a critical role in influencing the damping performance of the particle damper. Investigating the effect of particle shape on the vibration attenuation capability of a particle damper has been relatively rare and has yielded contradictory results. For example, Holkamp et al.[171] demonstrated experimentally that particle shape does not affect the vibration attenuation performance of a particle damper. A similar conclusion was reached numerically by Sanchez et al.[116]. In contrast, Terzioglu et al. [112] found through numerical studies that particle shape is crucial for reducing vibration amplitude, although its impact depends on the particle's motion mode. This chapter, however, emphasizes the critical role of particle shape in vibration attenuation. Nevertheless, to draw

definitive conclusions about the influence of particle shape on vibration mitigation performance, a comprehensive experimental analysis, where all parameters are held constant except for particle shape, is required.

Notably, the use of hard materials presents certain limitations. For instance, the additional mass associated with lead shot, steel balls, and steel chips is substantially greater compared to the rubber granulate utilized in RRPDs. The mass of lead shot exceeds ten times that of the rubber granulate "RG 4.6 mm" used in RRPDs. This significant increase in mass can be considered one of the major drawbacks of HMPDs, as it may limit their application in scenarios where weight constraints are a critical consideration. Overall, these findings contribute to a deeper understanding of how material properties, including type, shape, and mass, influence the effectiveness of damping systems in vibration control applications.

To harness the benefits of both RRPDs and HMPDs, this chapter uses the concept of hybrid particle dampers (HPDs). HPDs consist of a combination of two different types of granular materials. In the current study, soft materials, such as the rubber granulate "RG 4.6 mm", are mixed with hard materials, specifically lead spherical particles. The fundamental principle behind HPDs is to exploit the damping characteristics of both hard and soft granular materials, thereby enhancing the overall damping efficiency when compared to particle dampers that utilize a single type of granular material. It is essential to recognize that the damping efficiency of soft and hard granular materials can vary significantly across different frequency ranges. Therefore, the incorporation of HPDs has the potential to improve damping efficiency over a broader spectrum of resonance frequencies. By strategically combining these materials, HPDs can effectively mitigate the limitations associated with traditional particle dampers, providing superior vibration attenuation in a variety of applications. This innovative approach not only seeks to enhance damping performance but also aims to address specific challenges encountered in existing damping systems, ultimately contributing to more effective vibration control solutions.

The findings of this study indicate that the HPD composed of a mixture containing 25% lead shot and 75% rubber granulate "RG 4.6 mm" is capable of reducing the vibration amplitude of the test specimen by 18 dB. This significant attenuation demonstrates the effectiveness of the selected material composition in enhancing vibration control. Moreover, it has been observed that the combination of hard spherical particles with the irregularly shaped rubber granulate yields a greater reduction in vibration amplitude compared to mixtures that incorporate rubber powder with hard spherical particles. This disparity suggests that the viscoelastic deformation of the rubber particles during collisions with the hard spherical particles plays a critical role in enhancing energy dissipation rates. The lack of irregular shapes in the fine particles of rubber powder, in contrast to the more varied shapes of rubber granulate, contributes to their reduced effectiveness in diminishing vibration amplitudes. Therefore, it can be posited that the irregular geometries of the rubber granulate facilitate an increased number of contact points and collision interactions, as well as higher friction coefficients. These factors, in turn, enhance the viscoelastic deformation of the rubber, leading to improved energy absorption and overall damping performance.

The concept of HPDs is not entirely new but remains relatively unexplored, with studies conducted in different contexts by various researchers. For instance, Akbar et al. [179] developed an HPD by integrating a particle impact damper with a Coulomb friction damper, while Meyer [97] investigated different HPD configurations by varying the container material while keeping the particle material constant. However, among the existing studies, Chockalingam et al. [180] appears to be the only known work that has applied HPDs in a context similar to that presented in this thesis, specifically by mixing two different granular materials to create HPDs.

Building on these previous works, this study broadens the scope of HPDs by exploring a wider range of material combinations, laying the groundwork for future research focused on optimizing material mixing ratios. Such investigations can contribute to improving the damping efficiency of HPDs while

minimizing additional mass, particularly in configurations where reducing the added weight of RRPDs is a key design consideration.

The relationship between the vibration response of the system and the filling ratio of the granular material has been also systematically investigated in this study. To explore this correlation, the cavity of the test specimen was filled incrementally with the rubber granulate designated as "RG 4.6 mm". The results indicate that an increase in the additional mass of the system, achieved by adding rubber granulate "RG 4.6 mm," corresponds to enhanced vibration attenuation. This effect can be attributed to the increase in the quantity of filling material, which subsequently leads to a greater number of interactions among the rubber granulate particles themselves, as well as between the particles and the walls of the cavity. These additional interactions contribute to increased energy dissipation through mechanisms such as viscoelastic deformation and friction, ultimately resulting in improved vibration reduction performance. Overall, the findings suggest that optimizing the filling ratio of granular materials can be a critical factor in maximizing the vibration mitigation capabilities of the system.

Humidity is an another important parameter that can influence the damping performance of particle dampers. In this study, it was found that humidity has a negligible impact on the vibration response of the system when utilizing the preferred rubber granulate "RG 4.6 mm". However, humidity is likely to have a more pronounced effect on the damping characteristics of granular materials in powder form, such as stone powder, quartz powder, sand, and rubber powder, as briefly illustrated with sand in this investigation. The presence of humidity can lead to the adhesion of fine powder particles due to adhesive forces, resulting in the formation of clumps. This aggregation of particles can disrupt the particle damping mechanism, thereby compromising the overall effectiveness of the damper. The findings highlight the necessity of considering environmental conditions, such as humidity, when evaluating the performance of various damping materials, particularly those in powder form. Understanding these interactions is crucial for optimizing the design and application of particle dampers in diverse settings.

The findings of this chapter contribute to the advancement of particle-based damping technologies by providing engineers and researchers with a refined framework for material selection, performance optimization, and application-specific customization. Future research can build upon these insights to further optimize HPDs configurations, refine mixing ratios, and investigate advanced materials, ultimately facilitating the development of next-generation damping solutions for high-performance engineering applications.

6 Passive design approach to enhance granular motion in particle dampers

Chapter 5 presented a comprehensive experimental investigation of the vibration attenuation capabilities of various granular materials, a crucial factor in particle damper design. Having identified suitable materials, this chapter now focuses on how these materials can be effectively utilized within a particle damper to maximize the vibration attenuation of a structure.

Chapters 1 and 2 highlight that particle damper designs typically harness the vibrations of the main structure to activate granular material movement. This movement triggers particle-particle and particle-wall collisions, which effectively reduce the vibration amplitude of the primary structure. Nevertheless, Rongong et al. [175] explored the use of electromagnets to further enhance damping performance by actively manipulating the motion of granular particles. While this approach has demonstrated significant enhancements in damping efficiency, its effectiveness is mainly restricted to specific materials, thereby limiting its application. To overcome the limitations of electromagnetically induced motion, this chapter introduces three passive design variants: thin-wall cavity (TWC), thin-wall cavity with additional sheets (TWC-AS), and ring cavity (RC). These passive design variations are introduced with the objective of increasing the relative motion of granular materials, thereby enhancing the efficiency of the particle damper. This chapter expands upon the prior research presented in [208].

6.1 Laboratory test specimen design

The current chapter investigates various particle damper design strategies for L-shaped hollow steel structures, commonly used in wind turbine components, agricultural equipment, piping systems, and support structures for offshore construction, see Figure 6.1. Furthermore, the L-shaped hollow section offers an advantageous balance between structural complexity and practicality, ensuring the findings from this study to be applicable to a broad range of real-world scenarios. Moreover, their excellent resistance to bending, torsion, and buckling renders them ideal candidates for industrial applications. Additionally, the inner space of the hollow test specimen, as illustrated in Figure 6.1, provides the opportunity to design a particle damper within its confines. This approach enables the integration of particle dampers without compromising the integrity of the original structure.

As discussed in Chapter 5, the test specimen in this study was selected to facilitate the investigation of particle damper parameters while ensuring that the laboratory test results can be extrapolated to an industrial-scale wind turbine generator. Hence, in this chapter also, the geometry of the test specimen is inspired by a wind turbine and is derived from the stator arm of a direct-drive wind turbine. Specifically, the dimensions presented in Figure 6.1 represent a 50% scale reduction compared to the actual stator arm. While preserving key structural characteristics, minor simplifications were introduced to optimize the geometry for laboratory experimentation.

Although the test specimen is inspired by wind turbine stator arms, the passive design approaches presented in this chapter are not limited to this application. These methods can also be applied to other structures, including those used in automotive engineering. Further details on such applications are discussed in Chapter 12. It is essential to emphasize that the total weight of the test specimen without the particle damper is 100 kg.

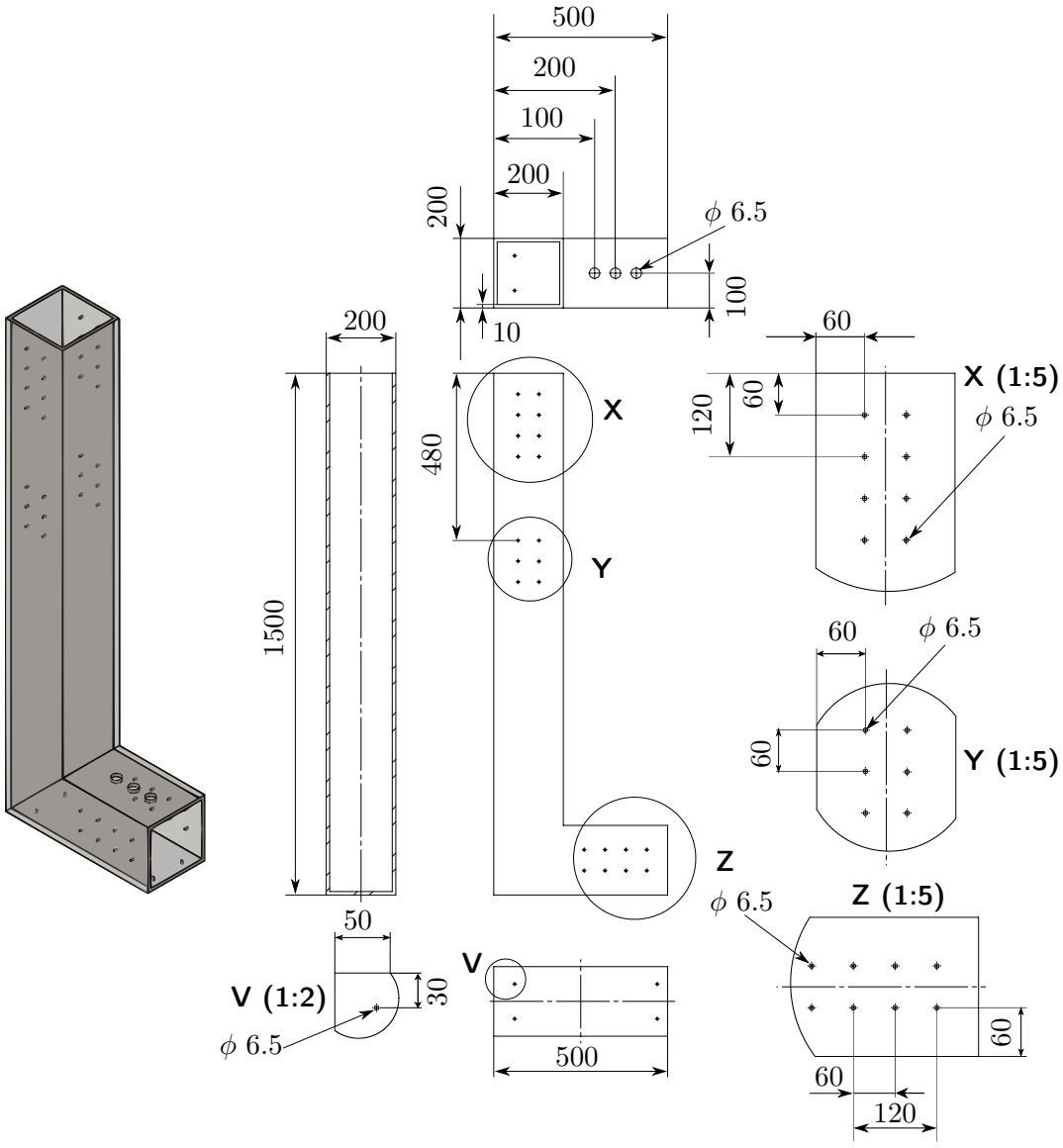

Figure 6.1: L-shaped test specimen geometry with dimensions in mm.

6.2 Design strategies

This section provides a comprehensive discussion on the design and conceptualization of the three design variants, namely: TWC, TWC-AS, and RC. These design modifications are aimed at improving the performance of particle dampers while ensuring that the granular materials remain enclosed within the hollow structure.

6.2.1 Thin wall cavity

The first design approach, referred to as the "thin-wall cavity (TWC)" variant, uses thin rectangular plates to form cavities within the test specimen for enclosing granular materials. The dimensions of the TWC are directly influenced by the mounting positions of the thin plates (see Figure 6.2 (left)). The test specimen has a total of 44 identical holes, each with a diameter of 6.5 mm, drilled across eleven distinct locations (L 1 - L 11), as illustrated in Figure 6.2 (left). Furthermore, the distance between adjacent holes is consistently maintained at 60 mm, see Figure 6.1. This arrangement allows

for the creation of TWCs in three different heights: 60 mm, 120 mm, and 180 mm. Although it is possible to design a larger TWC measuring $180 \times 180 \times 240$ mm by utilizing locations four (L 4) and five (L 5). However, this configuration would significantly increase the mass of the granular material. Consequently, the analysis within this study excludes the $180 \times 180 \times 240$ mm TWC.

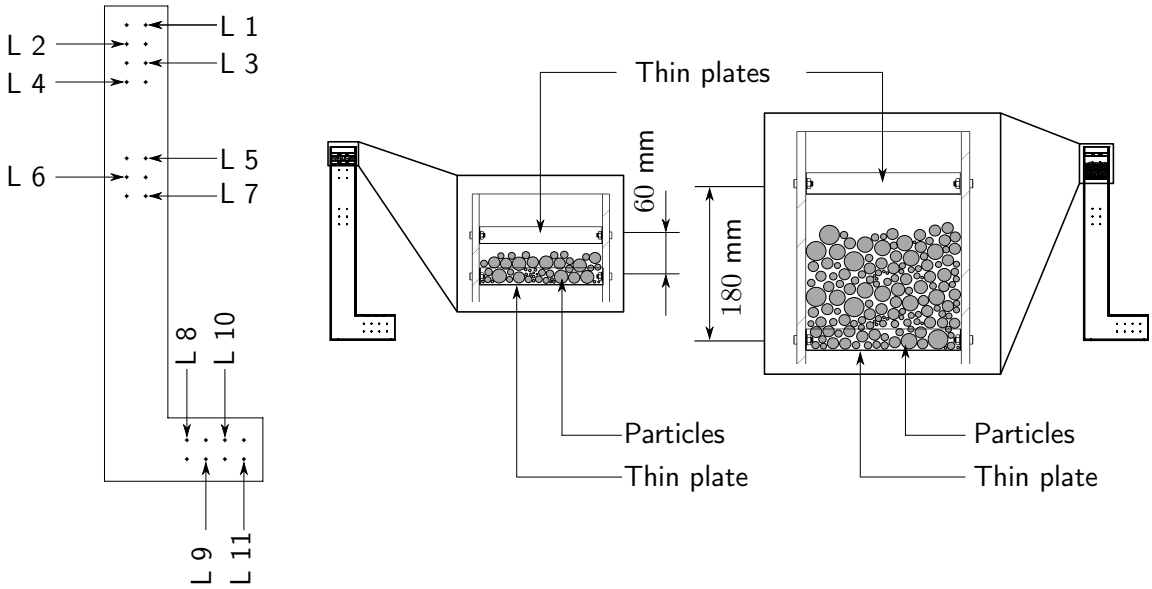

Figure 6.2: Left: Location numbers indicate the points of attachment for the thin sheet used to form a cavity inside the test specimen. Right: Illustration of the smallest and largest possible cavity sizes within the L-test specimen.

The design of a single TWC within the test specimen requires the integration of at least two thin plates, see Figure 6.2 (right). The selection of the cavity dimensions is primarily influenced by the objective of designing the particle damper volume in such a way that it minimizes the added mass of the granular material. In addition to this, it is crucial to ensure that the cavity contains a sufficient quantity of particles. This is essential not only to achieve the desired dampening effect but also to ensure a significant reduction in vibration amplitude, thereby enhancing the overall effectiveness of the particle damper in mitigating vibrations.

The concept behind incorporating thin plates in the TWC design is to induce additional motion to the particles. The wall thickness of these plates is significantly smaller than that of the test specimen. Consequently, the thin plates can vibrate with a greater amplitude, thereby offering supplementary motion to the particles in the granular material. Hence, this will increase the vibration attenuation capability of the TWCs compared to the conventional particle damper design, where the motion of the granular material enclosed in the particle damper occurs solely due to the vibration of the main structure.

The thin plates are securely fastened within the hollow section using identical bolts and nuts. A torque wrench is employed to ensure consistent tightening of all bolts across the TWC. Each bolt is fastened with a precisely controlled torque of 5 Nm. Furthermore, it is crucial to note that the positioning of the TWCs in the test specimen is strategically chosen to guarantee manual accessibility, thereby improving the convenience of the granular material filling and emptying process.

It is important to emphasize that, due to the fixed dimensions of the test specimen, the length and width of the TWC remain constant throughout this design study. However, the height of the TWC is variable, contingent upon the placement of the thin plates. Given the predetermined number of holes in the test specimen, it is feasible to design eight different TWC configurations at three specific locations: the top part (Figure 6.3 (a)-(c)), the middle part (Figure 6.3 (d)-(e)), and the bottom part

(Figure 6.3 (f)-(h)) of the L-shaped test specimen.

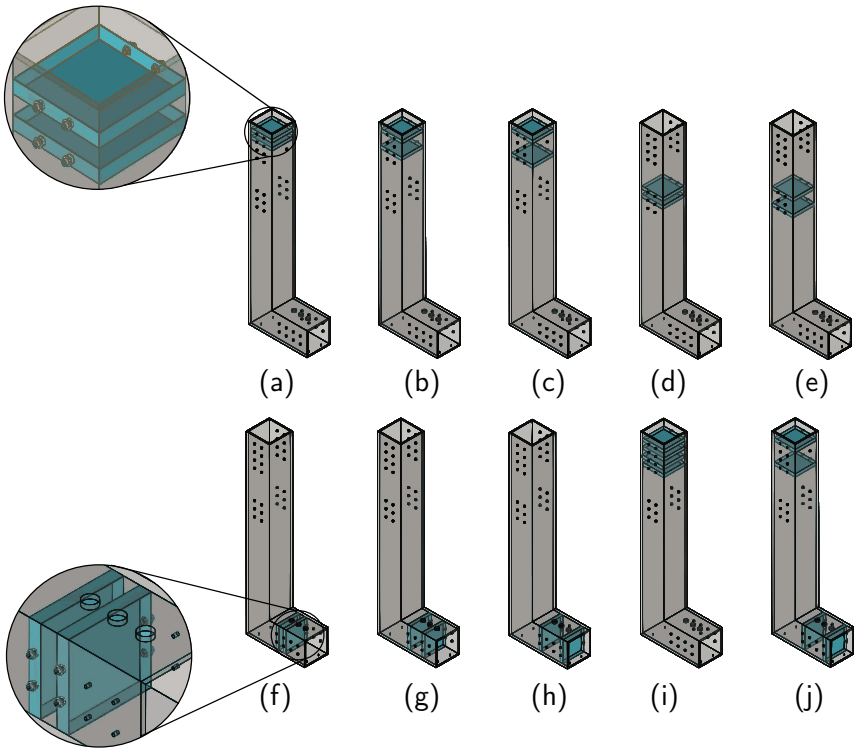

Figure 6.3: Locations, dimensions, and labels of the TWCs: (a) TWC 1, (b) TWC 2, (c) TWC 3, (d) TWC 4, (e) TWC 5, (f) TWC 6, (g) TWC 7, (h) TWC 8, (i) multi-unit TWC, (j) mix TWC.

Designing a TWC at the top and middle positions of the test specimen involves a three-step process. Firstly, affixing a thin plate to the underside of the cavity is initiated. Subsequently, the cavity is filled with granular material. Lastly, sealing the cavity is accomplished by using another thin plate identical to the one employed for the bottom part. As an example, consider designing TWC 1, as illustrated in Figure 6.3 (a). Initially, a thin plate is mounted at L 2 (see Figure 6.2 (left)). Subsequently, the cavity is filled with granular materials, and a thin plate is then affixed at location L 1 in the following step. In contrast, the design approach for a TWC located at the bottom section of the test specimen differs slightly from that used for TWCs in the upper and middle sections. This variation arises because the bottom section of the test specimen is fixed to the table, preventing the enclosure of the cavity after filling it with granular materials through the existing opening. In order to solve this issue, three holes, each with a diameter of 30 mm, have been drilled on the surface of the lower part of the test specimen. These holes facilitate the filling of granular materials within the TWCs (TWC 6, TWC 7, and TWC 8), which have been constructed by attaching two thin plates at distinct locations, as illustrated in Figure 6.3 (f)-(h).

Previous research has demonstrated that the design configuration of particle dampers, such as multi-unit (MU) and single-unit (SU) variations, can significantly impact their vibration attenuation properties [148, 209]. Consequently, this thesis incorporates a comparative analysis between SU TWCs and MU TWCs to elucidate the influence of design choice on performance. Several designs of MU particle dampers have been investigated in the literature. For example, Ye et al. [148] developed a MU particle damper comprising three rectangular containers, where the wall in the y-direction can be removed to facilitate the addition of particles. Additionally, they divided the cavities into three equal sub-cavities along the x-direction. In another study, Lu et al. [209] designed a MU particle damper by partitioning a

larger cavity into four equal square sections. In this chapter, The MU TWC is composed of two SU TWCs with identical dimensions measuring $180 \times 180 \times 60$ mm. The MU TWC has been designed at the upper part of the test specimen, utilizing four identical plates, as illustrated in Figure 6.3 (i). Furthermore, SU TWCs with comparable dimensions have been designed at both the upper and lower sections of the test specimen, as illustrated in Figure 6.3 (j). The reason for selecting the mix TWC configuration will be explained in detail in the results section.

The vibration characteristics of the thin plates employed in TWC design are dependent on various factors, with wall thickness of the thin plates playing a significant role in the damping efficiency of TWCs. Hence, to gain a deeper insight into the impact of TWCs wall thickness on the dynamic response of the system, plates with three different wall thicknesses, namely: 2.0 mm, 1.0 mm, and 0.5 mm have been chosen, see Figure 6.4. These rectangular plates feature rounded corners, facilitating their insertion into the test specimen. Additionally, all these plates are equipped with four identical holes for secure attachment within the hollow structure.

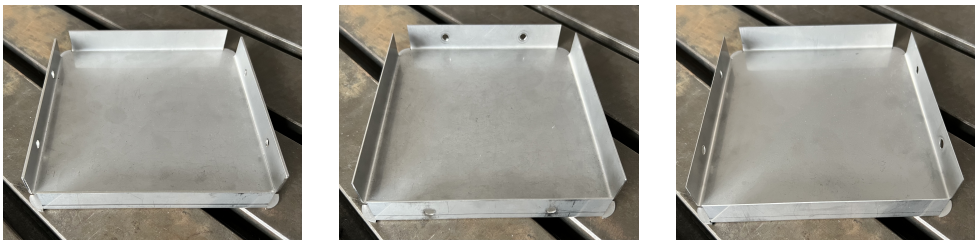

$t = 2.0$ mm $t = 1.0$ mm $t = 0.5$ mm

Figure 6.4: Thin plate design with three wall thicknesses for TWCs of various sizes and locations.

6.2.2 Thin wall cavity with additional sheets

This section introduces the concept of thin-wall cavity with additional sheets (TWC-AS) to enhance the effectiveness of TWCs in reducing vibration amplitude within a mechanical structure. The TWC-AS is designed by attaching a hanging sheet to a base plate that shares design similarities with the TWC, see Figure 6.5. The connection between the suspended sheet and the base plate is achieved through welding. Moreover, the wall thickness of the base plate remains consistent at 1.0 mm across all design variations of the TWC-AS. The reason behind selecting this particular thickness will become evident in the results discussion.

The introduction of a suspended sheet into the TWC variant is intended to enhance the interactions occurring among the particles within the granular material. The underlying hypothesis suggests that the vibrations caused by the suspended sheet will lead to an increase in the motion of the particles, thereby substantially boosting the likelihood of collisions among them. This heightened frequency of particle collisions is anticipated to produce a marked improvement in the damping effect. As a result, the vibration amplitude of the structure with the suspended sheet is expected to be considerably lower when compared to the unmodified TWC variant.

Similar to the TWC variant, the vibration response of the suspended sheets can be affected by a variety of factors, including the shape, size, quantity, and thickness of the sheets. It is important to note that alterations in the width and height of the suspended sheets can have a direct effect on the contact surface area between the particles of the granular material and the sheet itself, which may in turn lead to improved vibration attenuation. Moreover, variations in the shape and size of the sheets introduce distinct contact geometries, which can significantly influence the dynamic behavior of the entire system. To better understand these effects, the design of the suspended sheet and its corresponding impact on the system's vibration response have been subjected to detailed experimental investigation, as

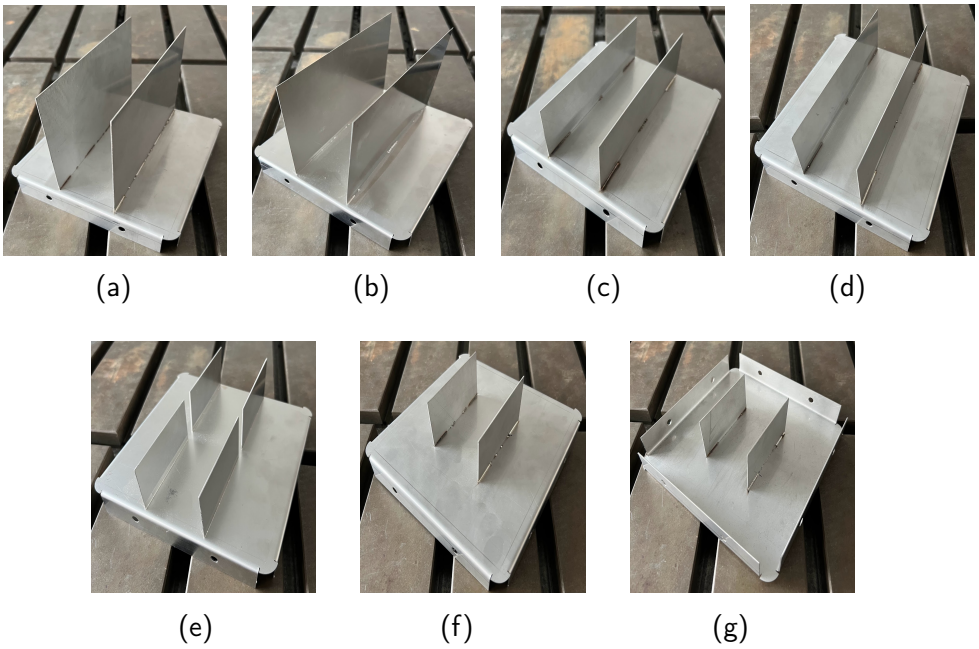

Figure 6.5: Design of TWC-AS with varying shapes, sizes, and thicknesses.

demonstrated in Figure 6.5. This examination aims to shed light on how different design parameters of the suspended sheet contribute to the overall efficiency of vibration reduction.

In this thesis, the TWC-AS system is explored through the examination of three distinct configurations of suspended sheets: the extended TWC-AS, the smaller TWC-AS, and the compact TWC-AS. The extended TWC-AS employs a larger sheet, measuring 170 mm in width and 105 mm in height, and is tested with two different wall thicknesses of 1.0 mm and 0.5 mm. Similarly, the smaller TWC-AS configuration retains the same width of 170 mm but features a reduced height of 45 mm, while still offering the same two wall thickness options (1.0 mm and 0.5 mm). In contrast, the compact TWC-AS configuration is distinct in that it exclusively utilizes sheets with a single wall thickness of 1.0 mm, with dimensions of 80 mm in width and 45 mm in height. In this configuration, an additional feature is the inversion of one sheet to examine the effect of sheet orientation on the system's ability to mitigate vibrations. It is also important to highlight that, while most TWC-AS configurations utilize two suspended sheets, one specific setup includes four suspended sheets attached to the base plate. Further details regarding the dimensions of the suspended sheets used in these configurations are provided in Table 6.1.

Table 6.1: TWC-AS dimensions, wall thicknesses, and number of hanging sheets.

Subfigure	Notation	Width [mm]	Height [mm]	Thickness [mm]	No. of sheet [-]
(a)	Extended TWC-AS	170	105	1.0	2
(b)	Extended TWC-AS	170	105	0.5	2
(c)	Smaller TWC-AS	170	45	1.0	2
(d)	Smaller TWC-AS	170	45	0.5	2
(e)	Compact TWC-AS	80	45	1.0	4
(f)	Compact TWC-AS	80	45	1.0	2
(g)	Compact TWC-AS inverted	80	45	1.0	2

6.2.3 Ring cavity

The additional mass introduced by granular materials in particle dampers presents a significant challenge for the widespread adoption of particle damping techniques across various industries. As discussed in Chapter 5, the selection of granular materials during the design phase plays a crucial role in determining the overall mass of the particle dampers. Despite the critical influence of material choice, once the granular materials are selected, it becomes difficult to reduce the added weight of the damper. In response to this challenge, the present chapter introduces the ring cavity (RC) design variant, which seeks to address the issue of excess mass while maintaining the effectiveness of the particle damping mechanism.

In the RC variant, the granular material can be distributed strategically to minimize its additional mass compared to traditional particle damper designs. The RC design, like its predecessors TWC and TWC-AS, boasts an enlarged contact surface between the wall and the granular material particles. Additionally, the vibration induced by the ring and its base plate further amplifies the probability of particle-particle collisions, enhancing the damping effect. The design of the RC used in this thesis can be seen in Figure 6.6. The RC design includes a rectangular ring with a square cross-section, along with a base plate. The base plate, with a wall thickness of 1.0 mm, is attached to the ring using a connection method similar to that utilized in the TWC-AS variant.

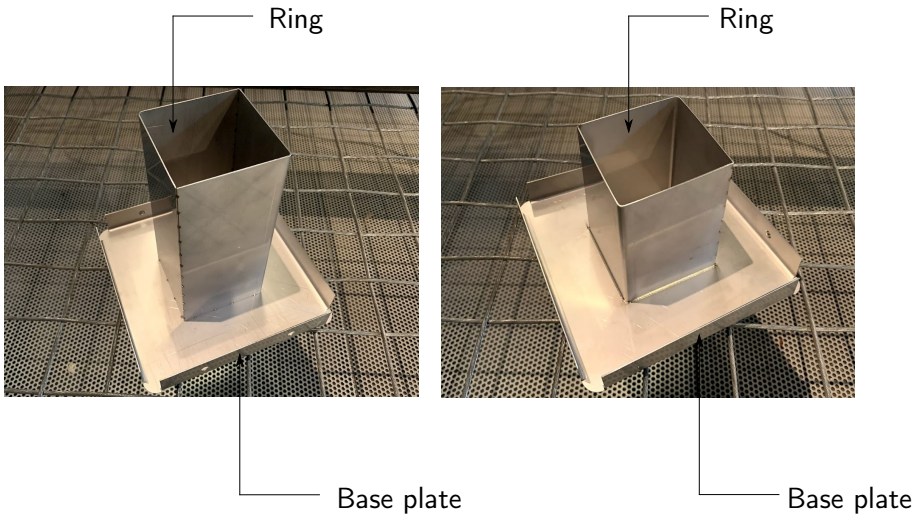

Figure 6.6: RC geometry: (a) large RC, (b) small RC.

This thesis investigates two distinct configurations of the Ring Cavity (RC) system, referred to as the large RC and the small RC. While both configurations maintain a consistent wall thickness for the base plate, they differ in the height of the ring component. The primary motivation for employing two different ring heights is to evaluate the influence of ring height on the system's ability to attenuate vibrations. By examining these variations, the study aims to provide a comprehensive understanding of how altering this particular geometric parameter impacts the overall vibration mitigation performance of the RC system. The specific dimensions of both the large and small RC configurations are provided in Table 6.2, offering detailed insight into the structural differences between the two setups.

Table 6.2: Height, width, and wall thickness of RCs.

Notation	Width [mm]	Height [mm]	Wall thickness [mm]	Base plate thickness [mm]
Large ring cavity	80	175	1.0	1.0
Small ring cavity	80	115	1.0	1.0

The distribution of the rubber granulate "RG 4.6 mm" within the RC can be arranged in three distinct configurations, namely: configuration 1, configuration 2, and configuration 3, as shown in Figure 6.7. In configuration 1, the rubber granulate is positioned along the outer wall of the ring, as depicted in Figure 6.7 (a). This specific arrangement allows the kinetic energy generated by both the test specimen and the RC vibrations is induced to the rubber granulate, potentially reducing the vibration amplitude of the test specimen. This reduction is attributed to the decrease in the extra mass of the granular material when compared to traditional particle damper designs.

(a) (b) (c)

Figure 6.7: Distribution of rubber granulate "RG 4.6 mm" in RC design variants:(a) Configuration 1: exterior ring wall, (b) Configuration 2: ring interior, (c) Configuration 3: both interior and exterior ring walls.

In configuration 2, the rubber granulate is partially filled inside the RC ring, further decreasing the overall mass of the granular material, as illustrated in Figure 6.7 (b). However, in this configuration, the rubber particles interact exclusively with one another and with the thin walls of the ring. This implies that the motion within the granular material is driven solely by the vibrations of the RC itself, rather than by any external excitation from the test specimen.

Lastly, configuration 3 involves the distribution of the rubber granulate "RG 4.6 mm" both inside and outside the RC ring, as shown in Figure 6.7 (c). While this configuration increases the mass of the rubber granulate compared to the first two configurations, it also has the potential to enhance vibration reduction in the test specimen. The additional mass may contribute to improved damping efficiency, offering greater vibration attenuation than configurations 1 and 2. The variation in these configurations highlights the importance of balancing mass and damping effectiveness in the design of vibration control systems.

6.3 Experimental set up

Various experimental configurations have been investigated to evaluate the vibration attenuation performance of the TWC, TWC-AS, and RC design variants. However, it was determined that the experimental setup described in Chapter 5 is also appropriate for this scenario. Therefore, a similar approach is adopted here. To avoid repetition, this chapter provides a concise overview of the experimental setup, with the understanding that certain details may overlap with those in Chapter 5 for the sake of completeness. The overview of the experimental setup is given in Figure 6.8.

Similar to the prior setup used to investigate the vibration attenuation capability of RRPDs, HMPDs, and HPDs (see Chapter 5), the present configuration also employs two identical beam-like structures to fix the test specimen to the measuring table. This approach remains consistent while acknowledging the necessity for increased beam thickness (10 mm) due to the substantial difference in the test specimen's dimensions and weight. Moreover, a reflective adhesive foil is attached to the measurement area of the

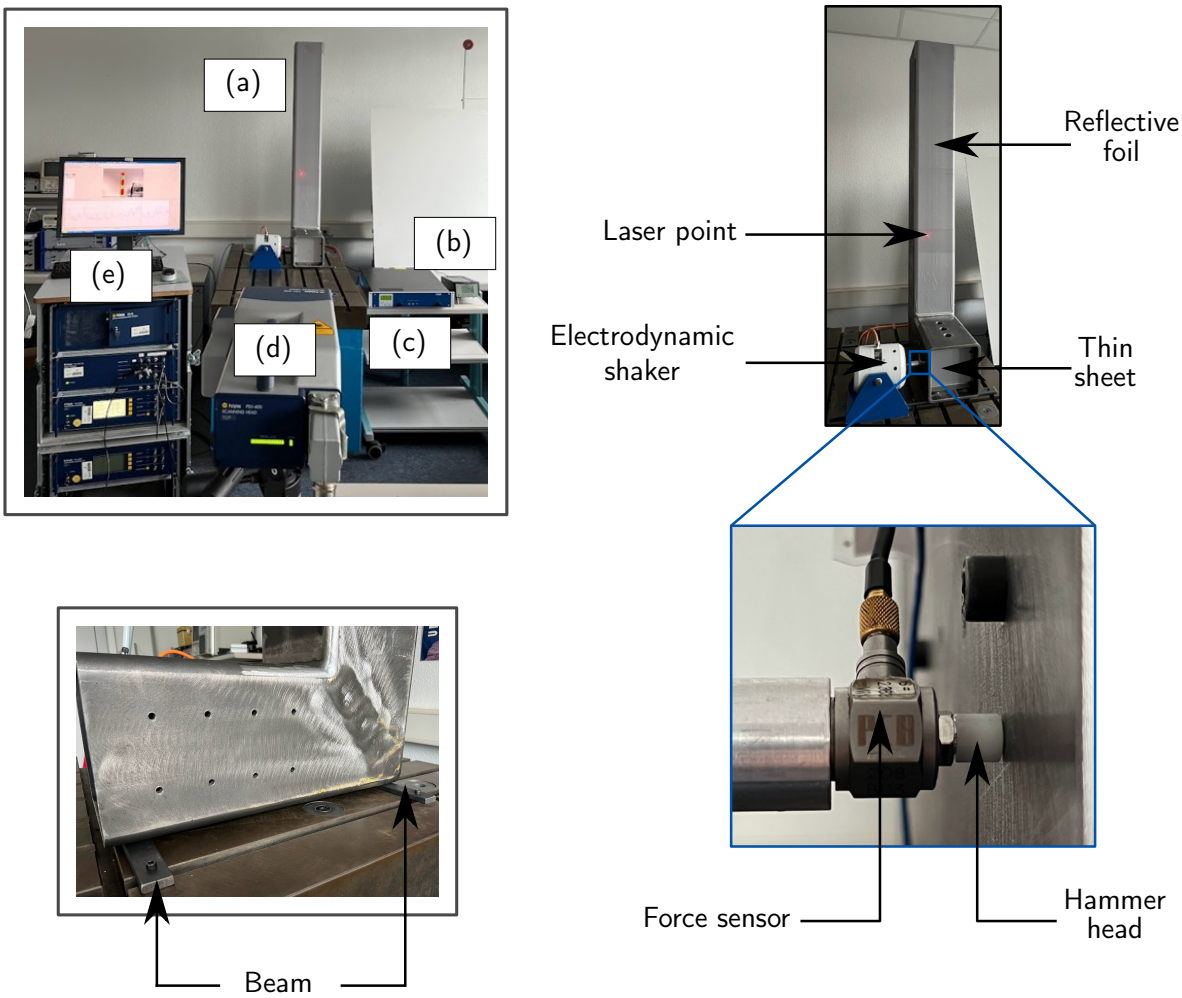

Figure 6.8: Experimental setup for vibration testing of TWCs, TWC-As, and RCs: (a) test specimen, (b) force sensor amplifier, (c) shaker power amplifier, (d) laser vibrometer scan head, (e) control and post-processing unit.

specimen to enhance the quality of the laser light reflection. The method for exciting the test specimen, the input signal, measuring the input force with the assistance of a force sensor, and measuring the surface velocity of the test specimen remains consistent with that described in Chapter 5.

The determination of the number of scanning points is based on empirical studies, which demonstrate that the selected quantity ensures sufficient measurement accuracy while minimizing the duration of the measurements. The scanning points are positioned along the elongated arm of the test specimen and remain consistent for every trial, as shown in Figure 6.9. This results in a well-defined grid of rectangular form, consisting of 302 measurement points, within the designated measurement area. The purpose of scanning the entire surface of the elongated arm is to capture the eigenform of the structure, which is essential for the analysis and design of the different particle damper variants. In addition to this, a parameter investigation was conducted on the reference test specimen to establish correlations between various parameters necessary for carrying out all experimental studies. The reference test specimen refers to the test specimen without any particle dampers. All parameters used in each experimental trial are listed in Table 6.3, providing an overview of the conditions under which the measurements were performed.

Chapter 5 highlights the critical role of reproducibility in ensuring the quality and reliability of experimental investigations. Consequently, a repeatability assessment is also carried out for this

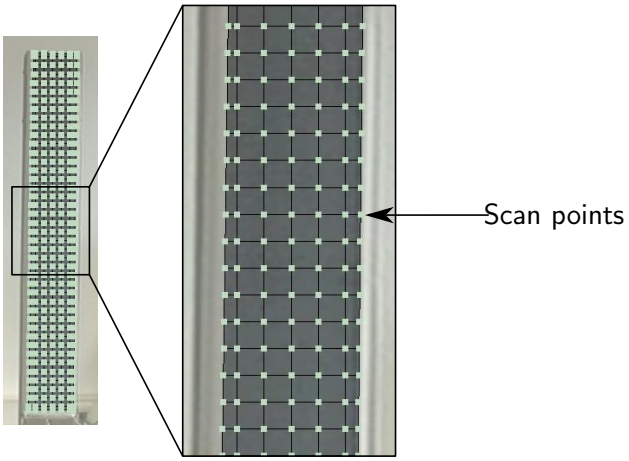

Figure 6.9: Grid of 302 scan points in rectangular arrangement

Table 6.3: List of parameters for data acquisition.

Parameter	Complex average	Cut-off frequency	Sampling frequency	Frequency resolution
Values	6	5000 Hz	25.6 kHz	1.5 Hz

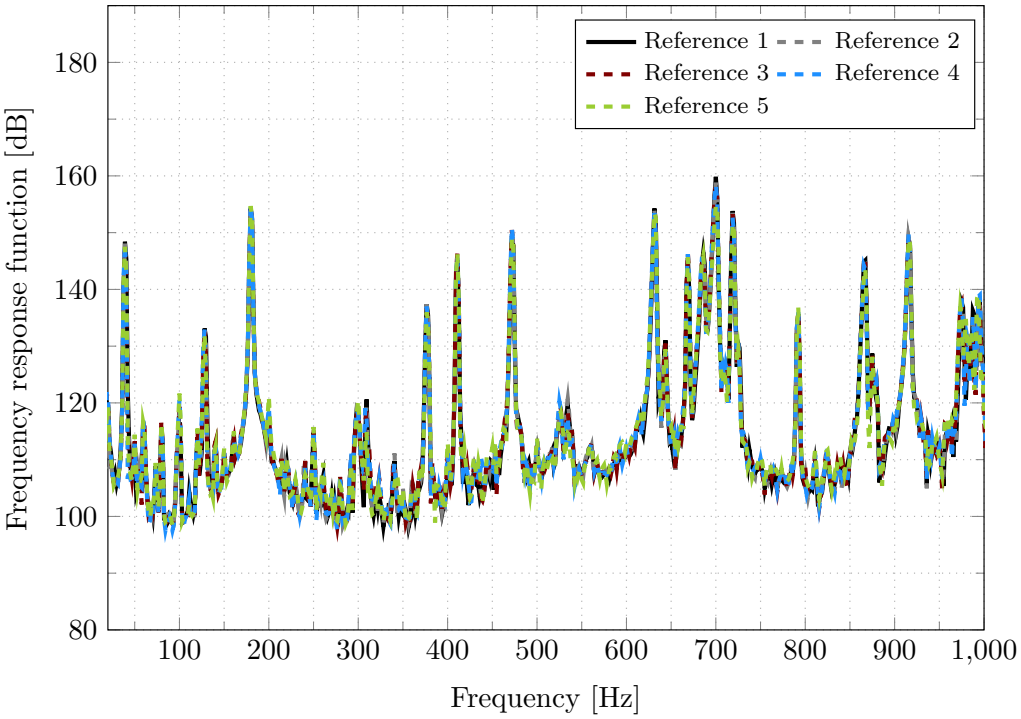

Figure 6.10: Repeatability of the experimental data.

experimental investigation. To ensure the reproducibility and repeatability of the experimental studies presented in this work, numerous tests have been conducted. These tests maintain uniformity in all experimental conditions, such as the positioning of scan points, the distance between the hammer head and the test specimen, the placement of the laser scanning vibrometer, and so forth. In order to verify the repeatability of the experiment, measurements are taken on the reference test specimen twice: once at the beginning and once at the end of the design study. Additionally, to evaluate the strength of the

experimental reproducibility, the vibration characteristics of the reference test specimen are monitored after performing a set number of measurements for design variables. The obtained findings confirm the reliability of the experimental setup in replicating the system's response, as depicted in Figure 6.10.

6.4 Results and discussion

As discussed in Chapter 5, the FRF of the test specimen in this chapter is also plotted both with and without granular materials, within a narrow frequency band spectrum as well as in a one-third octave band. The narrow-band spectrum enables detailed analysis of resonance peaks within the 20 Hz to 1000 Hz frequency range of interest. For reference, all narrow-band spectra are included in the appendix.

The selected frequency range is divided into two categories: a "low-frequency" and a "high-frequency" range. The lower boundary of the low-frequency range is conventionally set at 20Hz, although the upper boundary may vary depending on the specific application being studied. For example, Moller et al. [210] investigated noise emissions from large wind turbines within a frequency range of 20 Hz to 200Hz, while Zhou et al. [211] defined the low-frequency range as extending from 20 Hz to 300 Hz. In the context of this study, the low-frequency range is defined as spanning from 20 Hz to 300 Hz.

In order to quantify the reduction in vibration amplitude induced by particle dampers, an amplitude reduction plot within the one-third octave band is produced. This reduction in amplitude is determined by subtracting the vibration levels of a reference test specimen (without dampers) from those of a test specimen containing granular materials. In the resulting plot, a horizontal red line is used to denote 0 dB. Any region of the plot that lies above this line indicates an increase in vibration amplitude, whereas regions falling below the line signify a reduction in vibration amplitude. This visualization helps to clearly identify the effectiveness of the particle dampers in attenuating vibrations across different frequency bands.

Prior to evaluating the effectiveness of the various design variants, a baseline measurement of the reference test specimen was conducted to assess its dynamic behavior. The frequency response of the reference specimen is illustrated in Figure 6.11, where the resonance peaks, along with their corresponding eigenmodes, are presented. These eigenmodes are critical for understanding the vibrational characteristics of the structure and will serve as a valuable reference point for analyzing the performance of the particle dampers.

6.4.1 Influence of plate thickness on the damping performance of TWC

In the first design strategy, known as the TWC variant, the thin plates with three different wall thicknesses (2.0 mm, 1.0 mm, and 0.5 mm) were mounted to the uppermost position of the test specimen, denoted as L 1 in Figure 6.2. Mounting thin plates at this location creates a TWC with dimensions $180 \times 180 \times 60$ mm. This TWC is partially filled with 700 g of rubber granulate "RG 4.6 mm". It is important to highlight that the inclusion of the "RG 4.6 mm" in this specific scenario leads to a 0.7% increase in the overall system mass, which is significantly lower compared to particle dampers utilizing conventional materials such as steel balls and tungsten. While a minimum of two thin plates are necessary for designing a TWC, only one plate is utilized here to examine the impact of plate wall thickness on vibration attenuation capability. This decision is motivated by experimental convenience.

Initially, the experiment is conducted on the reference test specimen, i.e. specimen without a TWC. Following this, the frequency response of the system is measured for the test specimen featuring an empty TWC installed with thin plates of varying wall thicknesses at position L 1. This involves assessing the frequency response of the system housing a particle damper without granular material filling. Subsequently, measurements were taken on the test specimen incorporating a TWC partially

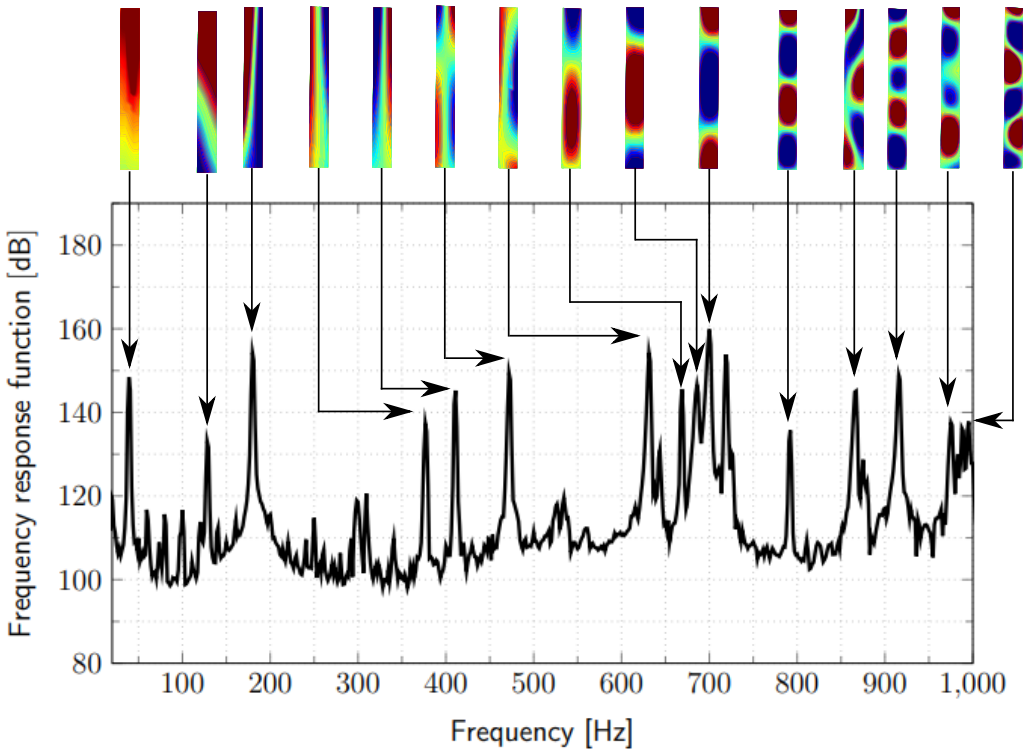

Figure 6.11: FRF and measured surface velocity of the reference specimen for normal direction.

filled with the rubber granulate "RG 4.6 mm" The results obtained for the TWC strategy are plotted in Figure 6.12 - Figure 6.13.

The narrow band spectrum illustrates that the presence of an empty TWC at location L 1 modifies the vibration behaviour of the primary structure (See Figure A2.4 in Appendix A2). This effect is noticeable within the torsional modes spanning from 410 Hz to 536 Hz. Additionally, the inclusion of thin plates at location L 1 impacts the bending modes of the main structure within the frequency band of 632 Hz to 718 Hz. These changes in frequency response manifest whether in frequency shifts or amplitude reduction. However, it should be highlighted that below 410 Hz, the impact of the empty TWC on the vibration behavior of the main structure diminishes significantly.

Across all tested configurations of TWCs, regardless of thin plate thickness, significant reductions in vibration amplitude were observed, see Figure 6.12. Interestingly, even an empty TWC exhibited amplitude reduction, as evidenced by the 0.5 mm and 1.0 mm thin plate configurations (blue and green dash-dotted lines, respectively) around the central frequency of 400 Hz. Conversely, at the same frequency, the empty TWC with a 2.0 mm thin plate (purple dash-dotted line) amplified the vibration amplitude of the main structure. Nevertheless, across the remaining frequency ranges, vibration reduction due to an empty TWC has been observed. Consequently, the precise degree of vibration reduction caused by a partially filled TWC is determined by subtracting the amplitude of the empty TWC from that of the partially filled one, see Figure 6.13.

The amplitude reduction plot clearly shows that the TWC with a 0.5 mm thick plate (indicated by the sky blue dashed line) achieves a maximum vibration attenuation of 3.7 dB at a resonance frequency of 400 Hz. Conversely, at the central frequency of 500 Hz, the TWC exhibits negligible vibration attenuation, while at 800 Hz, it amplifies the vibration rather than diminishing it. Furthermore, the maximum vibration mitigation achieved by the TWC featuring a 1.0 mm thick plate occurs at the central frequencies of 400 Hz and 800 Hz. Around these resonance frequencies, this particular TWC can achieve vibration reductions of up to 4.7 dB and 6.5 dB, respectively (light green dashed line). Moreover, the TWC equipped with a 2.0 mm thin plate, indicated by the orange dashed line, achieves

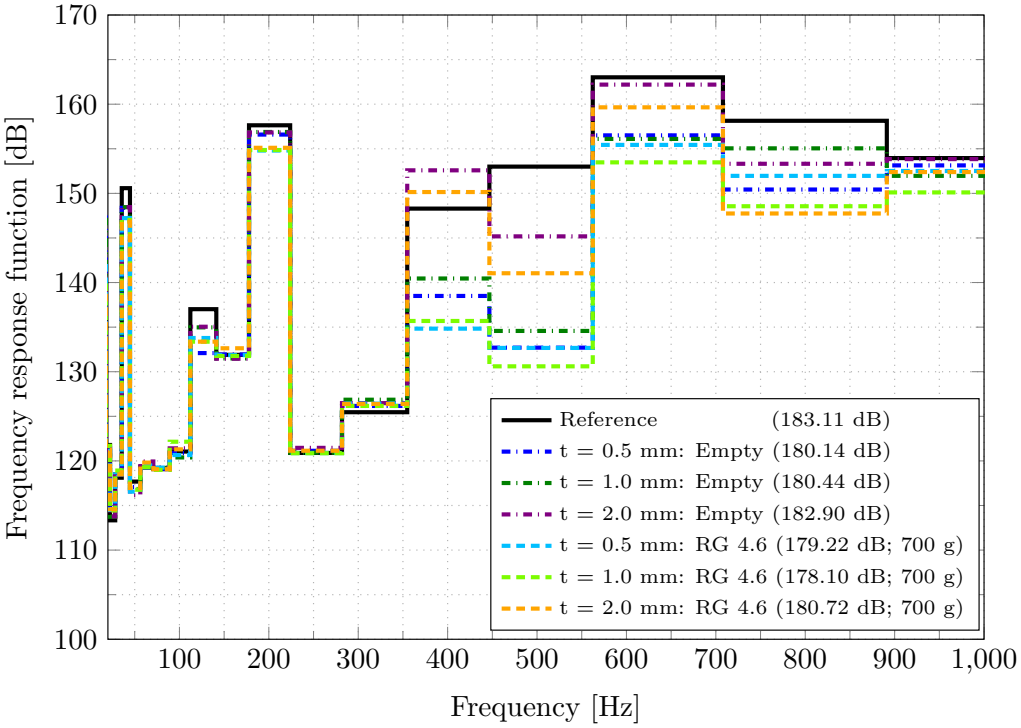

Figure 6.12: One-third octave band plot for empty and partially filled TWCs with different wall thicknesses (t). The SL values of surface velocity are presented in dB, and the mass of the granular filling materials is reported in grams (g).

peak vibration attenuation of 5.5 dB near the resonance frequency of 800 Hz, as shown in Figure 6.13.

A comparative analysis of the effectiveness of TWCs with varying wall thicknesses can be conducted using the SL values, as indicated in the legend of Figure 6.13. The results reveal that the SL value corresponding to the surface velocity of the TWC with a wall thickness of 1.0 mm is markedly lower than those of the other TWCs with different wall thicknesses. This finding suggests that the TWC with a wall thickness of 1.0 mm is more advantageous for designing a particle damper for the specified test specimen.

In Section 6.2.1, it was explained that the primary objective of TWC is to create a particle damper with a considerably thinner wall than that of the test specimen. Since thin plates are typically sensitive to vibrations, they can effectively transfer more kinetic energy to the granular materials. Therefore, it is reasonable to anticipate that the TWC with a 0.5 mm thin plate would offer significantly superior vibration damping compared to other plates due to its heightened vibration characteristics. However, contrary to expectations, it has been observed that the TWC featuring a plate with a 1.0 mm wall thickness demonstrates significantly enhanced damping performance. Consequently, it is conceivable that the vibration behavior of the plates is influenced by the mass of the rubber granulate. As a result, the kinetic energy transferred to the rubber granulate "RG 4.6 mm" by both the test specimen and the TWC with a 0.5 mm wall thickness proves insufficient in providing significant vibration mitigation, particularly within the high-frequency range.

The TWC design strategy presented in this chapter proves to be an effective approach for enhancing granular material movement within the particle damper, thereby improving its vibration attenuation capabilities. To ensure optimal performance, maintaining a uniform wall thickness in the TWC design is recommended, as it helps minimize the impact of granular material mass on the TWC's vibrational behavior. However, the ideal wall thickness depends on multiple factors, including the available hollow

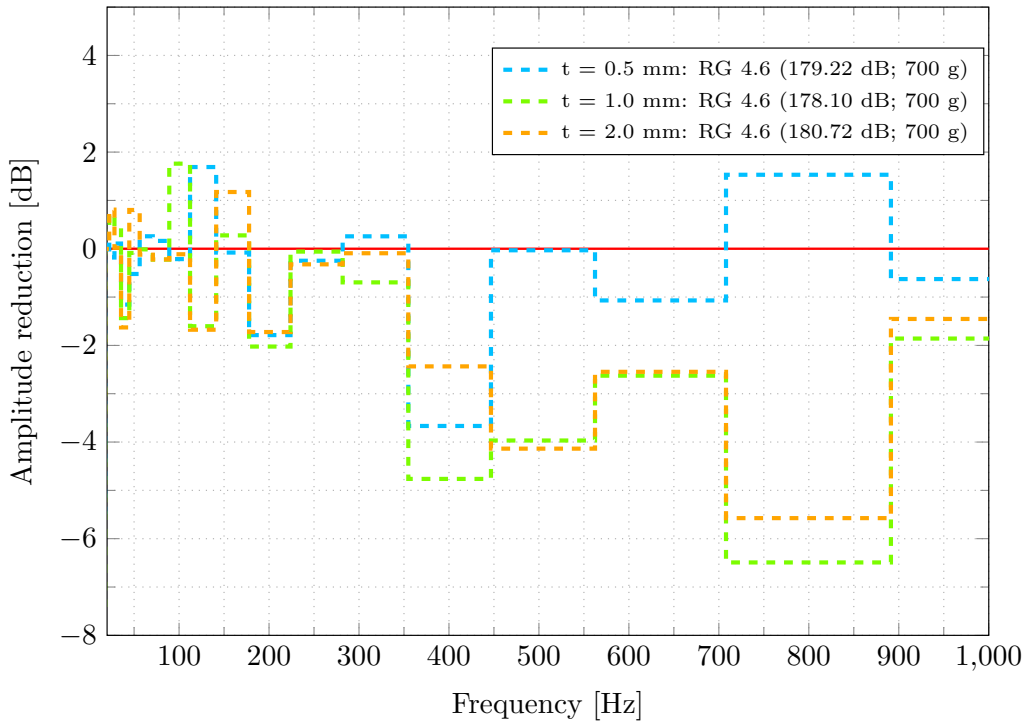

Figure 6.13: Amplitude reduction plot for a partially filled TWC with varying wall thicknesses (t). The SL values of surface velocity are presented in dB, and the mass of the granular filling materials is reported in grams (g).

space in the test specimen, the specimen's wall thickness, and the mass of the granular materials. Establishing an exact correlation between these parameters requires further extensive experimental investigations. Nonetheless, the key objective of this chapter was to demonstrate that integrating a passive design strategy like TWC into a particle damper can significantly enhance its damping efficiency, particularly in scenarios where structural vibrations are insufficient to effectively mobilize the granular materials within the damper.

6.4.2 Influence of location and dimension of the TWCs variant

The damping performance of particle dampers is influenced not only by their placement within the structure but also by the configuration and properties of the granular materials contained within them. In structures with relatively simple geometries, such as beams, it is often straightforward to estimate regions where displacement is more pronounced, which allows for the strategic placement of particle dampers. For instance, positioning a particle damper at the tip of a cantilever beam is highly effective, as the free end of the beam undergoes significant motion, making it an optimal location for vibration attenuation. However, in the case of more complex geometries, identifying the optimal location for placing particle dampers becomes far more challenging. Without prior experimental or computational investigation, it is difficult to predict the regions of maximum displacement, which are critical for ensuring the effectiveness of particle dampers.

In Chapter 5, it was noted that the vibration response of the system remains unaltered beyond a certain increase in the quantity of granular material within a particle damper. Furthermore, to optimize the design efficiency of TWCs while minimizing the added mass of granular material, it is essential to examine the impact of both the location and size of TWCs on the vibration response of the test specimen. Therefore, this section delves into investigating the damping effectiveness of TWCs at

different locations on the test specimen and examines how varying sizes of TWCs influence the vibration response of the L-shaped test specimen.

Experimental investigations conducted for the TWCs in Subsection 6.4.1 have demonstrated that a thin plate with a thickness of 1.0 mm is optimal for designing a particle damper for the hollow test specimen. Therefore, to analyze the influence of TWCs positioning on the test specimen and the impact of TWCs dimensions on vibration attenuation, thin plates of 1.0 mm thickness are employed in TWC design. It is crucial to emphasize that in exploring the influence of cavity sizes on vibration attenuation, a constant filling ratio is upheld within each cavity. Investigations (outlined in Chapter 9 and Chapter 10) have revealed that maintaining an 80% filling ratio proves most effective in reducing the vibration amplitude of the primary structure, while simultaneously minimizing the additional mass of the granular material. Various studies [8, 149] have also pointed out that a 100% filling volume is ineffective for vibration mitigation, as it restricts the relative motion of the granular materials within the cavity. Therefore, to examine how cavity sizes affect the damping performance of TWCs while ensuring a consistent filling volume, each cavity is filled with 80% rubber granulate "RG 4.6 mm". In this section, the placement of particle dampers at three distinct locations on the test specimen has been examined: the top, middle, and bottom, as illustrated in Figure 6.2. The positioning of the TWCs is chosen to facilitate manual filling and emptying of the granular material.

6.4.2.1 Top position of TWC

This section explores the impact of the dimensions of TWCs on structural vibration mitigation. Three distinct TWCs, designated as TWC 1, TWC 2, and TWC 3, are strategically positioned at the top of the L-shaped hollow specimen, as illustrated in Figure 6.3 (a)-(c). Each TWC possessed identical base dimensions of 180 mm $\times 180$ mm, while their respective heights differed, namely: 60 mm for TWC 1, 120 mm for TWC 2, and 180 mm for TWC 3. Furthermore, the internal filling of each TWC consisted of rubber granulate, with weights of 800 g, 1600 g, and 2400 g for TWC 1, TWC 2, and TWC 3, respectively. This filling constituted 80% of the total volume within each TWC.

Similarly to the results discussed in the previous section, it has been observed here as well that, regardless of their dimensions, the presence of empty TWCs alters the vibration characteristics of the primary structure, particularly affecting torsional modes within the frequency range of 410 Hz to 535 Hz (see Figure A2.5 in Appendix A2). Furthermore, the presence of empty TWCs also affects the bending mode of the test specimen at its resonant frequency of 668 Hz. Moreover, similar to observation in Subsection 6.4.1, here also empty TWCs have negligible influence on the dynamic response below 400 Hz.

A notable reduction in vibration amplitude is evident around the central frequencies of 400 Hz and 500 Hz due to the presence of empty TWCs, as illustrated in Figure 6.14. However, their effect on vibration attenuation of primary structure, particularly for bending modes, is considerably lower when mounted at the top position of the specimen. Therefore, to quantify the precise vibration reduction achieved by the top-positioned TWCs on the test specimen, an amplitude reduction plot was generated following the methodology outlined in Subsection 6.4.1. In essence, this plot represents the difference between the vibration levels measured with an empty and partially filled TWC, as illustrated in Figure 6.15.

Figure 6.15 demonstrates that all three partially filled TWCs positioned at the top of the test specimen, namely TWC 1, TWC 2, and TWC 3, have the ability to reduce vibration amplitude of the structure. However, within the frequency range of 354 - 562 Hz, TWC 2 (golden rod dashed line) outperforms TWC 1 (light coral dashed line) and TWC 3 (saddle brown dashed line) in mitigating test specimen vibration amplitude. Notably, TWC 2 achieves up to 15 dB reduction in vibration amplitude at the resonance frequency of 500 Hz, and 14 dB and 13 dB vibration reductions at 35 Hz and 400 Hz, respectively.

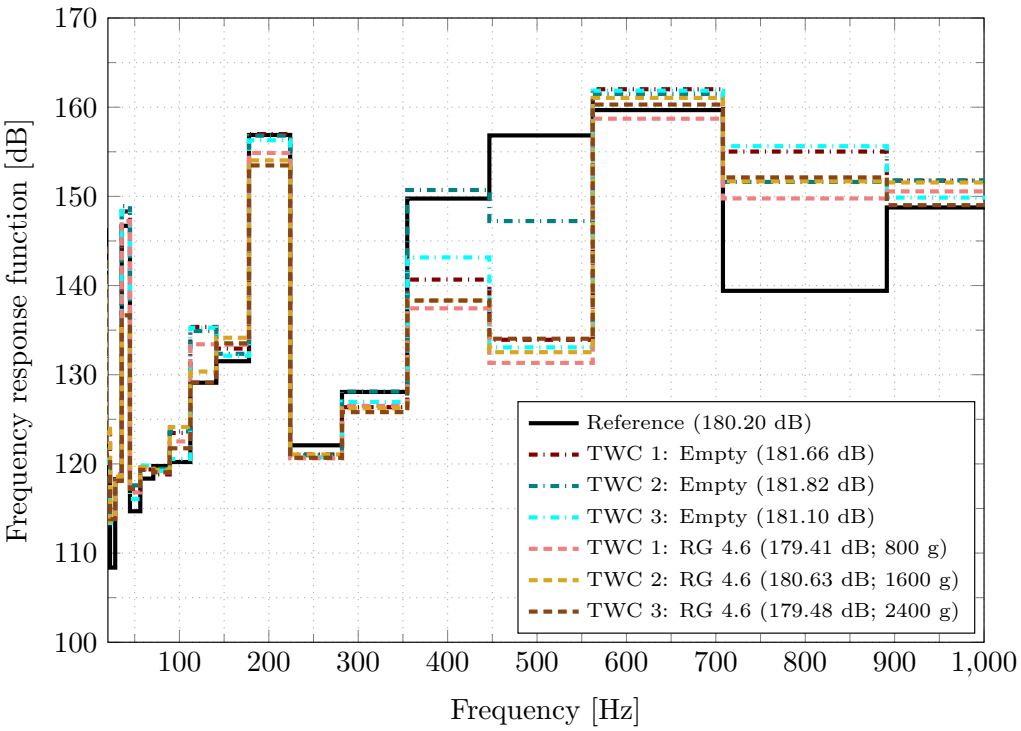

Figure 6.14: One-third octave band of empty and partially filled TWCs with different dimensions at the top position of the test specimen. The SL values of surface velocity are presented in dB, and the mass of the granular filling materials is reported in grams (g).

The improved damping performance of TWC 2 can be credited to its higher content of rubber granulate particles compared to TWC 1, with 800 g more "RG 4.6 mm" particles. This translates to more contact and collision points within the bulk material, enhancing friction and consequently, energy dissipation. On the other hand, although TWC 3 contains a greater quantity of rubber granulate "RG 4.6 mm" particles, its damping efficiency remains considerably lower than that of TWC 2. This can be attributed to the higher mass of granular materials in TWC 3, which may restrict the relative motion of the lower layer of rubber granulate particles. Consequently, it is possible that some rubber particles in TWC 3 do not actively contribute to the particle damping mechanism.

This analysis highlights that the observed reduction in vibration is mainly due to the particle damping mechanism, rather than solely increased mass. The optimized configuration of TWC 2 enhances particle interactions, resulting in superior damping performance across various frequencies.

6.4.2.2 Mid position of TWC

Considering the specific arrangement of holes in the middle section of the test specimen, it is possible to design two distinct TWC configurations, referred to as TWC 4 and TWC 5, as shown in Figure 6.3 (d) -(e). These configurations are constructed with dimensions of $180\times180\times60$ mm and $180\times180\times120$ mm, respectively. Both TWC 4 and TWC 5 maintain a uniform filling volume of 80% using rubber granulate "RG 4.6 mm", following the same methodology employed for the TWCs positioned at the top (TWC 1, TWC 2, and TWC 3).

In accordance with the findings discussed in Subsection 6.4.2.1, the presence of an empty TWC at the middle position exerts a clear influence on the vibration characteristics of the test specimen. This effect is visually represented in Figure A2.6 found in Appendix A2. While the general trends in how

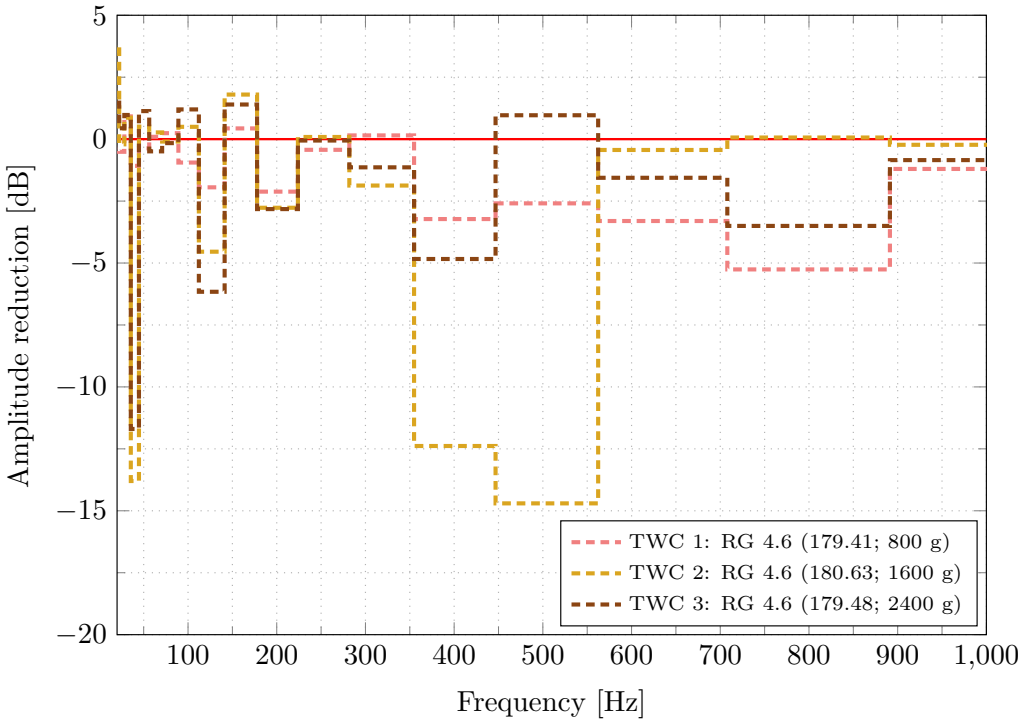

Figure 6.15: Amplitude reduction plot for partially filled TWCs with different dimensions at the top position of the test specimen. The SL values of surface velocity are presented in dB, and the mass of the granular filling materials is measured in grams (g).

the TWC configuration affects vibration are consistent between the top and mid positions (particularly for the central frequencies of 400Hz and 500Hz) there is a notable variation in the extent of amplitude reduction between these positions when empty TWCs are employed. As expected, a reduction in vibration amplitude has been observed due to the presence of an empty TWC at the middle position, a phenomenon that is further illustrated in Figure 6.16. Consequently, the amplitude reduction observed in this setup has been estimated using a method similar to that described in Subsection 6.4.1 and Subsection 6.4.2.1.

As shown in Figure 6.17, the vibration response of the system exhibits a consistent reduction across the entire frequency spectrum when employing the TWC with dimensions of $180 \times 180 \times 120$ mm (TWC 5). In contrast, the effectiveness of the TWC with smaller dimensions, measuring $180 \times 180 \times 60$ mm (TWC 4), is more limited, showing significant damping only at frequencies above 700 Hz. A similar damping pattern is observed when particle dampers of the same dimensions are placed at the top of the test specimen, further demonstrating the influence of TWC size and position on the vibration response, as depicted in Figure 6.17.

It is important to highlight that, although TWC 1 and TWC 4 possess identical dimensions and mass, TWC 1 demonstrates a markedly superior damping efficacy. Furthermore, TWC 2 effectively reduces vibration amplitudes by as much as 13 dB, 12 dB, and 15 dB at resonance frequencies of 35 Hz, 400 Hz, and 500Hz, respectively. In comparison, TWC 5, which is a particle damper of similar size placed at the midpoint of the test specimen, achieves vibration amplitude reductions of up to 11 dB, 8 dB, and 10 dB at the same resonance frequencies.

It is noteworthy that both TWC configurations incorporate a similar quantity of rubber granulate. However, at a resonance frequency of 800 Hz, TWC 5 reveals a significant reduction in the system's vibration response, achieving a reduction of 7.2 dB. In contrast, TWC 3, which shares the same

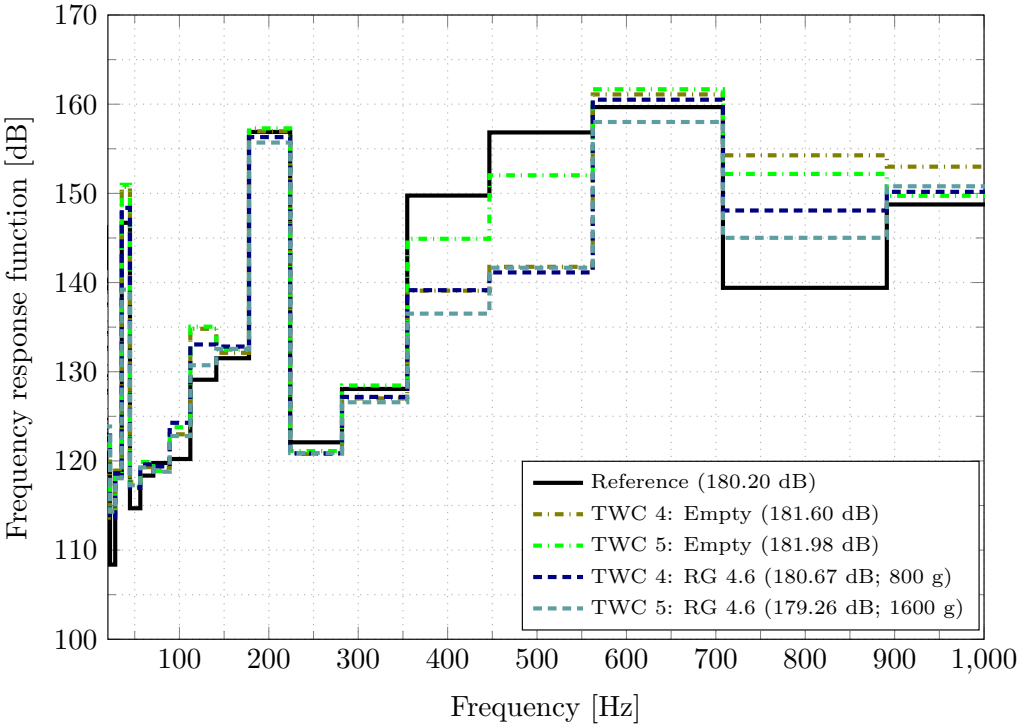

Figure 6.16: One-third octave band of empty and partially filled TWCs with different dimensions at the mid position of the test specimen. The SL values of surface velocity are presented in dB, and the mass of the granular filling materials is reported in grams (g).

dimensions and mass of filling material as TWC 5, does not exhibit substantial vibration attenuation at the 800 Hz resonance frequency.

The disparity in damping effectiveness may be attributed to the location of the bending mode shape's maximum displacement, which occurs at the midpoint of the test specimen, as illustrated in Figure 6.11. At the resonance frequency of 800 Hz, the peak bending displacement in the central region of the test specimen enhances the relative motion of the rubber granulate particles within TWC 5. Consequently, the frequency of particle-particle and particle-wall collisions is likely to increase, thereby enhancing the overall damping effect.

6.4.2.3 Bottom position of TWC

The third potential placement for the TWC is situated at the lower portion of the L-shaped hollow test specimen. As discussed previously, it is evident that the empty TWC can influence the vibration characteristics of the primary structure. Consistent with earlier observations, in this instance as well, the empty TWC at positions L 6 (TWC 6), L 7 (TWC 7), and L 8 (TWC 8) on the lower section of the test specimen alters the dynamic behavior of the main structure. However, the empty TWC in this scenario leads to a modification in the vibration characteristics of the test specimen below 400 Hz, particularly noticeable in the torsional mode around the resonance frequency of 200 Hz. This phenomenon is not observed when empty TWC is mounted at the top and middle positions of the test specimen, as illustrated in Figure 6.18. Nevertheless, within the frequency range of 410 Hz to 535 Hz, there is no notable frequency shift due to the empty TWCs, as observed in earlier cases. Moreover, above 500 Hz, both a frequency shift and a reduction in vibration amplitude were observed due to the absence of TWC. The plot illustrating the reduction in amplitude for this setup, see Figure 6.19, is also generated by subtracting the amplitude of the empty TWC from that of the partially filled TWC.

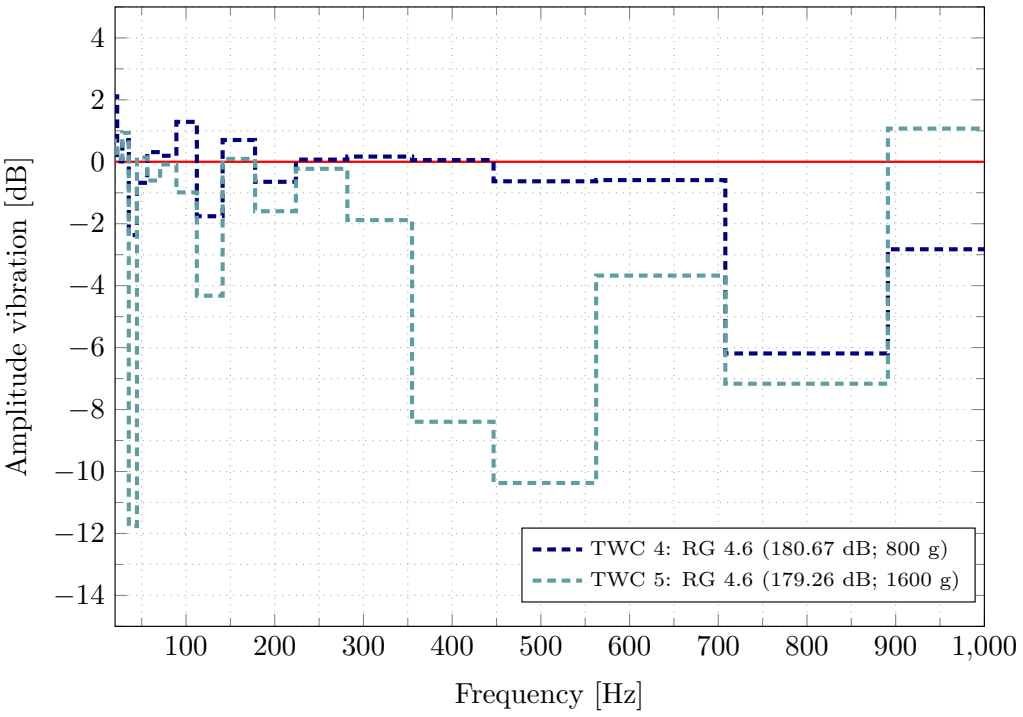

Figure 6.17: Amplitude reduction plot for partially filled TWCs with different dimensions at the mid position of the test specimen. The SL values of surface velocity are presented in dB, and the mass of the granular filling materials is measured in grams (g).

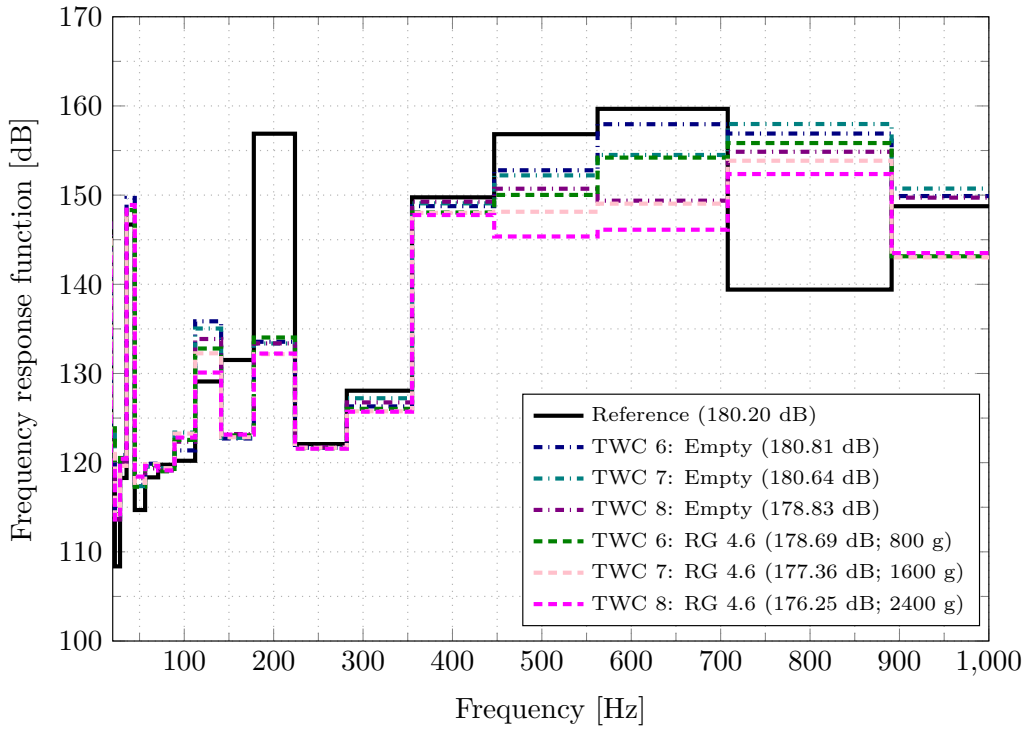

Figure 6.18: One-third octave band of empty and partially filled TWCs with different dimensions at the bottom position of the test specimen. The SL values of surface velocity are presented in dB, and the mass of the granular filling materials is reported in grams (g).

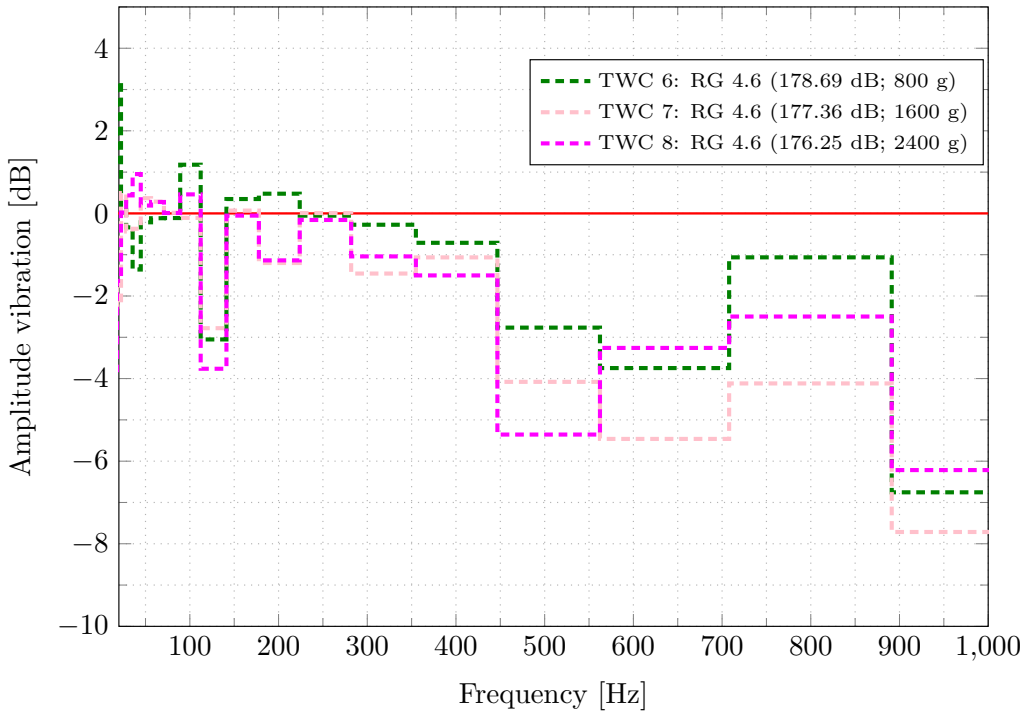

Figure 6.19: Amplitude reduction plot for partially filled TWCs with different dimensions at the bottom position of the test specimen. The SL values of surface velocity are presented in dB, and the mass of the granular filling materials is measured in grams (g).

Figure 6.19 demonstrates the significant vibration attenuation achieved by cavities mounted on the test specimen bottom section. Notably, these cavities achieve maximum reduction in vibration amplitude at specific frequencies: 100 Hz, 500 Hz, 650 Hz, and 900 Hz. It is worth mentioning that TWC 8 exhibits superior damping performance compared to TWC 7 below 550 Hz. Conversely, above 550 Hz, TWC 7 demonstrates better damping efficiency than TWC 8. Additionally, as anticipated, TWC 6 shows a notably lesser ability to reduce the vibration amplitude of the test specimen when compared to TWC 7 and TWC 8.

6.4.2.4 Conclusion

The preceding discussion indicates that positioning the TWC at the uppermost part of the test specimen yields a considerably more substantial reduction in vibration amplitude compared to when positioned at other locations. Moreover, the damping effectiveness of the TWC installed at the bottom of the specimen is significantly lower to that of the TWC installed at the top and middle positions. The poor performance of the TWC at the bottom position may be attributed to the boundary condition. As detailed in Section 6.3, the specimen's bottom section was rigidly fixed to the measuring table using identical steel beams to minimize experimental uncertainties and ensure result reproducibility. This fixed boundary condition, however, restricted the movement of rubber granulate particles within the bottom-mounted TWC, consequently leading to a significantly lower damping capability compared to other TWC configurations.

Analysis across Subsections 6.4.2.1, 6.4.2.2, and 6.4.2.3 reveals the critical role of TWC placement in mitigating test specimen vibration amplitude. Moreover, an analysis of various TWC locations reveals that positioning particle dampers in regions with higher displacement or surface velocity within the mode shape enhances vibration attenuation. This effect arises because placing the damper at locations with higher displacement introduces more kinetic energy into the granular material, thereby

increasing particle-particle and particle-wall interactions, which in turn improves the damper's overall vibration attenuation performance. A comparable finding regarding the optimal placement of particle dampers on a structure has been reported in the studies by Zhao et al. [177] and Koch et al. [150]. Their results, along with those presented in this chapter, confirm that positioning the particle damper in regions with higher displacement or surface velocity within the mode shape is most effective for vibration attenuation. This alignment in outcomes reinforces the understanding that such locations facilitate greater energy transfer into the granular material, enhancing particle interactions and thereby improving damping performance. Furthermore, filling ratios play a crucial role in the design of particle dampers. It has been observed that increasing the number of granular material particles enhances the vibration attenuation capability of the damper up to a certain threshold. In this study, a maximum attenuation is achieved at an 80% filling ratio, beyond which the damping performance declines. This reduction can be attributed to the restricted motion of the lower layer of granular particles due to the mass of the upper layers. A similar trend has also been observed in Chapter 5.

6.4.3 Multi-unit and single-unit TWC

The configuration of particle dampers, such as single-unit (SU) particle dampers and multi-unit (MU) particle dampers, are additional factors that can influence the vibration response of a system [148, 209]. To evaluate their effectiveness, a brief experimental investigation was conducted, analyzing the impact of both damper types on the damping performance of the TWCs. Based on the preceding discussion, the top position of the test specimen emerged as the optimal location for the TWC due to two key factors. Firstly, it exhibited the highest displacement value, indicating its potential for effective vibration mitigation. Secondly, mounting, demounting, filling, and refilling the TWC at this location proved significantly easier compared to other positions. Therefore, the top position was chosen for a comparative study evaluating the damping efficiency of SU and MU TWCs.

The design of the MU TWC involved mounting two thin plates of 1.0 mm thickness at locations L 2 and L 3, as shown in Figures 6.2 and Figure 6.3 (i). This contrasts with the SU TWC positioned at the top of the test specimen, which utilized a single cavity. Both TWCs contained the same amount of granular material (2400 g of rubber granulate). Notably, the MU TWC distributed this mass equally across its two cavities (800 g per cavity), while the SU TWC employed a single cavity filled entirely with 2400 g of rubber granulate "RG 4.6 mm".

It has been observed that the SU TWC exhibits significantly higher damping performance around the resonance frequencies of 40 Hz, 125 Hz, and 400 Hz compared to the MU TWC, see Figure 6.21. Interestingly, the MU TWC exhibits a significant rise in damping performance above 450 Hz. Moreover, the overall damping effectiveness of the MU TWC remains superior, as evidenced by the consistently lower SL values across the entire frequency range in Figure 6.21. The potential mechanisms behind the observed differences in damping performance can be attributed to the contrasting configurations of the SU and MU TWCs. As discussed in Section 6.4.2, the TWC containing 2400 g of rubber granulate exhibits lower performance compared to the TWC filled with 1600 g of rubber granulate. This can be attributed to the restricted motion of the lower layer of granular material due to the mass of the upper layer. However, the MU TWC, with an increased number of thin plates compared to the two present in the SU TWC, effectively divides the total cavity into two smaller cavities. This division reduces the pressure exerted on the lower layer of granular material by the overall mass. Additionally, the introduction of a third thin plate within the cavity contributes to the excitation of kinetic energy in the granular material. These two factors collectively enhance the vibration attenuation performance of the MU TWC significantly compared to the SU TWC.

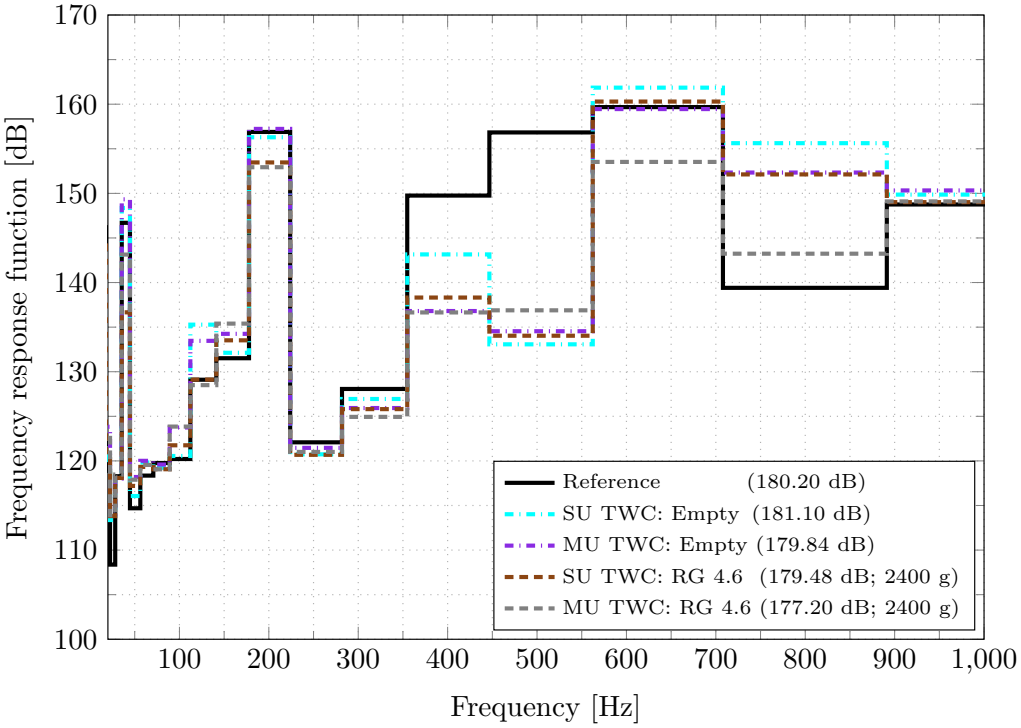

Figure 6.20: One-third octave band for empty and partially filled SU and MU TWCs. Surface velocity SL values are provided in dB, and the mass of the granular filling materials is in g.

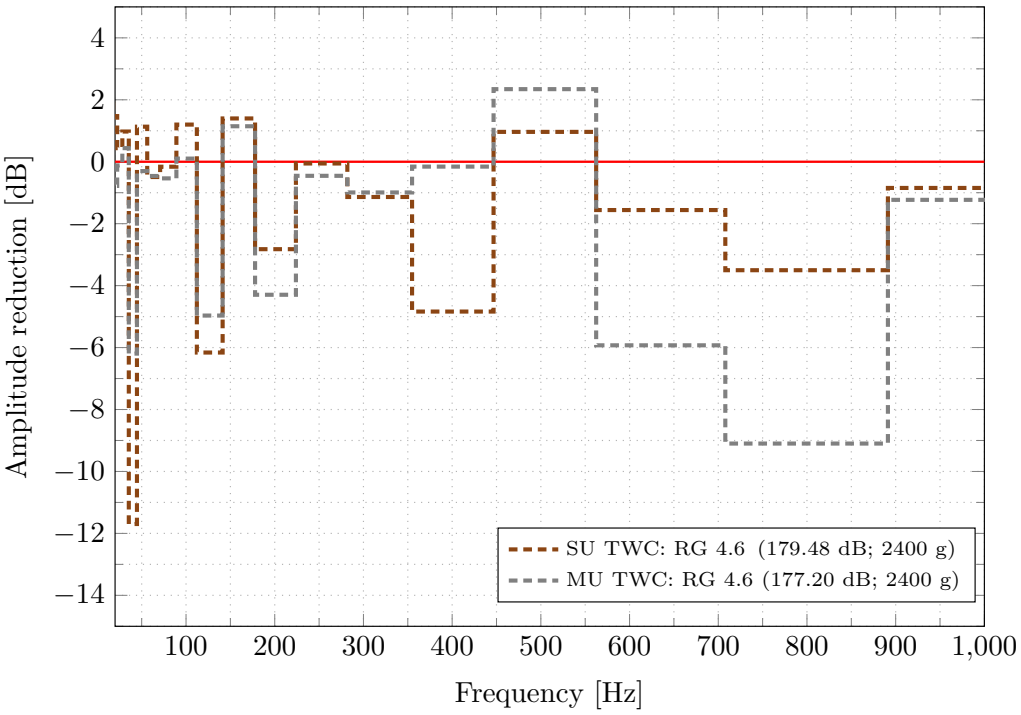

Figure 6.21: Amplitude reduction plot for empty and partially filled SU and MU TWCs. Surface velocity SL values are provided in dB, and the mass of the granular filling materials is in g.

6.4.4 Composition of TWC

Previous findings suggest that positioning the TWC at the uppermost part of the test specimen leads to a significant reduction in vibration amplitude compared to other locations. Conversely, mounting the TWC at the bottom of the test specimen was observed to be less effective. Hence, this section outlines a brief experimental investigation aimed at evaluating the effect of combining the most and least efficient TWC positions on vibration attenuation.

To accomplish this, two TWCs measuring $180 \times 180 \times 180$ mm have been simultaneously installed at the top and bottom positions of the test specimen, as depicted in Figure 6.3 (j). Moreover, these TWCs were filled partially with 2400 g of rubber granulate "RG 4.6 mm", and the outcomes of this setup are illustrated in Figure 6.22 and Figure 6.23.

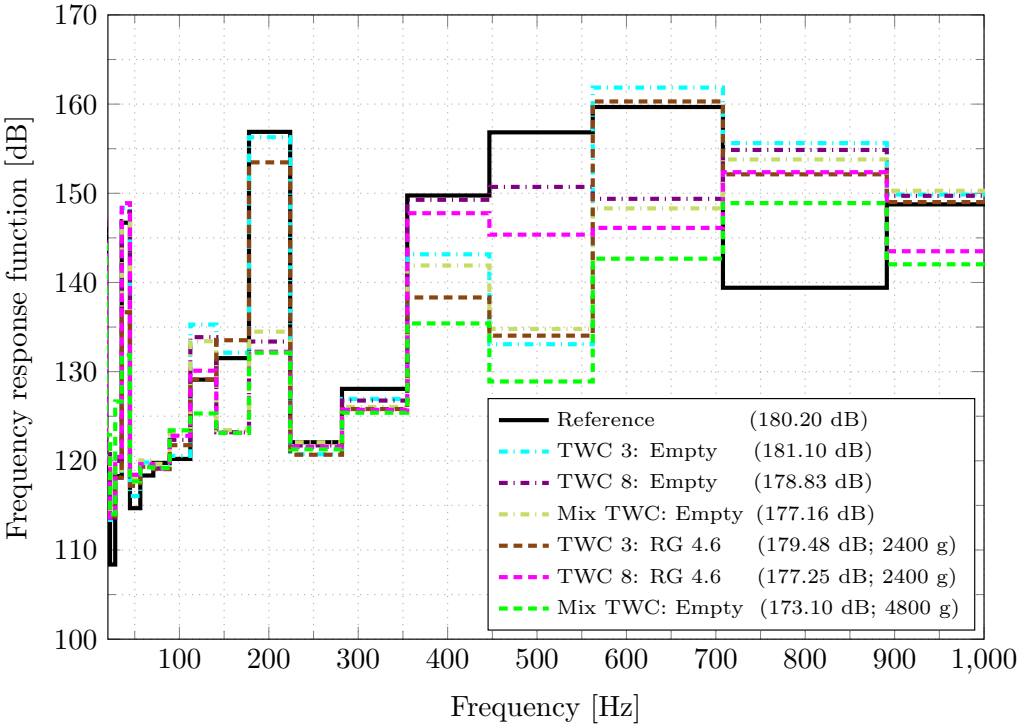

Figure 6.22: One-third octave band for the empty and partially filled SU and mix TWCs. The SL values of surface velocity are presented in dB, and the mass of the granular filling materials is provided in g.

To facilitate comparison, the FRF spectrum of TWC 3 and TWC 8 are also plotted in Figure 6.22 and Figure 6.23. Notably, TWC 3 occupies the top position of the test specimen, while TWC 8 is situated at the base. Importantly, both TWCs share identical dimensions of $180 \times 180 \times 180$ mm. The combined TWCs demonstrably achieve a significantly greater reduction in vibration amplitude compared to TWC 3 and TWC 8 individually. This enhanced performance can potentially be attributed to the increased number of rubber granular particles within the combined TWC cavities. Furthermore, a significant reduction in vibration amplitude is observed for TWC 8 compared to TWC 3 around 500 Hz, with similar trends noted at 650 Hz and 950 Hz. Therefore, it can be assumed that at these frequencies, the lower portion of the test specimen undergoes greater displacement around the corresponding eigenfrequencies compared to the upper section. However, to confirm this assumption, further analysis is required, including direct measurement of the surface velocity of the base part or a comprehensive numerical investigation.

Based on the preceding discussion, it can be concluded that the integration of TWCs results in a

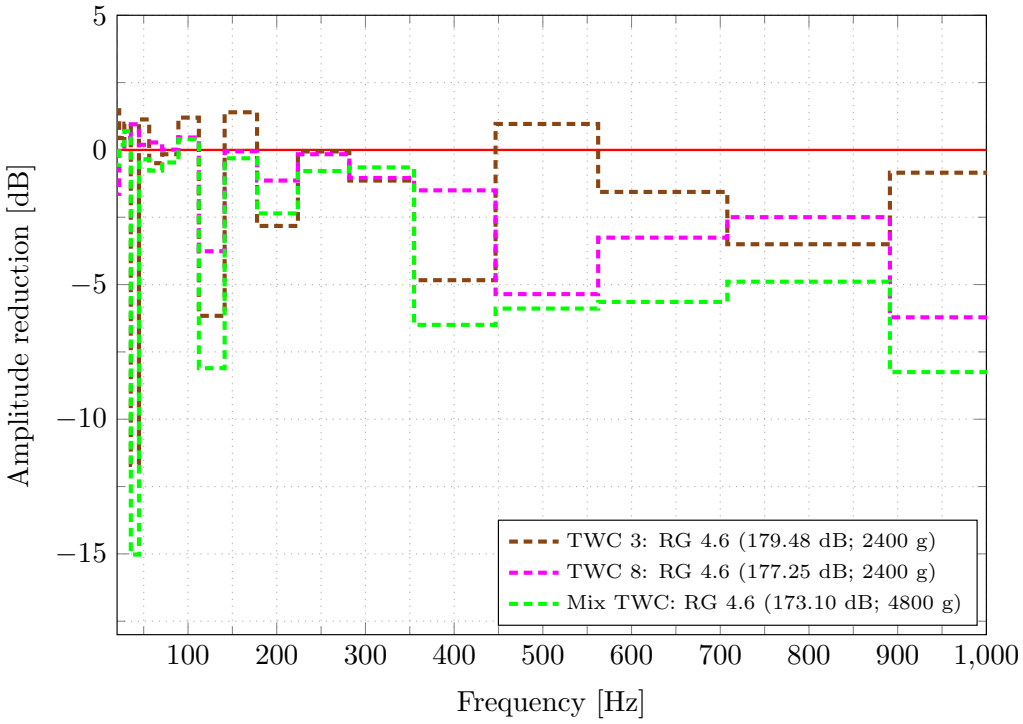

Figure 6.23: Amplitude reduction plot for the empty and partially filled SU and mix TWCs. The SL values of surface velocity are presented in dB, and the mass of the granular filling materials is provided in g.

substantial improvement in the overall vibration reduction of the system. This suggests that, rather than relying on a single particle damper, the attachment of multiple particle dampers to regions of the structure experiencing higher displacement would be more effective in enhancing vibration mitigation. However, it is important to consider that this configuration would also lead to a significant increase in the total mass of the granular materials used within the dampers. As a result, while the placement of several particle dampers may improve damping performance, the associated increase in mass must be carefully evaluated.

6.4.5 Thin-wall cavity with additional sheets (TWC-AS)

In the TWC-AS configuration, the thickness of the suspended sheet is significantly less than that of the main structural wall. Consequently, the suspended sheet is more flexible and susceptible to vibrations[1], thereby transferring more kinetic energy to the particles within the particle damper. This increased kinetic energy amplifies collisions both among particles and between particles and the walls. Hence, it is postulated that TWC-AS exhibits greater damping efficiency compared to conventional TWC setups.

The TWC-AS comprises two key components: a base plate with a thickness of 1.0 mm and variously sized hanging sheets. The selection of the base plate wall thickness is guided by findings from the TWC design analysis, which showed that a 1.0 mm wall thickness demonstrated superior overall vibration mitigation performance compared to designs with 0.5 mm and 2.0 mm thicknesses. Figure 6.5 illustrates the design and various configurations of the TWC-AS. Building upon the previous discussion, the top position of the test specimen emerges as the optimal location for mounting a particle damper. Consequently, the TWC-AS is specifically designed and positioned at this specific location to evaluate its influence on the dynamic response of the system.

[1]The vibration behavior is determined by material properties, boundary conditions, and external excitations.

To design the TWC-AS within the hollow test specimen, a thin plate measuring 1.0 mm in thickness is installed at position L 4. Following this, 2700 g of rubber granulate "RG 4.6 mm" is introduced into the cavity. Subsequently, the TWC-AS is affixed at position L 1 within the test specimen, facilitating the insertion of suspended thin sheets into the rubber granulate. This configuration enables maximum contact between the hanging sheet and the rubber granulate particles. Moreover, positioning the TWC-AS at location L 1 significantly streamlines the experimental procedure compared to its placement at position L 4. The dimensions of the TWC-AS closely resemble those of the TWC 3. It is well established that an empty TWC, designed from two 1.0 mm thin plates, alters the primary vibration characteristics of the test specimen. Since the TWC-AS design also incorporates base plates with the same 1.0 mm wall thickness, its attachment within the test specimen is expected to similarly affect the dynamic behavior, as observed with TWCs. Therefore, to assess the vibration attenuation provided by the empty TWC-AS, the empty TWC 3 is used as a reference measurement, represented by the black solid line, see Figure 6.24. For comparative analysis, the FRF of the partially filled TWC 3 is also plotted in the frequency response spectrum.

The current investigation reveals that all tested TWC-AS configurations achieved a significant reduction in the vibration amplitude of the test specimen, irrespective of their geometric characteristics, such as shape, size, and thickness. Notably, the majority of TWC-AS configurations demonstrated superior damping performance when compared to the reference TWC3, as illustrated in Figure 6.24 and Figure 6.25.

The enhanced performance of the TWC-AS can be attributed to the kinetic energy induced into the various layers of rubber particles by the thin suspended sheets. It has been observed that TWCs containing a higher volume of granular materials tend to become less effective in vibration attenuation. This reduction in effectiveness arises from the potential restriction of motion among the lower layers of granular material particles due to the weight of the overlying materials.

In contrast, the introduction of a thin sheet within the granular material significantly enhances the system's performance. The thin sheet can effectively induce kinetic energy into each layer of the granular material, with the extent of this energy transfer being influenced by both the length and thickness of the sheet. As a result, this mechanism facilitates improved vibration attenuation capabilities, thereby highlighting the critical role of suspended sheet characteristics in optimizing the performance of TWC-AS systems.

The plot showing the reduction in amplitude is presented in Figure 6.25. TWC-AS with a 1.0 mm suspended sheet thickness (orange-red dashed line) displayed significantly higher vibration attenuation compared to the 0.5 mm version (saddle brown dashed line) around resonance frequencies of 125 Hz, 400 Hz, and 800 Hz. It should be noted that both TWC-AS configurations possessed identical suspended sheet width and height. Interestingly, when comparing smaller TWC-AS configurations (170 mm $\times$ 45 mm), the 0.5 mm sheet thickness variant (SL value 178.77 dB) exhibited superior damping performance compared to the thicker 1.0 mm version (SL value 179.60 dB). This highlights the potential influence of sheet thickness on damping efficiency. Furthermore, a notable observation was the enhanced effectiveness of the "compact TWC-AS" with four suspended sheets (80 mm $\times$ 45 mm) in attenuating low-frequency vibrations (20 Hz - 300 Hz) compared to its two-sheet counterpart. In the low-frequency range, the compact TWC-AS featuring four suspended sheets (dark slate gray dotted line) demonstrates notable vibration attenuation, achieving reductions of 1.2 dB, 7.1 dB, and 6.6 dB around resonance frequencies of 40 Hz, 125 Hz, and 200 Hz, respectively. Conversely, the compact TWC-AS with two suspended sheets (cyan dotted line) proves highly effective in the higher frequency range. Specifically, around resonance frequencies of 400 Hz, 630 Hz, and 800 Hz, it achieves significant reductions in vibration amplitude of the primary structure, reaching 10.1 dB, 7.4 dB, and 7.8 dB, respectively. Furthermore, a compact TWC-AS damper in an inverted configuration was incorporated into the the test specimen. This involved mounting the 1.0 mm thin plate at L 1 and the inverted TWC-AS at L 4 of the test specimen. While this configuration exhibited significantly lower overall effectiveness compared to other TWC-AS designs, it demonstrated a remarkable improvement

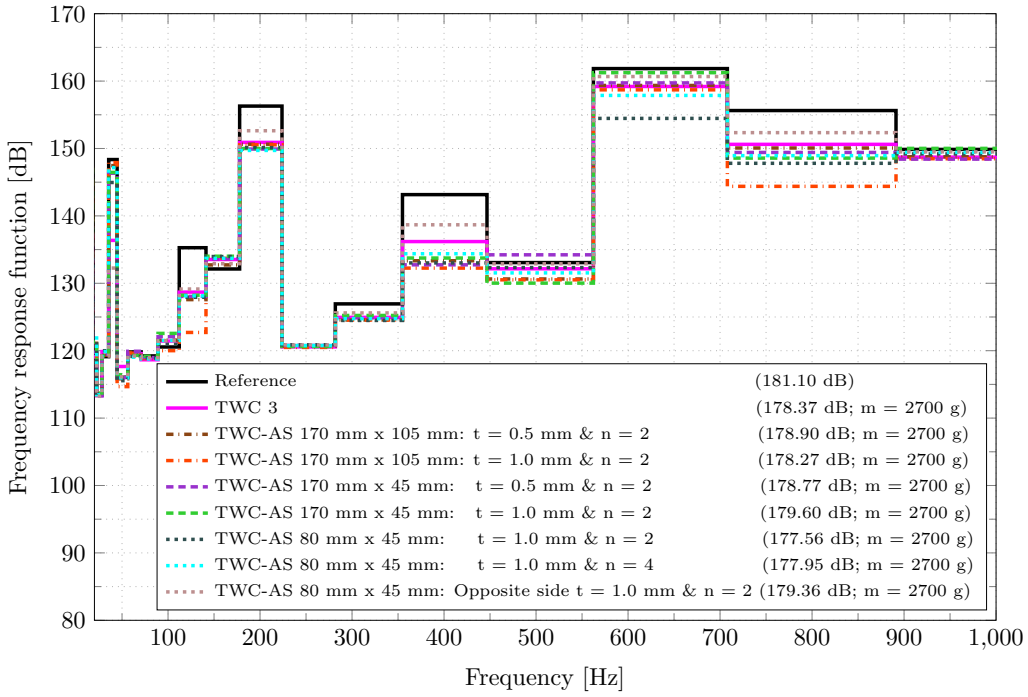

Figure 6.24: One-third octave band of the test specimen with TWC-AS. The SL values for surface velocity are provided in dB, and the mass of the granular filling materials is specified in g.

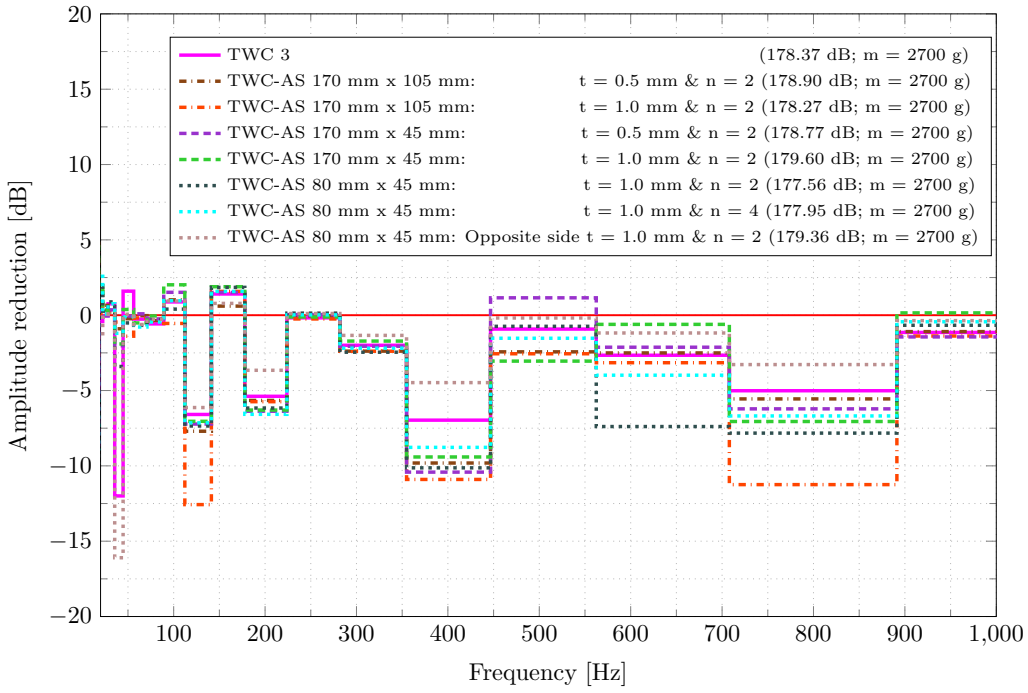

Figure 6.25: Amplitude reduction plot of the test specimen with TWC-AS. The SL values for surface velocity are provided in dB, and the mass of the granular filling materials is specified in g.

in vibration attenuation around the 40 Hz resonance frequency. Notably, it achieved a vibration reduction of up to 16.1 dB (rosy brown dotted line), surpassing the performance of all other TWC-AS

configurations at this specific frequency.

The findings demonstrate that the TWC-AS design strategy significantly outperforms the previously best-performing TWC configuration in reducing the test specimen vibration amplitude. This enhanced damping effect is attributed to the presence of the suspended sheets within the granular material. The sheet likely amplifies the transmission of vibration energy to the particles, thereby increasing particle-particle and particle-wall collisions, leading to a further reduction in the structure's overall vibration response.

In general, a thinner plate is more prone to vibration compared to a thicker plate, assuming both plates are made of the same material, have the same boundary conditions, and experience the same excitation. This is because the reduced bending stiffness of the thinner plate increases its flexibility, making it more susceptible to deformation under dynamic loading. However, the introduction of granular materials can substantially alter the vibration behavior. It is important to note that overly thick plates do not possess the required sensitivity to effectively excite particle motion. Thus, optimal particle damper performance is achieved by maintaining a precise balance between plate thickness and stiffness, avoiding extremes in either property. This finding aligns with the established principles of TWC design, where the specific sheet thickness of the TWC-AS is tailored to the mass of the employed granular material. Similar to the design variants of TWC, comprehensive experimental studies are also crucial in the case of TWC-AS to establish the precise relationship between sheet thickness and test specimen wall thickness in relation to vibration attenuation capability. However, it is important to highlight that the main objective of this chapter is to illustrate how the passive design variants presented here can improve the vibration mitigation performance of the particle damper.

The present study demonstrated the significant impact of suspended sheet size on the damping characteristics of TWC-AS configurations. The results indicate that longer sheets are associated with enhanced vibration amplitude reduction in the test specimen. This phenomenon can be attributed to the increased contact area between the suspended sheet and the granular material, which leads to a higher likelihood of particle-wall collisions and, consequently, improved energy dissipation.

In particular, the extended TWC-AS configuration, measuring 170 mm $\times$ 105 mm $\times$ 1.0 mm, demonstrated a higher reduction in vibration amplitude compared to its smaller counterpart, which has dimensions of 170 mm $\times$ 45 mm $\times$ 1.0 mm. However, it is essential to consider the relationship between sheet length and cavity height. While a longer sheet can effectively promote particle motion, it is crucial that its length does not exceed the cavity height to maintain unrestricted vibration within the TWC-AS system.

Additionally, similar to observations made with traditional TWC systems, the positioning of the TWC-AS plays a vital role in vibration reduction. For instance, installing the TWC-AS at position L 1 results in significantly greater vibration attenuation compared to mounting it at position L 4. These findings underscore the importance of optimizing both the dimensions and placement of the TWC-AS to maximize its damping effectiveness.

6.4.6 Ring cavity design variant (RC)

To assess the influence of RC on mitigating vibrations, two different sizes of RC (large and small) were selected and installed at position L 4 within the hollow space of the test specimen (refer to Figure 6.6). The concept behind RC aims to reduce the weight of the particle damper while either maintaining or enhancing its overall damping effectiveness. To empirically explore this concept, the rubber granulate "RG 4.6 mm" inside the RC was arranged in three configurations, namely: placed externally to the ring (configuration 1), placed internally within the ring (configuration 2), and positioned both internally and externally to the ring (configuration 3), see Figure 6.7.

The outcomes of the RC experiments are illustrated in Figure 6.26 and Figure 6.27. For ease of

comparison, the frequency spectrum of the TWC, comprising a single thin plate with a thickness of 1.0 mm and also installed at position L 4 on the test specimen, is plotted. Previous sections have established that both the empty TWC and the TWC-AS modify the vibration behavior of the primary structure. Similarly, the presence of an empty RC, irrespective of its ring height, also modifies the test specimen vibration characteristics, see Figure A2.10. Thus, to accurately quantify the vibration reduction solely attributable to the RC and TWC, the vibration levels measured with partially filled particle dampers are subtracted from those obtained with their empty counterparts.

Figure 6.27 reveals that around the resonance frequencies of 40 Hz, 315 Hz, and 500 Hz, the TWC with a single thin plate exhibits higher damping efficiency compared to both large and small RCs. Interestingly, for the large RC, vibration attenuation achieved by configuration 1 (yellow-orange dashed line) is nearly equivalent to configuration 3 (lawn green dashed line), see Figure 6.27. Furthermore, both configurations demonstrate the ability to reduce the test specimen vibration amplitude by up to 5.4 dB, 20 dB, and 4.6 dB at central frequencies of 200 Hz, 500 Hz, and 630 Hz, respectively. However, at 125 Hz, 800 Hz, and 1000 Hz, placing the rubber granulate solely outside the large RC ring proves more effective for vibration mitigation.

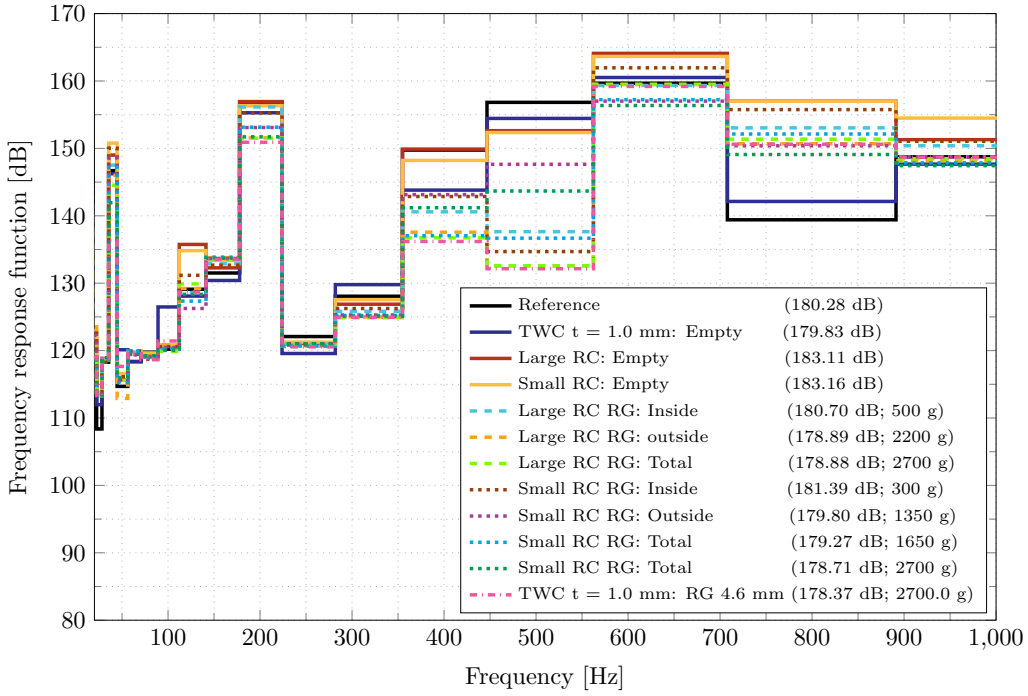

Figure 6.26: One-third octave band of the RC design variant. The SL values for surface velocity are provided in dB, and the mass of the granular filling materials is indicated in g.

Conversely, distributing the rubber granulate inside and outside the large RC ring enhances the RCs damping performance around the resonant frequencies of 40 Hz, 315 Hz, and 400 Hz. Nevertheless, the difference in vibration attenuation achieved by configurations 1 and 3 is marginally less. While configuration 2, with rubber granulate confined within the ring, exhibits some vibration reduction in the test specimen, its overall damping performance falls short compared to the other configurations. This observation can be attributed to the lack of direct particle contact with the vibrating structure. Consequently, kinetic energy transfer to the granular material likely occurs solely through the ring structure, limiting the damping effect. Furthermore, particle interactions within the ring are confined to collisions either with each other or with the ring walls, potentially hindering effective energy dissipation.

In contrast, configuration 1 and configuration 3, where the rubber granulate resides outside and inside

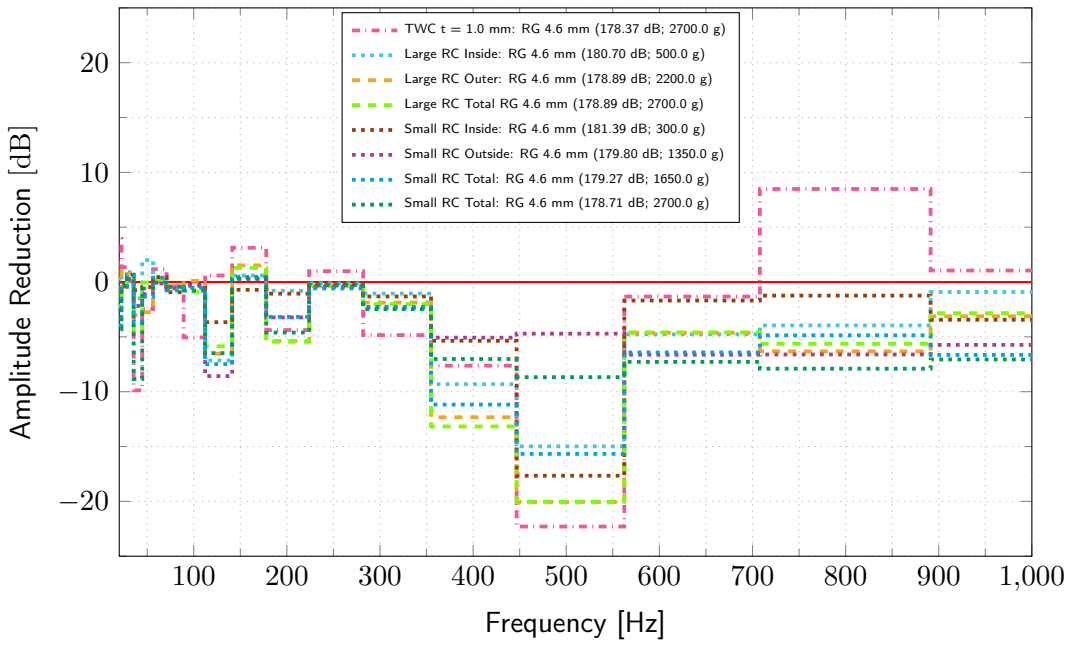

Figure 6.27: Amplitude reduction plot for the RC design variant. The SL values of surface velocity are presented in dB, and the mass of the granular filling materials is specified in g.

the ring, respectively, benefit from a dual excitation mechanism. The kinetic energy in the granulate is induced both by the thin walls of the ring structure and by the vibrations of the test specimen itself, significantly enhancing the probability of particle-particle collisions. This is further amplified by the potential for collisions between particles themselves, with the ring walls, and even with the primary structure walls. Consequently, these configurations exhibit superior damping capabilities compared to configuration 2. Notably, a similar trend in damping effectiveness was observed across all rubber granulate distribution patterns within the small RC, suggesting this principle applies consistently.

To further investigate the influence of RC size, comparative studies were conducted using both large and small RCs containing identical amounts of rubber granulate "RG 4.6 mm". For this purpose, configuration 3 is chosen that contains 2700 g of rubber granulate. The analysis revealed that the larger RC exhibited superior vibration damping performance at resonant frequencies of 200 Hz, 400 Hz, and 500 Hz. Compared to the similarly filled small RC, the large RC achieved significantly higher vibration amplitude reductions of 5.5 dB, 13 dB, and 20 dB, respectively. However, the trend reversed within the 600 - 1000 Hz frequency range, where the small RC proved more effective in dampening the structure. Despite this, the larger RC demonstrated superior overall damping efficiency, highlighting the trade-off between frequency-specific performance and broader damping effectiveness.

Figure 6.26 and Figure 6.27 clearly demonstrate that implementing the RC leads to significantly higher vibration attenuation compared to the TWC. Furthermore, the granular material distribution pattern offers a notable advantage in reducing mass. For instance, configuration 1, where the rubber granulate is placed solely outside the ring, boasts an 18% mass reduction compared to configuration 3, which distributes the granulate both inside and outside. Importantly, the distribution pattern also plays a crucial role in vibration attenuation. This suggests that the thin, rectangular ring, directly contacting the primary structure, and the vibration-sensitive granular materials work together to effectively induce kinetic energy into the particles. This increases the likelihood of particle-particle and particle-wall collisions, ultimately reducing system response. However, further optimization of the ring shape and size is necessary to push the boundaries of vibration attenuation.

6.5 Summary and conclusion

In this chapter, three distinct passive design strategies have been introduced to improve the vibration mitigation capabilities of a particle damper. These strategies include the thin-wall cavity (TWC), the thin-wall cavity with an additional sheet (TWC-AS), and the ring cavity (RC).

The proposed methodology for the TWC variant involves the strategic use of thin plates with varying wall thicknesses to form a well-defined cavity within the hollow section of the specimen. It is essential to ensure that the thickness of the plates used in the TWC is substantially less than that of the primary structural wall. This design consideration facilitates enhanced vibration dynamics and promotes increased kinetic energy transfer to the granular material, ultimately leading to improved damping efficiency.

The findings of this study indicate that the damping performance of the TWC is significantly affected by the thickness of the plates employed. Notably, the variant featuring a plate thickness of 1.0 mm demonstrated a superior overall vibration attenuation capability compared to those with thicknesses of 0.5 mm and 2.0 mm. This observation underscores the importance of maintaining an optimal plate thickness in the TWC design, as it minimizes the impact of the mass of the granular material on the vibration characteristics of the TWC.

Nevertheless, identifying the optimal plate thickness is a complex task that depends on several interrelated factors. These include the available hollow space within the specimen, the overall wall thickness, and the mass of the granular material utilized. Therefore, careful consideration of these parameters is crucial for optimizing the performance of the TWC variant in practical applications.

Beyond the design of the particle damper itself, its positioning and size significantly impact vibration attenuation. To explore this impact, three different locations and dimensions for the TWC variant were investigated. The results suggest that strategically placing the damper in regions with larger displacements or surface velocities leads to enhanced vibration attenuation. Investigations into the impact of TWC dimensions on vibration attenuation, while maintaining a fixed filling volume, revealed that TWC 2 ($180 \times 180 \times 120$ mm) outperforms both TWC 1 ($180 \times 180 \times 60$ mm) and TWC 3 ($180 \times 180 \times 180$ mm). This suggests that the sole factor influencing vibration reduction is not simply the mass of the granular material. In fact, a higher mass can even hinder the relative motion of particles within the lower layer. This implies that, in a TWC with a larger cavity size, a certain portion of the rubber particles might not actively participate in the damping mechanism.

This study demonstrates that the SU TWC is more effective at reducing low-frequency vibration amplitudes, while the MU TWC excels at high-frequency vibration attenuation. However, the MU TWC exhibits significantly higher overall damping performance compared to its SU counterpart. This could be attributed to the presence of more thin plates within the MU design, facilitating the transfer of higher kinetic energy into the granular material and leading to a substantial increase in damping efficiency. Additionally, mounting the particle dampers at both the most and least effective locations on the test specimen simultaneously yielded a remarkable outcome. This combined configuration outperformed single-location setups across the entire frequency range, albeit with the trade-off of increased additional mass.

To further enhance vibration attenuation, the TWC-AS variant was developed. This design incorporates two or more "hanging sheets" attached to a 1.0 mm base plate. The core concept lies in introducing an additional vibration-sensitive structure within the system, directly interacting with the granular material. This aims to maximize kinetic energy transfer to the particles, ultimately increasing damping performance. Several factors influence the TWC-AS effectiveness, including the shape, size, thickness, and number of suspended sheets. An experimental investigation explored the impact of these parameters on vibration attenuation capabilities. The results demonstrate that the TWC-AS significantly outperforms the best-performing TWC variant in reducing the test specimen vibration amplitude. This suggests that the additional suspended sheet effectively induces more kinetic energy into the granular material, leading

to the increased probability of particle-particle and particle-wall collisions, thereby enhancing damping. Similar to the TWC, the TWC-AS suspended sheet thickness is influenced by the mass of the granular material. Additionally, longer sheets, limited by the cavity height, have been observed to improve vibration attenuation.

This chapter also acknowledges the mass limitations associated with granular materials in practical, real-world applications and introduces the RC design variant as a solution. The RC design exhibits significantly improved vibration attenuation compared to the TWC variant, which contains the same quantity of rubber granulate "RG 4.6 mm". Additionally, the chapter explored different distribution patterns of the granular material within the RC design. The findings indicate that the additional mass of the granular material can be reduced by up to 500 g without compromising vibration reduction effectiveness, and in some cases, vibration attenuation is even enhanced at specific resonance frequencies. However, further refinement of the RC's ring geometry is necessary to optimize its performance. In particular, increasing the contact area between the RC and the primary structure has been identified as a potentially advantageous strategy for improving overall efficiency.

In this chapter, various design approaches for reducing vibration amplitudes in hollow-structured test specimens have been explored. It should be noted that these design concepts are not restricted to hollow structures but can be incorporated into conventional particle-based designs or adapted to other structural forms. In Chapters 11 and 12, it will be further demonstrated how these concepts can be utilized to enhance the vibration attenuation capabilities of particles in large-scale industrial structures. Through this, the potential for improving vibration control at an industrial scale will become clearer.

7 Particle damper performance under dynamic and thermal loads

Particle damper concepts, as explored in previous chapters, suggest that these devices encounter significant dynamic forces during operation. This raises concerns regarding potential degradation in their vibration attenuation capabilities over time. Consequently, evaluating a particle damper's performance after exposure to dynamic loads becomes critical before its real-world implementation.

Existing research has primarily focused on optimizing performance by analyzing the influence of factors such as filling ratio, excitation frequency, cavity size, and particle quantity (see Chapters 1 and 2). However, it is crucial to acknowledge that the enclosed granular materials within the damper are subjected to significant dynamic stresses during operation. These continuous dynamic loads have the potential to alter the properties of the granular media, impacting the wear, durability, and overall reliability of the particle damper. Given the high sensitivity of particle damper performance to the condition of the granular media, a focus on ensuring their long-term viability is paramount as their adoption in commercial applications expands.

This chapter aims to address this gap in knowledge by conducting a series of experiments to evaluate the vibration reduction characteristics of a particle damper. The damper will undergo millions of high-amplitude dynamic loads and temperature cycles over the course of several months. This will allow for the assessment of performance changes before and after the exposure. This chapter will provide crucial insights into the long-term performance and durability of particle dampers, ultimately aiding their reliable application in real-world scenarios. This chapter expands on the findings presented in a previously published paper [212].

7.1 Test specimen design

For evaluating the long-term durability of particle dampers, a dedicated laboratory test specimen was designed and manufactured. The specific details of this specimen, including its dimensions and configuration, are presented in Figure 7.1. A key objective during the design of the test specimen was achieving geometric simplicity. This approach offered several advantages. Firstly, it ensured a straightforward and cost-effective manufacturing process. Secondly, the design prevented granular material from spilling when mounted on a vibrating table and subjected to high-amplitude dynamic loads. Finally, a simple geometry facilitates the utilization of experimental results for the development and validation of numerical simulations in future studies.

These requirements were effectively met by using a box with a lid as the test specimen design. To further optimize the test specimen, a 4 mm thick, slender slab with two elongated holes was welded to the underside of the box. This design element served a dual purpose. Firstly, it provided rigid attachment to the measurement table, enhancing stability and minimizing experimental uncertainties. Secondly, it decoupled the box from the table, potentially mitigating unwanted vibration transfer. The elongated holes facilitated the secure mounting of the box onto the vibrating table during dynamic testing under high loads. The specific shape of the holes was necessitated by limitations in obtaining detailed setup information for the vibrating table used by the industrial partner during the initial design stage. Additionally, for secure closure during transport and testing on the vibrating table, the open top of the box was fitted with two square plates containing 8 mm holes. These plates facilitated lid

attachment using bolts. It is important to note that lids were used only when the partially filled boxes were mounted on the vibrating table to prevent the granular material from spilling. During vibration measurements, the boxes remained open to allow for unobstructed data collection.

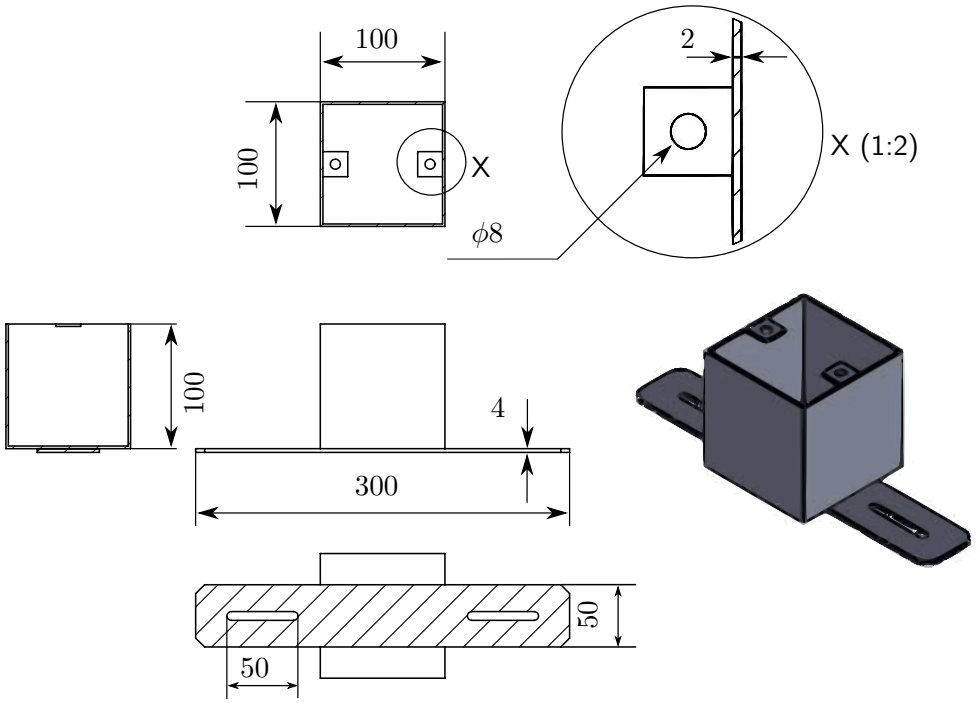

Figure 7.1: Test specimen design and dimensions for particle damper performance evaluation under high-amplitude dynamic loading and temperature fluctuations (All dimensions in mm).

This study utilized five identical steel boxes fabricated by WRD GmbH. One box was modified by incorporating two internal layers of polycarbonate (PC). This specific material selection was based on the anticipated increased wear susceptibility of PC compared to the steel walls.

7.2 Experimental setup to measure system response

Building upon the methodologies established in Chapters 5 and 6, this section details the experimental setup designed to investigate potential changes in the vibration characteristics of granular materials after getting exposed to intense dynamic loads and temperature variations, see Figure 7.2. This configuration mirrors the setup described in Chapter 5, ensuring consistency for comparative analysis. A Polytec LSV (model PSV-400) serves as the primary tool for measuring the system's dynamic response, replicating the approach used in previous chapters. A torque wrench is again employed to mount the test specimen, acknowledging the previously observed influence of bolt tightening on the dynamic response. To maintain consistency in specimen excitation and data acquisition, the methods outlined in Chapter 5 are meticulously followed. This includes utilizing an impulse signal from an electrodynamic shaker (TIRA) to excite the specimen, measuring the input force signal, and avoiding double strokes. Throughout the study, the experimental setup remained unchanged to ensure consistent frequency response. The out-of-plane surface velocity of the specimen was captured using the horizontally placed scanning head of the laser vibrometer.

A fine rectangular grid of 81 measuring points covered the designated measurement area, see Figure 7.3 (right). Four filled circles served as reference markers for consistent targeting across repeated measurements, including those conducted after a 20-month interval (Figure 7.3, left). The number of scanning

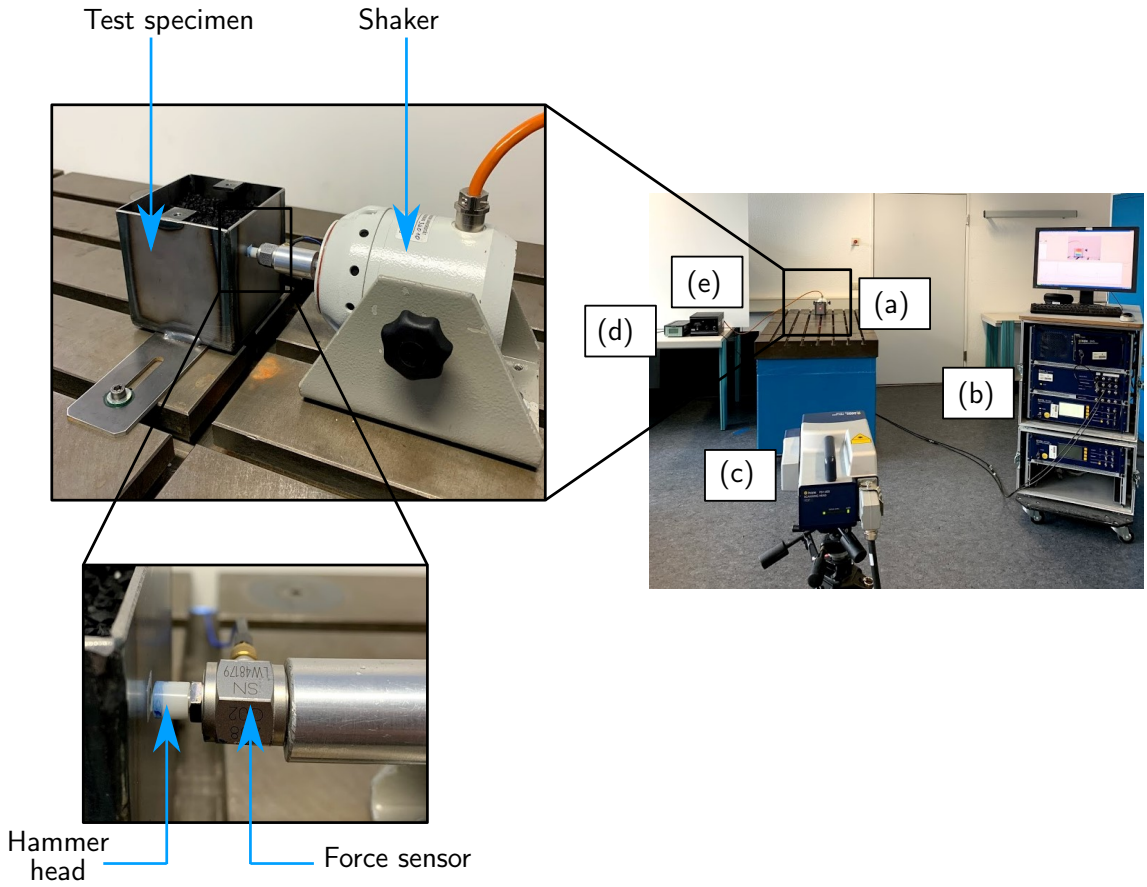

Figure 7.2: Experimental setup for dynamic testing: (a) test specimen, (b) control and post-processing unit, (c) laser vibrometer scan head, (d) force sensor amplifier, (e) shaker power amplifier.

points was determined through an empirical study, verifying its sufficiency for both measurement accuracy and capturing the accurate displacement shape of the test specimen.

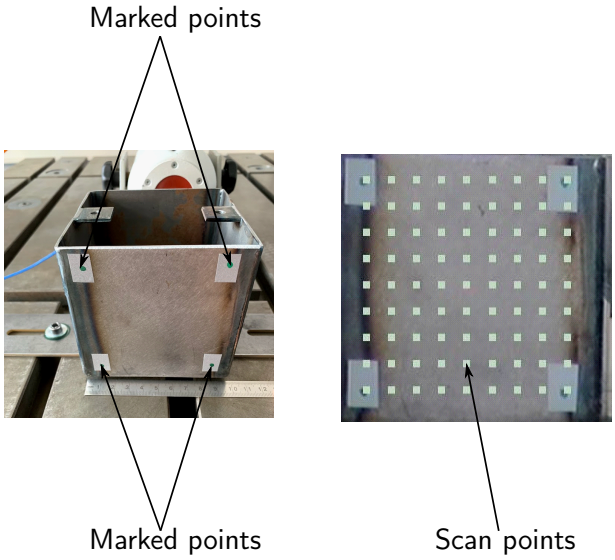

Figure 7.3: (Left) Marked points defining the maximum range for laser vibrometer scans on the test specimen surface. (Right) Square grid pattern with 81 scan points for detailed vibration measurement.

The experiment commenced with measurements on empty boxes, followed by tests on boxes filled with granular material at a 40% volume level. A parameter study on a reference specimen guided the data acquisition setup. To improve the SNR, six complex averages were acquired at each measurement point. Bandwidth limitations were applied using a low-pass filter with a 4 kHz cut-off frequency. For frequency spectrum calculations, a sampling frequency of 12.8 kHz and a resolution of 781.25 mHz were chosen. Finally, the Hann window function was utilized to minimize spectral leakage.

To ensure experimental replicability after a 20-month interval, meticulous documentation was undertaken. This documentation included details of the measurement surface area on the test specimen, the placement of bolt joints, the distance between the specimen and the laser scanning vibrometer head, and all other relevant configurations. Additionally, the granular material remained undisturbed within the securely sealed boxes throughout the entire study period, preventing any removal or addition of material.

7.3 Filling materials and packing ratio

To investigate the effect of high amplitude load and temperature cyclic load on the efficiency of a particle damper, two different materials were chosen: rubber granulate "RG 4.6 mm" and sand (see Figure 7.4). Sand is used as an alternative filling material in a steel box with a PC inner layer (Box 3) for comparative analysis, see Figure 7.4.

Rubber granulate Sand

Figure 7.4: Materials used to investigate particle damper behavior under dynamic loading and temperature fluctuations.

This chapter deviates from the optimal 80% filling ratio for vibration attenuation. The primary objective is not to achieve the absolute maximum reduction in vibration amplitude, but rather to investigate the impact of harsh operating conditions on the long-term performance of the chosen granular material. To achieve this, a filling ratio of 40% was deliberately chosen, see Figure 7.5.

This selection offers a twofold benefit. Firstly, it induces a measurable reduction in vibration amplitude at the outset. This initial mitigation serves as a baseline for evaluating potential changes in the material's damping capacity after exposure to high-amplitude dynamic loads and temperature cycling. Any deviation from the initial performance will indicate a potential degradation in the material's effectiveness. Secondly, the 40% filling ratio strategically introduces a larger void fraction (empty space) within the container. This increased void space is expected to promote more random interactions between the particles themselves and with the container walls during dynamic loading, particularly during dynamic loading on the vibrating table. This deliberate design choice allows us to assess the impact of wear, potentially induced by these increased particle motions, on the vibration attenuation capability. While direct wear measurements are not included in this study, the potential for accelerated

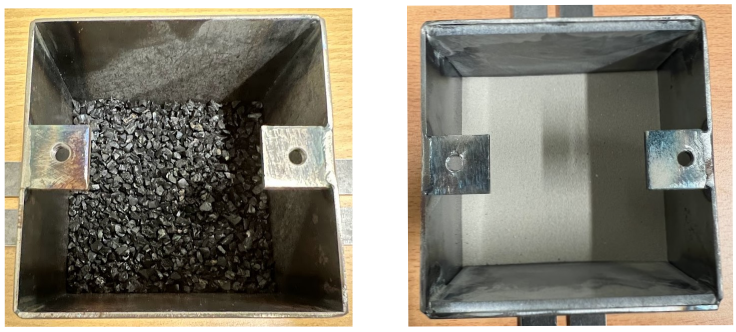

(a) (b)

Figure 7.5: Particle dampers: (a) steel box with rubber granulate "RG 4.6 mm", (b) steel box with PC layers filled with sand.

wear due to these increased particle interactions within the larger void spaces is acknowledged and serves as an additional point of investigation.

7.4 Long-term durability test condition

To assess the long-term durability of the particle dampers, three distinct dynamic load cycles were implemented, namely: 85 million, 165 million, and 330 million cycles. However, the application of these cycles was not uniform across the test boxes. Box 1 underwent the lowest load cycle of 85 million, while Box 2 experienced a more rigorous 165 million cycle exposure. The remaining three boxes (Boxes 3, 4, and 5) were subjected to the most demanding load cycle of 330 million cycles each.

It is important to note the unique pre-conditioning applied to Box 5 before it is exposed to the high-impact dynamic load. Prior to dynamic testing, Box 5 underwent a cyclic temperature load ranging from 30^oC to 120^oC, as detailed in Figure 7.6.

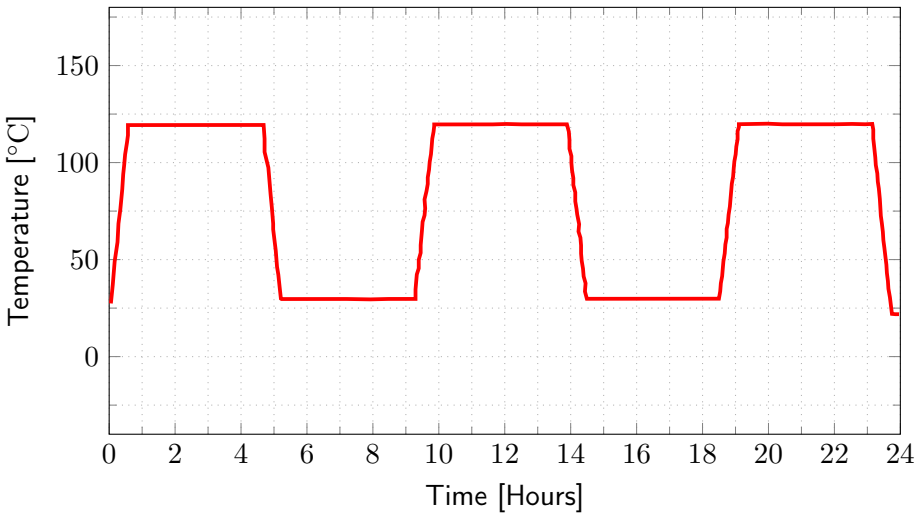

Figure 7.6: Cyclic temperature load over time applied to Box 5 before exposure to high dynamic load.

This pre-conditioning involved maintaining the partially filled box with the rubber granulate "RG 4.6 mm" under this temperature load for a period of 24 hours. Following this tempering process, the box was mounted on the vibrating table for dynamic load testing. Table 7.1 provides a comprehensive overview of the testing parameters for each container. This table shows the number of load cycles endured by

each box, the corresponding filling material used ("RG 4.6 mm" or sand), and whether the granular material was pre-conditioned through temperature cycling.

Table 7.1: Summary of boxes, filling materials, load cycles, and tempering status.

Specimen	No. of load cycles	Filling material	Tempered	Inner layer
Box 1	85 Million	RG 4.6 mm	No	No
Box 2	165 Million	RG 4.6 mm	No	No
Box 3	330 Million	Sand	No	PC
Box 4	330 Million	RG 4.6 mm	No	No
Box 5	330 Million	RG 4.6 mm	Yes	No

Beyond the number of cycles, the long-term durability test incorporated load frequencies ranging from 48 Hz to 76 Hz. To ensure clarity and effectively illustrate the application of varying amplitudes across these frequencies, the data is presented in Figure 7.7. Furthermore, the amplitude of the applied load increased proportionally with the frequency. For instance, the minimum load of 10.7 kN was applied at the lowest frequency of 48 Hz. Conversely, at higher frequencies (54 Hz and 55 Hz), the partially filled boxes experienced varying loads with three and four distinct amplitude values, respectively. This trend continued at the upper end of the frequency spectrum, where the load amplitude at 75 Hz ranged from 84 kN to 104 kN. Finally, at the maximum test frequency of 76 Hz, the load amplitude varied across ten different values, with the minimum being 104 kN and the maximum reaching 200 kN (see Figure 7.7). This sweep-frequency approach with varying amplitudes aims to comprehensively assess the performance of the particle dampers under diverse operating conditions.

The test boxes 3, 4, and 5 were subjected to their designated dynamic load profile at varying frequencies for pre-determined durations. Figure 7.8 illustrates the total exposure time for partially filled boxes at different frequencies. Notably, boxes experienced the load for 781 hours at 54 Hz. Conversely, the minimum exposure times were observed at frequencies of 48 Hz (26 hours), 57 Hz (2 hours), and 58 Hz (6 hours). Exposure durations increased at higher frequencies, with boxes experiencing 82 hours and 182 hours at 75 Hz and 76 Hz, respectively. The second-longest exposure occurred at 55 Hz, totaling 411 hours. In total, the partially filled boxes underwent vibration for 1602 hours, equivalent to approximately 67 days.

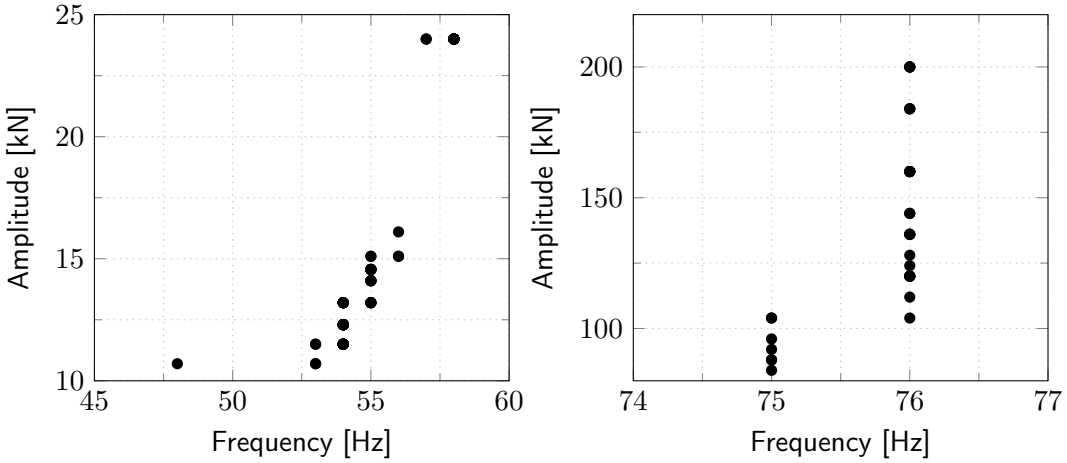

Figure 7.7: Amplitude and frequency variations for partially filled boxes.

The long-term durability testing was conducted in collaboration with an industrial partner at their facilities. The data provided by our collaborators regarding the dynamic load exposure duration for Boxes 1 and 2 was inconclusive. While it is obvious that there is a difference in exposure time compared to Boxes 3, 4, and 5 (as shown in Figure 7.8), the specific duration for Boxes 1 and 2 remains unclear.

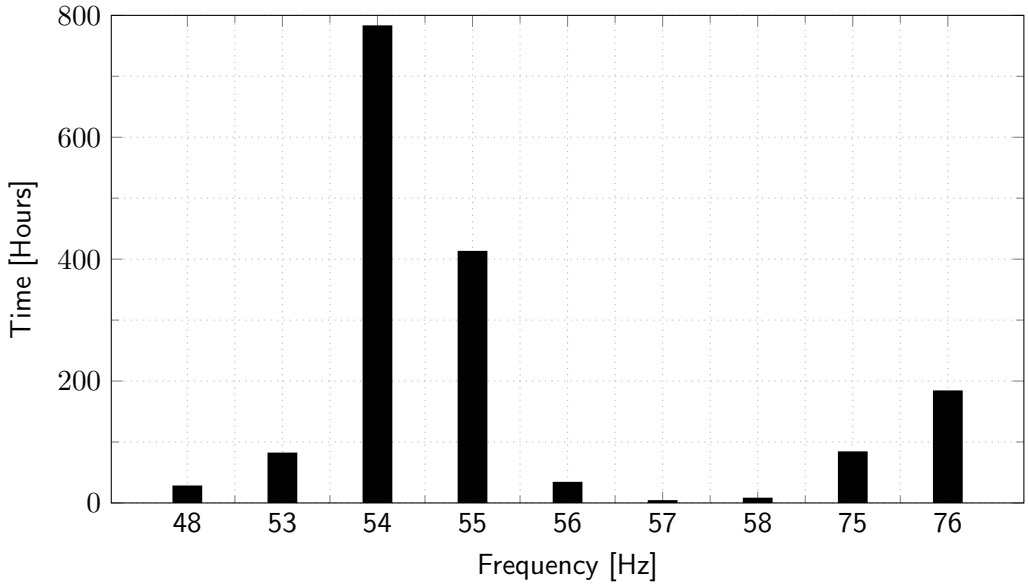

Figure 7.8: Time duration of boxes 3, 4, and 5 on the vibration table across different frequencies.

To ensure the test accurately reflects real-world conditions experienced by wind turbine components, the selection of load frequency and amplitude was guided by the partner's expertise. These parameters were chosen to mimic the life cycle characteristics of wind turbine components, allowing us to evaluate the vibration attenuation capability of the particle dampers throughout their projected operational lifespan. While specifics of the chosen frequencies and amplitudes are restricted by confidentiality agreements, it is important to note that this industry-informed approach ensures the test rigorously evaluates the long-term performance of the rubber granulate "RG 4.6 mm" within the relevant operating range of wind turbine components. Moreover, the long-term durability test conditions have been established to align with the lifecycle of wind turbines, as the concepts developed in this thesis will be tested on industrial-scale wind turbine components to demonstrate the transition from laboratory research to industrial application.

7.5 Comprehensive workflow

The experimental study examining the impact of high-amplitude dynamic loading and temperature fluctuations on the performance of particle dampers was conducted through a three-step experimental procedure, as illustrated in Figure 7.9. The initial phase (Step I) concentrated on establishing a baseline performance for vibration mitigation. Frequency responses were measured for both empty and partially filled boxes. The frequency response of the empty box is depicted by solid black lines, while that of the partially filled box is shown by green dashed lines. The vibration attenuation observed in this stage serves as the initial effectiveness of the particle damper (i.e., before exposure to cyclic loading) in reducing vibration amplitude.

Following the baseline measurements, the partially filled containers underwent a long period of high-amplitude cyclic loading (Step II). To replicate real-world operating conditions that could lead to wear or degradation of the particle damper material, these boxes were placed on a vibrating table for several months, see Figure 7.8. Notably, one of the boxes (Box 5) was also subjected to cyclic temperature loading, as illustrated in Figure 7.6, before being mounted on the vibrating table. In the final stage, the dynamic responses of both the empty and partially filled containers were measured again. This evaluation aimed to identify any alterations in the vibration attenuation properties of the granular materials within the partially filled containers attributable to the prior exposure to high-intensity dynamic loads in Step II. By comparing the vibration responses before and after exposure, this study

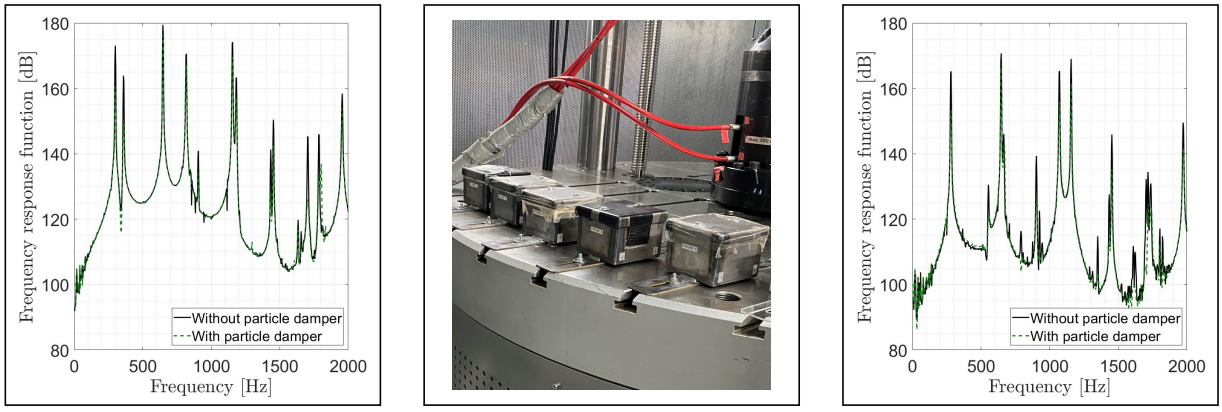

Figure 7.9: Key steps of the experimental workflow: Step I: Initial frequency response measurement of the granular material (before dynamic load), Step II: Exposure of the partially filled container to cyclic loads, Step III: Re-measurement of the frequency response of the granular material (after cyclic load).

sought to quantify any potential changes in the effectiveness of the particle dampers due to the cyclic loading.

This three-step approach facilitated a systematic investigation of the long-term durability of particle dampers under real-world-like operating conditions.

7.6 Results

To investigate the dynamic response of the boxes, their FRFs were measured within a frequency range of 20 Hz to 2000 Hz. This analysis identified the presence and number of resonance frequencies for both empty and granular material-filled boxes. Additionally, the FRFs facilitated the quantification of vibration attenuation around these resonant peaks. Figure 7.10 specifically showcases the narrow-band spectrum obtained for the empty Box 1, emphasizing its surface velocities primarily oriented in the normal direction of measurement.

The FRFs for empty and partially filled boxes demonstrate a significant reduction in vibration amplitude, attributed to the presence of granular materials (see Figure 7.11 (a) - (e)). After 1602 hours of exposure to high-intensity dynamic loading, the dynamic responses of the materials were reassessed (Figure 7.12 (a)-(e)). As previously stated, this study aimed to identify potential alterations in the vibration reduction capabilities of granular materials due to combined dynamic loading and temperature fluctuations. To achieve this, the experimental setups used for pre- and post-exposure FRF measurements were maintained as consistent as possible. While qualitatively similar trends are observed in both figures, minor variations exist between the FRF spectra of Figure 7.11 and Figure 7.12 for each box. These discrepancies are likely due to inevitable experimental variations occurring over a 20-month period. These variations may appear as shifts in resonance frequencies within the 20 - 2000 Hz range or altered amplitude values. Nevertheless, these variations do not hinder the assessment of the damping performance of the granular materials before and after dynamic loading.

The primary method for quantifying vibration reduction relies on comparing FRFs of partially filled boxes to their empty counterparts. This approach remains robust despite observed variations in resonance frequencies across experiments. However, directly comparing vibration amplitude reduction for each peak value in partially filled boxes, before and after cyclic loading, proves impractical due to the

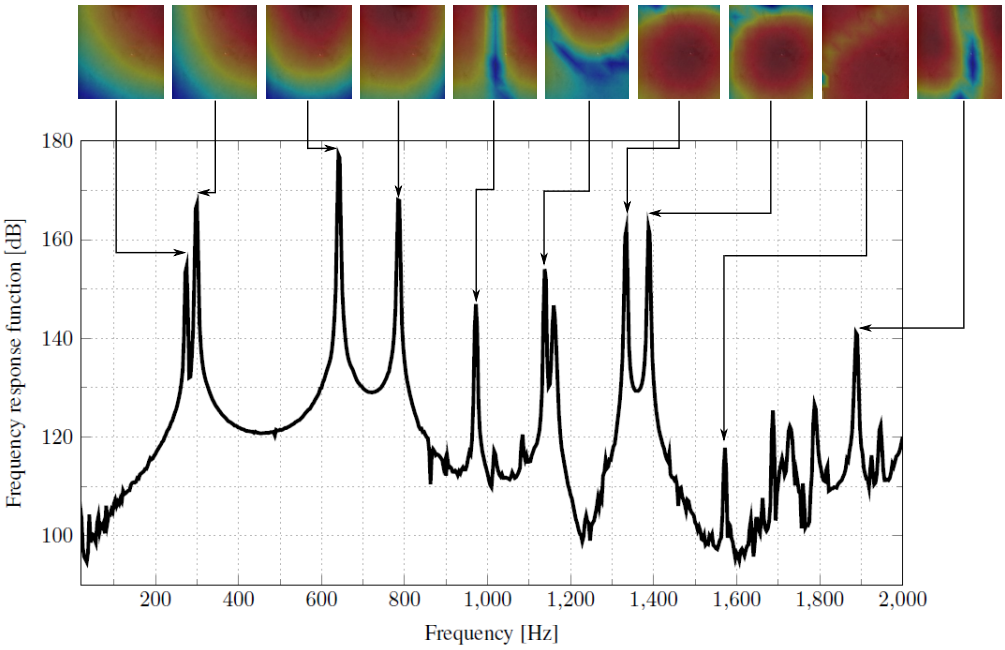

Figure 7.10: Frequency response function and surface velocity of Box 1 without granular material, centered on the normal measurement direction.

potential shift in the number of resonance frequencies. Therefore, the comparison of vibration reduction can be achieved by comparing the bending mode (around 650 Hz) of the box walls in each scenario, which also corresponds to the highest peak in the entire spectrum, see Figure 7.10. Furthermore, Table 7.2 summarizes the reduction in vibration amplitude observed in this first eigenmode of partially filled boxes.

Table 7.2: The reduction in vibration amplitude of partially filled boxes in their first eigenmode.

	First eigenmode frequency (Hz)		Amplitude reduction (dB)		
Specimen	**(Before cyclic load)**	**(After cyclic load)**	**(Before cyclic load)**	**(After cyclic load)**	**Difference (dB)**
Box 1	640.6	646.9	3.8	4.3	- 0.5
Box 2	646.9	646.9	3.2	3.6	- 0.4
Box 3	656.3	650.0	30.7	15.4	15.3
Box 4	640.6	640.6	2.4	6.6	- 4.2
Box 5	646.9	646.9	3.1	4.3	- 1.2

For example, Box 1 exhibits a bending mode at approximately 640 Hz. Here, the use of rubber granulate "RG 4.6 mm" leads to a vibration attenuation of 3.8 dB (Figure 7.11 (a) and Table 7.2). Interestingly, after experiencing 85 million cycles of dynamic loading, Box 1 filled with the same rubber granulate achieves an even greater vibration reduction of 4.3 dB in its first eigenmode (shifted to 646.9 Hz) (Figure 7.12 (a)). A vibration reduction performance almost identical to this has been observed for Box 2 after undergoing 165 million load cycles, see Figure 7.11 (b), Figure 7.12 (b) and Table 7.2. Furthermore, Box 4, filled with rubber granulate "RG 4.6 mm", also exhibited significant vibration attenuation even after enduring 330 million load cycles. It has been noticed that prior to enduring cyclic loading, the partially filled box (Box 4) can reduce vibration amplitudes by up to 2.4 dB around the resonance frequency of 640.6 Hz. Nevertheless, following exposure to 330 million cyclic loads, the damping performance of Box 4 significantly improves, reducing vibration amplitudes by 6.6 dB around the resonance frequency of 640.6 Hz. As previously explained, Box 5 investigated the effect of pre-conditioning on damping performance. The rubber granulate "RG 4.6 mm" within Box 5 underwent cyclic temperature fluctuations, spanning from 30^{o}C to 120^{o}C, before exposure to

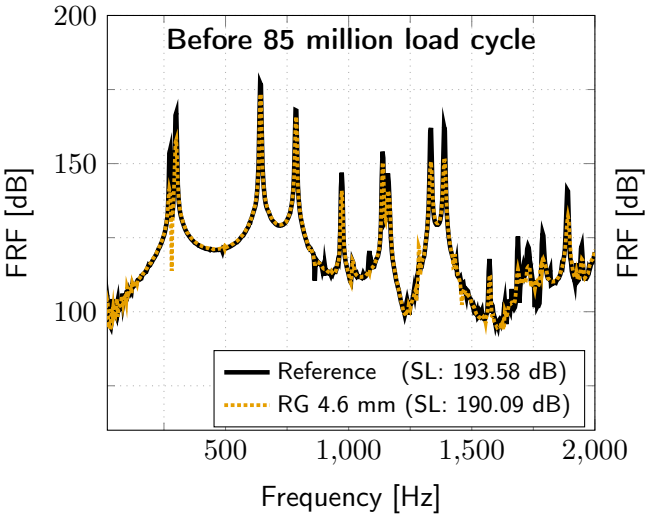

(a) FRFs of the empty and partially filled steel box (Box 1).

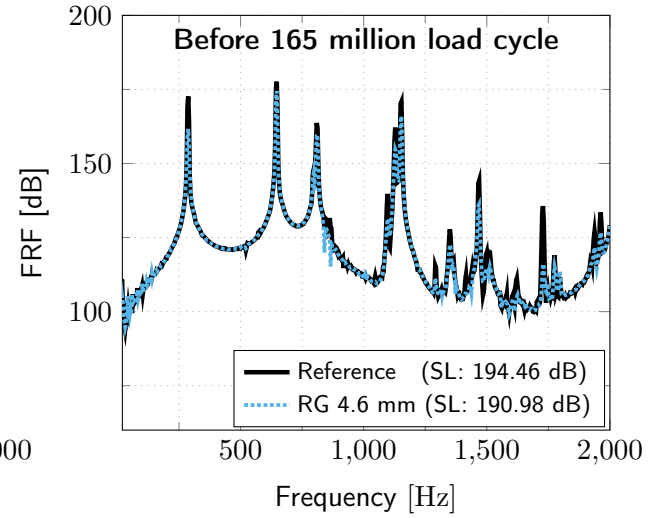

(b) FRFs of the empty and partially filled steel box (Box 2).

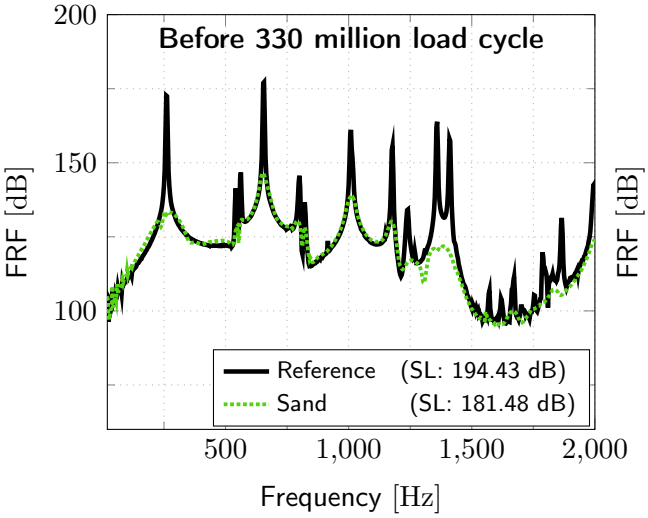

(c) FRFs of the empty and partially filled steel box with PC layers (Box 3).

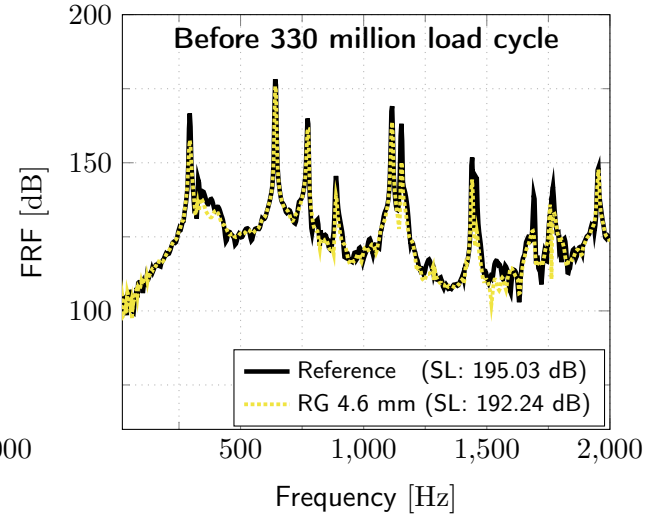

(d) FRFs of the empty and partially filled steel box (Box 4).

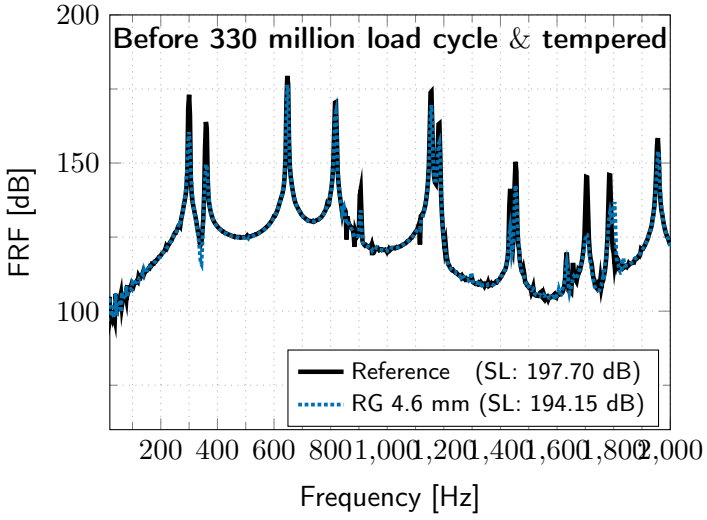

(e) FRFs of the empty and partially filled steel box (Box 5).

Figure 7.11: FRFs of empty and partially filled boxes before dynamic and cyclic temperature loading.

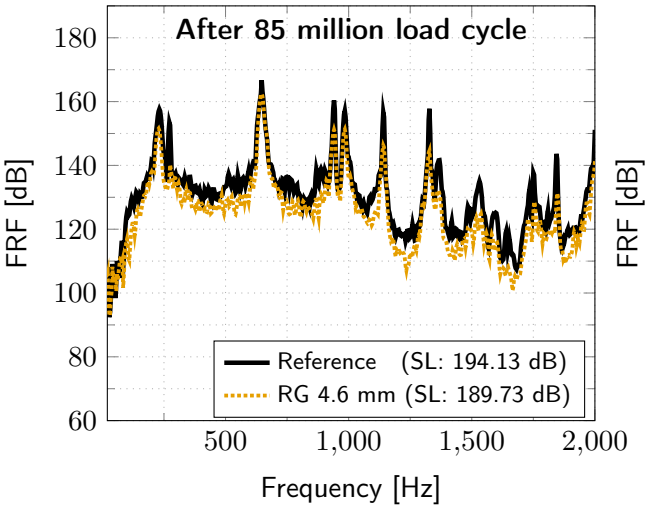

(a) FRFs of the empty and partially filled steel box (Box 1).

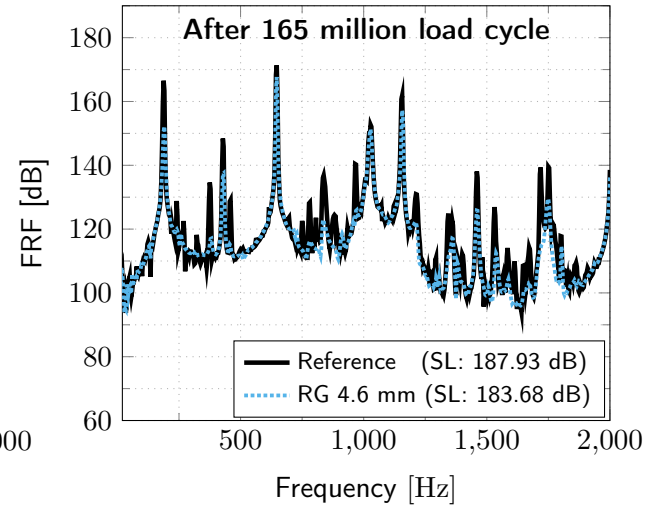

(b) FRFs of the empty and partially filled steel box (Box 2).

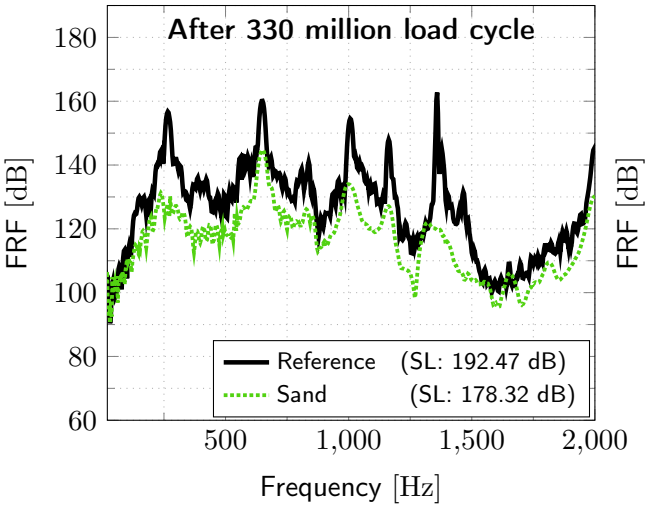

(c) FRFs of the empty and partially filled steel box with PC layers (Box 3).

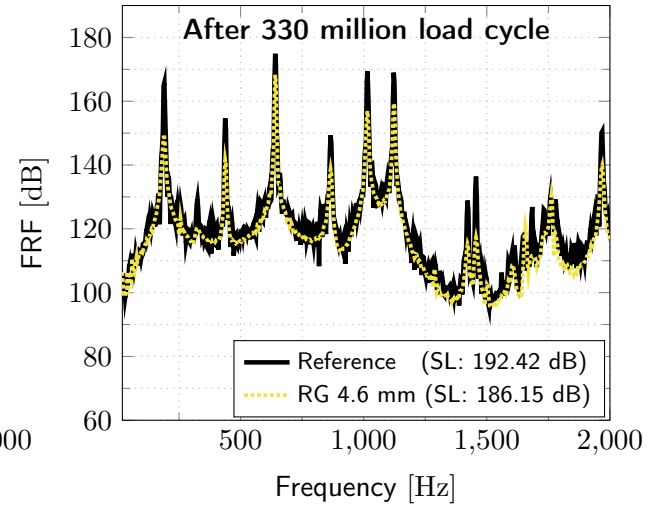

(d) FRFs of the empty and partially filled steel box (Box 4).

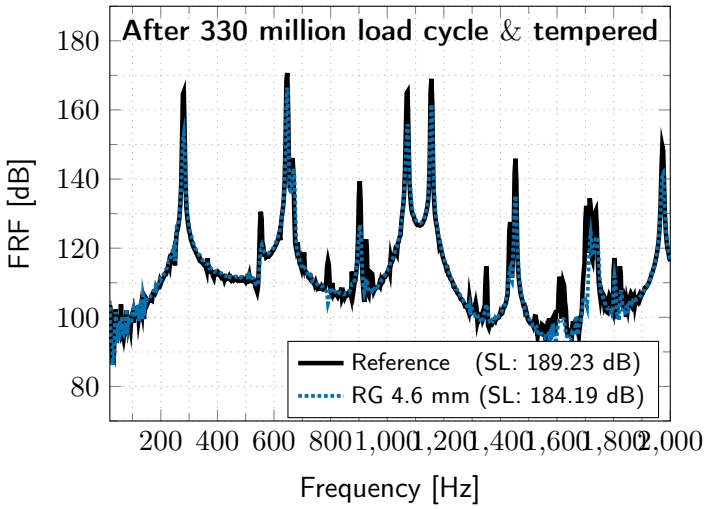

(e) FRFs of empty and partially filled steel box (Box 5).

Figure 7.12: FRFs of empty and partially filled boxes after dynamic and cyclic temperature loading.

dynamic loads. It has been observed that tempering the rubber granulate followed by 330 million load cycles resulted in a 3.0 dB lower vibration attenuation compared to the unconditioned rubber granulate, see Table 7.2. Interestingly, Box 5 exhibited lower vibration mitigation compared to Box 4, despite both undergoing the same number of load cycles. The key difference lies in pre-conditioning, i.e. rubber granulate enclosed in Box 5 was exposed to cyclic temperature fluctuations before experiencing high-amplitude loads. This observation suggests that the pre-conditioning process might influence the vibration attenuation properties of the rubber granulate "RG 4.6 mm". In contrast, Box 3 contained sand, which exhibited a significant reduction in vibration amplitude (30.7 dB) around its first resonance frequency (650 Hz) before cyclic loading. However, this damping effectiveness noticeably diminished after 330 million load cycles at the same resonance frequency. This finding suggests that sand's damping capacity might deteriorate under cyclic loading.

The results demonstrate that the rubber granulate "RG 4.6 mm" exhibits stable damping performance around its first resonance frequency. Even after exposure to cyclic loads and temperature variations, the damping effectiveness remains consistent. This suggests a high degree of resilience in the material's ability to reduce vibration amplitude.

Particle dampers are known for their ability to mitigate vibrations across a wide range of frequencies. To assess the impact of long-term durability testing on this broad-spectrum performance, this chapter also evaluates the damping capacity throughout the entire investigated frequency range (20 Hz to 2000 Hz). For this purpose, a comparison of the difference in the SL value of surface velocity before and after dynamic loading has been carried out. The computation involves subtracting the SL value of surface velocity from the test specimen containing granular materials from that of the empty boxes, which serve as the reference test specimen in each scenario. The SL values are provided in the legends of Figure 7.11 (a)-(e) and Figure 7.12 (a)-(e). Table 7.3 summarizes the SL values for each box before and after loading.

Table 7.3: Change in surface velocity sum level (SL) of partially filled boxes after cyclic loading, along with the corresponding cyclic loads each box endured.

Specimen	SL value (dB) (Before cyclic load)	SL value (dB) (After cyclic load)	Difference (dB)	Load cycle in million
Box 1	3.5	4.5	1.0	85
Box 2	3.5	4.3	0.8	165
Box 3	12.9	14.2	1.3	330
Box 4	2.8	6.3	3.5	330
Box 5	3.6	5.0	1.4	330

After undergoing 85 million and 165 million cyclic loads, the SL values for Box 1 and Box 2 are 4.5 dB and 4.3 dB, respectively, compared to identical pre-load values of 3.5 dB for both boxes. This suggests that the vibration attenuation capability of the rubber granulate "RG 4.6 mm" remains largely unchanged by these dynamic loads. Conversely, Box 4, filled with the same rubber granulate, displayed a noteworthy increase in damping performance (3.5 dB) after 330 million cyclic loads. Similarly, Box 5, subjected to a prior cyclic temperature load followed by 330 million cyclic loads, exhibited an improvement in damping (from 3.6 dB to 5.0 dB). These observations suggest potential performance enhancements for the rubber granulate "RG 4.6 mm" under specific extended loading regimes. Furthermore, Box 3, partially filled with sand, demonstrated an improvement in damping after 330 million cyclic loads.

From the above discussion, it can be concluded that the rubber granulate "RG 4.6 mm" exhibits consistent damping characteristics around its first resonance frequency and within the 20 Hz to 2000 Hz range following exposure to a low number of cyclic loads (85 and 165 million). This implies minimal impact on its damping performance under moderate dynamic conditions. However, a significant improvement in vibration mitigation performance was observed for the rubber granulate "RG 4.6 mm"

exposed to 330 million cyclic loads. This enhancement might be attributed to wear-induced changes in the rubber granulate's particle size distribution. An increase in particle size variation could lead to a higher number of particle-particle and particle-wall interactions, known to be key damping mechanisms in particle dampers. Furthermore, Chapter 5 demonstrates that rubber granulate with a wider distribution is more effective in vibration reduction. Interestingly, rubber granulate "RG 4.6 mm" and "RG 6.4 mm" exhibits a wider particle size distribution compared to other tested materials (Figure 5.5), potentially explaining its inherent damping capability. It is noteworthy that exceeding the number of load cycles (potentially beyond 330 million) might compromise the vibration attenuation performance of the rubber granulate. Hence, a further investigation is warranted to determine this threshold definitively. However, as previously established, the chosen load frequency, amplitude, and number of cycles in this study reflect realistic wind turbine component lifespans. Consequently, rubber granulate "RG 4.6 mm" rubber granulate presents itself as a highly suitable material for particle damper design. Nonetheless, it is crucial to prevent excessive wear that could degrade the granulate into a powder. Chapter 5 demonstrates that rubber powder exhibits significantly lower damping efficiency compared to its granular counterpart.

7.7 Conclusion

This chapter investigated the effects of dynamic and cyclic temperature loads on the performance of particle dampers, an area that has not been extensively explored in the existing literature. Steel boxes filled with rubber granulate "RG 4.6 mm" and sand were subjected to increasing levels of cyclic loading (up to 330 million cycles) and high-amplitude dynamic loads. Vibration response measurements were taken on partially filled boxes before and after these exposures, along with thermal cycling (30^oC to 120^oC) for one box. Additionally, final measurements were conducted on empty and filled boxes to assess changes in the vibration characteristics of the granular materials.

It has been observed that the rubber granulate "RG 4.6 mm" maintained consistent vibration reduction at 85 and 165 million cycles of cyclic loading. Interestingly, it showed improved vibration attenuation at 330 million cycles. This suggests wear-induced changes in the particle distribution, potentially leading to a wider range and improved vibration mitigation capability, as observed in Chapter 5. However, conducting a further experimental study is necessary to verify changes in the PSD of rubber granulate before and after cyclic loading, indicating the presence of wear. Furthermore, cyclic temperature loads were observed to potentially affect the damping capability of particle dampers in general. Nonetheless, no negative impact of temperature fluctuation was found on the performance of rubber granulate before or after cyclic loading. Hence, rubber granulate "RG 4.6 mm" proves to be an optimal choice for designing particle dampers, offering advantages in terms of vibration reduction capability, reduction in additional mass, and resilience to negative effects from cyclic loading and temperature fluctuation. Sand also exhibited improved vibration mitigation after cyclic loads. However, its additional weight and potential influence on humidity (see Chapter 5) pose challenges for real-world applications.

A limitation of this study is the combined effect of temperature cyclic loads and high-impact loads. Future research should focus on isolating the temperature effect by using controlled temperature exposure and vibration measurements, excluding high-amplitude cyclic loading, to better understand its impact on particle damper performance. Additionally, wear analysis of the granular materials after cyclic loading was not included in this study.

8 Particle damper in rotating systems

This study builds on previous chapters that analyzed the design parameters of particle dampers using non-rotating test specimens, which offered valuable insights into their behavior in static systems. However, to expand the potential applications of particle dampers, it is essential to investigate their performance in rotating systems.

Rotating systems exert centrifugal forces on dampers, significantly affecting the behavior of the granular materials contained within the particle damper. These forces can alter the contact dynamics between particles, resulting in changes in damping efficiency as the rotational speed varies. Such fluctuations are crucial, as they influence the overall effectiveness of the damper in vibration mitigation. Therefore, it is essential to conduct a comprehensive investigation into the behavior of particle dampers under the influence of centrifugal forces to understand their impact on performance. This chapter presents an experimental study aimed at exploring and quantifying these effects, providing valuable data for optimizing particle damper applications in rotating machinery. This chapter builds upon the results outlined in publication [213].

8.1 Design of test specimen and particle damper

Two simplified scaled wind turbine blades have been selected for the purpose of investigating the impact of centrifugal forces on the vibration reduction capabilities of a particle damper. These blades, as depicted in Figure 8.1, are composed of composite materials, specifically constructed with long glass fibers embedded within a nylon matrix. Each blade has a diameter of 533 mm and a total mass of 115 g. Although the wind turbine blade structure is used in the experimental study, the results obtained can be applied to any type of rotating machine components.

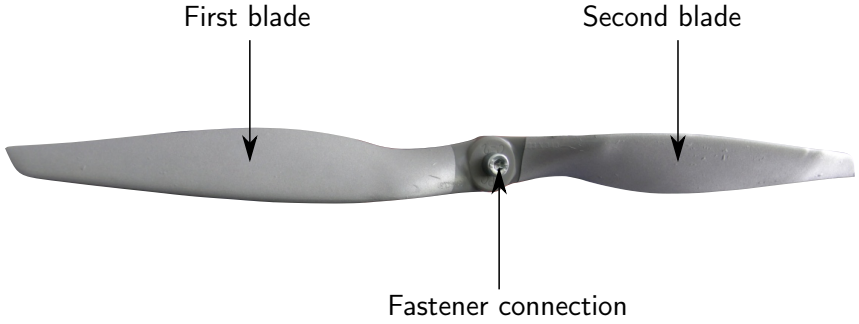

Figure 8.1: Blade test specimens joined using fastener connections.

Wind turbines are particularly vulnerable to lightning strikes, which can cause significant damage to critical components [214]. Statistics show that between 4% and 8% of European wind turbines suffer lightning damage each year, underscoring the need for effective risk mitigation [215]. As wind turbine blades continue to grow in size, reaching 60 meters and beyond, the risk of lightning strikes is expected to increase [215]. Conventional particle dampers using metallic particles have also been studied for reducing the vibration amplitude of rotating wind turbine blades [164]. While these dampers have been shown to positively affect vibration attenuation, the use of steel balls presents certain drawbacks.

The most notable concern is the substantial increase in the additional mass of the blade structure, which poses a critical design challenge. Additionally, the conductive nature of metallic particles can worsen the issue by increasing the likelihood of lightning strikes. By utilizing a non-metallic material like rubber granulate to design particle dampers for wind turbine blades, this approach addresses the dual concerns of vibration reduction and addressing lightning issues.

The particle damper used to investigate the influence of centrifugal force on its performance was designed with rubber granulate "RG 2.3 mm" as the damping material. Although "RG 4.6 mm" has demonstrated superior capabilities in reducing vibrations (see Chapter 5), its larger particle size made it unsuitable for this particular study. This limitation was due to dimensional constraints in the experimental setup, which necessitated the use of the smaller particle size in order to fit within the design specifications of the particle damper. The compact blade structure, necessitated by laboratory handling requirements, dictated a correspondingly sized cavity within the test specimen. This limited cavity volume could not accommodate the larger "RG 4.6 mm" particles. Consequently, "RG 2.3 mm" was selected as the filling material for this experiment, see Figure 8.2 (a). The cavity used in this design is constructed from a lightweight material in an elliptical shape and is partially filled with rubber particles (Figure 8.2 (b)). To ensure secure attachment to the wind turbine blade, the cavity is fastened to the blade's surface using screws. This fastening mechanism is carefully implemented to ensure that the cavity remains tightly sealed, preventing any spillage of particles during the rotation of the blade, see Figure 8.2 (c).

(a) (b) (c)

Figure 8.2: Material and cavity design of the particle damper attached to the blade specimen: (a) Rubber granulate "RG 2.3 mm", (b) partially filled cavity, (c) partially filled cavity attached to the balde.

As discussed in the previous chapter, the filling volume for the particle damper in this case is also set at 80%. This 80% fill corresponds to a total mass of 1 g of the rubber granulate "RG 2.3 mm", which results in an increase of approximately 1% in the overall mass of the wind turbine blade structure. Additionally, this amount of mass will help to maintain the balance of the blade during rotation.

8.2 Dynamic behavior of the test specimen

To determine the appropriate rotational speed (RPM) at which the scaled blade specimen should rotate in order to replicate the operational conditions of a full-scale wind turbine blade with a length of 51 meters, it is necessary to match the rotational dynamics. Typically, the full-scale blade operates at rotational speeds varying between 9 RPM and 12 RPM. In order to compute the corresponding RPM for the scaled blade, the centrifugal acceleration experienced by the wind turbine blade during operation must first be calculated. This acceleration can be determined using the following approach

$$a_{\text{blade}} = R_{\text{cavity}} \cdot \Omega^2 = R_{\text{cavity}} \cdot (2\pi f)^2 \,, \tag{8.1}$$

where R_{cavity} denotes the cavity's position on the blade, and Ω represents the blade's rotational speed.

To achieve a centrifugal acceleration comparable to that of a real wind turbine blade at its midpoint, a rotational speed of 180 RPM is required, if the cavity is positioned near the midpoint, at a radius of 0.115 cm.

Industrial wind turbine blades differ in length and rotational speed depending on the specific turbine model. In this thesis, a 51 m blade is chosen as a representative scale for experimental evaluation (see Chapter 11). The developed particle damper concept will be tested within this context to assess its practical effectiveness in real-world applications. Consequently, if the particle damper integrated into the scaled blade specimen demonstrates optimal performance within the 180 – 190 RPM range, it can be inferred that the design will function effectively in a full-scale wind turbine blade operating under comparable conditions.

8.3 Performance of particle dampers in non-rotating blades

Before investigating the effects of particle dampers on the dynamic behavior of rotating blades, an initial analysis was conducted to assess the blade's dynamic characteristics in a non-rotating state, both with and without particle dampers. This preliminary evaluation aimed to quantify the effectiveness of particle dampers under stationary conditions and establish a baseline for comparing performance changes during rotation.

8.3.1 Experimental set up

In this preliminary setup, the two blades were securely fastened to an electrodynamic shaker, manufactured by TIRA, using screws to ensure stability during testing. To minimize external vibrations and prevent interference from the testing environment, the shaker was isolated from the table by being mounted on four identical rubber bushings, as depicted in Figure 8.3.

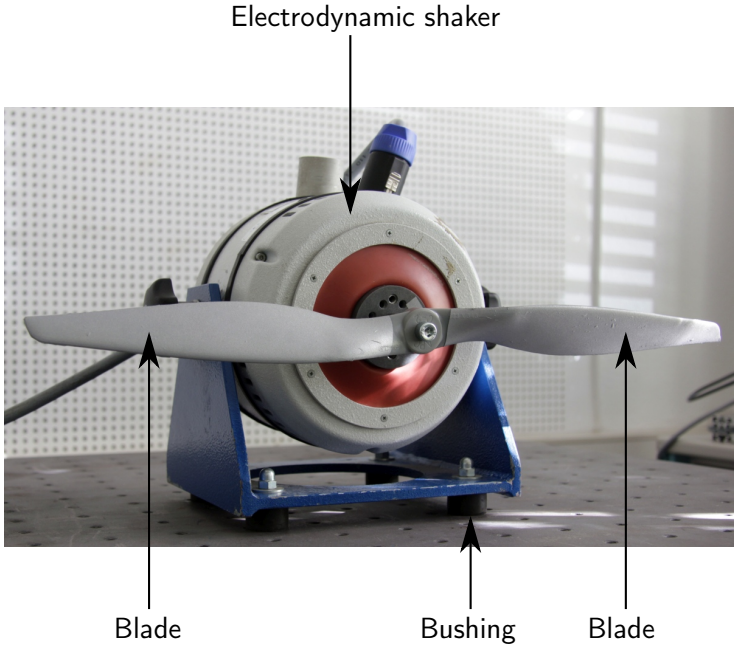

Figure 8.3: Blade test specimen mounted on a shaker for resonance frequency measurement in the non-rotating state.

This isolation setup ensured that only the intended vibrational forces were transmitted to the blade. The blade test specimen was then subjected to excitation through the shaker, with the blade remaining

stationary throughout the experiment. The surface velocity of the structure was carefully measured, yielding data on its vibrational properties in the stationary condition. The transfer function was computed from the reference point on the propeller hub to the blade surface.

$$H_i(\omega) = \frac{v_i(\omega)}{v_{\text{ref}}(\omega)}. \tag{8.2}$$

The experiment was conducted under two conditions: one with the particle dampers and one without. In the case where particle dampers were employed, two cavities consisting of rubber granulate "RG 2.3 mm" were affixed to the midpoint of each blade.

8.3.2 Results

The blade's FRF in a non-rotating state is shown in Figure 8.4. Four distinct resonance frequencies were observed during the analysis at 75 Hz, 168 Hz, 267 Hz, and 519 Hz. Notably, the particle damper exhibited the most significant vibration attenuation at the resonance frequencies of 267 Hz and 519 Hz, demonstrating its highest efficiency in reducing vibrations within these frequency ranges. However, around the remaining resonance frequencies the particle damper's ability to reduce vibration amplitude was limited, suggesting its lesser effectiveness in these frequency ranges.

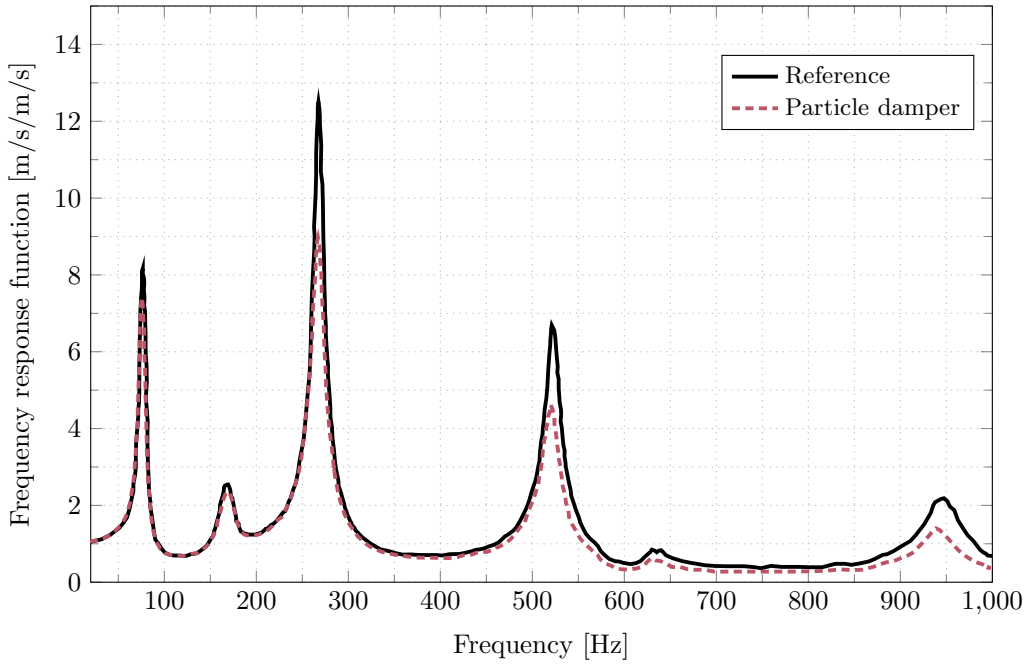

Figure 8.4: FRF of the blade in the non-rotating state, with and without the particle damper.

To investigate the ineffectiveness of the particle damper at resonance frequencies below 267 Hz, it is crucial to analyze the mode shapes of the blade. Figure 8.5 illustrates the mode shapes corresponding to each identified resonance frequency. In this figure, the location of the particle damper is marked by a black-filled circle. At the resonance frequency of 75 Hz, it is evident that the maximum displacement occurs at the tip of the blade, while the displacement around the particle damper's position is minimal. As a result, the rubber granules within the damper cavity are unable to move relative to each other, rendering the particle damper ineffective at this frequency.

Similarly, for the resonance frequency of 168 Hz, the displacement around the region where the particle damper is mounted remains minimal, which again limits the relative movement of the rubber particles

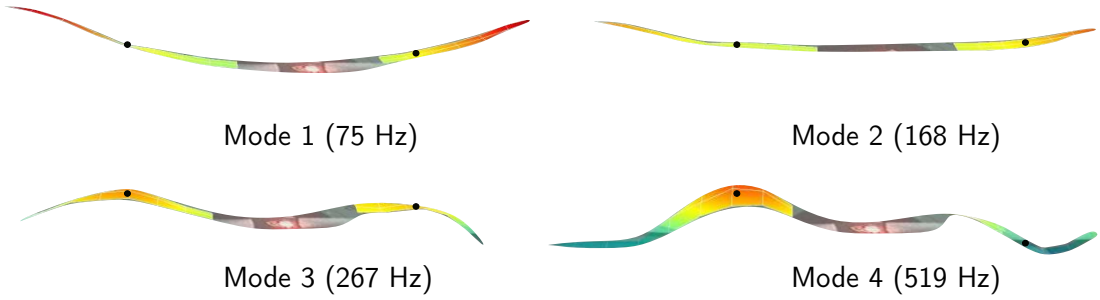

Figure 8.5: Mode shapes of the blade test specimen at their corresponding resonance frequencies. The black circle indicates the position of the particle damper on the blade.

inside the damper. Consequently, the particle damper is not effective at this frequency either.

In contrast, at the resonance frequencies of 267 Hz and 519 Hz, the displacement in the area surrounding the particle damper is significantly higher. This increased displacement allows the rubber particles to move relative to each other and against the cavity walls, enhancing energy dissipation. As a result, the particle damper demonstrates maximum effectiveness at these higher resonance frequencies.

A similar observation was made in Chapter 6, where TWCs were found to be most effective in regions where the structural displacement was at its maximum. This suggests that positioning the particle damper at locations with the highest structural displacement enhances its effectiveness. This finding aligns with results reported by Koch et al. [150], and others, who also observed that the performance of particle dampers is significantly improved when they are mounted at points of maximum displacement within the structure. Hence, this result further strengthen this conclusion, highlighting the significant impact of strategic damper placement on overall system performance.

8.4 Dynamic response of blade in rotating condition

This section presents the experimental setup and investigates the effect of a particle damper in reducing the vibration amplitude of a rotating blade.

8.4.1 Experimental set up

In order to accurately measure the vibrations of blades during rotation, a derotator unit is employed in conjunction with a laser scanning vibrometer, as illustrated in Figure 8.6. The derotator is an advanced optical device equipped with a rotating prism that redirects the laser beam from the laser scanning vibrometer, as well as the secondary reference vibrometer beam, onto the surface of the rotating object. The rotational speed of the prism is synchronized with the rotational speed of the propeller via an incremental encoder, which is connected to the motor located on the rear side of the setup.

For the derotator to effectively track the target point on the object, precise alignment of the rotational axis is crucial. Any misalignment introduces eccentricity, and even slight deviations from the correct axis alignment can result in a wobbling effect. Both of these issues cause the laser beam to deviate from the intended measurement point, leading to the measurement of additional, unintended movements. Consequently, these misalignments introduce measurement errors by capturing motion components that are not representative of the actual vibrational behavior of the blades.

Figure 8.7 illustrates the test rig in operation during the rotation of the propeller. In this setup, the inner laser beam is directed at the hub to measure a reference signal, which is crucial for obtaining

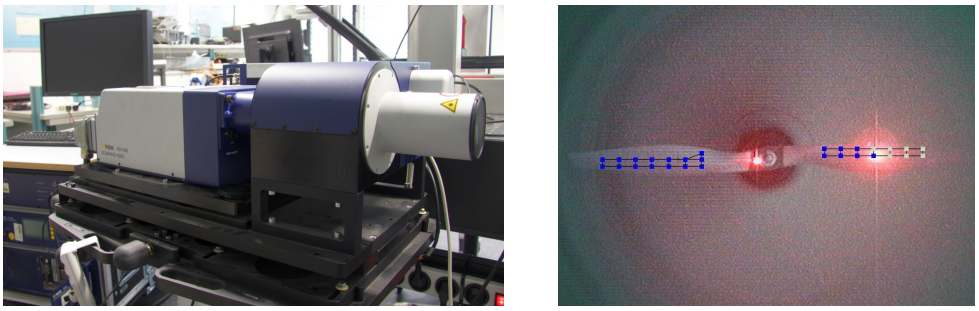

Figure 8.6: Laser scanning vibrometer with derotator unit (left) and view of the laser scanning vibrometer measuring a rotating object (right).

accurate phase information regarding the blade vibrations. Simultaneously, a second laser beam is used to capture vibration data at multiple locations across the surface of the blade. The measurement procedure involves systematically scanning these designated points, with each point being averaged over five complex measurements. This averaging process helps to account for potential variations in the object, which may arise from slight imperfections in the synchronization. The specific locations of the scan points on the blade surface can be observed in Figure 8.6 (right).

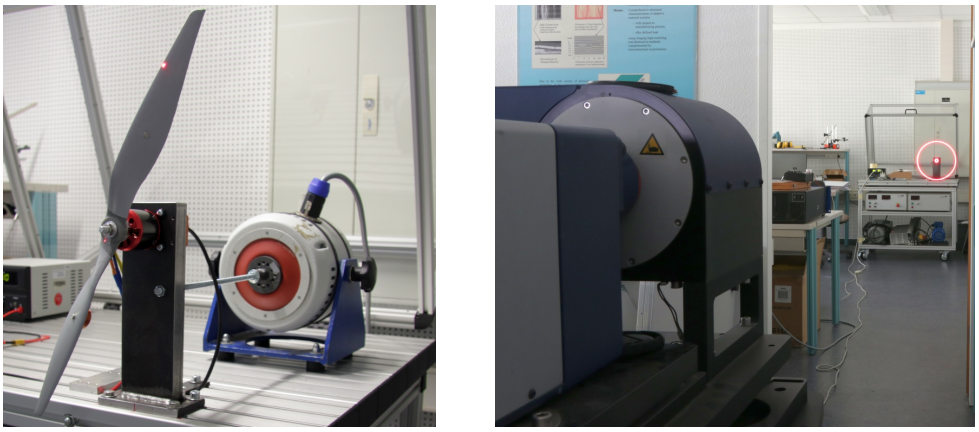

Figure 8.7: Propeller with motor and shaker setup (left), measurement during rotation (right).

To accurately determine the transfer function from measurement signals, it is essential to verify the frequency range of excitation. Here, vibration at the rotor hub serves as the reference. Without shaker excitation, vibrations at the blade hub are insufficient to excite all natural frequencies. Using a shaker with a pseudo-random signal generates adequate excitation up to 300 Hz. However, above this frequency, the transfer function cannot be reliably calculated due to the limited resolution of the AD converter in the scanning vibrometer. Consequently, all measured transfer functions are presented only up to 300 Hz, reflecting this excitation limitation.

8.4.2 Results

The effects of the particle damper on the rotating blade test specimen are presented in Figure 8.8. FRFs for the blade specimen are presented only up to 300 Hz, as excitation beyond this frequency range was insufficient to produce reliable measurements. The dynamic response of the blade was evaluated across four distinct rotational speeds: 120 RPM, 180 RPM, 660 RPM, and 1080 RPM, as illustrated in Figure 8.8. The findings reveal a pronounced dependency of particle damper effectiveness on rotational speed. Notably, at 180 RPM, the particle damper significantly reduces the blade's vibration amplitude.

In contrast, at the other speeds examined (120 RPM, 660 RPM, and 1080 RPM), the particle damper exhibits a minimal effect on vibration reduction.

The response was measured for different rotational speeds between 120 RPM and 1080 RPM. The limit speed to reach the same centrifugal acceleration as in a real wind turbine is 180 RPM so that the measured operating points are below and above the practically relevant boundary condition.

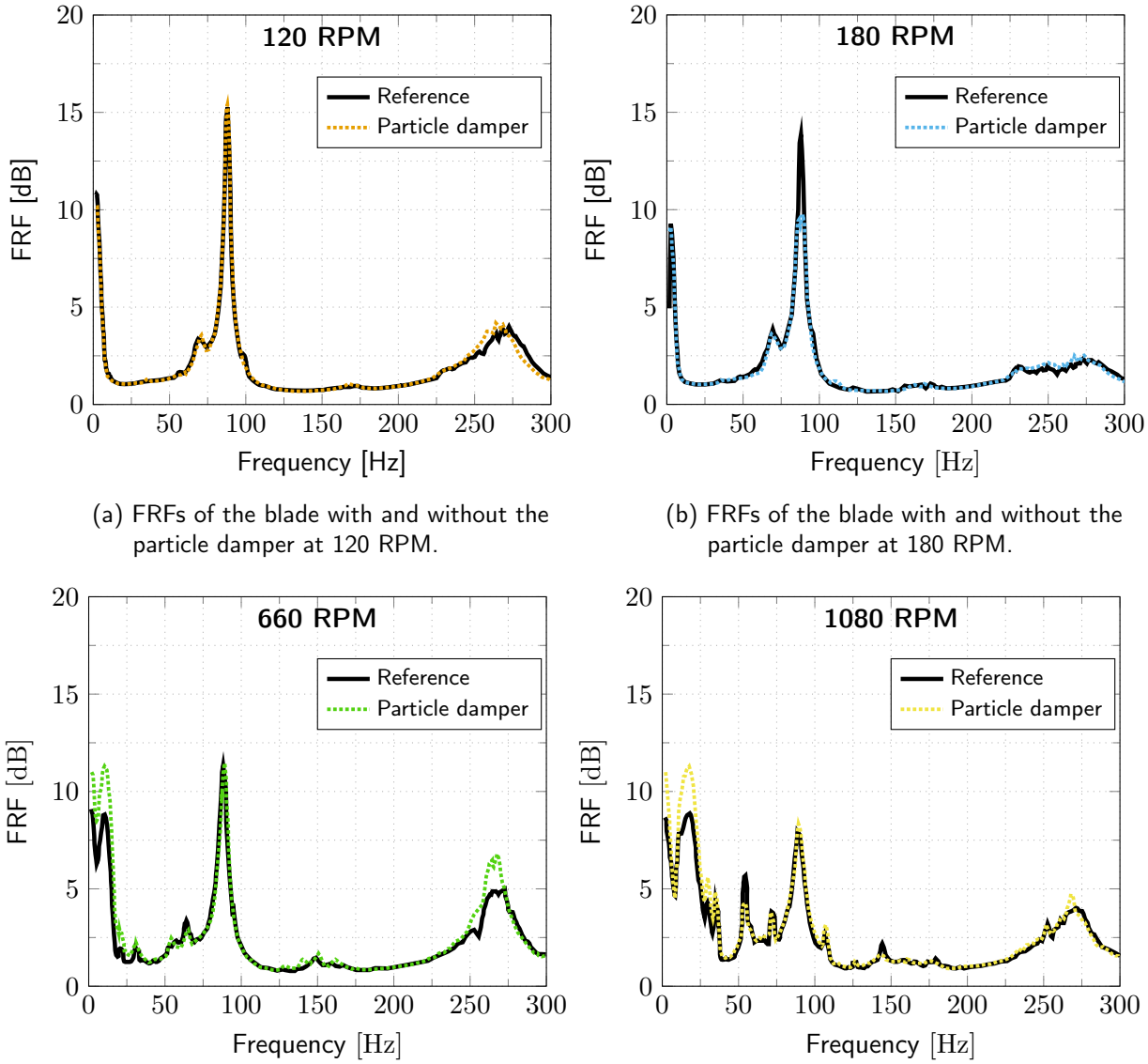

(a) FRFs of the blade with and without the particle damper at 120 RPM.

(b) FRFs of the blade with and without the particle damper at 180 RPM.

(c) FRFs of the blade with and without the particle damper at 660 RPM.

(d) FRFs of the blade with and without the particle damper at 1080 RPM.

Figure 8.8: FRFs of the test specimen at various rotational speed.

To investigate the ineffectiveness of the particle damper at rotational speeds of 120 RPM, 660 RPM, and 1080 RPM, it is essential to examine the motion behavior of the granular materials within the damper cavity. However, as discussed in Chapter 2, experimentally analyzing particle motion modes presents significant challenges. Consequently, researchers have relied on DEM simulations to study the influence of particle motion modes on the damping performance of particle dampers [98, 106, 109, 110, 139].

In Chapter 2, the varying optimal damping modes observed across multiple studies on particle dampers were explored in detail. While these studies show diverse behaviors under different conditions, a key similarity emerges: at higher excitation intensities, particles within the cavity enter a "collect and

collide" phase. In this phase, the particles group together into a clump, moving as a cohesive mass in a single direction before colliding with the cavity walls. This behavior minimizes relative motion among particles, resulting in a marked decrease in vibration attenuation capabilities since energy dissipation through inter-particle motion is minimized.

Another common observation across these studies is the behavior of particles at lower excitation intensities. Under these conditions, the particles exhibit a "solid-like" state, where there is minimal relative motion between the particles and the container. This lack of relative movement similarly reduces the particle damper's effectiveness, as energy dissipation through particle interactions is limited. Notably, it is important to highlight that all these studies were conducted on particle dampers subjected to either vertical or horizontal excitations and used spherical particles as the damping medium. This specificity in orientation and particle shape may influence the observed behaviors and should be considered when generalizing these findings to other damping configurations.

Therefore, it is plausible that at higher rotational speeds, the particles may enter a "collect and collide" phase, where the absence of relative motion among particles could substantially reduce the system's damping efficiency. The reduced effectiveness of particle dampers at higher rotational speeds was also observed by Sandanshiv et al. [164]. However, their study does not provide an explanation for this phenomenon. It is noteworthy that they used steel particles in their particle damper design, which may affect performance differently across varying rotational speeds. In contrast, Xiao et al. [158] investigated the influence of centrifugal forces on particle damper performance. They found that as rotational speed increases, the damping performance of the particle damper improves. This improvement is, however, closely related to the filling ratios, which vary in optimality across different rotational speeds.

As previously discussed, at lower excitation intensities, the particles within the cavity exhibit behavior similar to a solid state. However, at a rotational speed of 120 RPM, rubber granulate inside the cavity cannot behave like a solid. To validate the collect-and-collide mode phase at higher rotational speeds and to investigate particle motion at 120 RPM, where the particle damper has no effect, further experimental studies using high-speed camera analysis are necessary. These experiments would provide a detailed observation of particle dynamics under such conditions, offering deeper insights into the impact of rotational speed on damper performance. Nevertheless, the results indicate that the behavior of the particle damper in rotating systems is also nonlinear.

8.5 Discussion and conclusion

The particle damper effectively reduces vibrations in a scaled blade structure, significantly impacting eigenfrequencies up to 1000 Hz in non-rotating conditions. While its broad frequency effectiveness suggests potential for multi-mode vibration control, the damping effect is reduced under rotating conditions, affecting only certain eigenfrequencies.

To enhance accuracy in future studies, improving the test rig is crucial. The current setup's surface cavity alters airflow, potentially affecting aerodynamic and vibrational behavior. Using a larger blade specimen would allow direct piezoelectric actuator mounting, enabling transfer function measurement during rotation. This would overcome current excitation limitations, improving response accuracy above 300 Hz, a critical range for further analysis.

Additional tests with varied damper positions are also necessary to assess the impact of placement on vibration reduction. Installing multiple particle dampers across the blade could further reduce vibration amplitudes across all eigenfrequencies, improving overall damping performance. It is also crucial to capture and analyze the motion modes of particles within the damper cavity, as these modes vary with rotational speed and can significantly affect the damper's efficiency. Understanding the interaction between particle motion and rotational speed will provide deeper insights into optimizing particle damper configurations for rotating structures.

9 Lab-scale particle damper development for wind turbine generators

In the previous chapters, the key design parameters have been thoroughly investigated and analyzed. As mentioned in Chapter 1, one of the objectives of this thesis is to transition from laboratory studies to industrial-scale testing. To explore the use of particle dampers in reducing vibration amplitudes, wind turbine components have been selected as the industrial application. Before scaling up to industrial testing, the concept is first developed at the laboratory level using the design parameters from previous chapters. Therefore, this chapter introduces and evaluates these laboratory-developed concepts, intending to minimize vibrations in wind turbine generator test specimens.

This chapter opens with an overview of the growing importance of wind energy and the challenges it faces. It also includes a brief discussion of the latest trends in passive damping techniques used to mitigate vibrations in wind turbine components. Following this, an introduction to wind turbine generators is provided. The design of the test specimen developed for particle damper implementation is then examined, followed by a detailed analysis of the experimental study and the design concepts created for the generator. The chapter concludes with a comparison of the advantages and disadvantages of these design concepts. The current chapter is built upon the findings presented in previous publication [216].

9.1 Introduction

The pressing need to address environmental issues associated with conventional energy sources necessitates a transition from traditional fuels. This shift is crucial for meeting global energy demands while also reducing greenhouse gas emissions.

The rapid development of renewable energy sources, especially wind power, is transforming the energy landscape by providing a sustainable and eco-friendly alternative capable of fulfilling global energy requirements. Over the past two decades, the installed capacity of onshore wind turbines has experienced remarkable growth, increasing from 24 GW to 700 GW. This substantial expansion includes a notable 59% rise between 2019 and 2020, alongside the addition of approximately 78 GW of wind power capacity in 2022. These developments position wind energy as a vital player in assisting countries in achieving their net-zero emissions targets [217, 218].

However, undesired vibration and sound emissions can be one of the major hindrances to the growth of wind farms. The excessive vibrations of wind turbines hinder the conversion of wind energy into electricity and also contribute to the deterioration of structural components and fatigue life. In the most severe cases, these vibrations can ultimately cause the total collapse of wind turbines, posing a catastrophic risk [219, 220]. Additionally, sound emissions resulting from low-frequency vibrations can cause a range of health problems, including headaches, sleep disturbances, irritability, and fatigue [2–4].

Therefore, it is crucial to take into account the acceptance of nearby residents towards wind turbine sound emissions, primarily arising from low-frequency vibrations, during the development process. Consequently, to promote the continued growth of onshore wind farms, addressing and minimizing these vibrations and associated sound emissions is vital. As a result, each country worldwide has established its regulations to define the limits for sound emissions from onshore wind turbines. Consequently,

wind turbine manufacturers are placing increasing emphasis on implementing measures to reduce the undesired vibration and sound emissions from wind turbine components.

9.2 Vibration control of wind turbine components

Vibrations in wind turbines result from multiple mechanisms, primarily associated with the relative motion and interaction of mechanical components, as well as the dynamic responses of these elements under operational conditions. A prominent source of vibration-induced sound emission within a wind turbine is the generator. Specifically, vibrations are generated by electromagnetic interactions between the rotating poles of the rotor and the stationary stator. These vibrations travel through the turbine's structural components, leading to sound emissions that ultimately disperse into the environment.

To mitigate these vibrations, various passive damping techniques are employed across wind turbine components, including the tower, nacelle, and blades. For instance, the implementation of passive damper devices, such as a TMD and tuned liquid damper (TLD), has demonstrated its effectiveness in reducing the vibration amplitude of a wind turbine [221–223].

Significant research has focused on controlling vibrations in wind turbine towers through passive control devices. Among these, the TMD is a widely used passive system that effectively reduces vibration amplitudes in wind turbine towers. The TMD is tuned to the frequency of the tower's targeted vibration mode, causing it to resonate out of phase with the tower and effectively dissipate a significant amount of vibrational energy. Numerous studies have demonstrated successful vibration reduction by installing a single TMD in the nacelle [221, 222, 224]. This approach is particularly effective as the energy from wind and wave loads primarily occurs at low frequencies, typically exciting only the first vibration mode of the tower, with maximum displacement occurring near the tower top. Consequently, placing the TMD at the nacelle, where peak displacement is observed, optimally reduces wind- and wave-induced vibrations. Expanding on this, Zuo et al. [225] suggested installing multiple TMDs along the tower to target both the first and second vibration modes, further enhancing vibration control.

In addition to TMDs, tuned liquid column dampers (TLCDs) are frequently studied for controlling wind turbine tower vibrations. Unlike the TMD, a TLCD consists of a U-shaped container partially filled with liquid. Experimental studies have also explored the effectiveness of TLCDs in reducing the vibration amplitude of wind turbine towers [220, 226]. The TLD system is also commonly employed to mitigate tower vibrations [227–229]. This system typically comprises a tank partially filled with liquid, which can effectively reduce the primary structural vibrations by tuning the sloshing frequency of the liquid to match the frequency of the main structure. This tuning is accomplished by adjusting the water level within the tank. In addition to conventional TMDs, TLCDs, and TLDs, a range of alternative control devices has been developed to mitigate vibration amplitude in wind turbine towers. These devices include friction dampers [230], scissor-jack braced viscous dampers [231], and ball vibration absorbers [232].

A substantial body of research has focused on the use of passive design approaches to mitigate vibrations in wind turbine blades. A brief review of these passive damping methods, along with their advantages and limitations, will be presented in Chapter 10.

As discussed in Chapter 2, passive damping techniques have been found to be largely ineffective in mitigating vibrations in the low-frequency range. Additionally, these techniques generally lack the capability to provide broad-spectrum damping. The implementation of passive dampers, such as TMDs and TLCDs, also presents significant practical challenges, including the requirement for substantial installation space and the introduction of additional structural weight. Furthermore, in the case of TLCDs and TLDs, the potential leakage of liquid from the cavity during operation poses a critical reliability concern.

To overcome these limitations, this chapter explores the application of particle damping techniques

to attenuate the vibration amplitude of a wind turbine generator. While particle dampers have been extensively investigated for vibration suppression in various engineering domains (see Chapter 2), research focusing on their application in wind turbines remains extremely limited. To the best of the author's knowledge, no prior studies have reported practical implementations of particle damping in onshore direct-drive wind turbine generators. Therefore, this chapter examines two design variants based on the parameters identified in the previous chapters, aiming to integrate particle damping techniques for effective vibration amplitude reduction in wind turbine generators.

Chapter 5 established the vibration attenuation capabilities of different particle damper configurations, including RRPDs, HMPDs, and HPDs, offering valuable insights into material selection for specific applications. Chapter 6 further explored passive particle damper designs that enhance the mobility of granular materials, particularly in scenarios where primary structural vibrations alone are insufficient to induce particle motion. Additionally, Chapter 7 demonstrated that particle dampers incorporating rubber granulate maintain their vibration suppression performance even under high dynamic loads, confirming their long-term durability. These findings form a crucial foundation for the integration of particle dampers into industrial structures.

However, before these concepts can be applied to full-scale implementations, certain modifications are necessary to ensure feasibility and practicality. For example, the design variations explored in Chapter 6 have proven effective in enhancing granular mobility within particle dampers, a crucial aspect of optimizing vibration attenuation. Nevertheless, a key criterion for implementing particle dampers in large-scale wind turbine systems is that modifications to the existing generator subsystem should be kept to an absolute minimum. This constraint stems from essential engineering considerations, such as preventing extensive redesigns of critical components and maintaining cost-effectiveness. Additionally, since these concepts must be evaluated within an existing wind turbine generator subsystem, extensive modifications would not only be financially prohibitive but also significantly increase implementation time. Therefore, design adaption is required to fit within the current system with minimal structural changes is imperative for practical application.

Hence, in this chapter, two particle damping design variants were developed, namely: the honeycomb damping plate (HCDP) and the pre-existing cavity (PEC) concept. The HCDP concept is an adaptation of conventional particle dampers, where honeycomb cells are partially filled with granular materials and strategically positioned on the generator test specimen to enhance vibration attenuation. Initially, the HCDP variant will be tested on a scaled wind turbine generator specimen to evaluate its effectiveness in reducing vibrations. If the results demonstrate its viability, the TWC and TWC-AS design variations will be incorporated into the HCDP for further assessment in an industrial-scale wind turbine system. The PEC concept, on the other hand, leverages the existing hollow sections of the test specimen as enclosures for granular materials, eliminating the need for additional external dampers. While the PEC concept was initially introduced in Chapter 5 for evaluating the damping performance of granular materials, it is revisited here briefly for completeness and to facilitate a direct comparison with the HCDP concept. This systematic approach ensures that the most effective damping strategy can be identified for potential real-world application in wind turbine generators.

9.3 Wind turbine generator

The wind turbine generator is a fundamental subsystem responsible for converting mechanical energy from the blade rotation into electrical energy, making it essential to the overall energy generation process. In a direct-drive wind turbine, the generator speed matches the rotor speed due to the direct mechanical connection between the rotor and generator. Given the low rotational speed of the generator, multiple magnetic poles are incorporated to attain the desired high output frequency. Figure 9.1 (left) illustrates the generator subsystem of a direct-drive wind turbine, which is primarily composed of two critical components: the rotor and the stator. The stator, which remains stationary

during energy production, consists of the fixed elements within the generator. This chapter specifically explores the effectiveness of the HCDP concept and the PEC in enhancing the damping performance within direct-drive wind turbine generators. It should be noted, however, that with minor modifications, these damping concepts could be adapted for use with other types of generators as well.

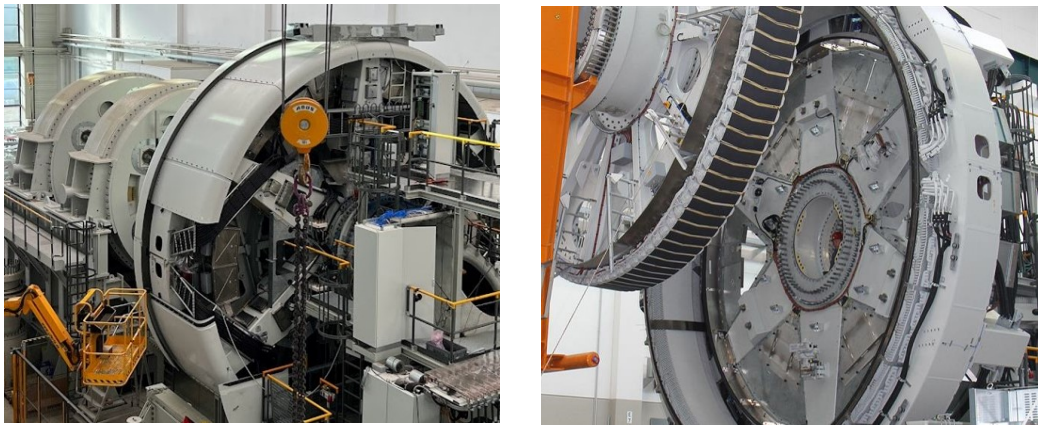

Figure 9.1: Left: Direct-drive wind turbine generator test bench, right: stator of the commercial annular generator [233].

The stator in a direct-drive wind turbine generator, often referred to as an annular generator, consists of a large stator ring and several stator arms, as depicted in Figure 9.1 (right). The stator arms, which are hollow, connect to the ring to provide structural support to the entire assembly. Within the stator ring, electromagnetic coils generate a magnetic field when an electric current flows through them. The interaction between this stationary magnetic field and the rotating poles of the generator induces vibrations within the system. These vibrations are subsequently transferred to other components of the wind turbine and can radiate into the surrounding environment.

Thus, the objective of the present chapter is to examine the damping effectiveness of the HCDP and PEC concepts specifically for reducing vibration amplitude within the WTS test specimen. This investigation is aimed at mitigating the transmission and radiation of vibrations from the generator to adjacent turbine components and ultimately to the external environment.

9.4 Test specimen design concept

As previously mentioned, the stator of an annular generator has been chosen for examining the effectiveness of the HCDP and PEC concepts in reducing the vibration amplitude of a wind turbine generator subsystem. This selection is driven primarily by the presence of hollow sections within the stator ring and arms. The hollow sections of the WTS offer an ideal environment for testing the damping efficiency of the PEC concept without necessitating any modifications to the existing structural framework.

Furthermore, since the stator is a stationary part of the generator, the influence of centrifugal forces on the performance of particle dampers can be effectively disregarded. This simplification leads to a reduced set of parameters that need to be considered in the design of the particle dampers. The primary goal of this study is to reduce the vibration amplitude in the areas surrounding the stator arm and ring (see Figure 5.1 for reference). By doing so, any unwanted structural disturbances are aimed to be prevented from propagating, thereby enhancing the overall performance and longevity of the wind turbine generator.

The test specimen used to assess the vibration attenuation capabilities of RRPDs, HMPDS, and HPDs (see Chapter 5) is also utilized to investigate the HCDP and PEC concepts. While Chapter 5 provides a comprehensive explanation of the test specimen development process, this chapter focuses on specific aspects of the design in relation to HCDP, clarifying the rationale behind the chosen test specimen and HCDP configurations.

Initially, the proposed design approach involved scaling down the original WTS by a specific factor to improve its feasibility for laboratory testing. However, this downscaling necessitates a proportional reduction in the HCDP geometry, including key parameters such as wall thickness and core dimensions (refer to Section 9.5 for the HCDP concept). This introduces significant challenges, as smaller HCDP cavities may become impractical to manufacture with the required precision. Additionally, reducing the core size restricts the free movement of granular materials within the HCDP, which is crucial for effective particle damping. Furthermore, decreasing the wall thickness of the honeycomb cores compromises the structural integrity of the HCDP, making it more susceptible to mechanical deformation. These factors highlight the complexities of scaling the WTS and emphasize the need for a careful balance between design trade-offs when developing a laboratory-scale test specimen alongside the HCDP.

To overcome the above-mentioned limitations, a reduced-scale test specimen was developed by selecting a small section of the original WTS and scaling it down, as illustrated in Figure 5.2 in chapter 5. In the commercial WTS, the stator arm is welded to the stator ring. However, in the laboratory-scale test setup, the stator arm is attached to the stator ring using four identical bolts. This bolted connection was deliberately chosen to facilitate the installation of the HCDP between the stator arm and stator ring. Additionally, multiple holes were drilled on all the faces of the stator ring to accommodate the attachment of the HCDP. The test specimen was constructed using steel, in line with the material used in the original WTS, ensuring material consistency between the experimental model and the commercial application. It is also important to note that the total mass of the laboratory-scale WTS test specimen is 8 kg.

9.5 Honeycomb damping plate (HCDP) concept

The HCDP is derived from the conventional particle damper design, featuring a distinct structural adaptation in which the granular materials are encased within a honeycomb core. This honeycomb structure facilitates an even distribution of granular materials throughout the damper cavity, while allowing unrestricted particle movement within the enclosure.

9.5.1 Honeycomb damping plate design

Figure 9.2 illustrates the design and dimensions of the HCDP. The HCDP structure consists of two thin face sheets, positioned at the top and bottom, which are affixed to a lightweight honeycomb core through adhesive bonding. This bonding technique is specifically selected for its capacity to connect surfaces with complex or irregular geometries without significantly altering the overall dimensions or geometry of the components. Additionally, adhesive bonding contributes minimal added weight to the materials being joined and facilitates rapid adhesion between diverse substrates, including those sensitive to heat [234]. To reduce the added mass of the particle damper, both the HCDP core and face sheets are constructed from aluminum. Notably, the wall thickness of the top and bottom face sheets, as well as the honeycomb cell walls, is uniformly set to 1 mm.

The effectiveness of seven HCDPs in attenuating vibrations in a scaled WTS has been systematically examined. All damping plates were designed to have identical length, width, and core height dimensions to ensure consistency across tests. To facilitate mounting the HCDPs at various locations on the WTS test specimen, six rectangular slots were cut into each HCDP to accommodate small steel blocks, each

with a thickness of 9 mm. These steel blocks were made slightly shorter than the height of the HCDP by 1 mm to prevent plastic deformation within the honeycomb core during the fastening process.

Each HCDP was then secured to the stator ring walls using a thin aluminum sheet and four identical bolts, see Figure 9.3 (right). This fastening method was selected to enable reuse of both the HCDPs and the WTS test specimen components, including the stator arm and stator ring, across multiple experiments. Additionally, mechanical fastening is a conventional and cost-effective joining technique, making it well-suited for industrial applications where cost reduction is crucial in large-scale manufacturing.

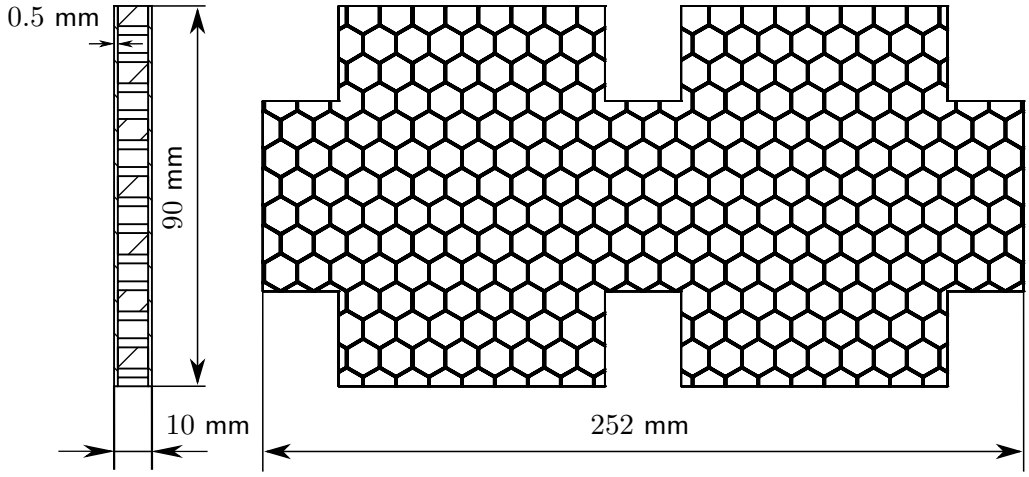

Figure 9.2: Design and geometry of honeycomb damping plate.

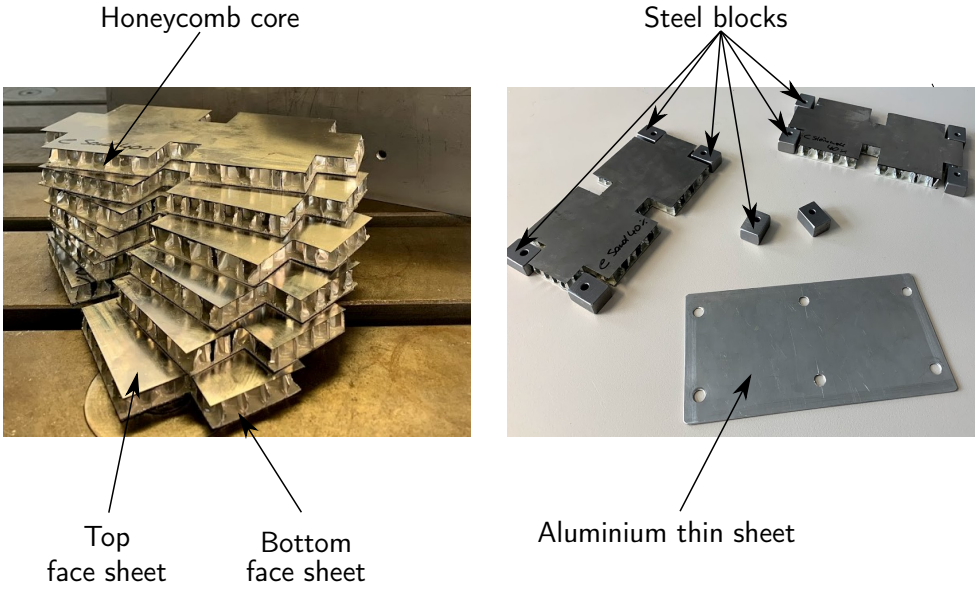

Figure 9.3: Left: Honeycomb damping plates (HCDPs) partially filled with granular materials. Right: steel blocks and thin aluminium sheet used for attaching HCDP to the WTS test specimen.

Chapter 5 presented an in-depth assessment indicating that rubber granulate "RG 4.6 mm" is a highly effective material for the design of particle dampers. However, its application in the current study is restricted by the size limitations of the HCDP cores, making it unsuitable as a filling material. To address this constraint, rubber powder has been selected as an alternative, as the granulates examined

in Chapter 5 exceed the maximum allowable particle size for the HCDP core. Among the available options, rubber powder "RP 0.5 mm" has been specifically chosen due to its superior ability to attenuate vibrations compared to rubber powder "RP 0.8 mm" (see Chapter 5). In addition to rubber powder, other materials such as stone powder, sand, and tungsten powder have been incorporated as fillers in the HCDP to evaluate their effectiveness in vibration mitigation. Among these, stone powder has exhibited a higher capacity for vibration reduction compared to rubber powder. However, despite its promising performance, practical implementation in real-world applications presents several challenges, as discussed in Chapter 5.

Although the damping characteristics of rubber and stone powders have already been analyzed in detail, their behavior is revisited in this study for two primary reasons. First, it is essential to determine whether the HCDP concept functions effectively under controlled laboratory conditions. Second, this study seeks to determine whether the vibration attenuation characteristics of these materials are affected by changes in the geometry of the test specimen, specifically the HCDP.

Furthermore, for comparative analysis, HCDPs are also partially filled with tungsten powder and sand. Similar to rubber and stone powders, these materials exhibit a non-uniform PSD, as detailed in Table 9.1. Notably, the sand used in this study differs from the sand analyzed in Chapter 5.

In addition to testing the fully assembled HCDP system, the vibration response of the WTS test specimen with an empty HCDP is also examined. By isolating the HCDP in an empty configuration, it is intended to demonstrate that the primary source of damping arises from the dynamic interaction with the granular media rather than from the structural design of the HCDP itself.

Table 9.1: Particle size of polydisperse granular materials for HCDPs design.

Material	d10 [mm]	d50 [mm]	d90 [mm]	Absoulte span [mm]	Bulk density [kg/m^3]
Tungsten powder	0.00074	0.00135	0.00305	0.00231	2630
sand	0.01014	0.06306	0.23111	0.22097	-

Alongside the investigation into the influence of different HCDPs on the vibration attenuation of the WTS test specimen, this study also systematically examines the effects of varying filling ratios on damping performance. Chapter 6 has demonstrated that an 80% filling ratio is effective for vibration mitigation. However, previous studies have reported varying optimal filling ratios for particle damper designs. For instance, Muthu et al. [156] found that a 50% filling ratio provided the best vibration attenuation, while Holkamp et al. [171] identified 45% as the most effective ratio for reducing vibration amplitude. Given these discrepancies, it is essential to further investigate the influence of filling ratio on HCDP performance. Since Chapter 6 has already established 80% as an optimal configuration, this chapter examines two additional filling ratios, namely: 20% and 40% to provide a more comprehensive understanding of how different fill levels affect vibration attenuation.

Similar to previous chapters, the filling ratio in this chapter is also defined as the proportion of the cavity volume occupied by granular particles relative to the total volume of the cavity. Granular materials are carefully introduced into each honeycomb cell to ensure an even and consistent distribution, achieving uniformity in the spatial arrangement of particles within the structure. This approach enables a controlled comparison of the impact of different filling ratios on the overall damping characteristics of the system. Furthermore, as discussed throughout this thesis, a 100% filling ratio is not considered optimal for the design of particle dampers, as it restricts the free movement of granular material particles, thereby diminishing their capacity to attenuate vibrations effectively. Consequently, this filling ratio is deliberately avoided in the design of HCDPs as well.

In Chapter 6, the influence of SU and MU particles on vibration attenuation was examined. In this section, the impact of this parameter will be further investigated. However, there is a notable distinction

in the design approach for the MU particle damper. Unlike in Chapter 6, where the MU particle damper was configured by inserting a thin plate within the SU TWC, the MU particle damper here will be constructed by combining two HCDPs. This approach of joining two HCDPs to create the MU configuration offers a streamlined design, simplifying the testing process for the MU particle damper.

Table 9.2 provides a summary of the filling materials used in the design of the HCDPs, including their respective filling ratios, the mass of each filling material, and the total mass of the HCDPs.

Table 9.2: List of filling materials, filling ratios, filling material mass, and total mass of the HCDP.

Material	Filling ratio [%]	Filling material mass [g]	Total mass of HCDP [g]
Empty			67.0 g
Sand	40	54.2	121.2
	20	25.8	92.8
Stone powder	40	46.7	113.7
	20	22.5	89.5
Rubber powder	20	16.1	83.1
Tungsten powder	20	49.9	116.9

9.5.2 Location of honeycomb damping plates

Chapters 6 and 8 highlights the significant impact that the placement of a particle damper can have on the reduction of vibration amplitude in the test specimen. Consequently, it is essential to assess the influence of HCDPs at all potential locations on the scaled WTS specimen prior to their implementation on full-scale WTS systems. To this end, HCDPs are mounted at all possible locations on the WTS test specimen. Figure 9.4 illustrates the various configurations of HCDPs applied to the WTS test specimen, enabling an investigation into the vibration reduction capabilities of the HCDP concept.

Both partially filled HCDPs and empty HCDPs are strategically positioned on the test specimen at every conceivable location to comprehensively evaluate their impact on vibration attenuation. The reference test specimen, which is the WTS test specimen without any particle damper, is depicted in Figure 9.4 (a). Initially, a SU HCDP is attached between the stator ring and stator arm to assess its influence on vibration attenuation, as shown in Figure 9.4 (b).

Building on these observations, the most effective partially filled HCDP identified at this location is paired with a corresponding HCDP featuring a different filling ratio, allowing for an examination of the effects of the MU HCDP on reducing the vibration amplitude of the test specimen (Figure 9.4 (c). Subsequently, the SU HCDP is affixed to the outer wall of the stator ring, positioned opposite the excitation point, as illustrated in Figure 9.4 (d). The performance rankings of the materials obtained from these tests are then utilized to design a MU HCDP configuration at the same location, depicted in Figure 9.4 (e).

In a similar approach, a MU HCDP arrangement is created by attaching it to the inner wall of the stator ring to evaluate its impact on vibration reduction in the WTS test specimen (Figure 9.4 (f)). Additionally, an SU HCDP is mounted on the inner wall of the stator ring to further investigate its influence on vibration attenuation (Figure 9.4 (g)). Based on the results obtained from the various HCDP placements on the WTS test specimen, additional investigations are conducted to assess the effects of three different combined configurations of the HCDP. These configurations referred to as Configuration 1, Configuration 2, and Configuration 3 are analyzed regarding their influence on transmission path damping, as illustrated in Figures 9.4 (h)-(j).

Configuration 1 involves the strategic selection of two distinct locations for the implementation of the HCDP. In this arrangement, a SU HCDP is securely fixed between the stator arm and the stator ring.

This is followed by the installation of a MU arrangement of the HCDP on the outer wall of the stator ring, positioned directly opposite the excitation point.

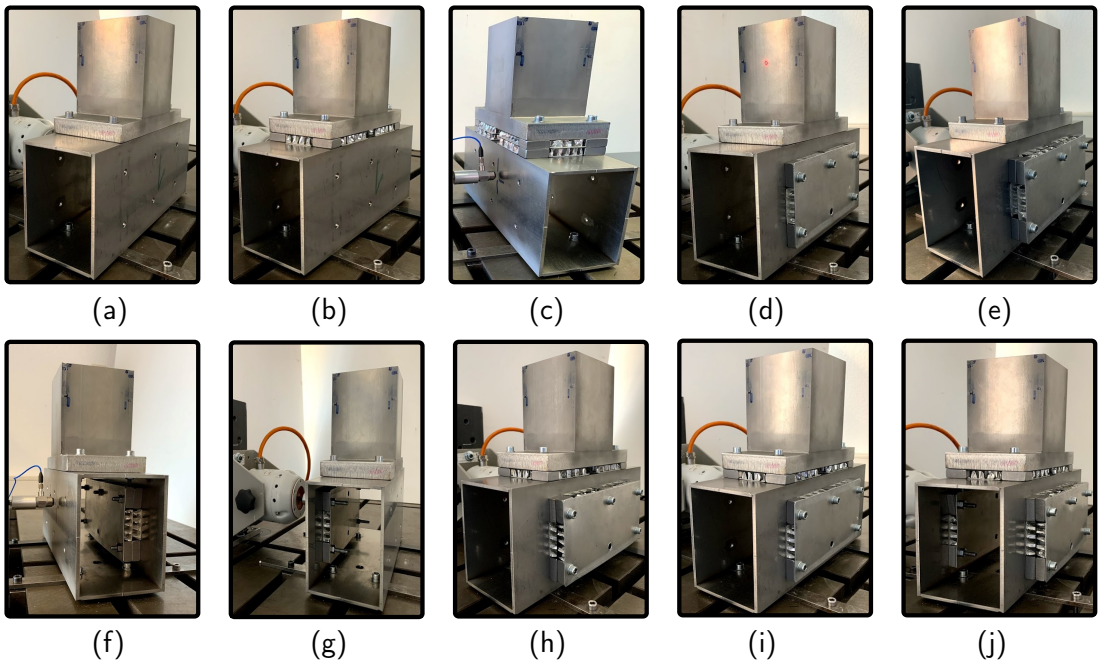

Figure 9.4: Location of HCDP on the WTS test specimen (a): Test specimen without HCDP (Reference test specimen), (b) SU HCDP mounted between the sator ring and stator arm (c) MU HCDP assembled between the sator ring and stator arm, (d) SU HCDP on the outer wall of the stator ring (opposite to excitation point), (e) MU HCDP on the outer wall the stator ring (opposite excitation point), (f) MU HCDP on the inner wall the stator ring (opposite excitation point), (g) SU HCDP on the inner wall of the stator ring (excitation point side), (h) Configuration 1, (i) Configuration 2, (j) Configuration 3.

Configuration 2 closely resembles Configuration 1, with the primary difference being the replacement of the MU HCDP with an SU HCDP mounted on the outer wall of the stator ring. This slight modification allows for an evaluation of the effects of a SU configuration in contrast to the multi-unit arrangement.

Configuration 3 presents a more complex combination of SU and MU HCDPs. Similar to Configuration 1, Configuration 3 includes a MU HCDP installed on the outer wall of the stator ring. Additionally, an SU HCDP is strategically placed on the inner wall of the stator ring, specifically on the side facing the excitation point, as well as between the stator arm and the stator ring. This multifaceted arrangement aims to explore the interaction between the various configurations of HCDPs and their collective influence on vibration attenuation in the test specimen.

9.6 Pre-existing cavity (PEC) concept

The incorporation of granular materials, empty HCDPs, fastening joining systems, thin aluminum sheets, and steel blocks in the HCDP results in an approximate 10% increase in the mass of the WTS test specimen. Furthermore, this design approach may presents challenges related to the manufacturing and production processes. To ensure the structural integrity and performance of the system, a comprehensive strength analysis and an examination of the bonding joining processes for the honeycomb damping plate are also critical. In response to these challenges, an alternative concept known as the pre-existing cavity (PEC) concept has been developed as a potential solution.

The PEC concept leverages the advantages of the existing cavity within the WTS test specimen arm to effectively enclose granular materials, as illustrated in Figure 9.5. Compared to the HCDP concept, the PEC concept offers several significant advantages. For instance, it simplifies the manufacturing process, avoiding any new challenges related to reliability and component safety that may arise from additional design complexities.

Additionally, the PEC concept facilitates a substantial reduction in the extra mass associated with the particle damper, thereby enhancing the overall efficiency of the system. Importantly, depending on the type and mass of the granular materials used, the PEC concept is designed to maintain the stiffness of the primary structure, ensuring that its structural integrity is not compromised. Moreover, the PEC concept presents a wide array of design opportunities for further exploration, as demonstrated in Chapter 5. This flexibility allows for innovative adaptations that can enhance the performance of the vibration damping system while maintaining the essential characteristics of the WTS test specimen.

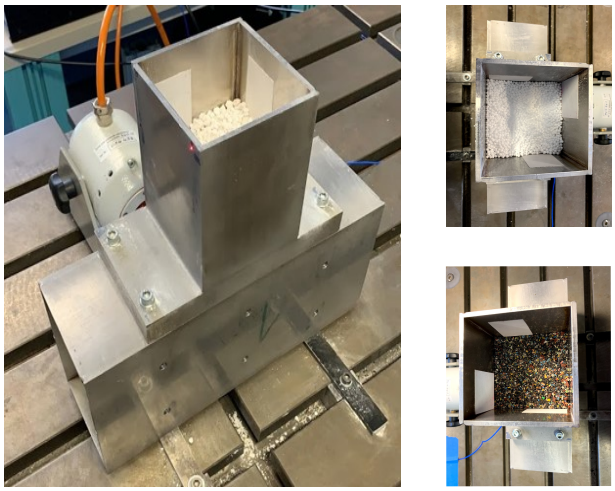

Figure 9.5: Pre-existing cavity concept configuration.

To enable a reliable comparison with the HCDP concept, conducting a new series of experiments is crucial. While the same approach has previously been used to evaluate the vibration attenuation performance of RRPDs, HMPDs, and HPDs, the experiments to test the PEC concept were conducted much earlier than the investigations in Chapter 5. As a result, the FRF spectrum exhibits noticeable variations in amplitude and resonance frequency. Without fresh experimental data, discrepancies could arise, making direct comparisons unreliable. Therefore, a new set of experiments has been conducted to ensure consistency and accuracy in the analysis. It is important to note that the PEC experimental study served as the basis for selecting the WTS test specimen arm as an enclosure for granular materials to systematically assess the vibration attenuation capability of various materials and their mixtures (see Chapter 5).

Rubber granulate "RG 3.0 mm" was selected as the filling material for the PEC concept. At the time these experiments were conducted, the rubber powder used in the HCDP was unavailable in sufficient quantity for the PEC setup. Therefore, "RG 3.0 mm" was used to enable comparative analysis between these concepts. Despite the difference in materials, a valid comparison remains possible.

It is also important to note that throughout the experiments, the WTS test specimen's stator arm in the partially filled configuration was left open, without a lid. Two scenarios were tested: the first with the arm partially filled with 150 g of rubber granulate, and the second with 250 g. Notably, the particle damper in the PEC concept remained approximately 70% lighter than the most effective configuration achieved with the HCDP concept.

9.7 Experimental setup and reproducibility test

The experimental setup outlined in Chapter 5 is utilized here to investigate the vibration attenuation capabilities of the HCDP and PEC concepts. To assess the effectiveness of the HCDP, the partially filled HCDP is mounted at various locations on the WTS test specimen, as discussed previously. This process necessitates the assembly and disassembly of each component of the test specimen after every series of experiments. This procedure is not only time-consuming but also introduces several uncertainties that can complicate the reproducibility of the experimental results.

Throughout the experiment, the stator ring remains stationary, while the stator arm is assembled or disassembled as required. However, to evaluate the efficiency of the PEC concept, both the stator ring and the stator arm are maintained in a fixed position throughout the study. This approach aligns with the methodology described in Chapter 5.

In a wind turbine generator, the excitation is generated by the stator ring and propagates through the arms of the structure. To accurately simulate real-world operating conditions, the outer surface of the WTS test specimen ring is selected as the excitation point. This choice allows for a more representative assessment of the excitation dynamics that occur in actual wind turbine systems. To quantify the effects of this excitation, the surface velocity of the arm is measured using the LSV, as detailed in Chapter 5. This method provides precise measurements of the vibration response, facilitating a thorough evaluation of the system's performance under conditions that closely resemble those encountered in practical applications.

As in previous chapters, before initiating the experiment to evaluate the damping performance of the HCDP and PEC concepts, it is critical to verify the reproducibility of the experimental results. Reproducibility tests were conducted on the reference WTS test specimen. By reassembling the stator arm of the reference specimen twice, while keeping the stator ring fixed, it was observed that the system response remained consistent across both instances, as shown in Figure 9.6. This confirms the robustness of the experimental setup used for the PEC concept.

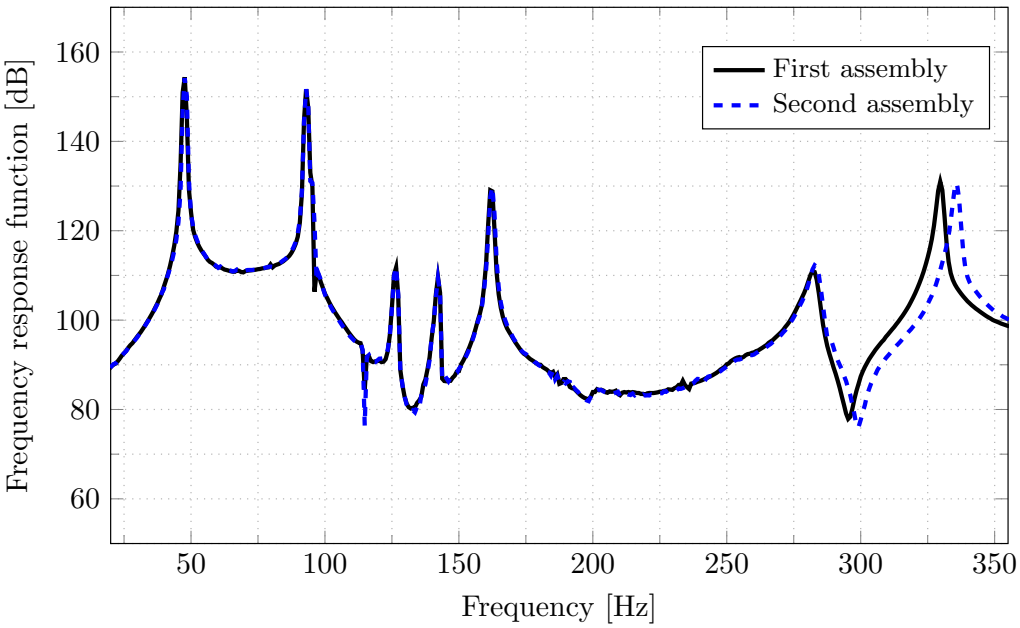

Figure 9.6: FRF of the WTS reference test specimen to validate the consistency and reliability of the experimental setup of PEC setup.

To verify the reproducibility and stability of the experimental setup for the HCDP concept, an empty

HCDP was mounted between the stator ring and stator arm. The assembly process involved four identical steel blocks, along with bolts, nuts, and washers to ensure consistent structural integrity. Results from this configuration confirmed the robustness of the setup in reproducing the system response, even after multiple reassemblies, with only a minor frequency shift observed around 350 Hz (see Figure 9.7). This slight shift at higher frequencies is considered negligible for the current study, as the primary focus in evaluating the particle damper's effect on vibration attenuation lies in the peak response values.

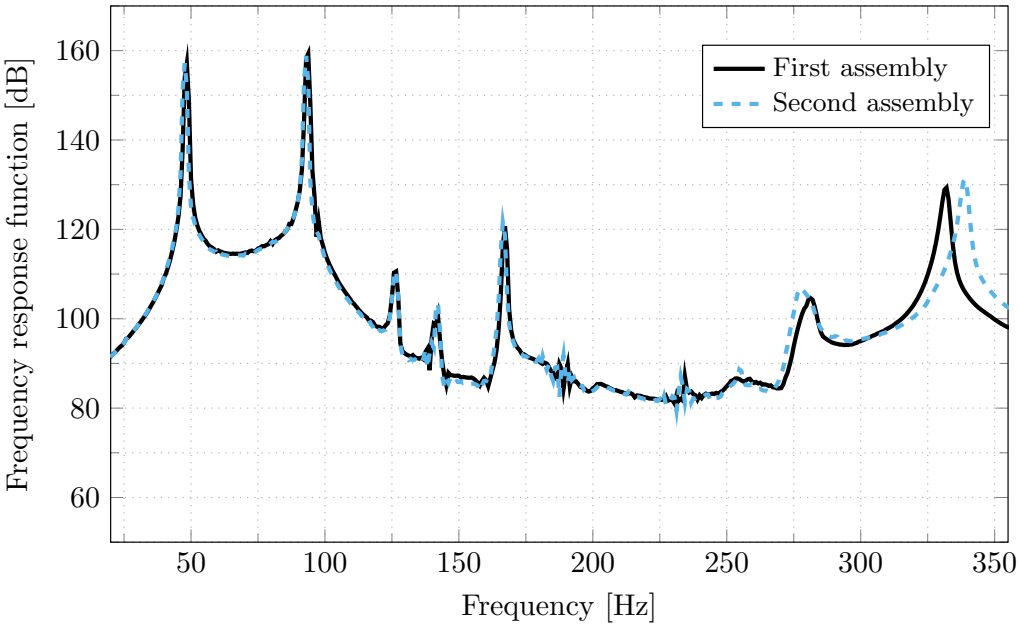

Figure 9.7: FRF of the WTS reference test specimen to validate the consistency and reliability of the experimental setup for HCDP cocnept.

9.8 Results and discussions for HCDPs concept

Figures 9.8- 9.10 present the FRF and corresponding vibration attenuation achieved by implementing the MU configuration on the outer wall of the generator ring, as depicted in Figure 9.4 (e). This MU configuration is formed by combining two SU HCDPs: one filled with sand and the other with stone powder, each with a filling ratio of 40%.

The reference test specimen displays resonance frequencies at approximately 47.7 Hz, 93.0 Hz, 126.6 Hz, 142.2 Hz, 162.5 Hz, 282.8 Hz, and 335.9 Hz (Figure 9.8). Additionally, a slight shift in the eigenfrequencies is observed when the WTS test specimen is equipped with the HCDP, though this variation is minimal. This frequency shift does not influence the current analysis, as the primary focus is on the peak values rather than frequency deviations to assess the particle damper's effect on vibration reduction. Similar to Chapter 5, only the prominent resonance peaks are considered, with gray patches in the FRF and amplitude reduction plots highlighting these key frequency ranges for enhanced visibility.

Furthermore, the one-third octave band plot clearly shows that installing the MU HCDP on the outer wall of the WTS ring resulted in reduced vibration amplitudes across the frequency range of 45 Hz to 355 Hz, see Figure 9.9 (blue dashed line).

The exact amount of vibration reduction due to the HCDP concept is illustrated in Figure 9.10. The amplitude reduction is determined by subtracting the level of the WTS test specimen with HCDP from

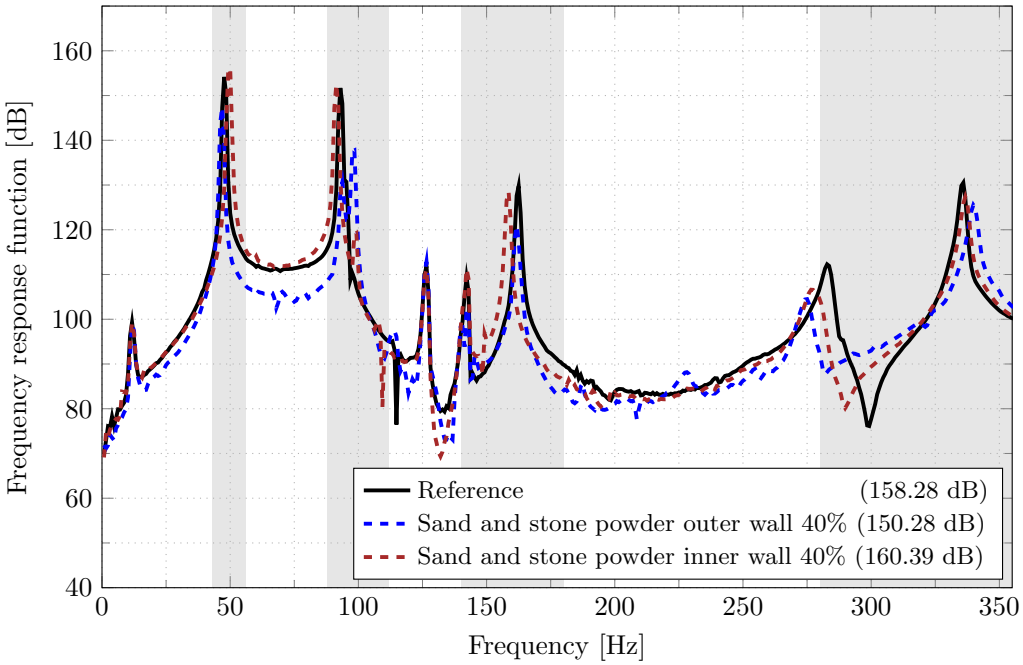

Figure 9.8: FRF of the WTS test specimen with the MU HCDP on the stator ring's outer wall. The SL value of surface velocity is given in dB, and the filling ratio is expressed as a percentage.

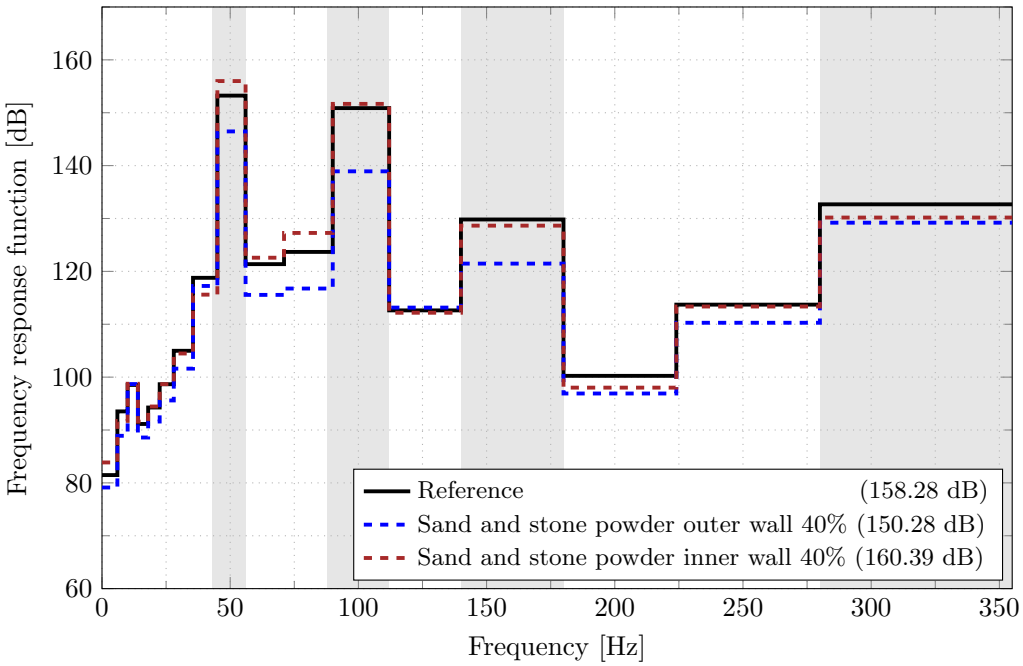

Figure 9.9: One-third octave band of the WTS test specimen with the MU HCDP on the stator ring. The SL value of surface velocity is given in dB, and the filling ratio is expressed as a percentage.

the reference WTS test specimen. In the amplitude reduction plot, a horizontal red line represents 0 dB. The area above the red line indicates an increase in vibration amplitude, while the area below the red line signifies a reduction in vibration amplitude. It has been observed that around the central frequency of 50 Hz, 100 Hz, 160 Hz, and 315 Hz the MU HCDP is capable of reducing the vibration amplitude up to 7 dB, 12 dB, 8 dB, and 3.5 dB (blue dotted line), see Figure 9.10. In contrast, when

the same MU HCDP configuration is attached to the inner wall of the WTS ring, it shows almost no efficiency in reducing the vibration amplitude. This phenomenon is also evident in the higher SL value (160.39 dB) observed in comparison to the SL value of the reference specimen (158.28 dB). These results highlight the critical importance of the HCDPs position on the WTS test specimen in reducing the vibration amplitude of a structure.

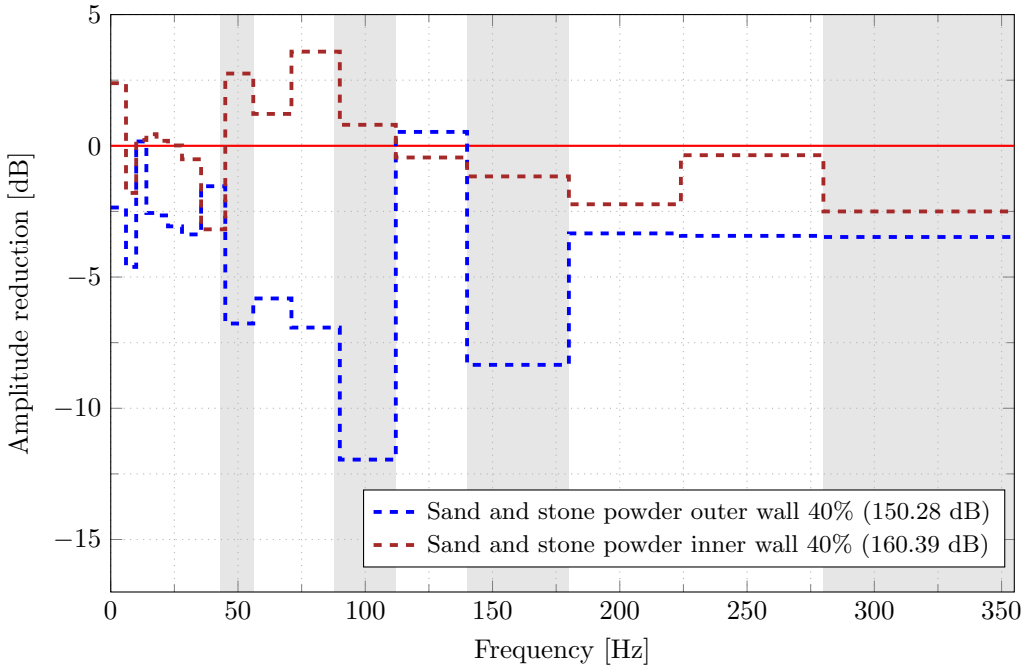

Figure 9.10: Amplitude reduction plot of the WTS test specimen with the MU HCDP on the stator ring. The SL value of surface velocity is given in dB, and the filling ratio is expressed as a percentage.

The vibration attenuation of the remaining configurations is briefly discussed in the Appendix A3, as their mitigation performance is significantly lower than that of the configuration presented above.

9.9 Results for PEC concept

The outcomes of the PEC concept are presented in Figures 9.11 - 9.12. The narrowband spectrum of the PEC is given in Figure A4.23. As anticipated, the results demonstrate that rubber granulate can substantially reduce the vibration amplitude of the WTS test specimen over the entire frequency range, as shown in Figure 9.11. The data further reveal that an increase in the mass of granular material correlates with enhanced vibration attenuation in the WTS test specimen, a trend also observed in Chapter 5. Specifically, around 50 Hz, filling with 250 g of rubber granulate reduces vibration amplitude by an additional 19% compared to 150g of granulate, as illustrated in Figure 9.12. At approximately 100 Hz, the difference in vibration attenuation between 150 g and 250 g of granulate increases by 51%. Similarly, near the third resonance frequency (around 160 Hz), vibration reduction improves by up to 31% with 250 g of rubber granulate compared to 150 g. However, within the 280 – 355 Hz frequency range, both material configurations exhibit comparable vibration attenuation capabilities. These findings highlight the PEC concept's strong potential to effectively reduce the vibration amplitude of the WTS test specimen.

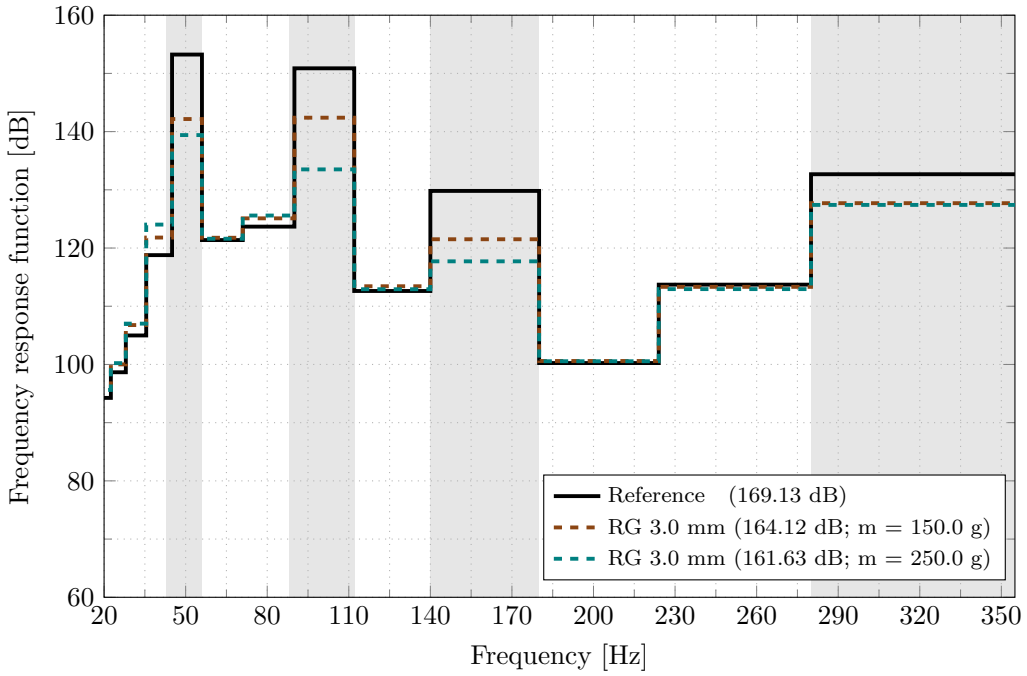

Figure 9.11: One-third octave band of the PEC concept. The SL values of surface velocity are given in dB, and the mass of the granular filling material is measured in g.

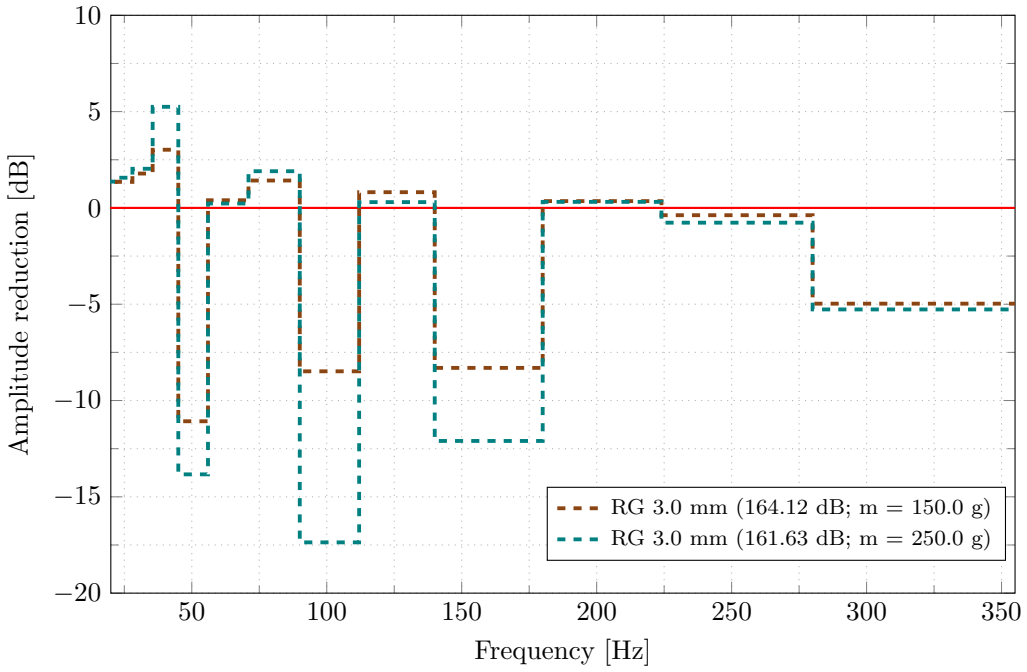

Figure 9.12: Amplitude reduction plot of the PEC concept. The SL values of surface velocity are given in dB, and the mass of the granular filling material is measured in g.

9.10 Comparison of HCDP and PEC concepts

As previously discussed, both the HCDP and PEC concepts have demonstrated significant potential in reducing the vibration amplitude of the WTS test specimen. It was additionally observed that the damping effectiveness of the HCDP concept varies depending on its placement on the specimen. To

enable a meaningful comparison, the most effective HCDP configuration, namely the MU HCDP setup mounted on the outer wall opposite the excitation point (as shown in Figure 9.4 (e)) was selected for analysis. Figures 9.13 - 9.14 illustrate a comparative analysis of both concepts.

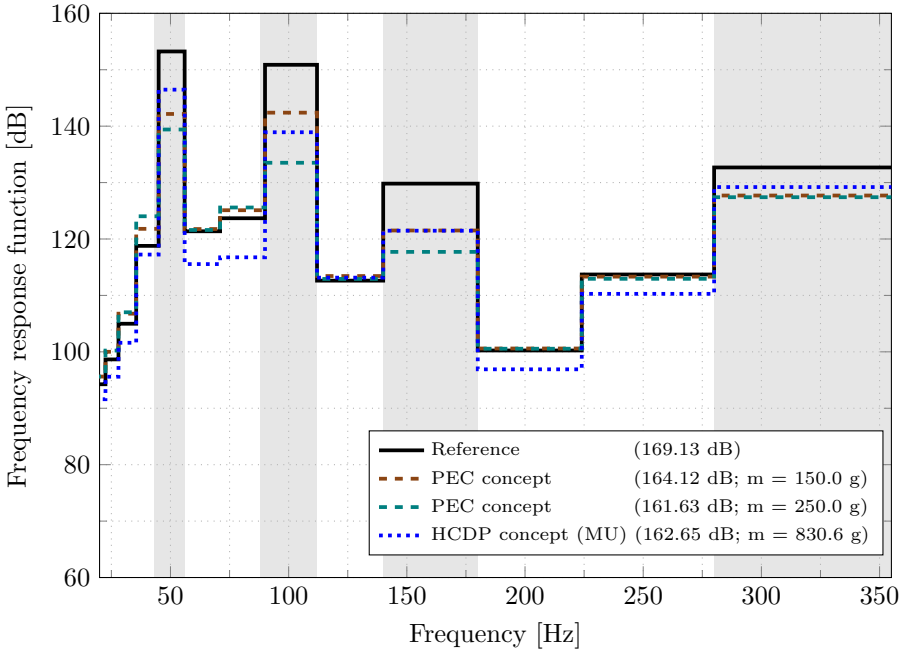

Figure 9.13: One-third octave band plot of vibration attenuation for HCDP and PEC concepts.

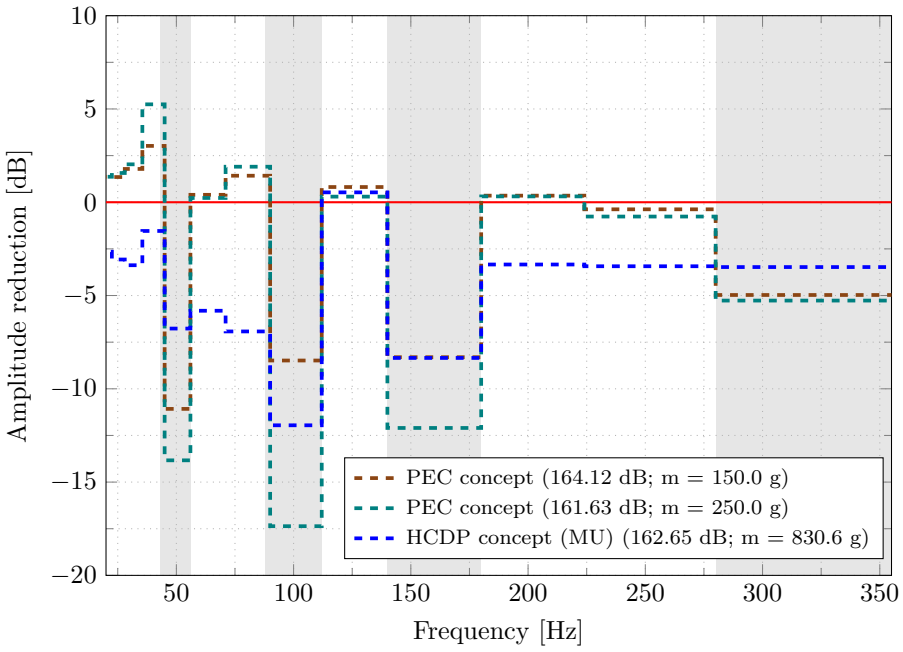

Figure 9.14: Amplitude reduction plot of vibration attenuation for HCDP and PEC concepts.

Experimental observations reveal that across the entire frequency range, the PEC configuration with 250 g of rubber granulate achieves substantial vibration amplitude reduction in the WTS test specimen compared to the best-performing HCDP configuration, as depicted in Figure 9.14. At the resonance frequency of 50 Hz, the most effective HCDP setup reduces the vibration amplitude by up to 6.7 dB. In contrast, at this same resonance frequency, the PEC configuration with 150 g of rubber granulate achieves a higher attenuation, reducing vibration by up to 11.1 dB. Around the second resonance

frequency, approximately 100 Hz, the HCDP outperforms the PEC configuration with 150 g of rubber granulate. In Chapter 5, it was also observed that stone powder outperforms "RG 3.0 mm" around 100 Hz, while sand exhibits a vibration attenuation performance similar to that of "RG 3.0 mm" at this resonance frequency. Combining both materials, therefore, results in superior performance compared to PEC. However, both the HCDP and PEC configurations with 150 g show similar damping performance near this frequency. Overall, these findings indicate that the PEC concept provides significantly enhanced damping performance compared to the HCDP concept. Additionally, the PEC concept demonstrates a substantial reduction in the additional mass required for effective particle damping.

9.11 Summary and conclusion

In this chapter, two concepts for reducing the vibration amplitude of a scaled wind turbine generator are introduced: the honeycomb damping plate (HCDP) concept and the pre-existing cavity (PEC) concept, both of which employ particle damping techniques. In the HCDP concept, the cells of the honeycomb structure are partially filled with granular materials, and the plates are strategically mounted at various locations on the WTS test specimen. Four mounting positions have been identified for optimal damping performance: between the stator arm and ring, on the outer and inner walls of the stator ring opposite the excitation point, and on the excitation side. Additionally, multiple HCDPs are installed simultaneously across these positions. Initial testing involves placing a single-unit (SU) HCDP at each location to identify the two most effective granular materials, which are then used to create a multi-unit (MU) HCDP configuration for enhanced damping.

The results of the experimental studies demonstrate a noteworthy reduction in vibration levels, achieving attenuation of up to 12 dB when a MU HCDP is installed on the outer wall of the wind turbine stator ring, specifically positioned directly opposite the excitation point. At this location, the SU HCDP filled with a combination of stone powder and sand was identified as the most effective configuration for mitigating vibrations, particularly at lower frequency ranges. Based on these findings, a MU HCDP was subsequently developed by integrating two HCDPs, which were filled to a ratio of 40%. This configuration aims to maximize the damping performance while utilizing the optimal granular materials identified in the preliminary experiments.

While the implementation of the HCDP concept has led to a notable reduction in vibration levels, the associated increase in mass raises concerns that warrant further consideration. The addition of the HCDP contributes an extra mass of approximately 10%, resulting from various components such as the granular material, the material used for the HCDPs, the fastening and joining systems, as well as the thin aluminum sheets and steel blocks employed in the assembly. This increase in mass not only impacts the overall dynamics of the WTS test specimen but also introduces potential challenges in the manufacturing and production processes. Furthermore, the integration of the HCDP necessitates comprehensive strength analyses to ensure structural integrity, as well as a detailed examination of the bonding and joining processes utilized for the HCDPs. These factors highlight the need for careful consideration and optimization in the design and implementation of the HCDP to balance the benefits of vibration attenuation against the implications of added mass and manufacturing complexity.

To address the concerns associated with increased mass and manufacturing complexity inherent in the HCDP concept, the PEC concept has been developed as an alternative approach. This innovative concept capitalizes on the existing cavities present within the primary structure to effectively contain granular materials. A notable application of this approach is the utilization of the hollow structure of the stator arms in an annular generator, which can be employed to house the granular materials necessary for vibration mitigation.

The implementation of the PEC concept results in a modest increase in the overall mass of the test specimen, ranging from 1% to 2.5%. This increase is significantly lower than the approximately 10%

additional mass associated with the HCDP concept. Moreover, the damping efficiency achieved through the PEC concept is markedly superior compared to that of the HCDP concept, offering enhanced performance in vibration attenuation.

Another advantage of the PEC concept is its negligible impact on the stiffness of the primary vibrating structure, ensuring that the dynamic characteristics of the system remain largely unaltered. Furthermore, the design of the PEC concept facilitates easier assembly and maintenance, contributing to its practicality in application. These attributes make the PEC concept a promising alternative for improving vibration control in wind turbine generators while minimizing the associated drawbacks of mass increase and structural complexity.

Chapter 11 will provide a comprehensive discussion on the application of these concepts in evaluating the efficiency of particle dampers within an industrial-scale wind turbine generator subsystem. This chapter will delve into the methodologies employed for testing, including the specific configurations of the HCDP and PEC concepts, and how they are integrated into the subsystem.

10 Lab-scale particle damper development for wind turbine blades

This chapter provides a comprehensive examination of various strategies developed for the application of the particle damping technique at the laboratory scale. These strategies are specifically intended to reduce the vibration amplitude of wind turbine blades. By examining the fundamental principles and methodologies behind these laboratory-scale strategies, the chapter aims to evaluate their effectiveness and feasibility for scaling up to industrial applications. The analysis includes a thorough investigation of the underlying concepts and how they can be adapted and optimized for use in large-scale wind turbine blades.

This chapter starts with a concise overview of the state-of-the-art passive damping techniques employed in wind turbine blades to minimize vibration amplitude. It then provides an introduction to the design of wind turbine blades before delving into a comprehensive discussion on the design strategies that have been developed and tested at the laboratory scale. The chapter presents the results of these strategies in terms of their effectiveness in reducing vibration amplitude, followed by an evaluation of their advantages and disadvantages. The findings presented in previous publication [197] form the basis of the current chapter.

10.1 Vibration control of wind turbine blade

Vibrations originating in a wind turbine's generator can propagate to the other components of the system. One possible scenario is that these vibrations may be transmitted to the wind turbine blades, resulting in sound emissions into the surrounding environment. The continuous vibration experienced by a wind turbine blade can also have a direct influence on its fatigue lifespan, leading to a significant decrease in the operational efficiency of the wind turbine. A particle damper design concept has previously been introduced to address vibration reduction within the generator subsystem. However, if this approach does not fully attenuate the vibrations, an additional damping solution may be required to counteract any residual oscillations that reach other components, including the blades.

In general, active vibration control, like blade pitch control [235, 236], shape change airfoil [237], and plasma actuators [238], has been widely used for reducing the vibration amplitude of the wind turbine blade [239]. However, implementation complexity, maintenance cost, and reliability issues of the active vibration control have motivated researchers to explore the passive damping technique to reduce the vibration response of the wind turbine blade.

Therefore, various passive damping methods have been developed to effectively reduce vibrations in blades. Robinson et al. [240] have proposed a viscoelastic damping material to reduce the vibration amplitude of a wind turbine blade. Zhang et al. [241] introduced a roller damper as a means to suppress the vibration response of wind turbine blades. A theoretical study was also carried out to demonstrate the effectiveness of a tuned liquid column damper to reduce the vibration amplitude in rotating wind turbine blades [242]. The findings indicate that as the rotor rotational speed decreases, the effectiveness of the tuned liquid column damper decreases as well. Basu et al. [243] presented a theoretical model for the application of a circular liquid column damper to attenuate vibrations in wind turbine blades. Meng et al. [244] have conducted numerical simulations to demonstrate the efficiency of a porous damping structure to mitigate the vibration of a wind turbine blade. The authors

adopted the structural characteristics of bamboo's vascular bundles as a basis for designing a porous damping structure, incorporating various pore diameters and densities. Sievers and Mullings have used viscoelastic material to dampen the wind turbine blade vibration [245].

Although the passive damping techniques discussed above have shown promising results, their application in wind turbine blades faces significant challenges. One primary limitation is the added mass these techniques introduce, a critical factor for turbine blade performance. Additionally, scaling these techniques poses difficulties, as they often require large installation space. Moreover, these methods have largely been studied in theoretical or laboratory settings and have yet to be implemented on an industrial scale. Addressing these issues, this chapter presents three alternative design strategies for integrating particle dampers to efficiently reduce vibration amplitude in wind turbine blades.

Previous studies, such as that by Sandanshiv et al. [164] (refer to Chapter 2), have successfully applied particle dampers to reduce blade vibration. However, as discussed in Chapters 2 and 8, the authors utilized steel particles in the particle damper design, which raises concerns about increased mass and lightning susceptibility. Research by Garolera et al. [246] has shown that wind turbines are expected to experience numerous lightning strikes over their operational lifespan, making the use of steel particles less practical. Consequently, the particle damper strategies proposed in this thesis specifically avoid steel or other metallic materials in their design, prioritizing safety and functionality in lightning-prone environments while still achieving effective vibration damping.

The insights gained from previous chapters regarding material selection, optimal filling ratios, and the effective mobilization of granular materials within a cavity provide a fundamental basis for designing particle dampers for industrial-scale wind turbine blades. These parameters play a crucial role in ensuring the feasibility and efficiency of the damping mechanism. However, before particle dampers are implemented in industrial-scale wind turbine blades, comprehensive studies of various design variants at the laboratory scale must be conducted. This preliminary step is critical as it enables the thorough evaluation of different design approaches, ensuring that the most effective and efficient solution is selected prior to scaling up. Tests and trials at the lab scale allow for the identification of the advantages and limitations of each design variant, ultimately refining the final design to be applied to industrial-scale blades. This process not only minimizes the need for significant modifications during industrial-scale implementation but also ensures that maximum vibration attenuation is achieved by the particle dampers. Hence, this chapter introduces three distinct design strategies for particle dampers, specifically tailored to mitigate vibration amplitudes in wind turbine blades.

10.2 Wind turbine blade design

The design of the wind turbine blade is crucial as it directly affects the extraction of energy, making it one of the critical elements in the entire wind turbine system. Structurally designing a blade involves several key stages, including the selection of suitable materials [247] and the evaluation of turbine loads [248]. However, this section will not explore the detailed design processes involved in the blade's development. Instead, it offers a concise overview of the blade's structural design and fundamental components. The purpose of this overview is to provide readers with a foundational understanding of the basic elements that make up the blade structure, ensuring clarity when interpreting the particle damper strategies discussed in the subsequent sections. Figure 10.1 presents a schematic representation of the various components that make up a wind turbine blade.

Wind turbine blades are predominantly manufactured using composite materials, with glass-fiber-reinforced plastic (GFRP) and carbon-fiber-reinforced plastic (CFRP) being the most commonly utilized. These materials consist of polymeric matrices reinforced with either glass or carbon fibers, which provide the necessary mechanical properties for structural integrity, durability, and fatigue resistance. In addition to the fiber-reinforced polymer composites, the blades often incorporate sandwich core materials such as polyvinyl chloride (PVC) foam or balsa wood, which contribute to enhanced stiffness and impact

resistance while maintaining a low overall weight. Furthermore, bonded joints are extensively employed in the assembly of blade components to ensure structural cohesion, while protective polyurethane coatings are applied to shield the surface from environmental degradation, including erosion, and moisture exposure. Additionally, wind turbine blades are equipped with integrated lightning protection systems, such as embedded conductors, to mitigate the risks associated with lightning strikes and ensure operational safety over their service life [249].

Structurally, wind turbine blades are designed with a hollow configuration, where the outer aerodynamic profile is formed by two primary shells. This hollow architecture is strategically employed for several critical reasons. First, it significantly reduces the overall weight of the blade, which is essential for improving the efficiency of the wind turbine and minimizing mechanical loads on the rotor and supporting structure. Second, the hollow design enhances the structural strength and stiffness of the blade while optimizing the distribution of aerodynamic and inertial forces during operation. Third, it plays a crucial role in achieving aerodynamic efficiency by maintaining an optimal airfoil shape while allowing for internal reinforcements that improve load-bearing capacity. Finally, from a manufacturing and cost perspective, the hollow configuration facilitates the integration of internal structural elements while ensuring economic viability in large-scale production. The two shells forming the outer blade surface are securely bonded together, and the internal structure is further reinforced using one or more structural webs. These structural webs serve to efficiently transfer and distribute shear forces between the shells, thereby enhancing the overall stability and mechanical performance of the blade [250].

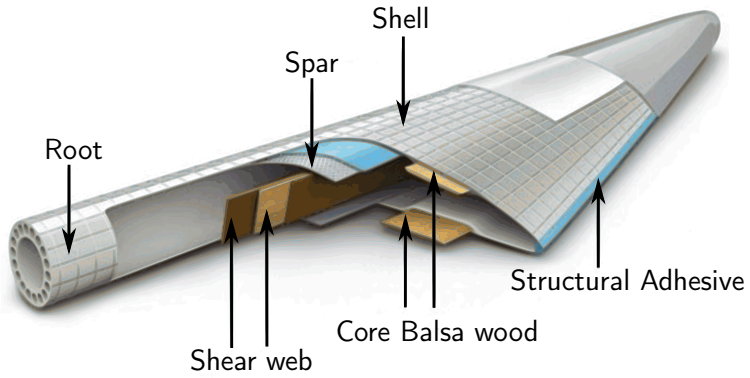

Figure 10.1: Schematic illustration of the components of a wind turbine blade [251].

In a wind turbine blade, the blade root plays a fundamental role as the primary structural interface between the circular hub and the initial aerofoil section of the blade. This region is subjected to significant mechanical loads, making its design crucial for the overall performance and longevity of the turbine blade. To accommodate the substantial load-bearing requirements, the blade root is typically designed with thicker aerofoil profiles, which enhance its ability to withstand the high bending moments and aerodynamic forces that arise during operation [252].

Furthermore, the structural integrity of the blade is reinforced by the spar cap or spar laminate, which are integral components specifically engineered to manage the complex loading conditions, including bending moments and shear forces, encountered throughout the blade's operational lifespan. These structural reinforcements are strategically incorporated to ensure that the blade remains both durable and lightweight, optimizing its performance while mitigating the risks of material fatigue and structural failure [253].

10.3 Implementation of particle dampers

This section presents several strategies for incorporating particle dampers into wind turbine blades to reduce vibration amplitude. Each concept is explored in detail, highlighting the underlying principles. Additionally, the section outlines the design of the test specimens utilized for experimental investigations and provides insights into the specific granular material chosen for the particle damper construction.

10.3.1 Sandwich core replacement

The concept of sandwich core replacement involves substituting the original sandwich core of the wind turbine blade, such as balsa wood, with a honeycomb-like structure. It is important to highlight that the cells within this honeycomb structure are partially filled with granular materials.

In order to experimentally assess the effectiveness of the proposed sandwich core replacement concept, a set of 12 test specimens was fabricated in a laboratory environment. Each test specimen consists of two thin sheets that encapsulate a lightweight core, as illustrated in Figure 10.2. The manufacturing process involves adhesive bonding, which securely attaches the two thin sheets to either side of the lightweight core. To evaluate the impact of core profile on damping performance, the test specimens were designed using two distinct core configurations, namely: honeycomb and tubus, see Figure 10.3.

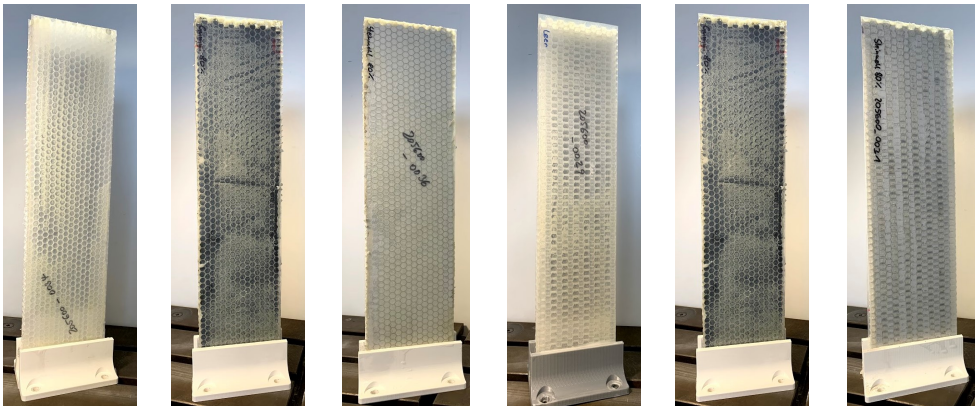

(a) (b) (c) (d) (e) (f)

Figure 10.2: Partially filled blade test specimen featuring a polypropylene sandwich core and layers: (a) Empty tubus core, (b) tubus core filled with rubber granulate "RG 2.3 mm" (80%), (c) tubus core filled with stone powder (80%), (d) honeycomb sandwich core empty, (e) honeycomb core filled with rubber granulate "RG 2.3 mm" (80%), (f) stone powder (80%) filled honeycomb core.

The external dimensions of the rotor blade test specimen were established at 500 mm $\times$ 120 mm $\times$ 25 mm. To ensure representative behavior and minimize the influence of individual cells, the width was set to include at least ten adjacent honeycomb or tubular cells. These dimensions were selected to facilitate laboratory handling while allowing the specimen to contain a substantial quantity of granular material.

While the length and width of all test specimens remain consistent, the diameter of the tubus core is slightly smaller than that of the honeycomb cell diameter, which is dictated by manufacturing constraints. Additionally, slight variations in the height of the honeycomb core and the tubus core are evident, reflecting their respective market availability. Despite these differences, it is important to note that the wall thickness of both core profiles is uniform, ensuring that the comparison between their damping performance remains valid.

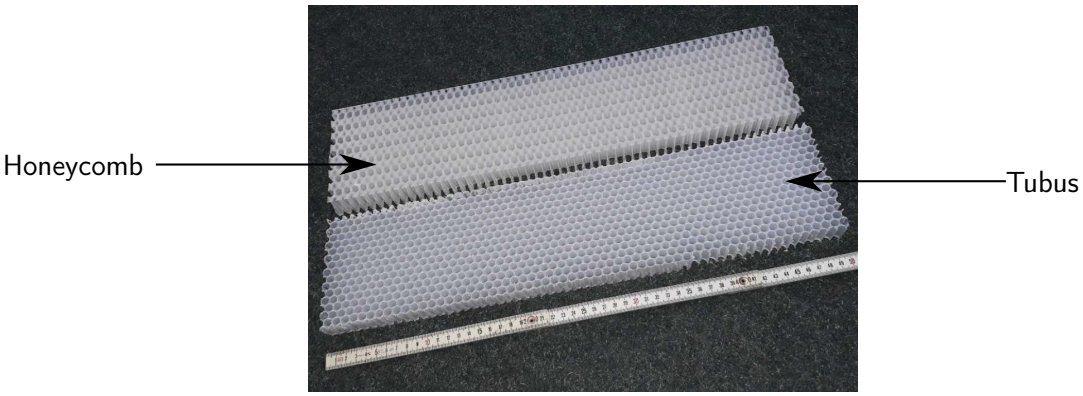

Figure 10.3: Honeycomb and tubus core profiles used in the design of the blade test specimen.

The sandwich core replacement variant focuses on investigating test specimens made from polypropylene (PP). The selection of this material for the test specimens is grounded in their lightweight properties, which are essential considerations in the design of wind turbine blades. Both PP and PC exhibit excellent resistance to corrosion and moisture, contributing to the longevity and durability of the blade structure. Furthermore, these materials possess superior damping characteristics compared to metals, which effectively minimizes sound emissions and vibrations within the structure. Importantly, it is necessary to ensure that wind turbine blades are constructed exclusively from non-metallic materials to comply with lightning safety standards. Therefore, the choice of PP and PC is deemed optimal for this application, as they align with the requirements for both performance and safety in wind turbine design.

In light of these findings, test specimens with a honeycomb core profile were partially filled with both rubber powder and stone powder. Following the positive results from the honeycomb core specimens, a similar approach was applied to the test specimens featuring the tubus core profile, which were also partially filled with rubber powder and stone powder.

It is essential to emphasize that, although Chapter 5 has already presented extensive experimental investigations on the vibration attenuation capabilities of various granular materials, two different granular materials are re-examined in this study. While rubber granulate "RG 4.6 mm" exhibited outstanding vibration attenuation performance, its application as a filling material in this specific context is impractical due to the dimensional constraints imposed by the tubus and honeycomb core profiles. Therefore, rubber powder is selected as a viable alternative, ensuring compatibility with the structural limitations. Additionally, stone powder is incorporated for comparative analysis.

As discussed in Chapter 9, this cahpter also aims to assess whether the vibration mitigation behavior of these materials remains consistent across different test specimen designs. Prior studies by Cempel et al. [168] has demonstrated that the packing configuration of granular materials significantly influences the performance of particle dampers. Furthermore, Ito et al. [114] investigated the effect of vessel shape on vibration attenuation. However, their study was entirely numerical, lacking experimental validation. Given these considerations, it is crucial to examine whether the materials analyzed in this thesis maintain a consistent vibration mitigation trend, regardless of the test specimen design.

The preceding chapters have shown that the filling ratio plays a crucial role in determining the damping performance of particle dampers. Based on this, two filling ratios, specifically 40% and 80%, were selected for experimental investigation in the wind turbine blade test specimen to evaluate their impact on vibration attenuation. While previous chapters have established that an 80% filling ratio is effective in reducing vibration amplitudes, this chapter further explores both filling ratios to determine whether

the effectiveness of the 80% filling ratio is consistent across different test specimen designs or if it is dependent on the specific design of the test specimen.

Additionally, it is essential to note that, irrespective of the specific implementation strategies employed, each test specimen is bonded to the 3D-printed structure using epoxy resin. This bonding process ensures a secure and stable connection between the test specimen and the 3D-printed support. The integration of test specimens into this 3D-printed structure not only provides a robust connection but also significantly streamlines the mounting process on the measurement table, thereby facilitating consistent positioning and reliable experimental setups.

10.3.2 Sandwich core modification

The design of the test specimen for the sandwich core modification strategy is illustrated in Figure 10.4. This method eliminates the need to replace the wind turbine blade's sandwich core with a honeycomb-like structure. Instead, the approach involves modifying the existing sandwich core to incorporate granular materials within its framework. To create a lightweight particle damping solution without substituting the original sandwich core, a reference prototype is used, consisting of a balsa wood sandwich core layered with GFRP.

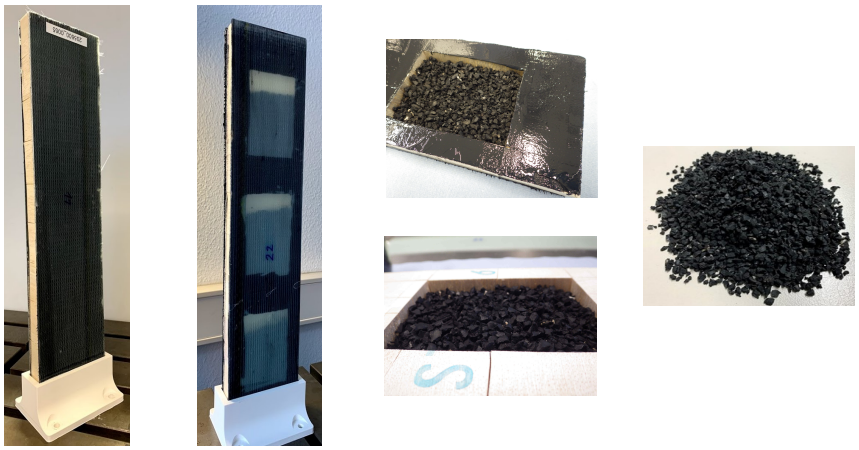

(a) (b) (c) (d)

Figure 10.4: Test specimen with balsa wood core and GFRP outer layers: (a) Balsa wood sandwich core (reference specimen), (b) balsa wood sandwich core filled with rubber granulate "RG 4.6 mm", (c) partially filled cavity, (d) rubber granulate "RG 4.6 mm" .

The GFRP layers are incorporated to simulate real-world conditions typical of rotor blade structures, where GFRP and balsa wood are bonded using epoxy or polyester resin. To accommodate the granular materials, three uniform rectangular cavities are designed within the balsa wood core (see Figure 10.4 (b)). These cavities are dimensioned to hold rubber granulate "RG 4.6 mm", known for its effectiveness in reducing vibration amplitudes, as discussed in Chapter 5. This cavity design ensures sufficient space for the granulate, allowing the modified sandwich core to effectively mitigate structural vibrations while maintaining the lightweight properties essential for wind turbine applications.

10.3.3 External cavity attachment

Balsa wood, utilized in the sandwich core modification approach for implementing particle dampers, is a common material in wind turbine blade design due to its excellent stiffness-to-weight ratio. However, the process of creating cavities in the balsa wood core to house granular damping materials may alter

this stiffness-to-mass ratio, potentially compromising the structural integrity of the wind turbine blade. Such modifications could lead to a weakened blade structure, affecting its durability and performance under operational loads.

To mitigate these challenges, a third design variant has been introduced, which takes advantage of the available empty space within the blade structure. This design is referred to as the "external cavity concept" because it utilizes the available empty space within the blade structure as an external cavity, as illustrated in Section 10.2. By utilizing this unoccupied space, the design aims to integrate particle damping technology without impacting the core's stiffness and mass balance, thereby maintaining the overall performance and reliability of the wind turbine blade.

The core principle of the external cavity attachment strategy involves integrating a partially filled cavity into the blade structure. This cavity is strategically placed in an area where the eigenmode exhibits significantly higher displacement, optimizing its effectiveness. Importantly, this approach does not necessitate modifications to the existing blade structure, as the available empty space within the blade can be utilized for the installation of the external cavity. As a result, this strategy is applicable to blades that are already in operation. The implementation of this method presents a cost-effective solution for incorporating particle damping techniques into wind turbine blades, simplifying the processes of manufacturing, assembly, and maintenance.

To illustrate the effectiveness of this concept, the reference test specimen utilized in the sandwich core modification strategy has been employed. In order to implement this approach at the laboratory scale, a system of reclosable plastic bags is utilized. These bags serve to enclose the granular materials, which are affixed to the test specimen at the location of maximum surface velocity, as shown in Figure 10.5.

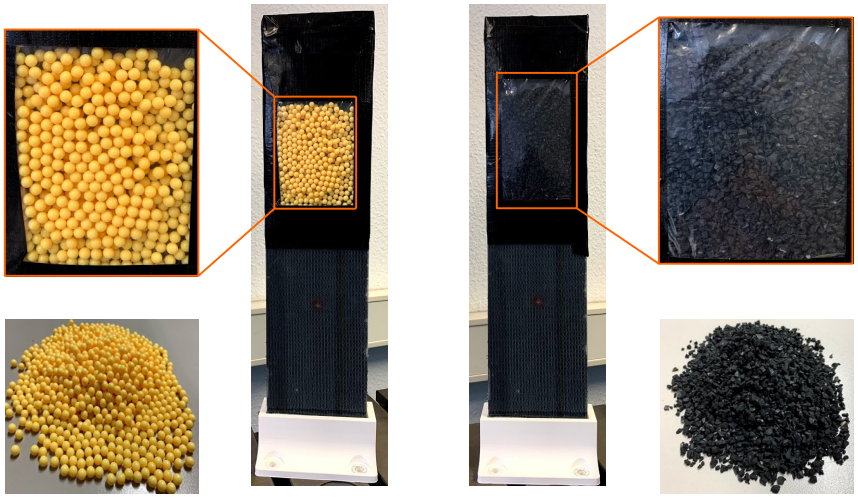

Figure 10.5: Test specimen with GFRP layers for external cavity attachment strategy.

Within each bag, the granular materials are distributed uniformly to ensure consistent damping performance. Furthermore, the plastic bags are secured to the test specimen in such a way that allows the granular materials sufficient space to move freely. This design consideration is crucial, as it helps to prevent the formation of large clumps that could arise from gravitational forces acting on the individual particles. By ensuring that the granular materials remain mobile, the experimental setup effectively simulates the conditions under which particle damping can enhance vibration attenuation in wind turbine blades.

To evaluate the effectiveness of the proposed approach, two distinct types of granular materials have been selected: rubber granulate "RG 4.6 mm" and plastic balls. The rationale for selecting the rubber

granulate "RG 4.6 mm" is detailed in Chapter 5. Additionally, plastic balls have been incorporated into the particle damper to illustrate that vibration attenuation is not solely governed by particle mass but is also influenced by the underlying damping mechanisms of the particle damper.

Table 10.1 provides a detailed overview of the filling materials utilized across all three methods, including their corresponding filling ratios and masses.

Table 10.1: Filling material along with their filling ratio and filling material mass for the test specimens.

Specimen	Filling material	Filling ratio [%]	Material mass [g]
PP honeycomb	Empty		
	RP 0.8 mm	80%	297.6
	Stone powder	80%	733.2
	RP 0.8 mm	40%	178.6
	Stone powder	80%	407.8
PP tubus	Empty		
	RP 0.8 mm	80%	344.8
	Stone powder	80%	875.5
	RP 0.8 mm	40%	211.4
	Stone powder	40%	446.5
Balsa wood with GFRP layers	RG 4.6 mm	80%	249.0
	RG 4.6 mm		97.9 and 57.0
	Plastic balls		97.9 and 57.0

10.4 Experimental setup

The experimental setup used to evaluate the effectiveness of the three strategies is shown in Figure 10.6. Consistent with the approach used in previous chapters, system response measurements were obtained using the Polytec LSV (model PSV-400). To secure the test specimen onto the measuring table, four identical bolts and sliding blocks were utilized, establishing a clamped boundary condition that closely mimics those found in real-world wind turbine blade applications. A torque wrench was used to apply a uniform torque of 2 Nm to each bolt, ensuring consistent preload across all bolts in each experimental configuration. This arrangement was carefully chosen to enhance reproducibility and maintain the reliability of the results.

The experimental setup for investigating the vibration attenuation effects of all the strategies mentioned is closely aligned with the setup described in Chapter 5. However, given the use of a different test specimen in this case, a detailed description of the experimental arrangement is provided here. The setup will be explained in a manner that minimizes redundancy with the previous chapter, though some overlap with Chapter 5 may be necessary for completeness. This approach ensures clarity and allows for a comprehensive understanding of the current experimental configuration.

To measure the surface velocity of the test specimen, the scan head of the laser scanning vibrometer is placed horizontally with respect to the test specimen. It should be emphasized that only the out-of-plane surface velocity has been measured. To excite the test specimen with a Dirac impulse, a TIRA electrodynamic shaker with an impact hammer head is used. Additionally, a PCB force sensor (Model 208C02) is installed between the hammer head and the shaker to accurately measure the applied load during the excitation of the structure. Throughout the experiment, the shaker is mounted on an aluminum frame to prevent unintended secondary vibration paths from occurring between the shaker and the structure. Moreover, maintaining the fixed position of the shaker is advantageous as it ensures a consistent excitation point for each test specimen. Furthermore, it is worth noting that the force sensor utilizes a Bruel Kjær amplifier of Type 2693, while the shaker is powered by a TIRA power amplifier of Type 50009.

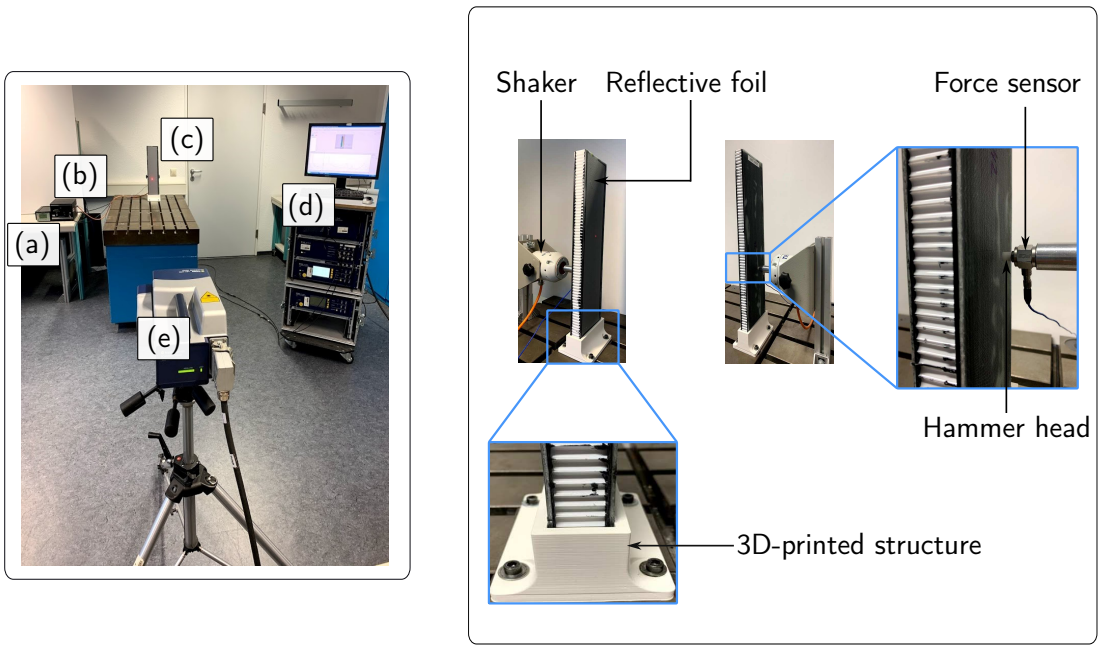

Figure 10.6: Experimental setup of the wind turbine blade test specimen for surface velocity measurement by using the LSV: (a) Force sensor amplifier, (b) shaker power amplifier, (c) test specimen, (d) control and post-processing unit, (e) scan head.

Besides this, it is necessary to maintain a sufficient distance between the hammer head and the test specimen to avoid double stroke, while also ensuring proximity to effectively excite the structure within the desired frequency range. Therefore, following an iterative process, the tip of the impulse hammer is maintained at a distance of 2 mm from the specimen. Moreover, to enhance the quality of the reflected laser light, an adhesive reflective foil is affixed to the measuring area of the specimen. The measuring area is divided into a rectangular grid of fine squares, comprising a total of 135 measuring points. The selection of this grid size is based on considerations of measurement accuracy and time efficiency. The number of measuring points is kept the same for each specimen and for each experimental setup.

To minimize measurement errors, the FRF is calculated by taking the average of the entire measured area. Furthermore, a parameter study is conducted on the reference test specimen to establish the parameters for data acquisition. To enhance the signal-to-noise ratio, six complex averages are performed per measuring point. A low-pass filter with a cut-off frequency of 1000 Hz is employed to restrict the bandwidth. The frequency spectra are computed using a sampling frequency of 12.8 kHz and a frequency resolution of 781.25 mHz.

10.5 Results

For all the strategies, the experiments are first carried out for the reference test specimen, i.e. test specimen without particle damper. Following that, the FRF of the reference test specimen is compared to the FRF of a test specimen that includes a particle damper, aiming to analyze the degree of vibration attenuation.

10.5.1 Sandwich core replacement

The experimental results for the sandwich core replacement strategy are presented in Figures 10.7 - 10.8. It was observed that all test specimens, regardless of core profile, exhibit two resonance frequencies below 250 Hz. In the current chapter, low-frequency vibration amplitudes are of particular interest,

as the primary vibration challenges in wind turbine blades occur in these frequency ranges, where conventional passive damping techniques generally prove insufficient.

The experimental investigation indicates that regardless of the shape and size of the core profile, partially filled test specimens have the ability to effectively reduce vibration amplitude. Besides this, a slight shift in the resonance frequency of the partially filled test specimen has been observed. This shift is a result of the added mass of the granular materials. Nevertheless, the observed frequency shift will not affect the outcomes of the current study, as the primary objective is to examine the impact of particle dampers on vibration attenuation solely in relation to peak values.

In the case of the PP honeycomb test specimen, it has been observed that rubber powder and stone powder can effectively reduce the vibration amplitude across the entire frequency range of interest, see Figure 10.7. Moreover, around the first resonance frequency of approximately 35 Hz, the rubber powder and stone powder has the capability to reduce the vibration amplitude of the test specimen by up to 10.5 dB and 6.6 dB, respectively. However, around the second resonance frequency, stone powder damping performance is significantly higher in comparison to rubber powder, see Figure 10.7. At this frequency, stone powder can effectively attenuate vibrations by up to 17.9 dB, while rubber powder only manages to reduce the vibration amplitude by up to 5.4 dB. This finding closely aligns with the results presented in Chapter 5, where it was observed that above 100 Hz, stone powder exhibited superior effectiveness in reducing vibration amplitude, whereas below 100 Hz, rubber powder demonstrated the highest attenuation performance. Therefore, it can be inferred that the vibration mitigation trend observed for these materials in this study remains consistent regardless of the test specimen design.

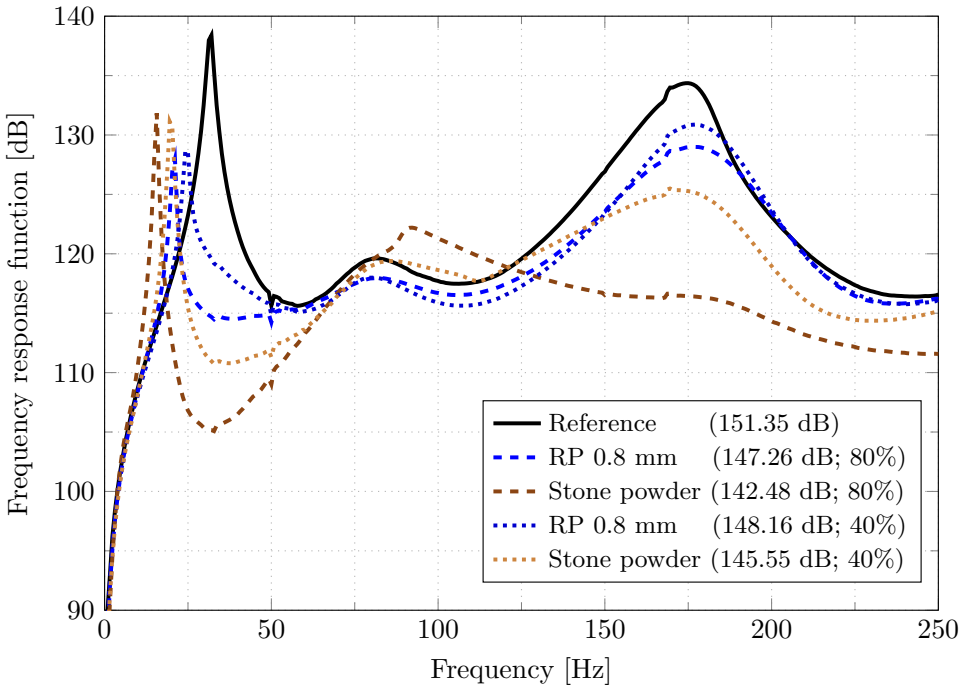

Figure 10.7: FRF of the PP honeycomb core test specimen with different filling ratios (80% and 40%). The SL values of surface velocity are presented in dB.

This effect may be attributed to the behavior of rubber powder near the second resonance frequency, where it likely enters the collect-and-collide phase. However, verifying this hypothesis would require high-speed camera experiments to capture the dynamic behavior of the particles. Additionally, the significantly higher quantity of stone powder particles compared to rubber powder particles increases both particle-particle and particle-wall collisions, thereby enhancing the vibration attenuation capability. In Chapter 5, it was observed that stone particles are less effective in the 20 - 50 Hz range, as these

frequencies are insufficient to overcome the inertia of the stone powder particles. Consequently, the stone powder's effectiveness is limited around the first resonance frequency.

The preceding chapters have demonstrated the significant impact of filling ratios on the performance of a particle damper. Therefore, the influence of the filling ratios on the vibration attenuation capability of the honeycomb-like structure has been also investigated. For this purpose, two different filling ratios are compared, namely: 80% and 40%. The experimental investigation of filling ratios has shown that the damping performance of 80% filling ratio is significantly higher in comparison to the 40% filling ratio. The reason for this can be the increased number of granular materials particles. Throughout this study, it has been consistently observed that, regardless of the test specimen design, a filling ratio of 80% is the most effective for vibration attenuation compared to other ratios. This suggests that the filling ratio is independent of the specific test specimen configuration. However, it is crucial to ensure that sufficient clearance is maintained within the cavity to allow for adequate particle movement, which is essential for effective damping performance.

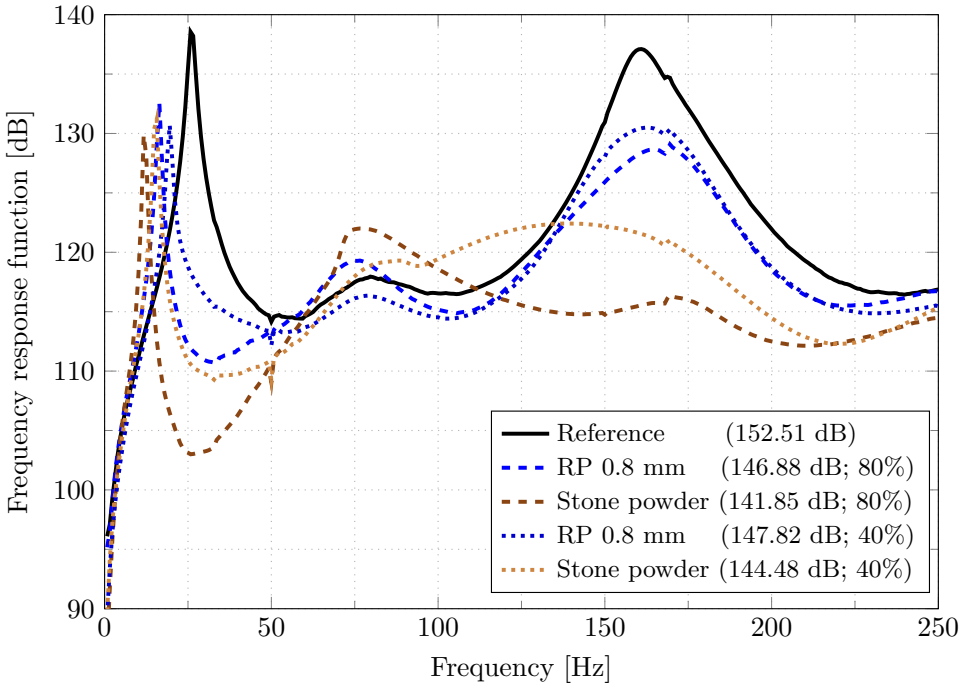

Figure 10.8: FRF of the PP tubus core test specimen with different filling ratios (80% and 40%). The SL values of surface velocity are presented in dB.

Another noteworthy observation derived from Figure 10.7 is that the influence of the filling ratio on test specimens containing stone powder is more evident in comparison to those filled with rubber powder. One possible explanation for this could be the smaller size of the stone powder particles. The stone powder particles are approximately 98% smaller than the rubber powder particles. Hence, the test specimen with a similar filling ratio contains more stone powder particles than rubber powder particles. As a result, the damping is increased. All the observations discussed above can also be verified by the SL values of surface velocity.

Based on the above discussion, it is evident that rubber powder exhibits greater effectiveness around the first resonance frequency and also demonstrates considerable vibration reduction capabilities around the second resonance frequency.

Similar to the PP honeycomb test specimen, the PP tubus specimen also exhibits two resonance frequencies below 250 Hz, see Figure 10.8. The first resonance frequency is approximately 26 Hz, while the second resonance frequency is around 160 Hz. In contrast to the PP honeycomb specimen, the

stone powder demonstrates a slightly more effective damping behavior, leading to an 8.7 dB reduction in the vibration amplitude of the PP tubus test specimen around the first resonance peak. The damping behavior of the stone powder is also enhanced around the second resonance frequency when compared to its vibration attenuation performance in the case of the PP honeycomb test specimen. The reason for this is the greater mass of the stone powder present in the PP tubus core profile test specimen. It should be noted that the test specimen consisting of the PP tubus core contains 19.4% more stone powder than the PP honeycomb core.

The influence of filling ratios on the system response of the PP tubus test specimen demonstrates a similar effect as seen in the PP honeycomb core test specimen. However, a direct comparison between the PP honeycomb core specimen and the PP tubus core specimen is not possible due to a slight difference in their core height, which significantly impacts the bending stiffness. Nevertheless, a conclusion can be drawn that regardless of the core profile, the stone powder is highly effective in reducing the vibration amplitude of the test specimen around the second resonance peak. Yet, in the first resonance frequency range, rubber powder proves to be more effective than stone powder in attenuating vibrations. Thus, it can be reaffirmed that the vibration attenuation characteristics of the materials remain consistent regardless of the test specimen design. Furthermore, it has been observed that the influence of the packing ratio on vibration attenuation remains consistent regardless of the core profile, and the filling ratio of 80% exhibits greater effectiveness in reducing vibrations compared to the filling ratio 40%. Hence, for further investigation, the filling ratio of 80% is selected as the preferred option.

10.5.2 Sandwich core modification

The results obtained from the sandwich core replacement strategy indicate a significant effectiveness in attenuating vibration amplitudes across the PP test specimens featuring both honeycomb and tubus core profiles. However, the proposition of substituting the original sandwich core of wind turbine blades with a partially filled honeycomb-like structure necessitates a thorough strength analysis to ensure structural integrity. Additionally, a comprehensive investigation into the bonding and joining processes involved in this modification is essential.

Moreover, the introduction of granular materials adds considerable mass, which presents a substantial challenge for practical implementation within industrial wind turbine blades. This added weight must be carefully considered in the overall design, as it could adversely affect the performance and efficiency of the turbine. Consequently, the application of this initial concept on an industrial scale faces significant barriers related to economic viability, production capabilities, manufacturing processes, and maintenance requirements. Therefore, while the results are promising in a laboratory setting, translating this approach into a viable solution for industrial wind turbine blades is not feasible[1].

To address these issues, an alternative approach has been experimentally investigated. In this approach, the original sandwich core of the wind turbine is used to enclose the granular materials, rather than replacing it entirely. Generally, balsa wood is one of the most favored core materials for wind turbine blades. Generally, the sandwich structure of a wind turbine consists of a core material that is thick and lightweight in nature and this core material is connected with laminate layers, which are thin and stiff. Thus, the concept behind the second approach is to utilize the balsa wood core to encapsulate the granular material. As mentioned above, the reference test specimen for this concept is the test specimen without granular materials, i.e. balsa wood test specimen without cavity with GFRP layers. Figure 10.9 illustrate the efficiency of the sandwich core modification strategy.

The results of the Sandwich core modification strategy show a remarkable reduction in the vibration

[1] Replacing the original sandwich core with a honeycomb-like structured core proved to be a highly time-consuming and financially challenging process. Additionally, the industrial partner faced significant difficulties in manufacturing a wind turbine blade based on this concept. Consequently, this approach could not be evaluated at the industrial scale.

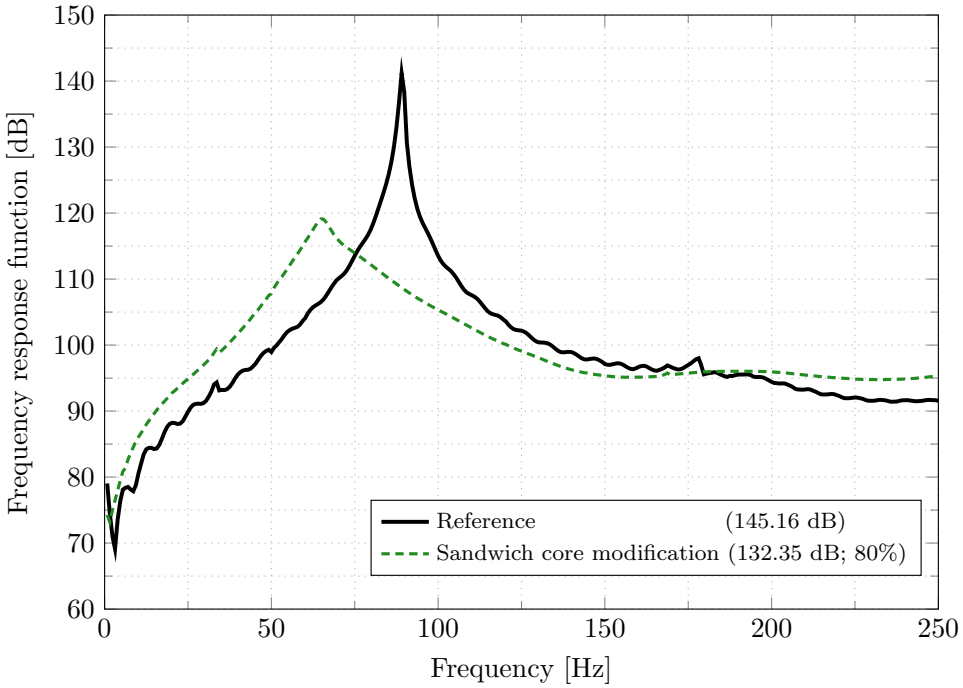

Figure 10.9: FRF for sandwich core modification startegy, showing the SL values of surface velocity in dB and filling ratios (%).

amplitude of the test specimen. It has been observed that the partially filled balsa wood test specimen can achieve a vibration attenuation up to 22.1 dB (green dash line), see Figure 10.9. A frequency shift has been observed in this concept, potentially resulting from the cavity introduced within the test specimen. Moreover, in this approach, the total mass of the reference test specimen is increased by 8.6%, which is significantly less in comparison to the sandwich core replacement approach. As mentioned previously, the balsa wood as a core material of a wind turbine blade serves the vital function of providing stability of the laminate structure against buckling and deformation. However, introducing a cavity in the balsa wood core can alter its vibration behavior and stiffness, which can make the load-bearing laminates of the wind turbine blade weaker. In order to address these concerns and further minimize the additional mass of the granular materials, a third strategy is being considered.

10.5.3 External cavity attachment

In external cavity attachment approach, a reclosable bag made of plastic is partially filled with granular material and is positioned at the location on the test specimen where the vibration amplitude is larger. For this approach also the balsa wood test specimen attached with GFRP layers is considered as the reference test specimen. The frequency spectrum for this strategy is plotted in Figure 10.10.

As demonstrated consistently in this thesis, it is once again evident that irrespective of granular materials a significant vibration attenuation has been observed. In particular, the results obtained from the external cavity attachment strategy demonstrate a remarkable vibration attenuation, reaching up to 16.9 dB. Notably, this reduction is achieved with an additional mass increase of only 5.5%, a fraction of the mass increment associated with the first and second strategies. This outcome underscores the effectiveness of the external cavity approach in achieving substantial vibration damping while minimizing mass addition, positioning it as a highly efficient alternative among the explored strategies.

To confirm that the primary contributor to vibration reduction is the damping effect of rubber granulate rather than merely the added mass, an experiment was conducted in which a plastic bag filled with

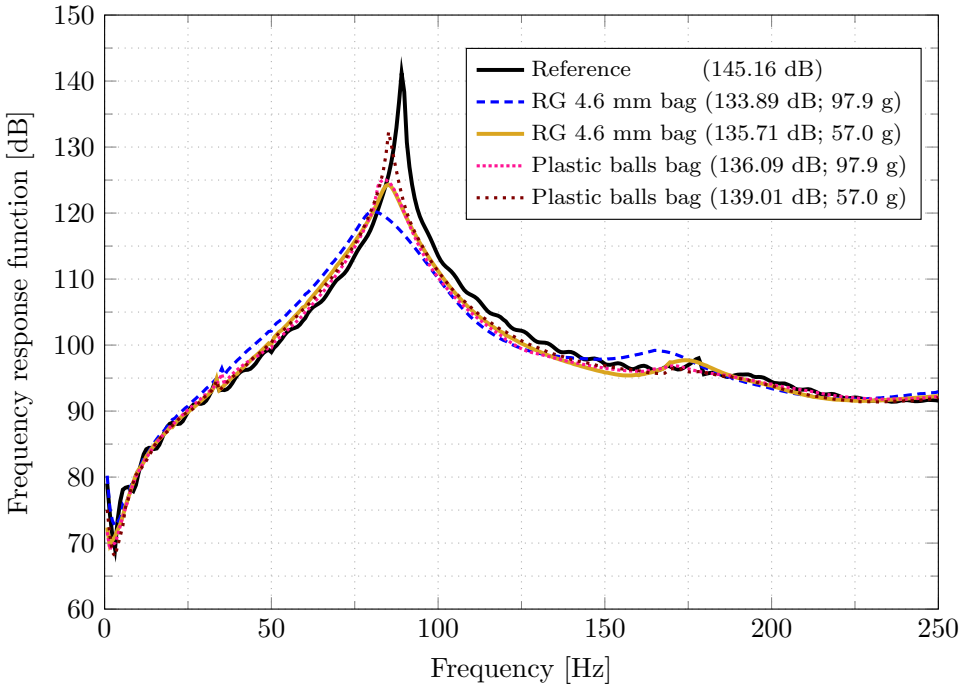

Figure 10.10: FRF for external cavity attachment startegy, showing the SL values of surface velocity in dB and filling ratios (%).

57 g of plastic balls was attached at the same location. The results reveal that, despite having a comparable mass, the rubber granulate achieved an additional 8 dB reduction in vibration amplitude compared to the plastic balls, underscoring the superior damping properties of the rubber material. Furthermore, to replicate the total mass of the setup where 97.9 g of rubber granulate "RG 4.6 mm" was embedded within three rectangular cavities in the balsa wood core, a plastic bag containing an equivalent 97.9 g of "RG 4.6 mm" rubber granulate was attached at the same location on the test specimen. This configuration enabled a direct comparison, reinforcing the effectiveness of the external rubber granulate placement in maximizing vibration attenuation.

The resulting vibration attenuation effect from both configurations, one with the rubber granulate "RG 4.6 mm" partially filled inside the balsa wood cavity (see Figure 10.9) and the other with a partially filled plastic bag containing the same rubber granulate "RG 4.6 mm" attached to the balsa wood test specimen, is very similar, see Figure 10.10. This similarity may arise because the rubber particles confined within the cavity at the base of the test blade are not fully engaging in the particle damping mechanism. In the first bending mode of the blade specimen, the largest displacement occurs near the blade tip, where particle damping would be more effective. Therefore, it can be concluded that, rather than creating an internal cavity within the balsa wood, it is more effective to attach an external cavity at the location with higher frequency response, maximizing the damping potential. This approach proves advantageous in preserving the stiffness-mass ratio of the sandwich core.

To facilitate comparison, a plastic bag containing 97.9 g of plastic balls is also attached at the same location. As anticipated, the rubber granulate proves to be more effective in reducing the vibration amplitude of the test specimen in comparison to plastic balls. Hence, it can be concluded that the external cavity attachment approach is beneficial in reducing the additional mass of the granular material significantly without compromising the stiffness or fatigue strength of the sandwich core or wind turbine blade. Additionally, this strategy offers the advantage of simplifying the manufacturing, production, assembly, and maintenance process, which will lead to a cost-effective solution for implementing the particle damping technique to a wind turbine blade.

10.6 Summary and conclusion

The primary objective of this chapter was to explore and evaluate multiple design variants based on the parameters studied in previous chapters before implementing one of the most effective concepts in an industrial-scale wind turbine blade. Conducting these investigations at the laboratory scale is crucial to minimize the need for extensive modifications when transitioning to industrial applications and to ensure maximum vibration attenuation efficiency.

In this chapter three different strategies to implement particle damper techniques to reduce the vibration amplitude of a wind turbine has been presented. The primary approach involves substituting the wind turbine blades original sandwich core with a partially filled honeycomb-like-structure. In this approach, two different sandwich cores are being studied, namely: honeycomb core profile and tubus core profile. The investigation focused on how the vibration response of the test specimens are affected by granular material, packing ratio, and particle size. The results from the first approach, i.e. from the sandwich core replacement strategy, indicate a significant reduction in the vibration amplitude of the test specimen, regardless of the type of granular materials used. However, soft particles like rubber powder are more effective for vibration attenuation in comparison to the stone powder in low-frequency range. Additionally, the vibration response of the test specimen with a filling ratio of 80% is significantly lower than the filling ratio of 40%. Similar results have been observed throughout this study, indicating that the effectiveness of the filling ratio is independent of the test specimen design.

Despite the promising damping performance of the sandwich core replacement strategy, its implementation in industrial-scale wind turbine blades is challenging due to factors such as increased mass, complex manufacturing and production processes, extensive strength analysis requirements, and time-consuming maintenance. Furthermore, the industrial partner faced significant difficulties in manufacturing wind turbine blades for this concept, making large-scale implementation impractical.

To address these challenges, the second approach, the sandwich core modification strategy, was explored. This method retained the original sandwich core while incorporating cavities within it to enclose granular materials. The experimental results of this strategy shows a vibration attenuation of 22.1 dB, which is significantly higher than the sandwich core replacement strategy. Furthermore, in comparison to the first strategy, the second approach results in a mere 8.6% increase in the mass of the primary structure, which is significantly lower than the mass increase observed in the primary approach. Nevertheless, milling cavities in the balsa wood sandwich core can alter the stiffness and vibration characteristics of the primary structure, potentially leading to reduced strength in the load-bearing laminates of the wind turbine blade.

To mitigate this issue, the external cavity attachment approach was introduced. In this method, an existing cavity within the hollow wind turbine blade is utilized to contain granular materials without altering the original laminate structure. To evaluate this concept, a reclosable bag system containing 97.9 g of rubber granulate "RG 4.6 mm" and plastic balls is affixed to the balsa wood sandwich core test specimen, positioned at the location with the highest vibration amplitude. This configuration achieved a damping efficiency, with a vibration reduction of 21.1 dB, comparable to that obtained through the sandwich core modification strategy. However, the damping performance of plastic balls is notably inferior to that of rubber granulate, underscoring that the observed vibration reduction is primarily due to the material's inherent damping properties rather than the effect of additional mass alone.

Overall, these findings provide strong evidence that both the vibration mitigation trend of granular materials and the optimal filling ratio are independent of the test specimen design. This consistency across different experimental setups suggests that these parameters can be reliably applied in larger-scale implementations without significant deviations in performance. The external cavity attachment approach, in particular, presents a promising alternative by effectively reducing added mass while maintaining high damping efficiency and preserving the structural integrity of the wind turbine blade.

By refining and optimizing this strategy, its applicability can be further expanded not only in wind turbine blades but also in other engineering applications where efficient vibration suppression is critical. The ability to integrate damping materials without altering the primary structural composition enhances the feasibility of this approach for industrial adoption, paving the way for broader implementation in various engineering disciplines. It is worth mentioning that the effect of centrifugal force on these concepts is outside the scope of this thesis, as testing the mentioned design variants in industrial rotating blades is not considered.

11 Evaluating particle dampers in industrial-scale wind turbine components

This chapter addresses the transition of particle damper technology from controlled laboratory conditions to the demanding environment of industrial applications. Building upon the successful demonstration of particle damper effectiveness in reducing vibration amplitude under laboratory settings (as detailed in previous chapters), this chapter presents a methodology for evaluating particle damper designs on a representative industrial scale, utilizing commercial wind turbine components. However, due to data confidentiality, some details about this transition phase will be excluded.

11.1 Introduction

Vibrations in wind turbines arise from the relative motion between their mechanical components and the dynamic forces that occur within these elements. A key contributor to these vibrations is the generator, which also serves as a significant source of sound emissions. Inside the generator, vibrations are primarily induced by electromagnetic interactions between the rotating rotor poles and the stator. These vibrations propagate through the turbine's structure, reaching components such as the blades, where they contribute to the emission of noise into the surrounding environment. Thus, this chapter transitions from laboratory studies to real-world applications, investigating the implementation of particle dampers for effective vibration mitigation in industrial-scale wind turbine generators and blades.

It is important to emphasize that the overarching objective of applying the particle damper concept, as explored in this thesis, to an industrial-scale generator was governed by certain key conditions. Firstly, the structural integrity of the existing generator should remain intact, meaning no significant modifications to its original design would be permissible. Secondly, the particle damper had to be implemented solely within the available space inside the existing generator, without the need for additional external modifications or expansions. These constraints were fundamental in shaping the approach to the practical application of the particle damper in an industrial setting. Consequently, the design parameters studied in this thesis were combined in such a manner that the additional mass from the granular material would not exceed 2% of the total mass of the stator.

11.2 Wind turbine generator

To assess the effectiveness of particle dampers in mitigating vibrations within the generator subsystem, the WTS component was specifically chosen for testing. The selection of this particular component is strategic, as applying a particle damper to this section of the generator offers several advantages. Notably, the influence of centrifugal forces can be disregarded, which significantly simplifies the design process. By eliminating the need to account for these forces, the number of design parameters is reduced, allowing for a more straightforward and efficient optimization of the particle damper. Furthermore, the stator contains numerous free surfaces that can be utilized for mounting particle dampers.

In the initial stage of designing a particle damper for industrial-scale WTS, the selection of an appropriate material is crucial. Chapter 5 presented an extensive study evaluating the vibration

attenuation capabilities of various granular materials. This investigation examined the effects of key factors such as particle size, particle size distribution, filling ratios, and humidity on the efficiency of vibration mitigation within the structure. The analysis identified rubber granulate "RG 4.6 mm" as the most effective material, surpassing the performance of all other tested materials. Additionally, long-term durability tests conducted over several months confirmed that the particle damper utilizing rubber granulate "RG 4.6 mm" can maintain its vibration attenuation performance over an extended period, as detailed in Chapter 7. This material meets the lifespan requirements of typical wind turbine components without significant degradation. Thus, rubber granulate "RG 4.6 mm" was selected as the material for the particle damper designed for commercial WTS.

After selecting the optimal material for the particle damper, the next critical consideration is how to effectively mobilize the granular material within the damper, particularly in cases where the vibration of the WTS may be insufficient to activate the damper's mechanism. To address this challenge, the concepts of TWC and TWC-AS were incorporated into the particle damper, as extensively discussed in Chapter 6. This chapter demonstrates that design variants such as TWC and TWC-AS are effective in reducing the vibration amplitude of the structure, thereby enhancing the damper's performance.

However, directly integrating TWC and TWC-AS variants into industrial-scale stator arms and rings is not feasible due to the increased testing time[1]. Consequently, the concept was proposed to integrate these design variants externally onto the stator. To evaluate this approach, HCDP concepts were tested on a scaled WTS test specimen to determine whether external attachment of the HCDP would reduce the vibration amplitude. The results, as discussed in Chapter 9, demonstrate that the design variants effectively mitigate the vibrations.

Therefore, TWC-AS is integrated into the HCDP, and the TWC and TWC-AS concepts are directly implemented at a specific location on the stator, namely where the stator arm connects with the stator ring. Nonetheless, it was observed that the wall thickness of the TWC and TWC-AS significantly influences the performance of the particle damper. To optimize the wall thickness for these designs, an additional experiment was conducted, similar to the study presented in Chapter 6. In this case, however, all dimensions of the test specimen were scaled down to half of those used in Chapter 6, including the scaling of the TWC dimensions and wall thickness. For example, in Chapter 6, the performance of TWCs with three different wall thicknesses, namely: 0.5 mm, 1.0 mm, and 2.0 mm was investigated. In this scaled experiment, the wall thicknesses of the TWC were reduced to 0.25 mm, 0.5 mm, and 1.0 mm, respectively. The experimental setup remained identical to the one described in Chapter 6, ensuring consistency in testing conditions. Additionally, the amount of rubber granulate inside the damper cavity was scaled down proportionally to maintain accuracy in the comparative analysis.

The results of this investigation, which offer insights into the effect of scaled wall thicknesses on the performance of the particle damper, are detailed in the Appendix (see Appendix A5). The findings reveal that the damping performance of the TWC with a wall thickness of 0.5 mm is particularly effective in reducing the vibration amplitude of the structure compared to other thicknesses tested. A similar trend was observed in Chapter 6, where the TWC with a wall thickness of 1.0 mm was highly efficient in attenuating vibrations in a structure with a wall thickness of 10.0 mm. Correspondingly, in the scaled experiment, the TWC with a 0.5 mm wall thickness effectively reduced the vibration amplitude of a structure with a wall thickness of 5.0 mm.

Building upon these observations, it is hypothesized that a TWC with a wall thickness of 2.0 mm would be well-suited for effectively mitigating vibrations in a structure with a wall thickness of 20.0 mm. Consequently, this assumption has served as a guiding principle in determining the appropriate wall thicknesses for both the TWC and TWC-AS designs in industrial-scale testing.

[1]The time allocated for industrial setup testing to evaluate potential particle damper configurations developed in the lab was limited. As a result, it was not feasible to integrate TWC and TWC-AS directly into the stator arm at various positions.

It is crucial to highlight that, although this study was conducted using scaled testing, further investigations involving additional parameter studies on scaled test specimens are necessary to comprehensively validate the scalability of the findings and to confirm the accuracy of the underlying assumptions. Scaling effects, material properties, and structural dynamics may introduce complexities that require deeper analysis to ensure the results can be reliably extrapolated to full-scale applications. Despite these limitations, the present study offers valuable preliminary insights into the selection of an appropriate wall thickness for a full-scale WTS particle damper.

All the aforementioned parameters were integrated and applied to the WTS, as shown in Figure 11.1. The red-marked box in the figure highlights the externally mounted particle dampers, which feature a combination of the HCDP and TWC-AS design variants. These dampers were carefully positioned at various locations on the stator, with placement decisions made based on the available space for external attachment. In addition, rubber granulate was introduced into the existing cavities of the stator, complementing the TWC and TWC-AS designs[2].

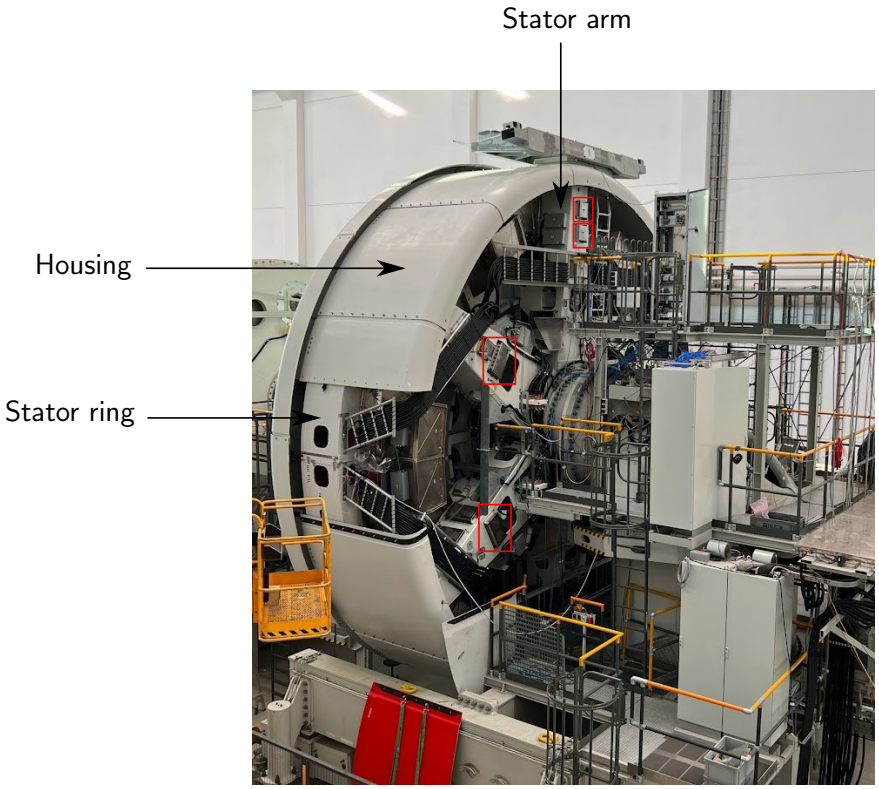

Figure 11.1: Particle dampers mounted on the industrial-scale wind turbine stator, used to investigate the efficiency of particle damping.

Table 11.1 presents the various particle damper configurations that have been investigated, detailing their positions on the WTS and corresponding filling ratios. The stator arm was divided into two primary sections for this study: the portion above the midpoint is referred to as the "stator arm above," while the section below the midpoint is termed the "stator arm below." A total of ten different particle damper configurations were tested, along with two reference measurements of the WTS operating without any particle dampers. This comprehensive testing setup allowed for a thorough evaluation of the damping performance across multiple configurations.

[2]It is important to note that due to confidentiality agreements with the industrial partner, specific details regarding the design and positioning of these particle dampers cannot be disclosed

Table 11.1: Configurations and filling ratios of particle dampers on a commercial WTS.

Position	Stator arm below	Stator arm above	Stator head	Stator ring
Configuration 1	0	0	0	0
Configuration 2	80	0	0	0
Configuration 3	80	80	0	0
Configuration 4	80	80	20	0
Configuration 5	80	80	40	0
Configuration 6	80	80	80	0
Configuration 7	80	80	80	80
Configuration 8	0	80	80	80
Configuration 9	0	0	80	80
Configuration 10	0	0	0	80
Configuration 11	0	0	0	0

11.2.1 Results

The full-scale tests conducted on the generator demonstrated promising results following the implementation of the particle damper concept. Although the system response of the WTS was measured at multiple locations, the results presented here will focus on two specific positions. First, data will be shown from a position where the acceleration sensor is directly attached to the particle damper. Second, results from a position where the acceleration sensor is placed at a certain distance from the damper will be discussed. This comparison illustrates that vibration attenuation is not limited to the immediate location of the particle damper but also leads to a reduction in vibration amplitude at other positions along the structure. Additionally, it is important to note that the results are presented in the time domain due to confidentiality restrictions imposed by the industrial partner.

Furthermore, it should be noted that this discussion will not cover the results for all tested configurations. Instead, only the configurations that demonstrated the best and worst performance are presented here. This approach provides insight into the significant role that particle damper performance plays in industrial-scale testing, with particular emphasis on the effects of the positioning and filling ratio of granular materials. By focusing on the most and least effective configurations, this chapter aims to illustrate how these factors influence the damper's overall efficacy in vibration reduction.

The findings for Configuration 6, which pertain to the two distinct sensor locations, are illustrated in Figures 11.2 and 11.3. The data indicate a significant reduction in vibration amplitude of the WTS due to the implementation of the particle damper. Notably, for the sensor positioned directly at the particle damper housing, the observed reduction in vibration amplitude is particularly pronounced, underscoring the damper's localized impact on vibration mitigation. Conversely, at the sensor located some distance from the particle damper, there is still a measurable reduction in vibration amplitude, albeit to a lesser extent than observed at the damper-adjacent sensor. This discrepancy in vibration reduction across sensor positions suggests that a detailed transfer path analysis is warranted. Such an analysis could elucidate the transmission pathways through which vibrations propagate from the ring to the stator arm, providing insights into whether vibrational energy in one stator arm may influence the vibrational behavior of adjacent arms. This understanding is crucial for optimizing particle damper placement and enhancing overall vibration reduction in the WTS.

Another possible reason for the reduced vibration damping could be that not all particle damper boxes are mounted in regions of the structure where the mode shapes exhibit higher displacement amplitudes. To verify whether the particle dampers are indeed positioned in areas corresponding to greater displacement, a detailed numerical model analysis of the WTS is required. This analysis would help determine the optimal placement of the dampers by correlating their positions with regions of higher vibrational displacement, ensuring maximum damping efficiency.

Observations indicate that not all configurations proved effective in reducing the vibration amplitude

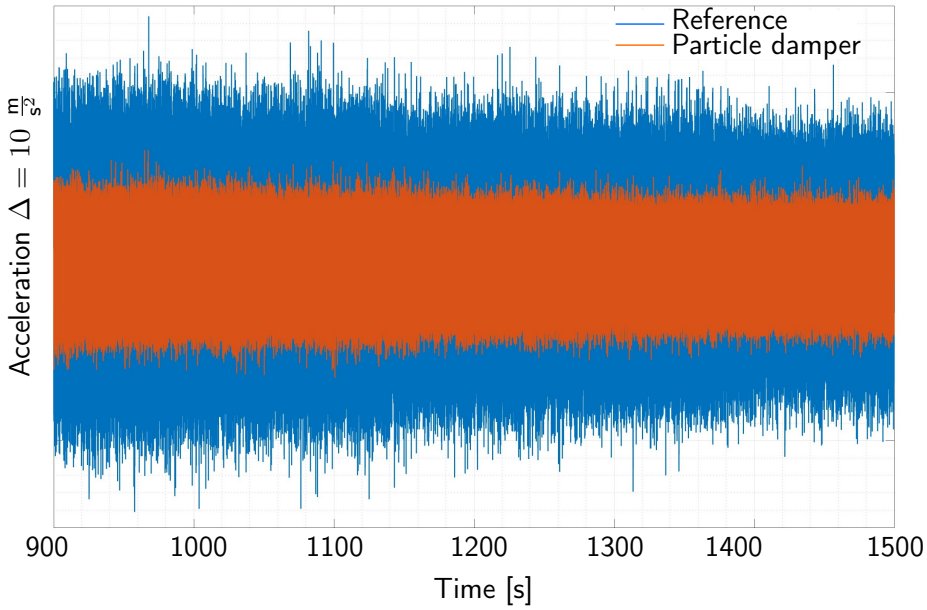

Figure 11.2: Time versus acceleration plot for the sensor located on a particle damper box on the WTS stator arm in Configuration 6.

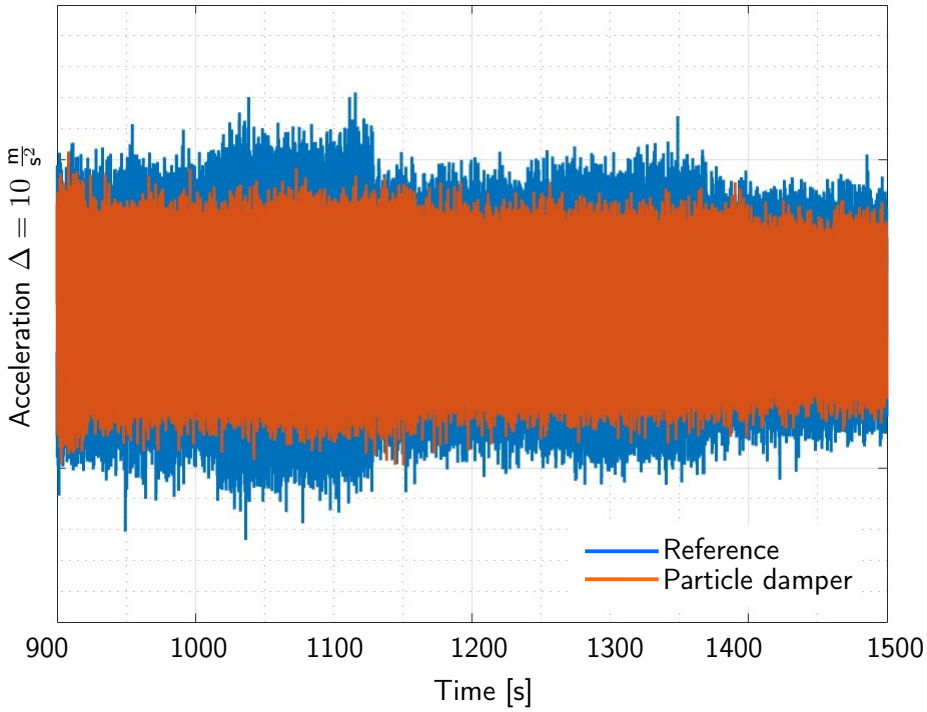

Figure 11.3: Time versus acceleration plot for the sensor located adjacent to a particle damper box on the WTS stator arm in Configuration 6.

of the generator. Specifically, when the particle damper (80% filling ratio) is only attached to the stator ring, the particle damper had a minimal effect on vibration mitigation, as demonstrated in Figures 11.4 and 11.5. This finding highlights the critical importance of optimizing the configuration of the particle damper, as some configurations demonstrate significantly greater effectiveness in reducing vibrations than others. The observed variations in damping performance across different configurations indicate that multiple factors, including the precise placement of the particle damper, play a crucial role in determining its overall efficiency. Improper placement or suboptimal design choices may lead to diminished damping performance, limiting the system's ability to effectively attenuate vibrations.

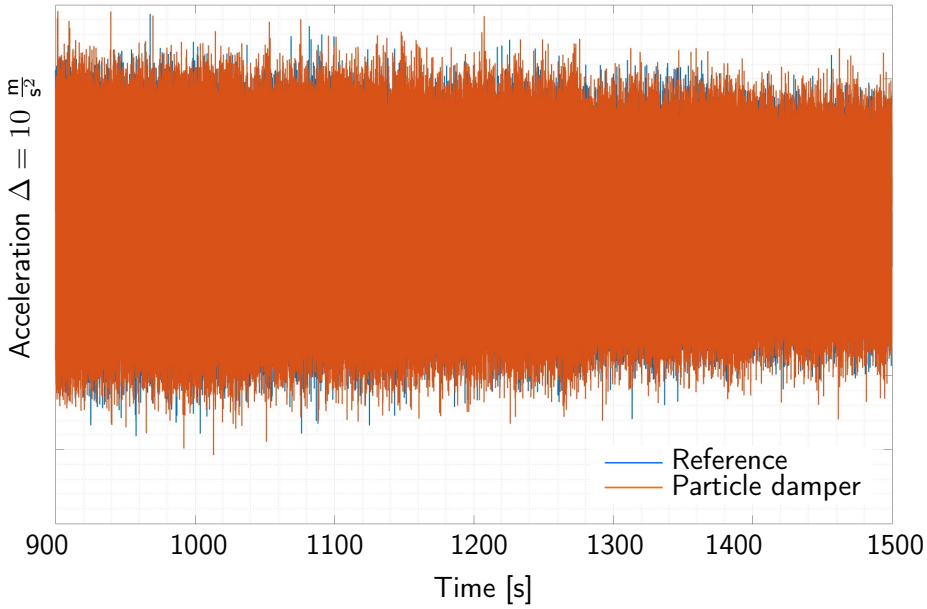

Figure 11.4: Time versus acceleration plot for the sensor located on a particle damper box on the WTS stator arm in Configuration 10.

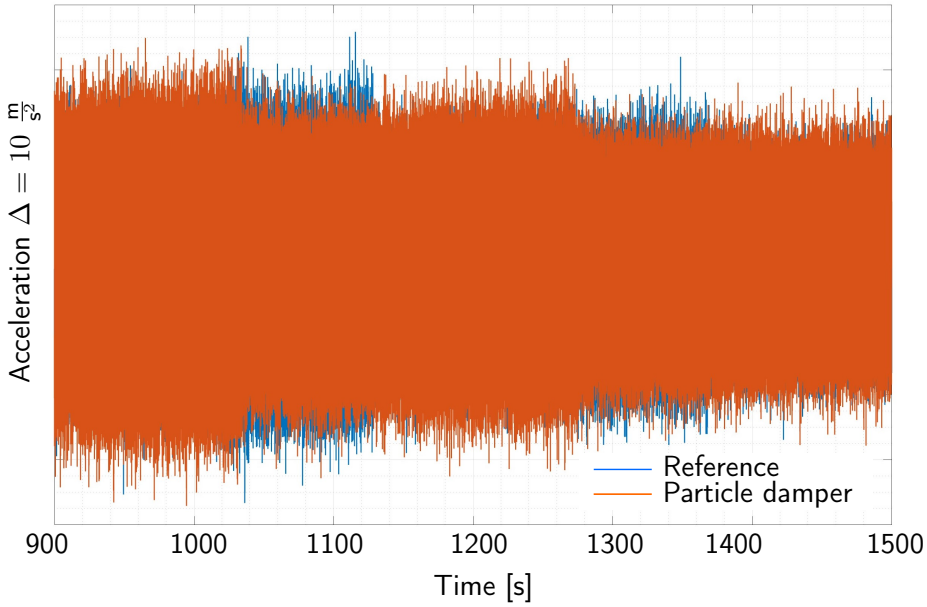

Figure 11.5: Time versus acceleration plot for the sensor located adjacent to a particle damper box on the WTS stator arm in Configuration 10.

Therefore, a meticulous approach to the selection and positioning of the damper configuration is essential to maximize its effectiveness. By carefully optimizing these parameters, the damping system can achieve superior vibration mitigation, ultimately enhancing the stability and operational reliability of the generator.

11.3 Wind turbine blade

In Chapter 10, three distinct approaches are thoroughly examined to mitigate the vibration amplitude of the blade test specimen, namely: sandwich core replacement, sandwich core modification, and external cavity attachment. Each of these strategies has demonstrated a notable reduction in the vibration amplitude of the test specimen, with its respective advantages and disadvantages. Furthermore, the discussion highlights how the external cavity attachment concept offers superior benefits compared to the other approaches, particularly in assessing the effectiveness of particle dampers for reducing vibrations in industrial-scale wind turbine blades.

In order to effectively implement the external cavity attachment concept in a 51 m long blade (see Figure 11.6 (left)), an extensive analysis of various encapsulation methods, arrangements, and fastening techniques for the rubber granulate has been conducted. This analysis included options such as enclosing the rubber granulate in rectangular boxes and lens-shaped containers, followed by their attachment to the blade structure. However, these methods were considered impractical due to challenges related to production and, more importantly, the complexities involved in arranging and securing these containers within the interior space of the rotor blade. Additionally, it is crucial that the encapsulation may increase the additional mass of the rotor blade. As a result, sealed plastic bags were chosen for implementation, reflecting their effective use in studies conducted with laboratory test specimens.

Figure 11.6: Left: An industrial wind turbine blade measuring 51 m in length. Right: A polyethylene plastic bag containing rubber granulate "RG 4.6 mm".

In order to implement the concept of utilizing plastic bags within large-scale wind turbine blades, polyethylene bags were selected as the appropriate enclosure for the rubber particles. Each bag is designed with dimensions of 500 mm by 500 mm, allowing for the containment of 9 kg of rubber granulate "RG 4.6 mm". The quantity of rubber particles within each bag has been carefully chosen to ensure that they can move freely, thus facilitating effective vibration mitigation.

The dimensions of the bags were intentionally chosen to prevent the formation of mass clumps among the rubber particles. If larger bags were utilized, the increased mass of the rubber granulate would likely impede the movement of the particles within the bag, adversely affecting the particle dampers vibration attenuation capabilities. Throughout this thesis, it has been demonstrated that merely increasing the mass of the rubber granulate does not enhance the vibration attenuation effectiveness of the particle damper.

On the other hand, opting for smaller bags could be beneficial for achieving higher vibration attenuation. However, this would lead to a significant increase in the total number of bags required to cover the same surface area of the blade. Consequently, this would complicate the experimental process and

increase the time needed for conducting the experiments. Therefore, a careful trade-off was established, resulting in the decision to utilize polyethylene bags of the specified dimensions and to contain the specified mass of rubber granulate within each bag. This balance ensures both the effective performance of the particle damper and the feasibility of the experimental procedures.

It is noteworthy to mention that all bags were partially filled with rubber granulate before being sealed using a foil welding device. The process of filling the materials into the bag and ensuring its proper sealing to prevent leakage during transportation and experimentation was carried out by IFAM in Dresden.

11.3.1 Experimental configuration

To evaluate the effectiveness of the particle damper, the wind turbine blade is suspended using bungee cords to establish a free-free boundary condition. Subsequently, a total of 20 polyethylene bags, each partially filled with granular materials, are strategically placed within the blade, see Figure 11.7 (left). These bags are secured using adhesive tape, ensuring that the rubber particles inside are uniformly distributed and do not aggregate into a clump.

The specific positioning of the bags is chosen to be near the root of the blade, as this region is critical for sound radiation into the surrounding environment. Additionally, this location is advantageous for maintenance purposes, as it allows for easy access while the turbine is in operation. This careful consideration of bag placement not only optimizes the performance of the damping system but also facilitates practical maintenance under operational conditions.

An impact hammer was utilized to excite the rotor blade, with six distinct locations selected for this excitation process. In conjunction with this, nine acceleration sensors were installed on the outer surface of the blade to capture the dynamic response. The placement of these sensors was strategically focused around the region where the particle dampers were affixed. Specifically, one sensor was positioned between the area of the particle dampers and the remaining eight sensors were mounted along the boundary of the particle damper region. These sensors were approximately 1 m away from the boundary of the particle dampers, allowing for precise measurement of the system's response in relation to the dampers' performance.

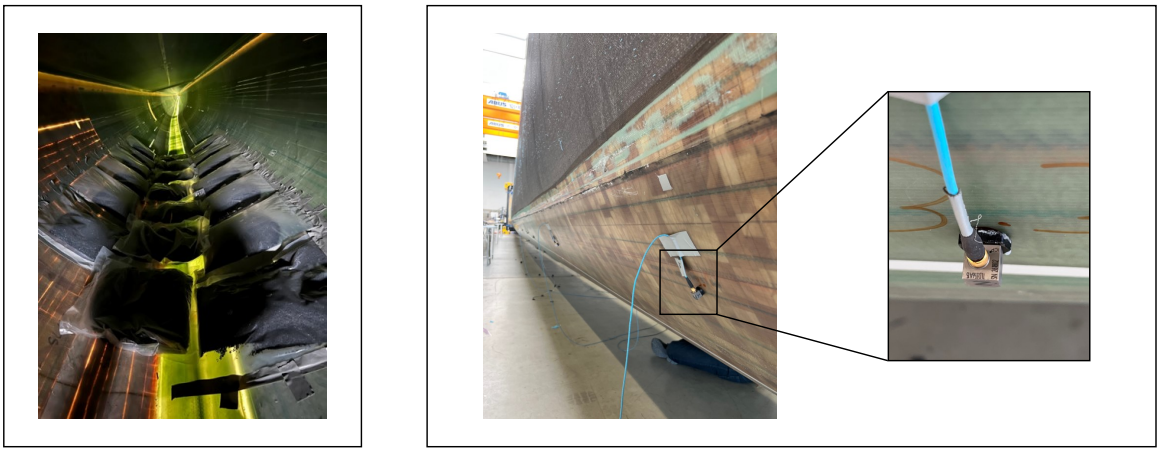

Figure 11.7: Left: Arrangement of 20 plastic bags partially filled with rubber granulate inside the blade. Right: Installation of 3D acceleration sensors on the outer surface of the blade to monitor the system's response.

It is important to note that the efficiency of the particle damper was not evaluated under rotating conditions. As a result, the influence of centrifugal force on the damper's performance in a 51 m

long blade could not be analyzed within the scope of this experimental study, and its assessment was beyond the objectives of this thesis. Nevertheless, it is intriguing to observe how a particle damper, initially tested on specimens with wall thicknesses ranging from 0.2 mm to 3.0 mm, could potentially be implemented in an industrial-scale blade, where the wall thickness at the root varies between 80 mm and 100 mm.

11.3.2 Results

The blade was excited near its root of blade using an impact hammer, and the acceleration response was measured at a location 5.5 m away from the excitation point. This measurement point was positioned 1 m beyond the end of the particle damper, while the excitation occurred 1 m before the damper's placement. Consequently, the sensor capturing the response was located 1 m away from the particle damper, ensuring that the recorded data reflected the damping effects without direct interference from the excitation input. The frequency response function is presented up to 100 Hz (see Figure 11.8), as the primary concern for wind turbine vibration and noise lies within the low-frequency range. Moreover, as previously discussed, passive damping techniques are generally more effective at attenuating vibration amplitudes in the high-frequency range. Therefore, it is particularly compelling to investigate whether the particle damper, as a passive damping method, can successfully reduce the vibration amplitude of an industrial-scale wind turbine blade within this low-frequency domain.

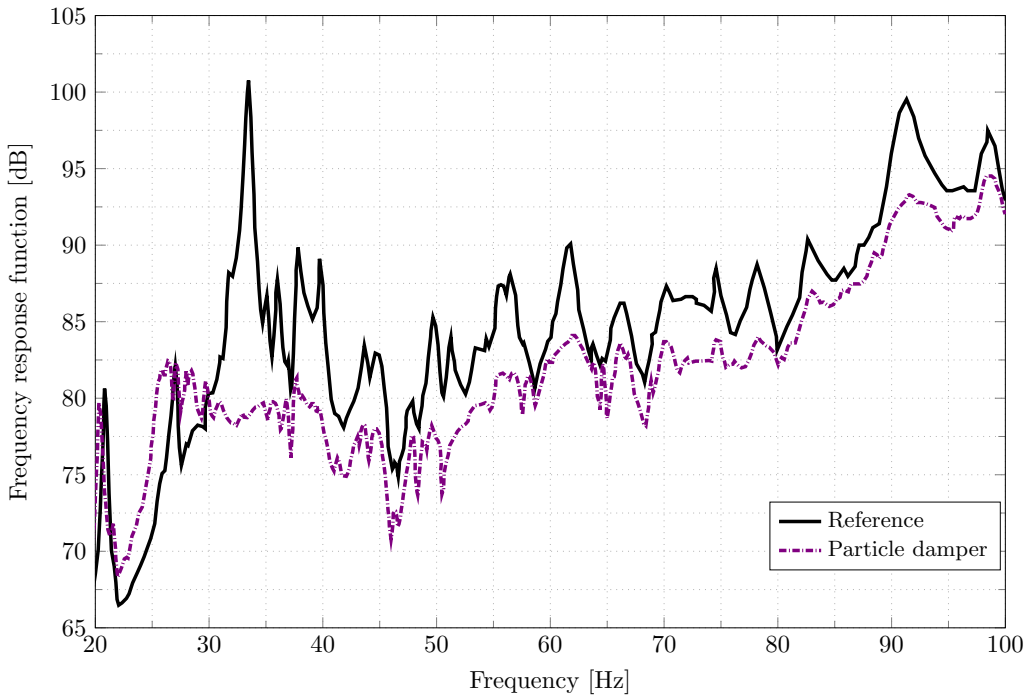

Figure 11.8: FRF of the industrial wind turbine blade with and without the particle damper.

In the frequency range of 20 Hz to 100 Hz, the particle damper consisting of rubber granulate "RG 4.6 mm" demonstrates a clear reduction in vibration amplitude across all resonance frequencies. The largest resonance peak is observed at 33 Hz, where the rubber granulate fully eliminates the vibration amplitude. The smallest vibration reduction is observed at the first resonance frequency of 20 Hz, with a decrease in vibration amplitude of 1 dB. However, there is an exception at 27 Hz, where the particle damper shows no noticeable effect on vibration attenuation. Apart from this, significant vibration reduction is consistently achieved at the remaining resonance frequencies within the tested range. To understand why the particle damper is ineffective around 27 Hz, it is necessary to analyze

the modeshape at this frequency. This analysis will provide insights into the vibration characteristics in the relevant region, helping to explain the observed behavior.

The particle damper concept developed in the lab, initially tested on a blade specimen measuring 500 mm in length, can indeed be scaled up for application in a commercial wind turbine blade measuring 51 m. However, for practical implementation in an operational wind turbine, it is important to consider modifications to enhance both sustainability and robustness. One proposed improvement is to enclose the rubber particles within a grid-like structure, which would then be attached to the areas where the plastic bags containing the rubber particles are currently placed. This design would prevent the risk of rubber particles escaping during the blade's rotation while potentially reducing the total mass of the rubber particles required.

It is also noteworthy that the total mass of rubber granulate used in this test amounts to 180 kg, which results in an increase in the overall blade mass by 1.02%. While this is a relatively small increase, further optimization of the particle damper design, particularly through the use of a grid structure, could offer both weight reduction and enhanced performance for long-term, reliable use in wind turbines.

11.4 Summary and conclusion

The objective of this chapter was to illustrate that the particle damper concepts developed in this thesis can be effectively implemented in industrial-scale wind turbine components for vibration mitigation, building upon findings obtained in a controlled laboratory setting. The results indicate that incorporating all the concepts introduced in this thesis, while carefully evaluating their respective advantages and disadvantages, can significantly reduce the vibration amplitude of the wind turbine stator.

Moreover, the vibration mitigation capability of the current particle damper design could be further enhanced by increasing the size of the cavity boxes attached to the stator arm. This adjustment would allow the dampers to cover a more substantial area of the stator arm surface, thereby improving their effectiveness. Additionally, designing the cavities in a flat configuration could help minimize the additional mass of the granular material while simultaneously increasing the overall efficiency of the system.

Furthermore, the placement of these cavities on the stator arm should be informed by the deflection modes of the stator, which can be accurately determined through FEM. This strategic positioning will optimize the performance of the particle dampers and enhance their contribution to vibration reduction in industrial applications.

The implementation of particle dampers in wind turbine blades has proven effective in reducing the vibration amplitude of a 51 m long blade. This investigation demonstrates that the concept, initially developed using a 500 mm long specimen with wall thicknesses ranging from 0.2 to 3.0 mm, can be successfully adapted for application in blades with thicker walls (varies between 80 mm and 100 mm) and significantly greater lengths. It is important to emphasize that all the tests conducted have been carried out under non-rotating conditions. Further research is required to assess the performance of the particle damper in a rotating environment for the 51 m blade. Nonetheless, the current findings suggest that, even in the absence of centrifugal effects, the particle damper may still demonstrate promising efficiency when applied to significantly thicker blade structures.

Additionally, the particle damper, designed using ELT rubber granulate, effectively minimizes the additional mass associated with its installation while also reducing vibration amplitudes in the low-frequency range during controlled laboratory tests. Notably, in industrial components, this design has demonstrated the capacity to achieve similar reductions in vibration amplitude in the low-frequency spectrum by increasing the mass of the structure by only 1%. This highlights the potential for the particle damper to enhance performance without significantly impacting the overall weight of the wind turbine blade.

12 Particle damper effectiveness in electric vehicles

This chapter focuses on applying the particle damper design parameters developed in this thesis to address vibration control challenges in electric vehicles (EVs). It begins by discussing the importance of Noise, Vibration, and Harshness (NVH) in EVs, followed by an overview of power electronic modules (PEMs) in the electric powertrain, which are key contributors to noise and vibration issues. Next, the chapter reviews state-of-the-art solutions for mitigating NVH in EV systems.

The chapter then experimentally validates the performance of particle damping techniques in reducing vibration amplitudes in an isolated PEM[1] setup, where the module operates independently from the electric powertrain. This analysis underscores the impact of the design parameters explored throughout the thesis, demonstrating their influence on the damper's ability to reduce vibrations. To extend the findings beyond laboratory conditions, full-scale tests are conducted on a modular electric drive under realistic operational environments. The research findings are grounded in previously published work referenced in [254].

12.1 The role of NVH in automotive design

Noise, vibration, and harshness (NVH) have emerged as critical factors in modern vehicle design as consumer expectations for a smooth driving experience continue to rise. Vibration, a longstanding concern, directly impacts reliability and quality. Noise, increasingly prevalent in vehicle environments, is a significant factor for consumers. Harshness, characterized by the transient nature of vibration and noise, further influences perceived quality.

NVH issues can originate from various vehicle components, such as the engine, pumps, drivetrain, wheels, and tires, or from integration challenges, such as misalignments between the powertrain, body, chassis, and suspension [255]. Controlling vehicle NVH is particularly complex due to the interconnected and speed-dependent nature of multiple vibration and noise sources, unlike many other mechanical systems. Increasingly stringent regulations on vehicle noise emissions and vibration control have been implemented to reduce environmental impact. Additionally, marketing demands and customer preferences have made NVH refinement a crucial part of vehicle design, serving as a competitive advantage in attracting potential buyers.

Similar to traditional vehicles, which have long faced numerous NVH challenges, EVs are now encountering a new set of NVH issues. In conventional vehicles, the internal combustion engine (ICE) serves as the dominant noise source, often masking other noises, so research efforts primarily focused on reducing engine noise, with less attention given to other sources. In contrast, EVs lack components such as the ICE, fuel tank, air intake, and exhaust systems. Instead, they have ample space for the electric drive unit and battery pack. Although EVs are quieter without a combustion engine, the need for NVH research has become even more critical. The absence of engine noise exposes various other sound sources that were previously masked but are now more noticeable and potentially annoying [256].

[1] Certain technical aspects and specific PEM design details are excluded from this chapter due to confidentiality, as in Chapter 11.

Recent research on EVs NVH has primarily focused on reducing noise and vibration caused by the powertrain, tires, wind, and ancillary systems.

In EV powertrains, NVH primarily stem from several key components, including the electric motor, power inverter, transmission with gear reduction, and various ancillary systems like cooling fans and pumps. Together, these elements play a significant role in generating both airborne and structure-borne noise within the vehicle [257]. The newly developed Volkswagen powertrain architecture is illustrated in Figure 12.1. The main propulsion system consists of a rear-axle-mounted permanent magnet synchronous motor, combined with a power electronic module and a single-speed transmission in an axle-parallel layout. This setup provides a peak power output of 150 kW, a maximum torque of 310 Nm, and can reach rotational speeds of up to $16,000$ RPM [258].

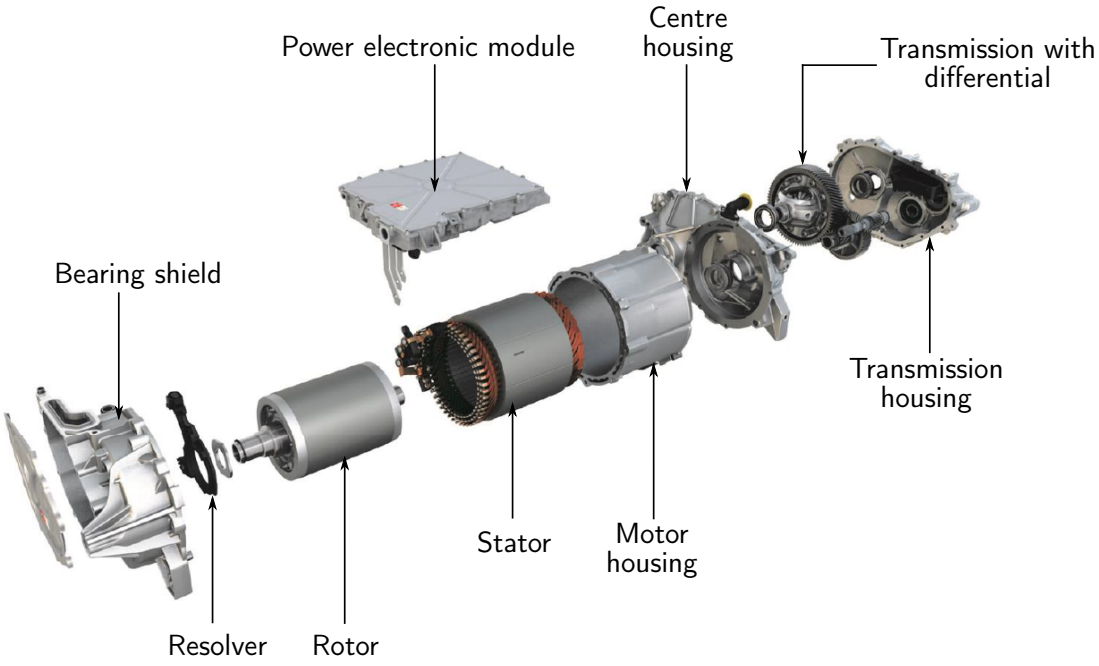

Figure 12.1: Powertrain configuration of the Volkswagen ID. vehicle family [258].

The electric motor, gearbox, and power electronic module (PEM) act as excitation sources, producing vibrations and noise that can propagate through different pathways [257]. Structural vibrations travel through the vehicle's framework, resulting in structure-borne noise, while airborne noise is transmitted through the surrounding air. The interaction between structural vibration transmission and noise radiation into the environment determines the resulting sound and vibration levels experienced by vehicle occupants.

At the heart of this experience is the human, which detects and interprets these sounds and vibrations. This perception significantly impacts the overall sensory experience and comfort for both the driver and passengers. Consequently, understanding and mitigating NVH in EVs is crucial for enhancing the ride quality and satisfaction of those inside the vehicle.

While it is essential to investigate all contributors to excitation in order to fully understand the NVH framework in EVs, this chapter will specifically focus on the vibration mitigation of the power electronic module using the particle damping technique. Noise reduction and psychoacoustics, though important aspects of NVH, are not within the scope of this thesis. As such, these dimensions of NVH will not be addressed or discussed in this work. The primary focus here will remain on the vibration aspects, particularly in relation to mitigating vibrations in the PEM. The decision to focus on the PEM is based on input from our industrial partner. According to their transfer path analysis, vibrations generated by the PEM are a key contributor to interior noise at higher frequencies.

12.2 Power electronic subsystem

PEMs, also known as inverters, serve as the central control units for managing various operational tasks. These PEMs incorporate power semiconductors, essential components that facilitate the conversion of electrical energy, as illustrated in Figure 12.2.

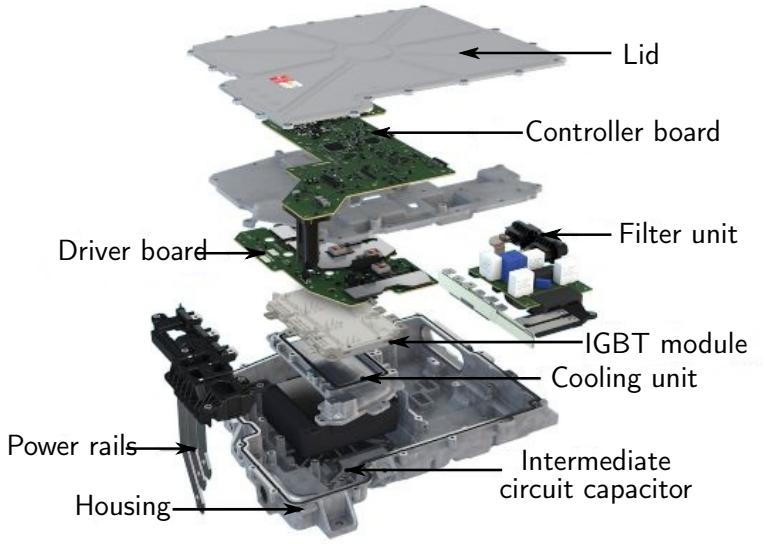

Figure 12.2: A detailed illustration of the physical layout of a power electronic module [259].

The fundamental purpose of power electronics is to ensure the efficient conversion and management of electrical energy. In electric vehicles, the main source of power is the battery pack, which provides a high-voltage direct current (DC) supply. However, electric motors require alternating current (AC) for propulsion. This necessary conversion from DC to AC is facilitated by power electronics devices [260]. The inverter plays a key role in transforming the DC power from the battery into the AC power that drives the motor. Beyond this primary function of power conversion, PEMs are also essential for controlling various aspects of vehicle dynamics [261]. They achieve this by regulating the alternating current supplied to the motor, which has a direct impact on the vehicle's performance. Specifically, the frequency of the AC current determines the speed at which the motor operates, while the amplitude of the current governs the motor's torque output. In this way, power electronics not only enable the conversion of energy but also actively control the motor's behavior, optimizing both speed and torque to meet the vehicle's demands.

In addition to the electric motor itself, PEMs are a major contributor to electromagnetic noise [262, 263]. A primary method used to convert DC from the battery to AC for the motor is pulse width modulation (PWM) [264]. The frequency at which this conversion occurs is known as the switching frequency, which generally remains constant across different operating conditions [261]. Furthermore, the non-sinusoidal output voltage and current generated by the inverter, containing high harmonic content due to switching, have been observed to cause high-frequency electromagnetic acoustic noise. The harmonics generated by the PWM inverter, influenced by the modulation technique, create radial force waves. These forces cause vibrations in the inverter, which can be transmitted to other components like the fan cowl, cooling duct, and terminal box [261, 262, 265]. If the frequency of these force waves aligns with the natural frequencies of the motor, resonance can occur, significantly amplifying noise levels in specific frequency ranges. The issue is further compounded by the fact that PEMs are often designed with thin-walled structures, making them particularly prone to vibrations.

These vibrations can travel through various components of the PEM and their mounting points, negatively affecting the overall system performance. The consequences of such vibrations can include diminished energy efficiency, accelerated wear and tear on the system components, and a reduction in the reliability of the system as a whole. Additionally, the vibrations may cause an increase in interior noise level, which can significantly impact passenger comfort.

12.3 Effective solution for reducing e-drive NVH

To address the issue of electromagnetic noise produced by power inverters, a number of strategies have been investigated. Among these, the optimization of PWM techniques has been a prominent approach [266, 267], as has the practice of adjusting the switching frequency [268, 269]. Both methods aim to reduce the noise generated during inverter operation. However, it may not be feasible to achieve this goal, and attempting to implement different modulation techniques across various output voltage regions of the converter would likely not produce the desired or optimal results. This approach, which involves varying the modulation strategies to maximize the efficiency of the drive system, may ultimately fail to deliver satisfactory outcomes due to inconsistencies or inefficiencies that arise when different methods are applied in different voltage ranges. However, a comprehensive analysis of these methods is beyond the scope of this thesis, which will focus primarily on passive damping techniques as a means of reducing noise.

A wide range of passive strategies have been thoroughly explored in an effort to address the challenges of NVH in electric drives. Researchers have investigated several approaches, including alterations to the design and functioning of the electric motor itself, as well as the influence of mesh gears and bearings, all of which have been identified as significant contributors to NVH problems. This section will provide a comprehensive yet concise overview of these innovative methods that are currently being examined in the field. Following this, the focus will shift to an in-depth analysis of the particle damping technique introduced in this thesis, demonstrating how it can effectively minimize vibration amplitudes within electric drives.

Tischmacher et al. [270] highlighted that power electronic converters can transmit vibration to the motor enclosure, potentially amplifying noise when the motor's eigenmode is excited. While the authors primarily focused on modifying the motor's cooling duct to reduce audible noise, they did not directly address the vibration source (power inverter) itself. Various cooling duct modifications were explored, including increasing the cover plate thickness, adding internal ribs, reinforcing side panels, and fixing a point at the duct center. The goal was to eliminate eigenmodes near 2 kHz. Although these modifications achieved some noise reduction, their effectiveness was significantly enhanced when combined with a decoupled fan cowl.

Lei et al. [271] highlight the critical role of gear micro-geometry in mitigating gear vibration and noise, particularly in the context of electric buses. Their innovative multi-objective optimization algorithm effectively addresses the challenges posed by gear meshing imperfections, manufacturing errors, and misalignment. By optimizing tooth surface micro-geometry, the proposed method significantly reduces noise levels and improves overall gear system performance. Experimental validation on a test bench further confirms the efficacy of this approach in achieving vibration and noise reduction in electric bus gearboxes.

Hu et al. [272] conducted a comprehensive analysis of noise and vibration in a hybrid electric vehicle operating exclusively in electric mode. The study was divided into two main phases. First, a frequency domain analysis was used to identify the primary sources of noise and vibration from the experimental data. The results highlighted that the main contributors were the gear engagement within the planetary gear set and the gear meshing between the external ring gear and the reducer. In the second phase, a theoretical investigation was conducted to optimize gear parameters such as mesh stiffness, tooth

error, and pitch error in order to reduce noise and vibration. The theoretical analysis showed significant potential for reducing vehicle noise and vibration levels.

Migal et al. [273] conducted experiments to find ways to reduce vibration in electric vehicle asynchronous motors. They looked at how the quality, size, and operating mode of the bearings affected vibration. They found that using higher quality bearings (P5 instead of P0) could significantly reduce vibration by up to 16 dB. They also found that reducing the rotating frequency of the bearings could help reduce vibration. Optimizing bearing preload resulted in a vibration reduction of 5 - 8 dB in the frequency range of 160 - 6300 Hz, while optimizing the bearing installation clearance within the housing led to a 5 - 10 dB reduction for most vibration frequencies.

Efforts to directly reduce vibration and noise generated by the power electronic converter have primarily focused on active-passive vibration control and acoustic shielding methods. Active-passive vibration control works by incorporating the inverter into the motor's isolation system, which helps to reduce the transmission of vibrations from the inverter to other components [274]. On the other hand, acoustic shielding aims to minimize noise by enclosing the inverter in sound-absorbing or sound-blocking materials [275]. These materials are designed to prevent airborne noise from spreading to surrounding areas, effectively lowering noise levels within the cabin and creating a quieter, more comfortable environment.

Rieß et al. [276] investigated the application of vibroacoustic metamaterials to a simplified power electronic lid, aiming to reduce vibration and noise. The lid's design was modified by removing stiffening ribs, resulting in a shift of its modal frequencies to lower values while maintaining overall structural behavior. Two distinct metamaterial configurations were tested: a sheet metal-based design and a plastic film-based design. For comparison, a conventional Alubutyl layer was also applied. The study demonstrated that both metamaterial configurations significantly outperformed the Alubutyl layer in reducing vibration and noise. Notably, the sheet metal-based metamaterial achieved a substantial reduction in vibration amplitude compared to the plastic film-based design. While the sheet metal metamaterial successfully lowered noise levels by 5 dB in a test vehicle, it's important to consider the associated mass increase. The sheet metal metamaterial added approximately 83% more mass than the simplified lid, whereas the plastic film metamaterial added 40%. In contrast, the Alubutyl layer increased mass by only 30%.

From the review of current research, it becomes evident that passive damping techniques are rarely applied to reduce the vibration and noise emitted by power electronic subsystems. Most studies have focused on other components of the electric drive powertrain, such as the motor [270], gears [271], and bearings [273]. This is largely due to the compact nature of the power inverter, where the limited available space makes it challenging to incorporate damping materials effectively. As a result, much of the research related to vibration and noise control for power inverters has concentrated on high-frequency adjustments [268] and control strategies [277]. Despite the limited application of passive damping techniques directly to the power electronic subsystem [275, 276], these methods have demonstrated a significant reduction in vibration amplitude and noise emission. However, their implementation faces practical challenges. The use of metamaterials adds excessive mass, making them less suitable for optimization in automotive applications, while acoustic shielding requires additional space, further complicating their integration into the already compact structure of the power inverter.

The primary aim of this chapter is to explore the application of particle damper concepts, which have been developed throughout this thesis and previously demonstrated to be effective in wind turbine components, to the power inverter lid. The goal is to reduce the vibration amplitude of the structure. In approaching this task, particular attention is paid to ensuring that the additional mass introduced by the particle damper remains as minimal as possible, and that the design of the lid is not significantly altered in the process. By successfully integrating the particle dampers into this automotive application, the chapter will showcase the adaptability and broader potential of the concepts developed in this thesis. It will demonstrate that these particle damper solutions can be effectively employed in a wide

range of applications where vibration control is crucial, thus highlighting their versatility beyond the initial focus on wind turbines.

12.4 Vibration mitigation of power electronic lid

As discussed earlier, the electromagnetic forces generated during operation can induce vibrations in both the PEM structure and its lid. According to insights provided by our industrial partner, these vibrations, particularly those affecting the lid, can manifest as audible noise within the vehicle cabin. Due to this, the PEM lid has been selected as the focus for further investigation, with the aim of studying how the implementation of particle dampers might help reduce the vibration amplitude within the powertrain system. Another reason for selecting the PEM lid for the implementation of particle dampers is the observation that there is insufficient free space within the PEM itself to effectively apply passive damping techniques, as shown in Figure 12.2.

The application of the particle damping technique to the PEM has been conducted in a structured, multi-phase approach, with each phase targeting different aspects of the system. The first phase of this process was dedicated to examining the specific effect of particle dampers when applied solely to the lid of the PEM, without considering the influence of other components within the system. By isolating the lid in this phase, a controlled environment was established, which enabled a focused and precise evaluation of the particle dampers' effectiveness in reducing vibrations in the lid itself.

The second phase of the study involved attaching the PEM lid, which had been outfitted with particle dampers during the first phase, to the power electronics casing. This stage focused on evaluating the performance of the particle dampers in reducing vibrations within the integrated system that consisted of the PEM and its casing. By simulating more realistic conditions, this phase aimed to assess how effectively the particle dampers could mitigate vibrations when applied to the complete module.

In the final phase of the study, the complete PEM assembly, now incorporating the dampened lid, was mounted onto the electric motor. The primary objective of this stage was to assess the performance of the particle dampers under real-world loading and boundary conditions. This crucial evaluation offered valuable insights into how well the dampers could function in an operational environment, where the PEM is exposed to the forces and vibrations generated during the motor's typical use.

It is crucial to emphasize that one of the key objectives of this study is to implement the particle damper without making any modifications to the existing structure. This approach stands in contrast to previous research, where modifications were made to facilitate the integration of vibration-reducing materials. For example, researchers in past studies, such as those by Riess et al. [276], simplified the design of the PEM lid to make it easier to incorporate vibroacoustic metamaterials. Likewise, in the work of Duvigneau et al. [149], particle dampers were applied to reduce the vibration amplitude of an oil pan, but they also altered the oil pan cover to improve the damper's performance. However, in Duvigneau et al. [149] study, the modified cover of the oil pan was significantly lighter than the original cover. In contrast, the aim of the current study is to achieve effective vibration reduction while preserving the integrity of the original structure, without the need for significant alterations.

As demonstrated in Chapter 5, rubber granulate "RG 4.6 mm" proved to be the most suitable material for designing a particle damper, outperforming other materials that were experimentally investigated in this thesis. This material has also been successfully tested in previous studies for its effectiveness in reducing the vibration amplitude of wind turbine generators and blades, see chapter 11. For these reasons, rubber granulate "RG 4.6 mm" is also used in this chapter to design a particle damper for the electric vehicle powertrain.

Figure 12.3 illustrates the PEM attached to the electric motor, along with the placement of the particle damper inside the PEM lid. The decision on the placement of the rubber granulate "RG 4.6 mm" was

made based on the design of the PEM lid and the available space within it[2].

To ensure the rubber granulate remains securely enclosed within the lid during the experiment, a very thin plastic sheet is used to seal the lid, preventing the granular material from escaping. This method is similar to the approach described in Chapter 10, where particle dampers were enclosed in plastic bags before being attached to blade specimens for testing. This sealing technique allows for accurate testing of the particle damper's effectiveness without compromising the integrity of the experimental setup.

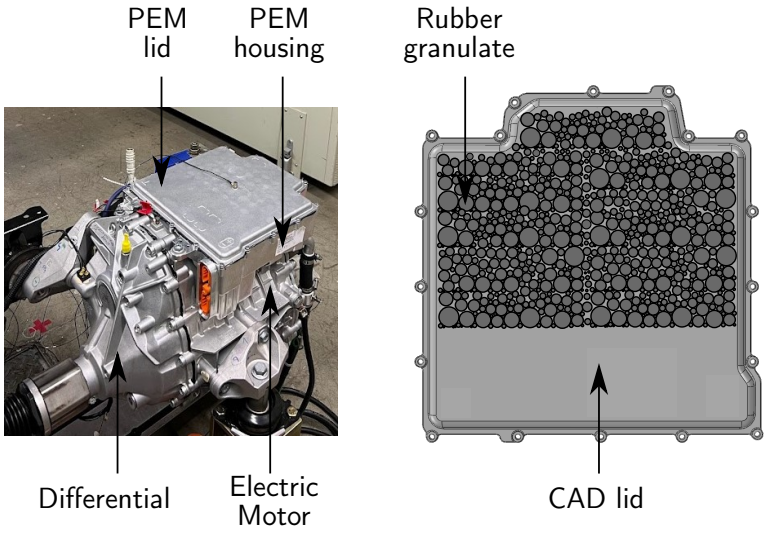

Figure 12.3: Left: A PEM mounted on an electric drive system. Right: A CAD model of the PEM's lid, filled with rubber granulate.

12.4.1 Experimental setup

Figure 12.4 presents the experimental setup created to examine how effectively a particle damper can reduce the vibration amplitude of the PEM lid. To ensure that the inherent dynamics of the PEM module were not affected by external factors, a free-free boundary condition was employed. This method involved suspending the module using a thin, elastic rope that was fastened to a dedicated hook affixed to a Bosch profile. By doing so, the experimental configuration successfully eliminated the clamping effects that are commonly associated with traditional mounting methods, allowing for a more accurate assessment of the particle damper's performance.

The dynamic response of the PEM lid was measured using four identical accelerometers, strategically positioned at various locations on the lid, see Figure 12.5 (right). The placement of these accelerometers was carefully selected to capture all potential dynamic responses of the lid, including both bending and torsion modes. To ensure reliable attachment, the accelerometers were affixed to the lid using super glue. A comprehensive study was conducted to determine the optimal adhesive material and gluing method. This study involved testing super glue under various temperature conditions, specifically at 20° C, 22° C, and 100° C, to evaluate its performance. Additionally, the timing of the measurements was considered, with acceleration data collected at different intervals following the gluing process. For instance, one set of measurements was taken 15 minutes after gluing the sensor, another set was taken 24 hours later, and a final set was recorded after 6 days. This thorough testing ensured that the selected adhesive provided consistent and accurate sensor attachment for reliable dynamic response measurements.

The lid is excited using a hammer equipped with a force sensor at its tip, allowing for precise measurement of the impact force applied to the structure under test. Two different excitation locations

[2]Due to confidentiality, the design of the backside of the lid cannot be disclosed

were selected for this process, as shown in Figure 12.5 (left). This choice was made to ensure that all possible eigenfrequencies of the structure within the range of 20 Hz to 1100 Hz are effectively excited. This frequency range is critical because it encompasses the frequencies at which vibrations from the PEM can generate audible noise inside the car cabin.

In order to capture all the measurement data from both the accelerometers and the force sensor, these devices were connected to the PAK MKII system manufactured by Müller BBM. This system served as the central hub for data acquisition, linking the sensors to the PAK 6.2 software installed on a connected computer, see Figure 12.4. The PAK 6.2 software was utilized to manage the data collection, perform in-depth analysis, and facilitate the evaluation of the measurements. This integrated setup ensured seamless data flow and processing, allowing for precise acquisition and thorough analysis of the sensor data.

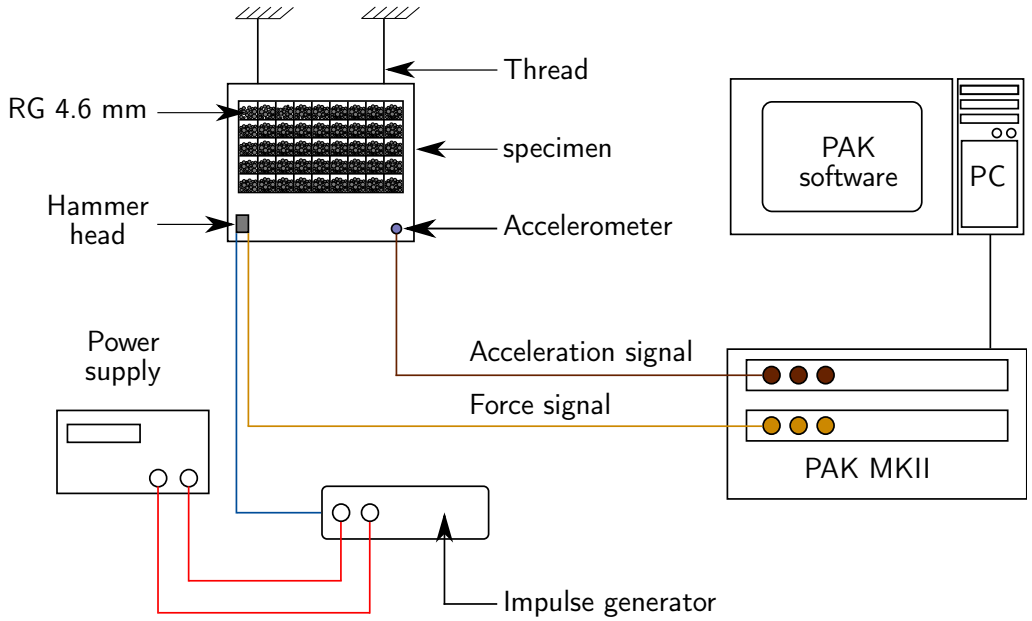

Figure 12.4: Experimental setup of particle damper for e-drive PEM vibration attenuation.

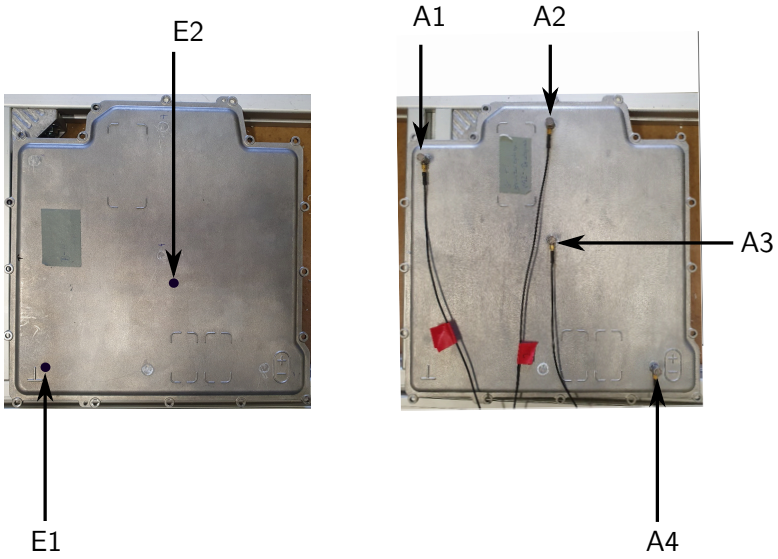

Figure 12.5: Excitation points (left) and accelerometer positions (right) on the lid.

The dynamic response of the PEM lid was measured under two distinct configurations: one with the

particle damper attached and one without. After these measurements, the lid was securely mounted to the PEM base using a set of 13 identical screws. As discussed in previous chapters, the tightening of bolts can have a significant effect on the vibration characteristics of structures. To minimize the influence of this factor, a torque wrench was used to ensure a consistent pre-load of 3 Nm was applied to each screw during the assembly process. Subsequently, the entire PEM module, with the lid in place, was suspended from the Bosch profile, as shown in Figure 12.4. This setup was carefully designed to evaluate the performance of the particle damper on the PEM lid, specifically focusing on its ability to attenuate vibrations. Additionally, the configuration allowed for an assessment of the lid's vibration behavior when it was attached to the PEM case. By utilizing this two-stage experimental approach, a detailed assessment of the particle damper's impact both on the PEM lid's vibrations and on the overall module's dynamic behavior was carried out.

12.4.2 Results

The results of the PEM lid for each acceleration sensor are depicted in Figure 12.6[3]. In these plots, the black spectrum represents the reference measurement, which corresponds to the structure without the particle damper in place. It is important to note that the results discussed in this section are for the scenario in which the lid, along with the PEM-attached lid, is excited by a hammer at the excitation position E1.

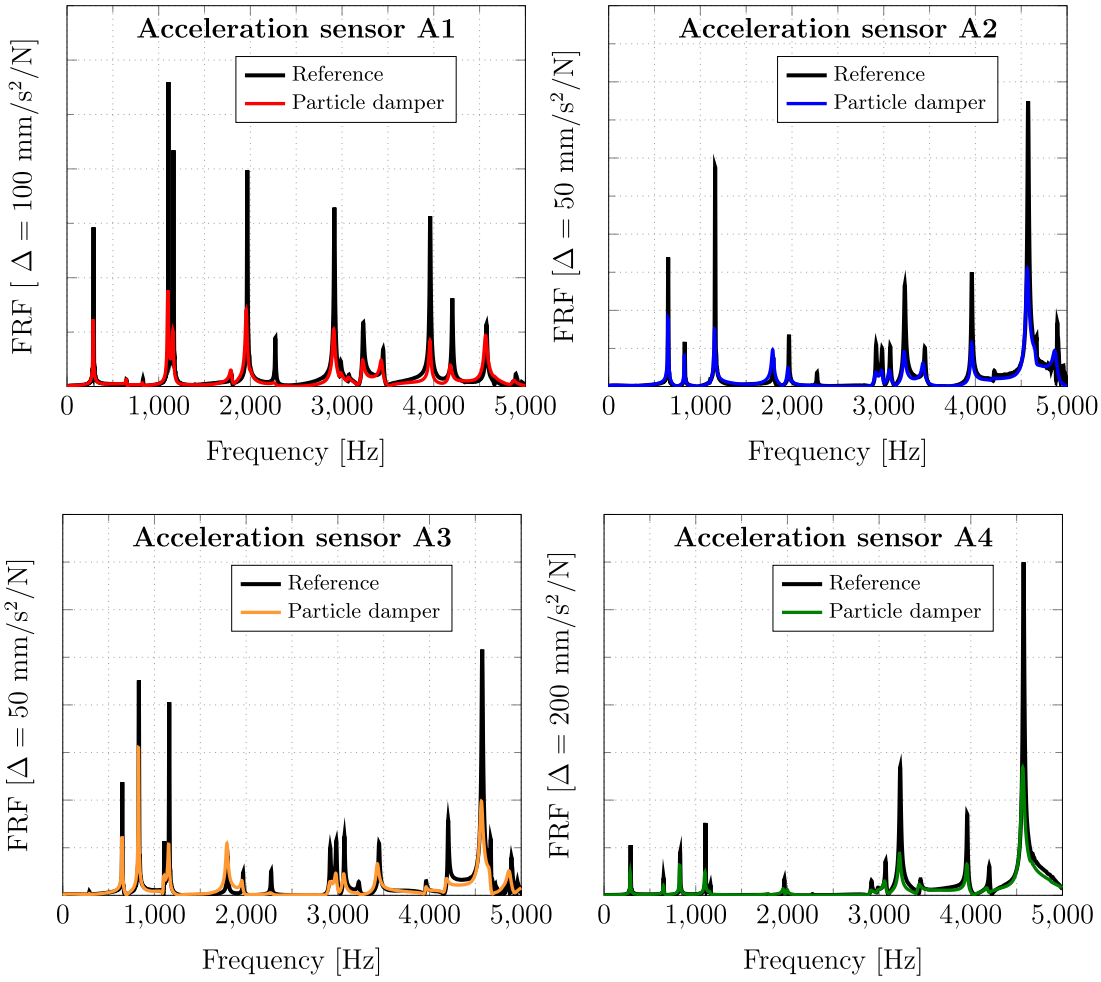

Figure 12.6: FRFs of all four acceleration sensors for the empty and partially filled lid.

[3]Due to confidentiality reasons, the exact values on the y-axis of these plots are not provided. Instead, a Δ value is given to offer a general understanding of the extent of vibration reduction achieved by the particle damper

In earlier chapters, it has been shown that rubber granulate "RG 4.6 mm" can effectively reduce the vibration amplitude of the structure within a frequency range of 20 Hz to 2000 Hz. In this case, however, the results indicate that the "RG 4.6 mm" can further reduce the vibration amplitude of the lid up to 5000 Hz. This suggests that the particle damper, designed with rubber granulate "RG 4.6 mm," is not limited to either low or high frequency ranges but instead operates as a broad-band damping concept. While particle dampers generally provide broad-band damping, conventional particle dampers designed with metallic particles tend to perform better in higher frequency ranges [32].

The results clearly demonstrate that the particle damper effectively reduces the vibration amplitude of the lid across all resonance frequencies, regardless of the sensor's position. For instance, low-frequency resonance peaks for sensors A1 and A4 have been observed around 290 Hz, and the introduction of the rubber granulate "RG 4.6 mm" has significantly reduced these peaks. In addition, for sensors A2, A3, and A4, the largest resonance peak occurs at approximately 4576 Hz. Here, too, the particle damper proves highly effective, reducing the vibration amplitude significantly around these peaks. For acceleration sensor A1, the most prominent resonance peak is seen at 1106 Hz, and once again, the rubber particles have been able to reduce its amplitude significantly.

The observed consistent and significant reduction in vibration amplitude, as measured across multiple sensors and spanning a range of resonance frequencies, provides strong evidence of the particle damper's effectiveness in suppressing vibrational responses. This outcome clearly demonstrates that the damper is not limited to mitigating vibration at specific frequencies but is instead capable of delivering reliable performance across a broad frequency spectrum. In particular, the use of rubber granulate as the damping medium proves to be highly versatile, as it successfully addresses both low-frequency and high-frequency resonance peaks. This dual capability ensures that the system experiences improved vibration attenuation in a more comprehensive manner, thereby enhancing its overall dynamic stability and operational reliability.

The dynamic response of the PEM-attached lid, both with and without the particle damper, is illustrated in Figure 12.7. In this analysis, the FRFs are plotted up to 1100 Hz. This upper limit was chosen because the most critical issues affecting the electric drive occur within the frequency range of 800 Hz to 1100 Hz. Addressing this specific frequency range is crucial for the optimal performance of the electric drive, as it is where the most significant vibration-related problems are likely to arise.

Figure 12.7 illustrates that the attachment of the lid, partially filled with rubber granulate "RG 4.6 mm", to the PEM base results in a pronounced reduction in the vibration amplitude of the system. This reduction is not confined to isolated measurement points but is consistently observed across all sensor positions, thereby providing strong evidence of the uniform effectiveness of the damping mechanism. The results suggest that the particle-filled lid contributes to a more globally distributed attenuation of vibrational energy within the structure, highlighting its capability to mitigate dynamic responses in different regions simultaneously. Such behavior further reinforces the suitability of particle damping as a reliable strategy for enhancing the vibrational performance of the overall system.

For the acceleration sensors A1, A3, and A4, it is evident that the resonance frequencies occur beyond 400 Hz. Specifically, for acceleration sensor A1, the most prominent resonance frequency appears around 700 Hz, where the particle damper significantly reduces the vibration amplitude at this peak.

In contrast, acceleration sensor A2 exhibits two types of resonance frequencies: one at a low frequency of 50 Hz and another occurring after 400 Hz. At this sensor position, the particle damper is effective in significantly reducing the amplitude of both resonance peaks. Notably, around the first resonance peak at 50 Hz, the particle damper completely eliminates the vibration amplitude, demonstrating its exceptional damping capabilities. Moving on to acceleration sensor A3, there are two distinct resonance peaks observed, specifically at 670 Hz and 704 Hz. The particle damper effectively reduces the amplitude of both of these resonance peaks as well. A similar effect has also been noted for acceleration sensor A4, where the particle damper continues to show effective vibration reduction.

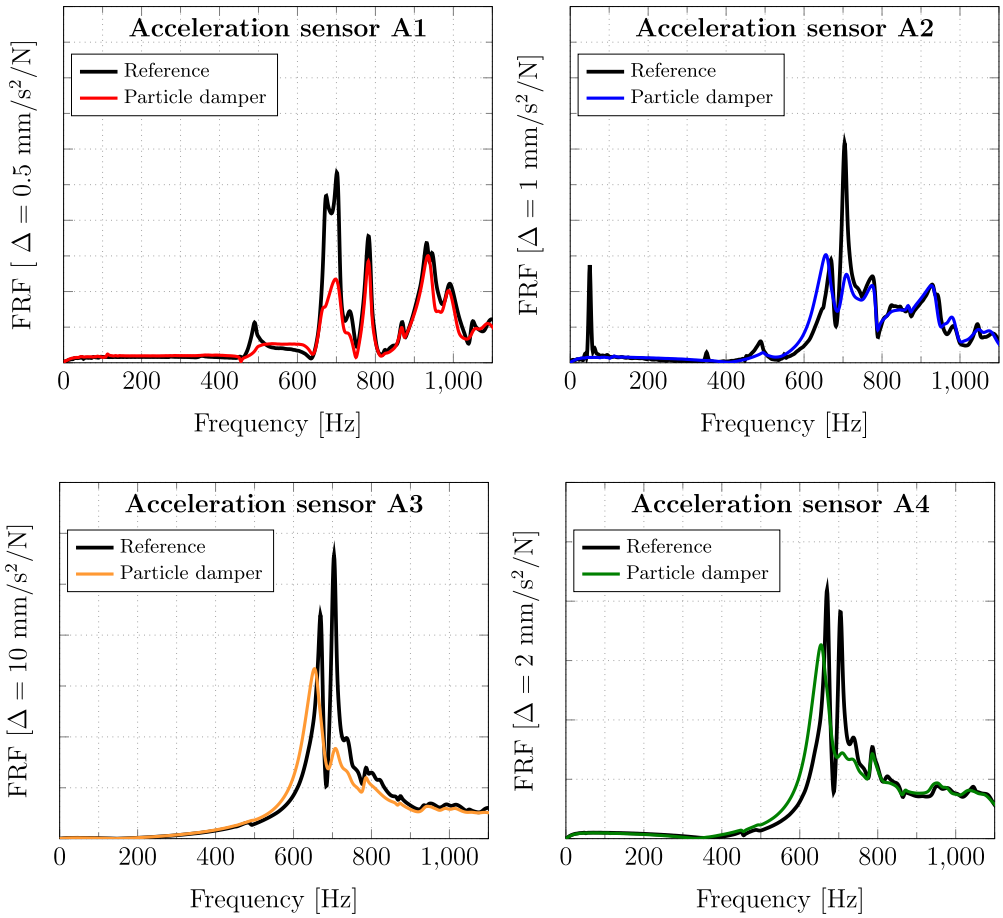

Figure 12.7: FRFs of all four acceleration sensors for the empty and partially filled PEM-attached lid.

12.5 Particle dampers for vibration mitigation in powertrains

In the previous section, the influence of the particle damper on the isolated PEM lid and PEM was successfully examined. In this section, the PEM will be integrated within the electric powertrain, and the effectiveness of the particle damper in mitigating vibrations will be experimentally evaluated under real-world load and boundary condition scenarios.

12.5.1 Experimental set up for e-drive

The experimental tests using hammer excitation on both the PEM lid and the PEM structure have demonstrated that the particle damper can effectively reduce the vibration amplitude of these components. While the previous section has demonstrated the effectiveness of particle damper designs in reducing PEM vibrations in laboratory conditions, this section explores their adaptation to more complex industrial environments. Figure 12.8 depict the experimental setup of electric powertrain test bench.

The e-drive test bench is designed to house various subsystems, including the dynamometer, measurement devices, and control systems, in an efficient and organized manner. To minimize potential noise disruptions and ensure an optimal testing environment, all subsystems, except for the power supply unit, dynamometer, and the test bench control system, are enclosed within an anechoic chamber. The test bench is divided into two distinct zones, namely the testing zone (anechoic chamber and brake

room) and the operator zone. The testing zone, which contains all the primary subsystems, is strictly restricted during testing to uphold the integrity and safety of the procedures. In contrast, the operator zone accommodates crucial equipment such as the power distribution cabinet, test control cabinet, and inverter cabinet, which allow for centralized monitoring of test activities. Additionally, the layout is designed with modularity and scalability in mind, enabling the seamless integration of additional components or subsystems as required by evolving customer demands or regulatory standards.

To withstand the increased operating temperatures, it is crucial to implement a sealing solution that is far more durable than the previously used thin plastic foil. In response to this requirement, the rubber granulate contained within the cavity of the PEM lid has been encased in a steel sheet with a minimal wall thickness of 0.15 mm.

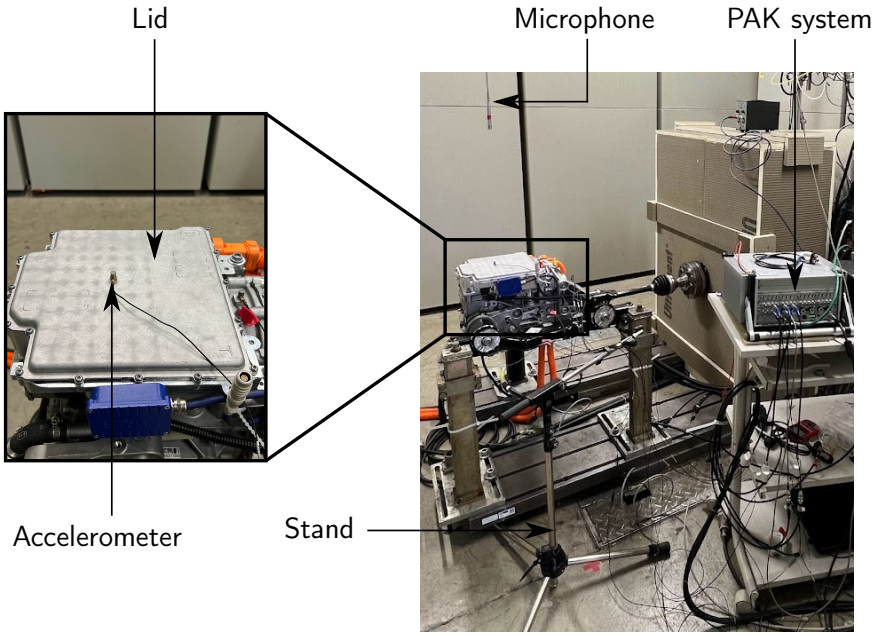

Figure 12.8: Experimental setup for assessing the vibration attenuation performance of the particle damper on the e-drive PEM.

This design decision is also influenced by the concept of TWCs discussed in Chapter 6. It has been observed that using a very thin sheet with a wall thickness much smaller than that of the primary structure leads to high-amplitude vibrations in the sheet. This phenomenon significantly enhances the transfer of kinetic energy into the granular material, which in turn improves the vibration mitigation capability of the particle damper.

To support the claim that enclosing the lid cavity with a thin steel sheet can enhance vibration reduction, comparative measurements were conducted using an alternative enclosure material, specifically a polyester fabric net. These tests were aimed at determining whether different enclosure strategies would have a noticeable impact on vibration attenuation. It was found that using the polyester fabric net as an enclosure method resulted in a negligible effect on vibration reduction (see Figures A6.27 - A6.28 in Appendix A6). This was observed despite the fact that the mass and distribution of the rubber granulate "RG 4.6 mm", remained identical in both cases, i.e. whether the granular material was enclosed within the thin steel sheet or the polyester fabric.

The observed phenomenon can be attributed to the superior internal damping properties of the polyester fabric, enabling it to dissipate vibrational energy more effectively than steel. Consequently, the kinetic energy transferred to the rubber granulate is markedly reduced compared to that induced in a thin steel sheet. Additionally, when exposed to vibrations, the fabric undergoes deformation, dispersing energy rather than oscillating in specific modes. In contrast, a thin steel sheet is prone to developing

pronounced resonant frequencies, which can amplify vibrational amplitudes. The higher stiffness of the steel plate also renders it more vulnerable to structural vibrations. Conversely, the fabric's lack of stiffness hinders efficient vibration transmission, instead promoting energy absorption and diffusion. Furthermore, the distributed fiber structure of the fabric facilitates rapid dispersion of vibrations, introducing additional damping effects. In contrast, vibrations propagate across the surface of a steel plate with minimal energy loss, resulting in higher amplitude oscillations.

The assessment of the particle damper's performance under real-world operating conditions was conducted through a two-phase experimental approach. In the first phase, the e-drive was operated at full load while performing a rotational speed sweep, beginning at 50 RPM and progressively increasing to $10,000$ RPM. This phase was designed to evaluate the damper's effectiveness across a wide range of operating speeds typically encountered in e-drive applications. The test also sought to identify the critical speed and corresponding frequency range where vibration and sound emission issues arise in electric vehicles. Furthermore, it aimed to verify whether these findings were consistent with the speed and frequency range specified by our industrial partner.

In the second phase, the e-drive was subjected to a stationary test, operating at a fixed rotational speed and torque, evaluated under a full-load testing scenario. This specific test condition was chosen to simulate a critical scenario in which vibration and sound emission issues pose significant challenges to driving comfort. By maintaining these parameters constant, the test provided valuable insights into the particle damper's ability to mitigate vibrations under demanding operating conditions.

12.5.2 Results

The acceleration-frequency plot for the full-load test scenario of the e-drive is presented in Figure 12.9. During the test, as the rotational speed of the e-drive test bench was progressively increased, three distinct acceleration peaks were observed within the frequency range of 400 Hz to 1100 Hz. These peaks occurred at approximately 557 Hz, 768 Hz, and 926 Hz. Notably, no significant acceleration peaks were detected below 400 Hz. Consequently, the frequency spectrum for this test was not plotted below 400 Hz, as no relevant data was available in that range.

It has been observed that at the third peak, the particle damper is capable of reducing the acceleration level by approximately 5.5 dB. According to our industrial partner, vibrations within the frequency range of 800 Hz to 1100 Hz are primarily responsible for generating audible noise inside the vehicle cabin. This observation is further supported by our experimental data on sound pressure level measurements. However, since acoustics is not the primary focus of this thesis, the corresponding results will not be presented here. Hence, it is evident that within this critical frequency range, the particle damper proves to be highly effective in mitigating vibrations, which could contribute to a significant reduction in interior noise levels.

However, at the first two acceleration peaks, the influence of the particle damper on vibration attenuation is negligible. This may be attributed to the distribution of the rubber granulate within the lid cavity. Since no design modifications to the lid are permitted, the distribution of the rubber particles is limited to the available spaces within the cavity. If the lid, which is bolted onto the PEM base, is considered as a clamped square plate, the first two eigenmodes would likely resemble circular patterns (2D) centered in the middle of the plate. In such a scenario, a significant portion of the rubber particles enclosed within the PEM lid may not be activated, thus limiting the effectiveness of the particle damper. However, to validate this hypothesis, further measurements would be required to analyze the eigenmodes of the lid under full-load test conditions.

Previously, the frequency range of 800 Hz to 1100 Hz has been identified as critical for e-drive vibrations. Therefore, this frequency range was selected for the stationary test to investigate the effect of the particle damper on vibration attenuation. The stationary test was conducted with the e-drive operating

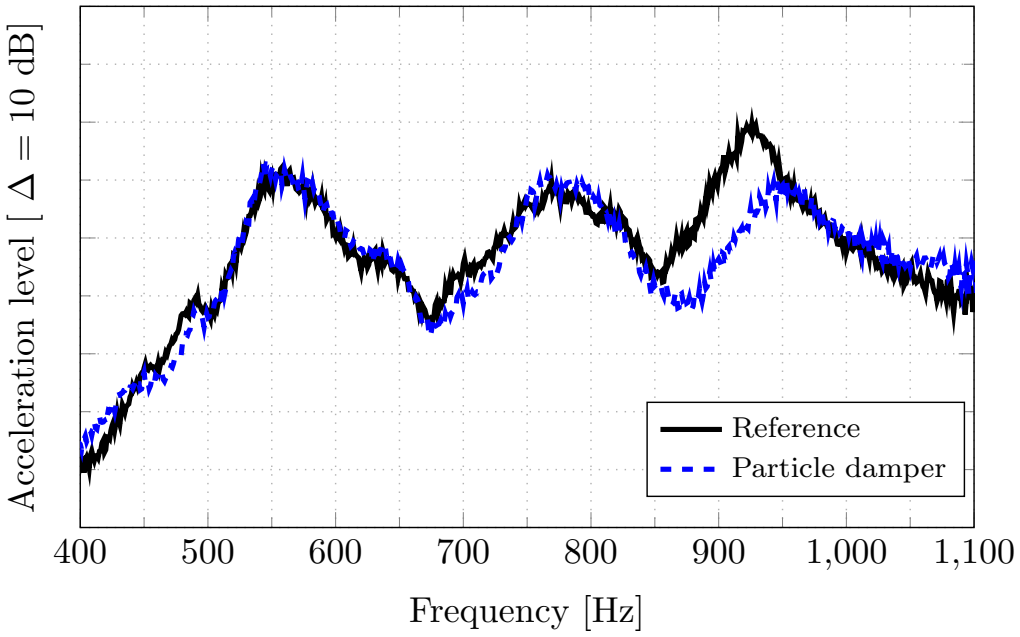

Figure 12.9: Acceleration levels of the PEM under full-load conditions, with a rotational speed sweep from 50 RPM to 1000 RPM.

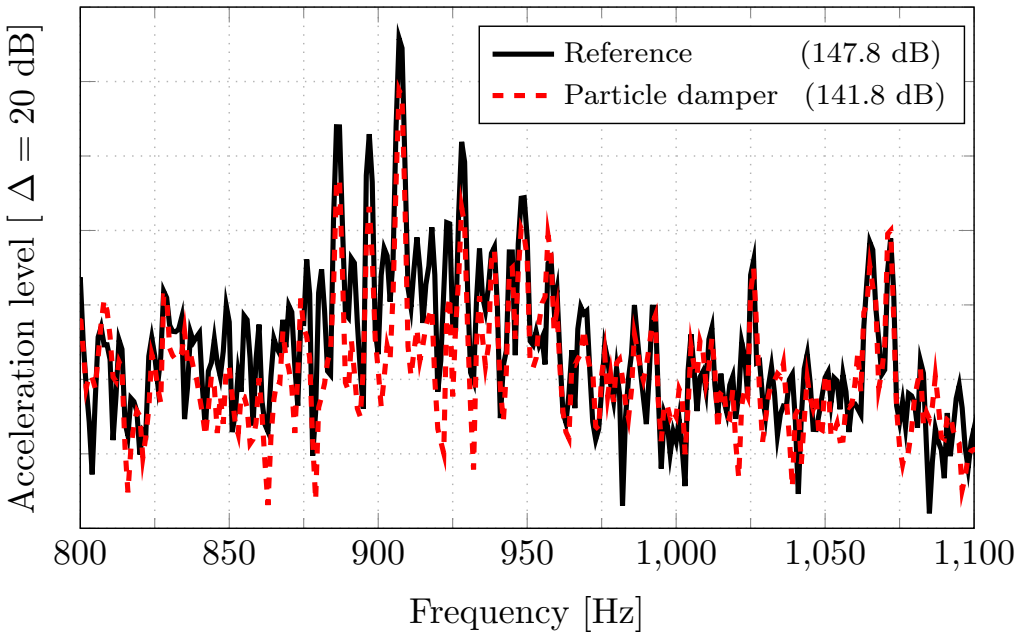

Figure 12.10: Acceleration of the PEM during a stationary test, maintaining a constant rotational speed and torque to simulate critical vibration conditions. SL values are expressed in dB.

at a fixed rotational speed and torque, both of which are known to be critical for the e-drive's NVH characteristics[4].

The acceleration value plot of the PEM during a stationary test is presented in Figure 12.10. It is

[4]Due to confidentiality agreements, the specific values for rotational speed and torque are not disclosed in this chapter.

evident that above 800 Hz, the rubber granulate "RG 4.6 mm" exhibits a significantly greater reduction in the vibration amplitude of the PEM. This effect is particularly pronounced at the resonance frequency of 897 Hz, where the particle damper achieves a maximum vibration attenuation of 9.7 dB.

Table 12.1 demonstrates a substantial reduction in vibration amplitude between 886 Hz and 1100 Hz for the PEM containing the rubber granulate. Furthermore, the overall damping performance of the particle damper in the stationary test is significantly enhanced, as indicated by the SL values, which are 147.8 dB for the reference PEM and 141.8 dB for the PEM equipped with the particle damper, reflecting a notable reduction in vibration levels.

Table 12.1: Vibration reduction of the PEM under stationary test conditions.

Frequency [Hz]	886	897	907	928	949	1026	1065
Reduction [dB]	7.0	9.7	7.3	8.8	4.1	1.1	3.2

12.6 Conclusion and discussion

This chapter evaluates the effectiveness of particle dampers in reducing PEM vibration amplitude. A key objective of this study is to examine the feasibility of applying the particle damper concepts developed and tested in this thesis to e-drive systems. As demonstrated in Chapter 11, these concepts have already proven effective in reducing vibrations in wind turbine components. The experimental investigations conducted in this chapter aim to determine whether these particle damper concepts can be directly implemented in e-drive applications without the need for additional parametric studies or modifications. Another critical aspect of this study is to preserve the structural integrity of the e-drive, following a similar approach used in wind turbine applications, where no modifications to the existing structure were made. The particle damper implementation is confined to utilizing only the available space within the current e-drive configuration, ensuring that no additional alterations or modifications to the system are required.

The experiments conducted to investigate the influence of particle dampers on e-drive vibration mitigation have been categorized into two main groups. In the first group, the lid and the PEM were isolated from the e-drive, and hammer testing was performed to analyze the effect of the particle damper. In the second group, the PEM was integrated with the e-drive, and the influence of the particle damper was studied under both full load and stationary load conditions.

The results indicate that the particle damper effectively reduces the vibration amplitude of the PEM lid across a range of resonance frequencies. Furthermore, the particle damper, initially tested in laboratory conditions, has been successfully adapted for use in complex industrial environments. To validate its effectiveness in real-world applications, a two-phase experiment was conducted. In the first phase, a rotational speed sweep, ranging from 50 RPM to 10000 RPM under full load, was performed to simulate various operating speeds encountered in electric drive systems. The second phase involved subjecting the e-drive to a fixed rotational speed and torque in a stationary state, replicating a critical condition prone to vibration and noise issues. These tests confirm the particle damper's efficacy in mitigating vibrations under diverse operating conditions, highlighting its potential for wider application in electric drive systems.

Particle dampers with rubber granulate "RG 4.6 mm" show strong potential for effective PEM vibration control in electric drives. The integration of particle dampers based on the TWC concept is further identified as a promising strategy to enhance the performance and reliability of e-drive systems by effectively suppressing vibrations. In addition, the correlation observed between the vibration reduction achieved in wind turbine components (Chapter 11) and the results obtained for e-drives highlights opportunities for future research. This connection points toward the development of a unified particle damper design approach with applicability across multiple industries.

13 Summary and Outlook

This chapter provides a comprehensive summary and discussion of the key findings presented throughout this thesis. It highlights the new insights gained from the research, emphasizing their significance and potential implications. Furthermore, the chapter explores the broader context of these findings, addressing their relevance to existing knowledge in the field. In addition to summarizing the main conclusions, an outlook on future research directions is presented, identifying potential areas for further investigation and development.

13.1 Summary and discussion

The objective of this thesis was to develop a comprehensive design framework for particle dampers by investigating their key design parameters at a laboratory scale. This study aimed to provide insights into the factors that influence the effectiveness of particle dampers, which have demonstrated robustness and utility in industrial-scale applications, particularly in wind turbine components and electric drives. Through rigorous laboratory experimentation, this research sought to identify optimal configurations and mechanisms within particle dampers, ultimately contributing to their reliable implementation in industrial-scale mechanical systems.

To establish the design framework, this research initially focused on evaluating the vibration attenuation effects of various granular materials. By systematically testing distinct materials, three particle damper concepts, namely RRPDs, HMPDs, and HPDs, were introduced, providing a foundation for a material ranking system tailored to specific applications.

Previous research on particle damper design has predominantly focused on monodisperse materials [8, 146], with limited attention given to the effects of polydispersity. While some studies have examined polydisperse rubber granulates for vibration mitigation [7, 147], they have not explicitly investigated the influence of particle size or particle size distribution (PSD) on damping performance. Additionally, prior research has generally reported that increasing the average particle size in polydisperse granular materials enhances vibration attenuation [32, 148]. However, this thesis reveals that this relationship does not always hold. To address this, this study not only examines the effect of median particle size but also investigates the role of PSD in vibration mitigation. The findings demonstrate that a broader PSD significantly improves the damping performance of RRPDs, suggesting that both median particle size and PSD must be considered for optimized damper design. This insight improves upon the conventional assumption that increasing particle size alone is sufficient to enhance damping efficiency. By explicitly analyzing these factors, this thesis offers a previously unexplored contribution to the field, providing a more comprehensive understanding of how particle characteristics influence vibration attenuation in RRPDs.

Furthermore, this study investigates the impact of nine hard granular materials on the vibration response of systems. A key finding of this study is that particle shape plays a critical role in influencing the damping performance of particle dampers. Previous investigations into the effect of particle shape on vibration attenuation have been limited and yielded conflicting results. For instance, Holkamp et al.[171] and Sanchez et al.[116] concluded that particle shape does not significantly impact damping performance, whereas Terzioglu et al.[112] found that particle shape is crucial for reducing vibration amplitude. This thesis, however, emphasizes the importance of particle shape in vibration mitigation.

Through an extensive experimental investigation into the effects of various granular materials and their mixtures on vibration attenuation, this thesis establishes that RRPDs present an optimal solution, balancing vibration mitigation, additional mass considerations, and sustainability due to their recyclable nature. Previous studies have demonstrated that higher-density granular materials are generally more effective in reducing structural vibration amplitudes [8]. On the other hand, Michon et al. [146] investigated the impact of lower-density materials on vibration mitigation and reported that while these materials are effective in the higher frequency range, their influence on lower frequency ranges is negligible. However, this research provides new insight by showing that lower-density materials, such as rubber granulate, can effectively attenuate vibrations not only in higher frequency ranges but also in lower frequency ranges, where high-density granular materials are typically less efficient.

After selecting a suitable material for the particle damper, another critical challenge addressed in this thesis is ensuring that the vibration of the main structure is sufficient to mobilize the granular particles inside the cavity. Most existing studies on particle dampers have overlooked this issue, as laboratory tests are typically conducted under high dynamic load conditions, such as on a shaker table. However, in real-world applications, structural vibrations are not always extreme, raising the concern that granular materials inside the cavity may remain stationary relative to each other, thereby diminishing their vibration-mitigation efficiency.

To solve this issue, Rongong et al. [175] proposed using a magnetic field to manipulate particle motion within the cavity to enhance damping efficiency. However, their approach is limited to specific types of granular materials. To address this broader challenge, this thesis shifts focus beyond material selection to the development of passive design variations that facilitate particle mobilization, particularly in scenarios where structural vibrations alone are insufficient to activate damping. In this context, several innovative passive design variants are introduced, namely TWC, TWC-AS, and RC. Experimental results demonstrate that these proposed designs significantly enhance the damping efficiency of particle dampers, providing a passive solution to a critical limitation in existing research and expanding the applicability of particle dampers in real-world conditions.

Building on the investigation of material selection and design variants for particle dampers, another key aspect that has not been explored in the existing literature is the long-term durability and sustained performance of particle dampers under prolonged dynamic loading. In response to this gap, this thesis presents a comprehensive experimental analysis conducted over several months, evaluating the vibration mitigation capabilities of a particle damper before and after exposure to high-amplitude dynamic loads. The results reveal that rubber granulate "RG 4.6 mm" retains stable vibration reduction even after 85 and 165 million cycles of loading. Remarkably, an improvement in vibration attenuation was observed at 330 million cycles, likely due to wear-induced changes in the particle distribution that enhance vibration control. Additionally, while cyclic temperature loading is known to influence damping behavior in particle dampers, no adverse effects were found for rubber granulate before or after exposure to cyclic temperature variations. These findings are unexplored in the literature and establish rubber granulate "RG 4.6 mm" as an efficient material choice for particle dampers, offering superior vibration reduction, minimal added mass, and exceptional resilience to both cyclic loading and temperature changes.

While laboratory results for particle dampers have been promising, their application in real-world settings has remained limited. To address this gap, this thesis takes a significant step forward by transitioning from controlled laboratory experiments to industrial-scale applications, specifically focusing on wind turbine components. Although few studies have explored particle dampers in real-world scenarios, typically limited to small-scale structures, this thesis addresses this gap by applying laboratory-scale design concepts to wind turbine components under realistic operational conditions. The successful transition from laboratory-scale studies to industrial-scale wind turbine components demonstrates the promising potential of particle dampers for large-scale applications.

This study also carried the exploration of particle dampers in the context of electric vehicle (e-

drive) systems, assessing whether these dampers could be implemented without the need for further adjustments to system parameters or structural modifications. By focusing on preserving the structural integrity of e-drive systems and utilizing only the available internal space, this approach avoids the need for any alteration to the existing configuration. The ability to seamlessly adapt particle dampers from laboratory environments to complex real-world settings, both in wind turbines and electric vehicles, marks a new direction in the practical application of vibration mitigation technologies, demonstrating their robustness, versatility, and potential for broad use across diverse industrial domains.

The findings presented in this thesis underscore the potential of particle dampers to be engineered as an effective solution for mitigating vibrations across a diverse array of industrial sectors. The research journey, which spans from controlled laboratory experiments to the development of concepts applicable at the industrial scale, has provided valuable insights into the complex dynamics that govern the efficiency of particle dampers. Key factors influencing their performance, such as the selection of appropriate materials, the design of optimal geometric configurations, and the formulation of effective deployment strategies, have been thoroughly examined and analyzed. These results not only deepen our understanding of the operational behavior of particle dampers but also lay the groundwork for their practical application in real-world engineering challenges.

13.2 Outlook

The methods and insights developed in this thesis offer a foundation for future research, advancing the field of particle dampers for complex industrial applications and paving the way for more resilient, efficient, and durable solutions to vibration challenges. Further research on hybrid particle dampers (HPDs) could significantly expand the scope of particle damper applications. By exploring optimal mixing ratios of hard and soft particles, it may be possible to enhance vibration mitigation while maintaining the low added mass characteristic of RRPDs.

This thesis has successfully demonstrated that passive design variants, such as TWC, TWC-AS, and RC, can effectively enhance vibration attenuation, particularly in scenarios where the vibration of the main structure is insufficient to mobilize the granular material within the particle damper. However, the optimal wall thickness of these structures in relation to the main structure remains an unresolved question. Numerical studies are required to fully establish this relationship. Such studies would enable the application of these concepts to various structural configurations without requiring additional testing. Moreover, the wall thickness of the TWC design can be adjusted to fine-tune its resonance frequency according to the specific requirements of the application. This tuning ability could prove especially valuable when precise damping at a targeted resonance frequency is needed, in addition to achieving broadband damping.

Preliminary results indicate that the particle damper, which was initially employed to reduce vibration amplitudes in e-drive applications, also holds promise in mitigating sound emissions within critical frequency ranges. As demonstrated in Figure 13.1, the particle damper effectively reduce sound emissions from the powertrain by 7 dB at the highest peak frequency of 907 Hz. Furthermore, at 897 Hz, a reduction of 9 dB in sound emission is observed. Therefore, the particle damper plays a significant role in reducing overall noise emissions from the electric powertrain, underscoring its potential for broader application in noise control.

A promising direction for future research involves investigating whether the design parameters optimized for vibration attenuation can also be effective in mitigating broadband sound emissions from mechanical structures. Exploring this potential could reveal the ability of particle dampers to serve dual purposes, effectively addressing both vibrational and acoustic challenges in industrial applications. Such research could significantly expand the utility of particle dampers, positioning them as valuable tools not only for reducing vibrations but also for controlling noise emissions. This would enhance the overall performance

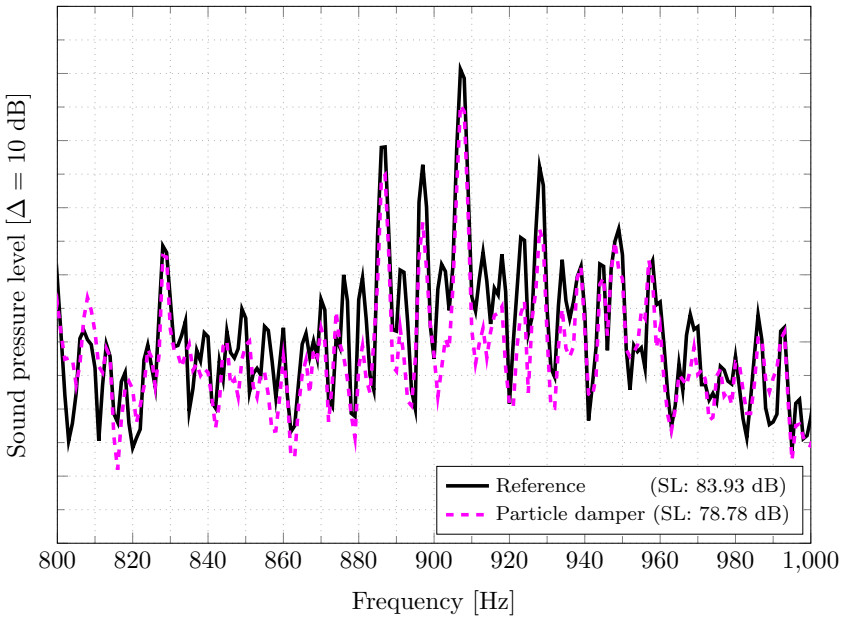

Figure 13.1: Noise reduction in the e-drive achieved through the use of a particle damper. The total sound level is given in dB.

and efficiency of mechanical systems, offering a more comprehensive solution to both vibration and noise control in various industries.

Bibliography

[1] Rezaee, M. and Aly, A. M. "Vibration control in wind turbines for performance enhancement: A comparative study". In: *Wind and Structures* 22, 2016. DOI: https://doi.org/10.12989/was.2016.22.1.107.

[2] Salt, A. N. and Hullar, T. E. "Responses of the ear to low frequency sounds, infrasound and wind turbines". In: *Hearing research* 268, 2010. DOI: https://doi.org/10.1016/j.heares.2010.06.007.

[3] Pedersen, E., Van Den Berg, F., Bakker, R., and Bouma, J. "Response to noise from modern wind farms in The Netherlands". In: *The Journal of the Acoustical Society of America* 126, 2009. DOI: https://doi.org/10.1121/1.3160293.

[4] Hansen, C. and Hansen, K. "Recent advances in wind turbine noise research". In: *Acoustics* 2, 2020. DOI: https://doi.org/10.3390/acoustics2010013.

[5] Qatu, M. S., Abdelhamid, M. K., Pang, J., and Sheng, G. "Overview of automotive noise and vibration". In: *International Journal of Vehicle Noise and Vibration* 5, 2009. DOI: https://doi.org/10.1504/IJVNV.2009.029187.

[6] Mayer, D. and Melz, T. *Advanced Materials in Automotive Engineering*. 1st ed. Elsevier, 2019.

[7] Koch, S., Duvigneau, F., Duczek, S., and Woschke, E. "Vibration reduction in automotive applications based on the damping effect of granular material". In: *Automotive acoustics conference 2017* 2, 2019. DOI: https://doi.org/10.1007/978-3-658-20251-4_3.

[8] Veeramuthuvel, P., Shankar, K., and Sairajan, K. "Experimental investigation of particle damper-based vibration suppression in printed circuit board for spacecraft applications". In: *Journal of Aerospace Engineering* 230, 2016. DOI: https://doi.org/10.1007/978-3-658-20251-4_3.

[9] Popper, A. N and Hawkins, A., eds. *The Effects of Noise on Aquatic Life*. Springer New York, NY, 2012. DOI: https://doi.org/10.1007/978-1-4419-7311-5.

[10] Baz, A. M. *Active and passive vibration damping*. 1st ed. John Wiley & Sons, 2019.

[11] Alkhatib, R. and Golnaraghi, M. "Active structural vibration control: a review". In: *Shock and Vibration Digest* 35, 2003.

[12] Min, C. "New semi-active vibration control with Serial-Stiffness-Switch-System based on vibration energy harvesting". PhD thesis. Technische Universität Ilmenau, 2018.

[13] Gardonio, P., Bianchi, E., and Elliott, S. "Design of a smart panel with multiple decentralized units for the control of sound radiation/transmission". In: *Smart Structures and Materials 2003: Smart Structures and Integrated Systems*. 2003, pp. 175–188. DOI: https://doi.org/10.1117/12.483393.

[14] Den Hamer, A., Angelis, G., and Roozen, N. "Broad-band active vibration suppression using PPF focused on industrial application". In: *IEEE/ASME Transactions On Mechatronics* 10, 20005, pp. 146–153. DOI: https://doi.org/10.1109/TMECH.2005.844718.

[15] Mahmoodi, S., Aagaah, M., and Ahmadian, M. "Active vibration control of aerospace structures using a modified positive position feedback method". In: *2009 American control conference*. 2009, pp. 4115–4120. DOI: https://doi.org/10.1109/ACC.2009.5159955.

[16] Prasad, B. B., Luft, T., Michaelsen, C., and Rottengruber, H. "Comparison of active and passive vibration control techniques for electric drive power electronic subsystem: Experimental validation". In: *INTER-NOISE and NOISE-CON Congress and Conference Proceedings*. 2024, pp. 71–82. DOI: https://doi.org/10.3397/IN-2021-1125.

[17] Jovanović, M., Simonović, A., Zorić, N., Lukić, N., Stupar, S., and Ilić, S. "Experimental studies on active vibration control of a smart composite beam using a PID controller". In: *Smart materials and structures* 22, 2013. DOI: https://10.1088/0964-1726/22/11/115038.

[18] Bronowicki, A., Abhyankar, N., and Griffin, S. "Active vibration control of large optical space structures". In: *Smart materials and structures* 8, 1999. DOI: https://10.1088/0964-1726/8/6/304.

[19] Simmers, G., Sodano, H., Park, G., and Inman, D. "Thermal protection for a self-sensing piezoelectric control system". In: *Smart materials and structures* 16, 2007, pp. 2492–2500. DOI: https://10.1088/0964-1726/16/6/053.

[20] Aridogan, U. and Basdogan, I. "A review of active vibration and noise suppression of plate-like structures with piezoelectric transducers". In: *Journal of Intelligent Material Systems and Structures* 26, 2015, pp. 1455–1476. DOI: https://doi.org/10.1177/1045389X15585896.

[21] Zoccolini, L., Bruschi, E., Cattaneo, S., and Quaglini, V. "Current trends in fluid viscous dampers with semi-active and adaptive behavior". In: *Applied Sciences* 13, 2023. DOI: https://doi.org/10.3390/app131810358.

[22] Dupont, P., Kasturi, P., and Stokes, A. "Semi-active control of friction dampers". In: *Journal of sound and vibration* 202, 1997, pp. 203–218. DOI: https://doi.org/10.1006/jsvi.1996.0798.

[23] Spencer, B., Dyke, S., Sain, M., and Carlson, J. "Phenomenological model for magnetorheological dampers". In: *Journal of engineering mechanics* 123, 1997, pp. 230–238. DOI: https://doi.org/10.1061/(ASCE)0733-9399(1997)123:3(230).

[24] Kunnath, S. *Structural Engineering and Geomechanics - Volume 3*. 1st ed. Encyclopedia of Life Support Systems(EOLSS), 2014.

[25] Soliman, A. and Kaldas, M. "Semi-active suspension systems from research to mass-market–A review". In: *Journal of Low Frequency Noise, Vibration and Active Control* 40, 2021, pp. 1005–1023. DOI: https://doi.org/10.1177/1461348419876392.

[26] Casciati, F., Rodellar, J., and Yildirim, U. "Active and semi-active control of structures–theory and applications: A review of recent advances". In: *Journal of Intelligent Material Systems and Structures* 23, 2012, pp. 1181–1195. DOI: https://doi.org/10.1177/1045389X12445029.

[27] Chatziathanasiou, G., Chrysohoidis, N., Kostas, G., and Saravanos, D. "Semi-active vibration control of aircraft structures". In: *AIAA Scitech 2021 Forum*. 2021. DOI: https://doi.org/10.2514/6.2021-1736.

[28] Rao, M. "Recent applications of viscoelastic damping for noise control in automobiles and commercial airplanes". In: *Journal of sound and vibration* 262, 2003. DOI: https://doi.org/10.1016/S0022-460X(03)00106-8.

[29] Marathe, A., Khot, S., and Nagler, J. "Development of low-cost optimal magneto-rheological damper for automotive application". In: *Journal of Vibration Engineering & Technologies* 10, 2022. DOI: https://doi.org/10.1007/s42417-022-00486-z.

[30] Ho, W., Wong, B., and England, D. "Tuned mass damper for rail noise control". In: *Proceedings of the 10th International Workshop on RailwayNoise*. 2012, pp. 89–96. DOI: https://doi.org/10.1007/978-4-431-53927-8_11.

[31] Soong, T. and Dargush, G. *Passive energy dissipation systems in structural engineering*. 1st ed. John Wiley & Sons, 1997.

[32] Panossian, H. "Structural damping enhancement via non-obstructive particle damping technique". In: *Journal of Vibration and Acoustics* 114, 1992. DOI: https://doi.org/10.1115/1.2930221.

[33] Shu, Z., You, R., and Zhou, Y. "Viscoelastic damper connected to adjacent structures involving seismic isolation". In: *Viscoelastic materials for structural dampers: A review* 342, 2022. DOI: https://doi.org/10.1016/j.conbuildmat.2022.127955.

[34] Matsagar, V. A. and Jangid, R. S. "Viscoelastic damper connected to adjacent structures involving seismic isolation". In: *Journal of civil engineering and management* 11, 2005. DOI: https://doi.org/10.1080/13923730.2005.9636362.

[35] Torvik, P. J. "Analysis of free-layer damping coatings". In: *Key Engineering Materials* 333, 2007. DOI: https://doi.org/10.4028/www.scientific.net/KEM.333.195.

[36] Kerwin, E. M. "Damping of flexural waves by a constrained viscoelastic layer". In: *The Journal of the Acoustical society of America* 31, 1959. DOI: https://doi.org/10.1121/1.1907821.

[37] Aumjaud, P., Smith, C. W., and Evans, K. E. "A novel viscoelastic damping treatment for honeycomb sandwich structures". In: *Composite Structures* 119, 2015. DOI: https://doi.org/10.1016/j.compstruct.2014.09.005.

[38] Hussaini, A. "Designing an Interior AppliedWaterborne Coating for Use in Automotive Paint Shops to Replace Sound Deadening Pads". In: *Proceedings of the SAE 2000 world congress*. 2000. DOI: https://doi.org/10.4271/2000-01-1391.

[39] Lilley, K. M., Fasse, M. J., and Weber, P. E. "A comparison of nvh treatments for vehicle floorpan applications". In: *Proceedings of the 2001 Noise and Vibration Conference*. 2001. DOI: https://doi.org/10.4271/2001-01-1464.

[40] Lu, J., Pyper, J., Weber, R., and Fisk, J. "Windshields with new PVB interlayer for vehicle interior noise reduction and sound quality improvement". In: *SAE transactions* 112, 2003.

[41] Gao, P. X., Zhai, J. Y., Qu, F. Z., and Han, Q. "Vibration and damping analysis of aerospace pipeline conveying fluid with constrained layer damping treatment". In: *Proceedings of the Institution of Mechanical Engineers, Part G: Journal of Aerospace Engineering*. 2018. DOI: https://doi.org/10.1177/0954410017692367.

[42] Henze, D., Karam, R., and Jeans, A. "Effects of constrained-layer damping on the dynamics of a type 4 in-line head suspension". In: *IEEE transactions on magnetics* 26, 1990. DOI: https://doi.org/10.1109/20.104757.

[43] Wang, L., Cheng, T., Tang, X., and Qian, J. "Vibration and damping analysis of carbon fiber wind turbine blade with viscoelastic damping treatment". In: *Advanced Materials Research* 1008, 2014. DOI: https://doi.org/10.4028/www.scientific.net/AMR.1008-1009.192.

[44] Yang, F., Sedaghati, R., and Esmailzadeh, E. "Vibration suppression of structures using tuned mass damper technology: A state-of-the-art review". In: *Journal of Vibration and Control* 28, 20222, pp. 812–836. DOI: https://doi.org/10.1177/1077546320984305.

[45] Frahm, H. "Device for damping vibrations of bodies". In: *US patent* 989, 1909.

[46] Hunt, J. and Nissen, J. "The broadband dynamic vibration absorber". In: *Journal of sound and vibration* 83, 1982. DOI: https://doi.org/10.1016/S0022-460X(82)80108-9.

[47] Zhang, M. and Xu, F. "Tuned mass damper for self-excited vibration control: Optimization involving nonlinear aeroelastic effect". In: *Journal of Wind Engineering and Industrial Aerodynamics* 220, 2022. DOI: https://doi.org/10.1016/j.jweia.2021.104836.

[48] Goodarzi, A., Pandarathil, N., and Esmailzadeh, E. "Vibration Control of Vehicles With Flexible Structure Using Optimum Tuned-Mass Dampers". In: *International Design Engineering Technical Conferences and Computers and Information in Engineering Conference*. 2010, pp. 121–128. DOI: https://doi.org/10.1115/DETC2010-28251.

[49] Stewart, G. M. and Lackner, M. A. "The impact of passive tuned mass dampers and wind–wave misalignment on offshore wind turbine loads". In: *Engineering structures* 73, 2014, pp. 54–61. DOI: https://doi.org/10.1016/j.engstruct.2014.04.045.

[50] Rahimi, F., Aghayari, R., and Samali, B. "Application of tuned mass dampers for structural vibration control: a state-of-the-art review". In: *Civil Engineering Journal* 6, 2020, pp. 1622–1651. DOI: https://doi.org/10.28991/cej-2020-03091571.

[51] Aly, A. "Vibration control of high-rise buildings for wind: a robust passive and active tuned mass damper". In: *Smart Structures and Systems* 13, 2014, pp. 473–500. DOI: https://doi.org/10.12989/sss.2014.13.3.473.

[52] Soto, M. and Adeli, H. "Tuned mass dampers". In: *Archives of Computational Methods in Engineering* 20, 2013, pp. 419–431. DOI: https://doi.org/10.1007/s11831-013-9091-7.

[53] Schönle, A. and Gnanasambandham, C. and Eberhard, P. "Broadband damping properties of particle dampers mounted to dynamic structures". In: *Experimental Mechanics* 62, 2022, pp. 1569–1578. DOI: https://doi.org/10.1007/s11340-022-00882-2.

[54] Pall, A., Marsh, C., and Fazio, P. "Friction joints for seismic control of large panel structures". In: *Journal of Prestressed Concrete Institute* 25, 1980. DOI: https://doi.org/10.15554/pcij.11011980.38.61.

[55] Jaisee, S., Yue, F., and Ooi, Y. "A state-of-the-art review on passive friction dampers and their applications". In: *Engineering Structures* 235, 2021. DOI: https://doi.org/10.1016/j.engstruct.2021.112022.

[56] Gagnon, L., Morandini, and Ghiringhelli, G. "A review of friction damping modeling and testing". In: *Archive of Applied Mechanics* 90, 2020. DOI: https://doi.org/10.1007/s00419-019-01600-6.

[57] Pesaresi, L., Stender, M., Ruffini, V., and Schwingshackl, C. "DIC measurement of the kinematics of a friction damper for turbine applications". In: *Proceedings of the 35th IMAC, A Conference and Exposition on Structural Dynamics*. 2017, pp. 93–101. DOI: https://doi.org/10.1007/978-3-319-54930-9_9.

[58] Perkowski, W. "Dry friction damper for supercritical drive shaft". In: *Journal of KONES* 23, 2016. DOI: http://dx.doi.org/10.5604/12314005.1217255.

[59] Sanati, M., Khadem, S., Mirzabagheri, S., Sanati, H., and Khosravieh, M. "Performance evaluation of a novel rotational damper for structural reinforcement steel frames subjected to lateral excitations". In: *Earthquake Engineering and Engineering Vibration* 13, 2014, pp. 75–84. DOI: https://doi.org/10.1007/s11803-014-0213-5.

[60] Bagheri, S., Barghian, M., Saieri, F., and Farzinfar, A. "U-shaped metallic-yielding damper in building structures: Seismic behavior and comparison with a friction damper". In: *Structures* 3, 2015, pp. 163–171. DOI: https://doi.org/10.1016/j.istruc.2015.04.003.

[61] Jugulkar, L. M., Singh, S., and Sawant, S. M. "Fluid flow modeling and experimental investigation on automobile damper". In: *Construction and Building Materials* 121, 2016, pp. 760–772. DOI: https://doi.org/10.1016/j.conbuildmat.2016.05.142.

[62] Narkhede, D. I. and Sinha, R. "Behavior of nonlinear fluid viscous dampers for control of shock vibrations". In: *Journal of Sound and Vibration* 333, 2014, pp. 80–98. DOI: https://doi.org/10.1016/j.jsv.2013.08.041.

[63] Pistek, V., Klimes, L., Mauder, T., and Kucera, P. "Optimal design of structure in rheological models: an automotive application to dampers with high viscosity silicone fluids". In: *Journal of Vibroengineering* 19, 2017. DOI: https://doi.org/10.21595/jve.2017.18348.

[64] Taylor, D. and Constantinou, M. "Testing procedures for high output fluid viscous dampers used in building and bridge structures to dissipate seismic energy". In: *Shock and Vibration* 2, 1995, pp. 373–381. DOI: https://doi.org/10.3233/SAV-1995-2503.

[65] Symans, M. and Constantinou, M. "Passive fluid viscous damping systems for seismic energy dissipation". In: *ISET Journal of Earthquake Technology* 35, 1998, pp. 185–206.

[66] Harris, D. *Noise Control Manual: Guidelines for Problem-Solving in the Industrial/Commercial Acoustical Environment*. 1st ed. Springer, 1991.

[67] Kelly, J. "Base isolation: linear theory and design". In: *Earthquake spectra* 6, 1990, pp. 223–244. DOI: https://doi.org/10.1193/1.1585566.

[68] Luca, A. and Guidi, L. "State of art in the worldwide evolution of base isolation design". In: *Soil Dynamics and Earthquake Engineering* 125, 2019. DOI: https://doi.org/10.1016/j.soildyn.2019.105722.

[69] Wenbin, S., Zhen-Hua, L., and Jianjun, S. "Finite element analysis of static elastic characteristics of the rubber isolators in automotive dynamic systems". In: *SAE transactions* 112, 2003, pp. 185–193. DOI: https://www.jstor.org/stable/44745387.

[70] Park, C., Shim, H., Choi, D., Kim, J., and Lee, S. "Shape optimization of rubber isolators in automotive cooling modules for the maximization of vibration isolation and fatigue life". In: *International Journal of Automotive Technology* 13, 2012, pp. 61–75. DOI: https://doi.org/10.1007/s12239-012-0006-7.

[71] Zolfagharian, A., Picken, P., Bodaghi, M., Fard, M., and Rolfe, B. "Additive manufacturing of composite foam metamaterial springs for vibration isolation". In: *Advanced Engineering Materials* 25, 2023. DOI: https://doi.org/10.1002/adem.202300356.

[72] Paget, A. L. "Vibration in steam turbine buckets and damping by impacts". In: *Engineering* 143, 1937.

[73] Rocke, R. and Masri, S. "Application of a single-particle impact damper to an antenna structure". In: *The Shock and Vibration Bulletin* 39, 1968.

[74] Ema, S. and Marui, E. "Damping characteristics of an impact damper and its application". In: *International Journal of machine tools and manufacture* 36, 1996. DOI: https://doi.org/10.1016/0890-6955(95)00073-9.

[75] Ogawa, K., Ide, T., and Saitou, T. "Application of impact mass damper to a cable-stayed bridge pylon". In: *Journal of wind engineering and industrial aerodynamics* 36, 1997. DOI: https://doi.org/10.1016/S0167-6105(97)00265-1.

[76] Galarza, F. A. M., Albuquerque, M. V. de, Antonialli, A. S., Pederiva, R., and Diniz, A. E. "Design and experimental evaluation of an impact damper to be used in a slender end mill tool in the machining of hardened steel". In: *The International Journal of Advanced Manufacturing Technology* 106, 2020. DOI: https://doi.org/10.1007/s00170-019-04786-9.

[77] Gagnon, L., Morandini, M., and Ghiringhelli, G. L. "A review of particle damping modeling and testing". In: *Journal of Sound and Vibration* 459, 2019. DOI: https://doi.org/10.1016/j.jsv.2019.114865.

[78] Lu, Z., Wang, Z., Masri, S. F., and Lu, X. "Particle impact dampers: Past, present, and future". In: *Structural Control and Health Monitoring* 25, 2018. DOI: https://doi.org/10.1002/stc.2058.

[79] Fowler, B. L., Flint, E. M., and Olson, S. E. "Effectiveness and predictability of particle damping". In: *Smart Structures and Materials 2000: Damping and Isolation*. 2000, pp. 356–367. DOI: https://doi.org/10.1117/12.384576.

[80] Chesa, O., Stelzer, R., Courtois, T., and Zogg, M. "Efficiency of particle damping on lightweight cfrp structures". In: *SAE Technical Paper*, 2019. DOI: https://doi.org/10.4271/2019-01-6000.

[81] Ma, C. and Zheng, L. and Wang, D. and Wang, Z. "Study on the damping mechanisms of a suspended particle damper attached to a wind turbine tower". In: *Wind. Struct* 33, 2021, pp. 103–114.

[82] Bapat, C. N. and Sankar, S. "Single unit impact damper in free and forced vibration". In: *Journal of Sound and Vibration* 99, 1985, pp. 85–94. DOI: https://doi.org/10.1016/0022-460X(85)90446-8.

[83] Friend, R. D. and Kinra, V. K. "Particle impact damping". In: *Journal of Sound and Vibration* 233, 2000, pp. 93–118. DOI: https://doi.org/10.1006/jsvi.1999.2795.

[84] Vinayaravi, R., Kumaresan, D., Jayaraj, K., Asraff, A. K., and Muthukumar, R. "Experimental investigation and theoretical modelling of an impact damper". In: *Journal of Sound and Vibration* 332, 2013, pp. 1324–1334. DOI: https://doi.org/10.1016/j.jsv.2012.10.032.

[85] Olson, S. E. "An analytical particle damping model". In: *Journal of Sound and Vibration* 264, 2003, pp. 1155–1166. DOI: https://doi.org/10.1016/S0022-460X(02)01388-3.

[86] Saeki, M. "Analytical study of multi-particle damping". In: *Journal of Sound and Vibration* 281, 2005, pp. 1133–1144. DOI: https://doi.org/10.1016/j.jsv.2004.02.034.

[87] Zalewski, R. and Szmidt, T. "Application of Special Granular Structures for semi-active damping of lateral beam vibrations". In: *Engineering Structures* 65, 2014, pp. 13–20. DOI: https://doi.org/10.1016/j.engstruct.2014.01.035.

[88] Szmidt, T. and Zalewski, R. "Inertially excited beam vibrations damped by Vacuum Packed Particles". In: *Smart Materials and Structures* 65, 2014, p. 105026. DOI: https://doi.org/10.1088/0964-1726/23/10/105026.

[89] Mishra, B.K. and Mehrotra, S.P. "A jig model based on the discrete element method and its experimental validation". In: *International Journal of Mineral Processing* 63, 2001, pp. 177–189. DOI: https://doi.org/10.1016/S0301-7516(01)00053-9.

[90] Alian, M. and Ein-Mozaffari, F. and Upreti, S.R. "Analysis of the mixing of solid particles in a plowshare mixer via discrete element method (DEM)". In: *Powder Technology* 274, 2015, pp. 77–87. DOI: https://doi.org/10.1016/j.powtec.2015.01.012.

[91] Cleary, P.W. "A multiscale method for including fine particle effects in DEM models of grinding mills". In: *Minerals Engineering* 84, 2015, pp. 88–99. DOI: https://doi.org/10.1016/j.mineng.2015.10.008.

[92] Ng, T. T. and Dobry, R. "Numerical simulations of monotonic and cyclic loading of granular soil". In: *Journal of Geotechnical Engineering* 120, 1994, pp. 388–403. DOI: https://doi.org/10.1061/(ASCE)0733-9410(1994)120:2(388).

[93] Chen, C. and McDowell, G.R. and Thom, N.H. "Discrete element modelling of cyclic loads of geogrid-reinforced ballast under confined and unconfined conditions". In: *Geotextiles and Geomembranes* 35, 2012, pp. 76–86. DOI: https://doi.org/10.1016/j.geotexmem.2012.07.004.

[94] Zhou, H. and Chen, Y. and Sadek, M.A. "Modelling of soil–seed contact using the Discrete Element Method (DEM)". In: *Biosystems Engineering* 121, 2014, pp. 56–66. DOI: https://doi.org/10.1016/j.biosystemseng.2014.02.006.

[95] Richter, C. and Roessler, T. and Otto, H. and Katterfeld, A. "Coupled discrete element and multibody simulation, part I: implementation, verification and validation". In: *Powder Technology* 379, 2021, pp. 494–504. DOI: https://doi.org/10.1016/j.powtec.2020.10.074.

[96] Cundall, P.A. and Strack, O. "A distinct element model for granular assemblies". In: *Geotechnique* 29, 1979, pp. 47–65.

[97] Meyer, N.-K. "Systematic design of particle dampers for passive vibration attenuation". PhD thesis. Technische Universität Hamburg, 2023.

[98] Zhang, K. and Chen, T. and Wang, X. and Fang, J. "Rheology behavior and optimal damping effect of granular particles in a non-obstructive particle damper". In: *Journal of Sound and Vibration* 364, 2016, pp. 30–43. DOI: https://doi.org/10.1016/j.jsv.2008.06.027.

[99] Romdhane, M. B. and Bouhaddi, N. and Trigui, M. and Foltête, E. and Haddar, M. "The loss factor experimental characterisation of the non-obstructive particles damping approach". In: *Mechanical Systems and Signal Processing* 38, 2013, pp. 585–600. DOI: https://doi.org/10.1016/j.ymssp.2013.02.006.

[100] Meyer, N. and Seifried, R. "Numerical and experimental investigations in the damping behavior of particle dampers attached to a vibrating structure". In: *Computers & structures* 238, 2020, p. 106281. DOI: https://doi.org/10.1016/j.compstruc.2020.106281.

[101] Biondani, F. and Morandini, M. and Ghiringhelli, G. L. and Terraneo, M. and Cordisco, P. "Efficient Discrete Element Modeling of Particle Dampers". In: *Processes* 10, 2022, p. 1247. DOI: https://doi.org/10.3390/pr10071247.

[102] Yang, M. Y., Lesieutre, G. A., Hambric, S. A., and Koopmann, G. H. "Development of a design curve for particle impact dampers". In: *Smart Structures and Materials 2004: Damping and Isolation*. 2004, pp. 450–465. DOI: https://doi.org/10.1117/12.540019.

[103] Wong, C. X. and Daniel, M. C. and Rongong, J. A. "Energy dissipation prediction of particle dampers". In: *Journal of sound and vibration* 319, 2009, pp. 91–118. DOI: https://doi.org/10.1016/j.jsv.2008.06.027.

[104] Duan, Y. and Chen, Q. "Simulation and experimental investigation on dissipative properties of particle dampers". In: *Journal of Vibration and Control* 17, 2011, pp. 777–788. DOI: https://doi.org/10.1177/1077546309356183.

[105] Trigui, M. and Foltête, E. and Bouhaddi, N. "Prediction of the dynamic response of a plate treated by particle impact damper". In: *Proceedings of the Institution of Mechanical Engineers, Part C: Journal of Mechanical Engineering Science* 228, 2014, pp. 799–814. DOI: https://doi.org/10.1177/0954406213491907.

[106] Meyer, N. and Seifried, R. "Toward a design methodology for particle dampers by analyzing their energy dissipation". In: *Computational Particle Mechanics* 8, 2021, pp. 681–699. DOI: https://doi.org/10.1007/s40571-020-00363-0.

[107] Guo, H., Ichikawa, K., Sakai, H., Zhang, H., and Takezawa, A. "Numerical and experimental analysis in the energy dissipation of additively-manufactured particle dampers based on complex power method". In: *Computational Particle Mechanics* 10, 2023, pp. 1–15. DOI: https://doi.org/10.1007/s40571-022-00540-3.

[108] Chen, T., Mao, K., Huang, X., and Wang, M. Y. "Dissipation mechanisms of nonobstructive particle damping using discrete element method". In: *Smart Structures and Materials 2001: Damping and Isolation*. 2001, pp. 294–301. DOI: https://doi.org/10.1117/12.432713.

[109] Salueña, C., Esipov, S. E., Pöschel, T., and Simonian, S. S. "Dissipative properties of granular ensembles". In: *Smart Structures and Materials 1998: Passive Damping and Isolation*. 1998, pp. 23–29. DOI: https://doi.org/10.1117/12.310696.

[110] Salueña, C., Pöschel, T., and Esipov, S. E. "Dissipative properties of vibrated granular materials". In: *Physical Review E* 59, 1999, p. 4422. DOI: https://doi.org/10.1103/PhysRevE.59.4422.

[111] Pourtavakoli, H., Parteli, E., and Pöschel, T. "Granular dampers: does particle shape matter?" In: *New Journal of Physics* 18, 2016. DOI: https://doi.org/10.1088/1367-2630/18/7/073049.

[112] Terzioglu, F., Rongong, J., and Lord, C. "Influence of particle sphericity on granular dampers operating in the bouncing bed motional phase". In: *Journal of Sound and Vibration* 554, 2023. DOI: https://doi.org/10.1016/j.jsv.2023.117690.

[113] Wong, C., Daniel, M., and Rongong, J. "Prediction of the amplitude dependent behaviour of particle dampers". In: *48th AIAA/ASME/ASCE/AHS/ASC Structures, Structural Dynamics, and Materials Conference*. 2007. DOI: https://doi.org/10.2514/6.2007-2043.

[114] Ito, T., Fujita, K., and Okaya, N. "Effects of vessel configurations on the damping effects of an impact damper using an elasto-plastic material". In: *Proceedings of the International Design Engineering Technical Conferences and Computers and Information in Engineering Conference*. 2007, pp. 179–186. DOI: https://doi.org/10.1115/DETC2007-35156.

[115] Lu, G., Third, J., and Müller, C. "Discrete element models for non-spherical particle systems: From theoretical developments to applications". In: *Chemical Engineering Science* 127, 2015, pp. 425–465. DOI: https://doi.org/10.1016/j.ces.2014.11.050.

[116] Sánchez, M., Carlevaro, C. M., and Pugnaloni, A. L. "Effect of particle shape and fragmentation on the response of particle dampers". In: *Journal of Vibration and Control* 20, 2014, pp. 1846–1854. DOI: https://doi.org/10.1177/1077546313480544.

[117] Terzioglu, F., Rongong, J., and Lord, C. "Motional phase maps for estimating the effectiveness of granular dampers". In: *Mechanical Systems and Signal Processing* 188, 2023. DOI: https://doi.org/10.1016/j.ymssp.2022.110038.

[118] Annabattula, R., Gan, Y., and Kamlah, M. "Mechanics of binary and polydisperse spherical pebble assembly". In: *Fusion Engineering and Design* 87, 2012, pp. 853–858. DOI: https://doi.org/10.1016/j.fusengdes.2012.02.033.

[119] Sinnott, M. and Cleary, P. "The effect of particle shape on mixing in a high shear mixer". In: *Computational Particle Mechanics* 3, 2016, pp. 477–504. DOI: https://doi.org/10.1007/s40571-015-0065-4.

[120] Stahl, M. and Konietzky, H. "Discrete element simulation of ballast and gravel under special consideration of grain-shape, grain-size and relative density". In: *Granular Matter* 13, 2011, pp. 417–428. DOI: https://doi.org/10.1007/s10035-010-0239-y.

[121] Pöschel, T. and Schwager, T. *Computational granular dynamics: models and algorithms*. 1st ed. Springer Science & Business Media, 2005.

[122] Ferellec, J. and McDowell, G. "A method to model realistic particle shape and inertia in DEM". In: *Granular Matter* 12, 2010, pp. 459–467. DOI: https://doi.org/10.1007/s10035-010-0205-8.

[123] Markauskas, D. and Kačianauskas, R. "Investigation of rice grain flow by multi-sphere particle model with rolling resistance". In: *Granular Matter* 13, 2011, pp. 143–148. DOI: https://doi.org/10.1007/s10035-010-0196-5.

[124] Coetzee, C. "Review: Calibration of the discrete element method". In: *Powder Technology* 310, 2017, pp. 104–142. DOI: https://doi.org/10.1016/j.powtec.2017.01.015.

[125] Parteli, E. "Using LIGGGHTS for performing DEM simulations of particles of complex shapes with the multisphere method". In: *EM6-6th International Conference on Discrete Element Methods and Related Techniques*. 2013, pp. 217–222.

[126] Elmqvist, H., Goteman, A., Roxling, V., and Ghandriz, T. "Generic modelica framework for MultiBody contacts and discrete element method". In: *Proceedings of the 11th International Modelica Conference, Versailles, France*. 2015, pp. 427–440.

[127] Sánchez, and Pugnaloni, L. "Effective mass overshoot in single degree of freedom mechanical systems with a particle damper". In: *Journal of Sound and Vibration* 330, 2011, pp. 5812–5819. DOI: https://doi.org/10.1016/j.jsv.2011.07.016.

[128] Balevičius, R. and Mróz, Z. "The combined slip and finite sliding models in a frictional contact interaction of two spherical particles". In: *Procedia Engineering* 57, 2013, pp. 167–174. DOI: https://doi.org/10.1016/j.proeng.2013.04.024.

[129] Holmes, M., Brown, R., Wauters, P., Lavery, N., and Brown, S. "Bending and twisting friction models in soft-sphere discrete element simulations for static and dynamic problems". In: *Applied Mathematical Modelling* 40, 2016, pp. 3655–3670. DOI: https://doi.org/10.1016/j.apm.2015.10.026.

[130] Lin, M. and Gottschalk, S. "Collision detection between geometric models: A survey". In: *Proc. of IMA conference on mathematics of surfaces*. 1998, pp. 602–608.

[131] Rousset, A., Checkaraou, A. W. M., Liao, Y., Besseron, X., Varrette, S., and Peters, B. "Comparing broad-phase interaction detection algorithms for multiphysics DEM applications". In: *AIP Conference Proceedings*. 2018, pp. 1–4. DOI: https://doi.org/10.1063/1.5043900.

[132] Mao, K., Wang, M. Y., Xu, Z., and Chen, T. "Simulation and characterization of particle damping in transient vibrations". In: *Journal of Vibration and Acoustics* 126, 2004, pp. 202–211. DOI: https://doi.org/10.1115/1.1687401.

[133] Mao, K., Wang, M. Y., Xu, Z., and Chen, T. "DEM simulation of particle damping". In: *Powder Technology* 142, 2004, pp. 154–165. DOI: https://doi.org/10.1016/j.powtec.2004.04.031.

[134] Lu, Z. and Masri, S. F. and Lu, X. "Parametric studies of the performance of particle dampers under harmonic excitation". In: *Structural Control and Health Monitoring* 18, 2011, pp. 79–98. DOI: https://doi.org/10.1002/stc.359.

[135] Meyer, N. and Seifried, R. "Energy dissipation in horizontally driven particle dampers of low acceleration intensities". In: *Nonlinear dynamics* 4, 2022, pp. 3009–3024. DOI: https://doi.org/10.1007/s11071-022-07348-z.

[136] Luo, B., Xu, Y., Xu, G., Liu, Q., and Xiao, "Research on Low Frequency Vibration Reduction of Transformers Based on Particle Damping". In: *2022 5th World Conference on Mechanical Engineering and Intelligent Manufacturing (WCMEIM)*. 2022, pp. 224–229. DOI: https://doi.org/10.1109/WCMEIM56910.2022.10021524.

[137] Song, C. and Han, Y. and Jia, B. and Xiong, X. and Jiang, Y. and Wang, P. and Liang, Y. and Fang, H. "Analysis of vibration reduction performance of vibration isolation system based on particle damping". In: *Journal of Low Frequency Noise, Vibration and Active Control* 17, 2024. DOI: https://doi.org/10.1177/14613484241235807.

[138] Zhang, K. and Chen, T. and He, L. "Damping behaviors of granular particles in a vertically vibrated closed container". In: *Powder technology* 321, 2017, pp. 173–179. DOI: https://doi.org/10.1016/j.powtec.2017.08.020.

[139] Yin, Z., Su, F., and Zhang, H. "Investigation of the energy dissipation of different rheology behaviors in a non-obstructive particle damper". In: *Powder Technology* 321, 2017, pp. 270–275. DOI: https://doi.org/10.1016/j.powtec.2017.07.090.

[140] Eshuis, P., Van Der Weele, K., Van Der Meer, D., Bos, R., and Lohse, D. "Phase diagram of vertically shaken granular matter". In: *Physics of Fluids* 19, 2007. DOI: https://doi.org/10.1063/1.2815745.

[141] Ansari, I. H. and Alam, M. "Patterns and velocity field in vertically vibrated granular materials". In: *AIP Conference Proceedings*. 2013, pp. 775–778. DOI: https://doi.org/10.1063/1.4812046.

[142] Lin, C., Alehashem, S., Wang, Y., and Ni, Y. "Model Development Of A New Rail Particle Damper And Parameter Optimization Using Fem-Dem Coupling Approach". In: *2022 8th world conference on structural control and monitoring (WCSCM)*. 2022, pp. 1–8.

[143] Liao, C., Chung, Y., and Weng, C. "A study on the energy dissipation mechanism of dynamic mechanical systems with particle dampers by using the novel energy method". In: *Nonlinear Dynamics* 111, 2023, pp. 15955–15980. DOI: https://doi.org/10.1007/s11071-023-08698-y.

[144] Xiao, W., Dai, Y., Peng, H., Zhang, X., Ren, X., and Liu, Q. "Research on vibration suppression of satellite bearing cylinder based on particle damping". In: *Advances in Space Research* 72, 2023, pp. 4485–4502. DOI: https://doi.org/10.1016/j.asr.2023.08.024.

[145] Simonian, S. "Particle damping applications". In: *45th AIAA/ASME/ASCE/AHS/ASC Structures, Structural Dynamics and Materials Conference*. 2004. DOI: https://doi.org/10.2514/6.2004-1906.

[146] Michon, G., Almajid, A., and Aridon, G. "Soft hollow particle damping identification in honeycomb structures". In: *Journal of Sound and Vibration* 332, 2013, pp. 536–544. DOI: https://doi.org/10.1016/j.jsv.2012.09.024.

[147] Bustamante, M., Gerges, S., Vergara, E., and Arenas, J. "High damping characteristics of an elastomer particle damper". In: *International Journal of Acoustics and Vibration* 21, 2016, pp. 112–121.

[148] Ye, H., Wang, Y., Liu, B., and Jiang, X. "Experimental study on the damping effect of multi-unit particle dampers applied to bracket structure". In: *Applied Sciences* 9, 2019. DOI: https://doi.org/10.3390/app9142912.

[149] Duvigneau, F., Koch, S., Woschke, E., and Gabbert, U. "An effective vibration reduction concept for automotive applications based on granular-filled cavities". In: *Journal of Vibration and Control* 24, 2018, pp. 73–82. DOI: https://doi.org/10.1177/1077546316632932.

[150] Koch, S., Duvigneau, F., Orszulik, R., Gabbert, U., and Woschke, E. "Partial filling of a honeycomb structure by granular materials for vibration and noise reduction". In: *Journal of Sound and Vibration* 393, 2017, pp. 30–40. DOI: https://doi.org/10.1016/j.jsv.2016.11.024.

[151] Liming, S., Wangqiang, X., Zeguang, L., Haiquan, G., and Zhe, Y. "Research on mining truck vibration control based on particle damping". In: *IOP Conference Series: Materials Science and Engineering*. 2018. DOI: 10.1088/1757-899X/324/1/012011.

[152] Xu, Z., Wang, M., and Chen, T. "A particle damper for vibration and noise reduction". In: *Journal of Sound and Vibration* 270, 2004, pp. 1033–1040.

[153] Sims, N. D., Amarasinghe, A., and Ridgway, K. "Particle dampers for workpiece chatter mitigation". In: *ASME International Mechanical Engineering Congress and Exposition*. 2005, pp. 825–832. DOI: https://doi.org/10.1115/IMECE2005-82687.

[154] Chan, K. W., Liao, W. H., Wang, M. Y., and Choy, P. K. "Experimental studies for particle damping on a bond arm". In: *Journal of Vibration and Control* 12, 2006, pp. 297–312. DOI: https://doi.org/10.1177/1077546306063257.

[155] Kumar S.M.and Mohanasundaram, K. and Sathishkumar, B. "A case study on vibration control in a boring bar using particle damping". In: *International Journal of Engineering, Science and Technology* 3, 2011, pp. 177–184.

[156] Muthu, E., Dashora, S., and Nandakumar, P. "Experimental Investigation of Particle Impact Damping On Machine Tools". In: *IOP Conference Series: Materials Science and Engineering*. 2020, pp. 1–6.

[157] Goehler, H., Jehring, U., Meinert, J., Hauser, R., Quadbeck, P., Kuemmel, K., and Stephani G.and Kieback, B. "Functionalized metallic hollow sphere structures". In: *Advanced Engineering Materials* 16, 2014, pp. 335–339. DOI: https://doi.org/10.1002/adem.201300057.

[158] Xiao, W., Huang, Y., Jiang, H., Lin, H., and Li, J. "Energy dissipation mechanism and experiment of particle dampers for gear transmission under centrifugal loads". In: *Particuology* 27, 2016, pp. 40–50. DOI: https://doi.org/10.1016/j.partic.2015.10.007.

[159] Jin, G., Zhao, Z., Liu, B., Cun, W., Zhao, Z., Hou, M., and Chen, G. "Design of a particle damper and experimental study on vibration damping of the pipeline". In: *Advances in Mechanical Engineering* 13, 2021. DOI: https://doi.org/10.1177/16878140211044923.

[160] An, S. Q., Zou, H. R., Li, W. H., and Deng, Z. C. "Experimental Investigation on the Vibration Attenuation of Tensegrity Prisms Integrated with Particle Dampers". In: *Acta Mechanica Solida Sinica* 393, 2022, pp. 1–10. DOI: https://doi.org/10.1007/s10338-022-00315-6.

[161] Wang, J., Juan, M., Yang, S., Zhang, D., Zhang, Z., Jin, J., and Yu, T. "Experimental Investigation of the Vibration Reduction of the Pipeline System with a Particle Impact Damper under Random Excitation". In: *Applied Sciences* 13, 2023. DOI: https://doi.org/10.3390/app13010618.

[162] Ye, F., Xue, X., Jiang, W., and Yin, X. "Mechanism and Experimental Investigation of Vibration Reduction for Container Cranes Based on Particle Damping Technology". In: *Actuators* 13, 2023. DOI: https://doi.org/10.3390/act13010011.

[163] Stauber, J., Ott, M., Snaith, M., and Puff, M. "Wind turbine noise attenuation using modal structural damping". In: *INTER-NOISE and NOISE-CON Congress and Conference Proceedings*. 2016, pp. 21–24.

[164] Sandanshiv, S. R. and Chavan, U. S. "Vibration suppression effects on rotating wind turbine blade using a particle damping method". In: *Vibroengineering Procedia* 29, 2019.

[165] Schmidt, H. "Die Schallausbreitung in körnigen Substanzen". In: *Acta Acustica united with Acustica* 4, 1954, pp. 639–652.

[166] Wolf, N. "Results of loss factor measurements on steel and concrete beams using a viscoelastic or sand damping system". In: *Wright-Patterson Air Force Base Tech. Documentary Report No. ASD-TDR-62-717* 152, 1962.

[167] Sun, J. C., Sun, H. B., Chow, L. C., and Richards, E. J. "Predictions of total loss factors of structures, part II: Loss factors of sand-filled structure". In: *Journal of Sound and Vibration* 104, 1986, pp. 243–257. DOI: https://doi.org/10.1016/0022-460X(86)90266-X.

[168] Cempel, C. and Lotz, G. "Efficiency of vibrational energy dissipation by moving shot". In: *Journal of Structural Engineering* 119, 1993, pp. 2642–2652. DOI: https://doi.org/10.1061/(ASCE)0733-9445(1993)119:9(2642).

[169] Papalou, A. and Masri, S. "Performance of particle dampers under random excitation". In: *Journal of Vibration and Acoustics* 18, 1996, pp. 614–621. DOI: https://doi.org/10.1115/1.2888343.

[170] Papalou, A. and Masri, S. "An experimental investigation of particle dampers under harmonic excitation". In: *Journal of vibration and control* 4, 1998, pp. 361–379. DOI: https://doi.org/10.1177/107754639800400402.

[171] Hollkamp, J. J. and Gordon, R. W. "Experiments with particle damping". In: *Smart structures and materials 1998: Passive damping and isolation* 3327, 1998, pp. 2–12. DOI: https://doi.org/10.1117/12.310675.

[172] Tomlinson, G. R., Pritchard, D., and Wareing, R. "Damping characteristics of particle dampers - some preliminary results". In: *Proceedings of the Institution of Mechanical Engineers, Part C: Journal of Mechanical Engineering Science*. 2001, pp. 253–257. DOI: https://doi.org/10.1243/0954406011520661.

[173] Yang, M. Y., Koopmann, G. H., Lesieutre, G. A., and Hambric, S. A. "Attenuation of high amplitude vibrations with particle dampers". In: *ASME International Mechanical Engineering Congress and Exposition*. 2002, pp. 113–118. DOI: https://doi.org/10.1115/IMECE2002-32689.

[174] Nayfeh, S. A., Verdirame, J. M., and Varanasi, K. K. "Damping of flexural vibration by coupling to low-density granular materials". In: *Smart Structures and Materials 2002: Damping and Isolation*, 2002, pp. 158–167. DOI: https://doi.org/10.1117/12.472652.

[175] Rongong, J. and Tomlinson, G. R. "Amplitude dependent behaviour in the application of particle dampers to vibrating structures". In: *46th AIAA/ASME/ASCE/AHS/ASC Structures, Structural Dynamics and Materials Conference*. 2005, pp. 71–82. DOI: https://doi.org/10.2514/6.2005-2327.

[176] Marhadi, K. S. and Kinra, V. K. "Particle impact damping: effect of mass ratio, material, and shape". In: *Journal of sound and vibration* 283, 2005, pp. 433–448. DOI: https://doi.org/10.1016/j.jsv.2004.04.013.

[177] Zhao, L. and She, G. Y. "Experimental Investigation on Dynamic Characteristics of NOPD Thin-Wall Frame Structure". In: *Applied Mechanics and Materials* 71, 2011, pp. 138–143. DOI: https://doi.org/10.4028/www.scientific.net/AMM.71-78.138.

[178] Booty, C., Bowyer, E. P., and Krylov, V. V. "Experimental investigation of damping flexural vibrations using granular materials". In: *International Conference on Noise and Vibration Engineering (ISMA 2014) Proceedings*. 2014, pp. 547–558.

[179] Akbar, M. A., Wong, W., and Rustighi, E. "A hybrid damper with tunable particle impact damping and coulomb friction". In: *Machines* 11, 2023. DOI: https://doi.org/10.3390/machines11050545.

[180] Chockalingam, S., Natarajan, U., and A., G. C. "Damping investigation in boring bar using hybrid copper-zinc particles". In: *Journal of Vibration and Control* 23, 2017, pp. 2128–2134. DOI: https://doi.org/10.1177/1077546315610946.

[181] Brunton, S. L. and Kutz, J. N. *Data-driven science and engineering: Machine learning, dynamical systems, and control*. 197th ed. Cambridge University Press, 2019. DOI: https://doi.org/10.1017/9781108380690.

[182] Serov, V. *Fourier series, Fourier transform and thier applications to mathematical physics*. 1st ed. Springer international publishing AG, 2017. DOI: https://doi.org/10.1007/978-3-319-65262-7.

[183] Pereyra, M. C. and Ward, L. A. *Harmonic analysis: from Fourier to wavelets*. American Mathematical Soc., 2012.

[184] Shin, K. and Hammond, J. *Fundamentals of signal processing for sound and vibration engineers*. John Wiley & Sons, 2008.

[185] Van Drongelen, W. *Signal processing for neuroscientists*. Academic press, 2018.

[186] Trimble, C. R. "What is signal averaging". In: *Hewlett-Packard Journal* 19, 1968, pp. 2–7.

[187] Tompkins, W. J. and Afonso, V. X. *Biomedical Digital Signal Processing: C-Language Examples and Laboratory Experiments for the IBM PC*. Prentice-Hall, 1993.

[188] Dodson, M. "Shannon's sampling theorem". In: *Current science* 63, 1992, pp. 253–260.

[189] Brandt, A. and Ahlin, K. "Sampling and time-domain analysis". In: *Sound & vibration* 44, 2010, pp. 13–17.

[190] Por, E., Kooten, M. van, and Sarkovic, V. "Nyquist–Shannon sampling theorem". In: *Leiden University* 1, 2019, pp. 1–2.

[191] Hoffmann, M. *Digital signal processing mathematics*. CERN, 2008.

[192] Tan, L. and Jiang, J. *Digital signal processing: fundamentals and applications*. 2nd ed. Academic press, 2018. DOI: https://doi.org/10.1016/C2011-0-05250-X.

[193] Karjalainen, M. and Paatero, T. "Frequency-dependent signal windowing". In: *Proceedings of the 2001 IEEE Workshop on the Applications of Signal Processing to Audio and Acoustics*. 2001, pp. 35–38. DOI: https://doi.org/10.1109/ASPAA.2001.969536.

[194] Braun, S. *Encyclopedia of vibration*. Academic Press, 2001.

[195] Kuttner, T. *Praxiswissen Schwingungsmesstechnik*. Springer, 2015. DOI: https://doi.org/10.1007/978-3-658-04638-5.

[196] Prasad, B. B., Duvigneau, F., Juhre, D., and Woschke, E. "Application of Particle Dampers on a Scaled Wind Turbine Generator to Improve Low-Frequency Vibro-Acoustic Behavior". In: *Applied Sciences* 12, 2022. DOI: https://doi.org/10.3390/app12020671.

[197] Prasad, B. B., Duvigneau, F., Juhre, D., and Woschke, E. "Experimental study of particle dampers applied to wind turbine blades to reduce low-frequency sound emission". In: *INTER-NOISE and NOISE-CON Congress and Conference Proceedings*. 2021, pp. 71–82. DOI: https://doi.org/10.3397/IN-2021-1125.

[198] Prasad, B. B., Duvigneau, F., Juhre, D., and Woschke, E. "Damping performance of particle dampers with different granular materials and their mixtures". In: *Applied Acoustics* 200, 2022. DOI: https://doi.org/10.1016/j.apacoust.2022.109059.

[199] Chong, Y. C. "Thermal analysis and air flow model-ling of electrical machines". PhD thesis. The University of Edinburgh, Edinburgh, Scotland, 2015.

[200] Rhodes, M. J. *Introduction to particle technology*. 2nd ed. John Wiley & Sons, 2008. DOI: https://doi.org/10.1002/9780470727102.

[201] Merkus, H. G. *Particle size measurements: fundamentals, practice, quality*. 1st ed. Springer Science & Business Media, 2009. DOI: https://doi.org/10.1007/978-1-4020-9016-5.

[202] Weiner, B. B. "What is a continuous particle size distribution". In: *Brookhaven Instruments, NY, USA*, 2011.

[203] Du, Y., Wang, S., Zhu, Y., Li, L., and Han, G. "Du, Yanchen and Wang, Shulin and Zhu, Yan and Li, Laiqiang and Han, Guangqiang". In: *Advances in Acoustics and Vibration* 2008, 2008, pp. 1–6.

[204] Popov, V. L. *Contact mechanics and friction: Physical principles and applications*. 2nd ed. Springer, 2010.

[205] Williams, J. A. and Dwyer-Joyce, R. S. *Modern tribology handbook, two volume set*. 1st ed. CRC press, 2000.

[206] Lee, W. K. and Jang, H. "Moisture effect on velocity dependence of sliding friction in brake friction materials". In: *Wear* 306, 2013, pp. 17–21. DOI: https://doi.org/10.1016/j.wear.2013.06.027.

[207] Corn, M. and Stein, F. "Re-entrainment of particles from a plane surface". In: *American Industrial Hygiene Association Journal* 26, 1965, pp. 325–336. DOI: https://doi.org/10.1080/00028896509342739.

[208] Prasad, B. B., Duvigneau, F., Reinboth, T., Juhre, D., and Woschke, E. "Design Strategies of Particle Dampers for Large-Scale Applications". In: *Journal of Vibration Engineering & Technologies* 12, 2024, pp. 5715–5746. DOI: https://doi.org/10.1007/s42417-023-01214-x.

[209] Lu, Z., Lu, X., Lu, W., and Masri, S. F. "Shaking table test of the effects of multi-unit particle dampers attached to an MDOF system under earthquake excitation". In: *Earthquake Engineering & Structural Dynamics* 41, 2012, pp. 987–1000. DOI: https://doi.org/10.1002/eqe.1170.

[210] Moller, H. and Pedersen, C. S. "Low-frequency noise from large wind turbines". In: *The Journal of the Acoustical Society of America* 129, 2011, pp. 3727–3744. DOI: https://doi.org/10.1121/1.3543957.

[211] Zhou, Z., Xue, L., Yang, F., Jiang, Z., Wang, K., Xie, M., and Chen, H. "Promising rare-earth high-entropy ceramic driving foamed silicon rubber composite to reduce 100–300 Hz low-frequency noise". In: *Materials Letters* 313, 2022. DOI: https://doi.org/10.1016/j.matlet.2022.131824.

[212] Prasad, B. B., Duvigneau, F., Bueschel, A., Göhler, H., Jehring, U., Juhre, D., and Woschke, E. "The impact of dynamic loading and cyclic temperature variations on the damping efficiency of particle dampers". In: *Journal of Vibration and Control*, 2024. DOI: https://doi.org/10.1177/10775463241264332.

[213] Daniel, C., Woschke, E., Prasad, B. B., and Duvigneau, F. "Effectivity of particle dampers with granular filling under rotating conditions". In: *Proceedings of SIRM 2023 - the 15th European Conference on Rotordynamics*. 2023, pp. 108–117. DOI: https://doi.org/10.26083/tuprints-00024057.

[214] Cotton, I., Jenkins, N., and Pandiaraj, K. "Wind Energy: An International Journal for Progress and Applications in Wind Power Conversion Technology". In: *Wind Energy* 4, 2001, pp. 23–37. DOI: https://doi.org/10.1002/we.44.

[215] Rachidi, F., Rubinstein, M., Montanya, J., Bermudez, J. L., Sola, R. R., Sola, G., and Korovkin, N. "A review of current issues in lightning protection of new-generation wind-turbine blades". In: *IEEE Transactions on Industrial Electronics* 55, 2008, pp. 2489–2496. DOI: https://doi.org/10.1109/TIE.2007.896443.

[216] Prasad, B. B., Duvigneau, F., Juhre, D., and Woschke, E. "Application of particle dampers on a scaled wind turbine generator to improve low-frequency vibro-acoustic behavior". In: *Applied Sciences* 12, 2022. DOI: https://doi.org/10.3390/app12020671.

[217] Council, Global Wind Energy. *GWEC Global Wind Report 2021*. 2021.

[218] Council, Global Wind Energy. *GWEC Global Wind Report 2023*. 2023.

[219] Chou, J. S. and Tu, W. T. "Failure analysis and risk management of a collapsed large wind turbine tower". In: *Engineering Failure Analysis* 18, 2011, pp. 295–313. DOI: https://doi.org/10.1016/j.engfailanal.2010.09.008.

[220] Zuo, H., Bi, K., and Hao, H. "A state-of-the-art review on the vibration mitigation of wind turbines". In: *Renewable and Sustainable Energy Reviews* 121, 2020. DOI: https://doi.org/10.1016/j.rser.2020.109710.

[221] Lackner, M. A. and Rotea, M. A. "Passive structural control of offshore wind turbines". In: *Wind energy* 14, 2011, pp. 373–388. DOI: https://doi.org/10.1002/we.426.

[222] Murtagh, P. J., Ghosh, A., Basu, B., and Broderick, B. M. "Passive control of wind turbine vibrations including blade/tower interaction and rotationally sampled turbulence". In: *Wind energy* 11, 2008, pp. 305–317. DOI: https://doi.org/10.1002/we.249.

[223] Colwell, S. and Basu, B. "Tuned liquid column dampers in offshore wind turbines for structural control". In: *Engineering structures* 31, 2009, pp. 358–368. DOI: https://doi.org/10.1016/j.engstruct.2008.09.001.

[224] Stewart, G. and Lackner, M. "Offshore wind turbine load reduction employing optimal passive tuned mass damping systems". In: *IEEE transactions on control systems technology* 21, 2013, pp. 1090–1104. DOI: https://doi.org/10.1109/TCST.2013.2260825.

[225] Zuo, H., Bi, K., and Hao, H. "Using multiple tuned mass dampers to control offshore wind turbine vibrations under multiple hazards". In: *Engineering Structures* 141, 2017, pp. 303–315. DOI: https://doi.org/10.1016/j.engstruct.2017.03.006.

[226] Buckley, T., Watson, P., Cahill, P., Jaksic, V., and Pakrashi, V. "Mitigating the structural vibrations of wind turbines using tuned liquid column damper considering soil-structure interaction". In: *Renewable energy* 120, 2018, pp. 322–341. DOI: https://doi.org/10.1016/j.renene.2017.12.090.

[227] Rahman, M., Ong, Z. C., Chong, W. T., Julai, S., and Khoo, S. Y. "Performance enhancement of wind turbine systems with vibration control: A review". In: *Renewable and Sustainable Energy Reviews* 51, 2015, pp. 43–54. DOI: https://doi.org/10.1016/j.rser.2015.05.078.

[228] Chen, J. L. and Georgakis, C. T. "Spherical tuned liquid damper for vibration control in wind turbines". In: *Journal of Vibration and Control* 21, 2015, pp. 1875–1885. DOI: https://doi.org/10.1177/1077546313495911.

[229] Zhang, Z., Staino, A., Basu, B., and Nielsen, S. R. K. "Performance evaluation of full-scale tuned liquid dampers (TLDs) for vibration control of large wind turbines using real-time hybrid testing". In: *Engineering Structures* 126, 2016, pp. 417–431. DOI: https://doi.org/10.1016/j.engstruct.2016.07.008.

[230] L., M. L., D., V. N., Chang, S., Kim, D., Cho, S. G., and Nguyen, D. D. "Vibration control of jacket offshore wind turbine subjected to earthquake excitations by using friction damper". In: *Journal of Structural Integrity and Maintenance* 4, 2019, pp. 1–5. DOI: https://doi.org/10.1080/24705314.2019.1565055.

[231] Zhao, Z., Dai, K., Lalonde, E. R., Meng, J., Li, B., Ding, Z., and Bitsuamlak, G. "Studies on application of scissor-jack braced viscous damper system in wind turbines under seismic and wind loads". In: *Engineering Structures* 196, 2019. DOI: https://doi.org/10.1016/j.engstruct.2019.109294.

[232] Zhang, Z. L., Chen, J. B., and Li, J. "Theoretical study and experimental verification of vibration control of offshore wind turbines by a ball vibration absorber". In: *Structure and Infrastructure Engineering* 10, 2014, pp. 1087–1100. DOI: https://doi.org/10.1080/15732479.2013.792098.

[233] Monthly, Windpower. *Windpower Monthly*. Apr. 2018.

[234] Brockmann, W., Geiß, P. L., Klingen, J., and Schröder, B. *Adhesive bonding: materials, applications and technology*. 2nd ed. John Wiley & Sons, 2009. DOI: http://dx.doi.org/10.1002/9783527623921.

[235] Qiao, Y., Han, S., Deng, Y., Liu, Y., Dong, J., Pan, L., Li, R., and Zhao, B. "Research on variable pitch control strategy of wind turbine for tower vibration reduction". In: *The Journal of Engineering* 13, 2017, pp. 2005–2008. DOI: https://doi.org/10.1049/joe.2017.0680.

[236] Bossanyi, E. A. "Individual blade pitch control for load reduction". In: *Wind Energy: An International Journal for Progress and Applications in Wind Power Conversion Technology* 6, 2003, pp. 119–128. DOI: https://doi.org/10.1002/we.76.

[237] Lachenal, X., Daynes, S., and Weaver, P. M. "Review of morphing concepts and materials for wind turbine blade applications". In: *Wind energy* 16, 2013, pp. 283–307. DOI: https://doi.org/10.1002/we.531.

[238] Moreau, E. "Airflow control by non-thermal plasma actuators". In: *Journal of physics D: applied physics* 40, 2007, p. 605. DOI: https://doi.org/10.1088/0022-3727/40/3/S01.

[239] Awada, A., Younes, R., and LLinca, A. "Review of vibration control methods for wind turbines". In: *Energies* 14, 2021, p. 3058. DOI: https://doi.org/10.3390/en14113058.

[240] Robinson, M. J. and Kosmatka, J. B. "Embedding viscoelastic damping materials in low-cost VARTM composite structures". In: *Smart Structures and Materials 2005: Damping and Isolation*. 2005, pp. 349–360. DOI: https://doi.org/10.1117/12.600421.

[241] Zhang, Z., Li, J., Nielsen, S. R. K., and Basu, B. "Mitigation of edgewise vibrations in wind turbine blades by means of roller dampers". In: *Journal of Sound and Vibration* 333, 2014, pp. 5283–5298. DOI: https://doi.org/10.1016/j.jsv.2014.06.006.

[242] Zhang, Z., Basu, B., and Nielsen, S. R. K. "Tuned liquid column dampers for mitigation of edgewise vibrations in rotating wind turbine blades". In: *Structural Control and Health Monitoring* 22, 2015, pp. 500–517. DOI: https://doi.org/10.1002/stc.1689.

[243] Basu, B., Zhang, Z., and Nielsen, S. R. K. "Damping of edgewise vibration in wind turbine blades by means of circular liquid dampers". In: *Wind Energy* 19, 2016, pp. 213–226. DOI: https://doi.org/10.1002/we.1827.

[244] Meng, J. and Sun, D. "Research on vibration suppression of wind turbine blade with a multi-layer porous damping structure based on bamboo wall microstructure". In: *Journal of the Brazilian Society of Mechanical Sciences and Engineering* 43, 2021, pp. 1–9. DOI: https://doi.org/10.1007/s40430-021-02888-8.

[245] Sievers, R. A. and Mullings, J. L. *Wind turbine blade with viscoelastic damping*. Jan. 2017.

[246] Garolera, A. C., Madsen, S. F., Nissim, M., Myers, J. D., and Holboell, J. "Lightning damage to wind turbine blades from wind farms in the US". In: *IEEE Transactions on Power Delivery* 31, 2014, pp. 1043–1049. DOI: https://doi.org/10.1109/TPWRD.2014.2370682.

[247] L., M., Branner, K., Petersen, H. N., Beauson, J., McGugan, M., and Sorensen, B. F. "Materials for wind turbine blades: An overview". In: *Materials* 10, 2017, p. 1285. DOI: https://doi.org/10.3390/ma10111285.

[248] Maalawi, K. Y. *Design Optimization of Wind Energy Conversion Systems with Applications*. IntechOpen, 2020. DOI: http://dx.doi.org/10.5772/intechopen.82111.

[249] Larsen, K. "Recycling wind turbine blades". In: *Renewable energy focus* 9, 2009, pp. 70–73. DOI: https://doi.org/10.1016/S1755-0084(09)70045-6.

[250] Jensen, F. M. and Branner, K. "Introduction to wind turbine blade design". In: *Advances in wind turbine blade design and materials*. 2023, pp. 3–53. DOI: https://doi.org/10.1016/B978-0-08-103007-3.00009-4.

[251] Oliveira, M. A., Simas Filho, E. F., Albuquerque, M. C. S., Santos, Y. T. B., Silva, I. C, and Farias, C. "Ultrasound-based identification of damage in wind turbine blades using novelty detection". In: *Ultrasonics* 108, 2020. DOI: https://doi.org/10.1016/j.ultras.2020.106166.

[252] Schubel, P. J. and Crossley, R. J. "Wind turbine blade design review". In: *Wind engineering* 36, 2012, pp. 365–388. DOI: https://doi.org/10.1260/0309-524X.36.4.365.

[253] Zhu, J., Cai, X., Pan, P., and Gu, R. "Optimization design of spar cap layup for wind turbine blade". In: *Frontiers of Structural and Civil Engineering* 6, 2012, pp. 53–56. DOI: https://doi.org/10.1007/s11709-012-0147-9.

[254] Prasad, B. B., Luft, T., Michaelsen, C., and Rottengruber, H. "Enhancing Vibroacoustic Performance of Power Electronic Subsystem in Electric Drives Using Particle Dampers". In: *DAGA 2024 - 50. Jahrestagung für Akustik*. 2024, pp. 503–506.

[255] Hua, X., Thomas, A., and Shultis, K. "Recent progress in battery electric vehicle noise, vibration, and harshness". In: *Science Progress* 104, 2021. DOI: https://doi.org/10.1177/00368504211005224.

[256] Ghosh, A. and Chatterjee, S. "An overview on various sources of vibration in electric vehicle and their identification techniques". In: *Journal of the Brazilian Society of Mechanical Sciences and Engineering* 45, 2023. DOI: https://doi.org/10.1007/s40430-023-04318-3.

[257] Horváth, K. and Zelei, A. "Simulating Noise, Vibration, and Harshness Advances in Electric Vehicle Powertrains: Strategies and Challenges". In: *World Electric Vehicle Journal* 15, 2024. DOI: https://doi.org/10.3390/wevj15080367.

[258] Blumenröder, K., Bennewitz, K., Lück, P., Tousen, J., and Estorf, M. "Der neue Modulare E-Antriebs-Baukasten von Volkswagen: Volkswagen's new modular e-drive kit". In: *Proceedings of the 40th Internationales Wiener Motorensymposium*. 2019, pp. 15–17. DOI: https://doi.org/10.51202/9783186811127.

[259] W., J. *Antrieb des Volkswagen ID.4: Ungewöhnlicher Motorenmix*. Accessed: 3 March 2025. 2020. URL: https://www.automotiveit.eu/cars/antrieb-des-volkswagen-id-4-ungewoehnlicher-motorenmix-244.html.

[260] Mehrgou, M., Madinabeiti, I. Garcia de, and Garmendia, J. "Simulation and Validation of Inverter-related NVH Issues in Electric Vehicle Drives". In: *ATZextra worldwide* 23, 2018, pp. 12–17. DOI: https://doi.org/10.1007/s40111-018-0005-4.

[261] Singh, R., Nalawade, A., Pande, M., and Singh, P. "Vibration and noise characteristics of an inverter for electric vehicle application". In: *Vibroengineering Procedia*. 2023, pp. 145–151. DOI: https://doi.org/10.21595/vp.2023.23563.

[262] Tsoumas, I. P. and Tischmacher, H. "Influence of the inverter's modulation technique on the audible noise of electric motors". In: *IEEE Transactions on Industry Applications* 50, 2013, pp. 269–278. DOI: https://doi.org/10.1109/TIA.2013.2268453.

[263] Körner, P. M., Stiegler, R., Meyer, J., Wohlfahrt, T., Waniek, C., and Myrzik, J. M. A. "Influence of inverter PWM control schemes on noise signature of electric powertrains". In: *18th International Conference on Harmonics and Quality of Power (ICHQP)*. 2018, pp. 1–6. DOI: https://doi.org/10.1109/ICHQP.2018.8378856.

[264] Sarrazin, M., Janssens, K., and Auweraer, H. Van der. "Influence of inverter PWM control schemes on noise signature of electric powertrains". In: *Proceedings of the 20th International Congress on Sound and Vibration*. 2013, pp. 7–11.

[265] Radha, V. and Ripin, Z. M. "Correlation between PWM modulation of an induction motor inverter and radiated electromagnetic acoustic noise". In: *IEEE International Conference on Control System, Computing and Engineering (ICCSCE)*. 2014, pp. 267–272. DOI: https://doi.org/10.1109/ICCSCE.2014.7072728.

[266] Na, S.-H., Jung, Y.-G., Lim, Y.-C., and Yang, S.-H. "Reduction of audible switching noise in induction motor drives using random position space vector PWM". In: *IEE Proceedings-Electric Power Applications* 149, 2002, pp. 195–200. DOI: https://doi.org/10.1049/ip-epa:20020244.

[267] Shao, R., Guo, Z., and Chang, L. "A PWM strategy for acoustic noise reduction for grid-connected single-phase inverters". In: *Twenty-Second Annual IEEE Applied Power Electronics Conference and Exposition*. 2007, pp. 301–305. DOI: https://doi.org/10.1109/APEX.2007.357530.

[268] Gilliam, J. E., Houldsworth, J. A., and Hadley, L. "Variable speed induction motor with integral ultrasonic PWM inverter". In: *IEE Colloquium on Microcomputer Instrumentation and Control Systems in Power Electronics*. 1988. DOI: https://doi.org/10.1109/APEC.1988.10555.

[269] Le Besnerais, J., Lanfranchi, V., Hecquet, M., and Brochet, P. "Characterization and reduction of audible magnetic noise due to PWM supply in induction machines". In: *IEEE Transactions on Industrial Electronics* 57, 2009, pp. 1288–1295. DOI: https://doi.org/10.1109/TIE.2009.2029529.

[270] Tischmacher, H. and Eichinger, B. "Sound optimization of a converter-fed drive system using an acoustic camera in combination with modal analysis". In: *COMPEL-The international journal for computation and mathematics in electrical and electronic engineering* 29, 2010, pp. 1106–1115.

[271] Lei, Y., Hou, L., Fu, Y., Hu, J., and Chen, W. "Research on vibration and noise reduction of electric bus gearbox based on multi-objective optimization". In: *Applied Acoustics* 158, 2020. DOI: https://doi.org/10.1016/j.apacoust.2019.107037.

[272] Hu, C., Tang, X., Zou, L., Yang, K., Li, Y., and Zheng, L. "Numerical and experimental investigations of noise and vibration characteristics for a dual-motor hybrid electric vehicle". In: *IEEE Access* 7, 2019, pp. 77052–77062. DOI: https://doi.org/10.1109/ACCESS.2019.2919113.

[273] Migal, V., Lebedev, A., Shuliak, M., Kalinin, E., Arhun, S., and Korohodskyi, V. "Reducing the vibration of bearing units of electric vehicle asynchronous traction motors". In: *Journal of Vibration and Control* 27, 2021, pp. 1123–1131. DOI: https://doi.org/10.1177/1077546320937634.

[274] Henderson, J. P., Plummer, A., and Johnston, N. "An electro-hydrostatic actuator for hybrid active-passive vibration isolation". In: *International Journal of Hydromechatronics* 1, 2018, pp. 47–71.

[275] Law, H., Law, J., and Kierzkowski, M. "Absorptive noise barrier development". In: *Proceedings of Meetings on Acoustics*. 2023. DOI: https://doi.org/10.1121/10.0023767.

[276] Rieß, S., Weber, A., Húlsebrock, M., López, J., Kleinfeller, N., Uszynski, O., and Atzrodt, H. "Vibration and noise reduction on a cover for power electronics for electric vehicles with vibroacoustic metamaterials". In: *INTER-NOISE and NOISE-CON Congress and Conference Proceedings*. 2024, pp. 71–82. DOI: https://doi.org/10.3397/IN-2021-1125.

[277] Subramaniam, U., Bhaskar, S. M., Almakhles, D. J., Padmanaban, S., and Leonowicz, Z. "Investigations on EMI mitigation techniques: Intent to reduce grid-tied PV inverter common mode current and voltage". In: *Energies* 12, 2019. DOI: https://doi.org/10.3390/en12173395.

Appendix

A1 Comparative analysis of RRPDs, HMPDs, and HPDs with constant material mass

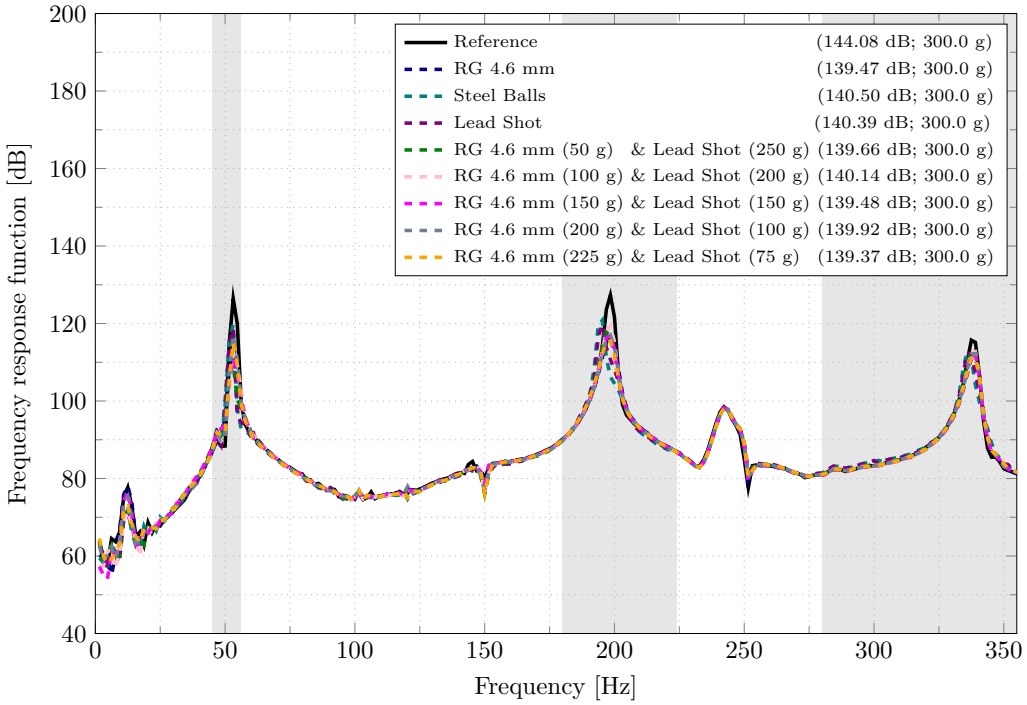

Figure A1.1: Narrowband spectrum of the test specimen filled with RRPDs, HMPDs, and HPDs at a constant material mass.

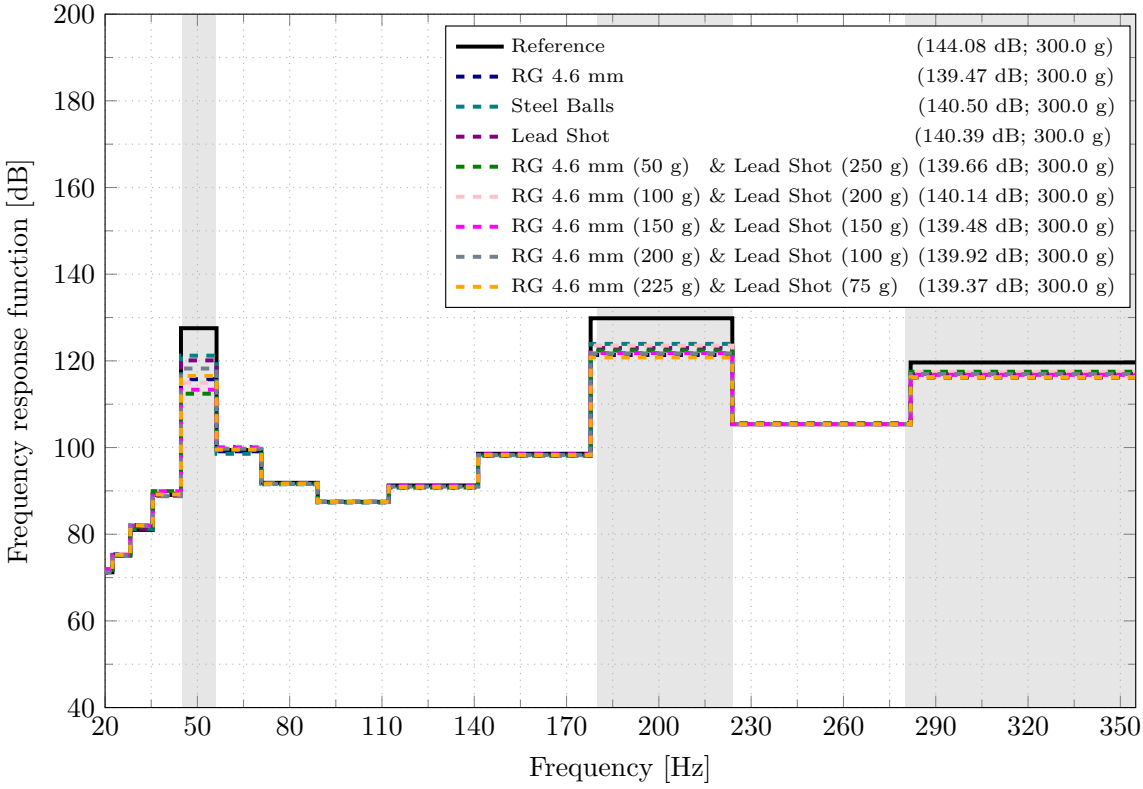

Figure A1.2: One-third octave bands of the test specimen filled with RRPDs, HMPDs, and HPDs at a constant material mass.

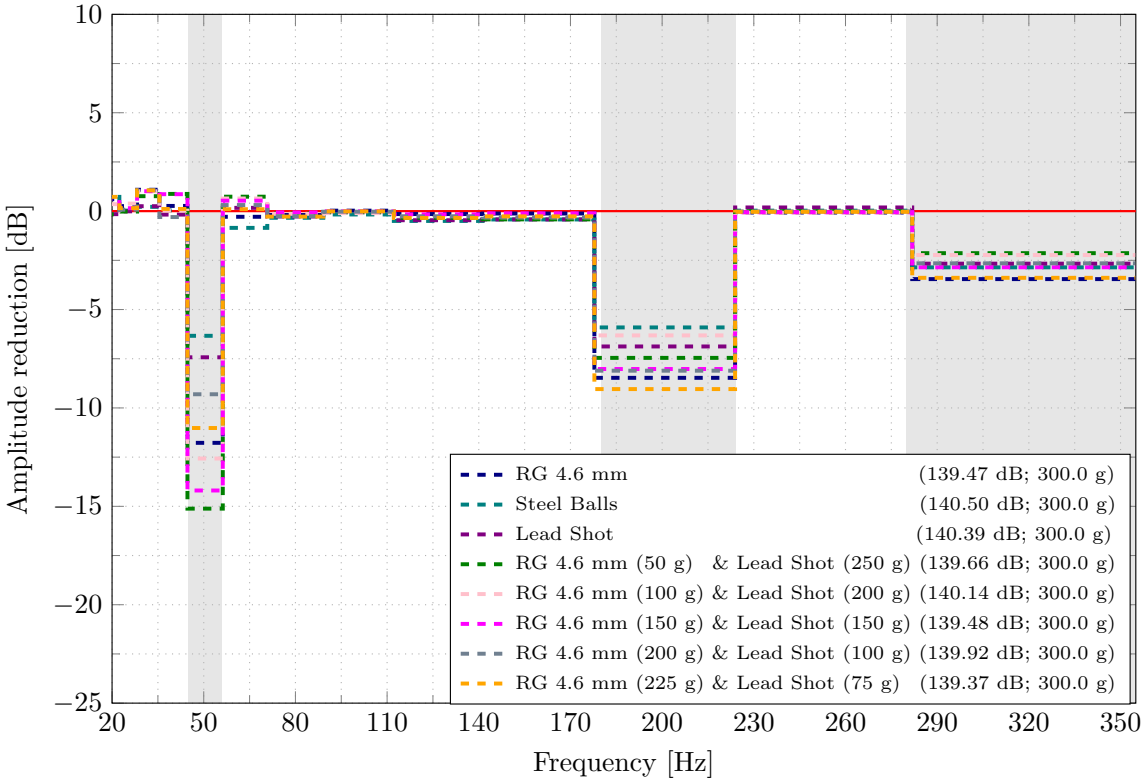

Figure A1.3: Amplitude reduction plot of the test specimen filled with RRPDs, HMPDs, and HPDs at a constant material mass.

A2 Narrowband spectrum analysis of TWC and TWC-AS design variants

This appendix presents the narrowband spectrum for the TWC and TWC-AS design variants.

A2.1 Narrowband spectrum of TWCs with varying wall thickness

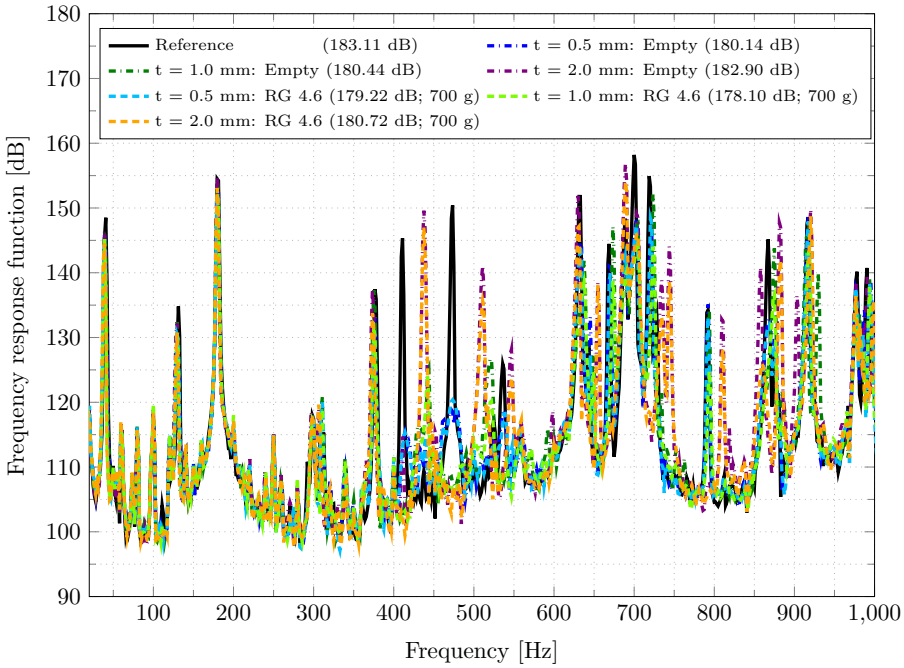

Figure A2.4: Narrowband spectrum of TWCs with varying wall thicknesses.

A2.2 Narrowband spectrum of TWCs with varying top dimensions

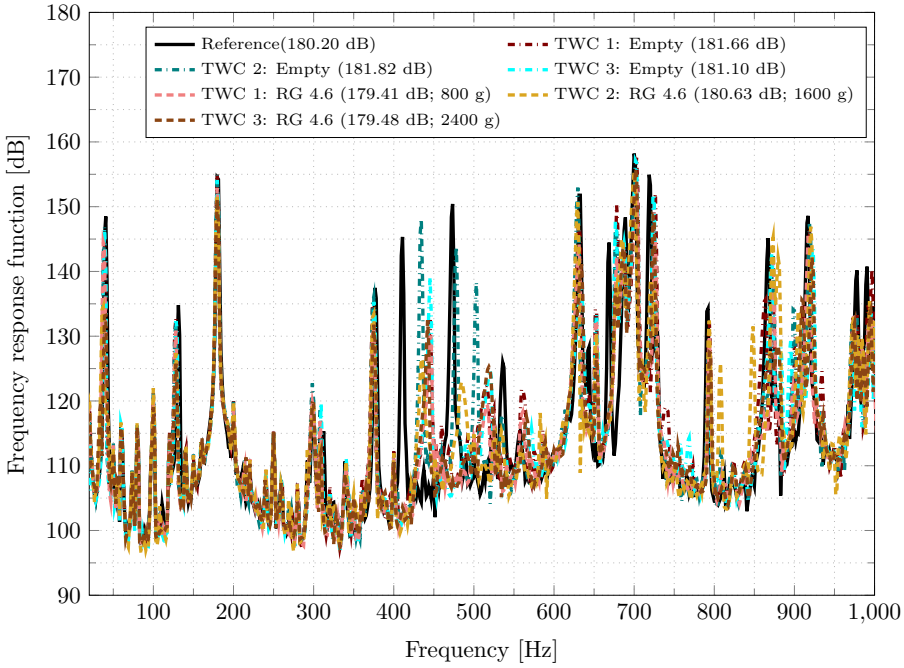

Figure A2.5: Narrowband spectrum of TWCs with varying dimensions at the top of the test specimen.

A2.3 Narrowband spectrum of TWCs with varying mid dimensions

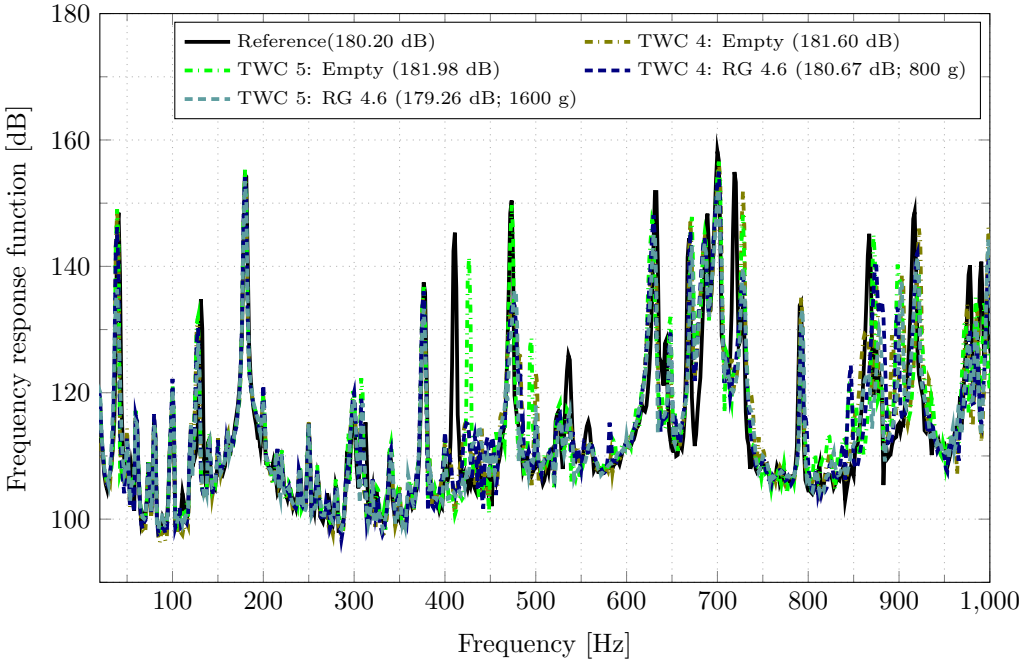

Figure A2.6: Narrowband spectrum of TWCs with varying dimensions at the mid of the test specimen.

A2.4 Narrowband spectrum of TWCs with varying bottom dimensions

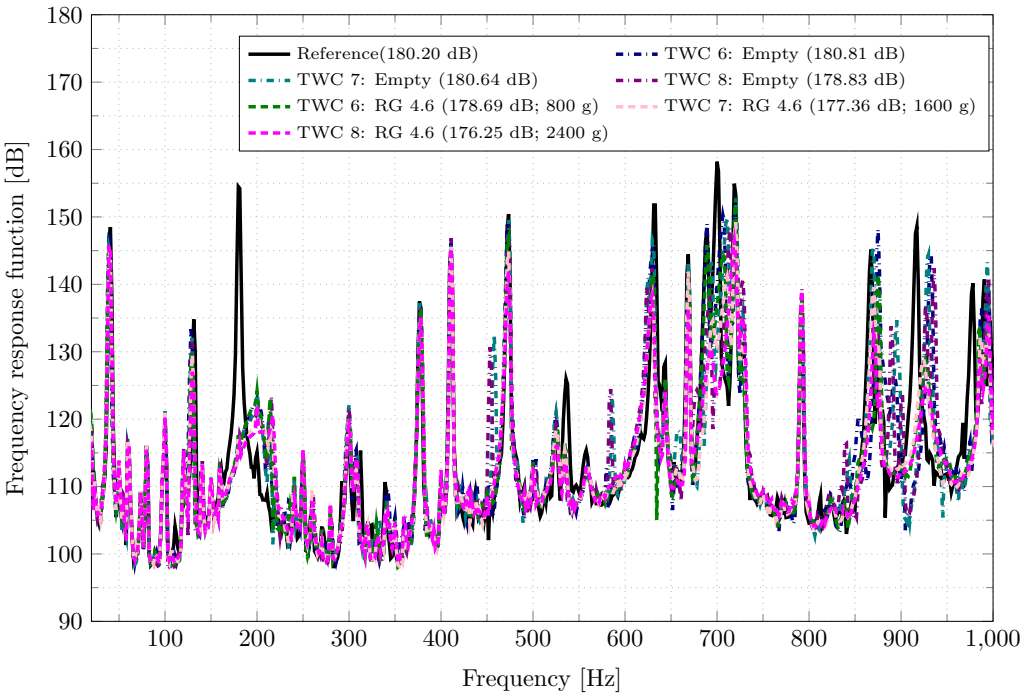

Figure A2.7: Narrowband spectrum of TWCs with varying dimensions at the bottom of the specimen.

A2.5 Comparison of narrowband spectra between MU TWC and SU TWC

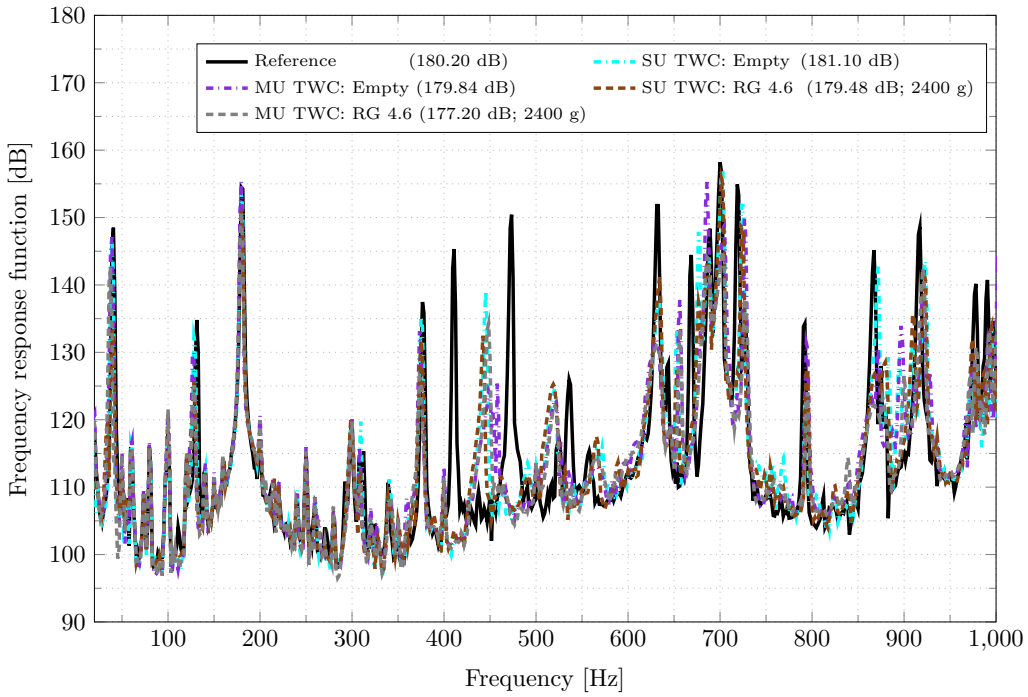

Figure A2.8: Narrowband spectrum of empty and partially filled SU and MU TWCs.

A2.6 Narrowband spectrum of TWC-AS design variants

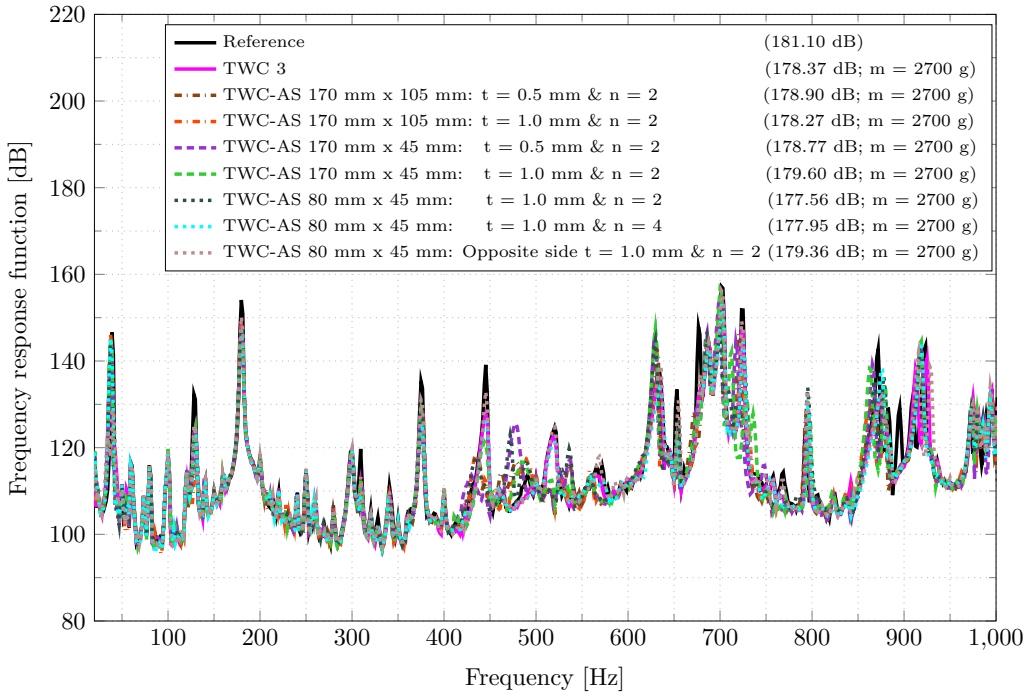

Figure A2.9: Narrowband spectrum of the test specimen with TWC-AS.

A2.7 Narrowband spectrum of RCs design variants

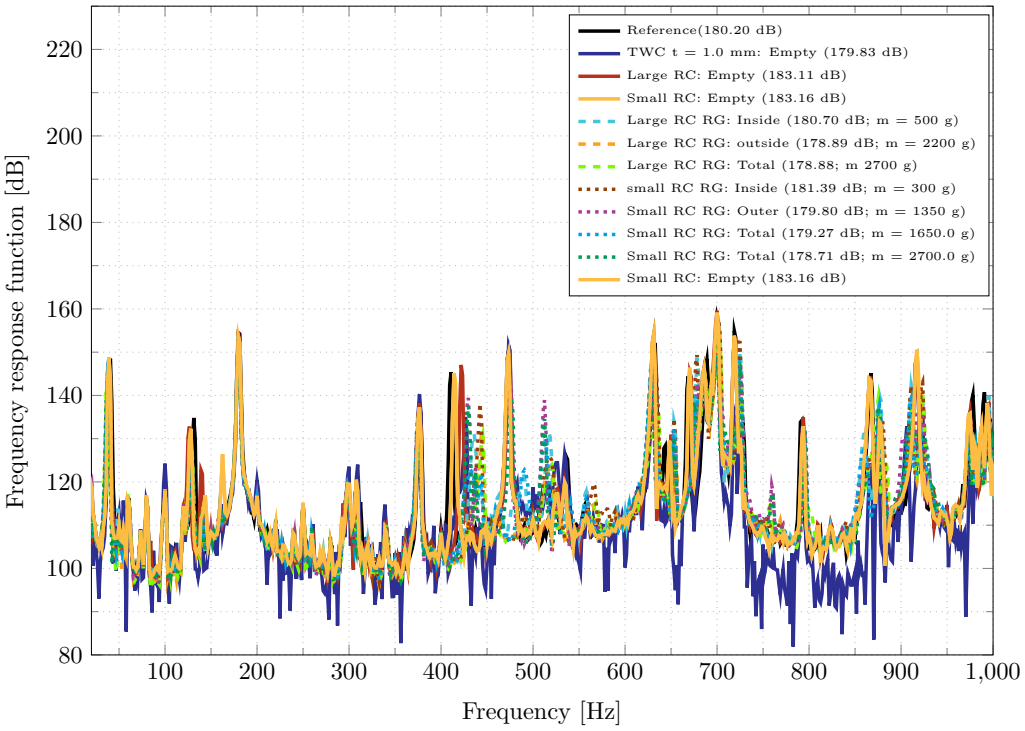

Figure A2.10: Narrowband spectrum of the test specimen with RCs.

A3 FRF of HCDP concept at various locations on WTS specimen

This appendix presents the FRFs and vibration attenuation achieved by the HCDPs mounted at different locations on the WTS test specimen.

A3.1 FRF of SU HCDP concept mounted opposite the excitation point

Figure A3.11 - Figure A3.13 present the frequency response of the WTS specimen when the SU HCDP is attached to the outer wall of the WTS ring, positioned opposite the excitation point. This arrangement of HCDP can be seen in Figure 9.4 (d). It can be observed that around the first resonance frequency, all the SU HCDPs are capable of reducing the vibration amplitude of the WTS test specimen. Moreover, it is observed that the SU HCDP filled with stone power (40%) and sand (40%) are particularly effective in attenuating vibrations at the first resonance frequency. These configurations lead to a reduction in vibration amplitude by 7.1 dB and 6.5 dB, respectively, see Figure A3.13. Furthermore, it has been also noticed that the attachment of the SU HCDP to the outer wall of the WTS ring results in a reduction of vibration amplitude near the third and fourth resonance peaks. However, in the case of the resonance near 150 Hz, the vibration amplitude of the WTS test specimen with the attached SU HCDP is higher compared to the reference values of the WTS test specimen. Furthermore, a slight frequency shift has also been observed, likely caused by the additional mass of the HCDP. Furthermore, the attachment of the SU HCDP at this specific location leads to an increase in vibration amplitude for the resonance peak around 100 Hz. However, it is worth noting that the overall damping characteristics of the SU HCDP filled with stone powder and sand are quite similar, as also evident from their SL values of surface velocity.

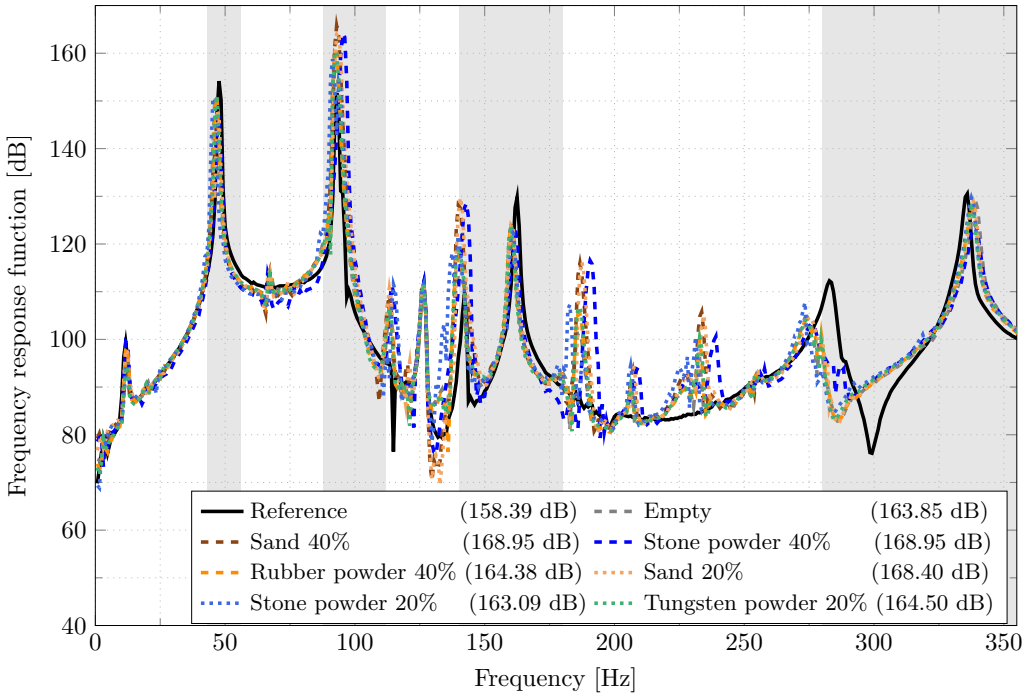

Figure A3.11: Narrowband spectrum of the SU HCDP mounted on the outer wall of the stator ring (opposite the excitation point).

Additionally, to demonstrate that the vibration attenuation is primarily due to the particle damping mechanism rather than just the added mass and design alternation, an empty HCDP is also attached to the WTS ring. The significance of the HCDP placement in vibration attenuation has been observed in the case of MU HCDP. Consequently, an investigation is conducted to examine the effect of an empty HCDP at various locations on the WTS test specimen for each SU HCDP configuration. From this

discussion and from Figure A3.11 - Figure A3.13, it can be concluded that the proposed configuration demonstrates a notable decrease in vibration amplitude at resonance peaks approximately around 50 Hz, 150 Hz, and 355 Hz. Moreover, it has been observed that stone powder and sand exhibit the highest vibration reduction near the first resonance peaks compared to other granular materials. However, it is evident that attaching the SU HCDP to the outer wall of the generator ring is not effective for achieving broadband damping, as reflected in the SL values of the SU HCDP in comparison to the SL value of the reference specimen.

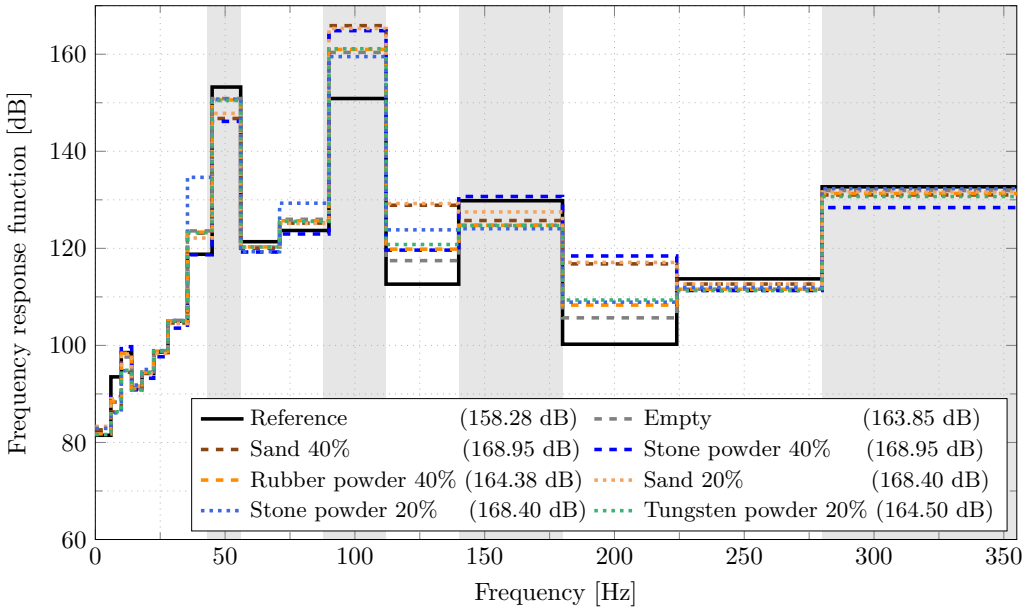

Figure A3.12: One-third octave band of the SU HCDP mounted on the outer wall of the stator ring (opposite the excitation point).

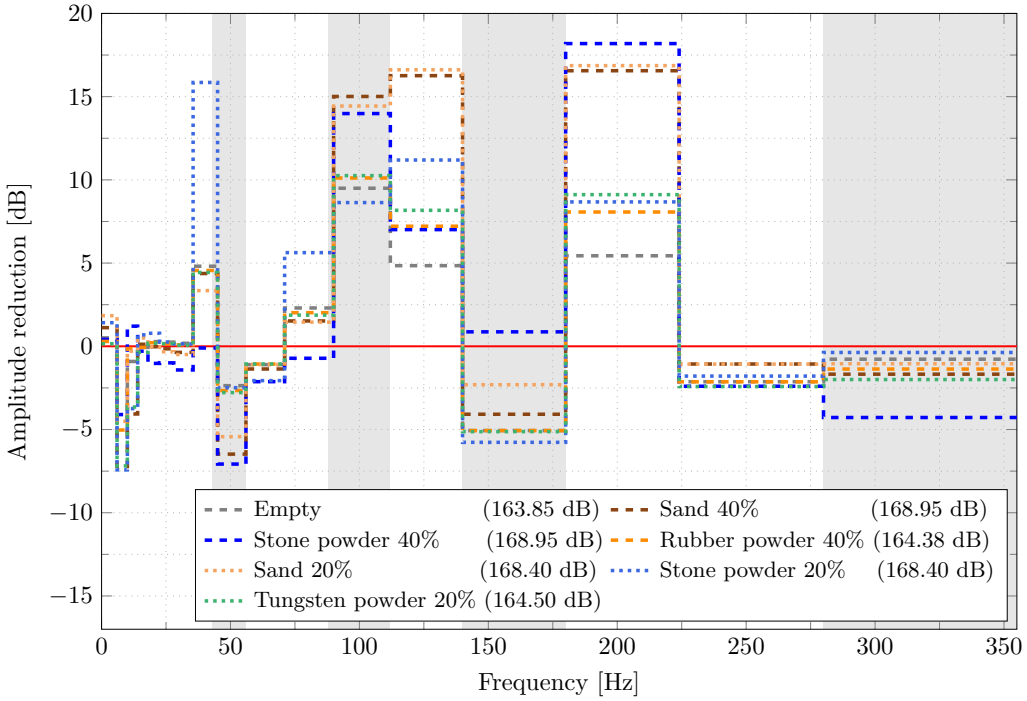

Figure A3.13: Amplitude reduction plot of the SU HCDP mounted on the outer wall of the stator ring (opposite the excitation point).

A3.2 FRF of SU and MU HCDP concepts mounted between stator arm and ring

The vibration attenuation capability of the HCDP, when placed between the stator arm and stator ring is plotted in Figure A3.14 - Figure A3.16. The attachment of the SU HCDP between the WTS arm and ring leads to a significant reduction in vibration amplitude near 150 Hz. Furthermore, a similar outcome has been observed around the resonance frequency of 355 Hz. However, around the first resonance frequency, i.e. near 50 Hz, only the SU HCDP filled with tungsten powder (green dotted line) and the MU HCDP filled with sand (violet dashed line) are effective in reducing the vibration amplitude, resulting in reductions of up to 3.5 dB and 1.49 dB respectively. The observation reveals that the empty HCDP (gray dashed line) generally either amplifies the vibration amplitude or exhibits a minimal damping effect. However, an exception can be seen for the resonance peak near 150 Hz, where the damping value caused by the empty HCDP is comparable to that achieved by attaching an SU HCDP filled with rubber powder at a filling ratio of 40% (orange dashed line). However, the attachment of an empty HCDP between the stator arm and ring leads to an increase in the overall vibration amplitude of the primary structure, as evidenced by the SL value of the surface velocity. While the placement of SU or MU HCDP between the stator arm and ring can effectively decrease the vibration amplitude, it is crucial to note that this configuration can be highly critical in real-world applications. The current industrial practice involves using welding processes to join the WTS arm and ring on a large scale. However, incorporating the partially filled HCDP at this specific location in the WTS would necessitate a comprehensive analysis of the fastening and joining procedures. Consequently, implementing this configuration at an industrial scale poses challenges for the manufacturing, production, and assembly processes.

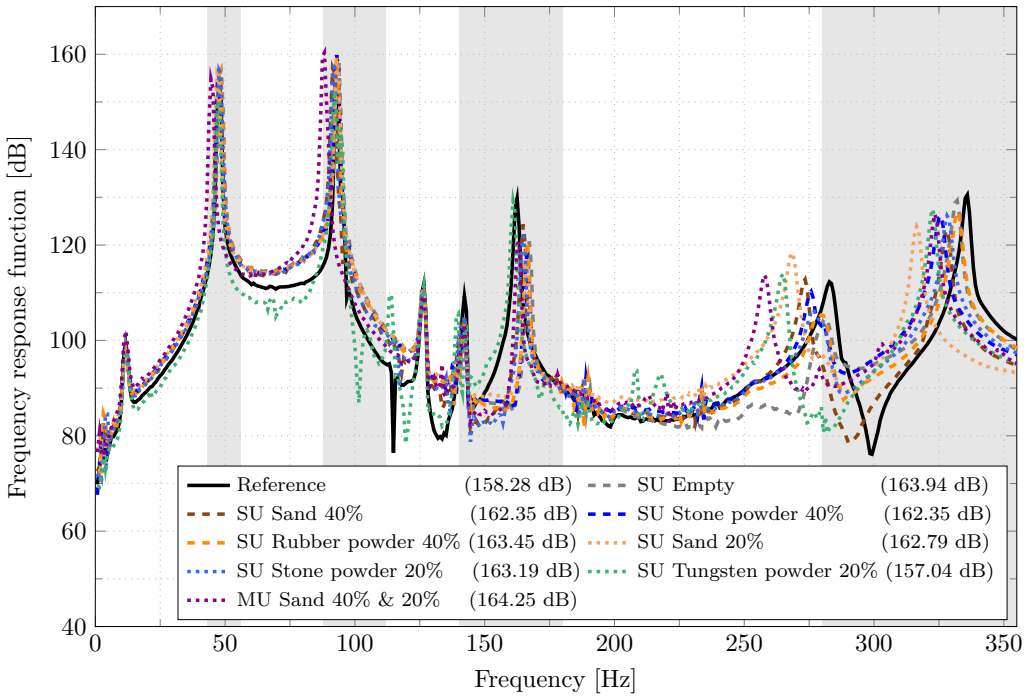

Figure A3.14: Narrowband spectrum of the SU and MU HCDP mounted between the stator arm and stator ring.

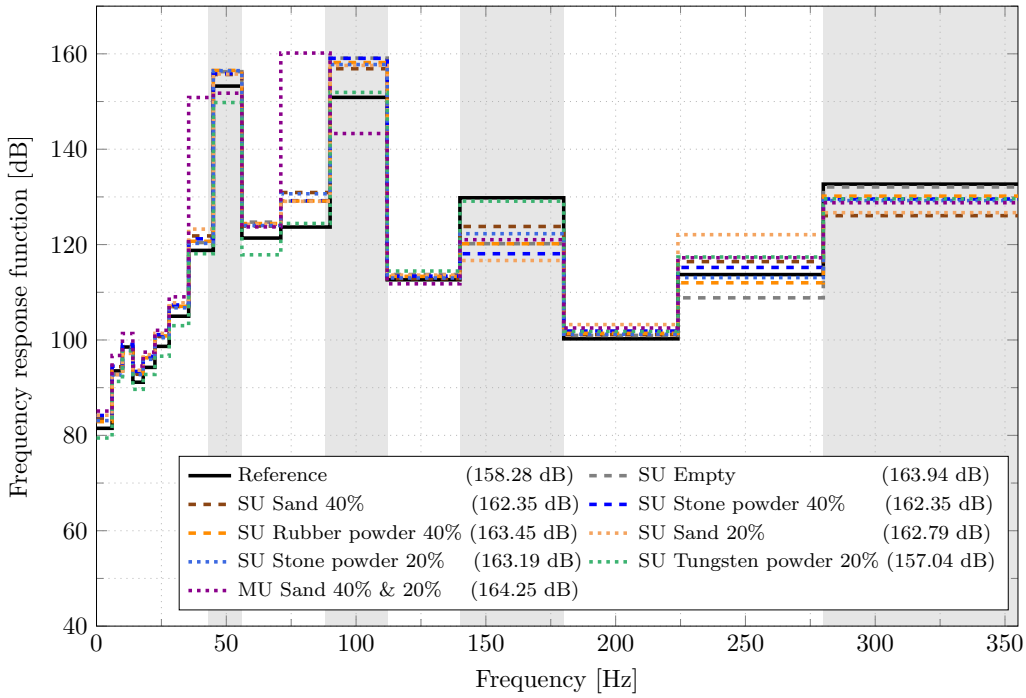

Figure A3.15: One-third octave band of the SU and MU HCDP mounted between the stator arm and stator ring.

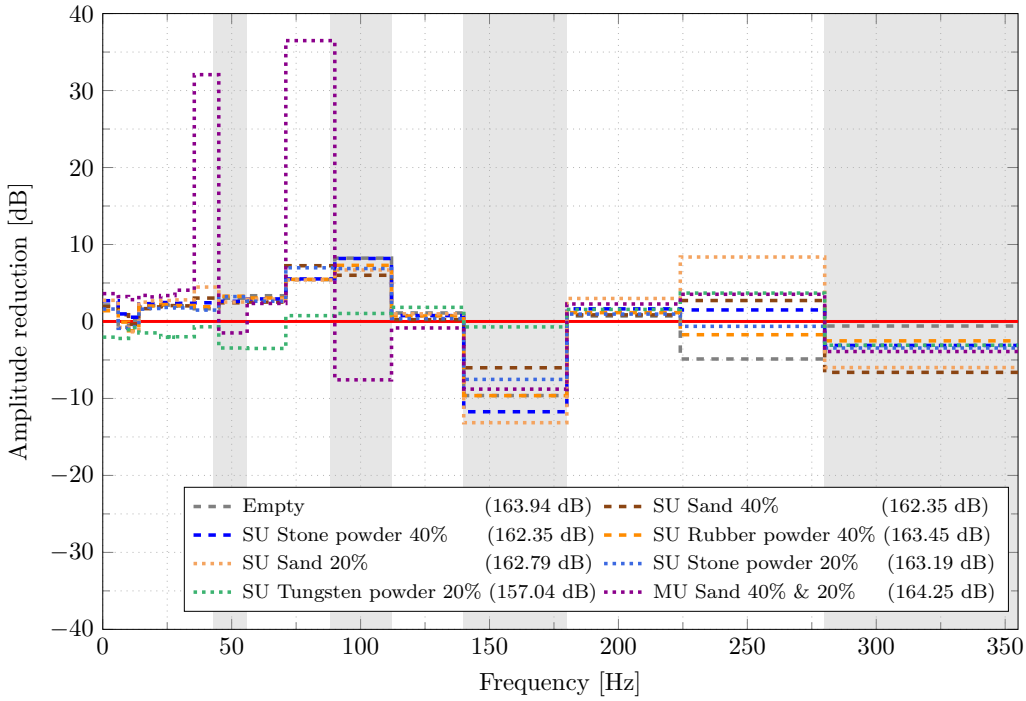

Figure A3.16: Amplitude reduction plot of the SU and MU HCDP mounted between the stator arm and stator ring.

A3.3 FRF of SU HCDP concept mounted on the excitation point side

To conduct a more in-depth examination of the impact of particle damper location on vibration attenuation, the SU HCDP is securely positioned on the inner surface of the WTS ring, precisely on the side where the excitation point is located, Figure 9.4 (g). The results of this configuration are given in Figure A3.17 - Figure A3.19. The observation made for this configuration reveals that mounting the SU HCDP at this specific location leads to a substantial reduction in vibration amplitude, especially around the resonance frequencies of 50 Hz, 100 Hz, and 355 Hz. Nonetheless, the vibration attenuation resulting from the presence of granular materials is not evident, as the reduction in vibration amplitude caused by the empty HCDP closely matches that of the partially filled HCDP. This observation is further supported by comparing the SL values of surface velocity. Furthermore, the filling ratios also show no influence on the vibration attenuation. Therefore, it can be assumed that the installation of HCDP at this specific location has the potential to enhance the bending stiffness of the primary structure, which plays a crucial role in vibration attenuation. This observation is reasonable since the width factor contributes linearly to both the resulting stiffness and mass of the system.

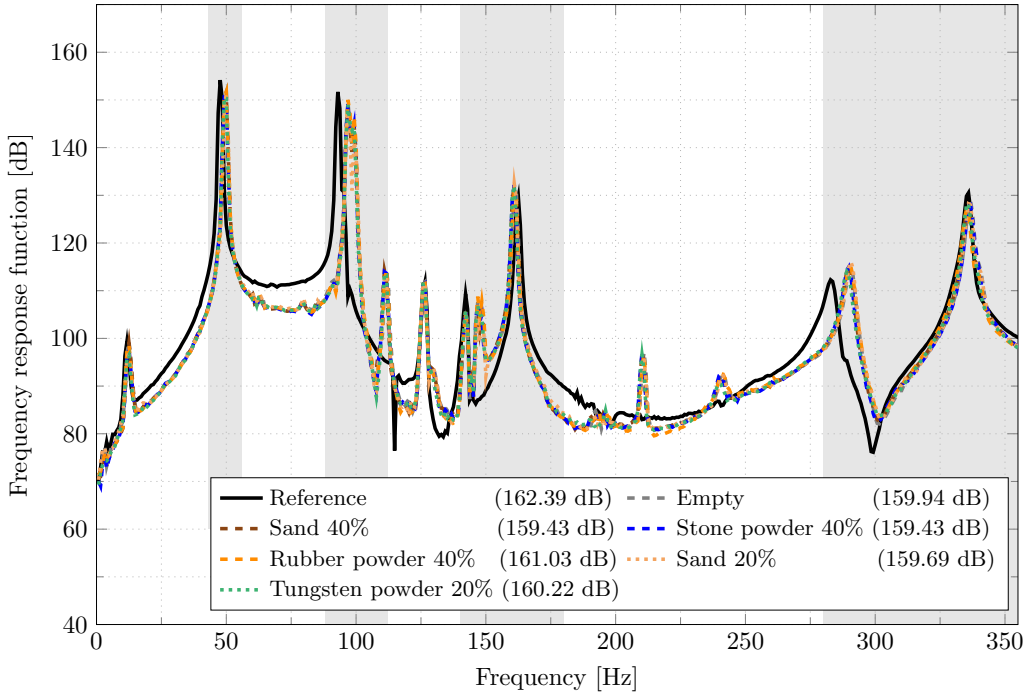

Figure A3.17: Narrowband spectrum of the WTS test specimen for the SU HCDP mounted on the inner wall of the stator ring (excitation point side).

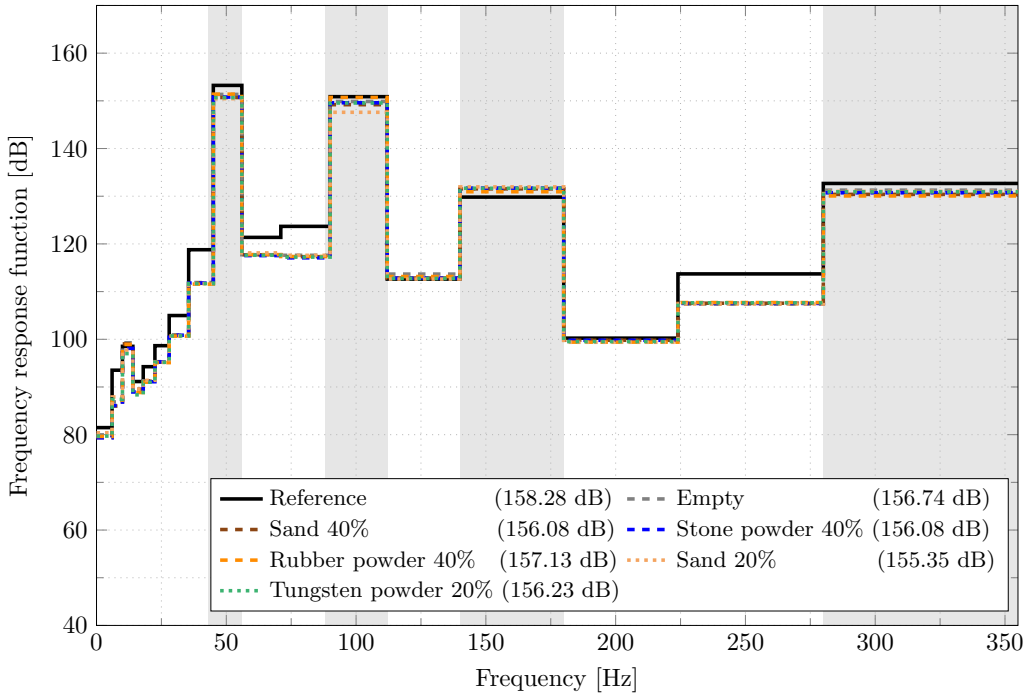

Figure A3.18: One third octave band of the WTS test specimen for the SU HCDP mounted on the inner wall of the stator ring (excitation point side).

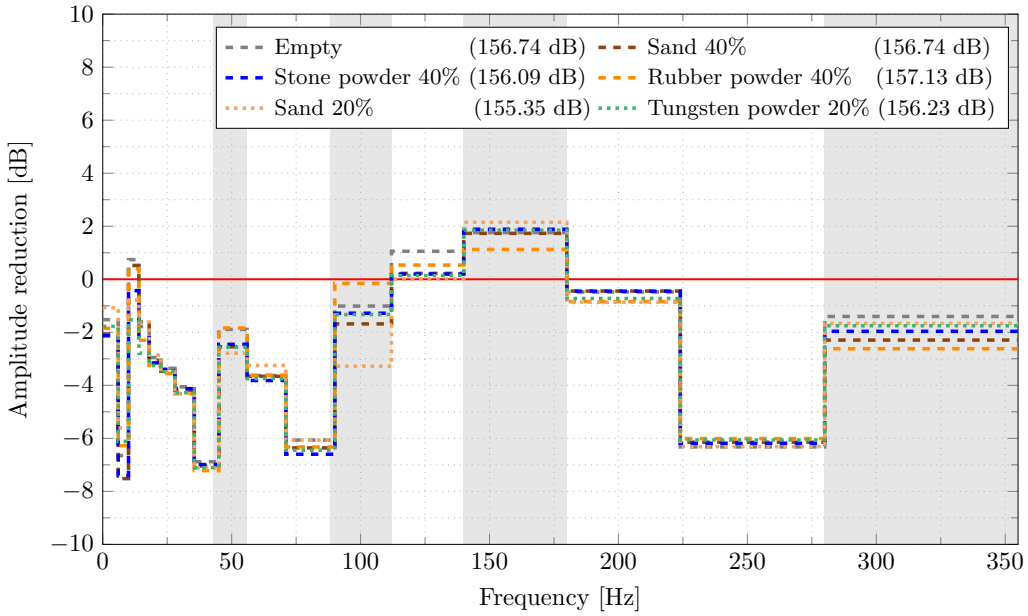

Figure A3.19: Amplitude reduction plot of the WTS test specimen for the SU HCDP mounted on the inner wall of the stator ring (excitation point side).

A3.4 FRF of HCDP concept in various configurations

As a subsequent step, both SU and MU HCDPs are simultaneously attached to different locations on the WTS test specimen, specifically referred to as configuration 1, configuration 2, and configuration 3.

For the configuration 1, the MU HCDP, which is partially filled with stone powder and sand is mounted on the outer wall of the ring. This particular combination of HCDP has been selected based on previous discussions, as it has demonstrated the highest level of vibration attenuation for the WTS test specimen. Additionally, a SU HCDP filled with tungsten powder is mounted between the stator arm and ring in order to take advantage of the broadband damping exhibited by tungsten powder at this specific location. Figure A3.22 illustrates the vibration attenuation achieved by this configuration. By implementing this configuration, the vibration amplitude is effectively reduced by 1.4 dB, 10.4 dB, and 15.0 dB at the resonance peaks located around 50 Hz, 150 Hz, and 355 Hz, respectively. Furthermore, the arrangement for configuration 2 closely resembles that of configuration 1, with the distinction that only a SU HCDP is affixed to the WTS test specimen, see Figure 9.4 (i). It has been observed that the configuration 2 is only effective around the resonance frequencies of 150 Hz and 355 Hz. Moreover, Configuration 3 builds upon the configuration 1, with the addition of an empty HCDP that is mounted onto the inner wall of the WTS ring, specifically on the side where the excitation point is situated, Figure 9.4 (j). The choice to attach an empty HCDP at this specific location was made because the damping effect in this area is primarily attributed to the increased bending stiffness of the primary structure, rather than the presence of granular materials. The damping behavior of this configuration closely resembles that of configuration 1. Additionally, the SL values of all three mentioned configurations are nearly identical and are larger than the SL values of the reference specimen (158.28 dB).

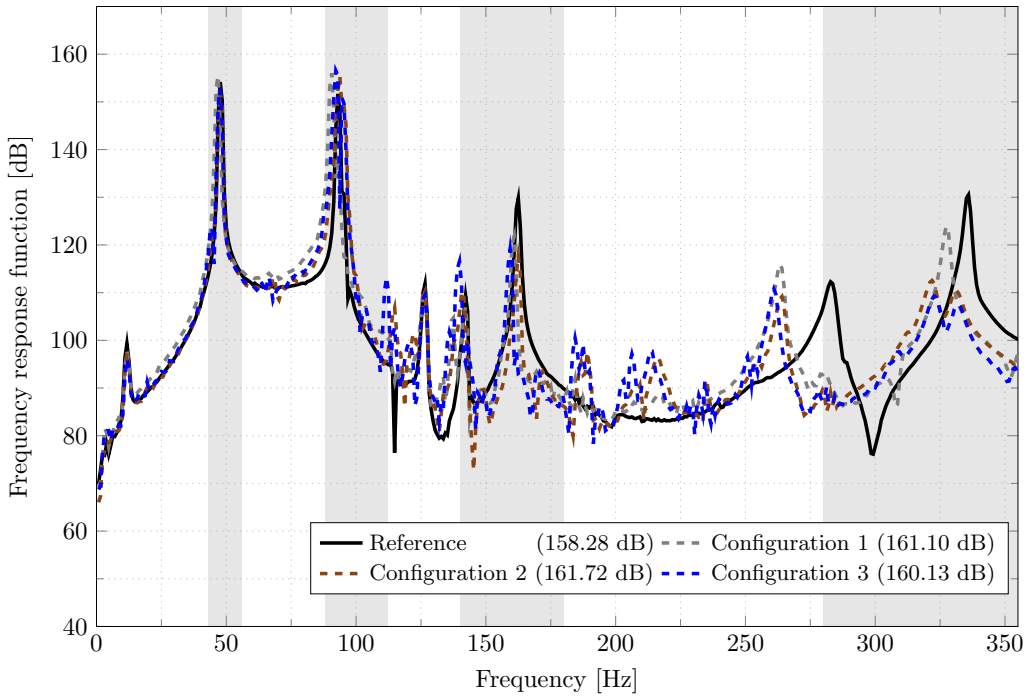

Figure A3.20: Narrowband spectrum of the WTS test specimen for three configurations.

A4 Narrowband spectrum of the PEC concept

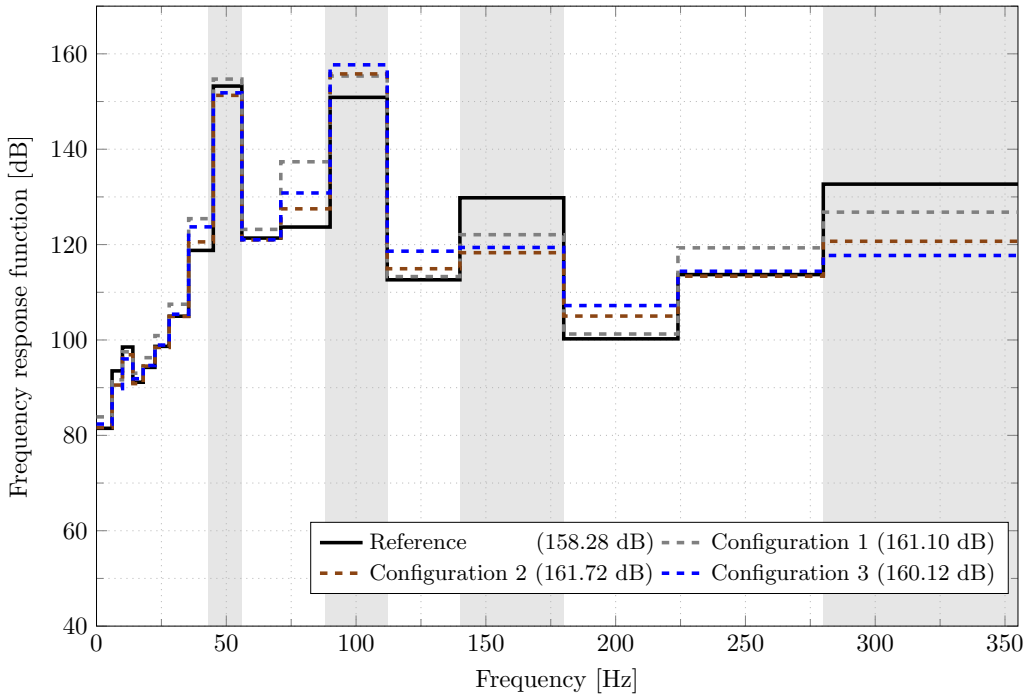

Figure A3.21: One-third octave band of the WTS test specimen for three configurations.

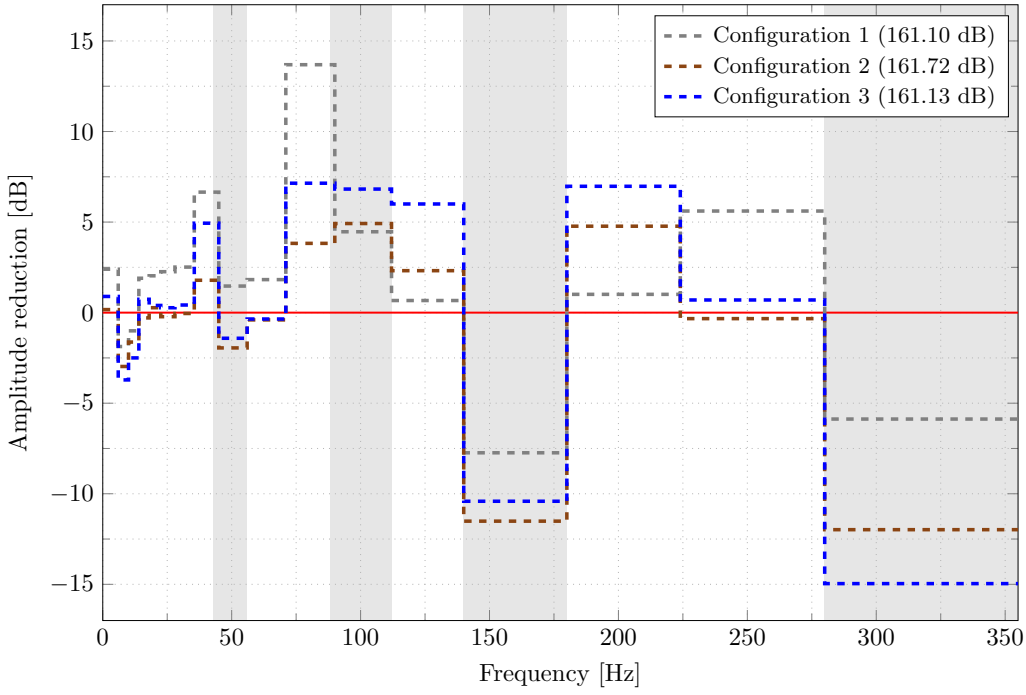

Figure A3.22: Amplitude reduction plot of the WTS test specimen for three configurations.

A5 FRF of half-scaled test specimen with TWC and varying wall thickness

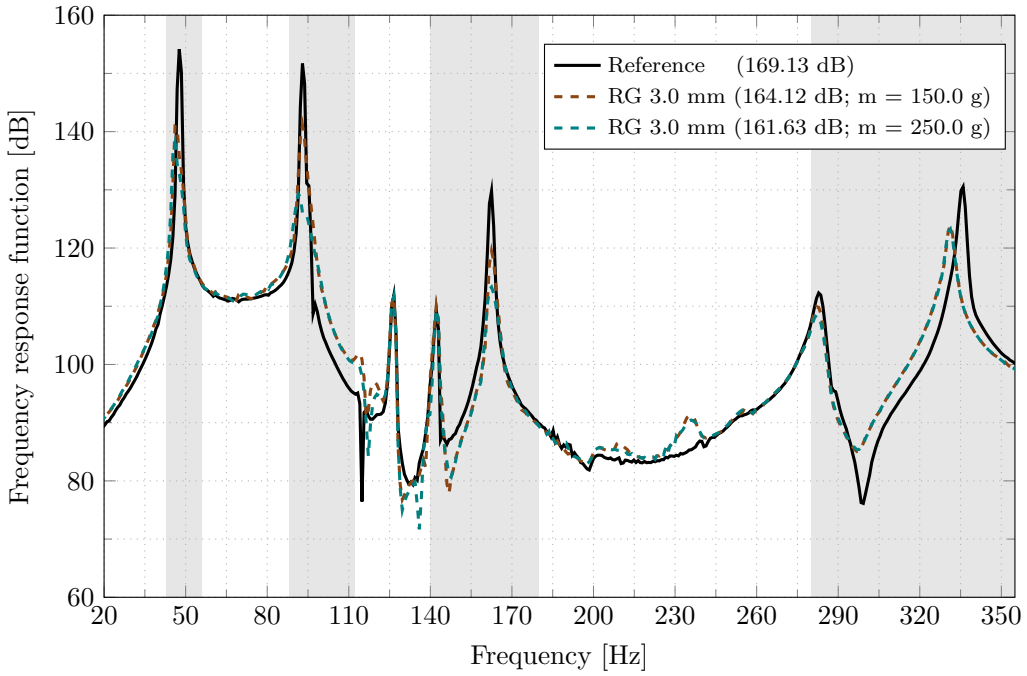

Figure A4.23: Narrowband spectrum of the PEC concept. The SL values of surface velocity are given in dB, and the mass of the granular filling material is measured in g.

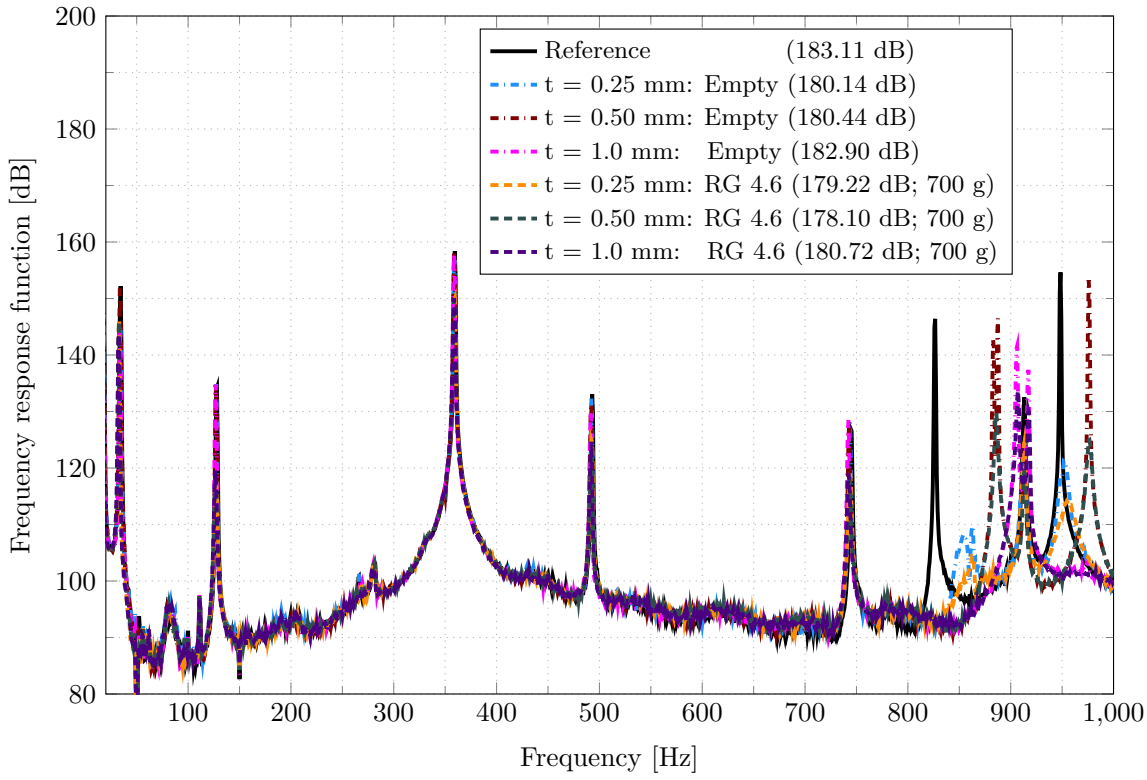

Figure A5.24: Narrow band spectrum of empty and partially filled TWC with varying wall thicknesses (t).

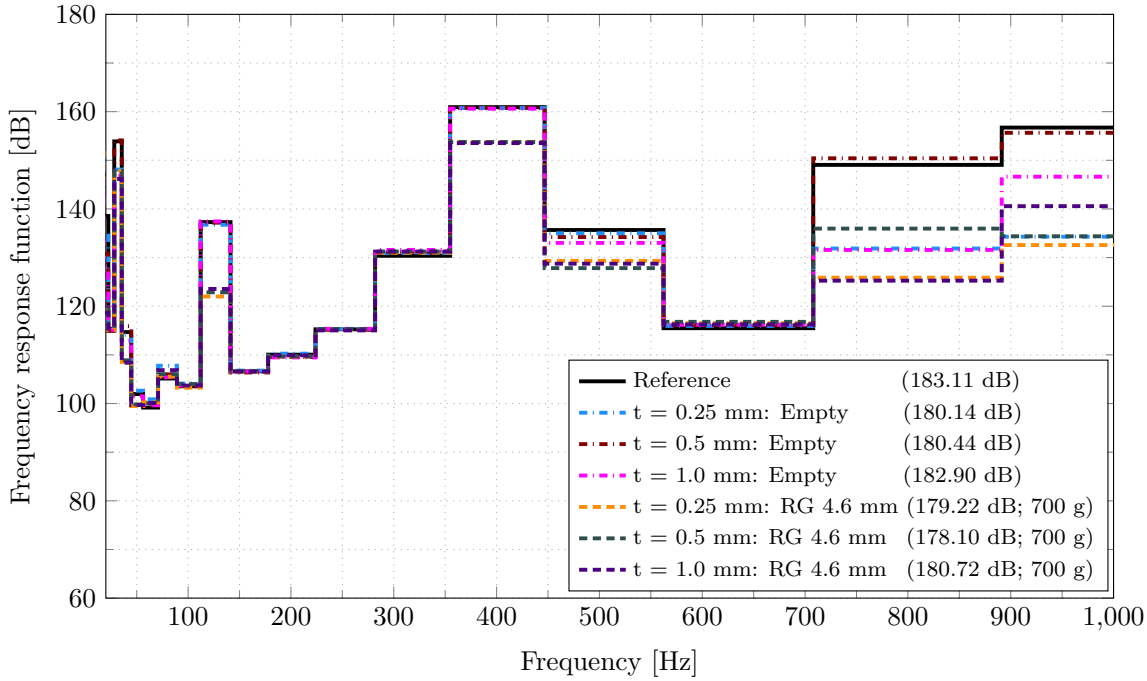

Figure A5.25: One-third octave band comparing empty and partially filled TWCs with varying wall thicknesses (t).

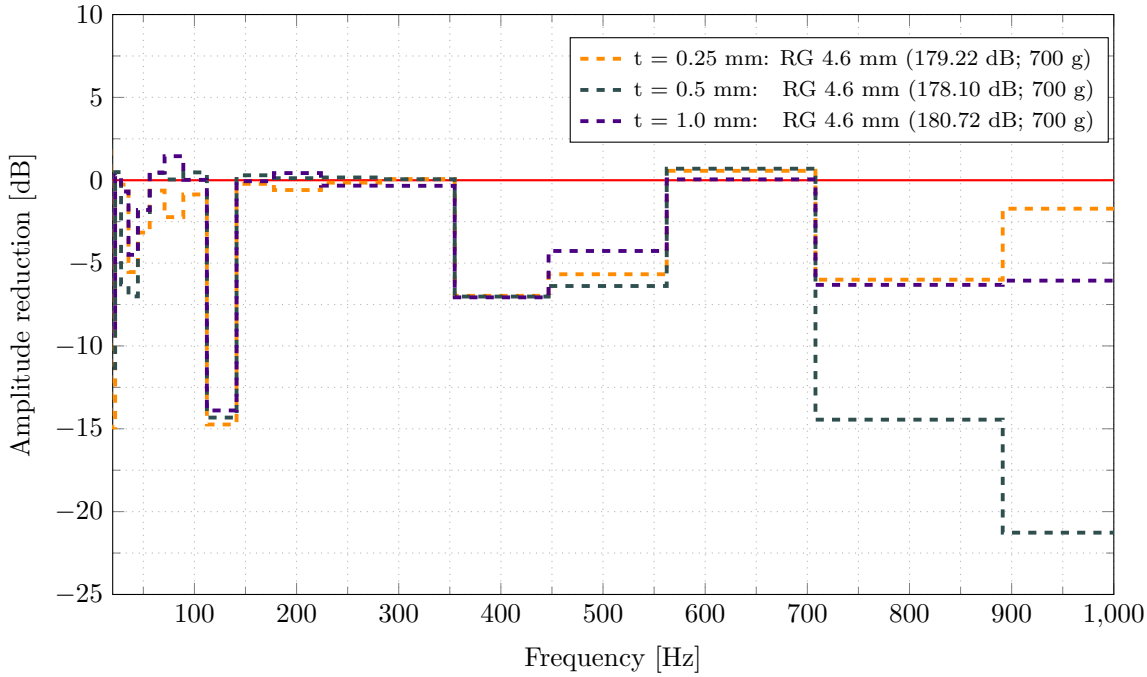

Figure A5.26: Amplitude reduction plot of partially filled TWCs with varying wall thicknesses (t).

A6 Particle damper performance with granular material enclosure using non-metallic nets

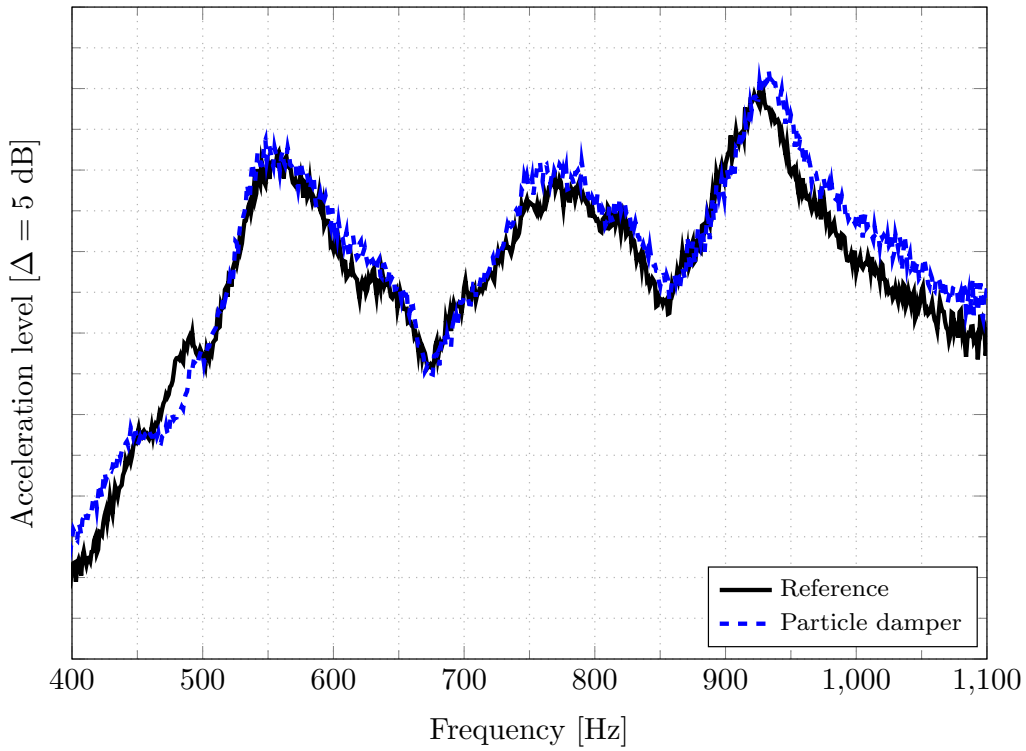

Figure A6.27: Acceleration levels of the powertrain under full-load conditions with rubber granulate enclosed in a net, during a rotational speed sweep from 50 to 10000 RPM.

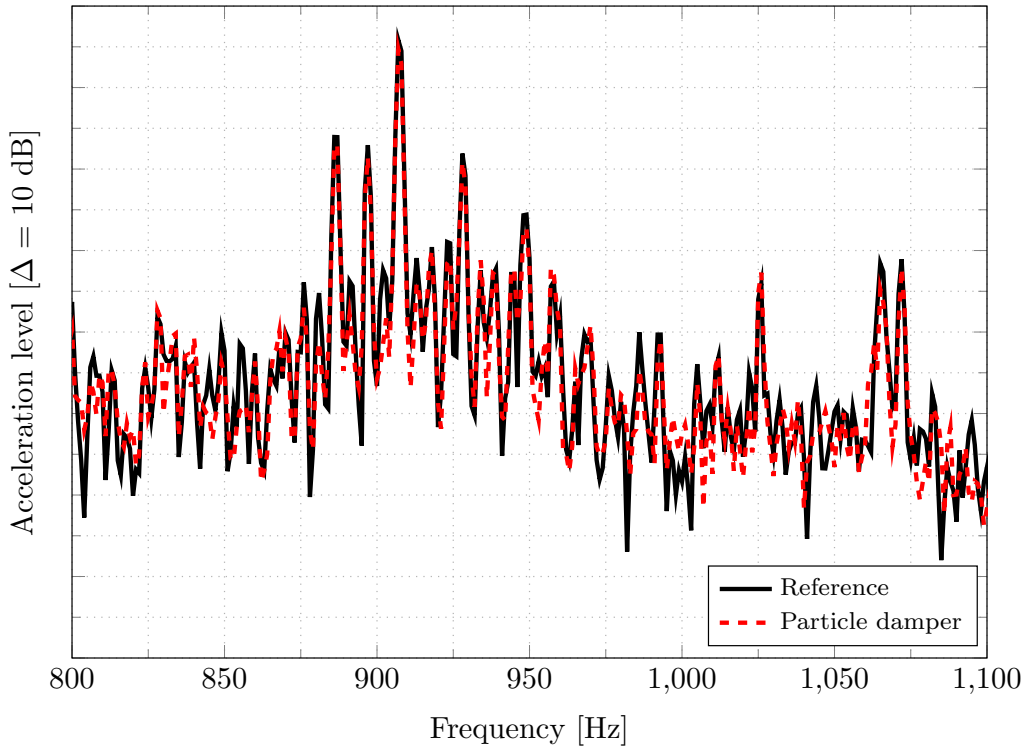

Figure A6.28: Acceleration levels of the powertrain under stationary test conditions with rubber granulate enclosed in a net.

Publications

Journal article

1. Prasad, B. B., Duvigneau, F., Bueschel, A., Göhler, H., Jehring, U., Juhre, D., Woschke, E.: „The impact of dynamic loading and cyclic temperature variations on the damping efficiency of particle dampers“. Accepted by: *Journal of Vibration and control*, 2024. DOI: 10.1177/10775463241264332

2. Prasad, B. B., Duvigneau, F., Reinboth, T., Juhre, D. and Woschke, E.: „Design strategies of particle dampers for large-scale applications“. Accepted by: *Journal of Vibration Engineering Technologies (JVET)*, 12, 2023. DOI: 10.1177/0309324718755956

3. Prasad, B. B., Duvigneau, F., Juhre, D. and Woschke, E.: „Application of Particle Dampers on a Scaled Wind Turbine Generator to Improve Low-Frequency Vibro-Acoustic Behavior“. Accepted by: *Applied Sciences*, 12, 2022. DOI: 10.1177/0309324718755956

4. Prasad, B. B., Duvigneau, F., Juhre, D. and Woschke, E.: „Damping Performance of Particle Dampers with Different Granular Materials and their Mixtures“. *Applied Acoustic*, 24, 2022, S. 226–238. DOI: 10.1177/0309324718755956

Conference paper

1. Prasad, B. B., Luft, T., Michaelsen, C. and Rottengruber, H.: „Comparison of active and passive vibration control techniques for electric drive power electronic subsystem: Experimental validation “. In: *INTER-NOISE and NOISE-CON Congress and Conference Proceedings, Nantes, France*, 2024, p. 71–82

2. Prasad, B. B., Luft, T., Michaelsen, C. and Rottengruber, H.: „Enhancing Vibroacoustic Performance of Power Electronic Subsystem in Electric Drives Using Particle Dampers“. In: *Proceedings of the 50. Deutsche Jahrestagung für Akustik, Hannover, Germany*, 2024, p.503-506

3. Daniel, C., Woschke, E., Prasad, B. B., Duvigneau, F.: „Effectivity of particle dampers with granular filling under rotating conditions“. In: *SIRM 2023 – 15th European Conference on Rotordynamics, Darmstadt, Germany*, 2023, p. 108-117

4. Prasad, B. B., Duvigneau, F., Jehring, U., Göhler, H., Bueschel, A. and Juhre, D. Woschke, E.: „Einsatz granularer Materialien zur passiven Schwingungsreduktion von Komponenten einer Windenergieanlage“. In: *Proceedings of the 49. Deutsche Jahrestagung für Akustik, Hamburg, Germany*, 2023, p. 1135-1138

5. Prasad, B. B., Duvigneau, F., Woschke, E. and Juhre, D.: „Application and damping mechanism of particle dampers“. In: *PAMM*, 2023, p. 135-1138

6. Prasad, B. B., Duvigneau, F., Woschke, E. and Juhre, D.: „Vergleich verschiedener granularer Materialien und Mixturen für die Anwendung in partikelbasierten Schwingungsdämpfern“. In: *Proceedings of the 48. Deutsche Jahrestagung für Akustik, Stuttgart, Germany*, 2022, p. 1358-1361

7. Prasad, B. B., Duvigneau, F., Woschke, E. and Juhre, D.: „Einsatz granularer Materialien zur passiven Schwingungsreduktion eines Generators einer Windenergieanlage“. In: *Proceedings of the 47. Deutsche Jahrestagung für Akustik, Vienna, Austria*, 2021, p. 573–576

8. Prasad, B. B., Duvigneau, F., Juhre, D. and Woschke, E.: „Experimental study of particle dampers applied to wind turbine blades to reduce low-frequency sound emission“. In: *INTER-NOISE and NOISE-CON Congress and Conference Proceedings, Washington, D.C., USA* , 2021, p. 71–82

9. Prasad, B. B., Duvigneau, F., Woschke, E. and Juhre, D.: „Wind turbine blade and generator test specimen for evaluating a passive vibration reduction concept based on granular materials“. In: *Proceedings of the ISMA*, 2020, p. 3525–3539

10. Prasad, B. B., Duvigneau, F., Juhre, D. and Woschke, E.: „Design of test specimen for wind turbines to evaluate passive vibration reduction concepts based on granular materials“. In: *Proceedings of the 46. Deutsche Jahrestagung für Akustik, Hannover, Germany*, 2020, p. 446–449